European Nuclear Young Generation Forum 2023

Book of Proceedings

ENYGF
KRAKÓW 2023

Kraków, Poland 8 -12May 2023

Organized by

The Polish Nuclear Society Young Generation

European Nuclear Young Generation Forum 2023

8–12 May 2023

Kraków, Poland

Book of proceedings

Sponsored by

świadomie o atomie
energia jądrowa w Polsce

Polskie Elektrownie Jądrowe sp. z o.o.

EDF

Westinghouse

urenco
The Energy to Succeed

OSGE
ORLEN SYNTHOS GREEN ENERGY

WORLD NUCLEAR ASSOCIATION

OAKRIDGE
SCIENCES & SERVICES

Partners and Sponsors

AGH
AGH University of Science and Technology

AGH CENTRUM ENERGETYKI

SOLARIS
NARODOWE CENTRUM PROMIENIOWANIA SYNCHROTRONOWEGO

enen

ZUOP

NEA
NUCLEAR ENERGY AGENCY

nuclear.pl PORTAL

BIZNES ALERT

Kraków.pl

NUCNET

Honorary Patronage

Ministerstwo Klimatu i Środowiska

Kraków
Mayor of the City of Kraków
Jacek Majchrowski

Technical commitee

Anna Talarowska
Chair of commitee

Filip Jędrzejek

Wojciech Kubiński

Tomasz Kwiatkowski

Maciej Lipka

Marek Migdal

Joachim del Roo

Table of Contents

Our ENYGF in Kraków

The ENYGF takes place every two years and is a week-long international event including key note speeches, panel sessions, interactive workshops, site tours, technical sessions (where delegates give presentations and display posters on their work) as well as formal and informal networking opportunities. It is seen as the main opportunity for young nuclear professionals to be heard on a global stage and facilitates the sharing of best practice, knowledge transfer and the building of professional networks.

Our ENYGF was the first after the pandemic and more than 300 people attended the conference. Our motto was „Neutrons for progress" as we think nuclear energy in technology can contribute to many issues faced by humanity. Selection of our motto has marked the 50th anniversary of famous „Atoms for Peace" speach by the US President Dwight D. Eisenhower which was celebrated in 2023.

After a comprehensive reviewing process, 68 submissions were accepted by the Technical Committee, and thus included in this proceedings book.

From the ENYGF Organizing Team, we hoped you enjoy this little piece of our conference.

ENYGF
KRAKÓW 2023

32% 68%

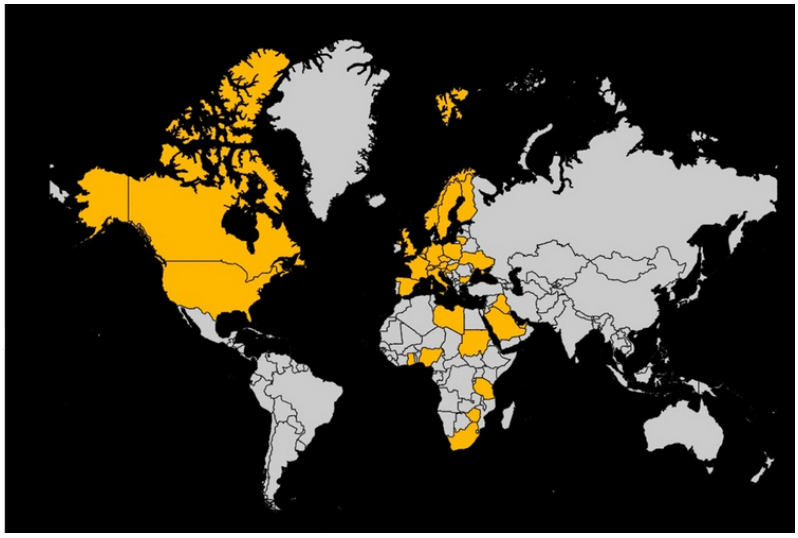

Acknowledgements

The Conference Organizers gratefully acknowledge the efforts of all of the volunteers who contributed to the organization of our conference

Anna and Maciej

Acknowledgements

Separately and by name, we would like to thank the following people who devoted their time to the process of reviewing articles:

Pau Aragón, Sofía Arfinengo del Carpio, Piotr Darnowski, Miriam Diaz Hernandez, Araceli Dominguez-Bugarin, Paweł Gajda, Ana Gonzalez Felgueroso, Jacob Home, Sophie Jackson, Filip Jędrzejek, Antonio Jiménez-Carrascosa, Barbara Kędzierska, Janez Kokalj, Tomasz Kwiatkowski, Elena Lagzdina, Eileen Langegger, Maciej Lipka, Santiago López, Lacey-Jo Elfreida Marsland, Olivia Mindrila, Fabio Nouchy, Sophie Elizabeth Osbourne, Krzysztof Piotr Otlik, Đorđe Petrović, Henry Preston, Prasoon Raj, Adam Rajewski, Thomas Romming, Luis Serra Lopez, Martin Sevecek, Raul Miguel Tacanho Marques, Anna Talarowska, Ronan Tanguy, Saralyn Thomas, Xavier van Huele, Carlos Vázquez-Rodríguez, Jake Nathaniel Williamson

Hot topics

Hot Topic 1– Energy Transition: The Role of Nuclear

Net zero needs nuclear. Mankind needs a reliable energy source that works regardless of the weather, working together with renewable energy, and its implementation is crutial to the successfulenergy transition.

Hot topic 2 – Neutrons for Progress

Nuclear energy is a powerful tool to support sustainable development throughthe scientific and medical applications of neutrons and other types of radiation. Research reactors and neutrons sources are irreplaceable for those purposes.

Hot topic 3 – Communication, Policy, and Education

Every success need a good story. Dissemination the peaceful use of nuclear technology and its benefits is crucial to its success. Together with education they form prosperous policies.

Hot topic 4 – Future Nuclear

Experimental and demonstration reactor designs present on drawing boards, that one day may be the everyday life of advanced energy with potential new features and applications.

Technical Tracks

Technical Track 1 – Reactor physics, Thermal hydraulics, and Simulation

All ideas to become a complete, safe project need a solid portion of calculations. Safe and effective operation is impossible without multiple computer codesfrom various physics areas.

Technical Track 2 – Nuclear Safety and Security

Ensuring nuclear reactors and radioactive sources safety and security remains a matter of global attention. Incidents and emergencies could have significant consequences thus the nuclear community is in constant need to achieve highest possible level of safety standards.

Technical Track 3 – Operation and Maintenance

Well-managed, safe nuclear power plants and installations continually and gradually improve their standards of operation and maintenance. Maintenanceincludes measures that ensure well-tempered functioning of structures, systems and components from construction to decomissioning

Technical Track 4 – Fuel Cycle and Radiation Protection

No machine can run without fuel, nuclear fuel needs to be handled properly. Community efforts are aimed at implementing the development of technical solutions for safe storage and circular economy

Hot Topic 1
Energy Transition: The Role of Nuclear

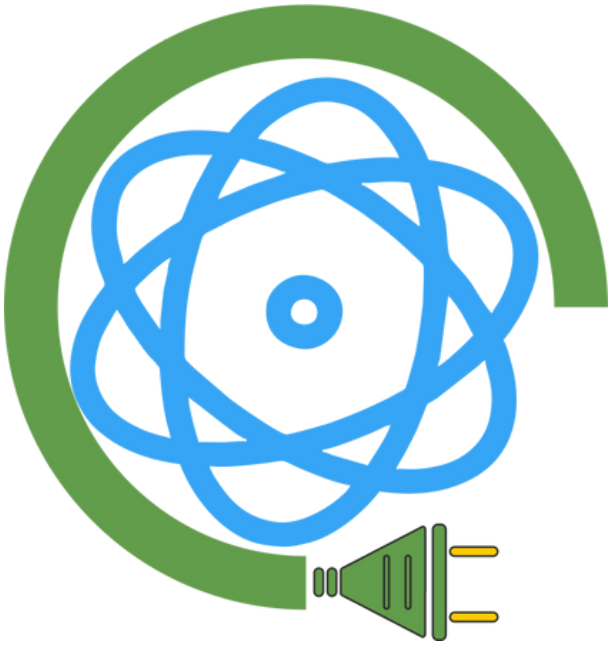

Proceedings of the European Nuclear Young Generation Forum
ENYGF'23
May 8-12, 2023, Kraków, Poland

Nuclear in comparison with other sources of energy: environmental, political, economic and legal aspects

Aksenova, Nataliia

Technical University of Berlin (TU Berlin), Germany

aksenovanataliia@gmail.com

I. INTRODUCTION

Nuclear energy is one of the cleanest energy sources with minimal carbon dioxide emissions. So why do some countries keep moving away from nuclear and new investment in nuclear?

When comparing different energy sources in terms of pollution and accidents, which types of energy are safer? Why the freedom to choose energy sources has **a political connotation,** it is not given the appropriate importance to a fact-based evaluation of safety concerns.

Other, no less important aspect, if we compare the **economic indicators and account investments** on all lifecycle phases of the nuclear power plant and other electrical generation plants (construction, operation, and decommissioning). In the long run, which type of the energy production is more efficient? Who pays back the costs spent on the extraction of raw materials and the construction of the energy generation plants faster?

The next issue that will be discussed in this article is **legislative regulation**. Making a preference for one or another type of energy, the state, on the example of European countries, creates a special legislative framework for these purposes, so that the development of other types of energy becomes less or more convenient for energy providers.

II. NUCLEAR IN COMPARISON WITH OTHER SOUCES OF ENERGY

A. Environmental Aspect

The energy production can have negative impacts on human health and the environment in three ways [1]

- **air pollution and greenhouse gas emissions:** fossil fuels and the burning of biomass – wood, dung, and coal – are responsible for the air pollution and, as a result, the people's deaths. At the same time, they are the main source of greenhouse gases (Figure 1), the primary driver of climate change.

Figure 1. Greenhouse gas emissions
Measures in emissions of CO2-equivalents per gigawatt-hour of electricity over the lifecycle of the power plant.
1 gigawatt-hour is the annual electricity consumption of 150 people in the EU

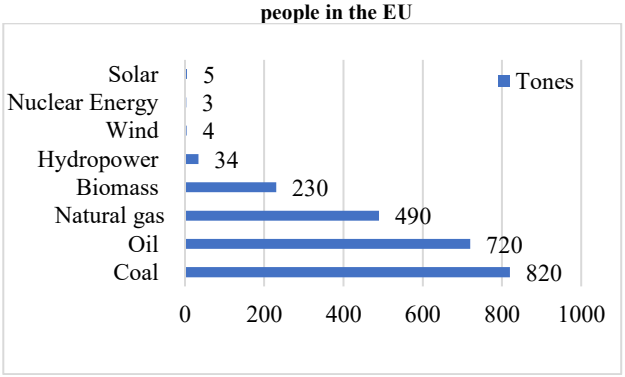

Source: https://www.thelancet.com/journals/lancet/article/PIIS0140-6736(07)61253-7/fulltext

- **accidents:** this includes accidents that happen in the mining and extraction of the fuels – coal, uranium, rare metals, oil, and gas, and, it also includes accidents that occur in the transport of raw materials and infrastructure, the construction of the power plant, or in the result of their maintenance. How we can see on the Figure 2, the main quantity of the deaths happens in the coal and oil industries.

Figure 2. Death rates per unit of electricity production
Death rates are measures based on deaths from accidents and air pollution per terawatt-hour (TWh) of electricity

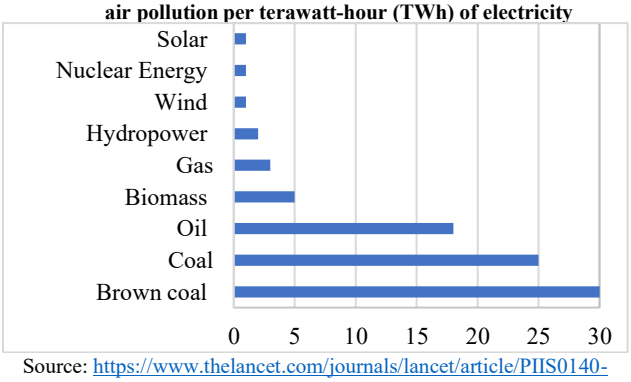

Source: https://www.thelancet.com/journals/lancet/article/PIIS0140-6736(07)61253-7/fulltext

B. Political Aspect

Under the political aspect assumes how countries make a choice between the different types of the energy sources, how geopolitical factors and the "energy" dependence of countries on each other influence on this choice.

The trend of recent years is to create an energy transition, to reduce emissions and the carbon footprint in order to limit global warming, leads to difficult choice of the current governments in ways how to solve the tasks and achieve carbon neutrality. And this problem is especially acute in the example of the European space, where extremely opposite views remain - from the complete abandonment of nuclear energy in some countries and the transition to renewable energy sources, while in other countries nuclear energy keeps the role of the main source of electricity (Figure 3).

Figure 3. Share of Nuclear Energy in Electricity Generation in Europe 2020 (%)

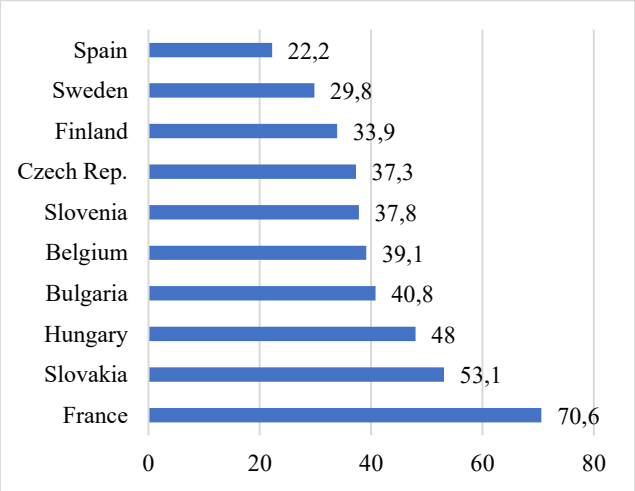

Source:https://pris.iaea.org/pris/worldstatistics/nuclearshareofelectricitygeneration.aspx

Despite the fact that such EU countries as Germany, Italy, Switzerland, Belgium, Spain are pursuing a long-term policy of abandoning nuclear energy, unlike France and Hungary, on the contrary, are increasing the share of nuclear energy and investing in this industry, in 2021 the European Commission added nuclear energy to the classification of clean energy sources [2].

Although nuclear energy is a low-carbon alternative to fossil fuels and represents a critical component in the energy mix of 13 of the 27 EU Member States, accounting for almost 26% of the electricity produced in the EU. However, in the aftermath of the 1986 Chernobyl disaster and the 2011 nuclear catastrophe in Fukushima, Japan, nuclear energy has become highly controversial [3].

As an analysis of the reasons for abandoning nuclear energy shows, in addition to the general fear of a repetition of the accident and the resulting radioactive waste, the "mood" of the current government is also a necessary factor.

The most striking example in this sense is **Germany**. The most active political force is the Green Party, which promotes renewable energy sources and forms of public opinion on the complete rejection of nuclear energy. Opposition to nuclear power is at the core of the activity that launched the Green Party in 1980, long before the Fukushima and even Chernobyl accidents, and continues to be its rallying cry.

And here we can consider **the phenomenon of Germany**, which is distinguished by freedom of speech and the ability of the society to publicly express their opinion and influence on the political decisions. Therefore, despite Germany's dependence on Russian fossil fuels, whose gas supplies account for 40% of imports, a sharp increase in electricity prices in recent years, Germany continues to close the existing nuclear power plants, relying on renewable energy and hydrogen in the long term.

We see the backlash and dependence on political power in **the example of France**. Polls have revealed an interesting feature - representatives of the left views are more likely to advocate a reduction in the share of nuclear energy, while the right, on the contrary, support the modernization of the corresponding infrastructure [4]. When a representative of right-wing views came to power, the preponderance leaned in favor of nuclear energy.

In November 2021, President Macron announced his intention to start building new nuclear reactors for the first time since 2002 and to modernize the energy sector for achieving energy independence, to access to cheap energy and carbon neutrality by 2050 as part of the fight against climate change [5].

Thus, on a vivid example of the European Union, we can talk about the significant influence of the current government on the choice of the preferred source of energy.

C. Economic Aspect

According to the NEA document “The Full Costs of Electricity Provision”, published in 2018, the costs of electricity provision fall into **three different, comprehensible categories**: plant-level costs of generation, grid-level system costs and the external social and environmental costs (Figure 4).

Figure 4. Different cost categories composing the full costs of electricity provision

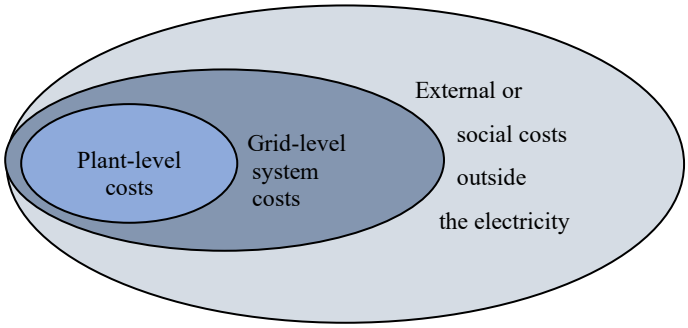

The first category is constituted of plant-level costs, which include the concrete and steel used to build the plant, and the fuel and the manpower to run it.

The second category concerns the costs at the level of the electricity system, linked through the transmission and distribution grid. It includes the costs that plants impose on the system in terms of extending, reinforcing or connecting to the grid, but also the costs for maintaining spinning reserves or additional dispatchable capacity when the

output of some technologies – typically wind and solar photovoltaic - is uncertain or variable.

The third, even broader, category includes items that impact the well-being of individuals and communities outside the electricity sector. Known as external or social costs, such costs include the impacts of local and regional air pollution, climate change, the costs of major, frequently not fully insurable, accidents, and land use or resource depletion. Social costs also include the impacts of different power technology choices on the security of energy and electricity supply, employment and regional cohesion or on innovation and economic development.

The Full Costs of Electricity Provision should be distinguished from **the Levelized Cost of Electricity (LCOE).** The LCOE indicates the discounted lifetime costs for different baseload technologies, averaged over the electricity generated. It has its purpose for informing the investment choices of electric utilities in regulated electricity systems, but it is less pertinent in deregulated electricity systems where revenues vary from period to period over an electricity generator's lifetime. The LCOE is an estimation of the cost of production of energy, thus it tells nothing about the price for consumers and is most meaningful from the investor's point of view [6].

According to the IEA report "Projected Costs of Generating Electricity", published in 2020, LCOE produced by nuclear is about $80 per MWh, this is one of the cheapest indicators among other types of energy (Figure 5).

Figure 5. LCOE by technology

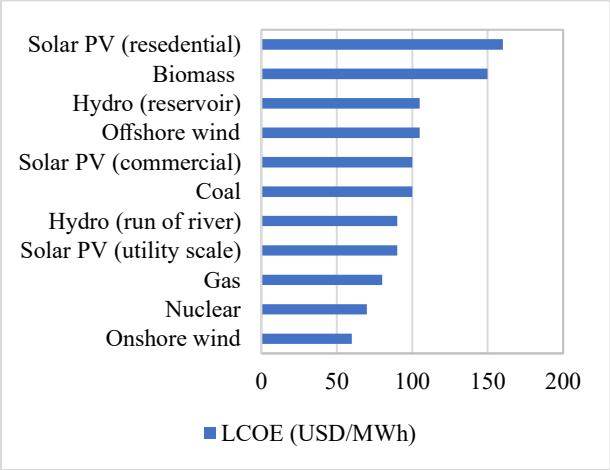

Source: https://iea.blob.core.windows.net/assets/ae17da3d-e8a5-4163-a3ec-2e6fb0b5677d/Projected-Costs-of-Generating-Electricity-2020.pdf

The cost of nuclear power is often broken down into **capital costs and operating costs.** Capital costs include site preparation, engineering, manufacturing, construction, commissioning, and financing. Operating costs include fuel costs (from uranium mining to fuel fabrication), maintenance, decommissioning, and waste disposal.

The capital costs of a nuclear power plant are much higher than for energy sources such as coal and natural gas - and the annual cost of repaying the initial investment is substantially higher than the annual operating costs. This is because nuclear power plants are **technically complex and must satisfy strict licensing and design requirements**.

The design and construction of a new nuclear power plant requires many highly qualified specialists and often takes many years, compounding financing costs, which can become significant. Nuclear power takes 5 to 17 years more time between planning and operation [7].

Because the capital costs of nuclear power are so significant, the most effective way to reduce the total price of nuclear energy is to design and construct plants more efficiently. The global trend is now moving toward **more standardized designs.** Standardization reduces design and construction uncertainties, as well as the time required to build future reactors, thus reducing capital costs.

In recent years, many nuclear power experts have called for **small modular reactors** where is possible to simplify safety systems and strict regulations, given their more simplified designs and passive safety measures. These reactors are also expected to have lower operating and maintenance costs [8].

Also, unlike coal and natural gas, nuclear power plants do not emit significant quantities of greenhouse gases. This environmental benefit can directly affect nuclear power economics in areas where **carbon credits or taxes** have been implemented or are being considered.

On the other hand, nuclear energy has by far the highest capacity factor of any other energy source. Capacity is the amount of electricity a generator can produce when it's running at full blast (Figure 6). This basically means **nuclear power plants are producing maximum power more than 92% of the time during the year**. That's about nearly 2 times more as natural gas and coal units, and almost 3 times or more reliable than wind and solar plants [9].

Figure 6. Capacity Factor by Energy Source in 2020

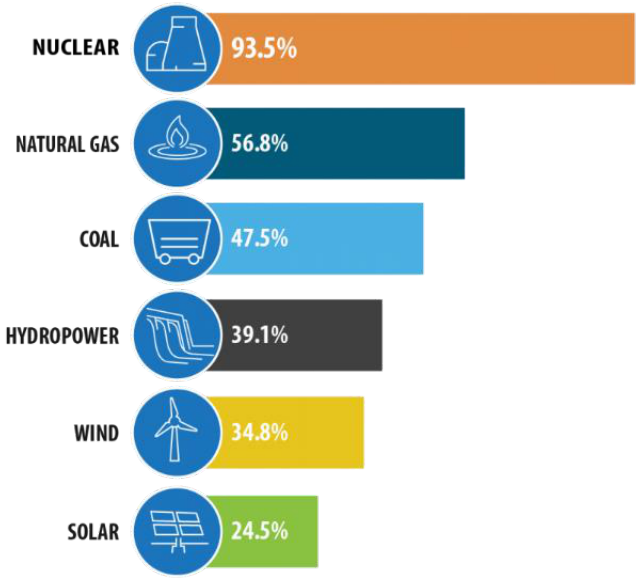

Source: https://www.iea.org/data-and-statistics/charts/global-government-clean-energy-spending-by-sector-and-technology-allocated-up-to-october-2021

D. Legal Aspect

Considering the legal aspect, there are two important issues: the first relates to state programs for subsidizing various energy sources, which are adopted through the approval of a legislative act, second relates to the peculiarities of regulatory framework of nuclear energy.

Today, combined **investment in energy efficiency, renewables and hydrogen and fuel cells is about twice that of nuclear**, but with less to show for it in terms of electricity supply. Since the turn of the century, research and development expenditure on renewables, energy efficiency and hydrogen and fuel cells has risen markedly.

As of October 2021, global government costs on clean energy reached USD 480 billion. The **USD 45 billion allocated to renewables** – including electricity, heat and fuels (biofuels, advanced biofuels and biogas) – accounted for about 9% of announced public spending on clean energy [10] (Figure 7).

Figure 7. Global government clean energy spending by sector and technology allocated up to October 2021 (USD billions)

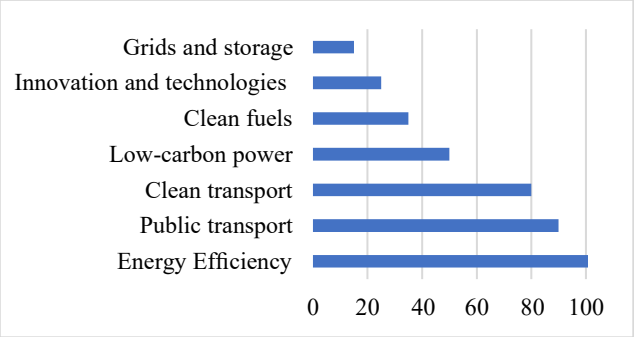

Source: https://www.iea.org/data-and-statistics/charts/global-government-clean-energy-spending-by-sector-and-technology-allocated-up-to-october-2021

Subsidies paid to renewable energy will peak just above $210 billion in 2030, before declining to about $170 billion by 2040. Over the period 2016-2040, cumulative subsidies to renewables are $4.7 trillion. Of total cumulative subsidies, about three-quarters go to solar PV and wind power, about 20% to bioenergy and the remaining portion to other renewables-based power plants [11].

Thus, now there is a tendency when the attention of states is directed to subsidizing and investing in renewable energy sources and creating an appropriate regulatory framework for this purpose. This picture is expected to change in the future.

Regarding the second issue is that the achievement and maintenance of a high level of safety during the lifetime of nuclear facilities and the duration of activities requires a **sound governmental, legal and regulatory framework**. The IAEA strives to strengthen such a framework in its member states through its Safety standards and review services.

A key aspect in the planning of new-built of a nuclear power plant is legal requirements about **licensing process.** The licensing process may introduce additional technical and operational requirements, which may lead to additional costs, and to challenges in relation to the time schedule for finalization of a project. So, the strict safety regulations and licensing imposed on the nuclear industry are the reason why other sources of energy are more attractive.

III. Conclusion

All energy sources have negative effects. But they differ enormously in size: as we saw, fossil fuels are the dirtiest and most dangerous, while nuclear and modern renewable energy sources are vastly safer and cleaner. From the perspective of both, human health and climate change, it matters less whether we transition to nuclear power or renewable energy, and more that we stop relying on fossil fuels.

There are many different electrical generation methods, each having advantages and disadvantages with respect to operational cost, environmental impact, and other factors – these all are the possibility of energy mixes modelling.

With nuclear power facing an uncertain future in many countries, the world risks a steep decline in its use in advanced economies that could result in billions of tonnes of additional carbon emissions. Some countries have opted out of nuclear power in light of concerns about safety and other issues. Many others, however, still see a role for nuclear in their energy transitions but are not doing enough to meet their goals.

Nuclear is still needed because renewables are intermittent and need natural gas for backup. Alongside renewables, energy efficiency and other innovative technologies, nuclear can make a significant contribution to achieving sustainable energy goals and enhancing energy security.

IV. References

[1] Markandya A, Wilkinson P. Electricity generation and health. The Lancet 2007.

[2] Regulation (EU) 2020/852 of the European Parliament and of the Council of 18 June 2020 on the establishment of a framework to facilitate sustainable investment, and amending Regulation (EU) 2019/2088

[3]https://www.europarl.europa.eu/factsheets/en/sheet/62/nuclear-energy

[4] https://www.ifop.com/publication/les-francais-et-la-sortie-du-nucleair

[5] https://www.world-nuclear-news.org/Articles/France-outlines-plans-to-speed-new-nuclear

[6] NEA (2018), The Full Costs of Electricity Provision, OECD Publishing, Paris

[7] IEA (2020), Levelised Cost of Electricity Calculator, IEA, Paris.

[8] https://thebulletin.org/2019/06/why-nuclear-power-plants-cost-so-much-and-what-can-be-done-about-it/

[9] https://www.iea.org/data-and-statistics/charts/average-annual-capacity-factors-by-technology-2018

[10] https://world-nuclear.org/information-library/economic-aspects/energy-subsidies.aspx

[11] https://www.iea.org/articles/how-much-will-renewable-energy-benefit-from-global-stimulus-package

Proceedings of the European Nuclear Young Generation Forum
ENYGF'23
May 8-12, 2023, Kraków, Poland

Safety, Security and Safeguard Consideration of Nuclear Power Plants in the Kingdom of Saudi Arabia

Alsafi, Osama[1], Alhamdi, Abdulwahab[1], Alsanea, Abdulaziz[1], Alsultan, Mohammed[1], Shams, Afaque[1,3], and Al-Athel, Khaled[1,2]

[1] King Fahad University of Petroleum & Minerals (KFUPM), Saudi Arabia

[2]Interdisciplinary Research Centre for Advanced Materials (IRC-AM), KFUPM, Saudi Arabia

[3]Interdisciplinary Research Centre for Renewable Energy and Power Systems (IRC-REPS), KFUPM, Saudi Arabia

*Corresponding author: s201827080@kfupm.edu.sa *(O. Alsafi)*

I. INTRODUCTION

Many countries worldwide share the ambition of adapting nuclear energy in their total energy mix. The Saudi government expressed interest in including nuclear energy as part of the overall energy mix in 2009. However, as of 2019, Saudi Arabia's energy mix consisted solely of fossil fuels producing 386 TWh of power, of which 56% was produced by burning natural gas and the remaining 40% by burning oil [1]. Nuclear energy became an essential component of the Saudi 2030 vision as a means to diversify the country's energy mix, produce clean energy to fight global warming, and meet the rising local demand for energy. This was due to the significant release of greenhouse gases to the environment and the need to abide by the Paris international climate change treaty signed in 2015. Saudi Arabia is taking serious steps to introduce nuclear energy as a contributor in the energy mix. Environmental conditions in the kingdom require extra attention since it has some unique phenomenon, such as heat waves, that not many countries share them. Additionally, nuclear energy is a highly developed technology since it must be operated under strict safety regulations without compromising its performance. The nuclear reactor could serve many purposes with different kinds of designs. As a result, the design that meets the safety consideration and regulation of Saudi Arabi is desired. To reach such a design, existing designs should be studied and compared to the government regulations and safety standards. Furthermore, the security of the power plant must be taken into account while planning to build new power plants. Security aspects include political tension in the area as well as cyber security infrastructure. Nowadays, cyber security is considered the main security measure. In addition, the best way to avoid accidents is to learn from the previous ones. Thus, it is important to consider previous accidents and study them when composing new regulations and evaluating existing designs. This article attempts to address potential challenges that might face Nuclear Power Plants (NPPs) in the kingdom with the safety evolution of promising designs, and provide lessons learned from past experience in NPP operation.

II. ENVIRONMENTAL CONDITIONS

Fossil fuelled power plants have become the backbone of modern civilizations, they have been around since electricity was first discovered in the late eighteenth century, unlike NPPs which have been first operated in 1950. Compared to fossil fuelled power plants, the site of an NPP must be carefully selected and evaluated such that it satisfies certain criteria, which are more stringent than any other power plant. For instance, the plant must be located near a reliable heat sink, which is embodied by a large water source in most cases. However, shall the heat sink temperature increase beyond safety margins, the plant becomes susceptible to several issues such as reduced efficiency and overheating to name a few. The Kingdome of Saudi Arabia lies on the equator; thus, both seawater and ambient temperatures are high year-round, which imposes a risk when the first NPP becomes commercial. Moreover, the kingdom's geographical location imposes several other environmental challenges such as seawater salt concentration, humidity, and sandstorms. This section is dedicated to briefly summarize the impact of such challenges on the operation of the first NPP in the kingdom.

A. Seawater Temperature

The existence of an ultimate heat sink is a major consideration for an NPP site. It is essential to cool the secondary coolant via the condensers of the plant. Although wet or dry cooling towers are an option,

drawbacks such as low heat capacity and water evaporation hinder their use.

In Saudi Arabia, the eastern coast is a viable candidate for the first NPP's cite in the kingdom, considering the presence of the Arabian Gulf Water (AGW). However, the AGW temperature is relatively high since it is mostly bounded by land and only small volumes of cool and freshwater flows from the Indian ocean. Figure 1 shows the average temperature of the AGW year-round. It is evident that during the summer (June through September), the water temperature becomes the highest in the year.

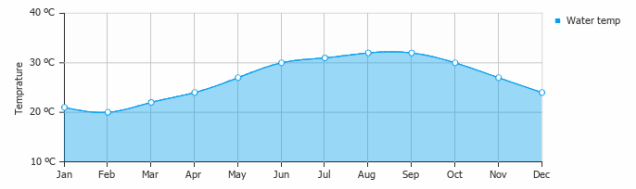

Figure 1. Average temperature of the AGW throughout the year [2].

The high seawater temperature could jeopardize the plant's cooling system, as the low cooling rate would propagate from the condenser to the secondary coolant, and eventually reaches the primary cooling system. This would lead to different scenarios to tackle the issue, among those is increasing the pumping power to allow more water to flow through the condenser and reject the heat. In the United Kingdom, the water flow rate through the condenser of a 1600 MWe reactor is roughly 90 m^3/s [3]. Therefore, the flow rate and the pumping power for an identical unit in Saudi Arabia would be higher, increasing the cost of operation. Moreover, another scenario would require the plant to operate at sub-nominal power, which renders the plant operation unfeasible. Additionally, high heat sink temperature affects the plant operation indirectly. Certain micro-scale organisms such as algae, clams, clumps of seaweed and jellyfish grow via metabolic reactions, which requires abundant energy in the surrounding medium. The high seawater temperature represents a perfect situation where such organisms can thrive. The excessive growth rate of such organisms may block the water intake to the condensers, which reduces the availability of water for cooling and consequently impacts the plant cooling system.

B. Seawater Salinity

The salinity of seawater is the amount of salt in grams dissolved in a kg of seawater, usually expressed as parts per thousand (ppt). The ocean water salinity ranges from 33-37 ppt. However, at high temperatures, the salt is isolated from the water as it evaporates, thus increasing the salinity of seawater [4]. In addition, with the low freshwater inflow from the ocean, the salt concentration grows even higher. Therefore, the Red Sea and the AGW are the saltiest ocean waters, with salinities approaching 40 ppt [4]. The high salt concentration increases the water viscosity and density, consequently, the pumping power to feed the condensers of the plant becomes expensive.

Furthermore, the seawater chemical composition includes free ions, which combine in a chemical reaction to produce different salts. Table 1 shows the principal constituents of seawater ionic composition for a 34.7 ppt salinity.

Principal constituents of seawater*

ionic constituent	g/kg of seawater	moles/kg**	relative concentration
chloride	19.162	0.5405	1.0000
sodium	10.679	0.4645	0.8593
magnesium	1.278	0.0526	0.0974
sulfate	2.680	0.0279	0.0517
calcium	0.4096	0.01022	0.0189
potassium	0.3953	0.01011	0.0187
carbon (inorganic)	0.0276	0.0023	0.0043
bromide	0.0663	0.00083	0.00154
boron	0.0044	0.00041	0.00075
strontium	0.0079	0.00009	0.000165
fluoride	0.0013	0.00007	0.000125

*Concentrations at salinity equal to 34.7.

**Ionic concentrations are conventionally expressed in molecular units. One mole per kilogram is equivalent to $6.023(10^{23})$ ions or molecules per kilogram of seawater. The relative concentrations in column 4 provide the number of ions of each constituent in one kilogram of seawater as compared to the number of chloride ions in one kilogram of seawater.

Table 1. The principal constituents of seawater ionic composition [5].

It is evident that Chloride (Cl^-) and Sodium (Na^+) ions are the most abundant ions in seawater. Upon combination, they form Sodium Chloride salt known as table salt (NaCl). The high NaCl concentration in the ultimate heat sink rapidly increases the corrosion rate of the plant's metallic equipment, as the dissolved ions interact with the free electrons of the metal, causing them to move faster. Therefore, considering the higher salinity of the AGW, the phenomenon is expected to magnify.

C. Humidity

Relative humidity is the ratio of water vapor content in the atmosphere to the maximum water vapor that can be retained without condensation at a given pressure and temperature [2]. The corrosion rate of metals in a humid atmosphere is relatively high compared to a dry atmosphere. The moisture-saturated atmosphere promotes Oxygen reaction with the free electrons of the metal, yielding high corrosion rates and eventually metal degradation [6]. This phenomenon occurs at the critical relative humidity, whose value is close to 80% for most conditions [6]. However, the relative humidity is not the root cause of corrosion, rather the temperature difference experienced by the metal at very high relative humidity. Therefore, the relative humidity is an important consideration for an NPP site.

D. Sandstorms

The Middle East geography mostly consists of deserts and oases; thus, wind activities would probably induce sand or dust storms, which may propagate to civilian and industrial cities. Sandstorms can be locally induced within a city;

thus, they are more frequent, and can displace a wind range of sand particle sizes at high speeds and short distances. On the other hand, dust storms are induced in open areas, and can displace small sized sand particles at low speeds, high altitudes, and over long distances. Considering the distinct characteristics of both storms, their impact on equipment and structures -including plants and factories- is expected to differ as well. In an NPP, they can damage the off-site emergency diesel generators, clog the cooling system filters, cause abrasion, damage the pump and pipe sealings and corrode metallic components. Therefore, since both storms yield wide undesirable effects, the resulting equipment failure may be sequential, and the overall consequence would probably be large.

III. DESIGN CONSIDERATIONS

Nuclear power generation is an advanced technology, and the necessity to operate nuclear installations with the highest safety standards, and without affecting its efficiency manifests that fact. Consequently, power reactors built around the world have different designs, adapting to a country's regulations, conditions, and goals. In 2009, the Saudi government has declared its interest to add nuclear energy as part of the total energy mix. However, as of 2019, the energy mix in Saudi Arabia relied totally on fossil fuels, with around 386TWh power, of which 56% is generated by combusting natural gas, and the rest by burning oil [1]. Considering the significant release of greenhouse gas to the environment, and to abide to the Paris international treaty on climate change signed in 2015, nuclear energy became a fundamental part of the Saudi 2030 vision, as to diversify the country's energy mix, produce clean energy to fight global warming, and cope with the increasing local demand on energy. This section will consider three different Generation III+ reactor designs, and a Small Modular Reactor (SMR) design, address their unique features, assess their compatibility with the Saudi nuclear program, and eventually propose a suitable option, based on an educated opinion.

A. Overview

The three considered designs all include extensive safety features for safe power operation, ensuring a good balance of active/passive systems, redundancy, and diversity. For instance, safety systems for emergency core cooling, residual heat removal, corium retention, and more are integrated. Moreover, the thermal power generated, and the output electrical power vary for each design. Therefore, the thermal efficiency of a design is determined by the quality of its thermal-hydraulic system, which includes the RCS and the feedwater system. Furthermore, the designs considered are two conventional pressurized LWRs, and one SMR. Therefore, it is expected that the construction time and capital cost would differ. Since SMRs technology has not matured yet, the initial investment in such designs could even surpass conventional large designs. For more technical design information, the reader is referred to [1], [7], [8], [9], [10], [11], [12], [13], [14], [15], [16].

B. Reactor Design Evaluation

An evaluation of the three reactor designs considered is conducted, based on the author's point of view. In addition, the evaluation criterion was selected based on design considerations. It covers aspects of safety, where the fundamental safety cultures are considered. Moreover, power, construction, and thermal hydraulic considerations are accounted for. The evaluation results for the three are summarized in Table 2.

			APR1400		AP1000		SMART	
Selection criteria		Weight	Rating	Weighting score	Rating	Weighting score	Rating	Weighting score
Safety	Redundancy	0.25	2	0.5	1	0.25	3	0.75
	Diversity	0.25	3	0.75	2	0.5	1	0.25
	Grace Period	0.25	1	0.25	3	0.75	2	0.5
	Systems Modes (Passive/Active)	0.25	2	0.5	3	0.75	2	0.5
Power	Power rating	0.1	3	0.3	2	0.2	1	0.1
	Thermal efficiency	0.1	2	0.2	1	0.1	3	0.3
Thermal Hydraulics	Complexity	0.05	3	0.15	1	0.05	2	0.1
	Coolant discharge	0.1	3	0.3	2	0.2	1	0.1
Construction	Time	0.05	2	0.1	1	0.05	3	0.15
	Cost	0.1	2	0.2	1	0.1	3	0.3
				3.25		2.95		3.05

Table 2. Design evaluation of three different reactor technologies.

IV. CYBER SECURITY

Cyber Security is the protection of technologies, data, or systems from digital attack by utilizing people, procedures, and policies [18]. Nowadays, it is considered as a high priority security measure. This fact is due to the highly sensitive data the enterprise store digitally and/or the cyber physical systems (CPS) which is a set of physical systems connected to each other by network that use computation, sensing, and controls to achieve certain function [19]. By performing cyber-attacks on these systems, the attacker could illegally access sensitive data or control cyber physical systems to cause certain harm for the facilities. An example of the later one, some unknown hacker in February of 2021, illegally and remotely controlled CPS in Florida water treatment plant and increased the amount of NaOH in water [19] but fortunately, the operator noticed the dangerous increase in NaOH level and acted to resolve the issue. Furthermore, cyber-attack could be on a way higher level during political tensions and wars. Therefore, the cyber security of NPP must be on high priority to ensure the safety of the plant during its life. The following points highlight possible cyber-attack mechanism on NPPs [18]:

- DDoS Attacks: In NPP, it is enough to disable a system to cause harm without the need to control it. One possible method of doing so is the DDoS attacks. In this method, the attacker sends massive amounts of useless data to the targeted network, causing traffic and hence disability of the network.
- Internet-facing Service Risks: This method depends on the direct penetration of the network defense walls. Even though this method is considered extremely difficult, its consequences are disastrous if the cyber security team fails to deal with it. This is due to the complete control of

the penetrator on the systems which he was able to penetrate or the data which can be accessed.

- Social-engineering-based Attacks: Social engineering focuses mainly on targeting the people who have access to certain data or CPS. The difficulty of this method depends on the awareness of the users who have access to certain data or CPS.

There is a different way to optimize Cyber Security by choosing the appropriate approach depending on the expected cyber-attack that an enterprise may receive. This section will consider only cyber-attacks that are expected on NPP. For the DDoS attack, the IP of network servers could be hidden from the public which is to be expected for sure for NPP network. Furthermore, the stronger is the servers and the more intelligent they are in receiving data, the higher is the difficulty to shut them or slow them down. Also, back up servers should be available during these circumstances to avoid critical situations if the main servers went down. For the Internet-facing service risks, if the cyber defense team and defense wall were on a high level of professionalism, the network would be extremely difficult to penetrate. Furthermore, it is best to have defense walls between different and redundant systems so that if the attack was successful, the situation does not go out of control. Lastly, the employee must be of high awareness and fully educated on the Social-engineering-based attacks so that they can realize the attack quickly and deal with it properly.

The following is a list of historical cyber-attacks on NPPs [20]:

- Ohio NPP: In 2003, Ohio Davis-Besse NPP servers were attacked by MS SQL 2000 malware. This is due to the open of one of the network lines to allow the transfer of data, which is normally not allowed.
- The Stuxnet Cyberweapon: In 2005, America and Israel cooperated to develop a cyberweapon malware named Stuxnet. The main goal of this weapon is to cause damage to the Iranian nuclear program.

National Cyber Security Authority is the governmental entity that is responsible for cybersecurity in Saudi Arabia [21]. Their goal is to develop, implement, and supervise strategies to ensure the security of cyber systems. The national strategy the authority aims on consist of the following 6 main concepts [21].

- Integration**:** Integrated cybersecurity governance at a national level.
- Regulation: Effective management of cyber risks at the national level.
- Assurance: Protecting cyberspace.
- Defence: Strengthening national capabilities in defence against cyber threats.
- Cooperation: Strengthening partnerships and cooperation in Cybersecurity.
- Construction: Building national human capabilities and developing the cybersecurity industry in the Kingdom

This strategy has been developed to ensure high cybersecurity level in the kingdom. Furthermore, the national authority has developed controls and policies which consist of four means in controlling cybersecurity. These means are [21]:

- Basic Cybersecurity Controls: 114 basic cyber security officers to reduce the risk of entities technology and information at the external and internal level.
- Sensitive systems controls: Support the basic cybersecurity controls by providing the minimum cybersecurity requirements for sensitive systems.
- Cloud computing controls: extension and complement to the basic cybersecurity controls which focus on the cybersecurity requirements for cloud computing.
- Cybersecurity controls to work remotely: This method developed during coronavirus epidemic which enabled the work remotely by workers and employees. In addition, National Cyber Security Authority has developed National programs and initiatives like the indicative Centre for Cybersecurity, Saudi Federation for Cybersecurity, and National Academy of Cybersecurity to improve awareness, capabilities, and technology for Cybersecurity.

V. LESSONS LEARNED

This section focuses on the main lessons learned from three-mile island, Chernobyl, and Fukushima accident from [23][24][25][26][27][28]. Taking these lessons into consideration when starting building NPP will help increase its safety by, for example, enhancing safety features, or establishing mitigation procedures. The lessons are summarized in the following points:

- Ensure availability, dependability, and redundancy of plant systems and equipment during environmental catastrophe.
- Negative void coefficient is safer than the positive.
- Xenon-135 cause serious power oscillation and thus it must be monitored carefully and considered in plant start up, operation and testing.
- Control rods scram should be fast (2 to 3 seconds).
- Develop emergency response procedures for accident scenarios.
- Enhance evacuation plans to account for factors other than radiation.
- Train staff for accidental situations and decrease the number of operators in the control room and connect them with technical supporters.

- Severe NPP accidents cost more money than that to build and operate one.

VI. CONCLUSION

In summary, this report touched different important considerations in selecting NPP specifically for Saudi Arabia. One of which is the safety based one Saudi Arabia environmental condition that may cause new problems in NPP fields including seawater temperature and salinity, humidity, and sandstorms. Another one is design consideration by evaluation between three modern technologies which are APR1400, AP1000, and SMART. The evaluation has been done as a comparison base with a weighted value for each feature. The highest were APR1400 (3.25) and the second is SMART (3.05) and lowest was AP1000 (2.95). In addition, security considerations also have been considered by focusing on three important concerns which are the general security in the country, security tension in the area, and cyber security. To conclude, the report listed several lessons learned from the biggest three NPP accident namely Three-mile island, Chernobyl, and Fukushima. The focus was on the design failure leading to the accident, the staff responsibility, and emergency response taken for the mitigation of the accidents.

VII. References

[1] "Nuclear Power in Saudi Arabia - World Nuclear Association," world-nuclear.org.

[2] "Climate and average monthly weather in Dammam (eastern province), Saudi Arabia," World Weather & Climate Information. [Online]. Available:

[3] World Nuclear Association, "Cooling Power Plants | Power Plant Water Use for Cooling - World Nuclear Association," world-nuclear.org, 2020.

[4] N. US Department of Commerce, "NWS JetStream - Sea Water," www.weather.gov.

[5] A. C. Duxbury and F. T. Mackenzie, "seawater | Composition, Salinity, Distribution, & Facts," Encyclopædia Britannica. Aug. 14, 2018. [Online]. Available:

[6] "Getting the Rust Out - Humidity and Corrosion - Latem Industries," latem.com.

[7] "Further delay in startup of Vogtle AP1000s : New Nuclear - World Nuclear News," www.world-nuclear-news.org.

[8] "Status report 81 -Advanced Passive PWR (AP 1000)." [Online]. Available:

[9] "PRIS - Reactor Details," pris.iaea.org.

[10] "Vogtle project update: Cost likely to top $30 billion," www.ans.org.

[11] "Status Report -APR1400 (KEPCO E&C/KHNP) KOREA 2020/05/15." [Online]. Available:

[12] "PRIS - Reactor Details," pris.iaea.org.

[13] "Emirates Nuclear Energy Corporation," www.enec.gov.ae.

[14] "Korea, Saudi Arabia progress with SMART collaboration: New Nuclear - World Nuclear News," www.world-nuclear-news.org.

[15] "Status report 77 -System-Integrated Modular Advanced Reactor (SMART)."

[16] djysrv "ROK / KSA deal for 100 MW SMART Reactor could be a model for U.S.," Neutron Bytes, Apr. 29, 2018.

[17] "What is Nuclear Security? | Integrated Nuclear Security & Safeguards Laboratory | UMass Lowell," www.uml.edu.

[18] *"What Is Cybersecurity?,"* Gartner.

[19] "Cyber-Physical Systems Must be Part of Your Security Strategy," *Gartner*.

[20] S. Kim, G. Heo, E. Zio, J. Shin, and J. Song, "Cyber attack taxonomy for digital environment in nuclear power plants," *Nuclear Engineering and Technology*, vol. 52, no. 5, pp. 995–1001, May 2020, doi: 10.1016/j.net.2019.11.001.

[21] "الهيئة الوطنية للأمن النووي والرقابة - المملكة العربية السعودية," *My.gov.sa*, 2022.

[22] "Why Chernobyl Exploded - The Real Physics Behind The Reactor," *www.youtube.com*.

[23] World Nuclear Association, "Fukushima Daiichi Accident," World-nuclear.org, May 2022.

[24] United States Nuclear Regulatory Commission, *"NRC: Backgrounder on Chernobyl Nuclear Power Plant Accident,"* Nrc.gov, 2008.

[25] "Chernobyl | Chernobyl Accident | Chernobyl Disaster - World Nuclear Association," *world-nuclear.org*.

[26] E. BLAKEMORE, "Chernobyl disaster facts and information," *Culture*, May 17, 2019.

[27] C. on, N. and, D. on, and National Research Council, "Summary," Nih.gov, Oct. 29, 2014.

[28] World Nuclear Association, "Three Mile Island | TMI 2 |Three Mile Island Accident. - World Nuclear Association," World-nuclear.org, Mar. 2020.

Proceedings of the European Nuclear Young Generation Forum
ENYGF'23
May 8-12, 2023, Kraków, Poland

Investigating the cooperation between nuclear power plants and renewable energy sources in Central Europe using high-resolution simulations

Biró, Bence[1*] and Aszódi, Attila[1]

[1] Budapest University of Technology and Economics, Institute of Nuclear Techniques (BME, NTI), Hungary

*Corresponding author: *bencebiro@edu.bme.hu*

I. INTRODUCTION

The energy supply faces many challenges in the short and long term. The main elements of these challenges are tackling climate change and achieving sustainability, while also meeting security of supply objectives. To achieve the decarbonization goals, the electricity system in European countries will have to undergo significant changes, taking into account technical, environmental, economic and social aspects. The path towards achieving the targets will be further complicated by the ongoing Russian-Ukrainian war, which has led to a rise in energy prices and has resulted in European countries aiming to reduce their dependence on Russian fossil energy imports. Taking all these factors into account it can be concluded that the most important task for European countries are to replace fossil fuels, reduce Russian fossil energy imports and keep prices at affordable levels. Renewable energy sources and nuclear energy can play a major role in this task. However, there is still little data on how these technologies work together, so a detailed analysis of the cooperating electricity systems is essential.

In this paper, we perform a numerical analysis of electricity system in Hungary and neighboring countries. Our work includes mapping the countries' system-level electricity consumption in year 2030 and planned power plant portfolios and building hourly resolution simulations in Energy Exemplar's PLEXOS modelling environment. Our simulations show highly relevant results for the operation of nuclear power plants in a future electricity system (e.g. in the 2030s) with increasing share of weather dependent renewable energy sources.

II. Data and methods

In a previous paper [1], we have already shown that models based on reference hours modelling (e.g. TIMES), which are the basis for many National Energy and Climate Plans, are methodologically not appropriate in many cases. They may underestimate the importance of security of supply and do not accurately represent the timely distribution of weather-dependent energy sources' production. For the reasons described in [1], we use here hourly resolution models to model the electricity supply of countries in this paper to reproduce the variability of renewable energy sources with sufficient accuracy.

The main task in modelling the electricity markets at hourly resolution is to simulate which energy sources can supply the electricity to the market in order to cover the electricity needs, taken into consideration the timely changes in consumption, the differences in production costs, and the changing availability of weather dependent sources. This task has to be done while optimizing the total operating cost of the system and taking into account the operational constraints of the system components. To perform these tasks, we have chosen Energy Exemplar's electricity market software PLEXOS [2].

PLEXOS is a commercial power system modelling tool used for power market simulations. Within the framework of this research, a model was built in the PLEXOS environment in which the electricity system of the countries under study is represented by a single node (the transmission network of the countries was not modelled within the framework of this research) and the cross-border capacities between countries is represented by a pair of cross-border transmission lines per country. The model built has a time horizon of 1 year and a resolution of 1 hour. The software calculates the behavior of the electricity markets for one whole calendar year with hourly resolution in 1-day steps, so that the optimization takes into account the 24 hours before and after the day actually being calculated. In the model, power plants are considered at the level of energy sources, thus neglecting unit sizes, plant maintenance and unexpected outages.

A. Country data

The future of a country's electricity system is projected by its National Energy and Climate Plan, which has to be prepared by the national governments, so we have based our models on these official documents. We have analyzed Hungary and its immediate neighbors, except Ukraine. Ukraine was excluded from this study because the country's electricity system was connected to the European grid just recently and the transboundary capacity to be sold on the market is very small at this moment. On this basis, we have

analyzed and modelled Austria (AT), Croatia (HR), Hungary (HU), Romania (RO), Serbia (RS), Slovenia (SI) and Slovakia (SK).

The countries' projected annual consumption and power plant portfolios at the source level for 2030 are defined in the model according to the countries' National Energy and Climate Plans. The consumption of countries in year 2019 and 2030 is shown in Figure 1, and the evolution of the installed capacity of energy sources is shown in Figure 2.

Figure 1 shows that all countries expect their electricity consumption to increase by 2030, driven by economic growth and the electrification of different sectors (industry, residential heating and cooling, transportation) according to their national strategies.

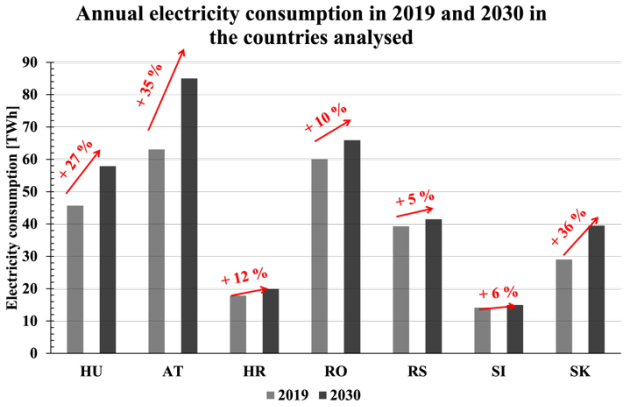

Figure 1. Annual electricity consumption in 2019 and 2030 in the countries studied (source of data for 2019 [3, 4] for 2030 [5–12], own representation)

The data presented in Figure 2 show that the installed capacity of electricity generators in the countries under study will increase significantly between 2019 and 2030. However, the energy source that the government of each country plans to use to cover this growth varies from country to country. Hungary and Slovakia plan to develop mainly nuclear and solar capacity, Romania plans to significantly increase its installed wind capacity, Croatia and Slovenia plan to invest in solar and natural gas, while in Austria and Serbia only solar and wind capacity is expected to increase in the coming years.

Cross-border interconnection capacity between the electricity systems of two countries provides a link between the two markets and creates the possibility for cross-border electricity trade. The interconnection capacities of the countries under study are defined according to [13].

To reproduce the effects of the pumped-storage power plants, it is not sufficient to define the installed capacity of these plants, but the turbine power, pumping power and reservoir capacity of the power plants must be given for each country concerned. Such precise data are not available in the National Energy and Climate Plan of the countries, therefore the above-mentioned parameters have been defined on the basis of the database referenced under [14].

Half of the electricity produced by the Krško nuclear power plant in Slovenia is used in Slovenia and the other half in Croatia (since Croatia owns 50% of the plant). By modeling this special circumstance in the Slovenian-Croatian interconnected grid a dedicated separate power line was assumed in the model between the two countries with a baseload operation exporting 348 MW (half of the installed capacity of the Krško NPP) from Slovenia to Croatia, and the Slovenian-Croatian cross-border capacity has been reduced by this 348 MW, to ensure a realistic utilization of the cross-border capacity.

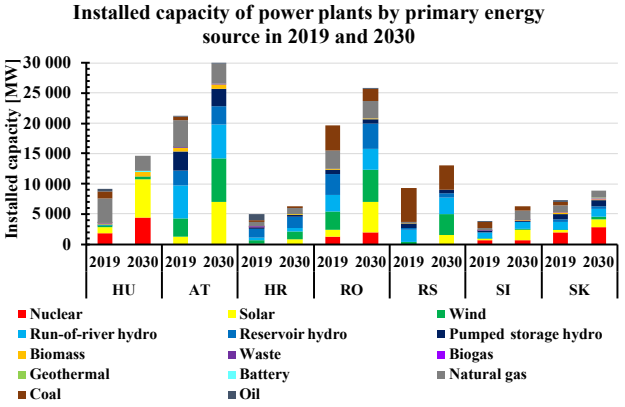

Figure 2. Distribution of installed capacity of power plants by energy source in 2019 and 2030 (source of data for 2019 [3,4] for 2030 [5–12], own representation)

B. Technical features of power plants

In order to describe the load variation limits of conventional power plants at the appropriate level, several technical parameters have been set for these capacities. The technical parameters are described as follows [15]:

- Minimum stable level [MW]/factor [%]: minimum stable production level for each production unit. Below this level, the production unit cannot operate and must be shut down. The factor is the minimum stable production level defined as a percentage of maximum capacity.
- Run-up / run-down rate [MW/min]: defines the rate at which the plant is ramped up from zero to the minimum stable level and ramped down from the minimum stable level to zero.
- Min up / down time [h]: The minimum number of hours in which the units must be in operation after being switched on / must not be in operation after being shut down.

For these parameters, the available literature was processed and the mean (column) and the minimum and maximum (error bars) of the values found in the literature were displayed in Figure 3. The mean values in Figure 3 were integrated into the model as input data. Since in this paper we model power plants only at the level of energy sources (not at the block level), the parameters presented in Figure 3 are also energy source specific.

C. Hourly data

We have also added hourly data to the model to simulate changes in electricity consumption and to reproduce fluctuations in weather dependent renewable energy production.

In order to determine the hourly consumption, the data for year 2019 were downloaded from the data publication website of the European Network of Transmission System Operators for Electricity (ENTSO-E) [3] for the neighboring

countries and from the website of the Hungarian Electricity Transmission System Operator Zrt. (MAVIR Zrt.) [4] for Hungary. To determine the hourly electricity consumption distribution in year 2030 the 2019 hourly load data series was divided by the 2019 annual consumption and multiplied by the 2030 annual consumption, assuming that day-by-day and the intraday relative change of electricity consumption in year 2030 will match the 2019 hourly relative consumption changes. A more precise estimate could only be made if we had data on weather conditions in 2030 and the hourly impact of economic growth and electrification on consumption, but these data are not available right now.

For solar and wind power plants, the hourly resolution capacity factors were downloaded from the Renewables.ninjas [16] database (described in studies [17, 18]) due to the shortcomings of the ENTSO-E database presented in [1]. For run-of river and reservoir hydropower plants – as no other data were available – the required hourly capacity factor values were generated using the 2019 hourly resolution generation and 2019 installed capacity, which were downloaded from the ENTSO-E [3] and MAVIR [4] databases.

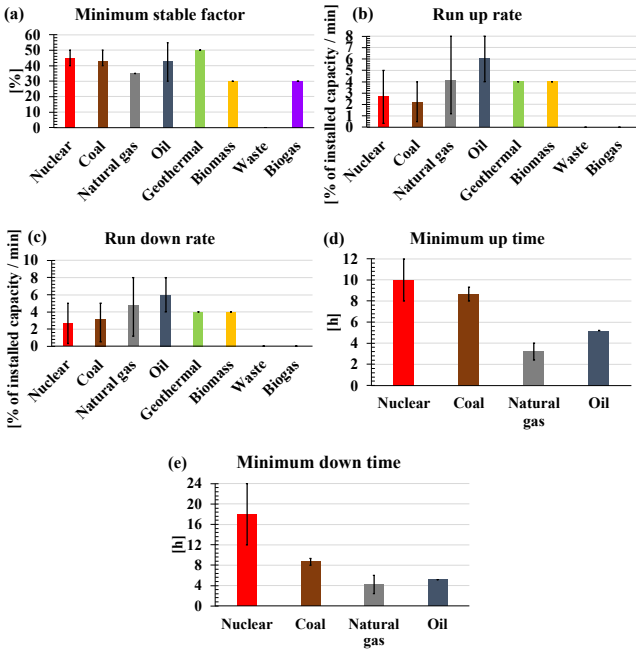

Figure 3. Minimum stable factor (a), run up rate (b), run down rate (c), minimum up time (d) and minimum down time (e) PLEXOS input for power plants (data source [19–22], own representation)

III. Results

We have already shown in previous studies [1, 23] that only countries that continue to rely on nuclear power will be able to meet the 90% carbon neutral electricity generation commitments set out in the European Green Deal [24]. These results therefore suggest that if countries really want to meet the commitments, they will need to apply nuclear power in addition to renewable power plants for their future electricity generation.

How renewable energy sources and nuclear power plants can co-exist will be crucial to the security of supply of future electricity systems, so in this article we have focused on the values associated with the operation of nuclear power plants in the results of our hourly resolution simulations. This study has resulted in very detailed data on the future capacity factor of nuclear power plants in the studied region.

First, we analyzed how the hourly capacity factor of nuclear power plants in concerned countries will evolve in 2030. The results of this analysis are summarized in Figure 4, where the specific frequency of utilization of nuclear units in four concerned countries is plotted. In Figure 4, we have treated separately the frequency associated with a hourly capacity factor of 0%, the other frequencies show values between 5 percentage points.

Our analysis in Figure 4 has the following main messages:

- Nuclear power plants in the region will continue to operate as baseload generators in 2030, as the capacity factor of each country's units will be 95% or higher for 99% of the hours of the year.
- Due to weather-dependent renewables and existing market mechanisms, nuclear plants will need to be dispatchable in 2030 to maintain system balance, so they will need to be ramped down to their minimum stable level for 40 to 45 hours of the year.
- As given in the results of the model calculations there are no system states in which the nuclear power plants are completely shut down. It means that – given the 18-hour minimum down time shown in Figure 3 – there is never a system state where the output of any country's nuclear units is not needed for more than 18 hours.

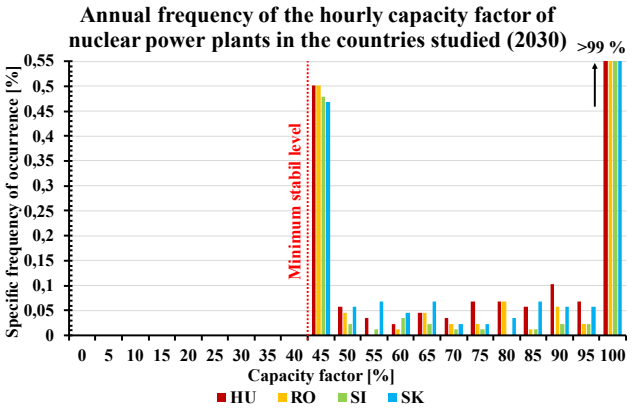

Figure 4. Annual frequency of the hourly capacity factor of the nuclear fleet of the countries under study in 2030

We also considered it important to analyze the hourly evolution of the capacity factor of nuclear power plants. For this purpose, the hourly capacity factor of nuclear power plants in 4 countries (HU, RO, SI, SK) for all 8760 hours of a calendar year is plotted in the form of a heat map in Figures 5 to 8. In Figures 5 - 8, the y-axis represents the hours of the day (1 - 24), while the x-axis the days of the calendar year (1 - 365), and the color of the given hour is defined by the color scale on the right y-axis. For the color scale, the values corresponding to a capacity factor of 45% are marked in white, and the values higher than 45% are plotted according to the color scale.

Our analysis presented in Figures 5 - 8 demonstrates that states where nuclear power plants are not operating at full capacity observed in Figure 4 can all be attributed to the May - July period within the year. The distribution of these system states within the day is more variable, but it is clear from our analysis that the vast majority of those system

states occur between 8 and 14 hours. This is of course explained by the fact that the capacity factor of solar power plants is the highest during these periods [1]. The analysis of these system conditions is important because these system states can be reduced or even eliminated by new investments in system-level energy storage (e.g. batteries, pumped storage hydro, hydrogen production by electrolysers).

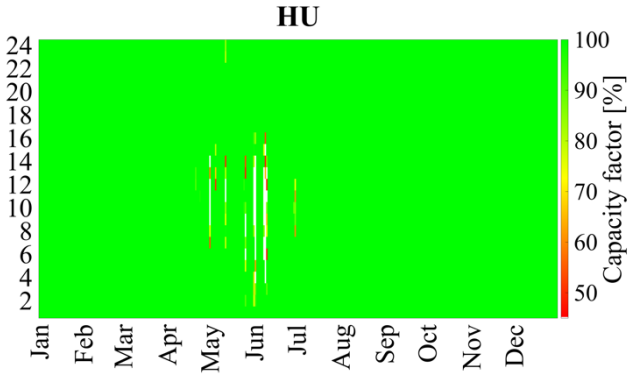

Figure 5. Hourly distribution of the capacity factor of the Hungarian nuclear fleet in 2030

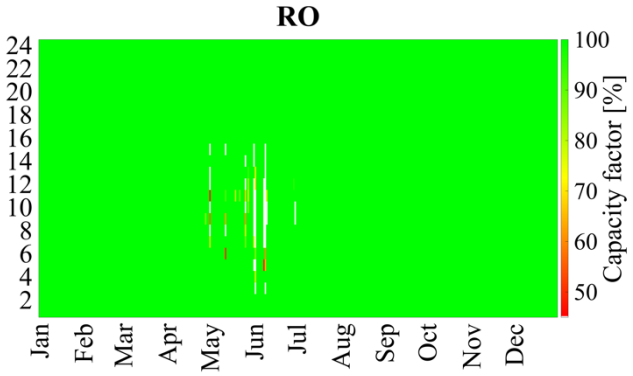

Figure 6. Hourly distribution of the capacity factor of the Romanian nuclear fleet in 2030

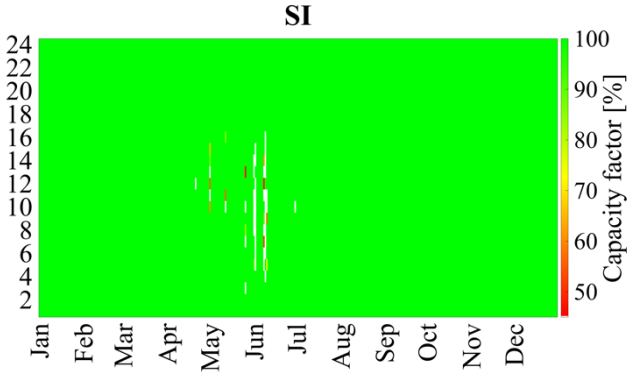

Figure 7. Hourly distribution of the capacity factor of the Slovenian nuclear fleet in 2030

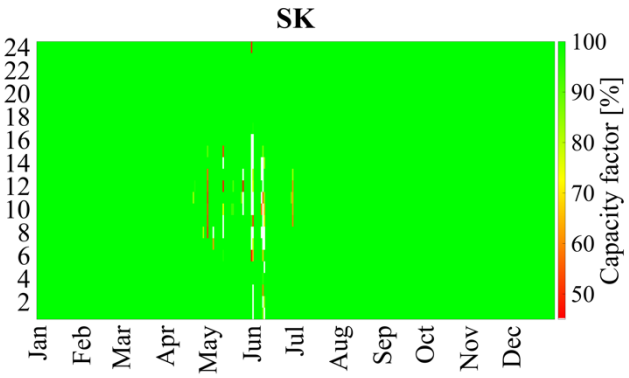

Figure 8. Hourly distribution of the capacity factor of the Slovak nuclear fleet in 2030

The Hungarian battery park with a capacity of 100 MWh and power output of 100 MW was also considered important to investigate. A one-hour storage was defined, as there is no corresponding data in the Hungarian NECP, and this research was not intended to investigate the capacity of storage under different scenarios, but it could be a promising topic for future research. To this end, we have plotted in Figure 9 whether the Hungarian battery park is empty (white), charging (red), discharging (blue) or storing energy (grey) at a given hour. The result in Figure 9 shows that on average there are about 500-550 charge-discharge cycles per year on a 100 MWh battery park, and from the analysis of the hourly data in Figure 9 it can be concluded that the Hungarian energy storage unit is charged at dawn and during the day and discharged during the morning and evening peak. The impact of the battery park on nuclear power plants could be determined by defining further scenarios, but these analyses were not in the scope of this research.

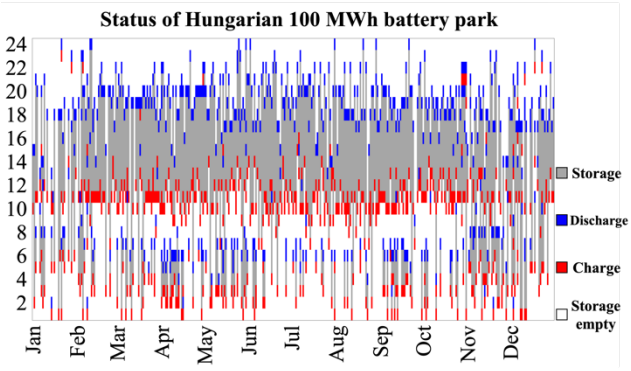

Figure 9. Hourly breakdown of Hungarian 100 MWh battery conditions in 2030

IV. Summary

In this paper, we have used very detailed, hourly-resolution simulations to investigate the future interaction of nuclear and renewable power plants in Central Europe. We have built a model to simulate the cooperating electricity markets of Hungary and its neighboring countries for year 2030 using the Energy Exemplar's PLEXOS modeling environment using data defined in the countries' National Energy and Climate Plans. The built model was also used to investigate the operation of a 100 MWh battery park in Hungary at high time resolution.

Our results clearly show that the nuclear power plants in the region will continue to play a baseload role for a significant

part of the year in 2030, however these capacities need to be prepared also for flexible operation to compensate adequately the volatile renewable production.

In this article, we have used heat maps to illustrate the hourly load factor distribution of nuclear power plants over the year 2030 and highlight those periods of the year in which they will need to operate more flexibly. Our analysis suggests that the problematic time period in the 2030s will be May, June and July. The results presented in form of heat maps also point out that, in the future the challenging time periods – when nuclear power plants will have to take part in system level control due to high feed-in of weather-dependent generators – energy storage (e.g. batteries, pumped storage hydro, hydrogen production) could be a solution if these technologies would be present in the electricity system of studied region.

V. Acknowledgment

The research reported in this paper is part of project no. BME-NVA-02, implemented with the support provided by the Ministry of Innovation and Technology of Hungary from the National Research, Development and Innovation Fund, financed under the TKP2021 funding scheme.

The research reported in this paper is also supported by the ÚNKP-22-2-I-BME-2 New National Excellence Program of the Ministry for Culture and Innovation from the source of the National Research, Development and Innovation Fund.

The research was also funded by the Sustainable Development and Technologies National Programme of the Hungarian Academy of Sciences (FFT NP FTA).

VI. References

[1] A. Aszódi et al., “Comparative analysis of national energy strategies of 19 European countries in light of the green deal’s objectives”, Energy Conversion and Management: X, vol. 12, p. 100136, Dec. 2021, doi: 10.1016/J.ECMX.2021.100136.

[2] Energy Exemplar, “PLEXOS - The Unified Energy Market Simulation Platform”, 2022, https://www.energyexemplar.com/plexos

[3] ENTSO-E, “Transparency Platform”, https://transparency.entsoe.eu/

[4] MAVIR, “Website”, https://www.mavir.hu/web/mavir/home

[5] Federal Ministry of Sustainability and Tourism, “Integrated National Energy and Climate Plan for Austria”, 2019, https://energy.ec.europa.eu/system/files/2020-03/at_final_necp_main_en_0.pdf

[6] Ministry of Innovation and Technology, “National Energy and Climate Plan”, 2020, https://energy.ec.europa.eu/system/files/2022-08/hu_final_necp_main_en.pdf

[7] Ministry of Economy, “Integrated National Energy and Climate Plan for 2021 to 2030”, 2019, https://energy.ec.europa.eu/system/files/2020-03/sk_final_necp_main_en_0.pdf

[8] Ministry of Economy and Energy and Business Environment, “The 2021-2030 Integrated National Energy and Climate Plan”, 2020, https://energy.ec.europa.eu/system/files/2020-06/ro_final_necp_main_en_0.pdf

[9] Republic of Slovenia, “Integrated National Energy and Climate Plan of the Republic of Slovenia”, 2020, https://energy.ec.europa.eu/system/files/2020-06/si_final_necp_main_en_0.pdf

[10] Ministry of Environment and Energy, “Integrated National Energy and Climate Plan for the Republic of Croatia for the period 2021-2030”, 2019, https://energy.ec.europa.eu/system/files/2020-01/hr_final_necp_main_en_0.pdf

[11] Ministry of Mining and Energy, Ministry of Finance and Department for Controlling and Financing of EU Funded Programmes, “Integrated National Energy and Climate Plan of the Republic of Serbia until 2030 with a vision until 2050”, 2022, https://www.mre.gov.rs/sites/default/files/2022/07/inecp_27_07_2022_eng.pdf

[12] Á. Beöthy et al., “SEERMAP: South East Europe Electricity Roadmap Country report: Serbia 2017”, 2017, www.seermap.rekk.hu

[13] ENTSO-E, “European Power System 2040 – Completing the map – Technical Appendix”, 2019, https://eepublicdownloads.entsoe.eu/clean-documents/tyndp-documents/TYNDP2018/european_power_system_2040.pdf

[14] Felice M de, “ENTSO-E PECD (European Climate Database) from MAF 2019 in CSV and Feather formats”, 2020, doi:10.5281/ZENODO.3702418

[15] Energy Exemplar, “PLEXOS Guide”, 2022

[16] Renewables.ninja, “Website”, https://www.renewables.ninja/

[17] S. Pfenninger and I. Staffell, “Long-term patterns of European PV output using 30 years of validated hourly reanalysis and satellite data,” Energy, vol. 114, pp. 1251–1265, Nov. 2016, doi: 10.1016/J.ENERGY.2016.08.060.

[18] I. Staffell and S. Pfenninger, “Using bias-corrected reanalysis to simulate current and future wind power output,” Energy, vol. 114, pp. 1224–1239, Nov. 2016, doi: 10.1016/J.ENERGY.2016.08.068.

[19] ENTSO-E. Mid-term Adequacy Forecast 2019 – dataset. 2019. https://www.entsoe.eu/outlooks/midterm

[20] J. Ho et al., “Regional Energy Deployment System (ReEDS) Model Documentation: Version 2020,” 2021, www.nrel.gov/publications.

[21] Nuclear Energy Agency, “The Costs of Decarbonisation: System Costs with High Shares of Nuclear and Renewables”, 2019, https://www.oecd-nea.org/jcms/pl_15000/the-costs-of-decarbonisation-system-costs-with-high-shares-of-nuclear-and-renewables?details=true

[22] Nuclear Energy Agency and International Energy Agency, “Projected Costs of Generating Electricity”, 2020, https://www.oecd-nea.org/upload/docs/application/pdf/2020-12/egc-2020_2020-12-09_18-26-46_781.pdf

[23] B. Biró and A. Aszódi, “Detailed numerical analysis of different energy scenarios and the role of nuclear energy in the decarbonization pathways of the Hungarian electricity system”, 2022, European Nuclear Young Generation Forum 2021 - Book of Proceedings, pp. 131–134, doi: http://dx.doi.org/10.13140/RG.2.2.12641.38245

[24] European Commission. Delivering the European Green Deal. 2022. https://ec.europa.eu/info/strategy/priorities-2019-2024/european-green-deal/delivering-european-green-deal_en

Proceedings of the European Nuclear Young Generation Forum
ENYGF'23
May 8-12, 2023, Kraków, Poland

Analysis of the socio-economic challenges that the Nuclear sector faces and how the industry can change public perceptions in order to reach global Net Zero targets

Chauhan, Shania[1*] and Jackson, Sophie[2]

[1] Abbott Risk Consulting Ltd (ARC Ltd), United Kingdom

*Corresponding author: shania.chauhan@consultarc.com, sophie.jackson@consultarc.com

I. INTRODUCTION

The public are headlined and bombarded on a daily basis with news about the latest extreme weather conditions and the effects of climate change which are rapidly starting to impact our lives. Most recently, the effects of the cost-of-living crisis, which is impacting millions of people across the globe, is a result of the reliance which we have on fossil fuels as our main source of energy. In 2020, over 110 countries set out to achieve a target of 0 carbon emissions by 2050, in order to decelerate climate change and provide clean energy to all. As an effective, sustainable and secure energy source, nuclear energy must be utilised in order to reach our global goal of Net Zero.

This paper will give an overview and examine the challenges and key factors which are preventing the growth of nuclear power from dominating the energy sector and reaching Net Zero in due course. The challenges analysed include a range of socio-economic factors such as funding, national priorities and environmental risks, focusing upon a comparative investigation between 3 countries which are actively invested in nuclear power, namely the United Kingdom, France and India, as well as Italy whose approach differs. A large factor which varies by country and impacts the growth of the nuclear industry is the public perception of nuclear risk. This paper aims to evaluate each countries approach, examining the reasons behind negative public perceptions and look at how individual country successes can be applied to the wider industry.

II. THE GLOBAL ROLE OF NUCLEAR ENERGY

Since nuclear power stations were first introduced in the 1950's, over 50 countries are now actively invested in using nuclear power to contribute to their sources of energy [1]. To better understand how to improve public perception and engagement in order to encourage the growth of the nuclear sector to reach Net Zero targets in time, the statistics and approaches of 4 different countries have been analysed and compared to better understand where the nuclear industry can improve and employ learning outcomes.

With new expertise entering the industry to aid in decommissioning, waste management and the design and build of new reactors, the demand and interest for employment in the UK nuclear industry is rapidly growing. In 2022, employment in the industry piqued at its highest level in five years with 'over 64,000 jobs' created 'across the UK nuclear supply chain' [25]. The UK currently has 11 nuclear reactors operating which provided 14.5% of the UK's electricity share in 2021 [1], [10], through the generation of 45.9 terawatt hours of electricity [3]. The UK has predominantly invested in Advanced Gas Reactors (AGRs) and Pressurised Water Reactors (PWRs), with two new European Pressurised Reactors (EPRs) currently under construction at Hinckley Point, aiming to provide an additional 25,000 jobs, each of 1630 MWe each [2]. Policies such as the British Energy Security Strategy are aiming to invest in nuclear power fourfold from around 6 GW to a total of 24 GW by 2050, supplying 25% of the UK's electricity [4].

Figure 1 shows how the UK public agreement is more in favour for nuclear energy than against it, however under each statement 47-55% of the population have stated they 'neither agree nor disagree' or 'don't know', thus suggesting that further education about the reality of nuclear energy is required to make a shift in public engagement and opinion. Recent publications released in the latest Spring Budget, alongside the launch of Great British Nuclear (GBN), suggest a UK movement towards greater use of nuclear energy as it was deemed 'environmentally sustainable'. These initiatives aim to help advocate for and target against common misunderstandings which prevent the nuclear industry from achieving further success [26].

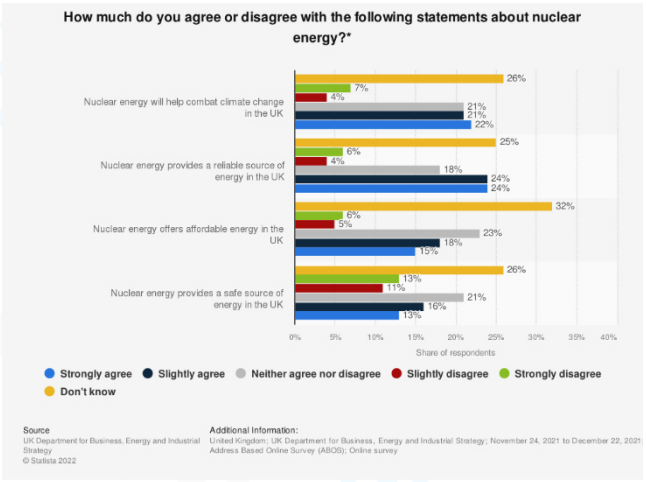

Figure 1 – Survey across the UK of the public opinion on nuclear energy [5]

Within Europe, for the last 30 years, the French have been the most successful in the implementation of nuclear energy, with a total of 56 operating reactors across the country, providing approximately 70% of the national electricity [1]. A further 20%+ comes from low carbon, renewable sources [6] leading to a 90%+ low carbon electricity grid. Despite this success, under the proposed energy policy, France is now looking to have a greater proportion of renewable energy sources, reducing the country's share in nuclear energy to 50% by 2035 [1]. Considering the historic success and investment into the nuclear industry, it poses the question as to why measures are being put into place to reduce nuclear capacity, despite still aiming for Net Zero by 2050. French nuclear energy predominantly utilises PWRs, with an EPR currently under construction and allows them to achieve their target of energy independence. Moving forward the French aims for the nuclear industry are to focus on EPR and Small Modular Reactors (SMR) design, whilst also re-examining the closed fuel cycle for using Mixed Oxide Fuel (MOX) within other reactor designs [6]. A higher percentage of renewable energy sources may provide the French greater security whilst developing other effective nuclear reactor designs.

India currently has 23 operating nuclear reactors, which are pre-dominantly pressurised heavy water reactors and boiling water reactors, providing around 3.2% of the country's electricity [1], [10]. Most recently, India has been looking to utilise its natural thorium reserve as a source of nuclear energy through the design of Advanced Heavy Water Reactors (AHWRs) [22]. India's current target for reaching Net Zero is 2070, putting it considerably behind other committed countries. Plans are being constructed to increase their nuclear capacity to 25% by 2050, [7]. India faces significant challenges in developing its nuclear capacity due to challenges such as a lower economic status and social poverty.

In contrast, Italy does not actively produce nuclear energy and instead chooses to import nuclear power from France and Switzerland into the country, accounting for 6% of the national consumption [14]. Previously, Italy has had 4 nuclear reactors, however post Chernobyl, all nuclear activity was ceased. Nuclear disasters such as Chernobyl and Fukushima have had a significant negative impact on the industry by re-introducing a further sense of fear and extreme risk which had previously been combatted and overcome. Through the rejection of new nuclear energy in Italy at referendums, both in 1987 and 2011 after the two accidents, it is evident that the perception of nuclear risk still remains high in Italy, thus contributing to the prevention of further new build operations from occurring. In 2020, Italy had imported 73.5% of its energy. Despite being committed to reaching Net Zero in 2050 and being the 4th largest producer of renewable energy in Europe, predominantly though mean of solar power [8], the sustainability and safety in relying on another country's generation and export for supply means that achieving Net Zero is out of their hands.

As shown in Figure 2, a comparison between Italy and France of the electricity generation to CO_2 intensity per country is shown. France's CO_2 intensity is around 1/5th of the intensity which Italy emits per year, whilst providing up to double the electricity output, further reinforcing the effectiveness of nuclear energy in decarbonisation and as a resource to reach Net Zero.

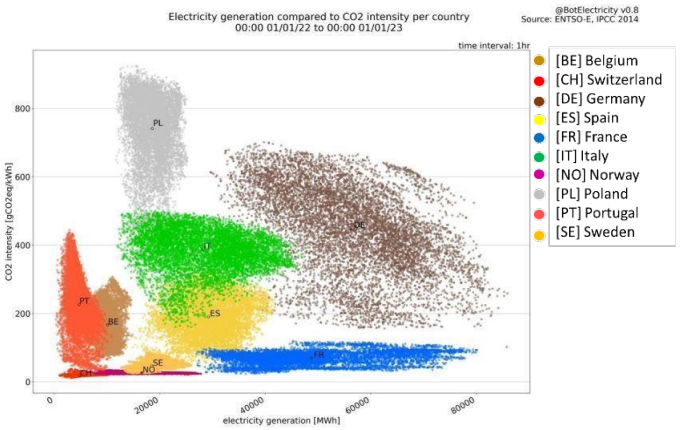

Figure 2 – Graph of the electricity generation compared to CO_2 intensity of 10 countries across Europe, including France and Italy [9]

III. PERCEPTION OF NUCLEAR RISK

The definition of risk is defined as a situation involving the exposure to danger. Actual risk is the quantifiable likelihood of an event or situation occurring. Perceived risk is the subjective judgment of a group or individuals on an event or situation occurring based on a variety of factors. The perception of risk can be detrimental regarding socio-economic decision making. For example, in a survey conducted in 1994, crime was falling, and yet the public perception of risk was increasing. This led to initiatives such as more police patrols and CCTV in shopping areas. Although these initiatives may have led to less actual crime, the police officers may have been diverted from other more effective methods of crime prevention [23].

With regards to nuclear power, the consequences of an accident occurring has global consequences, with the two major nuclear accidents being Chernobyl and Fukushima Daiichi [16]. The causes of both accidents have been reported and assessed extensively so will not be repeated here. The World Health Organisation initially estimated the death toll from the Chernobyl incident over the lifetime of emergency workers and local residents to reach ~4000 [17].

With regards to the Fukushima accident, “"No radiation-related fatalities or acute diseases have been observed among the workers and general public exposed to radiation from the accident. The doses to the general public, both those incurred during the first year and estimated for their lifetimes, are generally low or very low. No discernible increased incidence of radiation-related health effects is expected among exposed members of the public or their descendants" [18]. During the Fukushima accident, over 100,000 people were evacuated from their homes. With regards to the fall out in both cases, the clean-up cost and displacement of the public from their homes has been extensive. As defined by the World Nuclear Organisation, “there have only been two major accidents to have occurred in over 18,500 cumulative reactor-years of commercial nuclear power operation in 36 countries” [16]. The number of fatalities due to car accidents in Europe in 2021 alone is 19,800 [18], and when comparing this figure with the number of fatalities that have occurred due to civil nuclear then the reason behind the strong negative public opinion on nuclear power is not only to do with the potential health implications but also the social and economic impact of a nuclear accident.

Risk can be defined as:

Risk = Likelihood of an accident x consequence

Perceived risk = Perceived likelihood of an accident x consequence

For example, although the likelihood of a car accident is quite high, the consequence of a fatality is low. In 2021, there were 101,087 car accidents which lead to slight, serious or fatal injuries. Fatal injuries accounted for 1.5% of the total injuries recorded [24]. If there is a fatality due to a car accident, there is an economical cost associated with clearing the incident site and a social impact for the families of the deceased. If there is a major nuclear accident, the socio-economic factors are far greater due to the displacement of people and the financial cost of clean- up. The consequences of a disaster in the latter case are significantly higher than that of a car accident, but the risk of this occurring is significantly less.

The risk of an accident at a civil nuclear power plant is considered low. This is, in part ensured by robust safety legislation which is fed down from the IAEA into member states to ensure the safety of the operators and the public [19]. International cooperation and collaboration ensure that safety and security of nuclear power is met, with the legislation updated periodically to improve safety from learning from experience and innovation. Due to the consequences of a nuclear accident, the IAEA have ensured that in order to gain permissions and to continue operation of a nuclear power plant, there needs to be significant defense in depth to ensure that any incident that may lead to an accident is prevented, protected, and mitigated against, with multiple independent safety measures in place.

IV. DISCUSSION OF COMPARISONS AND RECOMMENDATIONS

Understanding the relationship between the individual success of countries which harness nuclear energy and the actual vs perceived risk of it may be a significant learning aspect in helping to reach global Net Zero targets. Despite a variety of socio-economic differences between these countries, collaboration can be utilised to apply lessons learnt and successful techniques to encourage growth of the nuclear industry and change negative public opinions which may prevent this.

As previously discussed, the analysis of the nuclear success which both France and UK have can be seen above and through the investment towards new build of nuclear reactors moving forward, such as in Hinckley Point C and Sizewell C in the UK and more EPRs and SMRs in France. Educating the public on the safety of nuclear energy has helped to change public perception and allow for this growth, despite there still being plenty of work to be done moving forward. France has tailored their approach through focusing on developing a rigid and closed nuclear fuel cycle, resulting in a 96% Uranium and Plutonium fuel recycle efficiency [6]. Fear of risk regarding nuclear energy also derives from the uncertainty of managing nuclear waste and the detrimental risk posed to the environment as a result of this in the cases of ineffective containment or leakage. Currently, the UK does not have a final disposal solution for nuclear waste despite six attempts to find an appropriate Geological Disposal Facility (GDF) [21]. It can be argued that negative public perception towards this is preventing a waste management strategy from moving forward, due to a lack of willingness from suitable communities to host a GDF due to scaremongering of being close to a radioactive facility despite thorough safety measures in place. Offering an incentive for reduced electricity bills for residents within a limited radius of the nuclear facility may be a beneficial method. Taking learnings from the French approach and investment into educating the public to understand the actual risk and safety procedures behind nuclear industry may help in aiding more development towards a nuclear waste management site.

The UK can also tailor their approach to Net Zero through taking advantage of the media and its representation of the nuclear and energy industry. The construction of Hinckley Point C has faced a number of negative headlines in news articles which further contribute towards a negative public perception of upcoming nuclear work. Headlines featured in The Guardian and The Telegraph include discussion of a ‘£3bn delay’ [12], and ‘risk of 11-year delay’ [13], with the agreed extension until 2036. Whilst stating the reality of a large project, this further emphasises reasons to the public as to why investment into nuclear may not be a favorable or high priority approach for the UK due to the high economical demands when ‘92% of adults’ have experienced a higher cost of living between ‘November to December 2022’ [11].

As discussed by A. Chowdhury [15], the extreme heatwaves faced in India encourages further usage of air conditioning systems, which is heavily relied upon to best prevent illness and deaths. In summer 2022, a coal shortage forced the country to import coal for 8 consecutive days [15], an extremely costly decision to

provide an immediate energy supply, made under desperate conditions. India faces a different and diverse climate compared to the other three countries being investigated. Investment into nuclear energy may not be considered a high enough priority in comparison to public health standards. Despite this perspective, investment into the nuclear industry will help to boost India's economy by providing a breadth of jobs in construction and engineering in the local areas, as well as increased security in a reliable low carbon energy source.

The discussion based on the actual vs perceived risk of nuclear energy highlights how Italy resent investing into nuclear power due to the perceived lack of safety and fear that this poses to the public. Work needs to be done moving forward in Italy to show the lessons learnt post Chernobyl and Fukushima, and to show the developments in nuclear safety legislation since these accidents, some 37 and 12 years ago.

V. CONCLUSION

This paper gives an overview of some of the challenges which the nuclear sector faces if it is to have a significant contribution in achieving global Net Zero. The analysis of approaches towards nuclear energy, taken by different countries has been examined to better understand learning aspects and how these can be further applied. It is key to acknowledge that due to socio-economic variations across the globe, certain approaches may not be applicable or suitable for all and that the barriers towards nuclear differ depending on location. As discussed, the resentment towards nuclear energy in Italy is based on the high perceived risk since accidents such as Chernobyl and Fukushima, a common perception also present in other countries, such as Germany. Whereas in India, the lack of funding and higher priorities such as national health figures prevent faster nuclear progression, despite the public enthusiasm towards it. In the United Kingdom, the nuclear industry face struggles with a lack of public education and fear towards the environmental risk of nuclear waste. Tailoring the approach towards the advantages of nuclear energy through focusing on the reduction in the cost-of-living crisis may be beneficial.

Moving forward, greater global collaboration must occur quickly to learn from other successes and give understanding to where knowledge and techniques can be adapted and utilised to best combat a negative public perception of the nuclear industry. Initiatives and reports such as Nuclear Week in Parliament in the UK and the Spring Budget are helping to encourage MPs to encourage discussions and invest into education to their local areas about the future of nuclear and its role towards Net Zero. This study discusses a snapshot of the current challenges faced and how best to combat these, however this study could be expanded further to give a greater insight towards reducing the perceived risk of nuclear as well as looking into how other active nuclear countries such as Korea, China and Japan have obtained their success.

VI. REFERENCES

[1] World Nuclear Association, Nuclear Power in the World Today, World Nuclear Performance Report 2021, 2021.

[2] World Nuclear News, 'Three-year extension agreed to Hinckley Point C contract,' 02 December 2022

[3] Electricity generated using nuclear fuel in the United Kingdom (UK) from 2005 to 2021, UK Department of Business, Energy and Industrial Strategy; 2005 to 2021, Statistica, 2023.

[4] HM Government, British Energy Security Strategy, April 2022, https://assets.publishing.service.gov.uk/government/uploads/system/uploads/attachment_data/file/1069969/british-energy-security-strategy-web-accessible.pdf

[5] 'How much do you agree or disagree with the following statements about nuclear energy?', UK Department for Business, Energy and Industrial Strategy, Statista 2022

[6] Country Nuclear Power Profiles, France, IAEA, 2022, https://cnpp.iaea.org/countryprofiles/France/France.htm

[7] G. Kuhika, J.T. Ripberger, A.S. Fox, H.C. Jenkins- Smith, C.L. Silva, 'The future of nuclear energy in India: Evidence from a nationwide survey', Volume 156, 2021, 112388

[8] Country Nuclear Power Profiles, Italy, IAEA, 2022, https://cnpp.iaea.org/countryprofiles/Italy/Italy.htm

[9] European Network of Transmission System Operators for Electricity (ENTSOE), 'Electricity generation (abscissa) compared to CO2 intensity (ordinate), IPCC 2014, 2023

[10] World Nuclear Association, 'Number of operable nuclear power reactors worldwide as of May 2022, by country', May 2022, Statista

[11] D. Harari, P. Bolton, B. Francis-Devine, M. Keep, 'Rising cost of living in the UK', House of Commons Library, 9428, 23 January 2023

[12] A. Lawson, 'Boss of Hinkley Point C blames pandemic disruption for £3bn delay', The Guardian, 20 May 2022

[13] R. Millard, 'Hinkley Point nuclear plant faces risk of 11-year delay', The Telegraph, 29 November 2022

[14] World Nuclear Association, 'Nuclear Power in Italy, July 2022, https://world-nuclear.org/information-library/country-profiles/countries-g-n/italy.aspx

[15] A. Chowdhury, 'How Nuclear Energy can aid India's Net-Zero Journey', Business World, 1st September 2022

[16] World Nuclear Association, 'Safety of Nuclear Reactors', March 2022, https://world-nuclear.org/information-library/safety- and-security/safety-of-plants/safety-of-nuclear-power-reactors.aspx

[17] World Health Organisation, Chernobyl: the true scale of the accident, UNDP 2005

[18] UNSCEAR 2013, 'Report of the United Nations Scientific Committee on the Effects of Atomic Radiation to the General Assembly', 2013

[19] European Commission, '2021 road safety statistics: what is behind the figures?', 2021

[20] IAEA, 'International Law and Nuclear Energy: Overview of the Legal Framework', March 1995

[21] GreenPeace France, 'The Global crisis of nuclear waste', 2018

[22] Country Nuclear Power Profiles, India, IAEA, 2016

[23] University of Sheffield, Public Perception of Risk, July 2004, https://griequity.astraea.net/resources/InvestmentIndustry/HowTo/riskbyforesight.pdf

[24] Department for Transport, 2021 Road Accidents, September 2022, https://roadtraffic.dft.gov.uk/custom-downloads/road-accidents/reports/b4602731-6a21-4afa-9695-5cf9c53ce749

[25] Nuclear Industry Association, Jobs Map 2022, 22nd September 2022, https://www.niauk.org/nia-jobs-map-2022/

[26] HM Treasury, Spring Budget 2023, March 2023, https://assets.publishing.service.gov.uk/government/uploads/system/uploads/attachment_data/file/1144441/Web_accessible_Budget_2023.pdf

Proceedings of the European Nuclear Young Generation Forum
ENYGF'23
May 8-12, 2023, Kraków, Poland

We officially need fission.

Fenwick, Hannah[1*]
1 Nuclear for Climate (N4C), Scotland, United Kingdom.

*Hannah Fenwick: *hannahdfenwick@outlook.com*

I. INTRODUCTION

Against the HT 1: Energy transition and the role of nuclear energy for the ENYGF 2023 Conference, in this paper I will:

- Investigate what the energy transition means for the climate crisis and prosperity of humankind;
- Comparatively assess nuclear as an energy source on the bases of carbon emissions, land use, raw material use, waste and safety;
- Explore public perception of nuclear energy; and,
- Look at alternative energy transition solutions.

II. WHAT IS THE ENERGY TRANSITION?

The demand for energy increases with the advancement of civilisation, enabling a better quality of life and socio-economic growth. In the developed world, living standards, and the energy demand to uphold them is ever increasing. The developing world seeks more energy for growth, prosperity, and the eradication of energy poverty. Electrification of carbon intense sectors such as heat and transport contribute to the ever-increasing global demand for energy [1]. Global energy consumption is expected to triple by 2050 [2].

Energy through access to electricity and industrialisation has brought many benefits to global society today however it has also depleted the world of finite resources, polluted the environment, and impacted the health of the same society and eco-system we co-exist in. The climate is changing, the global temperature is rising. In the current climate, energy must shift from carbon intense fossil fuels to low-carbon energy sources.

Energy is intrinsically linked with environmental impacts, and we have the choice to take energy down one of two paths: energy can remain a complicit villain in our probable doomsday, or it could be a hero, cleaning itself up and being a key to climate change mitigation and clean prosperity for the global community.

III. ENERGY CLIMATE ACTION

Individuals, communities, and nations worldwide are taking steps to tackle climate change. 195 United Nations members are parties to the United Nation Forum Convention on Climate Change (UNFCCC). The parties, having adopted the 2015 Paris Agreement to ensure that global warming doesn't exceed 1.5°C and the Kyoto Protocol (1995) to limit their greenhouse gas (GHG) emissions, countries are held accountable for their contributions to climate change. Without action, we face irreversible changes that are expected to have a drastic effect on the planet [3]. Extreme weather events, biodiversity loss, water scarcity, wildfire damage, food insecurity are all impacts expected with global warming [4].

So how much of the problem comes from our energy? A staggering 75% of GHG emissions come from energy. This includes the emissions from the production and consumption of electricity (40%), and emissions from other energy sources such as transportation, heating, and industrial processes (35%).

When considering lifecycle emissions of energy sources per GWh, wind and hydroelectric are found to be the best, with nuclear in third place - better than solar & biomass! (Figure 1).

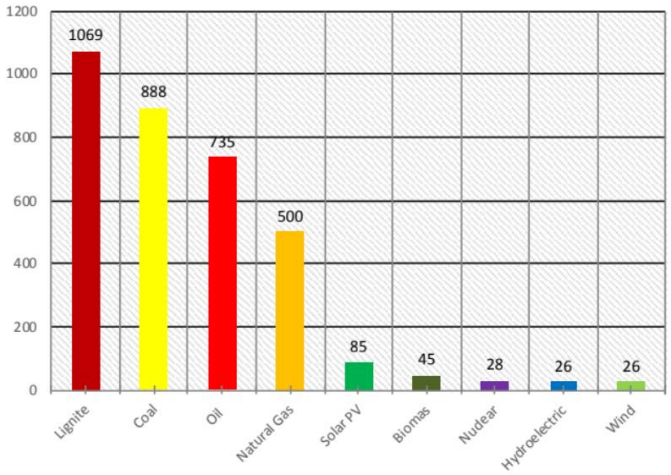

Figure 1 - Lifecycle emissions by energy source

Initial efforts to achieve national targets and to reduce our impact have focused on increasing the supply of renewable energy into the electricity mix which overall, can decrease carbon emissions.

Wind and solar energy are reliant on the weather meaning their supply is inherently irregular. One way to counteract the intermittency of renewables is using energy storage systems [5]. Whilst energy storage such as batteries continue to develop (which also come with their own lifecycle impacts), reliance on fossil fuel for a stable baseload of energy continues. Significant research is being undertaken on energy storage, with interest in making use of old electric car batteries [6]. This technology is not yet ready to deliver competitive seasonal storage of electricity for the grid [5].

This is where nuclear may have a larger role to play. Where nuclear and intermittent renewables differ is where they best complement each other.

The Intergovernmental Panel on Climate Change (IPCC) have reported that to meet the 1.5°C scenario, in all four pathways, nuclear energy supply must be included and increase on average by 300% (of 2020 levels) to 1,160 GW by 2050. The IPCC stated that the current time lag between the decision date and the commissioning of plants is 10-19 years [7].

This means that the best time to decide to build more low-carbon nuclear was decades ago. The next best time is now. For the benefit of human life with minimal impact to the planet [5], [8], [9].

A. ENERGY POVERTY

The developed world finds itself in a climate crisis caused by decades of over consumption. In parallel, energy poverty impacts people every day, effecting mortality and prosperity, predominantly in the global south and developing countries. 1 billion people live through energy poverty every day without adequate, safe access to energy [10].

Energy poverty impacts access to education and livelihoods. It perpetuates poor living conditions, leads to malnourishment, illness and even death. Providing equitable access to affordable low-carbon energy is not just a human rights issue; considering the resources taken from developing countries for the enrichment of developed countries, it is environmental justice. Tackling energy poverty aligns with the United Nations Sustainable Development Goal (SDG) 7: “ensure access to affordable, reliable, sustainable, and modern energy for all" [11].

The EU is by far the largest importer of energy, buying in ~ twice the US’s energy import and five times that of China. Import dependency is considered a problem in European energy policy [12]. Something that has come prominently into the public mind since 2022 following Russia’s invasion of Ukraine and the resulting energy crisis. In essence, rich countries are purchasing cheap fossil fuels, plunging under-developed countries into darkness through continued energy poverty. This leaves the exporting countries without the financial means to invest in cleaner energy alternatives.

I. NUCLEARS ROLE NOW

Nuclear power generation started in the 1950s, and today there are 30+ nuclear nations who operate nuclear power plants. Nuclear accounts for ~ 10% of the world's electricity and it ranks #2 after hydroelectric power for largest source of low-carbon electricity [13].

II. THE NUCLEAR LIFECYCLE

The civil nuclear industry, being under close scrutiny due to fear of radiation and non-peaceful uses of nuclear material, has not had the luxury to fail fast and learn quick. Long before other energy industries considered their carbon emissions or impact on the environment, the nuclear sector has had to manage the impact of its entire lifecycle. With extremely high regulation from mining, refining, enriching, operation, transportation, fuel reprocessing and storage & disposal – in every aspect of the sector, impacts are known and measured.

B. RESOURCES

A 100% renewable future, as idyllic as it sounds, is disputed in feasibility. One concern is that there is not sufficient raw material on planet earth to build a 100% renewable future.

All energy sources require raw materials - how does nuclear compare with renewables on this basis? As shown in Figure 2 and Figure 3 [14], nuclear has a comparatively low raw material requirement per GWh.

Figure 2- Advocacy tool to demonstrate raw material requirements of energy sources at COP27.

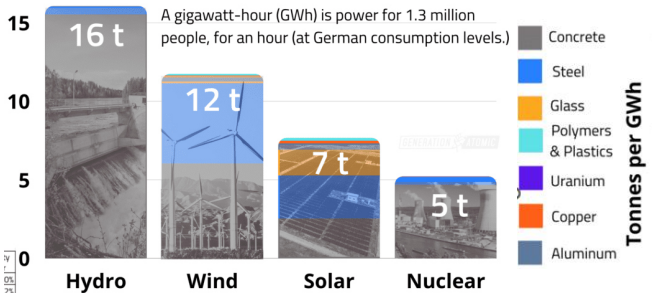

Figure 3 - Raw material requirements of energy sources

The volume of land used for generating energy has an impact on biodiversity of the local eco-system and alternative use of land (e.g., agricultural use, cultural significance). Nuclear, per GW has the lowest land use requirement of the low-carbon energy technologies [14].

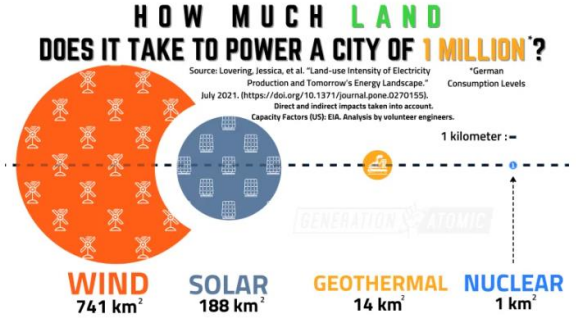

Figure 4 - Land use requirement for low-carbon energy sources

A. WASTE

All the waste generated from nuclear can be seen – we know where it is, and precisely how much of it we have, what has been done with it and we can contain it. The same cannot be said for other energy sources such as fossil fuels where waste in the form of GHG emissions are simply released to the atmosphere leading to air pollution.

Low-carbon energy sources such as solar unfortunately also have waste issues. Currently, we are without solution for recycling or safely disposing of photo-voltaic (PV) panels.

Expertise in long-term waste management, decommissioning and lifecycle impact is something that the nuclear industry can share with other sectors: with a time-tested understanding of cradle-to-grave waste management and decommissioning of power plants and reprocessing sites – the nuclear sector can lead the way in the future decommissioning of fossil fuel power plants.

Furthermore, the nuclear industry has an opportunity to share its far-sighted understanding of total impact from design to disposal with the renewable industry, tackling issues such as the toxic waste produced in the manufacture of solar panels [15].

B. BUT NUCLEAR KILLS…

No source of energy is without impact. Impact on the environment, including the eco-system and the humans and wildlife that inhabit the earth.

Wind turbines produce low-carbon electricity, but they also interrupt the eco-system and kill between tens to hundreds of thousands of birds per year in Europe [16]. However, domestic cats kill 84 million birds a year in Europe [17]. Cat's (see Figure 6) aren't intrinsically bad because they kill birds, and neither are wind turbines.

Figure 6 – Author's Cat: Loki, Scotland, United Kingdom. As an indoor cat, Loki's death-print of birds is estimated to be 0.

Death of our fellow human beings, including in their workplaces, is always a tragedy. Everyone deserves to return home from work safely. The effort of the energy workforce enables a high standard of living and prosperity to society by powering schools, hospitals, libraries and is essential to development of civilisation.

Engineers on wind turbines have died in tragic accidents as well as factory workers in manufacturing of solar panels. Many miners have lost their lives, plant operators and emergency responders have died in nuclear accidents and oil-riggers have lost their lives at sea.

A holistic view of the available energy sources shows unfortunately, human death is an impact of all energy sectors. Nuclear, managing its lifecycle to an extremely high standard, has the lowest "death-print" of all, something that is clear in Figure 5. This is inclusive of both direct deaths and epidemiological estimates, and the figures for nuclear include the deaths related to the Chernobyl accident [18].

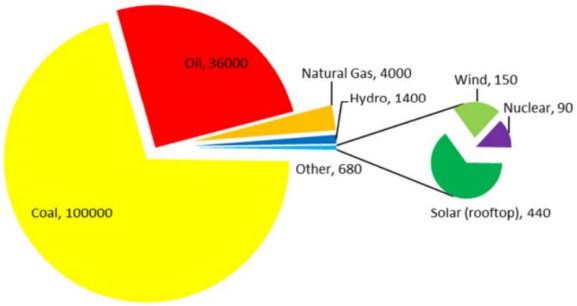

Figure 5 - Comparative death-print of different electricity generation methods.

C. NUCLEAR SAVES LIVES

In Europe alone, over 9 million patients a year benefit from nuclear medicine from diagnostic procedures and treatment. The benefits of radiation are widely accepted for treating cancers and detecting illness [19].

Beyond medicine, clean air is essential for healthy life and air pollution is a massive contributor to premature deaths and respiratory disease. Beyond the lowest death-print, nuclear energy saves lives. Nuclear, by displacing fossil fuel use has abated > 64 gigatonnes of GHGs from the atmosphere. To put this into perspective, that is double the 2016 global CO_2 emissions [20]. From this abatement, nuclear energy has in fact prevented many premature deaths; to be precise, 1.84 million of them [21].

D. PUBCLIC PERCEPTION

Based on the data alone, nuclear should be the environmentalists' choice with a major role in the low carbon energy future.

When the public considers energy policy, their appetite is for a greater share of renewables, but without increasing cost or reducing consumption. Comparing European countries shows that only the UK public are supportive of nuclear power as part of a future energy mix (Figure 7).

In Germany's energy transition policy: Energiewende 2010, the country committed to phasing out nuclear power, with all plants to be shut down, including early closure. It's estimated that these early closures of nuclear power plants in Germany have led to an additional 1,100 premature deaths per year from air pollution, mostly due to increased emissions from fossil fuels being used to replace the clean, zero-carbon energy that the nuclear power plants could have continued to produce safely and abundantly [22].

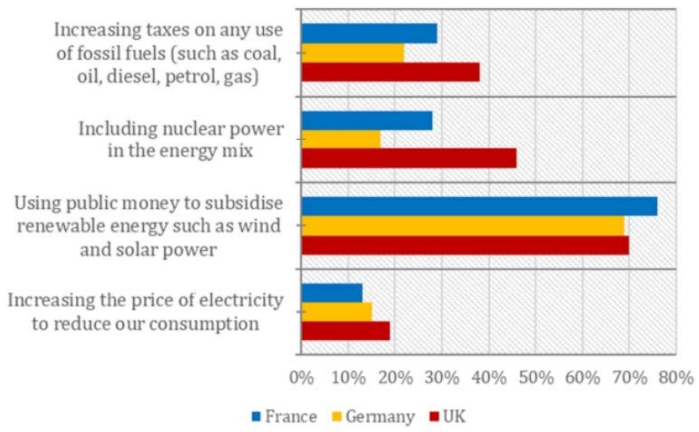

Figure 7 - To what extent do you support or oppose the following policies in [France/ Germany/ UK]? [39]

E. NON-ENERGY SOLUTIONS

Carbon Capture and Sequestration (CCS) is a technology that could reduce carbon emissions from the atmosphere [23]. Current forecasts of CCS implementation show that if all currently planned CCS facilities were deployed by 2030, they would only capture 17.5% of the carbon needed to achieve Net Zero [24]. To the author, focussing on CCS to enable the continued use of fossil fuels feels a little bit like grabbing a mop as the first line of defence when the bath is over-flowing. Focus should be directed to turning off the tap (see Figure 8).

Figure 8 - A person mopping a flood instead of turning off the tap [37]

However for hard-to-abate fossil fuel use such as high heat industrial processes, CCS could offer a solution in the short term whilst other energy technologies develop to replace fossil fuels in these scenarios.

III. SUMMARY

Ultimately: “no primary energy source, be it renewable or non-renewable, is free of environmental or economic limitations” [25].

The countries currently decarbonising their energy supplies most effectively are doing it with nuclear (France and South Korea), hydroelectricity (Brazil and Canada), and natural gas [26]. Governments around the world have recognised the requirement to include nuclear in their electricity mix. Developing countries such as UAE and China are fast-tracking nuclear programmes to meet increasing electricity demands [27].

Implementing proven, stable, abundant, reliable nuclear energy will enable access to energy for the prosperity and benefit of humankind in a sustainable way. Using nuclear to transition from fossil fuels will displace tonnes of carbon from the atmosphere whilst having minimal impact on land, material use and the environment.

IV. REFERENCES

[1] EIA, “Today in Energy: EIA projects 28% increase in world energy use by 2040,” 9 2017. [Online]. Available: https://www.eia.gov/todayinenergy/detail.php?id=32912.. [Accessed 4 2018].

[2] McKinsey & Company , “Global Energy Perspective 2022,” April 2022. [Online]. Available: https://www.mckinsey.com/industries/oil-and-gas/our-insights/global-energy-perspective-2022.

[3] Energy for Humanity, “Briefings, Climate Change: An Intro,” [Online]. Available: http://energyforhumanity.org/en/briefings/carbon-emissions/climate-change-basic-info/. [Accessed 18 3 2018].

[4] IPCC, “AR6 Synthesis Report Climate Change 2023,” 2023. [Online]. Available: ipcc.ch/report/ar6/syr/figures/summary-for-policymakers/figure-spm-4/. [Accessed 16 04 2023].

[5] European Academies' Science Advisory Council, “Valuing dedicated storage in electricity grids,” 2017.

[6] S. e. a. Tong, “Demonstration of reusing electric vehicle battery for solar energy storage and demand side management,” Journal of Energy Storage, vol. Vol. 11, pp. 200-210, 2017.

[7] IPCC, “Global Warming of 1.5°C,” IPCC, 2018.

[8] Orano, “All about the IPCC report on climate change,” Orano, [Online]. Available: https://www.orano.group/en/unpacking-nuclear/all-about-the-ipcc-report-on-climate-change. [Accessed 09 2022].

[9] Nuclear for Climate, “The fastest path to Net Zero for a sustainable & energy secure future for all - 2022 Position Paper COP27,” Nuclear for Climate, 2022. [Online]. Available: https://www.euronuclear.org/wp-content/uploads/2022/09/COP27-Position-Paper.pdf.

[10] Habitat for Humanity, “What is energy poverty: definition, statistics & effects on society,” www.habitat.org, [Online]. Available: https://www.habitat.org/emea/about/what-we-do/residential-energy-efficiency-households/energy-poverty. [Accessed 09 2022].

[11] United Nations Department of Economic and Social Affairs, “Sustainable Development - The 17 Goals,” United Nations Department of Economic and Social Affairs, [Online]. Available: https://sdgs.un.org/goals.

[12] F. Umbach, “Global energy security and the implications for the EU,” Energy Policy, vol. 38, no. 3, pp. 1229 - 1240, 2010.

[13] IAEA, “Nuclear power in the world today,,” IAEA, 2019. [Online]. Available: https://www.iaea.org/publications/factsheets/nuclear-power-in-the-world-today. [Accessed: Apr. 02, 2023]. . [Accessed 3 4 2023].

[14] Generation Atomic, “About> Why Nuclear Energy,” Generation Atomic, [Online]. Available: https://www.generationatomic.org/why-nuclear/. [Accessed 25 3 2023].

[15] Environmental Progress, “Are we headed for a solar waste crisis?,” Environmental Progress, 21 June 2017. [Online]. Available: http://environmentalprogress.org/big-news/2017/6/21/are-we-headed-for-a-solar-waste-crisis.

[16] BirdLife International, “The impacts of wind farms on birds in Europe,” BirdLife International, 2012.

[17] T. W. a. P. P. M. S. R. Loss, “The impact of free-ranging domestic cats on wildlife of the United States,” Nature Communications, vol. 4, p. 1396, 2013.

[18] IAEA, “Energy Snapshot Global carbon dioxide emissions, 1980 - 2016,” 2017. [Online]. Available: https://www.iea.org/newsroom/energysnapshots/global-carbon-dioxide-emissions-1980-2016.html.. [Accessed 5 4 2018].

[19] NuclearEurope, “Lifesaving nuclear medicine applications deserve better recognition and support at EU level,” NuclearEurope, 21 June 2021. [Online]. Available: https://www.nuclearеurope.eu/press-release/lifesaving-nuclear-medicine-applications-deserve-better-recognition-and-support-at-eu-level/. [Accessed 16 April 2023].

[20] International Energy Agency, “ Energy Snapshot Global carbon dioxide emissions, 1980 - 2016,” 2017. [Online]. Available: https://www.iea.org/newsroom/energysnapshots/global-carbon-dioxide-emissions-1980-2016.html.. [Accessed 5 4 2018].

[21] Hansen, “Prevented Mortality and Greenhouse Gas Emissions from Historical and Projected Nuclear Power,” Environmental Science & Technology., 2013.

[22] O. D. A. J. Stephen Jarvis, “THE PRIVATE AND EXTERNAL COSTS OF GERMANY'S NUCLEAR PHASE-OUT,” National Bureau of Economic Research, Cambridge MA, 2019.

[23] E. A. S. A. Council, “Carbon capture and storage in Europe,” European Academics Science Advisory Council, 2013.

[24] International Energy Agency, “www.iea.org,” September 2022. [Online]. Available: https://www.iea.org/reports/carbon-capture-utilisation-and-storage-2. [Accessed April 2023].

[25] R. K. P. P. Jeffrey Chow, “Energy Resources and global development,” Science, vol. 302, p. 5650, 2003.

[26] M. Goff, “Where Does Decarbonization Come From?,” The BreakThrough Institute, 4 12 2017. [Online]. Available: https://thebreakthrough.org/index.php/voices/where-does-decarbonization-come-from.. [Accessed 2 4 2018].

[27] Alaraby, “The New Arab. UAE to go nuclear as first reactor is completed,” Alaraby, 26 3 2018. [Online]. Available: https://www.alaraby.co.uk/english/news/2018/3/26/uae-to-go-nuclear-as-first-reactor-is-completed.. [Accessed 9 4 2018].

[28] IAEA, “World Energy Statistics and Balances,” 2019.

[29] IAEA, “Energy, Electricity and Nuclear Power Estimates for the Period up to 2050,” 2020.

[30] e. a. V Masson-Delmotte, “Global Warming of 1.5: An IPCC Special Report on the Impacts of Global Warming of 1.5 above Pre-Industrial Levels...,” 2018.

[31] American Nuclear Society, “Applications: Medical Applications,” American Nuclear Society, [Online]. Available: http://nuclear-connect.org/know-nuclear/. [Accessed 19 3 2019].

[32] e. a. Peter McCallum, “Critical impact of radiotherapy protocol compliance and quality in the treatment of advanced head and neck cancer: results from TROG,” Journal of Clinical Oncology, vol. 20, 2010.

[33] Ministere de la transition, Republique Francaise, Ministere de la transition ecologique et solidaire. Plan Climat, Ministere de la transition, Republique Francaise, 2017.

[34] DEFRA and DfT, UK, DEFRA and DfT. UK plan for tackling roadside nitrogen dioxide concentrations, UK Government, 2017.

[35] N. Z. M. &. T. N. C. Veziroglu, “From hydrocarbon to hydrogen-carbon to hydrogen economy,” International Journal of Hydrogen Energy, vol. 30, 2004.

[36] E. f. Humanity, “ Energy for Humanity,” [Online]. Available: http://energyforhumanity.org/en/.. [Accessed 2 4 2018].

[37] B. Meijer, “Dutch test the water for subsidy-free offshore wind farms,” Reuters, 15 December 2017. [Online]. Available: https://uk.reuters.com/article/.. [Accessed 17 March 2018].

[38] Francis, Matthew, “BBC Future,” BBC, 2014. [Online]. Available: http://www.bbc.com/future/story/20130726-will-we-ever-have-nuclear-fusion.

[39] Margaret Thatcher, “Speech to United Nations General Assembly,” November 1989. [Online]. Available: margaretthatcher.org. [Accessed 3 2018].

[40] European Network and Information Security Agency. , “Smart Grid Security,” 2012.

[41] https://www.fotor.com/features/ai-image-generator/, Artist, [Art]. Fotor, 2023.

[42] K. e. a. Steentjes, “European Perceptions of Climate Change: Topline findings of a survey conducted in four European countries in 2016.,” Cardiff University, Cardiff, 2017.

V. ACKNOWLEDGEMENTS

I’d like to acknowledge and extend my gratitude to Henry Preston and Allan Simpson, co-authors of a paper: “The Energy Transition: What is the role of nuclear technology in a world of growing alternative power and digital innovation?” for the 2017 – 2018 Spark! Contest. The general basis of this paper has come from the collaborative work with those co-authors.

Proceedings of the European Nuclear Young Generation Forum
ENYGF'23
May 8-12, 2023, Kraków, Poland

Future Polish zero carbon energy mix combining renewable and nuclear energy sources

Lipka, Maciej

National Centre for Nuclear Research (NCBJ), Poland

*Corresponding author: *Maciej.Lipka@ncbj.gov.pl*

I. INTRODUCTION

Poland, like other countries, must carry out an energy transformation in the coming years. Its goal is to participate in global efforts to stop climate catastrophe by reducing anthropogenic greenhouse gas emissions to achieve net zero emissions. Energy transformation, meaning departure from fossil fuels – not only coal but also natural gas, requires using the full spectrum of low-emission sources: nuclear, wind, solar and biomethane, and other available low-carbon sources. Nowadays, due to the Russian invasion of Ukraine and an increase in fossil fuel prices that followed it, departing fossil fuels is not only the climate but also a strategic necessity. The analysis demonstrates Poland's optimal zero-emission energy mix, determined from the point of view of the reliability of electricity supply and minimization of its carbon footprint. The system is mapped for the hypothetical year 2049. For the purpose of modelling, actual data on the availability of renewable energy in Poland and data from the Polish power system were used.

In this paper, a numerical analysis of the hypothetical power system in Poland is performed. The work combines hourly capacity factors of the renewable energy sources in Poland with Monte Carlo sampling, which enabled the selection of the optimal electricity mix.

II. DATA AND METHODS

The model relies on the hourly data of the electricity supply and demand sampled from the ENTSO-E Transparency Platform [1]. The year 2022 has been selected as the basis for the capacity factors calculation as the most recent that is available. They have been calculated by dividing the electricity generation by the monthly data about the installed power of onshore wind and photovoltaics (PV). As Poland currently does not operate offshore wind farms, data for the German offshore at the Baltic Sea were used (i.e. Arkona, Wikinger, EnBW Baltic 1 & 2) due to their geographical proximity to the Polish territory. The annual electricity demand has been set to 250 TWh as the mean value from the prognoses presented in Figure 1.

The hourly load was taken from the 2022 data and rescaled, so the current annual demand (173.5 TWh) will match that determined for 2049.

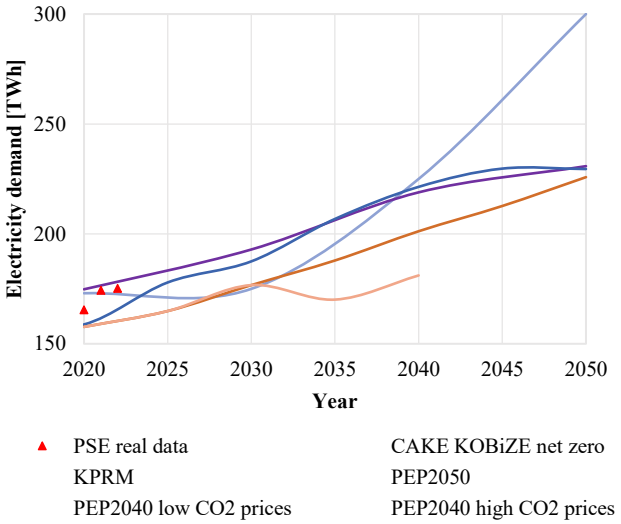

Figure 1. Increase of the Polish annual electricity demand [2]–[5]

For simplification, it was assumed that the nuclear fleet always operates at 100% installed power, but a fraction of the power units are taken offline every 18 months for refuelling. That generation decrease has been included in the calculation. As Poland currently does not have a nuclear strategy up to the year 2049, it was assumed that the installed capacity (12.1 GWe) will be proportionally higher than that described in Polish Nuclear Power Programme [6], i.e. up to 9 GWe in 2043 or, according to the press information about the new Poland's Energy Policy c.a. 8 GW– in 2040 [7].

Additionally, it was estimated that Poland should possess c.a. 15 GWe 'Fast burst' [8] biomethane or biogas sources, value which is technically feasible [9] and actually lower than the values presented in [7]. Moreover 4.2 GW/27 GWh pumped storage hydropower (PHES) will operate in the system (which is in line with the current national policy [10]) and additionally 7 GW/28 GWh of battery storage (proportional to the EU estimates [11]). The rest of the electricity demand is covered by the Demand Side Response

(DSR), which minimisation both in means of power and time is the optimisation goal (as too large DSR is temporary no more and means energy shortages). The system is accompanied by 1.5 GWe of biomass sources operating constantly and c.a. 890 MWe [12] hydropower plants with real hourly capacity factors.

Limit for the maximum installed capacity of photovoltaics, onshore wind and offshore wind farms has been applied as their maximum physical amount available in Poland [13]–[15]. Appropriate values are presented in Figure 2. It was also assumed that due to the high capital costs, offshore wind and nuclear in the 'nuclear scenario' compete with each other in a way, so, in that case, the maximum combined installed capacity of nuclear and offshore wind is capped at 28 GWe, which is maximum for the latter in Polish conditions.

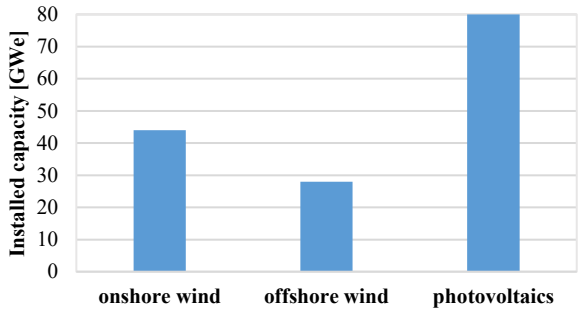

Figure 2. Maximum possible renewables installed capacity in the Polish conditions [13]–[15]

III. RESULTS

Set of 100,000 simulations with random installed capacity was runned, however, as it was noted, above 10,000 there was no increase in accuracy. Calculations outcome were the two data sets of installed capacities in two scenarios:

- Combining renewable and nuclear power (RENNUC)
- Renewable power only (RENONL)

In RENONL scenario, the installed capacities of renewables were determined by Monte Carlo to be equal to the actual physical limitations that can be seen in Figure 2. In RENNUC, they were determined by the same method but happened to be much lower.

Both scenarios have been presented in Table 1 below, together with the energy volumes required in 'Fast burst' sources and DSR. As it can be seen installed power in RENNUC scenario is 30% lower. Additionally 25% of power in DSR is needed. From the point of view of energy supply and consumption, nuclear scenario needs 63% less of DSR and 50% of gas amount.

In both scenarios part of the energy generated is inevitably wasted due to the impossibility of its storage. However in nuclear scenario the losses are 33% lower than in non-nuclear scenario (66 vs 100 TWh) due to the lower installed capacity in the intermittent renewable sources.

Both of the system, its load and electricity sources are presented in the daily resolution in the figures 3 and 4. Drops in the nuclear generation visible in figure 3 are due to the periodic refuelling of the reactors in modern, 18-months fuel cycle – procedure partially occurs in spring and partially in summer, due to the availability of intermittent sun and wind sources in those periods.

Operation of the PHES, electricity storage, 'fast burst' and DSR in both scenarios is presented in the figures 5 and 6. Negative values represent hours with loading of the energy storage sources.

Table 1. Calculated net-zero electricity mixes for Poland: nuclear and non-nuclear scenario

	RENNUC	RENONL
Nuclear [GWe]	12.1	0.0
PV [GWe]	35.0	80.0
Onshore wind [GWe]	35.0	44.0
Offshore wind [GWe]	15.0	28.0
DSR [GWe/TWh]	11.3/1.1	17.2/2.9
'Fast burst' [GWe/TWh]	15.0/14.0	15.0/28.5
Biomass	1.5	
Hydropower	0.9	
Energy storage	7.0	
PHES	4.2	

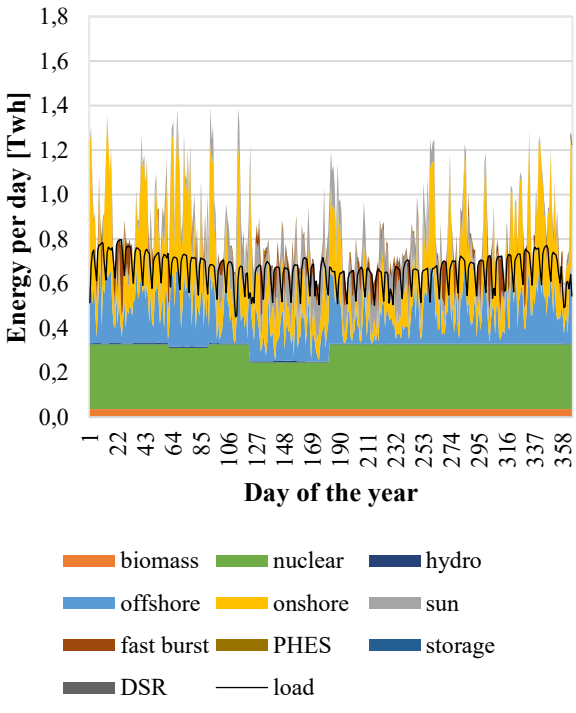

Figure 3. RENNUC electricity mix in daily resolution

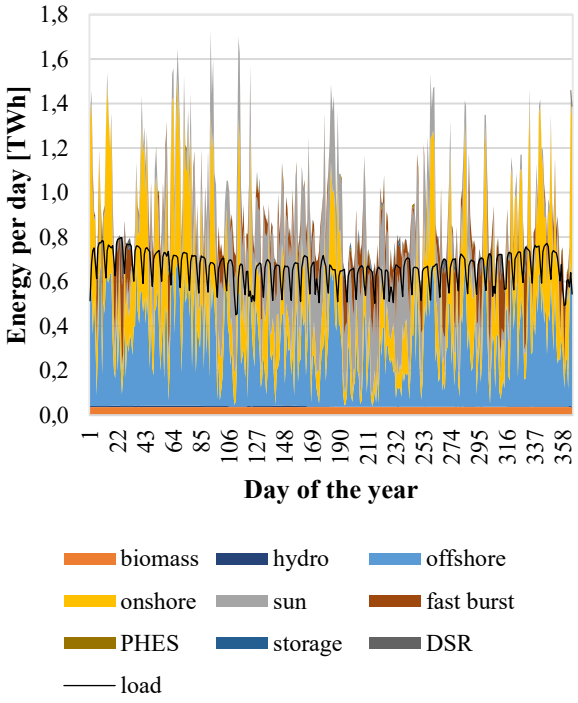

Figure 4. RENONL electricity mix in daily resolution

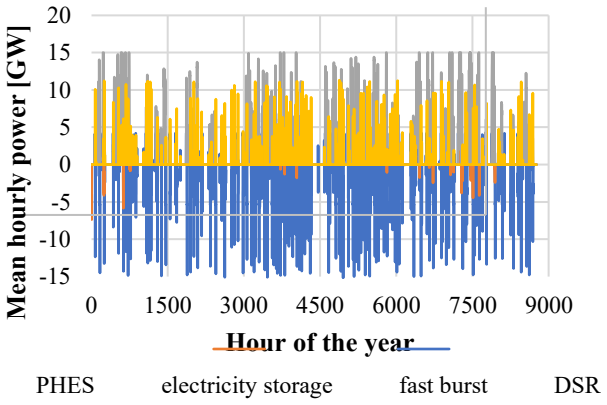

Figure 5. PHES, electricity storage, fast burst and DSR operation in RENNUC scenario

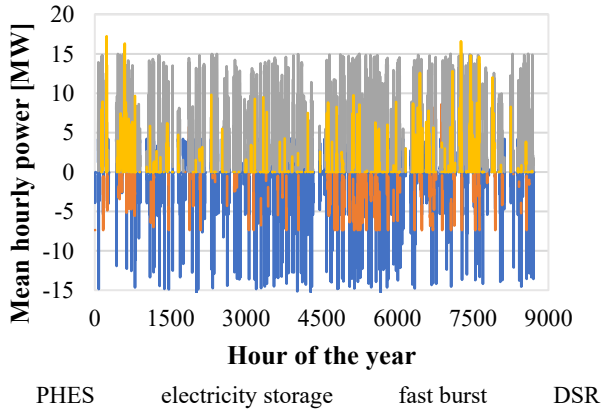

Figure 6. PHES, electricity storage, fast burst and DSR operation in RENONL scenario

To show DSR and fast burst performance in a more usual way, they both have been visualised below. In figure 7, the hourly needs of DSR in both scenarios are presented in an ordered manner. As it can be seen, the RENNUC scenario requires about 33% hours of energy savings and lower DSR capacity. Figure 8 presents the ordered manner of hourly gas power required in the two scenarios, as it can be seen, in the RENNUC needs are decreasing faster, i.e. smaller back-up is required for the intermitted sources. In the absolute terms, the amounts of energy stored in biomethane required in the 'fast burst' sources are c.a. 100% higher in RENONL scenario.

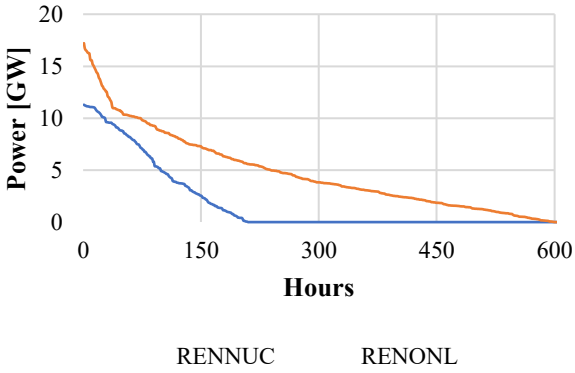

Figure 7. Ordered line graph of DSR needs in both scenarios

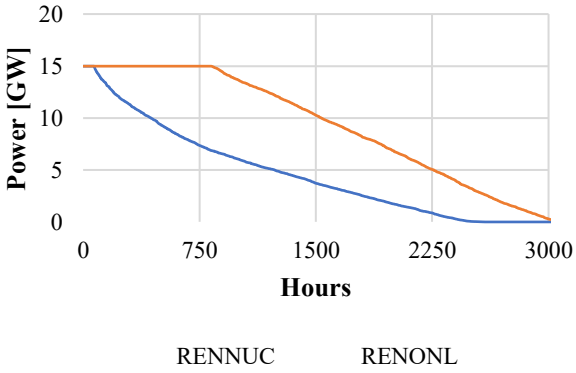

Figure 8. Ordered line graph of 'fast burst' needs in both scenarios

IV. CONCLUSIONS

The article compares two scenarios, determined by Monte Carlo modelling: cooperating nuclear and renewables, and renewables only. It has been determined that adding nuclear to the portfolio of clean energy sources limits the amount of the installed capacity and shortages of energy. The following research steps shall involve optimising the order in which the reserve sources (DSR, PHES, electricity storage and fust burst) join the system. Additionally, load following of the nuclear is going to be considered.

Moving away from fossil fuels is a necessity both because of the spectre of climate catastrophe and Poland's growing dependence on their imports. At the same time, it is a civilisational challenge to carry out the energy transition in such a way as to ensure a stable and reliable supply of electricity at reasonable prices. In every place on Earth, the circumstances will dictate the measures to achieve the goal.

Calculations presented in this article revealed that adding nuclear to the portfolio of technical means will make the

net-zero transition way easier than in the case without it. Both scenarios are presented in Figure 9. Net-zero must be based on renewable energy sources and large, proven nuclear units in Polish conditions. Additional pieces of the puzzle necessary for success are pumped storage power plants and other types of energy storage, as well as zero-emission peaking power plants, such as those using sustainably sourced biomethane. If any of those puzzle pieces fall out of the solution pool, the transition will fail, resulting in electricity shortages.

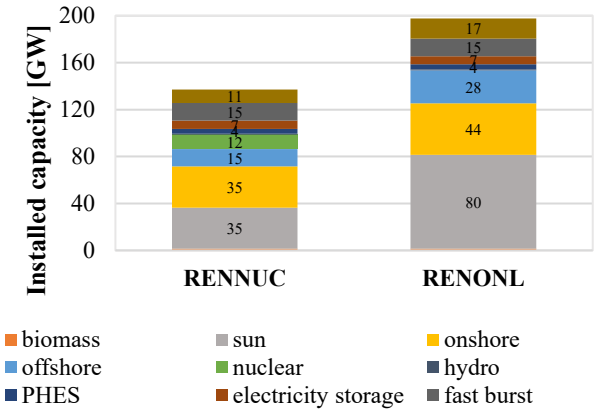

Figure 9. Installed power in both scenarios

V. Acknowledgements

I would like to express gratitude to Prof. Kacper Szulecki from Department of Political Science, University of Oslo and Mr Przemysław Stępień from Poland's Green Party 'Zieloni'. This research would never have been made if it wasn't for their essay about energy systems, which was not properly rooted in understanding how energy systems works.

VI. References

[1] 'ENTSO-E Transparency Platform'. https://transparency.entsoe.eu/ (accessed Mar. 18, 2023)..

[2] I. Tatarewicz et al., 'Transformacja sektora energetycznego Polski i UE do 2050 roku', Instytut Ochrony Środowiska - Państwowy Instytut Badawczy / Krajowy Ośrodek Bilansowania i Zarządzania Emisjami (KOBiZE), Warszawa, 2022.

[3] 'Projekt Polityki energetycznej Polski do 2050 roku', 2015. https://www.gov.pl/documents/33372/436746/DE_projekt_PEP2050_2015-08-03.doc/57c5150f-f50e-e8a7-6b27-49c330ab9d4d (accessed Mar. 18, 2023).

[4] Obwieszczenie Ministra Klimatu i Środowiska z dnia 2 marca 2021 r. w sprawie polityki energetycznej państwa do 2040 r. [Online]. Available: https://isap.sejm.gov.pl/isap.nsf/download.xsp/WMP20210000264/O/M20210264.pdf.

[5] 'Energy, Electricity and Nuclear Power Estimates for the Period up to 2050', International Atomic Energy Agency, Vienna, 2020.

[6] Program polskiej energetyki jądrowej. 2020. Accessed: Mar. 18, 2023. [Online]. Available: https://bip.mos.gov.pl/fileadmin/user_upload/bip/prawo/inne_projekty/PPEJ/Program_polskiej_energetyki_jadrowej.pdf

[7] 'Polska szykuje się na wojnę węgla z gazem w aktualizacji strategii energetycznej PEP2040', BiznesAlert.pl. https://biznesalert.pl/pep2040-strategia-energetyczna-aktualizacja-projekt-gaz-wegiel/ (accessed Mar. 29, 2023).

[8] N. A. Sepulveda, J. D. Jenkins, F. J. de Sisternes, and R. K. Lester, 'The Role of Firm Low-Carbon Electricity Resources in Deep Decarbonization of Power Generation', Joule, vol. 2, no. 11, pp. 2403–2420, Nov. 2018, doi: 10.1016/j.joule.2018.08.006.

[9] 'Raport Biogaz w Polsce', Biomass Media Group Sp. z o.o., Poznań, 2020. Accessed: Mar. 18, 2023. [Online]. Available: http://cdr112.e-kei.pl/cdr/images/2021/05/Raport-Biogaz-w-Polsce-2020-magazynbiomasa.pdf

[10] 'Rola elektrowni szczytowo-pompowych w Krajowym Systemie Elektroenergetycznym: uwarunkowania i kierunki rozwoju', Kancelaria Prezesa Rady Ministrów, Warszawa, 2022.

[11] Commission Staff Working Document Impact Assessment Report Accompanying the document Proposal for a Regulation of the European Parliament and of the Council concerning batteries and waste batteries, repealing Directive 2006/66/EC and amending Regulation (EU) 2019/1020. 2020. Accessed: Mar. 18, 2023. [Online]. Available: https://eur-lex.europa.eu/legal-content/EN/TXT/?uri=SWD%3A2020%3A335%3AFIN

[12] 'Informacja Statystyczna o Energii Elektrycznej'. https://are.waw.pl/wydawnictwa#informacja-statystyczna-o-energii-elektrycznej (accessed Mar. 18, 2023).

[13] 'Wizja dla Bałtyku. Wizja dla Polski. Rozwój morskiej energetyki wiatrowej w basenie morza Bałtyckiego', Polskie Stowarzyszenie Energetyki Wiatrowej, Warszawa, 2020.

[14] P. Czyżak, M. Sikorski, and A. Wrona, 'Co po węglu? Potencjał OZE w Polsce', Instrat Policy Paper 06/2021, 2021.

[15] 'Wind energy in Poland 4.0', Baker Tilly TPA / Polskie Stowarzyszenie Energetyki Wiatrowej / Kancelaria prawna DWF, 2022.

Proceedings of the European Nuclear Young Generation Forum
ENYGF'23
May 8-12, 2023, Kraków, Poland

Industry repowering with SMRs: key takeaways

Nouchy, Fabio[1*], Monette, Philippe[1], Piette, Célestin[1], and Touré, Anicet[1]

[1] Tractebel Engineering, Belgium

*Corresponding author: *Fabio.nouchy@tractebel.engie.com*

I. INTRODUCTION

Meeting the net-zero emission target by 2050 in order to counteract human-induced climate change is this century's challenge. Overcoming the climate crisis will imply reducing carbon dioxide emissions not only for electricity production, but rather for all the energy sectors. One particular sector hard to abate is the manufacturing industry, that in Europe totals about 13% of CO2 emissions.

Industrial plants often have stringent requirements in terms of reliability and availability, and may require both heat and electricity. Most of the industries are currently sourcing their power from dedicated coal or gas fired plants. From reference [1] it results that 157 GW of coal plants (about 7.5% of the worldwide figure) and 235 GW of gas-fired plants (13% of the worldwide figure) are currently operating in Europe. On the other hand, in 2020 in Europe, the industry used about 40% of the total coal consumption and 33% of the total gas consumption [2].

Only few options are available as low-carbon heat sources for industrial processes. Among the technologies to produce decarbonized heat, one can find heat pumps, fossil fuels properly abated via carbon capture and storage technologies, synthetic fuels via the Sabatier reaction and nuclear power. Among these technologies some are not able to reach the high temperatures required while others are merely energy vectors that need to be produced via electricity. Electricity supply can instead come also from Renewable Electricity Sources, such as wind power and photovoltaic plants, but in that case the industrial requirements on reliability imply the extensive use of back-up sources.

Focusing on nuclear power, some designs of Small Modular Reactors (SMRs) are promising solutions to replace conventional plants as they have a compatible footprint, high availability and can deliver high temperature process heat. Indeed, smaller footprints open the opportunity to colocalize the SMRs nearby existing industrial areas, either on the same brownfields occupied by the current technology, or on adjacent greenfield sites, i.e. previously undeveloped sites for industrial exploitation. The higher temperatures reached by the Generation IV technologies (steam can be supplied in a range between 500-600°C by High Temperature Gas Reactors [3]) can respond to the demand of high temperature steam supply, widely required in distillation steps of chemical and petrochemical processes. Tractebel has recently performed a few case studies for industries with different requirements, exploring the use of SMR technologies and assessing the most promising designs in technical and economic terms.

A. Goal of the case studies

The main goals of each study are to assess the suitability of the SMR solution in terms of economic competitiveness and technical integration, to assess if show-stoppers are present, and to down-select the best suited designs for the purpose.

The process followed to perform these assessments includes a definition of the suitability requirements, a down-selection of the best-suited designs, the ranking of the selected ones, the modelling of the balance of plant for the top-ranked to validate their adequacy to supply the required power and a cost estimation to compare their business case to the ones of competing fossil fuel fired solutions.

Rather than one specific study, this paper is a collection of findings for the consideration of the nuclear industry when planning industry repowering by SMRs. The paper includes also the methodology of the down-selection and ranking steps, as it has been standardized, while concerning system integration and cost estimation only key takeaways are given.

II. DESIGN DOWN-SELECTION

Since over five years Tractebel collected technical and business data from the SMR designs present on the market in a database, that at the moment of writing this paper contains entries on over 100 designs. For industries and utilities that look at SMRs as a possible solution to decarbonize their assets it would be a major effort to

collect the same broad vision on the SMR market and eventually choose the best solution.

The main reason to accurately perform a ranking exercise of these designs is that both their output parameters and the end-user requirements are scattered on a broad range of values, for which a matching endeavour is necessary.

A. Methodology

The down-selection is performed in three steps (see also Figure 1):

1. Identification of the exclusion criteria and application to the designs in the database;
2. Ranking of the retained designs by giving a score to each Critical Success Factor adapted to the project;
3. Perform a high-level assessment of the top-ranked designs.

Figure 1. Methodology of the down-selection process

At the project kick-off the first goal is to identify the suitability requirements together with the end user and ascertain which of those requirements are also exclusion criteria. For each project one can identify generic and specific exclusion criteria, where the former refer to conditions in the development status of the design which lead to its exclusion, while the latter can only be identified by studying the application and project specificities. Examples of generic exclusion criteria are evident lack of recent advancement or of support. Among specific exclusion criteria one finds the operating constraints (e.g. energy vector required and heat process temperatures), time-to-market constraints and layout requirements, e.g. footprint.

The term ranking criteria defines here all those factors that are used to set a score to the designs in the second phase of the down-selection. During the definition of the requirements all the ranking criteria are grouped into eight Critical Success Factors, aiming at characterizing the sufficient and necessary conditions for the success in the project from a techno-economic perspective. The ranking process is performed with the help of the SMR.FIT tool, developed within Tractebel, where every Critical Success Factor is analyzed and the ranking criteria are applied. Also in this case one can identify generic criteria, e.g. all those associated to safety, sustainability and delivery certainty, and specific ones, e.g. availability, reliability, temperature regime, module size, and all the parameters that are compared to end-user requirements, as well as some of the exclusion criteria .

SMR.FIT is a tool that helps in highlighting trends, but it still requires expert validation. Therefore after the ranking of the retained designs a validation of the results follows together with a complementary assessment of the top-ranked designs, where all the Critical Success Factors are discussed.

The final score that is given to each design is the result of a weighted sum of the partial scores given to the eight Critical Success Factors, where each weight is chosen with the end-user. Addressing the expectations of the end-user correctly is very important at an early stage and it translates into identifying exclusion criteria and into giving the correct weight to the Critical Success Factors.

B. Critical Success Factors

The SMR.FIT tool ranks the candidate designs for a project based on the list of ranking criteria, as grouped into the Critical Success Factors described in Table 1. A comprehensive list of ranking criteria is not given here as it is lengthy and project-dependent.

Table 1. Critical Success Factors and associated parameters used as ranking criteria to perform the down-selection

Critical Success Factor	Associated ranking parameters (non-exhaustive list)
Cost competitiveness	CAPEX, OPEX, construction time,…
Safety & Security	Divided in 4 sub-factors: Radiological consequences of accidents, grace period and coping time, sensitivity to internal initiating events, sensitivity to external hazards
Sustainability	Divided in 4 sub-factors: Fuel efficiency, resource use, waste production (including spent fuel), environmental management
Time to market	Projection for First-Of-A-Kind deployment, Technical Readiness Level, Research & Development status, Licensing status,…
Equity & Finance	Access to private funding, investments made, governmental funding, investors identified,…
Delivery certainty	Supply chain status, Research & Development plan, identified partners,…
Fitness for purpose	Power matching, footprint, parameters for process heat applications, service continuity,…
Geopolitical support	Governmental support, likelihood to obtain license in host country, public acceptance of technology proposed,…

C. Key takeaways

The importance to perform accurately a down-selection exercise derives from the need to find acceptable matches between design outputs and end-user requirements. From the experience gathered in recent projects, we identified the following main trends.

A company that is newly giving consideration to nuclear technologies often has a **perception** on designing, licensing and deploying a nuclear installation that is assimilated to the process for conventional units. A demystification effort is therefore necessary at the inception phase of the project so that the expectations are aligned with the reality, especially in terms of the flexibility of the solutions and their time to market.

Strong expectations are associated to the **time-to-market** factor, for which vendors communicating aggressive schedules attract the most attention independently of their current development status. Not fulfilling the expectations may have a backlashing effect on the whole market. Prudence is therefore urged from vendors.

The industrial plants are currently burning fossil fuels mainly to produce two **energy vectors**: heat and electricity. The latter can be equally supplied by SMRs or Renewable Energy Sources, but nuclear sources have a significative advantage, which is the higher reliability. As for the heat needs, wind and solar power are not an option, and the low-carbon energy sources that could replace fossil fuels are biomass fuels and nuclear. Biomass fuel being questionable in terms of sustainability and air pollution, the role of nuclear becomes of primary importance. However, heat extraction from nuclear fission cannot yet yield temperature levels and heat fluxes matching the ones from burning hydrocarbon flames. These are required by energy-intensive processes, as metal smelting and molecules cracking. To decarbonize these processes the solution is another energy vector: synthetic fuels, produced via hydrogen, carbon capture and subsequent Sabatier process. The role of an SMR in this case will be to supply the electricity needed for the electrolysis of water for hydrogen production.

Finally, when focusing on **power matching**, there seems to be a range between 50 and 150 MW_{th} in which the offer on the SMR market is reduced to less than a dozen designs. This is curious as that range is close to the power requirements from many industrials.

III. INTEGRATION

This chapter will introduce considerations on both system integration and layout integration of SMRs for industrial repowering. Tractebel performed quasi-static thermodynamic models of the SMR balance of plant using Thermoflow software, including the steam extractions for the industrial process, and preliminary site assessments.

The main objective of these assessments has been to investigate the possibility for retrofitting and, as a second solution, to dimension the balance of plant. In this context, a perfect retrofitting would mean to maintain all of the balance of plant installations and equipment downstream of the steam generator (turbine, piping, pumps, etc.) while limiting the replacement to the boiler with the SMR. Nevertheless, it would only make sense to replace a boiler before the old one is dismantled, as the most important aspect for the final user is production continuity. When retrofitting is not feasible, the project of repowering by SMR has to opt for deployment in adjacent land plots around the factory.

A. Key takeaways

The main finding of these assessments is that SMRs are generally suitable for industry repowering, while enabling high reliability and service continuity.

Fitting the construction site and the new asset in the **existing layout** can be challenging, especially on sites of very compact gas-fired facilities. Coal-fired boilers offer better possibilities, thanks to the large footprint of their fuel storage, which could be temporarily moved and phased out.

However, there are major technical obstacles that generally prevent the possibility for a retrofit: the main one is matching the **steam conditions** (flow, temperature and pressure) with a generic SMR design. Deviating on one of the steam parameters goes at the expenses of the plant efficiency and the economic interest of such a retrofit. On the other hand, specific designs are not worth the effort of re-designing and licensing for a limited market. If the need to feed a specific turbine cycle is removed and the main focus is limited to the supply of steam to the end user, the level of complexity decreases and a match of temperature and pressure parameters is more likely to be found. Overproduction of steam can instead be used to produce electricity for the grid. Using a turbogenerator as an alternative, instead of the main purpose, can indeed also provide flexibility by shifting a percentage of the process heat demand towards power production.

Optimizing the pressure ports of the turbine allows to increase the net power output. It was observed that **steam extractions** from the turbine at the targeted pressure(s) of the industrial process increases the power output, in certain cases by up to 10% when compared to extraction before the turbine inlet and expansion to the required pressure.

An advantage in terms of flexibility is presented by those reactors that decouple the nuclear island from the conventional island by design and introduce a **heat storage** set of tanks. The main advantage of this solution is an enhanced load following that can even respond to load peak demands if the turbine is over dimensioned, and besides the balance of plant can be designed with increased flexibility.

A new category of end users is searching for highly reliable and abundant electricity sources: the **data centres**. Although not industries properly speaking, their requirements in terms of proximity, costs and time to market are similar to those of industrial processes, and even more stringent their need for reliability, as their require up-times above 99.9999%. As no energy asset can guarantee such availability factors, an SMR is treated as any other technology: an additional asset within a dedicated micro-grid. The reactor itself does not guarantee

the availability, the microgrid with its diversified mix of assets and Uninterruptible Power Supply does.

Reducing the nuclear liabilities by design can be a winning feature for future technologies. For example, an important condition for industrials is the ease to re-establish a non-nuclear site, independently from it being originally a **greenfield** or a **brownfield** site. This condition leads them to look with interest at nuclear technologies with reduced footprint, having more chances to be deployed on brownfields, or, when smaller powers are at stake, to transportable technologies, as it is the case for a few Micro Modular Reactors (<10 MW_{el}) under development. In particular, floating reactors could be an attractive solution for coastal areas. In this particular case, however, solutions need to be developed to convey steam at high temperature and pressure (well over 400°C and 50 bar) out of the barge into a pipeline, a challenging condition due to the barge movement.

Another key takeaway is the need to conduct reciprocal hazard assessments for co-locating SMRs with potentially hazardous facilities. Such an assessment needs to be conducted early as part of the pre-feasibility stage.

IV. ECONOMIC ASSESSMENT

For a repowering project to be successful, the SMR designs proposed need to sell the energy at a competitive cost when compared to alternative technologies.

The economic assessment that Tractebel performs is based on the GIF guidance [4], where the Levelized Unit of Energy Cost (LUEC), aka Levelized Cost Of Energy, is regarded as the reference metrics to rank competitiveness. The application of LUEC is originally meant for electricity, but generally accepted to be extended to heat, or any other energy products. However, methodology issues arise in cases of joint-product generation and whenever the business model adopted does not involve a single owner-operator and a single end user.

Moreover, the estimation of LUEC is affected by large uncertainties originating from component costs heavily depending on external factors.

A. Key takeaways

Industrials generally wish to avoid the **risk to invest** in an activity that is clearly disconnected from their core business, as owning a nuclear asset. The general trend is to become an energy off-taker through a Power Purchase Agreement (PPA). Conventional assets can offer very short duration PPAs when compared to the nuclear installations, as required by their much longer lifetime, up to 60 years by design, and higher capital costs. Moreover, the difficulty to match the power requirements can lead to larger projects, as "energy hubs", where joint PPAs with several end-users are signed.

The situation complexifies further when a **joint production** of two or more products is planned. A generic fair cost repartition among the prices of the sold products has not yet been defined as it is generally assumed that electricity is the main product and the price of the side products is equivalent to the lost opportunity of unsold electricity. A fair attribution will have to take into account the proportions of core thermal power destined to the different products, weighted by the ownership shares in a Mankala-like model.

The reluctance of industrials to invest in SMR projects holds these same projects back. Some innovation in the offered ownership models is required from the vendors to entice industrials into investing.

The major causes for uncertainties in the LUEC are the unknowns of the Weighted Average Cost of Capital (**WACC**) and the **timeline** of the projects. The WACC, expressed in percentage, is the yearly average cost ratio of the capital expenditures. It varies greatly with the risk of a project and is commonly calculated with the following formula:

$$\mathrm{WACC} = f_{eq} R_{eq} + f_{deb} R_{deb} (1 - T_c)$$

Where f_{eq} and f_{deb} are, respectively, the fraction of equity and the fraction of debt that constitute the project capital, and R_{eq} and R_{deb} are, respectively, their rate of return. The last term of the equation is to take into account that businesses are able to deduct interest expenses from their taxes, T_c being the corporate tax rate.

Due to these uncertainties, the vendors are providing only Overnight Construction Costs (OCC) as capital expenditures, which are the equivalent of the amount that would be paid if the construction occurred overnight. The actual Total Capital Investment Cost (TCIC) has to include also price escalation and Interests During Construction (IDC). A simple change of construction starting date can impact the OCC, due to unexpected cost escalations of raw material and, on a lesser extent, inflation. Increases in OCC are generally accompanied by construction delays, which consequently make IDC increase, and eventually reduce in a sensitive fashion the profitability of the project [5].

On a positive note, SMR projects will decrease the impact of IDC on TCIC with respect to large nuclear projects with longer construction times and higher OCCs.

Finally, the cost competitiveness depends also on the market cost of **competing sources**, affected by policies, subsidies, associated carbon tax, etc.

V. CONCLUSION

SMR technologies are opening new possibilities for applications of nuclear energy beyond electricity generation, leading to big expectations from energy intensive users to have a solution to the current energy crisis. Even before delivering on the promises via concrete projects, demystifying a SMR plant delivery plan for a potential energy off-taker is a first step. At the same time, to foster the deployment projects of these technologies it is highly encouraged that end-users jointly invest in project companies.

SMRs are generally suitable for industry repowering, while enabling high reliability and service continuity. Although pure retrofitting may not always be possible, there is enough flexibility in the design of the balance of plant to respond to requirements. Moreover, we predict that the demand in electricity will increase, driven by the increase in hydrogen demand, wherever nuclear heat cannot cover the demand. Localized synthetic fuel production will not require redesigning endeavours at the plant interface, but well an additional cost for the electrolyser and the synfuel production facility. When the demand for steam is dominant at the end-users' side, nuclear technologies are only rivalled by biomass technologies. However, the low offer of SMR designs between 50 and 150 MW_{th} may exclude the interest of some end-users. Heat-only uses of SMRs would benefit from the parallel development of technologies enabling higher output temperatures, either via higher core output temperatures or augmented heat technologies, such as chemical heat pumps [6],

In terms of cost competitiveness, as the uncertainties are various and depending on external factors, some are left out from vendor's estimations. An international standard could be developed to guide the vendors in providing TCIC instead of OCC, as the capital cost remains the major contributor to the Levelized Unit of Energy Cost.

VI. References

[1] Global Energy Monitor, Global Coal Plant Tracker and Global Gas Plant Tracker Summary tables, https://globalenergymonitor.org/projects/, last consulted on 30 January 2023

[2] International Energy Agency, Europe data explorer, https://www.iea.org/regions/europe, last consulted on 20 January 2023

[3] International Atomic Energy Agency, "Advances in Small Modular Reactor Technology Developments", A Supplement to: IAEA Advanced Reactors Information System (ARIS), 2022 Edition

[4] GenIV International Forum, "Cost Estimating Guidelines For Generation IV Nuclear Energy Systems", Revision 4.2, prepared by the Economic Modeling Working Group of the Generation IV International Forum, September 26, 2007, GIF/EMWG/2007/004.

[5] Electric Power Research Institute, Inc, "Advanced Nuclear Technology: Economic-Based Research and Development Roadmap for Nuclear Power Plant Construction", Technical Report, June 2019, 3002015935

[6] American Nuclear Society, Nuclear Newswire, "Can chemical heat pumps for integrated energy systems and industrial applications change the world?", Vivek Utgikar, Piyush Sabharwall, and Brian Fronk, Fri, Aug 28, 2020, 10:27PM

Hot Topic 2
Neutrons for Progress

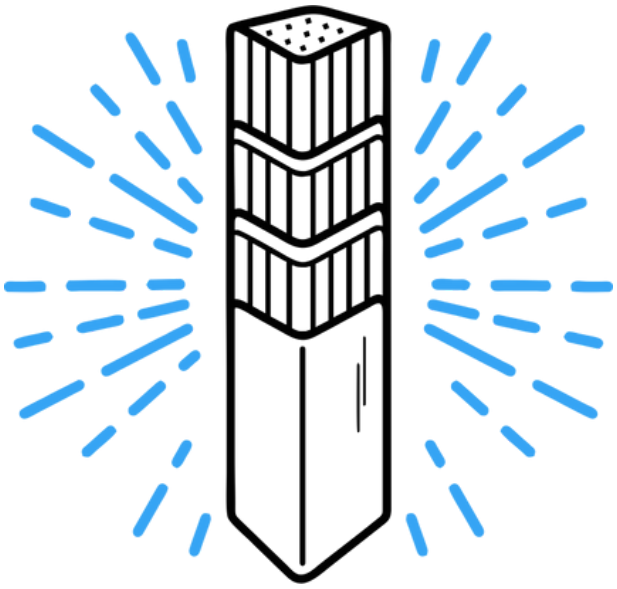

Proceedings of the European Nuclear Young Generation Forum
ENYGF'23
May 8-12, 2023, Kraków, Poland

Overview of Experiments at the Advanced Test Reactor

Horkley, Matthew[1*]: Hill, Jordan[1] and Skeen, Trevor[1]

[1] Idaho National Laboratory (INL), United States of America

* *matthew.horkley@inl.gov*

I. INTRODUCTION

The Advanced Test Reactor (ATR) is owned and operated under the U.S. Department of Energy (DOE) at the Idaho National Laboratory (INL). ATR has very robust irradiation capabilities and a high power-density that yields thermal and fast neutron fluxes up to $1x10^{15}$ n/(cm^2s) and $5x10^{14}$ n/(cm^2s), respectively[1]. With over 70 in-core experiment positions and a unique core design, ATR has a large capacity for experiments and the ability to irradiate many types of experiments. The most common experiment specimen types are placed in the following 3 categories: Fuel testing and qualification, materials irradiation testing, and isotope production.

Some of the most notable fuel testing and qualification experiments are United States High-Performance Research Reactor (USHPRR) experiments, Accident Tolerant Fuel (ATF) experiments, and Advanced Fuels Campaign (AFC) experiments. USHPRR experiments are designed to support the goal of converting several US reactors from high-enriched uranium (HEU) to low-enriched uranium (LEU). The goal of ATF experiments is to develop novel fuel and cladding types for light-water reactors that are safer under reactor accident conditions, which would include characteristics such as more resilience to melting and preclusion of hydrogen buildup. AFC experiments are supporting development of fast reactor programs that would ultimately help close the nuclear fuel cycle and eliminate transuranic waste.

The purpose of most materials testing experiments is to evaluate changes in material properties from neutron irradiation. Specific characteristics, such as reference transition temperatures, can be utilized to support qualification of new reactor vessels or other reactor core components. More commonly, materials are tested for scoping studies. Some examples of recently tested materials are high-entropy alloys and 3D printed alloys.

ATR is continuing to produce isotopes for multiple programs. High specific activity (HSA) cobalt is produced for a variety of uses, including stereotactic radiosurgery, scientific gamma irradiators, and other commercial applications. Pu-238 is produced for radioisotope thermoelectric generators (RTGs) for future National Aeronautics and Space Administration (NASA) missions such as the Dragonfly mission to Saturn's moon Titan.

II. FUEL AND TESTING

Many types of nuclear fuel are tested at ATR for a wide variety of test sponsors. Fuels are typically developed and tested under partnerships between DOE and other programs. Some of these programs include the ATF program, the AFC program, the USHPRR program, the Advance Gas Reactor (AGR) program, and the U.S. Naval Nuclear Propulsion Program (NNPP).

A. USHPRR Tests

USHPRR tests are being irradiated at ATR to support the goal of converting U.S. test and research reactors from HEU to low enriched U-Mo in support of non-proliferation efforts. USHPRR tests follow a tiered approach in support of generic and specific fuel qualification. Initially, mini-plate experiments are performed to down-select potential fuel designs, then full size plates and reactor-specific demonstration element experiments are performed. Currently, mini-plate experiments (Figure 1) are underway at ATR, and full-size plate experiments are to follow. A mini-plate experiment is a plate with dimensions of approximately 10cm x 2.5cm x 0.13cm. Four to eight of these plates are placed in a specimen holder and then configured in experiment holders to form a test assembly, which is irradiated in the 1.2m tall active core region of ATR. Post-irradiation examination (PIE) is performed on these plates after the desired fluence has been reached. If the PIE results provide data that indicate that plates perform within specified design criteria, the design will then be scaled up to perform tests on full sized fuel plates and, ultimately, full fuel assemblies. The first full sized LEU fuel assembly will be for the University of Missouri Research Reactor (MURR), which will support generic U.S. Nuclear Regulatory Commission (NRC) U-Mo fuel qualification and licensing for MURR. Irradiation is estimated to begin for this final qualification test in 2026, and other full size fuel assemblies will follow to allow for full LEU conversion of several U.S. reactors.

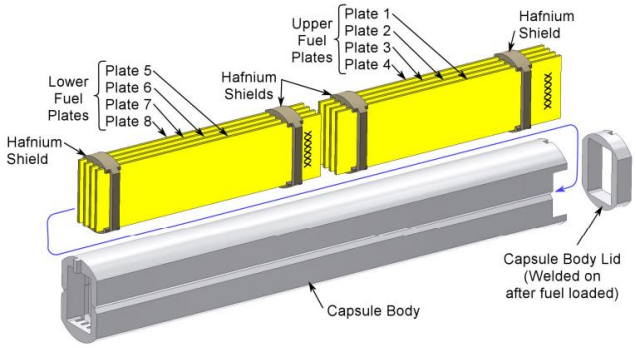

Figure 1. Mini-plate experiment assembly.

B. ATF Tests

The primary goal of ATF experiments is to develop novel fuel and cladding types for light-water reactors that are safer under reactor accident conditions, which would include characteristics such as more resilience to melting and preclusion of hydrogen buildup. Other goals of ATF experiments include increased enrichment, higher burnup and longer fuel life, improved corrosion resistance, and higher temperature resistance. These fuels are being developed primarily by Framatome, General Electric, and Westinghouse.

Uranium silicide, uranium oxide/chromium oxide mixtures, and traditional uranium oxide fuel are among the fuel types being tested. Uranium silicide is denser and can thus provide higher fuel loading and the potential for longer life, and uranium oxide/chromium oxide mixtures are expected to perform better at high temperatures. Most cladding types being tested are either silicon carbide or are composed of zirconium alloy that is coated with materials that help reduce hydrogen production, such as chromium[2].

ATF tests are being irradiated in small I-positions and in the center pressurized water loop (PWL) in ATR. Small I-positions are directly cooled by ATR primary coolant at ~140°F (60°C). PWLs are capable of controlling pressure, temperature, and chemistry to simulate conditions of a commercial pressurized water reactor (PWR). Test sponsors are able to use data from these tests to support licensing fuels through the NRC, and some fuel assemblies are being irradiated already in commercial reactors in support of fuel qualification. Licensing for full-core use of some ATF fuel assemblies is expected by 2026.

C. AFC Tests

The AFC program encompasses a wide variety of nuclear fuel and material testing, including ATF, advanced reactor (AR) concepts, and many others. At ATR, "AFC" is the experiment designator used solely for AR fuel tests. These tests are primarily designed to investigate fuels for sodium fast reactors (SFRs). Since ATR is a thermal light water reactor (LWR), AFC tests are usually placed in cadmium baskets during irradiation to filter thermal neutrons, which results in a more favorable neutron spectrum that is semi-representative of an SFR neutron spectrum.

Metallic fuels are being tested at "normal" to "high" burnup levels to test the viability of different fuel alloys and cladding types. HT9 and high-entropy alloys are among the cladding types being tested. Retention and migration of fission products and material embrittlement are some of the attributes that are examined in these tests after irradiation.

More recently, the Fission Accelerated Steady-State Test (FAST) approach has been adopted for some AFC tests. With these AFC-FAST tests, power density of fuel pins is increased by scaling the fuel pin down while maintaining the same linear heat generation rates. This has resulted in irradiation rates being accelerated by as much as six times. This will ultimately assist in more rapid development of AR fuels and support more rapid fuel qualification[2].

III. MATERIAL TESTING

Materials tests are routinely irradiated in ATR. In general, these tests are performed with the goal of determining changes in material properties as a result of irradiation. Neutron embrittlement, corrosion rates, and other material changes are determined during PIE. The obtained data are typically used for R&D but are also used for other purposes, such as qualifying new materials for use in commercial reactors.

A. NuScale Test

Qualification of new reactor vessel materials for small modular reactors (SMRs) is the purpose of the NuScale test, which is scheduled to begin irradiation in 2023. Tested materials will include SA-508 carbon steel and F6NM martensitic stainless steel. This test will have over 200 Charpy v-notch and tensile specimens that are cut from large weldments that simulate the most limiting reactor vessel welds. Standard material specimens, weld-region specimens, and heat-affected zone specimens will be irradiated to target fluence levels. Specimens will then be shipped for PIE. The results of this experiment will be used to determine changes in tensile properties and reference transition temperatures that will be used to support qualification of the new vessel materials through the NRC. The test is expected to be complete in mid-2024.

B. HDG-1 Test

Material tests are being performed for advanced graphite reactor programs. The high-dose graphite (HDG) experiment is being performed to evaluate graphite creep resulting from high fluence and high temperatures. The test is constructed with a hydraulic ram that maintains pressure on specimens. As shown in Figure 2, load cell and position indicators are also integrated in this system to monitor load and creep in real-time. The test is helium-cooled to maintain target temperatures of 600°C.

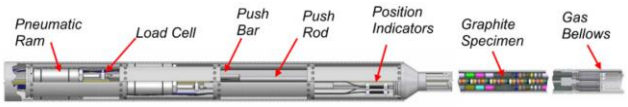

Figure 2. HDG-1 experiment assembly.

IV. ISOTOPE PRODUCTION

There are currently two isotopes being actively produced at ATR. Pu-238 is produced for use in RTGs to power spacecraft, and Co-60 is produced for uses such as stereotactic radiosurgery (aka gamma knife), scientific

gamma irradiators, and other commercial applications such as sanitization and non-destructive examinations.

RTGs are used by NASA as a power source for various space applications, such as the Mars Rover. The RTGs utilize heat created by alpha decay of Pu-238 coupled with an array of thermocouples to produce electrical power. These "space batteries" are capable of lasting for decades. An example of this longevity is shown with the Voyager space missions that were launched in 1977. The RTGs on both probes still have adequate power for continued communications and functionality after over 45 years of operation[3]. However, due to decay of Pu-238 and degradation of thermocouples, the RTGs currently have approximately 50% of their original capacity.

NASA is planning future missions, and the current Pu-238 supply is inadequate to support mission needs. To fulfill these needs, Pu-238 is being produced at ATR and the High-Flux Isotope Reactor (HFIR). Pu-238 is produced in these reactors by neutron irradiation of neptunium targets, and final assembly of the RTGs takes place at the INL.

Co-60 is produced in the form of very small pellets that measure 1 mm in diameter by 1 mm in length. These pellets are loaded and irradiated in capsules that measure 40.5 cm in length with a total of 6,120 pellets in each capsule (Figure 3). Capsules are irradiated for several operating cycles until specific activities of 200-400 Ci/g are reached. Once this activity is reached, the Co-60 is shipped from the ATR to a customer selected by the Department of Energy.

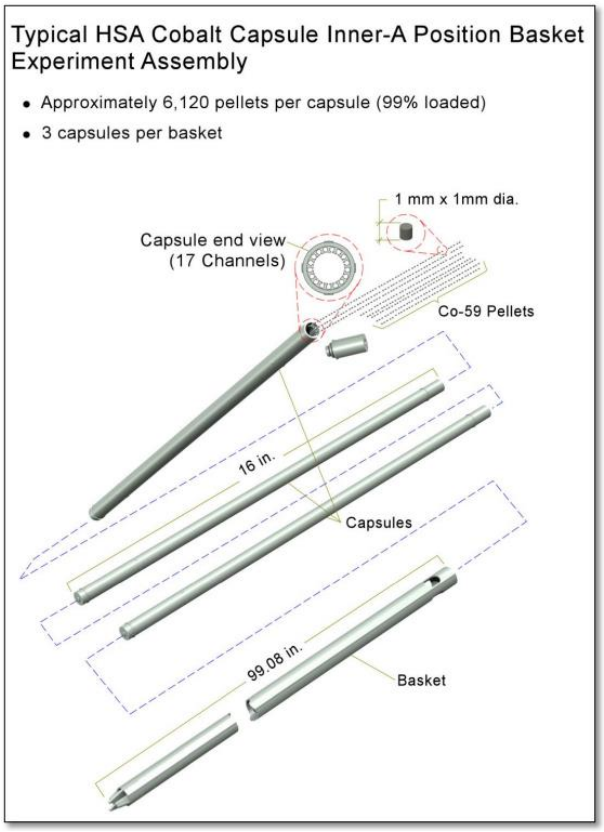

Figure 3. Typical cobalt capsule assembly.

V. CONCLUSION

In summary, ATR is continuing to provide unique irradiation capabilities that support nuclear fuel development and qualification, materials testing, and isotope production. New fuel developments will contribute to safer operation of nuclear plants and to non-proliferation efforts. Materials testing will assist in development of new cladding types, development of reactor component materials, and qualification of reactor components. ATR's isotope production capabilities contribute to space mission needs, radiopharmaceutical needs, and other commercial isotope needs. ATR, along with other test and research reactors around the world, will continue to perform a crucial role in the advancement of nuclear technology in order to help secure a safe, efficient, and reliable future for nuclear energy.

VI. References

[1] *Advanced Test Reactor User Guide*, Revision 24, Idaho Nat. Lab., Idaho Falls, ID, USA, 2021.

[2] P. King, et al, "Advanced Fuels Campaign 2021 accomplishments," *U.S. Department of Energy Office of Scientific and Technical Information*, November 2021, Available: U.S. DOE, https://www.osti.gov/biblio/1844229 [Accessed: January 26, 2023].

[3] National Aeronautics and Space Administration, "Voyager: Mission Status," *voyager.jpl.nasa.gov*, Available: https://voyager.jpl.nasa.gov/mission/status/ , [Accessed: January 28, 2023].

Proceedings of the European Nuclear Young Generation Forum
ENYGF '23
May 8-12, 2023, Kraków, Poland

Overview of the Advanced Test Reactor Irradiation Capabilities

Hill, Jordan[1*]: Horkley, Matthew[1] and Skeen, Trevor[1]

[1] Idaho National Laboratory (INL), United States of America (USA)

**jordan.hill@inl.gov*

I. INTRODUCTION

The Advanced Test Reactor (ATR), at Idaho National Laboratory (INL), is one of the most versatile operating research reactors in the world. The ATR has a long history of supporting reactor fuels and materials research for the United States (US) Department of Energy (DOE) Offices of Nuclear Energy, Science, and National Nuclear Security Administration; US Naval Nuclear Propulsion Program; National Aeronautics and Space Administration (NASA); universities; industry; and international customers.

The configuration of the ATR, a four-leaf clover shape, allows the reactor to be operated at different power levels in the corner lobes allowing for different testing conditions for multiple simultaneous experiments. This, combined with the typical operating power of greater than 100 MW (maximum power of 250 MW), provides unique testing opportunities.

There are three types of experiment configurations utilized in the ATR – the capsule, the instrumented lead, and the pressurized water loop (PWL) experiments.

- The simplest experiment is a capsule experiment. The fuel or material to be irradiated is typically encapsulated and placed in a holder that sits in a chosen experiment position in the ATR.
- The next level in complexity is an instrumented lead experiment, which provides active monitoring and control of experiment parameters during the irradiation period. Instrumented lead experiments contain a tube that runs from the experiment, in the reactor core region, up through a penetration in the reactor vessel and houses instrumentation connections that lead to a monitoring/control station.
- The PWL experiment is the most complex and comprehensive type of testing performed in the ATR. The experiment is isolated from the ATR primary coolant system via an inpile tube (IPT) with its own parameter monitoring/control (flow, temperature, pressure, and chemistry).

II. OVERVIEW OF ATR

The ATR design exploits a unique core configuration that offers a large number of experiment positions, including large experiment volumes in high-flux areas. Designed to permit simulation of long neutron radiation exposures in a short period of time, the maximum thermal power rating is 250 MW(Th) with a maximum unperturbed thermal neutron flux of 1.0 x 10^{15} n/cm^2-s (Figure 1). Since most contemporary experimental objectives generally do not require the limits of its operational capabilities, the ATR typically operates at much lower power levels. Occasionally, some loops of the reactor are operated at higher powers that generate higher neutron flux. The primary operating characteristics are listed in Table 1.

Table 1. ATR General Characteristics

Reactor	
Maximum thermal power	250 MW(Th)[a]
Maximum power density	1.0 MW/L
Maximum thermal neutron flux	1.0 x 10^{15} n/cm^2-s[b]
Maximum fast flux	5.0 x 10^{14} n/cm^2-s[b]
Number of flux traps	9
Number of experiment positions	77[c]
Core	
Number of fuel assemblies	40
Active length of assemblies	1.2 m (4 ft)
Number of fuel plates per assembly	19
Reactor Coolant	
Operating pressure	2.5 MPa (360 psig)
Design temperature	115°C (240°F).
Reactor coolant	Light water
Light water maximum coolant flow	3.09 m^3/s (49,000 gpm)
Coolant temperature (operating)	<52°C (125°F) inlet <71°C (160°F) outlet

a. Maximum design power. ATR typically operates near 110 MW(Th) level.
b. Parameters are based on the full 250 MW(Th) power level and will be proportionally reduced for lower reactor power levels.
c. Only 71 of the 77 are potentially available for experiments.

The ATR is cooled by pressurized (2.5 MPa [360 psig]) water that enters the reactor vessel bottom at an average temperature of 52°C (125°F), flows up outside cylindrical tanks that support and contain the core, passes through concentric thermal shields into the open upper part of the vessel, then flows down through the core to a flow distribution tank below the core. When the reactor is operating at full power, the primary coolant exits the vessel at a temperature of 71°C (160°F).

The unique design of ATR control devices permits large power variations among its nine flux traps using a combination of control cylinders (drums) and neck shim rods (Figure 2). The beryllium control cylinders contain hafnium plates that can be rotated toward and away from the core, and hafnium shim rods, which withdraw vertically, can be individually inserted or withdrawn for minor power adjustments. Within bounds, the power levels in each corner lobe of the reactor can be controlled independently to allow for different power and flux levels in the four corner lobes during the same operating cycle.

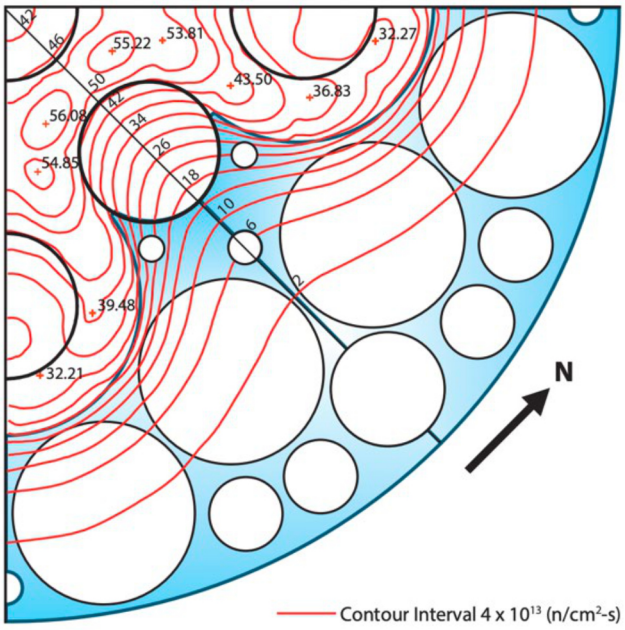

Figure 1. Unpertubed thermal neutron flux intensity distribution at the midplane in the east quadrant of the ATR for reactor power of 220 MW(Th).

III. EXPERIMENT POSITION OVERVIEW

The curved fuel arrangement of the ATR places reactor fuel closer on all sides of the flux trap positions than is possible in a rectangular grid. The ATR has nine of these high-intensity neutron flux traps and 68 additional irradiation positions inside the reactor core reflector tank, for a total of 77, each of which can contain multiple experiments.

The physical dimensions of the available experiment positions in the ATR range in size from 1.27 cm (0.5 in) in diameter to 12.7 cm (5.00 in) in diameter. The follow positions are available:

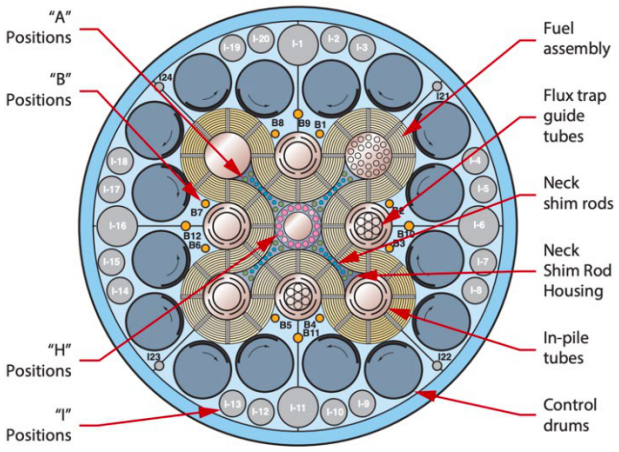

Figure 2. ATR flux traps and other irradiation positions in or near the core

- A Positions are in the cruciform-shaped neck shim housing; the inner eight positions (A-1 to A-8) have, in the past, been used mainly for long-term irradiations due to limited accessibility. However, a recent modification has made for better accessibility.
- B Positions are in the beryllium reflector surrounding the core, near the rotating control cylinders. The smaller B Positions are located close to the fuel elements and have considerably higher neutron flux than the large B Positions. The Hydraulic Shuttle Irradiation System has been used in space B-7 in the past and may be re-installed at a future date if a need is identified.
- I Positions are in the periphery of the beryllium reflector, outside the rotating control cylinders, thus the flux is lower than the other ATR positions, but these positions are larger than most others in the ATR.
- H Positions are in the center flux trap assembly. Positions H-3 and H-11 are used for N-16 monitors and are not available for irradiations. The other 14 H Positions extend 15 cm (6.0 in) below the active core for a total length of 272 cm (107 in), with 1.2 meters (47.2 inches). of active core.

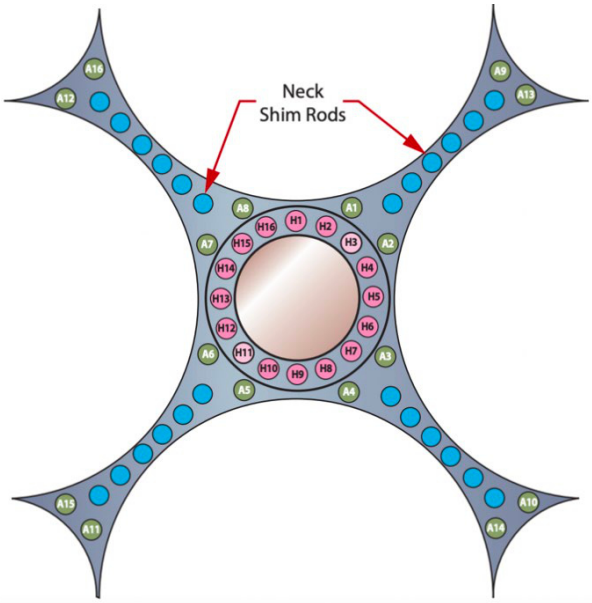

Figure 3. Detailed view of A positions (green) and H positions (pink) in ATR's neck shim housing and the center flux trap.

IV. CAPSULE EXPERIMENTS

Capsule experiments (Figure 4) are self-contained sealed encapsulations surrounding the irradiation specimens with an inert gas environment. Occasionally, experiment specimens are not encapsulated but are instead cooled directly by the primary coolant, which allows for lower specimen temperatures.

Capsule experiments typically include passive instrumentation such as flux wires for neutron fluence monitoring and/or melt wires for temperature monitoring during irradiation. In addition, the temperature of a capsule may also be controlled, within limits, by incorporating a small insulating gas jacket (filled with an inert gas) between the specimens and the outside capsule wall or pressure boundary. A suitable gas jacket width can usually be selected to provide the irradiation temperature desired by the experiment customer. The selected insulating gas and the heating rates of the capsule assembly are used to determine proper width of the gas jacket.

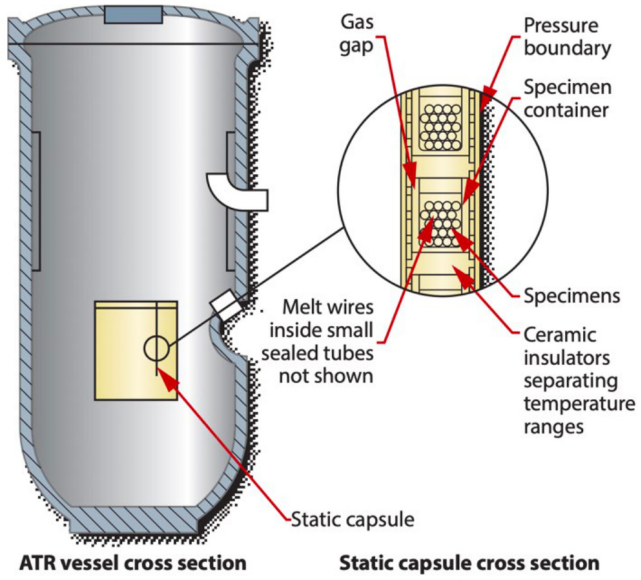

Figure 4. Capsule experiments are often stacked in aluminum baskets with the reactor core region shown in yellow on the left.

The capsules may vary in length from several centimeters to full core height of 1.2 meters (47.2 inches). They also may vary in diameter from 12 mm (0.47 inches) or possibly less for the small irradiation positions (or a portion of an irradiation position). The capsules are typically constructed of aluminum or stainless steel, but zircoloy has also been utilized. Depending on the contents and pressure of the capsule, a secondary containment may be included to meet the ATR safety requirements. The capsules are usually contained in an irradiation basket, which radially locates the capsules in the ATR experiment position. Occasionally, due to space limitations, a capsule has been used to also serve the function of the basket. In these cases, the capsules must fill the entire irradiation height and width and have a similar handling feature at the top of the capsule for installation and removal from the core.

The benefits of utilizing capsules for irritation testing include ease of removal/installation and ease of reconfiguration, which allows experiment sponsors to meet target fluence levels by selecting the most appropriate cycle, position, and experiment configuration. This configurability can also be utilized to relocate fueled capsule experiments to a higher power location to compensate for fuel burn-up. This type of testing is also less expensive than the other types of irradiation testing, and due to its simplicity, it requires the least amount of time to get specimens into the reactor. However, capsule testing has less flexibility and control of operating parameters (such as specimen temperature) during the irradiation and greater reliance is made on the design analyses since passive instrumentation can only provide snapshot values of the operating parameters during irradiation (e.g., melt wires can provide the maximum temperature attained during an irradiation but not the amount of time or when the maximum temperature was achieved).

V. INSTRUMENTED LEAD EXPERIMENTS

The next level of complexity in testing incorporates active instrumentation for continuous monitoring and control of certain experiment parameters during irradiation. These actively monitored and controlled experiments are commonly referred to as instrumented lead experiments, deriving their name from the active instrument leads (such as thermocouples or pressure taps) that they utilize.

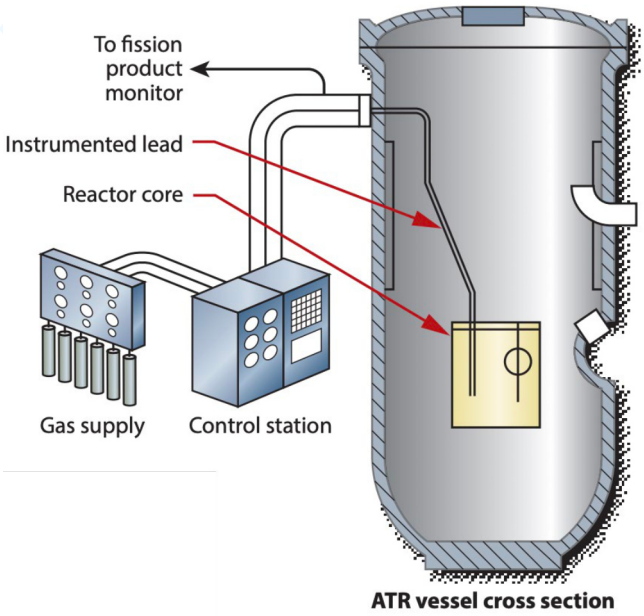

Figure 5. Illustration of an instrumented lead experiment.

An instrumented lead experiment containment is very similar to a capsule experiment, with the major difference being a tube connecting the experiment to a control system outside the reactor vessel (Figure 5). The tube is used to house the instrument leads (thermocouples, pressure taps, etc.) and temperature control gas lines from the irradiation position within the reactor core to the reactor vessel wall or top. The instrument leads and gas lines are then routed outside the reactor vessel to the control and data collection/monitoring equipment. An instrumented lead experiment may contain several vertically stacked capsules,

and specifically designed to meet the experimenter's needs. This is accomplished by selecting a suitable irradiation position, which will provide the necessary gamma and/or fission heating as well as the total neutron fluence within the available schedule, and then designing the tube routing necessary to connect the experiment to the reactor vessel.

The most common parameter to be monitored and controlled in an instrumented lead experiment during irradiation is the specimen temperature. The temperature of each experiment capsule is independently controlled by varying the thermal conductivity of a gas mixture in a very small insulating gas jacket between the specimens and the experiment containment. This is accomplished by blending a conductor gas with an insulator gas. Helium is used as the conductor gas and neon is typically used as the insulator gas. However, argon has also been used as an insulator gas (with helium as the conductor) when a larger temperature control band is needed, and the activity from the by-product Ar-41 does not affect the experiment data collection (i.e., monitoring of the experiment temperature control exhaust gas for fission gases, etc.). During normal operation, the gases are blended automatically to control the specimen capsule temperature based upon feedback form the thermocouples. The instrument leads allow for a real time display of the experiment parameters on an operator control panel. For any monitored experiment parameter, a data acquisition and archive capability can be provided.

VI. PRESSURIZED WATER LOOP EXPERIMENTS

Six of the ATR flux traps contain IPTs, which are connected to PWLs. The other three flux trap positions currently contain capsule irradiation facilities. An IPT is the reactor in-vessel component of a PWL, and it provides a barrier between the reactor coolant system water and the PWL coolant (Figure 6). Although the experiment is isolated from the reactor coolant system by the IPT, the experiment specimens within the IPT are still subjected to the high intensity neutron and gamma flux environment of the reactor. The IPT extends completely through the reactor vessel with closure plugs and seals at the reactor's top and bottom heads. This allows the top seals to be opened and each experiment to be independently inserted or removed. The experiments are suspended from the top closure plugs using a hanger rod. The hanger rod vertically positions the experiment within the reactor core and provides a pathway for test instrumentation. Anything from scaled-down reactor fuel rod bundles to core structural materials can be irradiated in these PWLs.

The great advantage of loop experiments is the ease with which a variety of samples can be subjected to conditions specified to any pressurized water reactor (PWR) design. Many samples can be tested at once with variation in the samples, thickness of cladding, etc., and the samples can be compared afterward for optimum design. Each IPT is connected to a separate PWL, which allows fuel or material testing at different pressures, temperatures, flow rates, water chemistry, and neutron flux (dependent of the location within the ATR core) with only one reactor.

Figure 6 is the cross section of a typical PWL experiment design. Three concentric tubes form the piping assembly for each water loop in the ATR. The assembly penetrates the reactor vessel's bottom closure plate and has an inlet and an outlet below the vessel. Coolant comes up through the flow tube, passes the experiment specimen, is redirected downward near the top of the IPT, and flows down between the flow tube and pressure tube.

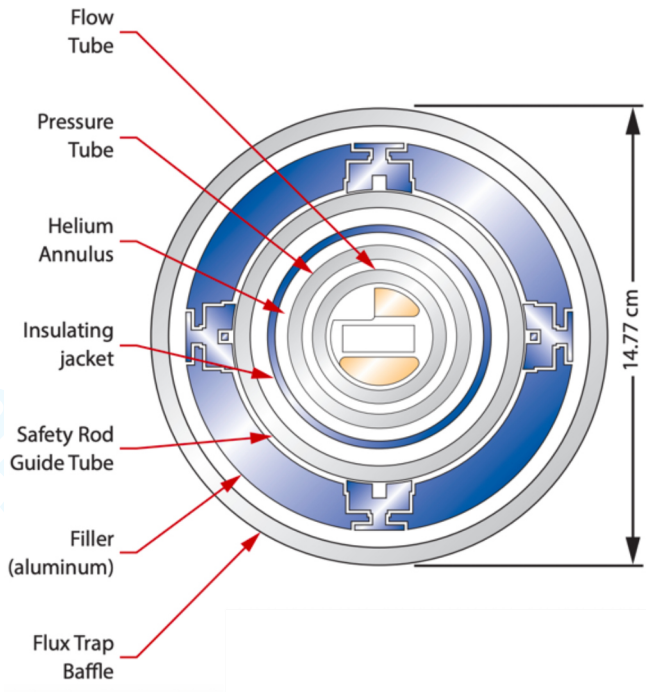

Figure 6. Cross section of the in-core position of a typical pressurized water loop experiment.

Helium flows through the annulus enclosed by the outermost tube, which also serves as the insulating jacket. Insulation is essential because the inside of the pressure tube is in contact with the loop coolant at temperatures much greater than primary coolant temperatures. The helium is monitored for moisture to detect any leaks in the tubes.

Loop out-of-pile equipment occupy the space around the reactor in two basements of the reactor buildings. The PWL equipment includes piping within the reactor vessel and pumps, heat exchangers, a pressurizer, and demineralizers within a shielded cubicle (Figure 7). The line heaters are capable of raising the loop coolant to desired operating temperatures in only a few hours. Normally, these heaters are used to capacity only when preparing the loop for startup. After reactor startup, fission and gamma heating of the samples provides much of the required heat.

The loops are connected to a computer control system. This system controls, monitors, and provides emergency functions and alarms for each loop.

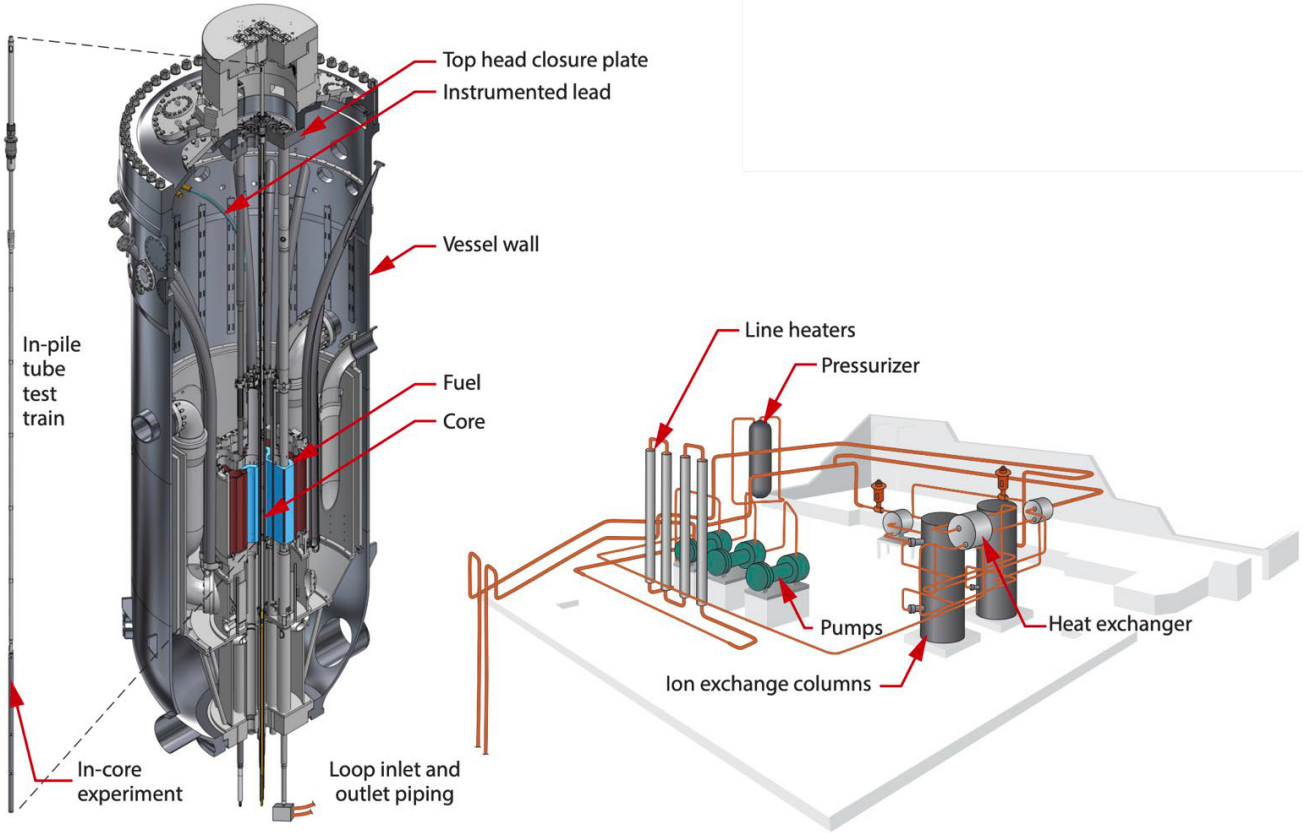

Figure 7. Pressurized water loop experiments provide environmental simulations for different reactor conditions

VII. I-LOOPS[3]

The permanent shutdown of the 60-year-old Halden Boiling Water Reactor (HBWR), put nuclear fuels testing in the US and Europe in a scramble. The US Accident Tolerant Fuels (ATF) Program was perhaps hardest hit by the shutdown of HBWR, prompting DOE research leaders and regulators to brainstorm a path forward. Though no single test reactor will be capable of replacing HBWR in all its functions, the DOE concluded that there was a need to increase capacity for steady-state and operational transient testing capabilities for fuels within its complex. The priorities were to expand water loop capacity in ATR by installing at least two I-Loops and continue use of the in-pile loss-of-coolant accident loop in Transient Reactor Test (TREAT) Facility.

Current irradiations for ATF concepts, provided by industry partners Framatome, General Electric, and Westinghouse, are happening in the center PWL and small I Positions (cooled directly from reactor primary coolant) of the ATR. Expanding water loop capacity into the underutilized I Positions in ATR's reflector (similar flux to HBWR's central core) is expected to provide BWR and PWR coolant conditions, ramping testing with instrumented specimens, and fuel failures testing.

VIII. CONCLUSION

The ATR has a long history in fuels and materials irradiations and will be fulfilling a critical role in future fuels and materials testing necessary to develop the next generation reactor systems and advanced fuel cycles. The capabilities and experiences at the ATR, as well as the other test reactors throughout the world, will be vitally important for the development of these new systems to provide the world with clean safe energy supplies.

IX. REFERENCES

[1] J. Campbell, "ATR User Guide," *U.S. Department of Energy Office of Scientific and Technical Information*, October 2012, Available: U.S. DOE, ww.osti.gov/biblio/1826354 [Accessed: January 4, 2023].

[2] F. Marshall, et al, "Advanced Test Reactor National Scientific User Facility Progress," *U.S. Department of Energy Office of Scientific and Technical Information*, October 2012, Available: U.S. DOE, www.osti.gov/biblio/1060978 [Accessed: January 4, 2023].

[3] M. DeHart, "Capabilities of the Halden Reactor and ATR Modifications to Partially Support Halden's Former Capabilities," *U.S. Department of Energy Office of Scientific and Technical Information*, September 2021, Available: U.S. DOE, www.osti.gov/biblio/1889855 [Accessed: January 4, 2023].

Proceedings of the European Nuclear Young Generation Forum
ENYGF'23
May 8-12, 2023, Kraków, Poland

Manufacturing of CoCrFeNi high-entropy alloy for potential nuclear application

Olejarz, Artur [1*], Huo, Wenyi [1], Zieliński, Maciej [1], Kalita, Damian [1], Wyszkowska, Edyta [1] and Kurpaska, Łukasz [1]

[1] NOMATEN Centre of Excellence; National Centre for Nuclear Research, A. Sołtana 7; 05-400 Otwock – Świerk

*Corresponding author: *artur.olejarz@ncbj.gov.pl*

I. Introduction

Nowadays, the most commonly used materials in nuclear reactors are different types of steel. They are a reference point for designing new, modern materials planned for the next generation reactors, e.g., High-Temperature Reactor (HTR) or Liquid Lead Fast Reactor (LFR). Pressure pipes for circulating coolant or containment vessels are mainly made of 304L or 316L austenitic stainless steel [1]. The main advantages of stainless steel are high corrosion resistance, excellent impact resistance, availability, and ease of fabrication. Although using steel is the most common in all nuclear-related applications, higher requirements force us to ask whether using steel in more harmful and demanding conditions and environment is still safe and can be done over prolonged operation time of the installation [2,3].

The main requirements for materials used in nuclear applications (such as fuel cladding elements) are higher shock resistance, elevated impact toughness, increased operating temperature, and lower mutual reactivity between the material and the fuel [2]. Recent studies suggest that the material evaluation will mainly focus on developing the Zircalloys coatings, which shall impede surface oxidation. Chromium coatings are regarded as an interesting point to start. For other applications, completely new alloys or metal-matrix composites are needed. One of the recent stars in the scientific community are medium and high entropy alloys (MEA and HEA) [2].

Traditionally, the materials design approach is based on adding alloying elements to the main material, which improves some properties. For example, ~10 % of Cr addition to ferritic steels enhances the material's corrosion resistance. This approach was shaken in 2004 when the concept of equiatomic five elements alloy was proposed for the first time. The synthesis of the CoCrMnFeNi revealed a solely single FCC phase, where each atom was embedded in a random place in a structure without segregation or intermetallic forming. Already at that time, there was a strong suggestion that the high configurational entropy restrains the atoms from segregation and is responsible for this effect [4,5]. This group of materials is named as high (>4 elements) and medium (2-4 elements) entropy alloys. The definition of high entropy alloys evolved. Now, non-equiatomic compositions, in situ carbides and oxides reinforced matrix, or even dual structures alloys are classified as high (or medium) entropy alloys [6]. Over time the studies of more complex compositions defined four basic effects describing this group of alloys: high entropy effect, sluggish diffusion effect, lattice distortion effect, and cocktail effect [4–6].

After designing the appropriate chemical composition of the material, choosing the manufacturing process is also extremely important. An arc melting technique attracts the most attention among many manufacturing methods for producing high entropy alloys [7]. This technique guarantees the excellent quality of manufactured samples. However, the most significant disadvantage of this method is a low perspective of applicability in the industry. As alternatives, powder metallurgy techniques [8] and 3D printing [9] are worth regarding. Thin layers in the form of coatings [7] or producing weld joints [10] from high entropy alloys are also becoming more common.

Starting from 2004, many chemical compositions were evaluated, revealing elevated mechanical properties and corrosion resistance [11]. The radiation resistance of some high entropy alloys was also analysed, and some successes were recorded [12].

Some literature data report that even materials commonly recognized as inconvenient for nuclear applications present better radiation resistance than austenitic stainless steel. For example, Duan et al. [12] showed that irradiation with 3.7 MeV Fe^{2+} ions at 300 °C CoCrFeNi alloy developed using the MA+SPS powder metallurgy process possesses similar properties to Fe-Cr-Ni austenitic stainless steel. Moreover, the Authors presented that increasing the temperature to 500 °C did not result in significant growth in the density and size of dislocation loops and voids. It was concluded that proper choice of material and production process could even inhibit

the negative effect of cobalt, which debris (e.g., corrosion debris) may transform into radioactive nuclides and, consequently, result in higher than necessary doses to the staff during operation [13]. The authors supposed that the effects of multiple grain boundaries with lattice distortion strengthening causing interstitial-vacancy recombination are responsible for this remarkable effect.

II. Experimental procedure

The CoCrFeNi composition was mainly developed and studied to better understand the interesting mechanical properties. Many publications have been made in the last few years [4,8,12,14]. Unfortunately, despite significant work already carried out, the discussion about manufacturing techniques of high entropy alloys is missing, especially for the synthesised samples. For this reason, we focused on the manufacturing parameters description of well-known composition to obtain the process efficiency versus economic aspects trade-off. This will help us to prepare other FCC high entropy alloys rarely described in the literature.

To do that CoCrFeNi equiatomic composition was mixed using planetary ball milling with different milling parameters. We analysed the milling time (10, 20, 30, and 40 hours) by simultaneously reducing the ball-to-powder ratio (BPR) to 5:1. The milling speed was 250 rpm, and 15 minutes breaks after 15 minutes of milling were introduced to cool down the system. BPR reduction may be an exciting way to obtain more powder for further synthesis, which may be particularly important for industrial applications. The Spark Plasma Sintering technique was chosen for powder consolidation. This method offers the internal heating source between powder particles during compression and an external heating source introduced through the graphite die by a direct current. The sintering temperature during the process was 950 °C, and the holding time was 10 minutes.

In order to optimize the manufacturing process, we tested the other milling parameters, like milling speed (350 rpm), milling intervals (15 minutes of milling vs. 5 minutes of break), or introducing short (10 hours) pre-milling process of fractions with lower diffusion rates presenting the very promising perspectives for further research.

The alloys' microstructure were observed using Olympus BX53M and Thermofisher Helios 5 UX Scanning Electron Microscope equipped with EDS and EBSD detectors. Structural studies were carried out on a Bruker D8 Advance diffractometer. The Bruker TOPAS program, based on fundamental parameters profile fitting (FPPF) and Rietveld approaches, was used to refine the models of the identified phases. To understand the mechanical properties of the material Vickers microhardness test and nanoindentation test were performed to obtain the material's response in two different scales.

III. Current studies

After the spark plasma sintering process, we revealed, by using XRD, a few FCC structures and promoted the dominant one at the expense of others as the milling time was enlarged (Fig. 1). SEM analysis presented in fig. 2 allowed us to detect the Cr-rich phase, which resulted from insufficient milling process efficiency.

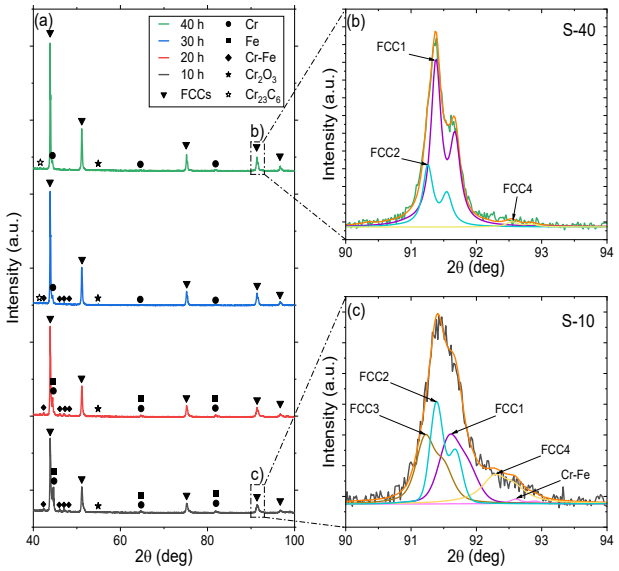

Fig. 1 XRD patterns of sintered samples

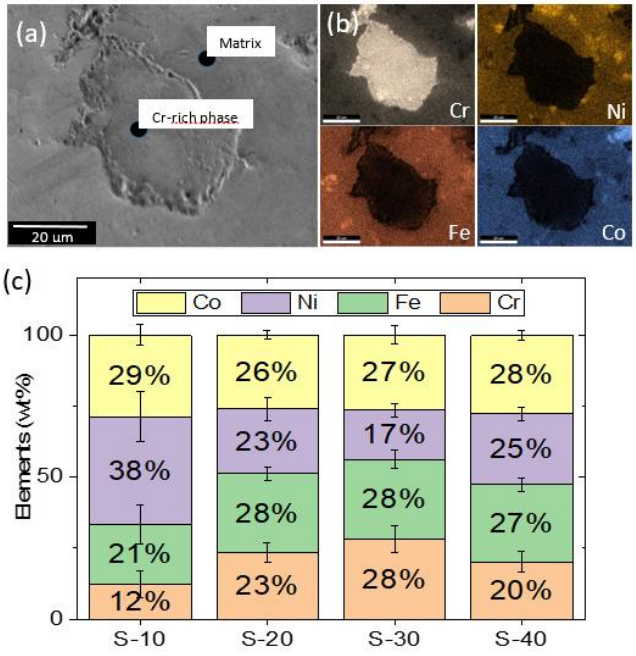

Fig. 2 (a) SEM image of Cr-rich phase after sintering with marked EDS detections spots, (b) EDS maps, and (c) quantitative (wt%) EDS results recorded during point analysis of the matrix.

However, heat-treated samples presented significant homogenization and almost all Cr-rich phase disappearance. Only the largest particles remain, as presented in fig. 3. Micro- and nanohardness results in fig. 4 demonstrated that the mechanical properties increase as a function of the milling time. Despite the hardness results being slightly below the average values reported in the literature, recorded process improvement allowed us to believe that efficient milling improves these materials' functional properties. We prepared the first paper on this topic, where we presented

our results. This work was already published in the Journal of Alloys and Compounds [15].

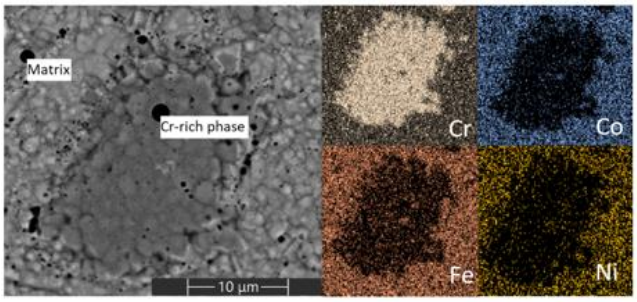

Fig. 3 SEM image of the representative Cr-rich phase obtained after annealing at 1050 °C for 12 h (left-hand-side) and recorded EDS maps of the Cr-rich phase and its nearest neighborhood matrix.

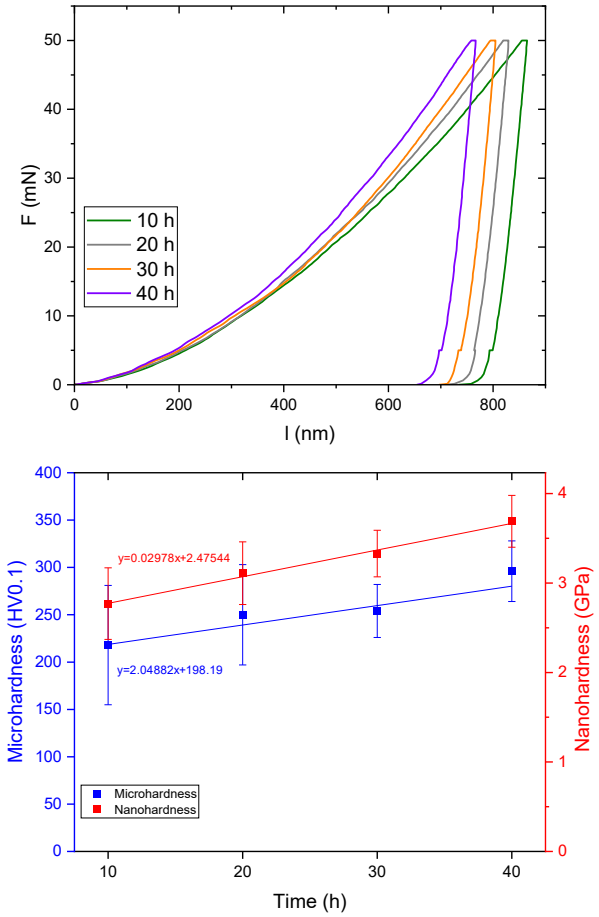

Fig. 4 (a) L-D curves recorded for all samples during the indentation test; (b) Micro- and nanohardness data comparison measured on the annealed samples.

IV. Conclusions and further plans

Our studies confirmed the gradual homogenization of the samples with increasing the milling time. The heat treatment employment results in further improvement of homogeneity. The results are consistent with the hardness increases, which shows the evolution in the strengthening mechanism of manufactured samples. However, a single FCC phase was not obtained even if the longest milling time was employed and the post-heat treatment process was performed.

The other process parameters were analysed to overcome this problem, as mentioned in part II. With the implementation of all the described parameters together, the material presents the microstructure almost free of the Cr-rich phase. The comparison of the samples after sintering from the previous section and described in the previous sentence is presented in Fig. 5. More research needs to be done to describe the evolution in a complex form.

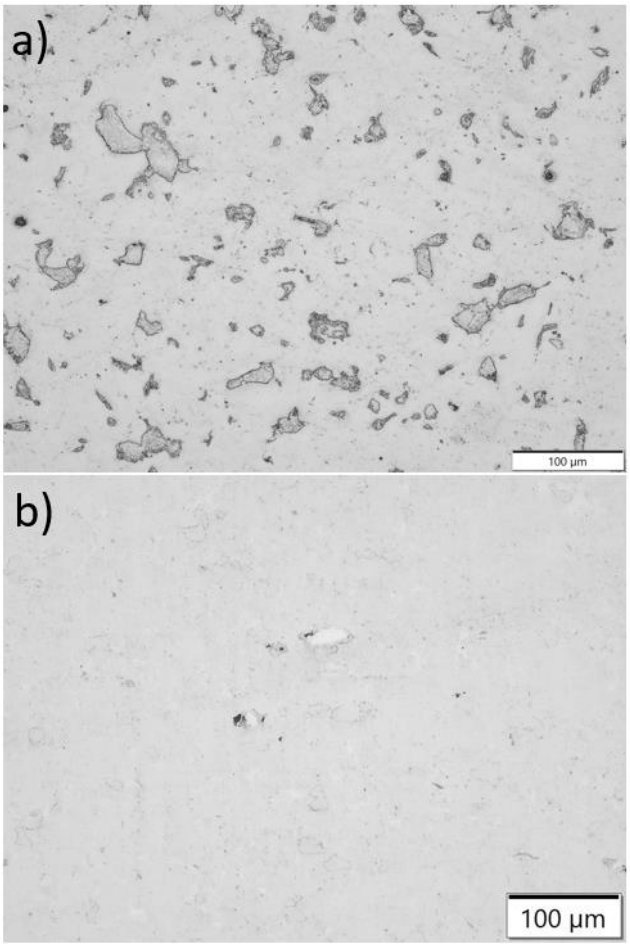

Fig. 5 (a) Microstructure of the sample in the first test cycle and (b) after a milling process improvement.

In parallel, we made the first samples by using arc melting. We prepared three equiatomic compositions: Fe-Ni, Cr-Fe-Ni, and Co-Cr-Fe-Ni, to analyse whether the production process used is proper. In the future, we will manufacture other samples with different chemical compositions (especially 15Cr-42Fe-15Mn-28Ni) using both methods. Based on the available literature data and numerical calculations made by our simulation group, this alloy composition should present very promising properties in a wide range of temperatures and elevated radiation resistance. We believe it may be considered a promising alternative to stainless steel and could be used in the next generation of nuclear reactors.

V. References

[1] Maziasz, P. & Busby, J.T.. (2012). Properties of Austenitic Steels for Nuclear Reactor Applications.

Comprehensive Nuclear Materials. 2. 267-283. 10.1016/B978-0-08-056033-5.00019-7., (n.d.).

[2] G.S. Was, D. Petti, S. Ukai, S. Zinkle, Materials for future nuclear energy systems, J. Nucl. Mater. 527 (2019) 151837. https://doi.org/10.1016/j.jnucmat.2019.151837.

[3] G.S. Was, P.L. Andresen, Radiation damage to structural alloys in nuclear power plants: Mechanisms and remediation, 2014. https://doi.org/10.1533/9780857097552.2.355.

[4] Y. Zhang, T.T. Zuo, Z. Tang, M.C. Gao, K.A. Dahmen, P.K. Liaw, Z.P. Lu, Microstructures and properties of high-entropy alloys, Prog. Mater. Sci. 61 (2014) 1–93. https://doi.org/10.1016/j.pmatsci.2013.10.001.

[5] J.W. Yeh, Alloy design strategies and future trends in high-entropy alloys, Jom. 65 (2013) 1759–1771. https://doi.org/10.1007/s11837-013-0761-6.

[6] D.B. Miracle, O.N. Senkov, A critical review of high entropy alloys and related concepts, Acta Mater. 122 (2017) 448–511. https://doi.org/10.1016/j.actamat.2016.08.081.

[7] B.S. Murty, J.W. Yeh, S. Ranganathan, Synthesis and Processing, High Entropy Alloy. (2014) 77–89. https://doi.org/10.1016/b978-0-12-800251-3.00005-5.

[8] A. Kumar, A. Singh, A. Suhane, Mechanically alloyed high entropy alloys: existing challenges and opportunities, J. Mater. Res. Technol. 17 (2022) 2431–2456. https://doi.org/10.1016/j.jmrt.2022.01.141.

[9] Y.O. Kuzminova, E.A. Kudryavtsev, J.K. Han, M. Kawasaki, S.A. Evlashin, Phase and structural changes during heat treatment of additive manufactured CrFeCoNi high-entropy alloy, J. Alloys Compd. 889 (2022) 161495. https://doi.org/10.1016/j.jallcom.2021.161495.

[10] Q. Yin, G. Chen, Y. Ma, B. Zhang, Y. Huang, Z. Dong, J. Cao, Strengthening mechanism for high-entropic weld of molybdenum/Kovar alloy electron beam welded joint, Mater. Sci. Eng. A. 851 (2022) 143619. https://doi.org/10.1016/j.msea.2022.143619.

[11] X. Yan, H. Guo, W. Yang, S.J. Pang, Q. Wang, Y. Liu, P.K. Liaw, T. Zhang, Al0.3CrxFeCoNi high-entropy alloys with high corrosion resistance and good mechanical properties, J. Alloys Compd. 860 (2021) 158436. https://doi.org/10.1016/j.jallcom.2020.158436.

[12] J. Duan, L. He, Z. Fu, A. Hoffman, K. Sridharan, H. Wen, Microstructure, strength and irradiation response of an ultra-fine grained FeNiCoCr multi-principal element alloy, J. Alloys Compd. 851 (2021). https://doi.org/10.1016/j.jallcom.2020.156796.

[13] Z. Que, M. Ahonen, I. Virkkunen, P. Nevasmaa, P. Rautala, H. Reinvall, Study of cracking and microstructure in Co-free valve seat hardfacing, Nucl. Mater. Energy. 31 (2022) 101202. https://doi.org/10.1016/j.nme.2022.101202.

[14] Z. Chen, R. Wang, Y. Shu, Y. Lin, Z. Liu, H. Deng, W. Hu, T. Yang, The interactions between dislocations and displacement cascades in FeCoCrNi concentrated solid-solution alloy and pure Ni, J. Nucl. Mater. 576 (2023) 154286. https://doi.org/10.1016/j.jnucmat.2023.154286.

[15] A. Olejarz, W.Y. Huo, M. Zieliński, R. Diduszko, E. Wyszkowska, A. Kosińska, D. Kalita, I. Jóźwik, M. Chmielewski, F. Fang, Kurpaska, Microstructure and mechanical properties of mechanically-alloyed CoCrFeNi high-entropy alloys using low ball-to-powder ratio, J. Alloys Compd. 938 (2023). https://doi.org/10.1016/j.jallcom.2022.168196.

Proceedings of the European Nuclear Young Generation Forum
ENYGF'23
May 8-12, 2023, Kraków, Poland

Study of the production processes of cobalt-60 in the core of a nuclear reactor

Świątkowska Julia[1*] and Darnowski Piotr[1]

[1] Warsaw University of Technology, Poland;

*Corresponding author: *Julia.swiatkowska1@gmail.com*

I. INTRODUCTION

Cobalt-60 is a radioactive isotope, which decays via β and γ radiation to Ni-60. Its history dates back to 1950s, when it was first used for medical purposes in Canada. Since then, because of its relatively long half-life of 5.27 years and high neutron capture cross section it has been widely used in sectors such as food irradiation, tumor treatment, radiotherapy or sterilization of medical equipment [1, 2]. Mostly due to growing population and research in medicine, the demand for this isotope is growing (and expected to grow) every year at a rate of about 6% [3].

It is produced from Co-59 isotope through neutron capture reaction ^{59}Co (n, γ) ^{60}Co, which can be conducted in a nuclear reactor core. The majority of the medical radioisotopes are made in research reactors only, however Co-60 is an exception due to its irradiating properties. The majority of its supply nowadays comes from CANDU reactors [4]. Almost 3/4 of all operating commercial reactors in the world however, are Pressurized Water Reactors and, out of another 57 currently under construction, 49 are also PWR [5]. Their dominance globally is therefore evident.

Thus, this work, investigates such type of a reactor to study a new way of developing the radioactive isotope of Co-60, what could possibly expand the production range. The model was based on AP1000 reactor by Westinghouse. Specifically, three different assemblies with five fuel enrichments and two burnable absorbers (BA) were taken from it. Four cases of each assembly were implemented, with either 0, 4, 6 or 8 cobalt rods inserted. All the simulations were run using Serpent2, code [6].

II. EXPERIMENTAL

A. Serpent2

Serpent2 is an effective tool in complex, reactor physics simulations and allows to determine multiplication factor, neutron flux, fuel burnup or reaction, fission, leakage and absorption rates. It implements the Monte Carlo method, which rather than solving transport or Bateman equations deterministically, obtains answers by simulating random particles and the final results are then inferred from the average behaviour of the simulated particles [7]. As an input it takes files including materials definitions, geometry and cycle parameters, as well as nuclear data libraries – in this case, ENDF/B-VII. As a result, output Octave/Matlab files are obtained for further analysis.

B. Materials

The most extensive part of the input file was materials' descriptions. In Serpent2, each material applied in the geometry, has to be defined with either atomic or mass density of each constituent isotope. All the compositions applied in the model can be found under this reference [8], however a few most important features will be discussed.

The fuel was UO_2 in a form of sintered pellets with density equal to 10.47 g/cc at temperature 900K. It was applied in five different enrichments: 1.58, 2.35, 3.2, 3.4 and 4.45 %wt (weight percentage of U-235). As a cladding for all the rods, optimized ZIRLO was used. It is a Zircaloy-4 derivative, with additional Nb supplement. It has high corrosion resistance and low neutron capture cross section [9]. Since its actual composition is not open to public insight, an estimated version was used.

Burnable absorbers, are elements in the reactor core, designed to absorb great number of neutrons in order to lower the multiplication factor k_{eff} quickly and effectively. They are made out of materials with high neutron capture cross section which, after absorption, decay into ones with low neutron capture cross section. An excellent example of such material is boron, which was introduced into the model in two ways. Firstly as the Integral Fuel Burnable Absorber (IFBA) in a form of a thin ZrB_2 layer around the fuel rod. Secondly, as separate borosilicate glass rods inserted into guide tubes. While both of the techniques fulfil their purpose, IFBA has a few advantages – most importantly it enables an unrestricted location in the assembly and a less drastic drop of the k_{eff}.

Finally, the moderator shall be discussed. Its purpose is slowing down fission neutrons, to thermal energies, in which the cross section values are highest. In the case of PWRs light water is used (typically borated) and put under high pressure of 155 bars in order to stay in the liquid phase at the temperature of 600K. Its density was set to 0.7194 g/cc.

C. Cobalt rods

The only naturally occurring isotope of Co-59. It does not exist in a pure metallic form on Earth, but is usually tied up with other elements forming minerals [11]. In the model it was implemented as a pure Co-59 pellet with density at 600K equal to 8.74 g/cc [12]. Its radius was the same as the fuel pellet with a thin, 0.125 cm aluminum coating [13]. The rods were inserted into the guide tubes in three different configurations, presented in Figure 1. [3].

Figure 1. a) Cobalt rods' positions in the assembly inserted into empty guide tubes (4 – yellow, 6 – additional green, 8 - additional burgundy); b) Geometries with IFBA rods replacing normal fuel rods (white, #2 assembly) and Pyrex inserted into guide tubes (dark blue, #3 assembly). #1 assembly had none of the BA mentioned.

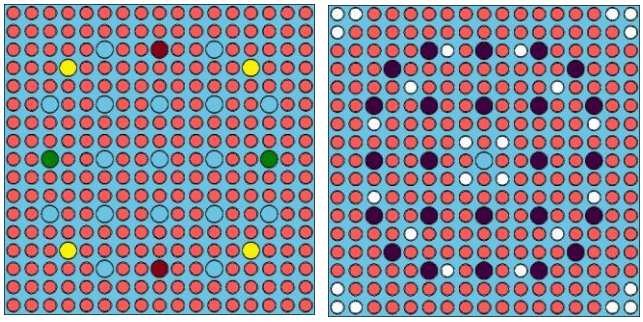

D. Simulation

The investigated assemblies were taken from the reactor's core and are shown in the Figure 2., named respectively: #1 with no BA, #2 with 28 IFBA rods and #3 with additional 24 Pyrex rods inserted into the guide tubes. One assembly was a 17x17 square lattice of pins, with 1.25984 cm pitch, yielding a total side length of 21.40204 cm. For each assembly, a reference case with no cobalt rods was run in order to compare the $k_{eff,}$ as well as the configurations with 4, 6 or 8 cobalt rods in the positions shown in Figure 1. The simulations were run for 500 active cycles, sampling 5000 neutrons in each and skipping additional first 20 cycles.

Table 1. AP1000 design parameters used in the simulation.

Parameter	Value
Fuel pellet radius	0.409575 cm
Fuel rod radius	0.47498 cm
Cladding thickness	900K
IFBA coating thickness	0.00258 cm
Pyrex rod inner radius	0.230505 cm
Pyrex rod outer radius	0.48387 cm
Number of fuel rods per assembly	264
Power density	0.35 kW/g

III. RESULTS AND DISCUSSION

A. Impact of the number of cobalt rods

Figure 2., shows the k_{eff} vs. fuel burnup for the 2.35%wt fuel enrichment for #1 geometry, from which can be concluded, that addition of cobalt rods into the model lowered the multiplication factor of the system. It is consistent with the expectations as indeed, cobalt acted as a neutron absorber and impacted neutron economy. Similar trend has been observed for other enrichments, but results are not reported in this paper. The k_{eff} values are of reasonable range, thus the model can be assumed to have worked properly.

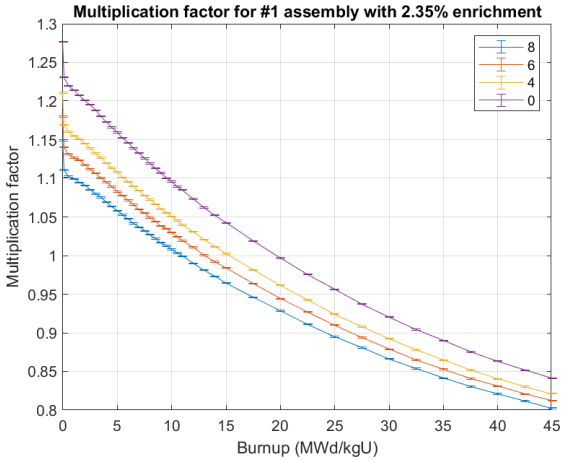

Figure 2. Multiplication factor plot for #1 assembly with 2.35%wt of U-235 with varying number of Co-59 rods.

Figure 3. shows the Co-60 mass during fuel burnup for the chosen geometry, to picture the overall trends, however, all the results for the #1 geometry can be found in the Table 2. Firstly, it is clear that the higher number of rods inserted, the higher amount of the isotope was produced and with no rods inserted, it was not detected at all.

Table 2. Final results for #1 assembly with varying number of cobalt rods – 8, 6 and 4 (presented for each fuel enrichment in this order).

Initial ^{59}Co mass [g/cm]	Final ^{59}Co mass [g/cm]	^{60}Co mass [g/cm]	^{60}Co [% of initial ^{59}Co]	Fuel enrichment [%wt]
36.7278	33.6532	**2.4943**	6.79	1.38
27.6790	25.3819	**1.8653**	6.74	
18.4017	16.8587	**1.2541**	6.82	
36.8763	34.2862	**2.1174**	5.74	2.35
27.5742	25.6445	**1.5790**	5.73	
18.4017	17.1121	**1.0563**	5.74	
36.7182	34.6242	**1.7186**	4.68	3.4
27.6998	26.1442	**1.2774**	4.61	

18.5238	17.4906	**0.8491**	4.58	
36.661	34.9138	**1.4347**	3.91	4.45
27.7438	26.4472	**1.0652**	3.84	
18.3353	17.4718	**0.7097**	3.87	

Secondly, for all cases the relation to fuel burnup was linear which means, that at no point in time the production rate was more favourable. Lastly, looking at the final Co-60 mass obtained after the cycle as the percentage of the initial Co-59 mass, it can be deduced, that the number of rods did not impact the amount of the isotope generated from each rod – it remained constant. It is due to the fact that the fuel material was treated as the same depletion material.

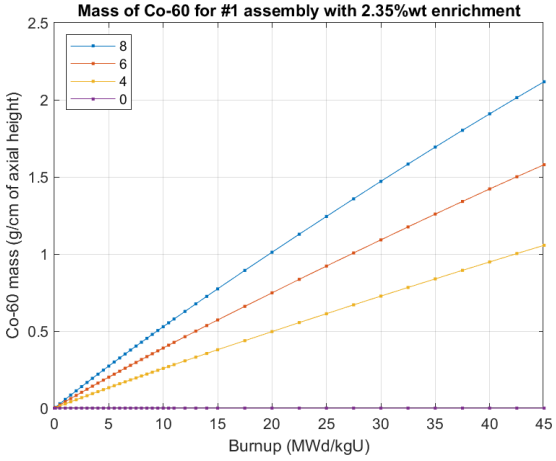

Figure 3. Co-60 mass for #1 geometry with fuel with 2.35%wt of U-235 for different number of cobalt rods inserted.

B. Impact of the fuel enrichment

The effect of the amount of U-235 in the nuclear fuel in the assembly on the multiplication factor was rather straightforward – its higher supplement resulted in more neutrons in the system and higher k_{eff}. For all the simulated cases, it had a downward tendency and it dropped below criticality at the end of simulation. The instance of the assembly with 8 cobalt rods is presented in Figure 4.

Looking at the final Co-60 mass however, an interesting conclusion can be drawn. Applying higher fuel enrichment actually increased the final amount of the radioactive isotope produced. The cumulative results for all cases are presented in the Table 2. The largest values of the Co-60 mass were observed for the 1.38%wt of the ^{235}U in the fuel and they decreased with the progression of the enrichment. It is presumably due to the fact, that with a higher percentage of the fissile material in fuel, neutrons produced from fission were more likely to be absorbed by it and not by Co-59, to then, via neutron capture, form Co-60. Accordingly, when the amount of fissile material was lower, neutrons had the opportunity to travel to guide tubes and react in the elements in there.

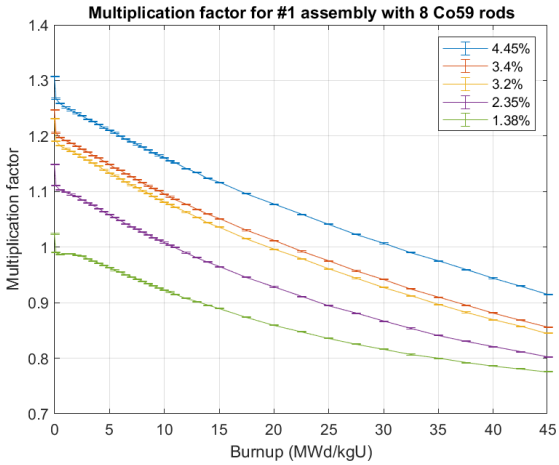

Figure 4. Multiplication factor for #1 geometry with 8 cobalt rods for different fuel enrichments.

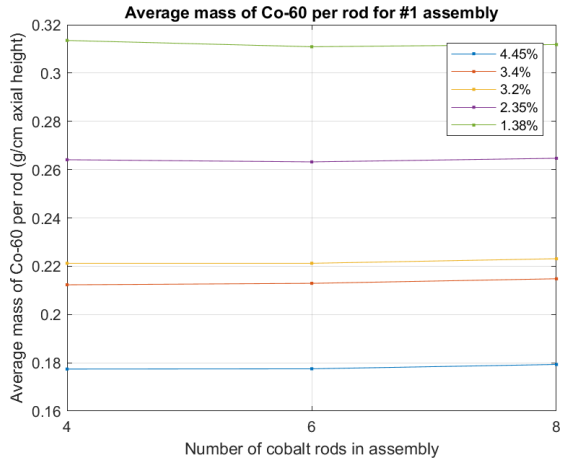

Figure 5. Average final Co-60 mass per rod for #1 geometry for five different enrichments.

A comparison of final Co-60 mass obtained per rod is presented in Figure 5. and confirms that it was not affected by the number of rods (it stayed constant) and higher for lower fuel enrichment. Based on these average values, its final amount per inserted rod was calculated for all five enrichments, presented in Table 3. The highest value achieved was 133.16g per rod for the assembly with 1.38%wt of U-235 in the nuclear fuel. The lowest was almost half of that – 76g per rod for 4.45%wt.

Table 3. Final Co-60 mass obtained per rod for #1 assembly with five enrichments.

Fuel enrichmen [%wt]	1.38	2.35	3.2	3.4	4.45
Av.Co-60 mass per rod [g]	**133.16**	**112.64**	**94.67**	**91.03**	**76.00**

C. Impact of the burnable absorbers

Results showed that an increased number of cobalt rods had a great impact on the k_{eff} for the #2 assembly, lowering it, whereas for the #3, adding the rods did not change the multiplication factor to such extent. It was most probably

due to the fact, that as the cobalt rods were inserted into the guide tubes' places, for the #2 assembly it was equivalent to an extra component absorbing neutrons. For the #3 assembly however, the guide tubes were already occupied by an absorbing neutrons material. This could mean that Co-59 could potentially replace Pyrex without a huge impact on the core's chain reaction.

Table 4. Final simulation results for #2 (blue) and #3 (orange) assemblies with varying number of cobalt rods – 8, 6 and 4 (presented for each case in this order).

Initial ^{59}Co mass [g/cm]	Final ^{59}Co mass [g/cm]	**^{60}Co mass [g/cm]**	^{60}Co [% of initial ^{59}Co]	Fuel enrichment [%wt]
36.9599	34.3859	**2.1014**	5.69	2.35
27.7638	25.8509	**1.5625**	5.40	
18.477	17.2006	**1.0439**	5,63	
36,7202	34,6265	**1.7165**	4,68	3.4
27,6902	26,1368	**1,2745**	4.52	
18,4069	17,3743	**0,8476**	4.60	
36,8747	34,4222	**1,9900**	5.35	2.35
27,6818	25,8557	**1,4820**	5.65	
18,3005	17,0858	**0,9858**	5.39	
36,7582	34,7196	**1,6628**	3.91	3.4
27,5466	26,0147	**1,2496**	3.84	
18,3673	17,3514	**0,8289**	3.87	

Table 4. shows similar results as in previous section for assemblies #2 and #3 with 2.35 and 3.4%wt of U-235 in fuel. Comparing the results to the ones obtained from #1 assembly, it is evident, that the assemblies with Pyrex rods produced less of Co-60. It can be attributed to the fact, that the neutrons were absorbed by borosilicate glass, instead of the cobalt rods. The same trend could be recognized for the IFBA, however the difference was much smaller.

Similarly as in the #1 assembly, for #2 and #3 the average value of final Co-60 mass obtained per single rod stayed constant for each number of them. Thus, for all cases an average was taken and multiplied by the height of the active core, yielding an estimate of the possible Co-60 mass that could be retrieved from a single rod inserted into the model, which is presented in Table 4.

Table 4. Final Co-60 mass obtained per rod for #2 and #3 assemblies with two enrichments.

Assembly: fuel enrichment [%wt]	#2: 2.35	#2: 3.4	#3: 2.35	#3: 3.4
Av.Co-60 mass per rod [g]	**111.53**	**90.87**	**105.57**	**88.67**

IV. CONCLUSIONS

This work intended to examine the production of the radioactive isotope of Co-60 in the nuclear reactor's core, based on AP1000 by Westinghouse. Individually, three assemblies were modelled with various fuel enrichments, BA and number of rods inserted. The results showed that for higher content of U-235 in fuel, the final mass of Co-60 obtained was lower. As far as burnable absorbers as concerned, assemblies with Pyrex rods inserted had an unfavourable effect on the production, while IFBA did not affect it to such extent. Number of the initial cobalt rods did not change the average mass of the isotope obtained per rod.

References

[1] John R. Cunningham. “Cobalt-60 Units for Radiotherapy.” John Wiley Sons, Ltd, 2006

[2] International Atomic Energy Agency (2006). “Gamma irradiators for radiation processing” (INIS-XA--862). International Atomic Energy Agency (IAEA).

[3] W. Zhang, et al., “Feasibility analysis of 60Co production in pressurized water reactors”. NUCL SCI TECH 30, 147 (2019)

[4] World Nuclear News, “Framatome and Exelon to explore Co-60 production”, 05 January 2022

[5] IAEA, Power Reactor Information System (PRIS): https://pris.iaea.org/PRIS/WorldStatistics/OperationalReactorsByType.aspx, Vienna (Accessed 16 Dec 2022)

[6] Leppänen, J., et al., "The Serpent Monte Carlo code: Status, development and applications in 2013." Ann. Nucl. Energy, 82 (2015) 142-150.

[7] A. Judaibi & A. Soliman, “Simulation of cobalt-60 production in research reactors using OpenMC Monte Carlo code”. Kerntechnik, 87(2), 230-236.

[8] P. Darnowski, et al. “Simulations of the ap1000-based reactor core with serpent computer code”. Archive of Mechanical Engineering, vol.65 no. 3) 295–325, 2018.

[9] https://info.westinghousenuclear.com/blog/the-art-of-innovation- optimized-zirlo-cladding

[10] Royal Society of Chemistry. https://www.rsc.org/periodic-table/element/27/cobalt.

[11] K. Thurnay. “Thermal properties of transition metals.” May 1998.

Hot Topic 3
Communication, Policy, and Education

Proceedings of the European Nuclear Young Generation Forum
ENYGF'23
May 8-12, 2023, Kraków, Poland

Nuclear fission energy initiatives in the kingdom of Saudi Arabia

Alruwaished, Abdulaziz[1*], Alshehri, Sultan[1], Mukhrish, Abdulkarim [1], Shams, Afaque[1,3] and Al-Athel, Khaled [1,2]

[1] King Fahad University of Petroleum & Minerals (KFUPM), Saudi Arabia

[2] Interdisciplinary Research Center for Advanced Materials (IRC-AM), KFUPM, Saudi Arabia

[3] Interdisciplinary Research Center for Renewable Energy and Power Systems (IRC-REPS), KFUPM, Saudi Arabia

*Corresponding author: s201833440@kfupm.edu.sa *(A. Alruwaished)*

I. INTRODUCTION

In 2010 the Kingdom of Saudi Arabia took its initial move into the nuclear power field by establishing King Abdullah City for Atomic and Renewable Energy (KA CARE). Since then, KA CARE has worked on regulating and studying how to implement nuclear power plants in the Kingdom. Also, in 2016 when the Kingdom introduced its vision 2030, which is a strategy to decrease the Kingdom's reliance on oil and diversify its economy. The Kingdom announced a variety of plans and projects to achieve its vision, and one of these projects is the green and renewable energy initiatives, part of it is the interest of this report which is nuclear power initiatives. Thus, this report will discuss the position of nuclear power in Saudi Arabia's 2030 vision, the project requirements, possible locations, and the Kingdom's plan to build and implement its nuclear project.

II. BACKGROUND

A. The Saudi energy sector in vision 2030

Vision 2030 is a sustainable vision for the future of Saudi Arabia where sustainability is the main mover of all sectors. In the energy sector Saudi plans to achieve an optimum energy mix by 2030, in which 50% of produced energy is comprised of renewables and natural gas. Saudi Arabia aims at reaching net zero carbon emissions by 2060, these ambitious goals are to be attained through diversifying the energy sector with different forms of clean energy. [1]

Renewable energy is an optimistic clean energy source for the future, but it comes with disadvantages that affect its integrity as a sustainable source. Capacity factors of different energy sources are found in [2], Solar, wind, and hydropower have the lowest capacity factors compared to their peers. This makes it challenging to rely solely on renewables, such an action would require a reduction of energy consumption, which comes against the expected increase of energy consumption in Saudi Arabia to 120GW by 2032. In addition, wind, solar, and hydropower produce a total of 52 tons of greenhouse gas emissions [2]. Being said it is difficult to achieve the kingdom's 2060 zero carbon emissions goal by relying on renewables solely. Rather Saudi renewable energy must be supported by a stronger energy source, that proves sustainability.

B. The role of nuclear energy in the Saudi energy mix

Choosing a suitable energy source is a crucial decision that depends on the needs and capabilities of the country. Energy demands in Saudi Arabia have grown across all industrial and residential sectors of the kingdom. The total energy consumption in Saudi Arabia has reached 359 TW.h in 2020 [3]. Choosing Nuclear energy as a leader in the Saudi energy mix proves to be the most beneficial decision. Nuclear energy has the highest capacity factor [2], which makes it the most reliable energy source. The utilization of nuclear energy will help the Kingdom reach sustainability and meet its energy needs without relying heavily on oil.

Nuclear energy is a clean energy source since it is based on nuclear fission rather than chemical burning, thus there is no direct carbon emission which is the main cause of global warming. When comparing the greenhouse emission of nuclear with the combination of renewable power in [5], nuclear proves to be the cleanest with 3 tons of greenhouse emissions while combined renewables (solar, wind, and hydropower) produce 52 tons of greenhouse emissions, that is nearly 17 times more than nuclear. It is estimated that the kingdom contains around 60,000 tons of uranium, based on preliminary studies [4]. By relying on nuclear energy supported by renewables the Kingdom can optimize its oil and natural gas resources for other useful uses, or it could export it to other countries and reinvest in clean energy.

III. Recommendations

A. Create an outstanding nuclear power program

According to the IAEA, a successful nuclear power program requires a national commitment of 100 years [6], during

these 100 years there will be a rapid digital and technological change in the world, and not keeping up with these digital changes will lower the chances of program success and development. Accordingly, KSA must intensify its digitalization efforts to create a robust, distinctive digital infrastructure to assure a continuously sustainable development program that will put Saudi Arabia on the list of leading nuclear-powered countries. This is achieved through three main objectives that should be considered before building nuclear power plants, create a digitalization committee, develop digital twins, and ensure that digital capabilities are part of the first nuclear power plant.

The Saudi ministry of energy and the Saudi ministry of communication and information technology must cooperate to create a committee between the Saudi nuclear power holding company and the Saudi Authority for Data and Artificial Intelligence (SDAIA). The responsibility of this committee is to:

- Compose a technical and financial feasibility study on the effectiveness of digitalization of the nuclear power industry
- Develop programs that facilitate the digitalization of the nuclear power industry.
- Ensure that proper infrastructure is available for such programs through any form of cooperation with third parties.

Once the digitalization committee agrees on the digitalization program, digital twins (DT) must be developed as a first step. A digital twin is a digital representation of a physical system or a process, it collects and store data in a database and then simulates data in different models. This simulation results in an overview of the past, present, and future performance of the system or process that aids critical decision-making in the design or operational phase. KSA must facilitate the atomic energy strategy progress, by utilizing Digital Twins' capabilities in the construction and operations phase. During this DT will be fed with data or plans, and it will simulate and analyze them to give out optimal strategic decisions. During the construction phase, DT can simulate different construction plans, this will help engineers detect possible project issues resolving them early. DT will be a vital support in the operational phase, by collecting operational data continuously and implementing them into its simulation capabilities that will predict sudden maintenance operations or possible future failures in the plant. These two applications will optimize time and reduce costs.

Since the first nuclear power plant in Saudi Arabia will be based on an external nuclear power vendor, then the contract agreement between Saudi Arabia and the vendor must include a clause that assures the development of a digitalized nuclear technology with a strategy provided by the Saudi digitalization committee and other related parties.

B. Ensure a sustainable nuclear power program through education

A proper level of education is an important aspect throughout the lifespan of a nuclear power program since it is present before, during, and after building nuclear power plants. Education affects the program's success, as a nuclear power program requires high levels of education, experience, and societal awareness. In the following sections educational issues in Saudi Arabia will be discussed in addition recommendations will be given on societal views, expert building, training, and research centers.

Society view

Society views are essential factors that affect nuclear power program development, various studies were carried out to understand the effects globally, limited of which were intended for Saudi Arabia. A study was performed in [7] to examine the acceptance of nuclear energy in Saudi Arabia and examine the factors affecting acceptance levels. The objective of the research was to help policymakers identify public views on nuclear power plants, and further studies are required to support the claims.

Hence, a different survey is conducted by the authors of this article, to investigate society views in Saudi Arabia. The survey aims to study the overall social acceptance of the nuclear industry. There were 213 respondents both males and females, educational levels varied as high school, diploma, bachelor, and higher levels of education. The survey consisted of the following questions:

- In your opinion, what type of energy is the best option for the future?
- What comes into your mind when you hear the word "Nuclear Energy"?
- Do you think that Saudi Arabia needs Nuclear Energy?
- Your background level in nuclear power plants is:
- In terms of safety, in your opinion nuclear power plants are:
- In your opinion, the cost of building nuclear power plants is
- In your opinion, the cost of electricity produced by nuclear power plants is
- Do you support building nuclear power plants?
- Would you accept to work or (have a relative/friend work) in the nuclear power industry?
- Would you live in a city that has a nuclear power plant?

The survey data showed the following observations:

- 47% of respondents believe that nuclear power is the best option for the future, and 47% believe in the wind and solar energy.

This tells that people do believe in nuclear power to a level that makes it favorable to renewables such as solar and wind. These high levels of belief come from the fact that these energy sources are of high interest in vision 2030 which aims at reaching net zero carbon emissions by 2060.

The misconception about nuclear energy

- 31% of respondents have mixed between nuclear power and nuclear weapons
- 74% of all respondents have low or no knowledge of nuclear power plants.

When analyzing the previous two points, it has been observed that 82% of people with low or no knowledge mix between the term nuclear power and nuclear weapons. This

shows that there is a clear proportional relation between lower backgrounds on nuclear power and the misconception of nuclear power and weapons.

Awareness levels

- 89% believe that KSA needs to use nuclear energy
- 58% of total responders prefer not to live in a city that has NPP
- 84% of the total survey population support building NPP

When analyzing previous data, it is observed that 49% of those that support building NPP are willing to live near NPP. While 51% are not willing to. These results show that people are aware of the importance of nuclear energy, but the majority are in favor of not having it near their area.

- 15% of total respondents believe that an NPP is safe and 21% believe they are extremely dangerous
- 54% of respondents would accept to work in NPP
- 64% believe that the construction cost of NPP is very high
- 36% believe that the cost of nuclear electricity is very high

These statistical observations can be directly related to two main factors. The first is that there is a lack of educational knowledge on nuclear power in Saudi society. The second factor is that for years the media has been providing misleading information on the uses of nuclear energy which has created a misconception of the term nuclear energy. Unless these two factors are resolved, fear and national rejection of nuclear power programs will obstruct the Saudi national atomic energy plan (SNAEP). To avoid such an obstruction, levels of awareness and education must be increased through proper methods of psychological treatments for nuclear energy fear.

A proposed solution is to educate people at early educational stages on the civil uses of nuclear energy, which includes electricity production, water desalination, and the production of radioisotopes for cancer treatment. This is the role of the government led by the ministry of energy, and the ministry of education to create educational video content and update school curriculums with the various applications of nuclear energy. To reach out to a wider audience it is recommended to use social platforms to advertise these civil applications of nuclear fission energy. Furthermore, it is the role of nuclear power engineers to shift society's views on nuclear power by lighting on the high levels of safety and security found in nuclear power plants and teaching people proper methods of information evaluation.

Building experts

To start a nuclear program, we mainly need people who are highly expertise in this field. It is worth noting that human development efforts were initiated by KA CARE, where different level university students were sent to international training institutions to learn more about the nuclear field. This is a leading step toward the future, but in the long term, this will be a drawback because such a program has a high cost, and it involves the transfer of assets outside the kingdom. A solution to this manner would be to attract experts from outside the kingdom and build a strong human infrastructure by educating university-level students on the most modern technological advancements found in the nuclear industry. Such a step would create a self-independent program that graduates Saudi nuclear power experts that will benefit the Saudi nuclear program, in all aspects.

Training centers

To initiate a new industry, a tremendous community must be present that is well-knowledgeable and trained in this industry. In the nuclear industry, this principle is more crucial than others. The nuclear industry is more sensitive especially when talking about the safety aspect. Therefore, to create a nuclear community Saudi training centers must be created. Training centers will provide highly educated generations of NNP operators, technicians, engineers, and scientists. Not only that but also, these centers will ensure the continuity and improvement of NNP workers' proficiency. These training centers must follow international standards, and to build such centers the kingdom must cooperate with an expert country in the nuclear field such as France. Due to its long-life experience of France in the nuclear field, France has highly advanced training facilities. INSTN (National Institute for Nuclear Science and Technology) is an example of a French institute that provides training programs related to the nuclear Field. The trainees in INSTN can experience similar tasks to the tasks conducted in a real NPP. Advanced educational platforms and equipment are used to achieve this purpose. EVOC is an example of a multimodal platform that has been used in INSTN to simulate the operation event of a nuclear research reactor. Therefore, such training programs should be included in the Saudi nuclear program.

The training centers aim to guarantee the implementation of the highest international requirements of safety and quality in the operation of NPPs. The centers should include highly advanced programs in radiation protection since its one of the biggest concerns in the nuclear field. Additionally, to meet the goal of these centers, supremely advanced nuclear reactor simulators should be provided. The simulators will train the operators, engineers, regulators, technicians, and students on many important subjects related to the nuclear field. Most importantly, they will be well educated in the physics and engineering design of nuclear reactors, and they will train to act properly in the case of accidents using these simulators.

Research centers

The Saudi nuclear power industry needs strong research centers. The exigency of having these centers increases because the environment and weather in the kingdom differ from those found in most of NNPs around the world. Moreover, the Kingdom plans to build its NNPs with the highest technology, which means that a huge amount of research is still needed to support such reactors. The research centers can:

- Provide innovative technologies that serve NPPs.

- Promote the aspect of nuclear safety.
- Severe Accident analysis.
- Provide studies regarding fuel.
- Improve waste management strategies.
- Promote studies on the new reactors' designs
- Have a mock-up of NPPs.

KA CARE and KACST (King Abdulaziz City for science and technology) are researching nuclear issues and how to initiate the Saudi nuclear industry. However, more specialized research centers are required. Establishing training and research centers should be one of the first objectives of the Saudi nuclear power plan.

C. Ensure a sustainable nuclear program through regulations

The nuclear regulator is the regulatory body that is responsible for commissioning licenses to protect public health and the environment by ensuring safe nuclear operations. The regulatory authority in the kingdom is the Nuclear and Radiological Regulatory Commission. However, a nuclear regulatory authority cannot work alone, it needs to rely on other organizations and entities for expertise and security. That will lead to the creation of the following two organizations, a technical support organization (TSO), and a nuclear safety specialized entity.

Technical support organization (TSO)

The technical support organization is an organization or organizational unit recognized by the government and the regulatory authority, to support nuclear and radiation safety and all related technical and scientific issues by providing expertise and services [8]. Moreover, an indispensable characteristic of the TSO is to conduct research and development to help and support the regulatory authorities and other public authorities. The maintenance of expertise supporting the regulatory authorities' works and utilities, and the communications between the technical support organization and the regulatory authority identified by the IAEA as a key pillar of the framework for safety. Being said a question arises does Saudi Arabia need a technical support organization for its nuclear project? The answer is certainly yes, as stated above the role of a TSO is irreplaceable. Despite a safe operation of an NPP is mainly the responsibility of the organization that is operating it, the TSO must provide all the needed expertise to insure a safe operation. Also, by having a TSO the kingdom can share and receive information and experience with other TSOs around the world through the Technical Support Organization Forum (TSOF). TSOF is a platform established by the IAEA in 2010 to help to share information and experiences among TSO worldwide [8].

Nuclear safety specialized group

For the nuclear regulatory authority to insure a safe and secure operation of a nuclear power plant, it must establish an independent organization specialized in this task. The role of such an organization is to respond as fast as possible in case of an emergency. For example, after the Fukushima accident in 2011, EDF established a specialized entity called the Nuclear Rapid Action Force FARN, to ensure the availability at any time of all the equipment and human resources that are needed to prevent any release into the environment in case of a serious accident in a nuclear power plant. FARN's mission is to supply the power plant with electricity, air, and water to maintain the functionality of the site. Moreover, such an organization can help in other accidents other outside of an NPP if needed. Thus, establishing a similar entity will help ensure the safety and security of NPPs and the surrounding environment.

D. Ensure sustainability of the nuclear fuel sector

Nuclear fuel is one of the main issues in the nuclear energy industry, it has its dangers and requires intensive strategic planning that considers the whole fuel life cycle starting from uranium mining to waste disposal. The kingdom has two different choices regarding its nuclear fuel, it could buy the fuel from an international source, or it could start mining and enriching nuclear fuel inside the territories of the kingdom, each plan has its advantages and disadvantages that affect the whole life cycle of the Saudi nuclear program.

Depending on an international source

If the kingdom decides to buy and dispose of its nuclear fuel by cooperating with an expert international source, the burden of mining, enriching, and disposal operations will be relieved but that comes with consequences that are:

- Transportation of assets outside the kingdom
- Saudi will not be able to utilize its natural resources of uranium
- The Saudi nuclear energy program will lack sustainability

These issues will weaken the national economy and national GDP, which makes this option an opposition to the commitment of vision 2030 to create a mining sector that contributes to the national economy at its full potential.

Mining and enriching in KSA

Mining and enriching natural uranium in Saudi Arabia will come with big benefits for the country. New jobs will be created for both the mining, enriching, and waste disposal industries, and other related jobs would increase. The Saudi NP program will be self-sustaining, and it will be independent of international circumstances. Furthermore, Saudi would export uranium and sell it to other countries, this money could be reinvested into the Saudi nuclear program to make it self-sufficient and independent. As a result, Saudi Arabia must create a national waste disposal program that considers all types of waste, such a program requires high levels of experience which are currently unavailable, hence modern solutions must be created to avoid the delay of the Saudi nuclear energy program.

Suggestion

To reach an outstanding nuclear energy program, Saudi should depend on these two resources in a four-stage process (figure 14). The first stage would involve initiating the uranium exploration efforts in cooperation with an expert country. In addition, waste disposal facilities must be defined in a preliminary phase. Once uranium resources are confirmed, stage two begins where waste disposal and fuel enrichment facilities are built with the highest standards. In the meantime, the first NPP in Saudi Arabia must begin operations using international uranium, which will help the Saudi nuclear program develop and gain experience. As the program reaches sustainability and NPP operations are stable, Saudi should start using a mixture of its national fuel and international fuel to operate its NPPs. As the enriching and waste disposal sectors develop in KSA, national fuel must be utilized for the Saudi NPPs, and it must be exported for commercial uses.

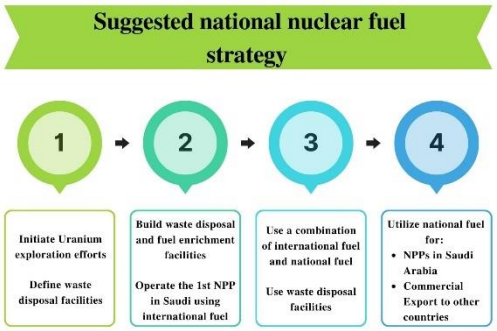

Figure 14. Suggested nuclear fuel strategy

IV. Concluding remarks

Saudi Arabia holds a commitment to reach net zero carbon emissions by 2060, the plan is to create a diverse clean energy mix that serves the upcoming energy demand. This ambitious goal cannot be achieved unless nuclear energy is chosen as an energy mix leader. The Saudi nuclear energy initiatives are optimistic, but many issues are recommended to be developed and worked on. An outstanding nuclear power program must be established on a strong national digital infrastructure that facilitates the development of digital technologies such as digital twins. To assure sustainability, national issues must be resolved, these include societal misconceptions and low awareness levels of nuclear energy. Additional efforts are required to prepare safe and reliable operations of nuclear power plants, by building research and training centers to develop nuclear experts and engineers. A regulatory framework must be developed such that the nuclear and radiological regulatory commission (NRRC) is supported by a technical support organization (TSO) and a specialized nuclear power plant safety entity. Furthermore, a nuclear fuel strategy is suggested, such that nuclear fuel resources are utilized at maximum potential, without causing any further delays in the Saudi National Atomic Energy Plan (SNAEP).

V. References

[1] Government of the Kingdom of Saudi Arabia. Vision 2030. (2016)

[2] USA, N.R.C. (2020) Infographic - capacity factor by energy source - 2019, Energy.gov.

[3] International energy agency, IEA. (2020) Saudi Arabia - countries & regions, IEA.

[4] Mansouri, Noura. (2020). The Saudi Nuclear Energy Project. KS—2020-CO17. Riyadh: KAPSARC.

[5] Ritchie, H. (2020) What are the safest and cleanest sources of energy? Our World in Data.

[6] Milestones in the development of a national infrastructure for nuclear power. — Vienna: International Atomic Energy Agency, (2015). p. ; 24 cm. — (IAEA nuclear energy series, ISSN 1995–7807 ; no. NG-G-3.1, rev. 1)

[7] Alzahrani. S., Alwafi. A., Alshehri. S., (2022, November 21). A framework of examining the factors affecting public acceptance of nuclear power plant: Case study in Saudi Arabia.

[8] International Atomic Energy Agency, IAEA Technical and Scientific Support Organizations Forum (TSOF) (n.d.).

Proceedings of the European Nuclear Young Generation Forum
ENYGF'23
May 8-12, 2023, Kraków, Poland

The "Jóvenes Nucleares" model: The Young Generation is active in the Spanish Nuclear Sector

Domínguez-Bugarin, Araceli[1], Díaz, Miriam[1], Aragón, Pau[1] and Carrasco, Alejandro[1*]

[1] *Jóvenes Nucleares (JJNN), Spain*

*a.carrasco@jovenesnucleares.org

I. INTRODUCTION

The Spanish Young Generation Network (JJNN) places a strong emphasis on organizing activities that promote the awareness and understanding of the numerous applications of nuclear science and technology. Over the years, key activities such as school talks, university courses, advanced reactor seminars, and technical visits to nuclear facilities have become integral to JJNN's mission. In order to reach a wider audience, the organization actively engages with social media and values the contributions of young professionals, who bring fresh perspectives and ideas to the table. As we look towards a return to normalcy after the Covid-19 pandemic, JJNN continues to expand its range of activities and initiatives. This paper aims to highlight five recent efforts, emphasising their motivation and alignment with our strategic goals.

II. DEAD OPERATORS SOCIETY

The inspiration to launch a debating club arose from the growing involvement of JJNN in mass media (TV, radio, podcasts, press, etc). Like in the 1989 film "Dead Poets Society" directed by Peter Weir, where students of a non-conventional teacher secretly gather to read poetry in a cave, the board members of JJNN come together once a month to weigh the advantages and disadvantages of nuclear energy. The primary aim of this effort is to advance our technical understanding of nuclear science and technology, as well as to develop our communication and public speaking abilities.

In each session, participants are presented with a series of anti-nuclear arguments and are encouraged to respond to them. The achievement of the first objective is based on the exchange of knowledge and sharing of experiences among the board members of JJNN, who come from a diverse range of backgrounds in the nuclear sector, including engineers, physicists, lawyers, and communication graduates. This diversity in expertise allows for a variety of perspectives and an opportunity to always learn something new, regardless of one's level of specialization in a particular subject. The valid arguments discussed during technical debates are later documented in a report called "The Nuclear Case." It is important to note that this document encompasses more than just a collection of pro-nuclear arguments and seeks to address the limitations of nuclear energy to effectively advocate for its use.

Figure 1. Dead Operators Society kick-off meeting.

The main anti-nuclear arguments have been grouped into four blocks, presented in order of increasing complexity:

1. Greenhouse gas emissions
2. Nuclear safety and waste management
3. Integration with renewables
4. Cost

Regardless of their prior knowledge, it is crucial for participants to learn to develop a comprehensive debate strategy. This will enable them to steer the conversation towards the topics they are most comfortable with. Given the time constraints, not all topics are covered in equal depth. The most commonly discussed issues (such as greenhouse gas emissions, safety, and waste management) are given higher priority and participants are encouraged to attain a deeper technical understanding of these subjects.

To attain the second objective (to enhance our communication and public speaking skills), each session dedicates its latter half to hands-on exercises. These exercises are designed to stimulate participation and

provide an opportunity to apply the concepts covered in the technical discussion. To accomplish this, activities that imitate real-life scenarios such as interviews or debates are frequently introduced. For instance, the first practical exercise involved conducting unexpected interviews. Upon arrival at the meeting point, members of Dead Ops Society were paired with two individuals, one of whom asked questions while the other recorded the interview for future review. Finally, a compilation of videos was reviewed and discussed by the entire group at the end of the session.

At such crucial times for our future well-being, JJNN continues strengthening its position as a staunch advocate of nuclear energy through this initiative.

III. PINT OF SCIENCE

Pint of Science is a global festival of events where researchers and scientists come together to share their work with the general public in local bars, promoting the communication of science in a relaxed and social environment.

We had the opportunity to participate in Reus, with the talk about “SMR: pocket-sized nuclear reactors”, in Tarragona, with “Uranium Alchemy: transmutation” and in Madrid we were able to participate two days during this last year’s Pint of Science with two talks. These talks were about "Nuclear energy: why is it trendy again?", where we talked about the renaissance in relevance that nuclear energy has been getting these past few years, and "A connection route between Nuclear and Aviation", where we explored the similarities between the aviation industry and the nuclear industry.

Figure 2. Pint of Science in Tarragona.

IV. SCIENCE WEEK

During Spanish science week (11-20 November) several activities were organised in both Madrid and Catalunya to motivate the knowledge of nuclear technology and its applications to a more general public. Since Spain is a country where nuclear is not always well received, these types of activities are essential for the good dissemination of the capabilities and uses of nuclear technology and for creating awareness about the benefits of this technology, not only in the energy sector but also in other fields such as medicine, industry, etc.

Since this initiative was celebrated during the expand of a week and a half in two different locations, the organization between the two branches of Spanish YGN and the different activities that were developed was key for reaching as many fronts as possible without affecting the scope of any of them.

A. Trillo NPP Simulator

In Madrid, the first activity program for this week was the visit to Trillo NPP simulator. Due to the size of the simulator, this activity was limited to 14 people and they were selected by registration order exclusively to prioritize equity in the selection process. The activity consisted of 2 parts, first an introduction to nuclear-based energy production and a practical example of several accidents on the simulator. The public there was taught how a NPP operator should react in case of an accident, how to use the operational manuals and the different jobs inside the control room of a NPP.

B. Seminar in Nuclear Medicine

At the Technical School of Industrial Engineers of the Universidad Politécnica de Madrid a seminar about nuclear medicine was held. This seminar was focused on radioisotopes and their use in medicine, for both diagnosis and therapy, as well as their production and the availability of these substances in Europe. For this activity, we counted on the help of several professionals from the field who work with these radiopharmaceuticals daily. Although this activity possessed a higher technical knowledge, both students and the general public participated in it since this seminar was designed to be easy to follow and precise.

C. Nuclear is “green”, now what?

In this activity we talked about the new wave of nuclear technology that has been growing in the recent years in the world. We talked about the new taxonomy in terms of economy, politics, institutional back-up, etc. This activity was conducted at Comillas University in Madrid. Thus, the target audience were students and people with previous knowledge on the economy and industry. Here we explored the future of nuclear technology in both Spain and Europe based on the actual tendencies of the industry and the predictions for the following years.

Figure 3. Nuclear is "green", now what? poster.

D. From Neuroscience to AI: A walk hand in hand with Ramón y Cajal

This year Science Week was dedicated to Santiago Ramon y Cajal, Spanish doctor and scientist who won the Nobel prize in 1906 thanks to his works in neuroscience and neural networks. As an homage to this great character, we organized a workshop where we talked about the neuronal networks and their similarities with Artificial Intelligence (AI). We explored the capabilities of both systems and how a better knowledge in neuroscience could lead to better AI performance and better future applications of this technology.

E. Visit to Vandellós II simulator and Vandellós I NPP

On November 11th, as part of the activities of the Science Week in Catalonia we organized a visit to the Vandellós NPP simulator, where attendees were able to experience what it was like to be an "Operator for a Day".

Figure 4. Visit at the Vandellós II simulator.

During the activity, concepts of nuclear energy were combined with demonstrations carried out by the audience themselves, such as scramming a reactor, loss of external electrical supply, and starting the emergency diesel generators.

We received very good feedback from the attendees, who were delighted to be able to put their newly acquired knowledge into practice and resolve any doubts they had about Nuclear Power Plants.

Then, we visited the site of Vandellós I, decommissioned nuclear power plant. It was the first commercial nuclear power plant in Spain and began operating in 1972. The plant consisted of one pressurized water reactor with a capacity of 435 MW. The plant operated for more than three decades. Today, the site serves as a museum, and continues to provide important lessons for the safe and efficient operation of nuclear power plants.

V. JJNN SOCIAL MEDIA

Jóvenes Nucleares is present on the major social media platforms such as Facebook, LinkedIn, and Instagram, with the largest number of followers on Twitter. In fact, in 2022, JJNN reached 12,000 followers on Twitter, and to celebrate this milestone, we hosted "Twitterfest", an Open Mic about the threads that generated more engagement between our followers.

Posts promoting events and initiatives receive very positive feedback, with many followers expressing interest in attending and supporting the organization. In addition, we have created several new sections, such as "Comic Fridays", where we post some original comics about nuclear energy, which have a great engagement between our followers, new infographics, short videos to show our activities and technical visits, and an advent calendar for Christmas.

Overall, Jóvenes Nucleares has a strong social media presence and a positive reputation among its audience. By continuing to post engaging content and expanding our presence on other platforms, they can further increase their reach and engagement with their target audience.

Figure 5. "Comic Friday" example.

VI. NUCLEAR TECHNOLOGY: SEMINAR AND WORKSHOP

The Young Generation are often the first to know about the latest technologies and with this new yearly seminar and workshop, Jóvenes Nucleares will bring the latest in the nuclear sector to the Spanish Public.

Neural networks have the potential to enhance the safety, reliability, and economics of nuclear power plants. However, their present applications are little known among most professionals in the nuclear sector and the general public. In this light, JJNN organized a seminar in which representatives from Tecnatom, ENUSA, IDOM, and Westinghouse explained how their respective companies benefit from the use of neural networks. Applications ranged from the design and optimization of a nuclear reactor core to lowering the cost of nuclear fuel fabrication. The event was attended by over 50 people and concluded with a cocktail aiming to promote knowledge transfer between attendees and speakers - one of the basic pillars of our organization.

The Workshop compliments the seminar as a more interactive counterpart, assistants to the Spanish Nuclear Society's main yearly congress could interact firsthand with the latest advances from 13 different companies big and small: ALISYS, ANAV, Azisa, Boost4pro, Enusa, Framatome, GE Hitachi, Iberdrola, Inetec, Innomerics, Siali, Tecnatom and Westinghouse. These innovative applications included robotics and drones for nuclear inspection and intervention, artificial intelligence applied to computer vision, and visual and augmented reality applied to plant visits, digital twins and training. This interactive experience was highly appreciated by both the companies and congress participants, touching and playing with technology is usually the best way to present it to the wider public.

Figure 6. Nuclear Technology workshop.

VII. Conclusions

The Spanish Young Generation in Nuclear, Jóvenes Nucleares, was founded in 1996 and has been active for more than 25 years of ever-increasing activity. 2022 was no exception, with increased social media presence, conferences, media appearances, bar talks, seminars, and a large list of other activities.

In particular this paper looks to summarise 2022's efforts by describing 5 activities:

1. Dead Operators Society: a debate club organised to train JJNN members for media appearances. In it, the main pro and anti-nuclear arguments are discussed, while undergoing debate practice sessions and drills.
2. Pint of Science: JJNN continues to contribute to this now classic event in our agenda, participating in its bar talks in Madrid and Catalonia.
3. Science week: several activities were organised in both Madrid and Catalonia to promote nuclear technology knowledge, including conferences and technical visits for the general public.
4. Social Media presence: JJNN continued to have increased social media presence in 2022, creating many engaging new initiatives for its followers.
5. Nuclear Technology seminar and workshop: a new yearly pair of activities of seminar and workshop on the latest and greatest nuclear technologies was launched in 2022.

JJNN will continue to promote the awareness and understanding of the numerous applications of nuclear science and technology in the coming years, by bringing together its activities and members, the organisation's two central pillars.

Proceedings of the European Nuclear Young Generation Forum
ENYGF'23
May 8-12, 2023, Kraków, Poland

NOMATEN Centre of Excellence in Multifunctional Materials for Industrial and Medical Applications — An international breakthrough partnership

Järvenpää, Jenna[1]*, Oksa, Maria[1], Alava, Mikko[2], Dollé, Frédéric[3], Gallé, Christophe[3], Moutiers, Gilles[3], Iljin, Kristiina[1], Jóźwik, Iwona[2], Kurpaska Łukasz[2], Papanikolaou, Stefanos[2] and Pruszyński, Marek[2]

[1] VTT Technical Research Centre of Finland Ltd (VTT), Finland; [2] National Centre for Nuclear Research of Poland (NCBJ), Poland; [3] French Alternative Energies and Atomic Energy Commission (CEA), France

*Corresponding author: *jenna.jarvenpaa@vtt.fi*

I. INTRODUCTION

Advanced multifunctional materials are essential for many industrial sectors. They enable advanced manufacturing processes for harsh environmental applications including, high temperature and pressure, corrosion and radiation, without adverse effects on infrastructure maintenance costs, energy consumption, and product purity. These materials meet also specific requirements on, e.g., light weight, recyclability, and biodegradability, which are also further needed in medical technologies, such as in cancer therapy.

The NOMATEN Teaming Phase 2 project is an international breakthrough partnership between the National Centre for Nuclear Research of Poland (NCBJ) and two leading non-Polish institutions: the French Alternative Energies and Atomic Energy Commission (CEA) and the VTT Technical Research Centre of Finland Ltd (VTT). It is funded by the Research Executive Agency (REA) under the powers delegated by the European Commission, and it supports the establishment of a world-class international Centre of Excellence (CoE) in Poland [1].

Together these NOMATEN Partners possess exclusive knowledge and long-term experience in material and radiopharmaceutical sciences for the front-line nuclear sector and close the gap between nuclear and non-nuclear applications. With four material and one radiopharmaceutical research groups of the NOMATEN CoE and the expertise of CEA and VTT, the NOMATEN Teaming Phase 2 project will foster Poland´s R&I performance and increase the international cooperation between Poland, Finland and France.

The established NOMATEN CoE in Multifunctional Materials for Industrial and Medical Applications will serve the needs of the growing energy, chemical, and pharmaceutical industries as well as nuclear medicine in Poland and the EU for innovative multifunctional materials via the generation, application, and dissemination of breakthrough research and innovation outputs. It also provides training for the next generation of experts (Masters and PhDs) and solutions for the challenges faced by the EU, such as increased energy consumption and increasing disease burden.

II. EXPERIMENTAL MATERIAL RESEARCH

Two of the NOMATEN material research groups focus on experimental research. The Functional Properties Group conducts X-ray diffraction experiments and data analysis with focus on materials subjected to high temperatures and radiation, integration of the results from structural and mechanical tests, multi-scale mechanical tests and predicting the material properties in real industrial installations. This research covers studies of structural elements used in nuclear reactors, e.g., fuel cladding and materials for the pressure vessel, chemistry and pharmaceutical industries. The research group also develops and conducts standardized tests and performs high-temperature mechanical, structural and thermal in-situ studies as a pioneer in Poland.

The research covers investigation of mechanical and structural properties of PLD manufactured amorphous alumina coatings, manufacturing of high entropy alloys via powder metallurgy techniques combined with Spark Plasma Sintering (SPS) and Arch Melting (AM) technique and studying the impact of radiation damage on functional properties of High Entropy Alloys (HEAs). The research group also studies the influence of specific features of Fe-Cr alloys on the microstructural changes induced by neutron surrogate to identify the features causing low-temperature hardening and subsequent embrittlement in F/M steels.

The research group studies the impact of radiation damage on mechanical and structural properties of newly developed HEA-ODS alloys as well as the impact of both radiation and temperature on corrosion kinetics of pure zirconium. It studies the behaviour of zirconium-based alloys used in nuclear reactors, the impact of the nanoprecipitate chemical composition on structural and mechanical properties of Oxide Dispersion Strengthened (ODS) steels and the impact of radiation damage on functional properties of NiFe single crystals.

It works in close cooperation with the NOMATEN Partners and other research groups, such as the Materials Characterization Group. The Materials Characterization Group is specialized in using a wide range of techniques, such as TEM

analysis, SEM/FIB/ESBD/EDX, to characterize, analyse and develop advanced multifunctional materials.

This research group uses a Helios 5 UX (Thermo Fisher Scientific) (Figure 1), which is a fully digital, Extreme High Resolution (XHR) Field Emission Scanning Electron Microscope (FE SEM) equipped with Focused Ion Beam (FIB) technology, Energy Dispersive X-ray Spectroscopy (EDS) and Electron Backscatter Diffraction (EBSD). This FE SEM allows the NOMATEN CoE to fast characterize nanometre-sized details and to use various analysis techniques, such as 2D, elemental (qualitative and quantitative) and crystallographic analysis (Figure 2).

The Materials Characterization Group´s research focuses on mechanical and electrical properties of polymer materials exposed to ionizing radiation, detailed characterization with Raman imaging of purity and degree of order of various types of graphitic materials intended for application in HTGR (high temperature gas reactor) technology, in-situ temperature studies of structural evolution of graphite as well as on surface and in-depth distribution of defects. Moreover, the research covers mechanically driven structural changes in model materials, and in-situ Raman spectroscopy study of the phase transformations in materials.

The research also includes, e.g., XRD study of the stress/strain and phase transformations in materials, structural studies of irradiated Fe, alumina coatings and HEA (NiFe binary systems) (Figure 3), SEM/TEM study of the tensile/stress influence on the irradiation defect formation in materials, in-situ SEM/EBDS studies of materials deformation and study of plastic deformation in Ni-based alloys with application of SEM-FIB-EBSD 3D reconstruction. These studies incorporate, e.g., the characterization of microstructure of different materials, such as pure Fe, steels, HEAs, and polymers, as well as studies on degradation of cable insulations at a nuclear power plant environment.

III. COMPUTATIONAL MATERIAL RESEARCH

The experimental research groups are supported by two computational material research groups. The Materials Structure, Informatics and Function (MASIF) Group focuses on four research avenues. The first avenue includes modeling of nanoindentation for advanced alloys by using state-of-art strategies and machine learning and the second avenue focuses on development of machine learning interatomic potentials (MLIP) for multiscale modeling applications. The third avenue covers material design by using machine learning methods. Its focus has been on hydrogen-related projects using density functional theory methods. Through these general methods, the MASIF Group has widen its international cooperation in the European Research Area (ERA) by co-authoring a M-ERA-NET project for hydrogen energy research. The fourth avenue consisting of web-app and software development for material informatics purposes is mainly targeted to the NOMATEN experimental material research.

The MASIF Group has a leadership position in Poland for materials informatic research and development of machine learning interatomic potentials (MLIP). It has organized the first Materials Informatics Conference in Poland in the NOMATEN premises (June 2022) and works systematically on state-of-art multiscale modeling approaches for advanced materials destined to be applicable at extreme conditions, such as high temperature and irradiation.

By contrast, the Materials´ Complexity Group works mainly on applying advanced computational, experimental, and data-analysis techniques including machine learning to nonlinear materials behavior. The research group´s recent examples include simulations of plasticity at fine dislocation densities to look for strengthening mechanisms and advanced, e.g., creep and fatigue, experiments where fractography and digital image correlation are exploited to look at how the material properties influence crack growth. The analysis of such data is conducted by artificial intelligence trials aimed to predict sample-to-sample response and ultimately the sample strength and lifetime.

This research group advances the NOMATEN CoE understanding of modern materials by offering computer simulations, concentrating on several key material systems, such as high-entropy alloys and metallic glasses, collaborating extensively within the NOMATEN partnership and with foreign collaborators, and by designing certain material characteristics, such as the strength properties.

Figure 1. Helios G5 UX by ThermoFisher Scientific at NOMATEN.

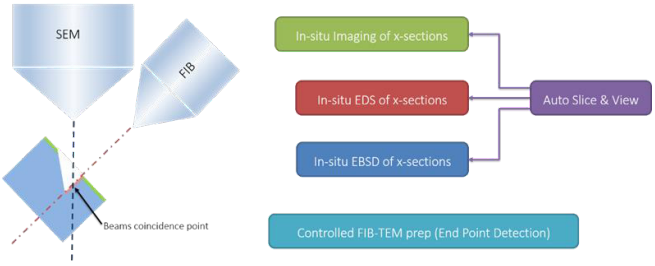

Figure 2. Schematics of the dual-beam concept (FIB-SEM).

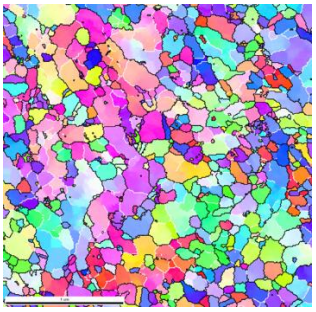

Figure 3. EBSD orientation imaging microscopy map of HEA obtained in transmission mode (Transmission Kikuchi Diffraction).

IV. RADIOPHARMACEUTICAL RESEARCH

The NOMATEN CoE and the Partners work together on development and translation research (pre-clinical and clinical trials) of imaging (PET, SPET) and therapeutic radiopharmaceuticals. As such, original low-molecular-weight molecules (< 500 Da) as well as engineered biomolecules (peptides, proteins including antibodies and derivatives) and nanoparticles are developed, all bearing dedicated radionuclides, to serve early detection of diseases as well as their better management in theranostic approaches.

The Radiopharmaceutical Research Group, together with researchers from CEA / JOLIOT (Service Hospitalier Frédéric Joliot (SHFJ) / BIOMAPS unit and Medicines and Healthcare Technologies department / Molecular labeling and bio-organic chemistry (SCBM) unit) focuses on the design, synthesis, and preclinical evaluation of novel diagnostic and therapeutic molecular radiopharmaceuticals for targeted, personalized medicine.

The research group has access to the Reactor Maria (and POLATOM facilities) and a modern 30 MeV cyclotron being installed this year as part of the CERAD project. This emerging research infrastructure of the NCBJ is unique on a national and European scale. As part of the NOMATEN partnership, it allows scientists access to reactor- and cyclotron-produced commercial radionuclides and gives the opportunity to initiate production of new radionuclides. This allows the NOMATEN CoE to become a leader in innovative drug technologies, notably for the treatment of cancer. The research group and its partners specialize in development of various chelating agents, prosthetic groups, labelled biomolecules and nanostructures, e.g., micelles and liposomes.

These nanostructures (especially those developed at CEA/SCBM) may be used as carriers of radionuclides and different chemotherapeutics or compounds which make cancerous cells more sensitive to, e.g., ionizing radiation or magnetic field. These nanostructures may also be decorated with biomolecules, permitting efficient *in vivo* targeting. The latter biomolecules may also be "directly" labelled with various radioisotopes. The consortium built around this research group is of utmost importance. A biosensor group from VTT has a unique expertise and access to invaluable production facilities of antibodies (full IgG) and derivatives (scFv) and CEA / BIOMAPS has already investigated and developed a series of labelled biomolecules.

The Radiopharmaceutical Research Group focuses also on target´s material preparation, radiochemical separation and target recovery, development of methods for radiolabelling and translation research. It will organize the first Radiopharmaceuticals Conference in Poland in the NOMATEN premises (October 2023) and is already sharing a first co-directed PhD with ADI Université Paris-Saclay co-tutelle program.

V. THE NOMATEN COOPERATION

The NOMATEN partnership between NCBJ, CEA, and VTT tackles two major challenges: maintenance of Europe´s long-term competitiveness in nuclear research and technologies and the translation of cutting-edge knowledge from the nuclear sector to provide results important for general industry and healthcare. Each Partner has its responsibilities in the NOMATEN Teaming Phase 2, e.g., NCBJ leads project management, research infrastructure and strategic research and innovation agenda, whereas CEA is responsible for capacity building programme and VTT for innovation-based sustainability work package. Each Partner is further introduced in the following subchapters.

A. The National Centre for Nuclear Research of Poland (NCBJ)

The National Centre for Nuclear Research (NCBJ, Narodowe Centrum Badań Jądrowych) represents fundamental/applied research profile that combines nuclear power-related studies with various fields of sub-atomic physics (elementary particle physics, nuclear physics, hot plasma physics etc.). The Centre is strongly involved in developing nuclear technologies and promoting practical applications of nuclear physics methods. Major market products manufactured in the Centre include radiopharmaceuticals and a range of particle accelerators for science, various industry sectors and medicine. The Centre is an IT and R& D background infrastructure, which provides expert support for decision-makers in developing nuclear power industry in the coming years in Poland. National Centre for Nuclear Research is the largest research Institute in Poland having over 1000 employees, about 70 Professors, holders of the Dr. hab. and post-doctoral degree as well as over 150 PhDs. NCBJ is also the only Polish research institution operating the only nuclear reactor (the MARIA reactor) in Poland.

B. The French Alternative Energies and Atomic Energy Commission (CEA)

The Atomic Energy and Alternative Energy Commission (CEA, Commissariat à l'Énergie Atomique et aux Énergies Alternatives), is a public establishment devoted to scientific, technical and industrial research and development, under the authority of the Ministries of Energy, Research, Industry and Defence [2]. CEA is today a major player in research, development and innovation in four areas: defense and security, low-carbon energies (nuclear and renewable), technological research for industry and fundamental research (material and life sciences). It conducts a part of its research in the framework of the French nuclear deterrent program. It also provides technology to strengthen security in the face of new hazards such as terrorism and cyberattack.

As a key player for energy research, CEA mobilizes its expertise and multidisciplinary competencies to propose innovative technological solutions to address major societal challenges, such as energy transition, nuclear and renewable energy, and understanding the mechanisms of climate change. CEA follows a research strategy encompassing the whole energy system, focusing simultaneously on means of electrical power production, both nuclear and solar, improving energy efficiency and dynamic adjustment of supply and demand through energy storage, the use of hydrogen, or smart power grids. Through the activities of the Division of Energies (DES), CEA is a key contributor to the development of 4th generation reactors, Small Modular Reactors

(SMR) and research reactor (JHR). It has, e.g., the internationally recognized JANNuS-Saclay triple ion beam facility, which can be used to study materials under irradiation.

CEA also mobilizes its expertise and multidisciplinary competencies to biotechnologies and biomedical innovations. Challenges linked to personalized medicine and technologies for the medicine of the future are priorities, and dedicated research are conducted in the field of *in vivo* molecular imaging probes, diagnostic tools and molecules for therapeutic or theragnostic uses. Methodologies devoted to isotopic labelling remains a specificity of CEA, both serving drug development and radiopharmaceutical development.

When *in vivo* imaging with Positron Emission Tomography (PET) is concerned, CEA (SHFJ / BIOMAPS) run dedicated laboratories (Figure 4) specialized for radiochemical processes and manufacturing of radiopharmaceuticals. These facilities are surrounded by preclinical and clinical imaging laboratories, all equipped with state-of-the art tomographs (Inveon (Siemens) µPET and µPET/CT, HRRT (Siemens) and Biograph (Siemens) PET, Signa (GE) PET/IRM).

C. VTT Technical Research Centre of Finland Ltd.

VTT Technical Research Centre of Finland Ltd is the leading research and technology company in the Nordic countries [3]. VTT uses its research and knowledge to provide expert services for the domestic and international customers and partners, and for both private and public sectors. VTT has over 2000 experts to develop new technological solutions. VTT's mission is to help customers and society to grow and renew through applied research. With over 80 years' experience supporting the clients' growth with top-level research and science-based results, VTT develops new smart technologies, profitable solutions and innovation services. VTT cooperates with the customers to produce technology for business and build success and well-being for the benefit of society. VTT has high variety of infrastructure for experimental work to support the cooperation within NOMATEN, including the irradiated and non-irradiated materials, as well as the research facilities for antibody development research in radiopharmaceuticals. There are two large research facilities on the energy materials: the Centre for Nuclear Safety (CNS) and the Research hall. The VTT Centre for Nuclear Safety is Finland's recent infrastructure to ensure safety and efficiency in nuclear power generation and radwaste management, including both experimental and computational R&D services. Unique set of sophisticated experimental facilities, like modern hot cells (Figure 4), analysis and modeling software can be used to cover research topics like new-built projects, operation and maintenance, decommissioning and waste management.

VI. CONCLUSIONS

Although material and radiopharmaceutical research and innovation topics of the NOMATEN CoE seem to be highly different, they still provide answers to similar research questions mainly related to using solids in extreme environments. The research and innovation outputs of the NOMATEN CoE will constitute a pedestal for future technologies in novel materials resistant to high temperature, corrosion, and radiation for industrial applications and in novel radiopharmaceutical materials for medical applications.

The international breakthrough partnership between NCBJ, CEA and VTT together with the continuous management of the strategic research and innovation agenda are the key to the NOMATEN CoE excellence and impact on Polish and European economy and society. The multidisciplinary nature of the research extends the NOMATEN partnership to other research institutes, such as the Institute of Nuclear Chemistry and Technology (ICHTJ) and the Radioisotope Centre POLATOM, as well as to external collaborations at industrial, national and international level, including Horizon Europe and Euratom instruments.

It is expected that these regional and global networks will result in establishing robust and long-lasting collaborations in nuclear materials investigation with leading institutions and preparing project proposals for the new Horizon Europe perspective.

Figure 4. Hot Cell facilities at CEA (top) and VTT (bottom).

VII. ACKNOWLEDGEMENTS

This project has received funding from the European Union's Horizon 2020 research and innovation programme under grant agreement No 857470.

VIII. REFERENCES

[1] NOMATEN. (2023). *NOMATEN MEANS NOVEL MATERIALS AND RESEARCH EXCELLENCE* [Online]. Available: https://nomaten.ncbj.gov.pl/

[2] CEA. (2023). *From research to industry* [Online]. Available: https://www.cea.fr/english

[3] VTT. (2023). *Welcome to VTT* [Online]. Available: https://www.vttresearch.com/en

Proceedings of the European Nuclear Young Generation Forum
ENYGF'23
May 8-12, 2023, Kraków, Poland

Global best practices to create a sustainable human resource pool as a guarantee of nuclear safety and security

Khuzhazhinova, Kamila[1]*and Verkhoturova, Vera[1]

[1] Tomsk polytechnic university (TPU), Russian Federation

*Corresponding author: *kamilakhuzhazhinova@gmail.com*

I. INTRODUCTION

The nuclear industry is currently undergoing a renaissance in those countries that once favored renewable energy. Thus, the number of nuclear and radiation f acilities will increase in the future [1]. Moreover, high-tech systems at these facilities are developed, which require a certain availability of qualified personnel pool, that should be trained in the shortest possible time.

An additional challenge for the nuclear industry is that in the near future the developing major high-tech corporations will be one of the main competitors in the labour market.

This, in turn, could affect the shortage of qualified personnel, which would consequently create problems in the sustainability of nuclear knowledge, leading to a conflict with the basic principle of the nuclear industry - ensuring safety and security.

Thus, this synopsis describes global best practices f or the nuclear and radiation regulators and companies to create a sustainable human resource pool in the nuclear industry as a guarantee of nuclear safety and security. The implication is that interactions with the younger generation will be effective when nuclear and radiation regulators and companies collaborate.

II. INFLOW OF YOUNG SPECIALISTS TO THE NUCLEAR INDUSTRY

The training of a qualified human resource is ba sed on a certain level of motivation among the younger generation who enrol in nuclear educational programs [2]. This factor can be influenced by the promotion of activities to f orm the public acceptance of nuclear technologies.

One non-obvious fact is that the sustainability of human resources in the industry depends on projects to form public acceptance of nuclear technologies [3]. Figure 1 details the impact of such projects, targeting different a ge groups, on the influx of specialists to the industry:

– kindergarten and school. At this level, the child's mindset is formed, an interest in nuclear technology and STEM are created;
– university level. It is the main subject of nuclear knowledge transfer. After university, students are employed in the nuclear industry;
– adults can both influence their children on the acceptability of nuclear technology and decide to apply to nuclear universities for further employment in the industry.

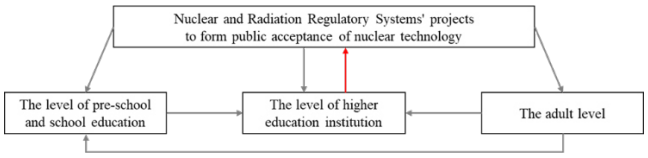

Figure 1. Schematic of the impact of public acceptance projects on the inflow of specialists to the nuclear industry

The following is a more detailed review of possible age-appropriate social acceptability projects based on the world's best practices. In parentheses are organizations with the names of projects that are currently being successfully implemented

A. Preschool and school education

At this stage it is important to create a positive thought image of nuclear technologies for the child through master classes. Schoolchildren from the age of 16 will begin to prepare for choosing a further educational institution, so it is recommended to take children of this age to enterprises under construction and in operation, to acquaint them with possible future professions (Électricité de France "Young HPC" and "Inspire", "Get to Know Nuclear is a Girl Scout" of the American Nuclear Society) [4, 5]. These m easures will attract young people to study STEM, a nd additional free online and offline courses in mathematics and physics will give them an equal access to educational resources ("Achieving Together with Optimistic Mentoring Program" mentor program of Dublin secondary school) [6]. The cut scene from the advertisement video of the "Young HPC" initiative of the EDF is shown in the Figure 2.

Figure 2. "Young HPC" program's advertisement video

To maintain the level of motivation in the study of the sciences will allow to conduct competitions with subsequent prizes:

– international nuclear quiz. The project is recommended to be held in an annual format, as a result of which it is possible to win an excursion to one of the operating NPPs, a trip to a children's camp ("International Nuclear Quiz" of Russia, the poster of which is shown in the Figure 3) [7];
– organization of a children's summer camp. Lectures on nuclear technologies will help familiarize the young generation with the basics and principles of the nuclear industry ("Appealing Light" of China national nuclear corporation (CNNC)) [8].

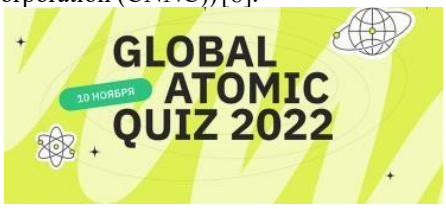

Figure 3. Poster of "Global Atomic Quiz" 2022

As a result of these activities, a pool of schoolchildren with a loyal attitude to nuclear technologies and a high STEM score will be formed. From this number of children by means of specialized tests can be selected students of the program to nuclear universities and on target training with the subsequent obligatory employment with the established time interval for working off the contract.

B. University

This level of the educational system is the main subject of nuclear knowledge transfer. Possible measures to in teract with current students are the following:

– scholarship programs to encourage the continuation of studies in the nuclear industry. This financial support will allow the student to cover basic needs by focusing on learning new material;
– olympiads and events of a competitive nature in the level of knowledge with subsequent prizes or opportunities for internships and practical tra in ing in the organization;
– career fair to introduce the current organizations for further employment in the nuclear industry;
– providing internship and practical training programs for students;
– creation of a community of nuclear university students to promote the image of nuclear education and the nuclear industry as a whole;
– holding thematic forums and events (the logotype of the "Workforce industry training" of Warton high schoolis shown in the Figure 4) [9].

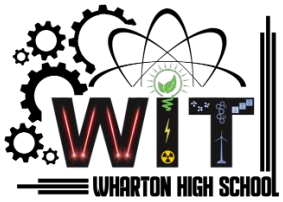

Figure 4. "Workforce industry training" logotype

All of the above measures are common practices already in use around the world.

C. Adult generation

In addition to the fact that the adult generation may decide to enroll in a nuclear university to begin a career in the nuclear industry, it may also affect family members, children included.

Interaction with this age group is possible through the following communication channels:

– a video project that presents on behalf of current workers in the industry about the opportunities of employment in the nuclear industry;
– a show in which scientists or nuclear industry employees answer the most popular questions f rom the public regarding nuclear technologies;
– a competition. One of the outstanding cases in the world history of shaping public acceptability is the challenge to the Leningrad NPP. In order to prove to the general public the safety of the plant, Russia organized fishing competitions in the water reservoirs closest to the NPP. After measuring the catch with dosimetry equipment, the participants were shown that the background radiation does not exceed permissible levels. Now, starting in 2019, such events, called "Crazy Flying Fishing", are held annually [10]. The Figure 5 shows a photo which was taken during this competition in 2022.

Figure 5. "Crazy Flying Fishing" competition

Successful cases of interaction with different age groups include the following:

– techno-art exhibition dedicated to innovation, engineering of the future and the people who create it ("Engineering as Art" of Informational Center of Atomic Energy) [11];
– information centers. Such centers can be located in the regions of the country to organize events educating the population in the field of nuclear technology and engineering (Informational Center of Atomic Energy of Russia) [12].

A distinctive approach to form public acceptability belongs to the China National Nuclear Corporation in organizing a series of anti-poverty projects. CNNC provides students with access to information resources and mentoring

programs. In addition, this corporation also provides funds to sponsor infrastructure and industrial development projects in nearby cities and poor villages. The use of goods and products from nearby villages, which are needed to supply employees during working hours a t the plants, allows consumption to be allocated in favor of supporting local production [13].

III. CONCLUSION

As a result of this synopsis, the following should be highlighted:

- the future human resource challenges f acing the nuclear industry can be addressed by increasing the motivation of young people to enrol in nuclear education programs through more activities to form public acceptance, starting from kindergarten;
- different age groups have certain fears and stereotypes about nuclear technologies. Also, the wa ys in which information can be effectively perceived are different depending on age, so a graded approach is recommended when organizing public acceptance activities for each age group;
- the implementation of effective measures to involve the younger generation into to the field of nuclear science and technologies will increase in the future of those, who will be employed in nuclear industry a nd thus will provide the industry with sustainable human resource pool for the future.

IV. References

[1] V. V. Velikorosov, E. V. Genkin, “Problems and prospects of nuclear power”, Economics and management: problems and solutions, vol. 2, no. 5, pp. 43-51, Feb., 2019.

[2] International Atomic Energy Agency, Knowledge Management and its Implementation in Nuclear Organizations , IAEA Nuclear Energy Series No. NG-T-6.10/ IAEA, Apr., 2016 [Online]. Available: https://www-pub.iaea.org/MTCD/Publications/PDF/Pub1724_web.pdf .

[3] D. Xia, Y. Li, Y. He, T. Zhang, Y. Wang, J. Gu, “Exploring the role of cultural individualism and collectivism on public acceptance of nuclear energy”, Energy Policy, vol. 132, pp. 2018 - 215, Sept., 2019.

[4] EDF Energy, EDF Inspire program [Online], Apr., 2021. Available: https://www.edfenergy.com/energy/nuclear-new-build-projects/hinkley-point-c/for-teachers-students-and-educators/inspire.

[5] The American Nuclear Society, Girl Scouts Get to Know Nuclear [Online], March, 2021. Available: http://nuclearconnect.org/know-nuclear/talking-nuclear/girl-scouts-get-to-know-nuclear-patch.

[6] Dublin secondary school, Achieving Together Optimistic Mentoring (ATOM) [Online], March, 2021. Available: https://www.dublinisd.us/Page/2347.

[7] Atomic energy 2.0, World Science Global Atomic Quiz [Online], Nov., 2021. Available; https://www.atomic-energy.ru/news/2021/11/09/119218.

[8] Social Responsibility Report, Appealing Nuclear power Beautiful China [Online], Apr., 2021. Available: https://en.cnnc.com.cn/pdf/AppealingNuclearPowerBeautifulChina.pdf.

[9] Wharton High School, Workforce industry training [Onlin e] , March, 2021. Available: https://www.whartonisd.net/domain/418.

[10] Rosatom Country, Fishing near the Leningrad PP [Online], Sept., 2022. Available: https://strana-rosatom.ru/2022/09/20/ryba-iskala-gde-glubzhe-kak-proshla-ryba/.

[11] Atom Calendar, Nuclear technologies in a modern art [Online], Aug., 2020. Available: https://calendar.atom75.ru/25-sentyabrya/kollaboratsiya-iskusstva-i-inzhiniringa.

[12] MyAtom, About Informational Center of Atomic Energy [Online]. Oct., 2022. Available: https://myatom.ru/%d0%be%d0%b1-%d0%b8%d1%86%d0%b0%d1%8d/.

[13] CNNC, CNNC promotes poverty alleviation [Online], Jun e, 2019. Available: https://en.cnnc.com.cn/2019-06/05/c_548206.htm

Proceedings of the European Nuclear Young Generation Forum
ENYGF'23
May 8-12, 2023, Kraków, Poland

Competence Building for Accelerated SMRs' Deployment

Ozerina, Milana[1*]

[1] National Research Nuclear University MEPhI

*Corresponding author: *milanaozerina24@gmail.com*

I. INTRODUCTION

Globally, policymakers, energy analysts, and the machinery industry, including private sector enterprises, are showing increasing interest in the potential of small modular reactors (SMRs) as a competitive element of low-carbon technologies to be used in future integrated power systems. The SMRs embody hopes for inherent safety, simplification, and standardization properties that can substantially facilitate and make more cost-effective commissioning of advanced nuclear power plants (NPP) based on SMRs [1].

According to the International Atomic Energy Agency (IAEA), as of December 2022, there are 83 SMR projects in the world that are at different stages of development [2]. Some projects are planned to be implemented until 2030; others that are in the early stages of development will be implemented until 2050, which is stimulated by countries' commitment to the Paris Agreement. Nevertheless, regardless of the timing of the implementation of SMR projects, it is obvious that a large amount of qualified human resources will be needed for their deployment.

The development of an effectively competent workforce is one of the fundamental conditions of success for any nuclear power programme (NP programme). Without capable manpower, no NPP can be designed, built, or operated appropriately, and nuclear safety and reliability of power production cannot be assured. The amounts and qualifications of manpower required for a successful NP programme are usually underestimated, and the resulting shortage of manpower is a restraint on the development of nuclear technology, especially in developing countries. A newcomer country must determine its true manpower requirements within the context of the proposed NP programme and assess the existing organizational, educational, and industrial capabilities for meeting these requirements before embarking on its first NP programme. Manpower development for domestic participation in the NP programme should be considered within the broad context of the national industrial development strategy and its overall manpower requirements [3].

The topic of competence building for accelerated SMRs' deployment is necessary to help strengthen management systems, human resource development, and stakeholder involvement for nuclear infrastructure in embarking states, as well as provide support to expanding NP programmes and assure safe, reliable, and sustainable NPP operations. To keep up with the timeline, since 2011 courses in SMRs have been developed in Russia with the goal of raising awareness among participants about the use of SMRs and various processes associated with their performance. This article analyzes existing Russian competence-building programmes, which were originally aimed at large NPPs, and makes recommendations for adapting them to SMR deployment.

II. FORECAST OF NUCLEAR TECHNOLOGIES DEVELOPMENT

In 2022, the share of nuclear generation in the energy mix was 10% [4]. According to the IAEA's high projections, global nuclear electricity generating capacity will increase by 82% by 2050 to 715 GW(e), accounting for 11% of global electricity generation. The low case projected a decrease of 7% to 363 GW(e), representing a 6% share of global electricity generation [5] (see Figure 1).

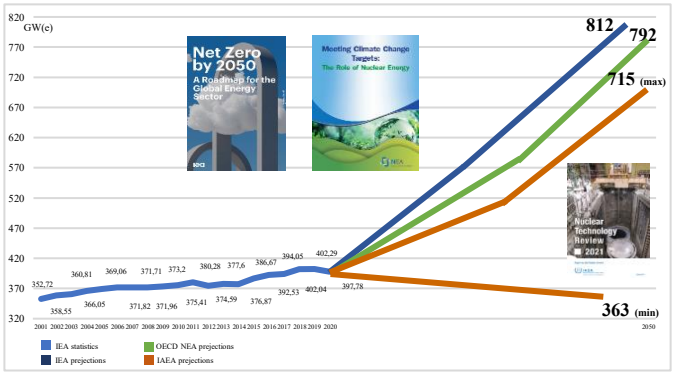

Figure 1. Global nuclear electricity generating capacity projections [5][6][7]

The International Energy Agency (IEA) projects an increase to 812 GW(e) by 2050, representing a 2% share of global electricity generation [6].

The OECD (Organization for Economic Co-operation and Development) Nuclear Energy Agency (NEA) projects the global nuclear electricity generating capacity to be 792 GW(e) by 2050 [7].

Within the identified share of global electricity generation, nevertheless, the majority of projections assume a significant increase in nuclear power generation capacity. In this case, the most realistic way to achieve this goal is through accelerated SMR deployment.

Among the drivers of SMRs' development are some of their specific characteristics. They can be deployed gradually to match rising energy demand, resulting in moderate financial costs. SMRs show the prospect of significantly reducing costs through their modular design, which should reduce construction time and costs. SMRs are also considered for several non-electrical applications, like hydrogen production and municipal and industrial heat generation. Some designs may also serve niche markets, for example, by deploying micro-reactors to replace diesel generators on small islands or in remote regions. SMRs are also a good option for replacing existing coal plants worldwide, thereby reducing the carbon footprint.

The market expectations for SMRs are also associated with exports to countries with weak energy networks and little experience in the development of nuclear energy, which is possible due to the small size and peculiarities of the passive safety systems. Nowadays, primarily developed countries are pursuing a green energy transition policy. But the prospects of non-power applications, cogeneration, and applications for electricity production in remote places are incentives for SMR market development in other countries. A reduced footprint of NPPs with SMRs allows not only to expand the circle of customers who can afford a NPP financially and in terms of compatibility with the size of their power grid, but also to change the attitude of the population towards nuclear energy.

According to estimates by the National Nuclear Laboratory (NNL) of the United Kingdom (UK), by 2035, the SMR's market will be between 300 and 500 billion dollars. For comparison, the size of the global renewable energy market by 2035 will be approximately 650 billion dollars, according to IEA estimates [8].

Below are several examples of the national SMR-related programmes with the objective of achieving a substantial share of the future market.

In 2017, the NNL conducted an analysis of the technical maturity and applicability of the existing SMR projects in the world at that time according to the criteria of their readiness for justifying safety according to existing approaches, technical risks, resources available to developers, and economic prospects [9]. As a result, in 2018, a programme was launched to create an infrastructure for SMRs, which includes, first, setting up legislation to simplify their licensing process.

In Canada, in 2018, a roadmap for SMRs aimed at creating a SMR industry was published, and it projects the construction of SMRs between 2025 and 2040 [10]. As in the UK, the work so far is aimed at optimizing the licensing process, reducing the technical risks and costs of SMRs, and breaking the deadlock of Canada's nuclear industry, which has unique experience in building heavy water reactors that finally lost the market to light water reactors about 15 years ago.

The United States of America (USA) is actively engaged in SMRs' development, demonstrating this by the large number of projects, as one can see in Figure 2.

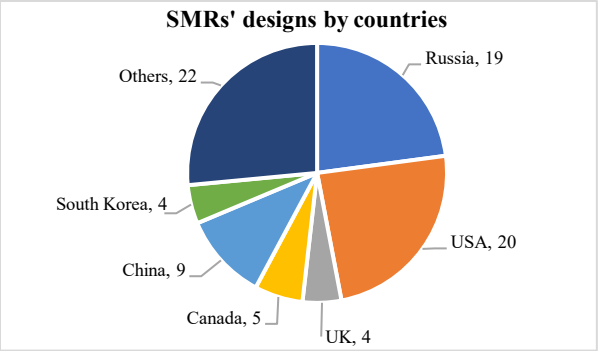

Figure 2. Number of SMRs' designs by countries as of January 2023 [2]

Recently, the USA introduced an initiative named the Foundational Infrastructure for the Responsible Use of Small Modular Reactor Technology (FIRST) with the aim to ensure that nations around the world can build and expand civil nuclear programmes with safe, secure, and transparent partnership options [11].

In the European Union, there is a well-accentuated trend to establish an industrial alliance to promote European SMR NUWARD, which is a French design, in cooperation with regulatory bodies of Finland and the Czech Republic [12].

As for the designs under construction, it is worth mentioning the CAREM project in Argentina, an illustrative example of new vendors with ambitions to achieve a substantial share of the market [13].

Within the SMRs currently being operated, the Chinese projects HTR-10 and HTR-PM started in 2000 and 2022, respectively. The last one belongs to the Generation IV family [14].

The main advantages of Russia in SMR domain are commercial operation of floating NPP (FNPP) (KLT-40S started in 2020), serial production of RITM-200 for the icebreaking fleet, and construction of the fast lead-cooled BREST-300, which started in 2020, see Table 1. Among the Russian projects under development are SHELF, VITYAZ, ATGOR, SVBR-100 and ABV-6.

Table 1. SMRs in operation [2]

№	Name	Capacity	Reactor type	Company and country	Fuel
1.	KLT-40S	35 MW(e)	PWR	OKBM Afrikantiov, Russia	HALEU (18,6%)
2.	HTR-PM	210 MW(e)	HTGR	INET, Tsinghua University, China	HALEU (8,5%)
3.	HTR-10	2,5 MW(e)	HTGR	INET, Tsinghua University, China	HALEU (17%)
4.	HTTR	30 MW(t)	HTGR	JAEA, Japan	HALEU (6%)
5.	RITM-200	50 MW(e)	PWR	OKBM Afrikantiov, Russia	HALEU (14%)
6.	KLT-40	35 MW(e)	PWR	OKBM Afrikantiov, Russia	HEU (30–40%)

III. READINESS OF SMRs FOR ENTRY INTO THE MARKET OF NUCLEAR POWER REACTORS

According to the IAEA, 55% of SMR projects will use HALEU fuel (High-Assay Low-Enriched Uranium, with enrichment between 5% and 20% with U-235), see Figure 3 [2].

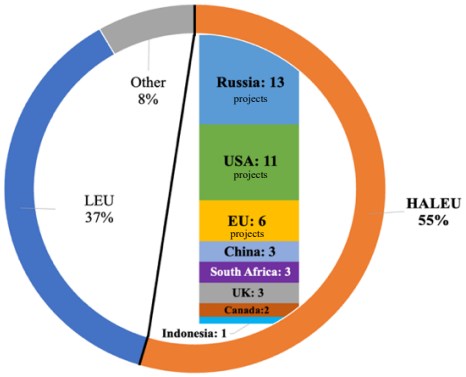

Figure 3. Fuel for SMRs [2]

Currently only Russia can commercially produce HALEU fuel. In the future, the USA plans to create an infrastructure for the independent production of HALEU fuel. For experimental reactors and the first SMRs in the USA at the turn of 2030 and later, fuel was planned to be purchased from Russia. However, in October 2022, the USA announced that it was trying to replace Russian HALEU fuel [15]. According to TerraPower plans, they are oriented on the independence of Russian HALEU supply, which leads to a delay in the commissioning of the Natrium reactor (345 MW) for at least 2 years [16].

Licensing is also an important issue for the deployment of SMRs, since the cost of a license for development, construction, and operation is comparable to the cost of large reactors. The existing regulatory framework is designed for large reactors and may deter the potential deployment of SMRs. In particular, the requirements for each site may present difficulties for assembling identical units based on the reference design.

As innovative technological concepts and designs, including SMRs, are technically diverse, the IAEA is working to create a technologically neutral safety framework to promote harmonization of international approaches based on existing IAEA safety standards [17].

IV. CAPACITY BUILDING FOR ACCELERATED SMRS' DEPLOYMENT

A. Training courses on SMRs in Russia

Training courses on SMRs has been conducted since 2011, when the technical workshop on «The Development of Curricula for Training of Foreign Specialists in Small-Power Nuclear Plants in Russia» was held. In 2013, a five-day training seminar on «Introduction to the Liquid Metal Fast SMR Technology» was held, where 14 specialists from Italy, Poland, China, Spain, Germany, Turkey, the Czech Republic, Malaysia, Serbia, and Singapore took part. It was the first public-private partnership in competence building for the advanced fast reactor SVBR-100, which is a civil application of navy propulsion technology. In 2015, a five-day training course on «The Assessment of Advanced Pressurized Water Reactors Utilization in New-Comer Countries» was conducted for ASEAN (Association of South East Asian Nations) countries. In 2016, a scientific visit on floating NPP and fast reactor SMR technology was organized in cooperation with the IAEA. And in 2017, four events on the topic of SMRs were held: three training courses on HTGR/SMR technology and a scientific visit on SMRs and floating NPP for ASEAN countries. In February 2020, a four-day training course on «Simulation Codes for Safety Assessment of SMR and VVER-type reactors» was organized on the premises of the Indonesian Polytechnic Institutes of Nuclear Technology.

In 2022, using distance learning methods, a hybrid Interregional Training Course on Fuel Design Optimization and Fuel Cycle Options for SMRs was successfully held, in which 35 specialists (17 in person and 18 online) from 18 countries took part. As part of the training course, a technical tour was organized, where the participants got acquainted with the technological processes for the manufacture of fuel pellets, fuel elements, and fuel assemblies for further delivery to NPPs.

B. Training courses on SMRs abroad

The IAEA, being a global hub for exchange in peaceful nuclear technologies is spearheading training programmes with the development and distribution of simulation software and training courses. In 2016 a joint IAEA- Arab Atomic Energy Agency SMR Safety and Licensing was held with the main focus on the status of development of selected SMR designs, the safety requirements in the USA, Canada and South Korea, siting and environmental issues, and the historical licensing process in the USA, and its evolution [18]. Later in 2016 the same workshop was orginized with the Forum of Nuclear Regulatory Bodies in Africa, it also featured economic considerations as calculated by the OECD NEA [19]. In 2017 the subject workshop was held in Jakarta, Indonesia and was hosted by BAPETEN, the Indonesian nuclear regulator [20]. In this regard, it can be concluded that these courses are aimed more at regulators and do not include important aspects of the nuclear fuel cycle (NFC).

C. Experience in training personnel for floating NPP with KLT-40S

The world's only FNPP «Akademik Lomonosov» was commissioned in Russia in 2020 [21]. This project has no analogues anywhere in the world. The NPP consists of a floating power unit (FPU) and coastal infrastructure. Two icebreaker PWR reactors KLT-40S are installed on board. In 2018, the first FNPP crew was trained. In September 2022, Russian specialists carried out work to analyze the vulnerability and assess the effectiveness of the physical protection system of the FNPP.

Thus, Russia has accumulated unique experience in training personnel for NPPs both for the Russian Federation and for

foreign countries on a bilateral basis or with the cooperation with the IAEA.

D. Lessons learned

To improve the quality of events, feedback is collected from participants after each event. Thus, for all training activities on the topic of SMRs, the highest assessment was obtained from participants, including regarding training programs and the selection of lecturers.

As possible improvements, there were suggestions regarding waste management issues for spent nuclear fuel from SMRs, safeguadrability of SMRs, including BREST-300, which provides an option of a closed NFC within the perimeter of a NPP, and an assessment of the economic feasibility of SMRs for remote places based on the cost of the final product, for example aluminum production from bauxite to smelting.

In 2023, it is planned to hold seven more training courses on SMRs on a wide range of topics (see Table 3). All courses will be conducted jointly with IAEA with focus on developing countries.

Table 3. Training courses on SMRs in 2023.

№	Type	Title
1	Training course	Integrated justification of SMRs' development within the national energy system, including the formation of strategies for the decarbonization of the energy sector, using the IAEA INPRO tools
2	Training course	Cost-effective Solutions in the Radioactive Waste Management for Near-Term Deployable SMRs; Decommissioning by Design
3	Training course	Application of INPRO NESA Methodology for Sustainability Assessment of SMRs and Microreactors
4	Training course	Energy planning and use of Agency tools to model electricity systems meeting demand and climate objectives for SMRs
5	Workshop	Specific Design Considerations of Nuclear Cogeneration Projects using SMR\MR
6	Training course	SMR Safety Training (technology specific aspects including design safety, safety analysis, waste management and decommissioning)
7	Training course	Design Features of Transportable SMRs

V. CONCLUSION

Now, Russia is one of the leaders in the nuclear energy technology market as a whole and a leader in the construction of SMRs. The SMR market is only in its infancy. However, with carbon price pressure on traditional power, competition to acquire a share of the market is already underway around the world. Milestones of this competition are already well-defined by the Paris Agreement, and the first referent SMRs will start opearion around 2030. It means now is the time for human resources development and staff training. It is a time-consuming process, and for the world to be ready for the full-scale implementation of the SMRs, not only from a technical point of view but also from the point of view of rich personnel potential, we need to start now.

Based on the study, it is also possible to draw the conclusion that, at the moment, in the world, there are not so many courses on SMRs. It is necessary to change this situation by exchanging experiences between countries with competencies in this area. Existing international initiatives are mainly aimed at simplifying the licensing process and harmonizing regulations, but it is necessary to think about an initiative in terms of knowledge management. Existing international initiatives (e.g., NHSI – Nuclear Harmonization and Standardization Initiative [22] and FIRST) are mainly aimed at simplifying licensing and harmonization, but it is necessary to think about an initiative in terms of knowledge management and human resources development. Such an initiative under the IAEA could bring together countries involved in the development of SMR projects and strengthen dialogue between them in order to form training courses, scientific visits, and other educational activities. In this regard, Russia could play a significant role within such an initiative considering the vast experience it has not only in the development, manufacturing, and operation of SMRs but also in conducting training activities on this topic.

VI. REFERENCES

[1] IAEA, Small Modular Reactors: A new energy paradigm, Pre-print, Access: https://nucleus.iaea.org/sites/smr/Shared%20Documents/SMR%20Booklet_22-9-22.pdf

[2] IAEA, Advances in Small Modular Reactor Technology Developments, A Supplement to: IAEA Advanced Reactors Information System (ARIS), 2022 Edition, September 2022

[3] IAEA, Manpower Development for Nuclear Power, A Guidebook, Technical reports series No. 200, Vienna, 1980

[4] World Nuclear Association, Nuclear Power in the World Today, January 2023, Access: https://world-nuclear.org/information-library/current-and-future-generation/nuclear-power-in-the-world-today.aspx

[5] IAEA, Nuclear Technology Review 2021

[6] IEA, Net Zero by 2050, A Roadmap for the Global Energy Sector, 2021

[7] OECD NEA, Meeting Climate Change Targets: The Role of Nuclear Energy, 2022

[8] IEA, Energy Technology Perspectives 2023, January 2023

[9] National Nuclear Laboratory, Small Modular Reactors: Techno-Economic Assessment, 7 December 2017, Access: https://www.gov.uk/government/publications/small-modular-reactors-techno-economic-assessment

[10] Natural Resources Canada, A Call to Action: A Canadian Roadmap for Small Modular Reactors, Canada, November 2018

[11] U.S. Department of State, Joint Statement on the New Clean Energy and Nuclear Security Collaboration under the Foundational Infrastructure for Responsible Use of Small Modular Reactor Technology (FIRST) Initiative, 4 April 2022, Access: https://www.state.gov/joint-statement-on-the-new-clean-energy-and-nuclear-security-collaboration-under-the-foundational-infrastructure-for-responsible-use-of-small-modular-reactor-technology-first-initiative/

[12] EDF, NUWARD™ SMR, leading the way to a low-carbon world, 2023, Access: https://www.edf.fr/en/the-edf-group/producing-a-climate-friendly-energy/nuclear-energy/shaping-the-future-of-nuclear/the-nuwardtm-smr-solution/the-solution

[13] World Nuclear News, Construction of Argentina's CAREM-25 unit to restart, 8 November 2021, Access: https://www.world-nuclear-news.org/Articles/Construction-of-Argentinas-small-CAREM-25-unit-to

[14] World Nuclear News, China's demonstration HTR-PM reaches full power, 9 December 2022, Access: https://www.world-nuclear-news.org/Articles/China-s-demonstration-HTR-PM-reaches-full-power

[15] Reuters, U.S. developing domestic uranium strategy, 26 October 2022, Access: https://www.reuters.com/markets/us/us-developing-domestic-uranium-strategy-energy-secretary-2022-10-26/

[16] Nuclear Newswire, TerraPower announces delay due to lack of fuel availability, 19 December 2022, Access: https://www.ans.org/news/article-4589/terrapower-announces-delay-due-to-lack-of-fuel-availability/

[17] Official web-site of the IAEA, Accelerating SMR Deployment: New IAEA Initiative on Regulatory and Industrial Harmonization, 1 April 2022, Access: https://www.iaea.org/newscenter/news/accelerating-smr-deployment-new-iaea-initiative-on-regulatory-and-industrial-harmonization

[18] International Regulatory Development Partnership, Workshop on Small Modular Reactor (SMR) Safety and Licensing, 2016, Access: https://www.irdp-online.org/news/workshop-small-modular-reactor-smr-safety-and-licensing

[19] International Regulatory Development Partnership, Workshop on SMR Safety and Licensing for FNRBA, Access: https://www.irdp-online.org/news/workshop-smr-safety-and-licensing-fnrba

[20] International Regulatory Development Partnership, Workshop on SMR Safety and Licensing for ANSN, Access: https://www.irdp-online.org/news/workshop-smr-safety-and-licensing-ansn

[21] Rosatom Newsletter, FNPP in Operation, June 2020, Access: https://rosatomnewsletter.com/2020/06/29/fnpp-in-operation/

[22] Official web-site of the IAEA, IAEA Initiative Sets Ambitious Goals to Support the Safe and Secure Deployment of SMRs, 4 July 2022, Access: https://www.iaea.org/newscenter/news/iaea-initiative-sets-ambitious-goals-to-support-the-safe-and-secure-deployment-of-smrs

Hot Topic 4
Future nuclear

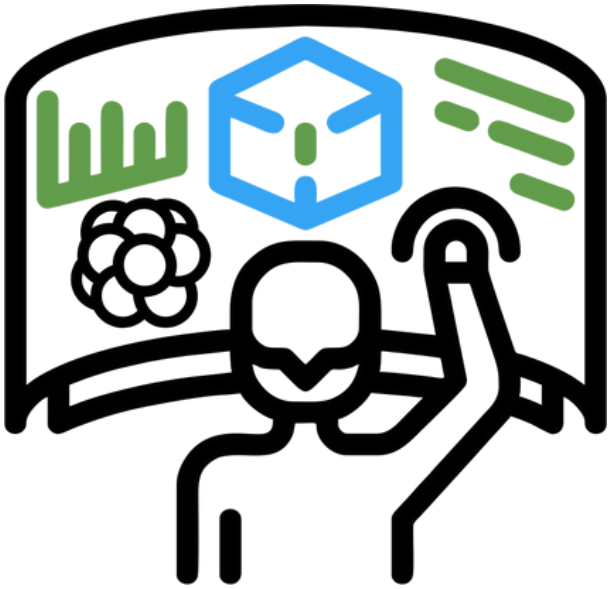

Proceedings of the European Nuclear Young Generation Forum
ENYGF'23
May 8-12, 2023, Kraków, Poland

Small Modular Reactors (SMRs) for the Future and Development of Saudi Arabia

Al-Salhabi, Abdalaziz[1*], Alhabib, Ahmad[2], Alharbi, Talal[1], Aljohani, Mohammed[1], Shams, Afaque[1,3] and Al-Athel, Khaled[1,4]

[1]Mechanical Engineering Department, King Fahd University of Petroleum & Minerals, Dhahran 31261, Saudi Arabia; [2]Chemical Engineering Department, King Fahd University of Petroleum & Minerals, Dhahran 31261, Saudi Arabia; [3]Interdisciplinary Research Center for Renewable Energy and Power System (IRC-REPS), KFUPM, Dhahran 31261, Saudi Arabia; [4]Interdisciplinary Research Center for Advanced Materials (IRC-AM), KFUPM, Dhahran 31261, Saudi Arabia

*Corresponding author: Abdalaziz.alsalhabi@gmail.com

I. INTRODUCTION

Nuclear energy (NE) is essential to establish a powerful carbon-free supply. NE can substitute power sources that emit CO_2, such as oil and coal since the emissions produced by these sources are increasing daily with the increase of population worldwide. While NE, a very clean energy source, contains almost no air pollution content while operating. Furthermore, NE is a more reliable power source due to the high-capacity factor compared to natural gas, wind, and solar, and also due to less maintenance required and a more extended refuelling period.

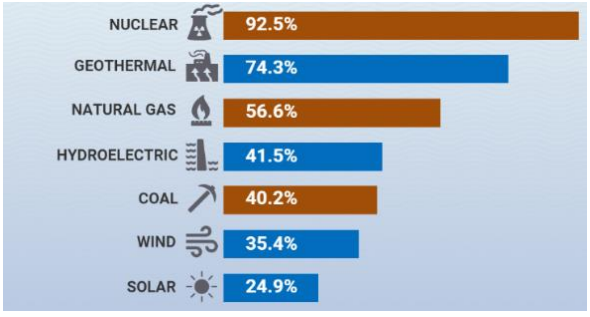

Figure 1. Capacity factor by energy source – 2020 [1]

Although nuclear power is safe, few disasters have been encountered previously. The significant events of the three known disasters related to nuclear power that frightened the people, TMI, Chornobyl, and more recently, Fukushima, accelerated the process of enhancing and improving nuclear technology. For example, improving and implementing more advanced safety systems with redundancy, diversity, and independence, reducing the construction time for building a nuclear reactor, and designing new innovative nuclear technologies that can provide more flexibility and safety for more applications than large reactors.

For instance, Small Modular Reactors (SMRs) are smaller nuclear fission reactors with a unique design having an electrical power of around 300 MW_e and up to 1000 MW_{th}. With small footprints, SMRs have the potential to be built more quickly and safely in factories with less construction time and can fit in trucks and shipping containers. In addition, SMRs could reduce costs, even the start-up cost, by starting with a single unit and adding additional units incrementally if the load on the grid increases. Moreover, SMRs have the potential to decrease the risk of delays in the construction of the power plant and provide many distinguished technological advances due to the flexibility of modular construction compared to large nuclear power plants [2].

On the other hand, the Kingdom of Saudi Arabia (KSA) depends mainly on fossil fuels to produce electricity. As a result, the CO_2 emissions in 2020 were around 575 million tonnes. However, with Saudi Arabia's 2030 vision, the Kingdom will reach net zero carbon emissions by 2060. To fulfill this plan, a clean and sustainable power source in Saudi Arabia is required, and the Kingdom selected nuclear power along with other sources.

Furthermore, KSA has the potential to produce the Yellowcake, which is a mixture of powder form of uranium oxides with almost 85% of U_3O_8 that can be converted to a suitable fuel. Also, KSA already built the uranium extracting facility to meet the future vision [3].

Nuclear energy will be necessary for Saudi Arabia's development by departing from fossil fuels. SMRs, as part of it, will contribute considerably to the Kingdom for various applications. For instance, to develop desalination, to increase the power for existing power plants, and to

provide power for far-distanced places in the Kingdom with zero carbon emissions.

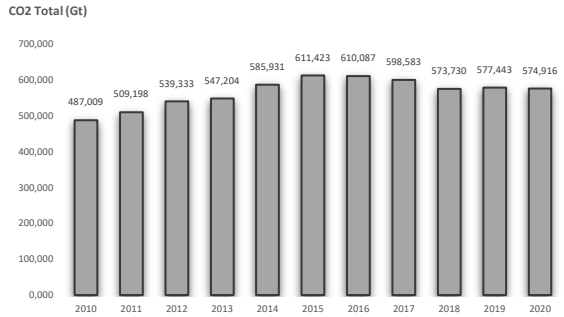

Figure 2. CO_2 total emissions in KSA for the last decade [4]

II. TECHNOLOGIES USED IN SMR CONCEPTS

SMR concepts use large reactor technologies with enhanced safety and higher operational performance. The concept behind SMRs varies depending on the type of the reactor, which could be water-cooled reactors like PWR or Advanced Modular Reactor (AMR) using generation IV technologies such as LFR, HTGR, SFR, and MSR. Furthermore, the concept is called Micro Modular Reactor (MMR) if the generated power is limited between 1 to 20 MW_e. The variation is not restricted to the type because the coolant also plays a huge role. The selected type of coolant (water - gas - liquid metal - molten salt) is based on the reactor type, design, and application.

III. DESIGNS OF SMRS

Currently, two reactor designs in operation are classified as SMRs. Firstly, the KLT-40S reactor by Russia for a floating nuclear power plant (NPP) [5]. This reactor, a twin unit for the plant configuration, produces 2 x 35 MW_e for Russian marine propulsion. KLT-40S uses PWR as a type and light water as a coolant and moderator. The second SMR reactor design in operation, using helium gas as coolant and graphite as a moderator, is HTR-PM by China, which produces 210 MW_e to supplement PWRs and co-generation using HTGR technology. For both reactor designs, there are two reactors of each in operation.

Also, there are reactors under construction, like the CAREM reactor and the ACP100 reactor, and both use PWR type. Furthermore, many conceptual designs exist regarding the design of SMRs, for example, the integral SMR and Aurora reactor.

IV. SAFETY, FUEL CYCLE AND WASTE MANAGEMENT

Safety is essential for any power plant, especially when discussing NPP. Through the years, NPPs have devoted enormous efforts to provide design solutions and innovative features that can improve safety. SMRs, as advanced reactors, have some innovative features that potentially will enhance safety. For most SMRs, one of the features is the passive cooling system, in which no electrical supplies are required to cool the reactor because electrical supplies are a significant issue during accidents. Nevertheless, the passive safety system allows the achievement of the cooling process using gravity and natural convection. This passive system can reduce the cost and the maintenance required for the reactor.

The experience gained from current reactors and NPPs developed the reactors regarding the fuel cycle and waste management. The operation cycles extended between refuelling in many SMR concepts compared to large reactors. Different examples of SMRs with long refuelling cycles, such as KLT-40S, which has a refuelling cycle of 30 to 36 months, are mentioned in [6]. Some ideas propose the usage of reprocessed fuel coming from LWRs to decrease the amount of spent fuel further.

Spent fuel from SMRs is dealt with similarly to that from large plants. For countries that have existed nuclear power programs, the process of dealing with spent fuel should be manageable due to the experience. On the other hand, countries that are new to nuclear energy need to think carefully about spent fuel management and set up a suitable infrastructure.

V. SMRS AGREEMENTS IN SAUDI ARABIA

The nuclear power program began in Saudi Arabia in 2010 through KACARE (King Abdullah City for Atomic and Renewable Energy). KACARE has been established to take responsibility for initiating oil alternative sources, nuclear energy, and radiation waste programs. In addition, a virtual nuclear reactor was built in Riyadh for research at King Abdul-Aziz City for Science and Technology (KACST). Furthermore, the Saudi Nuclear Energy Holding Company (SNEHC) has been created to administrate the nuclear power program in the Kingdom. Within this period, Saudi Arabia has made many contracts and agreements with several countries to contribute to building nuclear reactors with different power outputs.

Regarding large reactors, the objective is to construct the first two nuclear reactors with a capacity of 3.4 GW by 2032. According to authorities, the new facilities will be created with the most up-to-date technical standards and the strictest safety procedures [7].

Regarding SMRs, KSA has made a couple of agreements about construction in the country. Starting with the agreement signed in 2015 between South Korea and KSA regarding specific SMR type designed by KAERI SMART (System Integrated Modular Advanced Reactor) [8]. SMART is a passive safety system reactor that can produce up to 330 MW_e gross, refuelling time estimated every three years. The reactor has a design life of around 60 years and three years of construction, which is low compared to large reactors. SMART has a distinct design from other reactors. The steam generators and the pressurizer are inside the vessel. The core is 2 m in length and consists of 57 fuel assemblies. The design allows some of the heat produced in the reactor to be used for water desalination. Furthermore, SMART is composed of four safety injection systems, two shutdown cooling systems, two emergency diesel generators, four residual heat removal systems, and a containment spray system.

Also, two agreements were signed with China in 2016 and 2017 to initiate and facilitate building of a new small

modular reactor called HTR-PM (High-Temperature reactor pebble-bed module). The first agreement is for constructing the reactor in Saudi Arabia. In contrast, the second was signed in March 2017 to study the project's feasibility. The construction duration of the reactor is estimated to be five years. China started building the reactor in late 2012 in Shandong Province to be fully operational by the end of 2017.

Argentina is another country that signed an agreement with Saudi Arabia in 2015 to launch an Argentinian-designed modular reactor, a new type of SMR called (CAREM). The agreement came from the cooperation between Saudi company "Taqnia" with Argentinian one "Invap" to establish a joint-venture company called "Invania," which is the responsible company for developing this PWR nuclear reactor [9]. The electrical capacity of CAREM is 27 MW_e, and the enrichment of the fuel is about 3.4% of Uranium-235. The refuelling process is annual. One of the advantages of this SMR is the natural circulation, meaning no requirements for pumps.

VI. USES AND APPLICATIONS OF SMRS IN SAUDI ARABIA

There are many uses for SMRs in KSA that will help to reach the future vision. For example, the energy demand has been increasing for the past two decades and is expected to grow even more with all the planned projects like Alula, Abha, and Neom. Hence, more supplies of energy are needed to compensate for this demand. Also, this demand must be covered with as low as possible carbon emissions, as the KSA vision states.

A. Desalination

The Kingdom of Saudi Arabia is the largest producer of desalinated water. It has the largest reverse osmosis water desalination plant, Rabigh Three (Guinness World Records). The Kingdom relays on desalinated water since there are no other sources of fresh water like rivers and lakes. As a result, this emphasizes the need for desalination plants. In the Kingdom, desalination plants use oil & gas as a source of energy, which are significant producers of CO_2. Another source of energy that has fewer CO_2 emissions with a high technological level, which serves the vision of KSA for net zero CO_2 emission, is nuclear energy.

Moreover, since conventional nuclear power plants occupy a large area, SMRs can solve this issue with much smaller size, advanced technology and safety, and the energy needed for desalination. Therefore, SMRs can be used in desalination plants in the Kingdom to provide the energy required for desalination and electricity. More than 150 reactors and years of experience have proven that integrated nuclear desalination plants are feasible. Examples are Kazakhstan, India, and Japan. For example, between 1973 and 1999, the BN-350 at Aktau, in Kazakhstan, produced 80,000 m^3/d of potable water and generated 135 MW_e of electricity.

According to the Saline Water Conversion Corporation's (SWCC) annual report for 2019, Saudi Arabia is the largest producer of desalinated water worldwide. SWCC produced 1890x 10^6 m^3 in 2019, an increase of 4% over the year before, accounting for 22% of global production [10]. KSA produced this quantity of water from 33 water desalination plants along the Red Sea and Arabic Gulf, and it was delivered to KSA regions by a massive pipeline system with a length of 7,700 Km. Due to varied topography in different areas, there is an average rise in sea level of 900 m – 1100 m. The Corporation has constructed 63 pumping stations to provide water to every home in Saudi Arabia due to the length of this pipeline and the height above sea level.

In 2019, SWCC consumed 40 million MW_h, or in terms of power (power calculations in average value)

$$P = \frac{40 \text{ x } 10^6 MW}{365 \text{ x } 24} = 4570 \text{ MW} \quad (1)$$

(14.7% on the red sea and 85.3% on the Arabic Gulf). According to the report, one of the challenges SWCC faces is the low price of the electricity it produces when they sell it. The report also claims that one of SWCC's challenges is the company's high electricity production costs.

Using a diesel generator to generate 4600 MW of power has several drawbacks, including high CO_2 emissions and unstable costs. Since SWCC has 96 locations, some in remote areas, SMR and microreactors can be used instead of diesel generators in response to the demand for electricity in pumping stations. Additionally, this will assist SWCC in lowering its CO_2 emissions from 266.5 g CO_2/kW_h to 16 g CO_2/kW_h. Since SWCC generates about 48% of KSA's electricity and meets the country's target of having net zero CO_2 emissions by 2060, this will aid in lowering CO_2 levels there. Also, in terms of cost, the average cost of producing 1 KW_h by diesel generator can range from 0.80 $ – 5.00 $ per KW [11] due to fluctuating oil prices, while the cost of producing 1 KW_h by NPP is 0.46 $ per KW [12].

B. Electricity Production

SMRs can produce up to 300 MWe, and this considerable power can take responsibility for a small town or part of a city in KSA. Hence, using SMRs in Saudi Arabia to generate electrical power can be treated as the primary and additional energy source. Nowadays, the electrical energy transferred from power plants to the delivery point is highly efficient. However, when transferring the power to far-distanced places, the reduction in efficiency may be huge. Hence, building SMRs for such sites is highly recommended.

$$P_{total\ per\ hour} = \frac{Total\ Energy\ Consumed}{Hours\ in\ One\ Year} \quad (2)$$

$$P_{consumption\ per\ person} = \frac{Power\ Consumed}{KSA\ Population} \quad (3)$$

$$N_{No.\ of\ familes} = \frac{One\ SMR\ Power}{Power\ Consumption\ per\ Family} \quad (4)$$

The total average energy consumed in 2020 in KSA is 289,333 GW_h, and the average power consumption per hour, using **Eq.2**, is 33.03 GW. **Eq. 3** provides an estimate for the average power consumption per person in KSA, 943.71 W,

which is W/hr consumption by each person. The average family in KSA consists of 5.7 people [13], and the average power consumption per family in KSA is 5.43 KW. **Eq. 4** concludes that only one unit of 300 MW_e SMR can generate enough electricity for around 55,248 families (314,913 people). Furthermore, SMRs can be multi-units, with each unit of the same power. Hence, SMR reactors can be used for far-distanced places in Saudi Arabia.

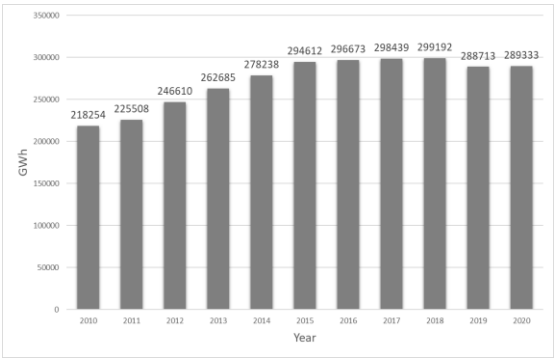

Figure 3. Annual electricity consumption in KSA for the last decade [14]

In 2020 the amount of energy produced is around 335,445 GW_h. One unit of SMR can produce 0.783% of the total energy produced in KSA.

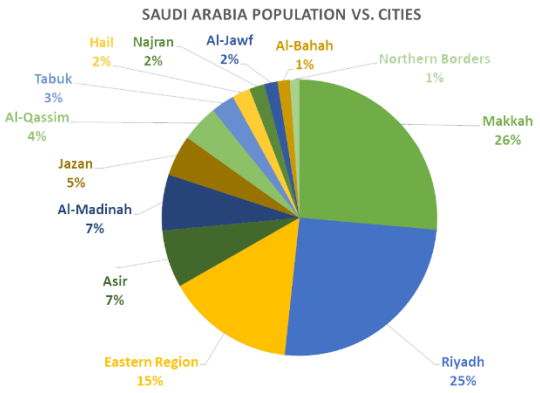

Figure 4. Saudi Arabia population vs. cities – 2021

Saudi Arabia has a population of 34.2 million, and the distribution around the Kingdom in Fig.4. Implementing the SMR concept in KSA can cover the people and cities in Table.1. For example, two units of 300 MW_e SMR can cover Al-Bahah city or the Northern Borders in the Kingdom. Also, SMR can be an extra unit for an existing power plant. Adding up the power of SMR to the plant can be a smooth solution if the plant does not provide enough power. For example, one of the two large nuclear reactors that will be built in KSA in 2032 has a 1.7 GW capacity, covering 5.27% of the population. Adding SMR units, in addition to renewable energy sources, will increase the population covered.

In KSA, the CO_2 produced directly correlates with fossil fuel energy production. Therefore, if the energy produced comes from an environmentally friendly power source, KSA can fulfill its vision of zero-carbon emissions by 2060.

Table 1. Study of % of the population with possible cities covered with No. of SMRs in KSA.

Units of SMR (300 MWe)	% of the Population in KSA	Possible Cities Covered
2	1.86	Al-Bahah; Northern Borders
4	3.72	Tabuk; Hail; Najran; Al-Jawf
6	5.58	Jazan; Al-Qassim
8	7.44	Asir; Al-Madinah

SMRs can also be used for steam production for industrial applications. For such purposes, light water reactors are suitable such as PWR. In addition, steam can be used for drying, heating, and sterilizing.

VII. FUTURE OF SMRS WITH RENEWABLES IN KSA

By the year 2030, renewables and natural gas will make up 50% of the energy mix, based on Saudi Arabia's vision [15]. For example, more than ten projects, such as Saad, Laila, and Al-Rass, are for solar energy. Moreover, projects for wind energy, such as the Dumat Al-Jandal project, to reach net zero emissions by 2060. Although renewable energy is a promising clean energy option for the future, it has drawbacks that compromise its sustainability. The dependency on variable sources, such as wind and sun, limits the reliability of renewables due to the fluctuation in power. Also, the low-capacity factor of some of the renewables, as stated in Fig.1, shows the challenges of renewables to accomplishing the 2030 vision [16].

Furthermore, compensating for such shortcomings is resolved by using mainly diesel generators. Hence, for a cleaner solution, SMRs can be studied to be used effectively with renewable energies for the plans in KSA. Using SMRs can balance the fluctuation in power and reduce the energy storage system size in renewable plants in KSA, besides implementing the large reactors for a primary power source.

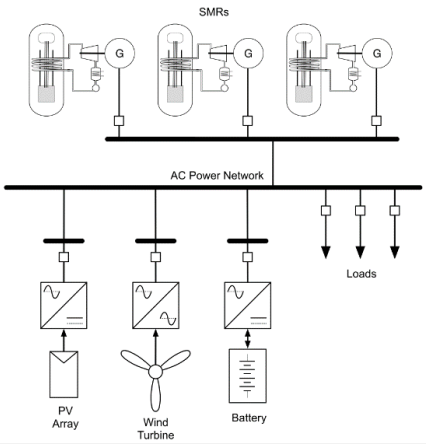

Figure 5. Example of SMR - renewable microgrid configuration [17]

VIII. CONCLUSION

To conclude, SMRs, with electrical power reaching 300 MW, in Saudi Arabia can be helpful and facilitate reaching

net zero carbon emissions by 2060, as the 2030 vision states. Saudi Arabia will develop even more by using such technology for desalination and power production. Using SMR instead of a diesel generator in desalination will help reduce CO_2 emissions from 266.5 g CO_2/kW_h to 16 g CO_2/kW_h. Also, the cost of producing 1 KW_h in NPP is 0.46 $, while it ranges between 0.8 $ – 5.0 $ using a diesel generator. Furthermore, in electricity production, one unit of SMR can generate enough electricity for 0.93% of KSA's population. Also, one unit of SMR can produce 0.78% of the total energy produced in KSA. Moreover, SMRs can be the primary power source since two units could cover Al-Bahah city or be an addition to an existing power source. Even more, SMRs can integrate with renewable energy sources due to the possible drawbacks compromising renewable sustainability.

Saudi Arabia is ready to host such technological concepts since the uranium extracting facility has already been constructed, also the agreement between Saudi Arabia and South Korea was signed for launching the SMART reactor in KSA. In the end, SMRs will be one of the reasons for the development of Saudi Arabia toward a future free of CO_2.

IX. References

[1] Nuclear Information Center, "Capacity factor – it's a measure of reliability," 18 May. 2021. https://nuclear.duke-energy.com/2021/05/18/capacity-factor-it-s-a-measure-of-reliability

[2] IAEA, "What are Small Modular Reactors (SMRs)?," 04 Nov. 2021. https://www.iaea.org/newscenter/news/what-are-small-modular-reactors-smrs

[3] A. Yosri, "Saudi Arabia has built yellowcake uranium processing plant: WSJ," 05 Aug. 2020. Aljazeera. https://www.aljazeera.com/economy/2020/8/5/saudi-arabia-has-built-yellowcake-uranium-processing-plant-wsj.

[4] Country Economy, "Saudi Arabia - CO2 emission," 2021. https://countryeconomy.com/energy-and-environment/co2-emissions/saudi-arabia

[5] IAEA, "Small Modular Reactors: A new nuclear energy paradigm. International Atomic Energy Agency," 22 sep. 2022. [Online]. Available: https://nucleus.iaea.org/sites/smr/Shared%20Documents/SMR%20Booklet_22-9-22.pdf.

[6] IAEA, "A Supplement to: IAEA Advanced Reactors Information System (ARIS). International Atomic Energy Agency," 2020. [Online]. Available: https://aris.iaea.org/Publications/SMR_booklet_2022.pdf.

[7] Government of the Kingdom of Saudi Arabia. Vision 2030. (2016). https://www.vision2030.gov.sa/media/rc0b5oy1/saudi_vision203.pdf

[8] World Nuclear News, "Korea, Saudi Arabia progress with SMART collaboration. World Nuclear News," 07 Jan. 2020. https://world-nuclear-news.org/Articles/Korea-Saudi-Arabia-progress-with-SMART-collaborati.

[9] World Nuclear News, "Saudi Arabia and Argentina form R&D joint venture," 09 Mar. 2015. https://www.world-nuclear-news.org/NP-Saudi-Arabia-and-Argentina-form-joint-venture-0903158.html.

[10] SWCC, "Annual Report of 2019. Saline Water Conversion Corporation (SWCC)," 2019. https://www.swcc.gov.sa/uploads/ANNUAL_REPORT_2019.pdf

[11] C. Nordstrom, "Cost of a Kilowatt – Diesel Generator Analysis," 17 Dec. 2021. Uprise Energy. https://shortest.link/8EMo.

[12] World Nuclear Association, "Economics of Nuclear Power," Mar. 2020. https://world-nuclear.org/information-library/economic-aspects/economics-of-nuclear-power.aspx.

[13] Argaam, "Study of the population in the Kingdom," 05 Aug. 2016. https://www.argaam.com/ar/article/articledetail/id/438807#

[14] STATS, "Electrical energy statistics 2020. General authority of Statistics, Kingdom of Saudi Arabia," 2020. https://www.stats.gov.sa/sites/default/files/Electrical%20Energy%20Statistics%202020EN_0.pdf.

[15] Government of the Kingdom of Saudi Arabia. Vision 2030. (2022). https://www.vision2030.gov.sa/v2030/v2030-projects/saudi-green-initiative/

[16] Office of Nuclear Energy, "Nuclear Power is the Most Reliable Energy Source and It's Not Even Close," 24 Mar. 2021. https://www.energy.gov/ne/articles/nuclear-power-most-reliable-energy-source-and-its-not-even-close

[17] D. Michaelson and J. Jiang, "Review of integration of small modular reactors in renewable energy microgrids," Renewable and Sustainable Energy Reviews, vol. 152, p. 111638, Dec. 2021, doi: https://doi.org/10.1016/j.rser.2021.111638.

Proceedings of the European Nuclear Young Generation Forum
ENYGF'23
May 8-12, 2023, Kraków, Poland

The Prospect of Nuclear Power Integrated Desalination Plants in Saudi Arabia

Alsubhi, Abdulaziz[1*], Balabaid, Abdallah[1], Al-Qahtani, Khaled[1], Al-Gazlan, Osamah[1], Shams, Afaque[1,3] and Al-Athel, Khaled[1,2]

[1]King Fahd University of Petroleum and Minerals (KFUPM), Saudi Arabia

[2]Interdisciplinary Research Center for Advanced Materials (IRC-AM), KFUPM, Saudi Arabia

[3]Interdisciplinary Research Center for Renewable Energy and Power Systems (IRC-REPS), KFUPM, Saudi Arabia

*Corresponding author: s201761950@kfupm.edu.sa

I. INTRODUCTION

With the Kingdom of Saudi Arabia's urban and industrial expansion, the Kingdom's natural renewable water resources are insufficient to supply the Kingdom's need for freshwater due to its geographical location and desert environment. The World Bank's Freshwater Development Indicators estimate that Saudi Arabia has an internal renewable freshwater resource of 2.4 cubic kilometers per year and that Saudi Arabia withdraws about 21.2 billion cubic meters of freshwater annually [1]. With a significant disparity between domestic renewable freshwater supply and increasing demand for freshwater, the Kingdom of Saudi Arabia is challenged with a situation that necessitates long-term solutions to meet the country's growing water demand. One of the solutions in which the Kingdom of Saudi Arabia has invested heavily is the desalination of seawater and converting it into fresh water suitable for human use.

Saudi Arabia has invested in desalination and relied on it as the country's primary supply of fresh water due to its economic capacity to fund seawater desalination plants and its 3,400 km coastline on the Arabian Gulf and the Red Sea. The main entities Saudi Arabia relies on for desalination are the Saline Water Conversion Corporation (SWCC) and the Saudi Water Partnerships Company (SWPC). Together, they produce approximately 8,442,272 cubic meters per day of fresh water. The Saline Water Conversion Corporation in Saudi Arabia produces approximately 5,900,272 cubic meters per day, while the Saudi Water Partnership Company produces approximately 2,542,000 cubic meters per day [2, 3]. Desalination facilities in Saudi Arabia utilize a variety of processes, with multi-stage flash distillation (MSF) accounting for 57.8% of domestic Saudi production, multi-effect distillation (MED) accounting for 13.2%, and reverse osmosis (RO) accounting for 29% [4]. However, according to Sustainable Development Goals (SDGs) provided by SWCC, the dependency on reverse osmosis will increase by Replacing thermal plants with environmentally friendly reverse osmosis plants in the near future [5].

Despite its accomplishments in water desalination, Saudi Arabia is constantly trying to expand its capability and improve its sustainability to fulfill the growing demand for fresh water. According to the SWCC Sustainable Development Goals (SDGs), to accomplish the objective of sustainable cities, desalination plants must be equipped with cutting-edge technology to meet the requirements of a sustainable generation of electricity and the desalination industry [5]. The Sustainability Report presented by the SWCC also emphasizes the continuous need for development to ensure compliance with the requirements of the Kingdom's Vision 2030 [5]. Among the primary goals of the Kingdom's Vision 2030, which the kingdom's desalination plants must comply with, is to reduce carbon emissions to 278 million tons annually by 2030 and to reach net zero emissions by 2060 [6]. These goals drive Saudi Arabia to search for solutions to the carbon emissions of desalination plants and to try to find sustainable and reliable solutions for decades to come.

The problem of carbon emissions in desalination facilities has several possible solutions, one of which is nuclear energy. We can define nuclear desalination as a description of when a nuclear reactor is utilized to operate a desalination plant that provides drinkable water from seawater or brackish water. Nuclear power has been successfully implemented in desalination and is being promoted as an alternative option to reduce fossil fuel use and carbon dioxide emissions [7]. Nuclear water desalination has also proven to be the most feasible in terms of economic cost, as proven in studies conducted by The International Atomic Energy Agency (IAEA) [7]. The growing demands for nuclear energy and the danger posed by carbon emissions from fossil fuels used in desalination plants prompted countries to consider nuclear desalination as a possible

solution and alternative to ensure water security for decades to come without risking the nation's environmental future.

II. ECONOMICS

Many studies have been developed on integrating desalination plants with renewable energy sources such as solar PV and wind. However, recently, the focus on nuclear desalination has increased dramatically. The use of integrated desalination and nuclear plants has shown, in addition to low carbon emissions, a substantial reduction in the cost of water. As the largest country in the field of desalination, the consumption of energy is dramatically increasing due to the increase in demand. Consequently, the establishment of alternative, less costly sources of energy is essential. Moreover, conventional sources of energy and some renewable sources are unreliable. Therefore, the use of nuclear desalination is the most appropriate approach to mitigate this issue. Table 1 shows the energy consumption per day for some of the RO desalination plants along with their capacity in Saudi Arabia. The distillation processes the energy demands of MSF and MED are higher than those of the RO and include both thermal and electrical energy. Primarily electrical energy is required to power the system in RO, and little heat energy is used. Consequently, the technology focused on in this analysis is RO technology. Furthermore, the vision of Saudi Arabia is to shift all the focus to the RO desalination plants.

Table 1: Capacity and Estimated Energy Consumption of Some Desalination Plants in KSA [8,10,11].

Region/ City	Technology	Capacity (m3/day)	Energy consumption (MWh/day)	Power consumption (MW)
Khobar	RO	210,000	1050	43.75
Jeddah (3)	RO	240,000	1200	50
Khafji	RO	60,000	300	12.5
Yanbu 4 (2023)	RO	450,000	2250	93.75
Jubail 3 (A) (2022)	RO	600,000	3000	125
Jubail 3 (B) (2024)	RO	570,000	2850	118.8
Rabigh 3	RO	600,000	3000	125
STPC-IWP	RO	250,000	1250	52.08
SEPCO-IWP	RO	150,000	750	31.25
SqWEC-IWPP	RO	212,000	1060	44.17
Shuqaiq 3	RO	450,000	2250	93.75

The plant's ability to produce water, the location's features, the type of energy used, and the desalination technology are only a few of the variables that affect the overall cost of water. However, the capital cost of the water module, the O&M cost, and the cost of energy are often added together to get the overall water cost [8]. A factor of 5 (kWh/m3), was taken as an average value for the consumption of electricity per meter cubed of desalinated water from [9] , was used to approximate the consumption of each desalination plant in table 2, where E is the energy consumption (MWh/day), C is the capacity of the plant, divided by a factor of 1000 to convert from kWh to MWh.

A. Conventional Desalination Plant

Conventional desalination plants normally use natural gas and Liquid fuels such as crude oil, heavy fuel oil (HFO), and diesel to get electric power. [12], using the data for the capacity of the desalination plants, as well as the average electricity consumption factor specified earlier the Levelized Cost Of Water (LCOW). The LCOW represent the final cost of a meter cubed of desalinated water. Using the relation in equation 1 the LCOW was calculated to be 0.4$/m^3, where the value 0.3 SR/kWh represents the cost of electricity in KSA [13]. To check the validity of the LCOW calculated for the technology, it must be comparable to the data provided by SWCC. Table 2 shows a comparison between the theoretical value estimated and the values provided by the SWCC. the estimation, provides reasonable error margins when compared to actual plants data.

$$\boldsymbol{LCOW} = \frac{\mathbf{5\ (kWh/m^3)} * \mathbf{0.3\ (SR/kWh)}}{\mathbf{3.75}\ (\boldsymbol{SR}/\$)} \quad (1)$$

Table 2: Conventional LCOW Literature vs Theoretical

Region/City	LCOW ($/m3) (for conventional power plant) (literature)	LCOW ($/m3) (for conventional power plant) (theoretical)	%Difference
Yanbu 4 (2023)	0.464	0.4	14
Jubail 3 (A) (2022)	0.411	0.4	3
Jubail 3 (B) (2024)	0.424	0.4	6
Rabigh 3	0.531	0.4	25
Shuqaiq 3	0.52	0.4	23

B. Nuclear Desalination Plant

For nuclear desalination plants, equation (3) represents the cost of water relative to the LCOE for each nuclear technology, Where LCOW is in $/m3. Table 3 shows the LCOE for different nuclear power plants technologies. Those costs were estimated for the advanced technologies present in recent years. Table 4 shows the LCOW for different nuclear technologies coupled with RO technology, assuming a discount rate, a measurement of the value of future outcomes relative to immediate ones, of 5%. Nuclear power generation was much less expensive than the substitutes in every country at a discount rate of 3%; at 7%, it was equivalent to coal and still less expensive than CCGT; and at 10%, it was like both [14]. In line with the US Federal Reserve's move, the Saudi Central Bank increased both of its repo rates by 75 basis points to 4.5 %. The Saudi repo rate is higher than

the 3.1% inflation statistic from September 2022. Due to the Riyal's tie to the dollar, Saudi Arabia normally adheres to Fed policies (see figure 1) [9]. Therefore, based on the maximum and minimum values of the discount rate within

the last 22 years, the value of the discount rate will not affect the competency of the nuclear desalination.

$$LCOW = \frac{5\ (kWh/m3)\ *\ (\text{LCOE}\ (\$/\text{MWh})}{1000} \quad (2)$$

Table 3: Levelized cost of electricity (5% discount rate) [12]			
Nuclear ($/MWh)			
SMR	EPR	APWR	AP1000
50	56.42	48.23	36.31

Table 4: Levelized cost of water conventional and Nuclear					
Tech	Normal ($/m^3)	Nuclear ($/m^3)			
		SMR	EPR	APWR	AP1000
RO	0.4	0.25	0.2821	0.24115	0.18155

To compare the two technologies, all parameters were fixed and a comparison between LCOW was conducted. Table 5 shows that the LCOW was decreased by more than 25% and up to 54.6% when using nuclear power as source of electricity.

C. Conventional vs Nuclear

Using the energy consumption calculated before, the LCOW can be calculated and compared between conventional and nuclear desalination. From table 5, it can clearly be seen that the LCOW using nuclear power plants is more economical compared to the conventional plants. However, even with small size and low construction cost, the LCOW of the SMR is not the lowest out of the nuclear technologies. This indicates that for recent designs of SMRs, the technology cannot be utilized efficiently.

Table 5:							
Region /City	Capacity (m3/day)	Energy consumption (MWh/day) (averaged)	LCOW ($/m3) (for conventional power plant)	NPP type	LCOE ($/MWh)	LCOW ($/m3) (NPP)	%Diff
Khobar	210,000	1050	0.4	SMR	50	0.25	37.5
Khobar	210,000	1050	0.4	EPR	56.42	0.2821	29.5
Khobar	210,000	1050	0.4	APWR	48.23	0.2412	39.7
Khobar	210,000	1050	0.4	AP1000	36.31	0.1816	54.6

III. ENVIRONMENTAL IMPACT

A. Paris Agreement

In 2015 Saudi Arabia joined efforts with 195 other parties, to reduce CO_2 emissions to limit the increase in temperatures to below 2 °C, compared to pre-industrial levels, and pursue further efforts to limit the increase to 1.5 °C [15]. In 2016, Saudi Arabia submitted its first Nationally Determined Contribution (NDC) which promised to cut CO_2-e emissions (CO_2- equivalent) by 130 million tons. In 2021 Saudi Arabia, has updated its NDC and increased it to 278 million tons of CO_2-e by 2030, which is more than twice the previously declared value [16]. This increase comes due to a change in internal policies and other factors which are outside of the scope of this study. One crucial factor that is essential to this study is the phase out of energy intensive technologies such as MSF and MED, while simultaneously investing more in SWRO technology.

B. Current Environmental Impact

To have a better understanding of the change in the environmental impact, an examination of the current state of CO_2 emissions is necessary. Due to the current phase out of thermal desalination technologies, little focus will be placed on them in what is to come, while most will be placed on SWRO. There are two ways in which desalination contributes to CO_2 emissions, one is through burning of fossil fuels, natural gas, to provide thermal energy. This is used in both MSF and MED. The other is electrical coupling between the grid and the desalination plant. This is done in SWRO.

Table 6 shows the extent to which these different technologies contribute to CO_2 emissions. We can see that even though SWRO contributes to what is approximately third of the water capacity in the kingdom, it only contributes to 5% of the total emissions. This is due to low emission factor of CO_2, which accounts to, 3.4 kg CO_2/m_3. On the other hand, we see an almost 1:1 and 3:4 contributions of MED and MSF, respectively. This is the result of a high emission factor, 18 kg CO_2/m_3, 23.4 kg CO_2/m_3 for MED and MSF, respectively. Using these emission factors and the yearly capacity of production, one could easily obtain the total CO_2 emissions to be, 75.18 million ton/year. This accounts for 18% of the total emissions in the kingdom [4].

Table 6: Technologies contribution to water capacity and CO_2 emissions.		
Technology	% Water capacity contributed	% CO_2 emissions contributed
SWRO	29.0%	5.8%
MSF	57.8%	80.1%
MED	13.2%	14.0%

C. Future Environmental Impact

Nuclear power generation is known for its high-volume electricity generation and low CO_2 emissions. These emissions are mainly due to transportation, nuclear fuel cycle, and construction & decommissioning. However, those parameters differ from one reactor design to another. The reactor designs to be considered for the coupling process with SWRO are, SMR, AP1000, EPR. The emission factor for these designs differs due to the different sizes and electricity output. Table 7 shows the emission factors for the respective designs compared to the grid averaged value for SWRO. To show the extent of this reduction in emissions, table 8 shows what if some of the current SWRO plants were operated on nuclear energy instead of fossil fuels. It can be seen that a reduction of 2.85 Mton of CO_2/ year in the case of Rabigh 3 can be achieved. Well, what if this transformation is carried out on all operating desalination plants with a total capacity of 3.08E09 m^3/year? Taking a non-conservative approach by choosing the SMR emission factor as basis (As shown in equation 4).

$$3.08 \times 10^9 \ \frac{m^3}{Year} * SMR\ emission\ factor \frac{kgCO_2}{m^3} = \frac{kgCO_2}{year}. \quad (4)$$

Then, 0.111 Mton of CO_2/year is produced. Comparing this to the current value of 79.34 Mton CO_2/year, we can see a reduction of 99.86% of all emissions. This would help in decreasing the desalination sector's contribution to the kingdom's CO_2 emissions from 18% to 0.03%.

Table 7: Emissions factors for the grid and different nuclear technologies. [17]

	Grid average value (current)	EPR	SMR	AP1000
CO_2 emission factor from SWRO ($kgCO_2/m^3$)	3.4	0.018	0.036	0.033

Table 8: Change in emissions, before and after nuclear conversion. [4]

Region/City	Capacity (m3/day)	Energy consumption (MWh/day) (averaged)	NPP type	Current emissions (Fossil fuels) in Mton co2/yr	Nuclear energy emissions. In Mton co2/yr
Khobar	210,000	840	AP1000	0.9	2.58E-03
Haql	17,000	68	SMR	0.01	2.26E-04
Rabigh 3	600,000	2400	EPR	2.86	4.03E-03

IV. LIFETIME

The lifetime of electricity production plants is one of the most critical variables influencing decision-makers' decisions to invest in and develop new technologies that differ from those currently in use. Electricity production plants that rely on oil and natural gas derivatives are currently used in the Kingdom of Saudi Arabia, for a variety of reasons, including the Kingdom of Saudi Arabia's ability to provide sufficient oil derivatives and gas used in electricity production, as well as to ensure production sustainability. The other reason is that oil and gas-based electricity production plants can continue to produce electricity if suitable maintenance and human resources are provided for up to 30 years for gas-powered electricity production stations and up to 43 years for stations producing electricity with oil derivatives [18].

When we talk about nuclear power plants, one of its most important features is the plant's long production period, which may exceed 60 years, and this makes nuclear power plants an alternative that many industrialized nations rely on to create electricity [19][20][21]. However, the data can often be misleading. Although there haven't been any nuclear power plants that have operated for 60 years, it is true that this is their expected lifespan. To operate for 60 years, the highest maintenance requirements must be followed. Additionally, you must uphold these standards for 60 years and provide the greatest possible training for engineers and technicians. Although nuclear power reactors are widely acknowledged to be extremely dependable, they also come with a variety of regular maintenance, training, and safety regulations, this pushes decision-makers to examine several alternatives before excessively depending on them.

V. Safety

Before desalinated water is transported to be used, it must comply with strict quality specifications, which are compatible with the World Health Organization (WHO) guidelines. SWCC monitors the quality of the water thorough their network through collecting samples from pumping stations and tanks. These samples are tested for pH, turbidity, chlorine dioxide residues and electrical conductivity [3]. This requires the desalination plants to have rigorous safety procedures to ensure the safety of their output water. Thus, ensuring constant water quality. Similarly, a Nuclear Power Plant has the containment of radioactive materials as one of its three main safety concerns. Therefore, a great deal of effort has been made to ensure the safety of both industries individually. In terms of design and operation, the challenges to be considered are solely ones that arise from the coupling of a Nuclear Power Plant with a sea water desalination plant. On the other hand, in terms of public opinion, mentioning nuclear desalination would present unwarranted safety concerns. Tackling these safety concerns would benefit from an easy-to-explain solution for the design safety.

Unlike other desalination technologies such as MSF and MED, that use thermal energy as well as electrical energy, which along with the power they generate, complicates safety and comparison. RO requires only electricity to function properly. This presents a uniquely simplified coupling scheme. The electricity can be delivered from the NPP to the desalination plant either directly through a connection to the NPP, or indirectly through a connection to the power grid. A direct connection would be valid for remote desalination plants that require little energy. This task can be handled by an SMR type reactor fittingly. The larger types of reactors such as the EPR and AP1000, should have an indirect connection due to the excess power they provide. In this manner, the electricity not used by the desalination plant will transfer to the power grid directly. Furthermore, this simplified scheme -a wire connection for electricity- presents the needed easy-to-explain coupling process to trivialize the unwarranted concerns of the lay person.

VI. RECOMMENDATIONS

After analyzing the data and discussing the results, several decisions are clear to be the best fitting for Saudi. The first, which is due to the plan to phase out thermal desalination technologies, is to focus on electrical based desalination technologies such as RO. This will simplify both comparing and justifying the use of NPPs. For a lay person, the concept of using nuclear power to desalinate water might wrongfully come across as dangerous. This is a further incentive to use RO technology as a simple connection to electricity would be the best for public acceptance and further normalize the use of nuclear energy in the public eye.

The deciding factors in desalination through conventional means against nuclear are the levelized cost of water (i.e., the least expensive) and CO2 emissions (i.e., more environmentally conscious). For the first factor we recommend using an AP1000 reactor, as it provides the cheapest power for the desalination process at 0.18155 $/m^3$

which is more than 50% cheaper than conventional. For the second factor, all technologies reduced CO2 emissions by more than 99% per meter cubed. SMRs had the highest emissions of the three technologies considered, with the EPR having the least emissions.

VII. CONCLUSION

In conclusion, the switch from conventional desalination to nuclear desalination offers several favourable benefits. The simple coupling method of a RO/SWRO desalination plant with an NPP does not depend on water quality or plant efficiency. The deciding factor is purely the levelized cost of electricity of the NPP. Thus, the analysis depends only on the NPP, but the results include all RO desalination Plants. By switching to nuclear desalination, Saudi Arabia could save up to 37.5%, 29.5%, 39.7% or 54.6% on the price of desalinated water using a SMR, EPR, APWR or an AP1000, respectively. Furthermore, the use of NPPs will also lower CO2 emissions from desalination plants per meter cubed by 99.93%, 99.87%, and 99.86%when coupled with an EPR, AP1000 or an SMR, respectively. This will be a significant step in the country's vision of zero emissions, reducing desalination-based emissions from 18% to at least 0.03%of the total emissions.

References

[1] "World Development Indicators | The World Bank," wdi.worldbank.org. http://wdi.worldbank.org/table/3.5# (accessed Dec. 24, 2022).

[2] [Saline Water Conversion Corporation, "Production Systems." https://www.swcc.gov.sa/en/ProductionSystems (accessed Dec. 24, 2022).

[3] Saudi Water Partnerships, https://www.swpc.sa/ (accessed Dec. 24, 2022).

[4] A. Hamieh, F. Rowaihy, M. Al Juaied, A. Nabil Abo-Khatwa, A. Alafifi, and H. Hoteit, "Quantification and analysis of CO2 footprint from industrial facilities in Saudi Arabia," Energy Conversion and Management: X, p. 100299, Sep. 2022, doi: 10.1016/j.ecmx.2022.100299.

[5] Saline Water Conversion Corporation, "Sustainability Report 2021," Saline Water Conversion Corporation, 2021. Accessed: Dec. 24, 2022. [Online]. Available: https://www.swcc.gov.sa/uploads/SustainabilityReport2021(English).pdf

[6] "Saudi & Middle East Green Initiatives," Saudi & Middle East Green Initiatives. https://www.greeninitiatives.gov.sa/about-sgi/sgi-targets/reducing-emissions/reduce-carbon-emissions/

[7] N. Y. Mansouri and A. F. Ghoniem, "Does nuclear desalination make sense for Saudi Arabia?," Desalination, vol. 406, pp. 37–43, Mar. 2017, doi: 10.1016/j.desal.2016.07.009.

[8] Saudi Water Partnership Company, "IWP-Projects," Saudi Water Partnership Company, Jan. 12, 2011. https://www.swpc.sa/en/ (accessed Dec. 20, 2022).

[9] M. A. Abdelkareem, M. El Haj Assad, E. T. Sayed, and B. Soudan, "Recent progress in the use of renewable energy sources to power water desalination plants," Desalination, vol. 435, pp. 97–113, jun. 2018, doi: 10.1016/j.desal.2017.11.018.

[10] INTERNATIONAL ATOMIC ENERGY AGENCY, Introduction of Nuclear Desalination, VIENNA: INTERNATIONAL ATOMIC ENERGY AGENCY, 2000.

[11] Saline Water Conversion Corporation, "Sustainability Report 2021," Saline Water Conversion Corporation, 2021. https://www.swcc.gov.sa/uploads/SustainabilityReport2021(English).pdf (accessed Dec. 20, 2022).

[12] A. Al-Karaghouli and L. L. Kazmerski, "Energy Consumption and Water Production Cost of Conventional and renewable-energy-powered Desalination Processes," Renewable and Sustainable Energy Reviews, vol. 24, pp. 343–356, Aug. 2013, doi: 10.1016/j.rser.2012.12.064.

[13] S. E. Company, "Tariffs and Connection Fees," Saudi Electricity Company, 1 1 2018. [Online]. Available: https://www.se.com.sa/en-us/customers/pages/tariffrates.aspx. [Accessed 12 19 2022].

[14] World Nuclear Association, "Economics of Nuclear Power," world-nuclear.org, Aug. 2022. https://world-nuclear.org/information-library/economic-aspects/economics-of-nuclear-power.aspx

[15] "The Paris Agreement," Unfccc.int, 2016. [Online]. Available: https://unfccc.int/process-and-meetings/the-paris-agreement/the-paris-agreement. [Accessed: 20-Dec-2022].

[16] "KSA updated first nationally determined contribution," UNFCC, 2021. [Online]. Available: https://unfccc.int/sites/default/files/resource/202203111154---KSA%20NDC%202021.pdf. [Accessed: 20-Dec-2022].

[17] A. Simons and C. Bauer, "Life cycle assessment of the European pressurized reactor and the influence of different fuel cycle strategies," Proceedings of the Institution of Mechanical Engineers, Part A: Journal of Power and Energy, vol. 226, no. 3, pp. 427–444, Mar. 2012, doi: 10.1177/0957650912440549.

[18] Nuclear Energy Agency and International Energy Agency, "Projected Costs of Generating Electricity - 2015 Edition," Nuclear Energy Agency, Paris, 2015. Accessed: Dec. 24, 2022. [Online]. Available: https://www.oecd-nea.org/jcms/pl_14756/projected-costs-of-generating-electricity-2015-edition?details=true

[19] W. Cummins, "THE ADVANCED PASSIVE AP1000 NUCLEAR PLANT-COMPETITIVE AND ENVIRONMENTALLY FRIENDLY." Accessed: Dec. 24, 2022. [Online]. Available: https://repository.lib.ncsu.edu/bitstream/handle/1840.20/30915/S1845.pdf?sequence=1&isAllowed=y

[20] International Atomic Energy Agency, "System-Integrated Modular Advanced Reactor (SMART)," International Atomic Energy Agency, Apr. 2011. Accessed: Dec. 24, 2022. [Online]. Available: https://aris.iaea.org/PDF/SMART.pdf

[21] International Atomic Energy Agency, "The Evolutionary Power Reactor (EPR)," International Atomic Energy Agency, Apr. 2011. Accessed: Dec. 24, 2022. [Online]. Available: https://aris.iaea.org/PDF/EPR.

Proceedings of the European Nuclear Young Generation Forum
ENYGF'23
May 8-12, 2023, Kraków, Poland

Overview of Microreactors and their potential applications in Saudi Arabia

Altanam, Musaad [1]*, Alnewirah, Anas [1], Alnasser, Akbar[1], Alrubayyi, Sufyan[1], Alruwaished, Abdulaziz[1] , Al-Athel, Khaled[1,2] and Shams, Afaque [1,3]

[1] King Fahad University of Petroleum & Minerals (KFUPM), Saudi Arabia

[2] Interdisciplinary Research Center for Advanced Materials (IRC-AM), KFUPM, Saudi Arabia

[3] Interdisciplinary Research Center for Renewable Energy and Power Systems (IRC-REPS), KFUPM, Saudi Arabia

*Corresponding author: s201926890@kfupm.edu.sa (Altanam, Musaad)

I. Introduction

As a result of growing worries about climate change and environmental damage, many nations are shifting towards nuclear energy as a carbon-free energy source to reach their net zero. The Paris Agreement establishes a worldwide framework aimed at mitigating the impacts of climate change by setting targets to limit global warming to significantly below 2°C, with a specific goal of striving for a limit of 1.5°C [1]. Despite the huge development of nuclear power plants worldwide, conventional nuclear power plants, which is large scale facilities and can produce more than 700 MWe are unpreferred by some sectors and countries due to their high capital costs, design complexity, large size, and construction delays. Microreactors with a capacity of less than 50 MWe can represent a distinct and innovative approach for several conditions and applications that will be presented in the text. MRs can operate in conjunction with the electric grid, autonomously, or as a component of a microgrid, making them a favorable choice for diverse sectors, including industries, military, and remote areas. Currently, microreactors remain a theoretical possibility as there has not yet been a single instance of construction or licensing of such devices. The coming sections will point out the main expected gains of microreactors and their associated challenges, an overview of developed microreactor design, and the possible applications of microreactors in Saudi Arabia.

II. Why should microreactors be the future of clean energy?

A. Fundamental design features

One of the major differences between nuclear power plants and microreactors (MR) is that they require large land areas, which provides more safety processions but is challenging in terms of capital cost. The small size of MR designs enables the adoption of more ambitious modularization schemes and manufacturing techniques, reducing construction time, minimizing capital costs, and shortening installation times. Moreover, the simple layout allows design modifications for various applications such as submarines, spacecraft, and remote areas as will be explained further in the coming sections. Despite the licensing process, the smaller design of microreactors allows faster transportation and connection to the grid, which is a significant decrease in installation time when compared to large-scale nuclear power plants. Due to the reduced reactor dimensions, the reactor could be constructed in a facility under regulated environmental circumstances and quality control processes.

Furthermore, microreactors are expected to be simply and swiftly removed, replaced with a new one, or transferred to a different location. Although the smaller size of MR means easier transportation, safety challenges arise regarding the reactors fuel content during transportation [2]. Mehran and Adkins [2] Identified two options for MR transportation, a separate transportation method where fuel is removed from the vessel to a transportation package specially designed for that fuel. A second option presented by [2] is the transportation of microreactors with their fuel, but that is not feasible unless equivalent safety is demonstrated through PRA. Complete assembly in the plant could boost reactor component production rates, lower costs through enhanced economies of scale, and shorten installation time in the field. According to GAO [3], Turbines, generators, and various other related components could also be made as modular components in a facility and assembled on-site. However, this claim needs more research and experiment to support as some components are difficult to manufacture in a modular size such as the generator's stator.

Microreactors are special in that they can be used to recover electricity in the event of environmental catastrophes or system outages in emergency cases, such as hurricanes,

floods, and earthquakes, where no proper infrastructure is available. Currently, generators running on gasoline, diesel, or other fuels are used in these cases, but they have an average running time of half a day, and they need to be resupplied with fuel continually for a long period, which is expensive and challenging to carry. However, microreactors are designed to provide flexible operations and complement intermittent energy sources to provide power and heat either independently or in a microgrid with a refueling process of twenty years. In addition, the small size of microreactors allows ease of transportation to locations where it is difficult to extend and deliver an electricity network where electricity generators are used such as villages above mountains. Table 1 illustrates a comparison between diesel generators, micro-reactors, and renewable energy in terms of application, size, CO2 production, electricity generation prices, and capital costs. Note that microreactor has the lowest electricity generation cost, at the smallest size, which enhances its ability to be shipped and transported simply for remote areas.

Table 1. Comparison among microreactor technologies and diesel generators and renewable sources in microgrids. Source: [4]

Source	Electricity generation costs	Capital cost
Microreactor	0.14 $/kWh and 0.41 $/kWh	5000 and 20,000 $/kWe
Diesel generators	0.15 $/kWh and 0.60 $/kWh	200-2000 $/kWe
Renewable sources	0.15–0.30 $/kWh	3000-5000 KWe

B. Microreactors are high safety

The microreactor serves as a walk-away safe reactor [5], in the event of any mishap, the core will not melt because the entire heat escapes quietly toward its surroundings with no movement of components as well as water, regardless of the situation. This means that the facility does not require operating heat removal devices. However, this claim requires further study to support it, maybe through thermal hydraulics analysis. Because of the low power, the reactor can cool despite the involvement of a supervisor as well as any operational cooling device. Furthermore, USNC [5] claims that the facility requires no external services, such as electrical power, to function securely. However, it is believed that the facility requires at least a coolant purification building as well as a start-up boiler room.

All chemicals and cooling fluids used in the microreactor tend to be non-interactive as well as chemically suitable. Helium is used in some microreactors because it is a noble gas that is radiologically clear and of one phase which means that it cannot flare or boil. Helium has no molecular reaction with the propellant or the reactor core parts, and its pressure can be easily measured and controlled. The Fully Ceramic Microencapsulated fuel guarantees pure helium devoid of fission products [5]. Microreactors will be able to protect themselves due to simple as well as flexible design concepts. They will not necessitate an abundance of specialist workers and will rely on inactive protection mechanisms to avoid overheating as well as reactor failure.

C. Applications

By using nuclear microreactors, electricity can be generated without emitting greenhouse gases or other harmful pollutants, thus reducing carbon emissions, and meeting global energy demands in regions that require MR features. Microreactors can be used to power small communities or military bases, providing reliable and secure energy. Despite safety concerns and regulatory obstacles, microreactors have potential benefits, which need to be addressed before wide adoption occurs. With continued development and investment in microreactors, a sustainable and secure electrical energy future is to be achieved.

Microreactors are predicted to be used for propulsion fuelling submarines and spacecraft. Ofek [6] stated that a prototype of a mobile microreactor will be built at the Idaho National Laboratory by the US Department of Defense to secure the nation's energy supplies in the future. The cost-effectiveness and reliability of microreactors to power submarines are still being investigated and debated in the scientific community. Due to the microreactor's small size, submarine designs can be more flexible and efficient. Power plants in conventional submarines are typically located in the aft section, limiting space available for other equipment and systems. The microreactor, on the other hand, can be placed more centrally, freeing up more space for other uses in the submarine's aft section. Having the weight and systems distributed evenly throughout the submarine can improve its overall efficiency.

Moreover, in a similar fashion to large-scale nuclear power plants microreactors can be designed to use different types of fuel, including low-enriched uranium or even thorium, which is a more abundant and less hazardous material, and their advanced nuclear technology ensures that they produce minimal radioactive waste, making them more environmentally friendly. As a result, the use of microreactors in submarines is seen as a promising solution to many of the challenges facing modern naval forces, such as reducing dependence on fossil fuels and improving underwater mobility and endurance.

Utilizing microreactors in aerospace propulsion systems can potentially transform the sector away from Chemical propulsion. Faster journeys to distant planets can be achieved with this technology, and crewed missions could be completed in a shorter amount of time. There are still challenges to be overcome before microreactors can be widely adopted for aerospace propulsion systems. Despite their potential to offer higher energy density than chemical propulsion systems, microreactors also pose significant technical and practical challenges due to their weight, size, and safety concerns. Nuclear power was first attempted in aerospace applications with the Aircraft Shield Test Reactor and the Tupolev Tu-95LAL, but both were ultimately abandoned due to safety concerns. It has been more than 40 years since these programs were developed in the 1950s and 1960s, and technology has greatly evolved since that time, which suggests that reconsidering these applications

in research is crucial for nuclear propulsion. Microreactors can be used on ion propulsion systems or thermal propulsion systems. In ion propulsion systems, electricity ionizes propellants resulting in a charged gas that is accelerated using electromagnetic fields achieving high speeds. In nuclear thermal propulsion, microreactors can be used to create high-pressure gas by heating a propellant, such as hydrogen, which will be expelled from the nozzle producing thrust. According to NASA [7], nuclear thermal propulsion provides high thrust while doubling the efficiency of chemical rocket propellants. NASA studied nuclear thermal propulsion in the 1960s and 1970s, and it is now being re-examined as a potential technology for crewed missions to Mars.

III. Overview of various nuclear microreactor designs

Multiple microreactor designs have been developed and studied recently. This section will discuss some of these designs and a comparison is provided at the end in Table 2.

A. MoveluX

MoveluX is a 10 MW(t) class multipurpose microreactor known as the Mobile-Very-small reactor for Local Utility in X-mark. To cool the central core, a heat pipe is employed, which simplifies the system while also providing passive safety. To increase nuclear security and non-proliferation, MoveluX employs low-enriched uranium fuel with a level of enrichment of less than 4.99 weight percent. To shrink the core size, moderator material is needed. The multipurpose microreactor also needs a high-temperature operation to function properly. As a result, a moderator material made of calcium-hydride (CaH2) that can operate up to 800o C is chosen [8].

B. U- Battery

The advanced small modular reactor (AMR/SMR) known as U-Battery uses high-temperature gas reactor technology that has already been successfully developed. The main novelty is its compact size, which enables a variety of new uses and markets. Its energy production can be scaled from 10MW thermal to 4MW electric, and its footprint is under 350m2 (about 1.5 tennis courts). A U-Battery driven by accident-tolerant TRISO fuel reduces the requirement for backup shutdown mechanisms by preventing the leakage of radioactive material Figure1. It is made up of three layers of spherical uranium fuel particles. A coating of pyrolytic carbon is applied to a uranium center, followed by a layer of silicon carbide and a final layer of carbon. Because of its design and spherical form, TRISO fuel can endure harsh circumstances without losing its integrity [9].

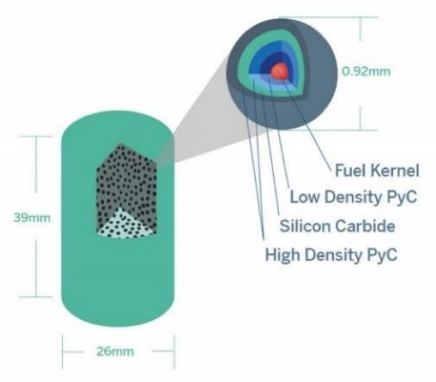

Figure 1. TRISO fuel particle used in U-Battery [9]

C. Aurora

The Aurora is made to offer microgrid-scale, reasonably priced, consistently available, carbon-free power. Power will be provided by Oklo which has tried to license the design of the reactor, but NRC has denied the application for licensing in 2022 [10]. Aurora produces relatively small power; hence it produces small de-cay heat. This decay heat will disperse by the heavy metal used in the reactor, in addition to tons of shielding and other structural material used in the reactor [11].

D. Westinghouse eVinci

The Westinghouse eVinci microreactor is designed with many safety factors. A solid steel monolith that serves as the foundation of the distinctive core design has channels for heat pipes and fuel pellets. For efficiency and redundancy, three heat pipes are placed next to each fuel pin in the core with a ratio of 1 to 2 heat pipes to fuel pins. The many in-core heat pipes are meant to improve system dependability and security. Heat pipes connected to the decay heat exchanger can be used in removing the decay heat [12].

E. MMR

The MMR system is a compact modular system that serves remote areas of mines, industries, and towns with safe and cost-effective power and heat. Energy production has two systems a nuclear plant that works independently and an adjacent plant that contains equipment and instruments that are used to convert heat into electricity or any other form of energy. It produces around 15 MW(t) of process heat, which might be used to create heat or electricity for a small town [13].

Table 2. Comparison of Main Characteristics of Microreactor Designs [11]

Reactor	*eVinciTM*	*MMR*	*U-Battery **	*Aurora*	*MoveluX™*
Institution	Westinghouse	Ultra Safe Nuclear Corporation	Urenco	OKLO	Toshiba Corporation
Country	United States	United States	United Kingdom	United States	Japan
Coolant	Heat pipes	Helium	Helium (primary) Nitrogen (secondary)	Liquid metal	None (Sodium heat pipe cooled)
Moderator	Metal hydride	Graphite	Graphite	N/A	Calcium hydride (CaH2)
Thermal output, MW(t)	7 – 12	15	10	4	20
Electrical output, MW(e)	2-3.5	5	4	1.5	3-4
Enrichment %	5 - 19.75	9 – 12		19.75	4.8 – 5.0
Fuel cycle, months	> 36	Continuous		Up to 20 years	Continuous
Reactivity Control	Ex-core control drums	Control rods		N/A	Lithium Expansion Module
Design status	Conceptual	Conceptual/Basic	Conceptual	Accepted combined license application by the US NRC	Conceptual

IV. Microreactors in Saudi Arabia

Utilizing microreactors in Saudi Arabia is a leading step toward the future, where this clean energy source can be helpful for multiple applications in the oil sector, urban living, and remote areas. The cost of extracting one oil barrel in Saudi Arabia is around 10$ [14], this cost is divided over employee salaries, transportation, and oil boiling. This cost might be reduced if a microreactor is used in the boiling process, by providing heat at a lower cost. If so, Saudi Arabia will have more oil to sell, and less extraction cost, which leads to higher profit. At the same time, microreactors can help decarbonize the oil refinery sector in Saudi Arabia which accounts for 49 metric tons of CO2 per year [15]. Furthermore, MR can be a green replacement for diesel generators used in various applications in the kingdom. Diesel generators operate using fossil fuel with 0.6 $/kWh of electricity generation cost. However, MR is low in greenhouse gasses with 0.41 $/kWh [5]. The use of MR extends to urban living projects such as The Line, which is a city being built in Saudi Arabia aiming to be 100% eco-friendly. The current plan in The Line is to use renewable energy as a main energy source, but renewables such as solar and wind have their imperfections and are limited to the climate status, hence it will be difficult to rely solely on these sources. A microreactor can be provided to complete these imperfections and sustain constant power generation ensuring sustainability. A study in [16] has been performed to explore suitable energy solutions for The Line in NEOM, results of the study have shown that Westinghouse's eVinci reactors are a possible candidate with an estimated cost of 24.6 $/MWh.

Due to portability, microreactors may be used for remote areas across the kingdom. According to the annual report of the Saudi electricity company in 2017, the company provided 41 new villages with electricity in one year. Placing MR near these villages as a replacement for electricity generators or network extensions is an aid towards the Saudi ambitious goal of net zero by 2060. In addition, microreactors if allowed to be transportable may be used for oil, gas, and mineral exploration missions in the empty quarter or other regions.

V. Conclusion

To conclude, microreactors have the potential to be part of the decarbonization of Saudi Arabia, not solely but rather through supporting other clean energy sources. These smaller reactors offer greater flexibility and scalability than large-scale nuclear power plants making them ideal for remote areas, and isolated residential regions. Compared to traditional reactors, they require much less fuel and can operate for up to 20 years without recharging making them a sustainable and cost-effective energy source. Microreactors can be efficiently produced in factories due to their modular design, which reduces construction time and capital expenditures compared to large-scale nuclear projects. Also, the portability of microreactors makes them more easily deployed at different locations. Even though microreactor technology is still relatively new, several designs have already been created and are currently in production, including MoveluX, U-Battery, Aurora, Westinghouse eVinci, and MMR. The utilization of microreactors in Saudi Arabia will contribute to generating low-carbon energy and responding to global climate change concerns.

VI. References

[1] United Nations Framework Convention on Climate Change (UNFCCC). (2015). Paris Agreement. Retrieved from https://unfccc.int/process-and-meetings/the-paris-agreement/the-paris-agreement

[2] Maheras SJ and HE Adkins, Jr. (2021). Microreactor Transportability Challenges - 21072. WM2021: 47 Annual Waste Management Conference, United States

[3] U.S. Government Accountability Office (February , 2020). Science & Tech Spotlight: Nuclear Microreactors.

[4] Testoni, R., Bersano, A., & Segantin, S. (2021). Review of nuclear microreactors: Status, potentialities and challenges. Progress in Nuclear Energy, 138, 103822. https://doi.org/10.1016/j.pnucene.2021.103822

[5] Ultra safe nuclear. (2022, September 25). Micro Modular Reactor - Advanced Nuclear HTGR. Ultra Safe Nuclear. Retrieved April 19, 2023, from https://www.usnc.com/mmr/

[6] Ofek, R. (Ed.). (2020). Mobile Nuclear Microreactor Develop-ment: A Military-Civilian Symbiosis. The Begin Sadat Center for Strategic Studies. https://besacenter.org/wp-content/uploads/2020/05/1584-Mobile-Nuclear-Microreactors-Ofek-English-final-1.pdf

[7] Skelly, C. (2021, February 12). Nuclear Propulsion Could Help Get Humans to Mars Faster. NASA. https://www.nasa.gov/directorates/spacetech/nuclear-propulsion-could-help-get-humans-to-mars-faster

[8] ARIS, "Status Report – MoveluX (Toshiba Energy Systems & Solutions) Japan," IAEA, https://aris.iaea.org/PDF/MoveluX_2020. pdf (Sept. 30, 2019).

[9] Design and Technology | U-Battery. (n.d.). https://www.u-battery.com/design-and-technology

[10] United states nuclear regulatory commissions. Combined Lísense Application Documents for Aurora – Oklo Power Plant Application. 2022

[11] International Atomic Energy Agency (2020). Advances in Small Modular Reactor Technology Developments A Supplement to: IAEA Advanced Reactors Information System (ARIS) 2020 Edition (INIS-XA--20K0995). International Atomic Energy Agency (IAEA)

[12] Westinghouse Global Technology Office, "Westinghouse eVinci™ Micro Reactor," www.westinghousenuclear.com/Portals/0/new%20 plants/evincitm/GTO-0001_eVinci_flysheet_RSB_03-2019_003.pdf?ver=2019-04-04-140824-613 (March 2019).

[13] Ultra Safe Nuclear Corporation, "MMR Energy System," https:// usnc.com/mmr-energy-system (accessed Mar. 27, 2023).

[14] Jawadi, F., & Ftiti, Z. (2019). Oil price collapse and challenges to economic transformation of Saudi Arabia: A Time-series analysis. Energy Economics, 80, 12–19. https://doi.org/10.1016/j.eneco.2018.12.003

[15] Hamieh, A., Rowaihy, F., Al-Juaied, M., Abo-Khatwa, A. N.,Afifi, A. M., & Hoteit, H. (2022). Quantification and análi-sis of CO2 footprint from industrial facilities in Saudi Arabia. Energy Conversion and Management: X, 16, 100299. https://doi.org/10.1016/j.ecmx.2022.100299

[16] Khan, S. U., & Khan, R. (2022). Techno-economic assessment of a very small modular reactor (vSMR): A case study for the LINE city in Saudi Arabia. Nuclear Engineering and Technology, 55(4), 1244–1249. https://doi.org/10.1016/j.net.2022.12.015

Proceedings of the European Nuclear Young Generation Forum
ENYGF'23
May 8-12, 2023, Kraków, Poland

ALFRED neutronics benchmark

Álvarez-Romero, David[1,2*], Romojaro, Pablo[1] and García-Herranz, Nuria[2]

[1] Belgian Nuclear Research Centre (SCK CEN), Belgium; [2] Technical University of Madrid (UPM), Spain

*Corresponding author: *david.alvarez.romero@sckcen.be*

I. INTRODUCTION

Lead-cooled Fast Reactors (LFRs) are one of the reactor technologies proposed by the Generation IV International Forum (GIF) [1] to address future international energy needs. This type of reactor is meant to accomplish the four objectives set by the GIF, i.e.: sustainability; economics; safety and reliability; and, proliferation resistance and physical protection. The capability of LFRs to operate in a closed fuel cycle is important for achieving the stated goals, as it allows for the breeding of new fissile material and the consumption of transuranic elements, either from spent nuclear fuel or produced within the cycle itself [2]. LFRs can also operate as burners, using fertile materials such as Thorium to produce transuranic elements or minor actinides [2].

One of the motivations for using Lead or Lead-Bismuth Eutectic (LBE) as coolant lies in its reduced capability to moderate neutrons and its low absorption cross section, so that the reactor can operate in a fast neutron spectrum [2].

But the advantages of Lead go further [2]:

- it does not react chemically with water and air, which allows to have the steam generators inside the reactor vessel;
- it acts as a shield for gamma radiation and fission products, reducing the dose received by workers;
- its high boiling point (1745 °C) reduces the risk of voiding the central part of the core, reducing the relevance of the positive void feedback;
- it allows the vessel to operate at atmospheric pressure;
- and, the high temperature of the coolant allows the reactor to operate with a higher thermodynamic efficiency, and to have access to other industrial applications.

Despite that, other challenges have to be faced before the industrial implementation of the technology [2]:

- liquid Lead is opaque, making fuel handling and in-service inspections and repairs of internal components difficult;
- the production of Polonium-210 in reactors using LBE [3];
- the fluid dynamic design of the pumps due to the high density of the Lead;
- the corrosion of different elements of the reactor with Lead at high temperatures;
- and, the lack of operational experience in Europe.

In Europe, the design of the European LFR (ELFR) was proposed by the European Commission under its 7th Framework Programme Lead-cooled European Advanced DEmonstration Reactor (LEADER) Project [4]. However, the lack of operational experience in Europe with this reactor, as well as the challenges outlined above, have motivated the development of a demonstration reactor to verify the proper operation of this technology. This is the objective of the Advanced Lead-cooled Fast Reactor European Demonstrator (ALFRED) [5].

In Table 1, the power and the efficiency of both reactors are shown, and as can be seen, ALFRED has a similar power to a Small Modular Reactor, although it is not its intended purpose.

Table 1. Comparison between ALFRED and ELFR power and efficiency [6].

	ALFRED	ELFR
Power [MW_{th}]	300	1500
Power [MW_e]	~ 125	~ 625
Efficiency [%]	~ 44	~ 43

In order to familiarize interested institutions in the LFR concept with the physics and neutronics of an LFR core, and to assess the capability of current tools of simulating an LFR core, a benchmark of ALFRED is carried out under the guidance of the OECD/NEA Expert Group on Physics of Reactor Systems (EGPRS) [7]. The present paper describes the work carried out in this benchmark.

II. ALFRED

ALFRED is a pool type reactor, that is meant to be the demonstrator of LFR technology. Figure 1 provides a schematic representation of the reactor.

The coolant, which moves by forced circulation, operates over a wide temperature range, allowing the reactor to reach higher efficiencies than the current Light-Water Reactors, and goes from 400 °C in the core inlet, to 520 °C in the core outlet. The high boiling point of Lead, together with its good conductivity coefficient, allows the fuel to reach an average temperature of 900 °C [8].

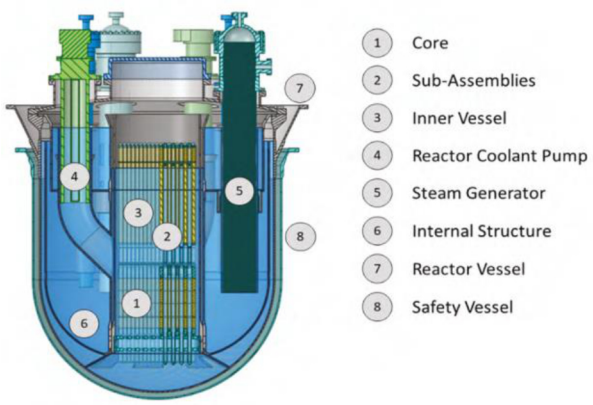

Figure 1. ALFRED primary system configuration [9].

The core map distribution is shown in Figure 2, and is composed of the following 253 Sub-Assemblies: 56 inner Fuel Assemblies (FAs); 78 outer Fuel Assemblies; 12 Control Rods (CRs); 4 Safety Devices (SRs); 1 Test Assemblies (TA); and, 48 reflector and 54 shield Dummy Assemblies (DA).

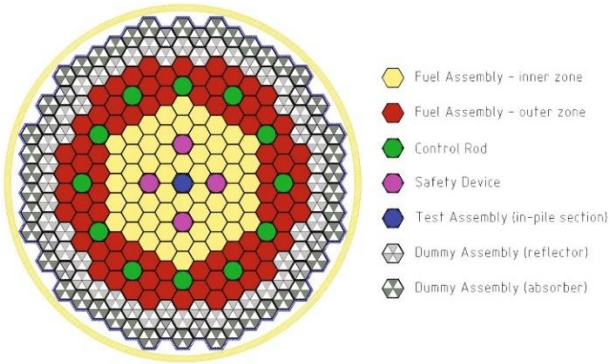

Figure 2. Radial view of the ALFRED core [9].

Mixed oxide (MOX) fuel with depleted Uranium is used in ALFRED. The core has two different enrichment zones in order to flatten the power distribution and have an homogeneous distribution of the burnup, with the inner-core FAs having an enrichment of 20.5 wt.%, while the outer-core FAs have an enrichment of 26.2 wt.%.

An axial view of the fuel rods is presented in Figure 3. Fuel pellets have an inner hollow filled with Helium (as the gap) and the cladding of the rods is made of AIM1 austenitic stainless steel.

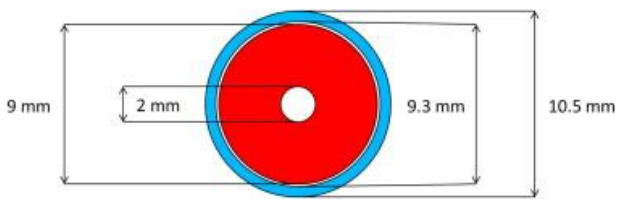

Figure 3. Radial view of a fuel pin. [9]

The fuel assemblies consist of 126 fuel rods arranged in a hexagonal lattice (shown in Figure 4), with a dummy pin in the centre, made of Yttria-Stabilized Zirconia (YSZ), that consists of Y_2O_3 and ZrO_2.

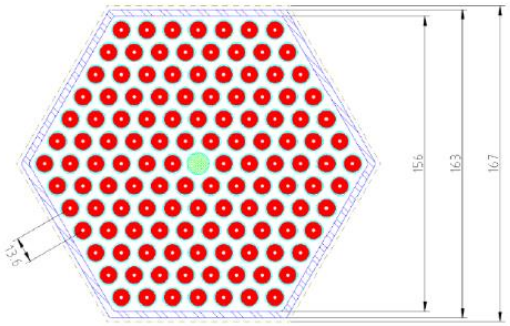

Figure 4. Radial view of a Fuel Assembly [9].

The CRs, that enter the core from below, are made of Boron-Carbide (B_4C) with two different enrichments: the upper zone, which first enters the active region of the core, and is responsible for the control of the reactor in normal operation, has an enrichment of 42 at.% Boron-10; and the lower part, which only enters the active region of the core if the reactor shutdown is needed, has an enrichment of 90 at.% Boron-10. The SRs are made of the same material and enrichment as the lower part of the CRs (B_4C and 90 at.% of Boron-10), as their function is the same, i.e., to shut down the reactor.

The TA located in the centre of the core works for in-pile irradiation experiments, and the DA of the outermost part of the core are made of YSZ.

III. BENCHMARK

Although the benchmark is divided into 3 phases (Phase I - Fuel Pin, Phase II - Fuel Assembly and Super Cell, and Phase III - Full Core), this paper will focus only on Phase III - Full Core. For this purpose, criticality analyses (k_{eff}) have been carried out at Beginning of Life (BoL), and CR worth has been derived, with steps of 5 cm. For BoL, some requested one group cross sections have also been obtained for certain isotopes (section B). Additionally, the radial distribution of the power in the core has been calculated.

Three different nuclear data libraries have been used for the calculations: JEFF-3.3 [10], ENDF/B-VIII.0 [11] and JENDL-4.0u [12]; in order to verify and compare the different results obtained using the libraries mentioned.

IV. RESULTS

The calculations in this benchmark were performed using Serpent 2.2.0 [13], a Monte Carlo neutron transport code developed by the Finnish Reactor Laboratory and the VTT Technical Research Centre of Finland.

A. Criticality analysis

When using the JEFF-3.3 library, the highest reactivity values are obtained, followed by JENDL-4.0u and ENDF/B-VIII.0. Therefore, depending on the libraries,

sub-criticality is achieved at different depths of insertion of the CRs: 25 cm of insertion would be required with JEFF-3.3, 20 cm with JENDL-4.0u, and 15 cm when using ENDF/B-VIII.0 nuclear data library, as shown in Table 2. Figure 5 shows that the CR Integral Worth (IW) at BoL is similar among the different libraries studied, so the fact that the sub-criticality appears at different moments is due to the difference between k_{eff} in the initial position of the CRs, which is with an insertion in the active region of 280 mm.

Table 2. keff for different positioning of the control rods, being 5.4 pcm the maximum relative statistical error observed in calculations. The initial position of CRs is 0 cm, and 55 cm is fully inserted.

Position CRs [cm]	JEFF-3.3	ENDF/B-VIII.0	JENDL-4.0u
0	1.02728	1.01995	1.02240
5	1.02042	1.01292	1.01546
10	1.01315	1.00584	1.00836
15	1.00640	0.99895	1.00161
20	1.00009	0.99257	0.99531
25	0.99437	0.98696	0.98957
30	0.98960	0.98202	0.98476
35	0.98565	0.97825	0.98096
40	0.98268	0.97528	0.97802
45	0.98086	0.97344	0.97606
50	0.97953	0.97219	0.97504
55	0.97918	0.97187	0.97457

The value of the IW is the amount of anti-reactivity added to the system at a given position of withdrawal, and it is given by the following equation:

$$IW\ [pcm] = \frac{10^5}{N}\int_0^z dz \frac{\partial k}{\partial z}(z) = 10^5 \frac{\Delta k}{N} \qquad (1)$$

Where the factor 10^5 is used to change the reactivity into pcm, Δk is the difference between the k_{eff} of a certain position and the initial one, and N is the amount of control rods (12).

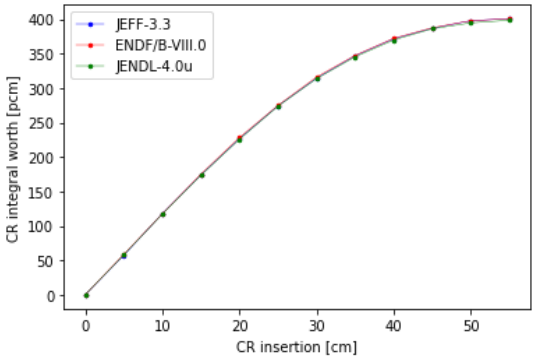

Figure 5. IW or CRs insertion at BoL from the initial position to fully inserted.

B. Cross sections

In Table 3 the fission and capture cross sections for different isotopes present in the core are shown. Only fission and capture cross section are discussed in this paper.

Table 3. Fission and capture cross sections for the different libraries, with a maximum relative statistical error observed of 18 pcm.

	JEFF-3.3		ENDF/B-VIII.0		JENDL-4.0u	
Isot.	**σ fis [b]**	**σ cap [b]**	**σ fis [b]**	**σ cap [b]**	**σ fis [b]**	**σ cap [b]**
^{239}Pu	1.788	0.428	1.776	0.450	1.781	0.446
^{241}Pu	2.422	0.440	2.425	0.411	2.416	0.438
^{235}U	1.839	0.544	1.838	0.510	1.807	0.450
^{238}U	0.045	0.255	0.045	0.260	0.046	0.262
^{56}Fe	-	0.011	-	0.012	-	0.011
^{208}Pb	-	4.14E-4	-	6.18E-4	-	4.14E-4

The cross section that differs the most from one library to another is Lead-208 capture cross section, with the value obtained with ENDF/B-VIII.0 library being higher than the cases of JEFF-3.3 and JENDL-4.0u by ~50%. This is due to differences in the experimental data used for the evaluation, since ENDF/B-VIII.0 does not take into account the data from H. Beer *et al.* [14]. JEFF-3.3 evaluation is based on JENDL-4.0u, so Lead-208 capture cross section in these libraries are identical. For the rest of the isotopes, a good agreement is found with differences lower than 2% for fission cross sections and lower than 12% for capture cross sections.

C. Radial power distribution

The Power Peaking Factor (PPF) is defined as the ratio between the greatest Local Power Density (LPD) and the average power density of the core, and is important in order to ensure that the hottest element does not melt [15].

$$PPF_i = \frac{Power\ FA_i}{Average\ FA\ power} \qquad (2)$$

The radial power peaking map of the ALFRED core at BoL, considering 1/4th symmetry, is shown in Figure 6.

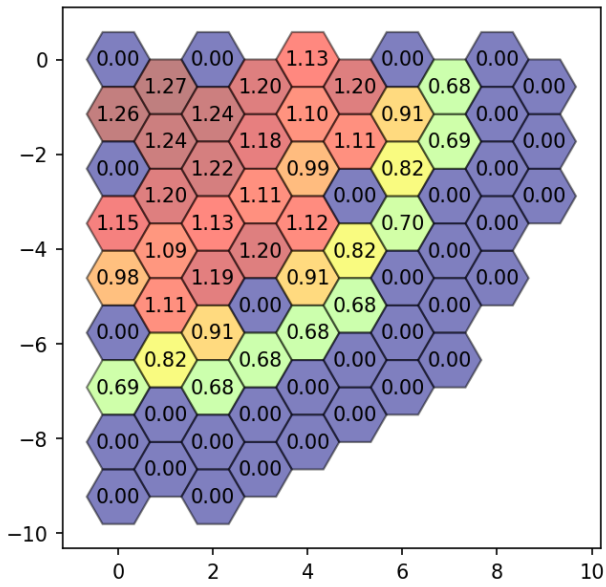

Figure 6. Radial power peaking map at BoL for ¼ of the core.

As could be expected, the elements with the highest power are located in the inner ring of the core (PPF of 1.27), while the lowest powers appears in the outer-core region.

An hypothetical case was performed (Figure 7), following the same procedure, but using inner-core enrichment throughout the entire core, to compare the power distribution in both scenarios and see how the different enrichment flattens the power map.

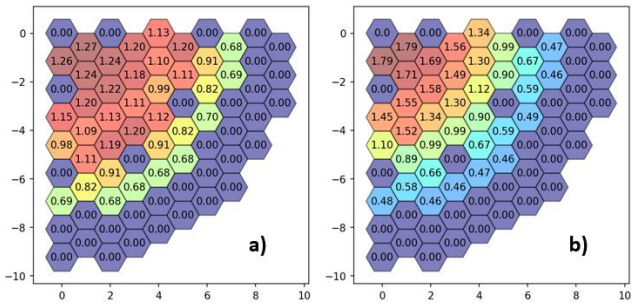

Figure 7. Comparison of the radial power peaking map between the real case (a) and the hypothetical case (b).

Increasing the enrichment of the outer-core elements allows the power map to flatten, resulting in a more homogeneous distribution of power, energy and burn-up. The greatest relative difference appears in the inners FAs, being of 42.06 % higher in the hypothetical case.

V. CONCLUSIONS

For the third phase, the requested criticality values and cross-sections have been obtained. The criticality was found to be highest when using the JEFF-3.3 library, followed by JENDL-4.0u, and the lowest values were reported for ENDF/B-VIII.0. The integral worth of the CRs is almost the same for all three libraries. Because of this, criticality is reached at different levels of insertions of the CR, with the calculations performed with JEFF-3.3 requiring more insertion than the others, and ENDF/B-VIII.0 reaching criticality with less insertion.

A high difference in the Lead-208 capture cross section between libraries could be seen, due to the fact that ENDF/B-VIII.0 does not follow the same experiments as JEFF-3.3 and JENDL-4.0u evaluations.

The power distribution map of the core has been calculated, where the highest values are found in the centre of the core. Later, an hypothetical case in which the same fuel enrichment have been used in all the core was presented. The importance of having two different enrichments for the different zones of the core, in order to keep the power distribution as uniform as possible, and therefore guarantee a more homogeneous burnup, and also to reduce the PPF value of the hottest element, has been shown.

Next step is to perform an End of Cycle (EoC) analysis, followed by sensitivity analysis to understand which parameters affect the k_{eff} the most, along with uncertainty analysis, in order to determine whether or not a Target Accuracy Requirement (TAR) analysis is necessary. TAR analysis allows to set the nuclear data requirements to keep the reactor parameters within a certain range of uncertainty to ensures the proper optimization of the reactor.

VI. ACKNOWLEDGMENTS

Authors would like to acknowledge the support of the Fostering ALfred CONstruction (FALCON) consortium for the realisation of this benchmark. For more information, see reference [16].

VII. REFERENCES

[1] GenIV International Forum, “Annual Report 2021”, GIF, 2021.

[2] A. Alemberti *et al.*, “Lead-cooled Fast Reactor (LFR) System Safety Assessment”, 2020.

[3] D. Lilin *et al.*, ‘Multi-Physics Model Development for Polonium Transport Behavior in a Lead-Cooled Fast Reactor’, *Frontiers in Energy Research*, vol. 9, p. 711916, 2021.

[4] D. De Bruyn et al., “Main achievements of the FP7-LEADER collaborative project of the European Commission regarding the design of a Lead-cooled Fast Reactor”, *Korean Nuclear Society*, vol. 4, p. 281, 2013.

[5] A. Alemberti, “Advanced Lead Fast Reactor European Demonstrator--ALFRED PROJECT”, in *GEN-IV International Forum-Webinar*, 2018, vol. 26, pp. 2018–2011.

[6] A. Alemberti, L. Mansani, and M. Frogheri, “The ELFR Industrial Plant and ALFRED Demonstrator” in *Fourth conference on Heavy Liquid-Metal Coolants in Nuclear Technologies (HLMC-2013),* Obninsk, Russia, 2013.

[7] Expert group on physics of reactor systems (EGPRS). https://www.oecd-nea.org/jcms/c_12860/expert-group-on-physics-of-reactor-systems-egprs. (accessed: Jan. 18, 2023).

[8] A. Alemberti *et al.*, ‘ALFRED reactor coolant system design’, *Nuclear Engineering and Design*, vol. 370, p. 110884, 2020.

[9] M. Tarantino, “ALFRED Overview and Safety Features” in *Ninth Joint IAEA-GIF Technical Meeting/Workshop on the Safety of Liquid Metal Cooled Fast Reactors*.

[10] A. J. M. Plompen et al., ‘The joint evaluated fission and fusion nuclear data library, JEFF-3.3’, *The European Physical Journal A*, vol. 56, no. 7, pp. 1–108, 2020.

[11] D. A. Brown et al., ‘ENDF/B-VIII.0: The 8th Major Release of the Nuclear Reaction Data Library with CIELO-project Cross Sections, New Standards and Thermal Scattering Data’, *Nuclear Data Sheets*, vol. 148, pp. 1–142, 2018.

[12] K. Shibata *et al.*, ‘JENDL-4.0: A New Library for Nuclear Science and Engineering’, *Journal of Nuclear Science and Technology*, vol. 48, no. 1, pp. 1–30, 2011.

[13] J. Leppänen, M. Pusa, T. Viitanen, V. Valtavirta, and T. Kaltiaisenaho, ‘The Serpent Monte Carlo code: Status, development and applications in 2013’, *Annals of Nuclear Energy*, vol. 82, pp. 142–150, 2015.

[14] H. Beer, W. Rochow, F. Käppeler, and T. Rauscher, ‘The 208Pb (n, γ) cross section’, *Nuclear Physics A*, vol. 718, pp. 518–520, 2003.

[15] I. H. Bae, M. G. Na, Y. J. Lee, and G. C. Park, ‘Calculation of the power peaking factor in a nuclear reactor using support vector regression models’, *Annals of Nuclear Energy*, vol. 35, no. 12, pp. 2200–2205, 2008.

[16] A. Alemberti, G. Villabruna, P. Agostini, G. Grasso, I. Turcu and M. Constantin, “ALFRED and the FALCON Consortium”, in *Third International Scientific and Technical Conference "Innovative designs and technologies of nuclear power" (ISTC NIKIET2014)*, Moscow, Russia, 2014.

Proceedings of the European Nuclear Young Generation Forum
ENYGF'23
May 8-12, 2023, Kraków, Poland

An overview on harnessing the power of nuclear energy for an H_2 economy.

Chourashiya, Muralidhar[1*], Sotniczuk, Agata[1], and Baron-Wiechec, Aleksandra[1, 2, 3]

[1] NOMATEN Centre of Excellence (CoE), National Centre for Nuclear Research (NCBJ), 05-400 Otwock, Poland; [2] Technion-Israel Institute of Technology, Haifa 32000, Israel; [3] Guangdong Technion - Israel Institute of Technology (GT-IIT), 515063 Shantou, China.

*Corresponding author: muralidhar.chourashiya@ncbj.gov.pl

I. INTRODUCTION

The role of nuclear energy in achieving the goal of a net-zero future is of utmost importance. Nuclear power provides a reliable source of energy that works regardless of weather conditions and may complement renewable energy sources in the transition to a low-carbon economy. According to the United Nations Economic Commission for Europe (UNECE), "nuclear power is an important source of low-carbon electricity and heat that can contribute to attaining carbon neutrality and hence help to mitigate climate change". Nuclear power has been instrumental in reducing global CO_2 emissions, having avoided around 74 gigatons of CO_2 emissions in the past 50 years. This figure is almost two years' worth of total global energy-related emissions, highlighting the significant role that nuclear energy has played in mitigating climate change [1]. The International Atomic Energy Agency (IAEA) also recognizes the role of nuclear power in mitigating climate change. In 2018, nuclear power produced about 11 percent of the world's electricity (Figure 1) and contributed to the leveling of global CO_2 emissions at 33 gigatons in 2019 [2]. The IAEA states that "nuclear power – as a dispatchable low carbon source of electricity – can play a key role in the transition to a clean energy future" [3]. It is important to note that while nuclear power is considered a low-carbon source of energy, it is not entirely "carbon neutral". However, its potential to contribute to attaining carbon neutrality and mitigating climate change is widely recognized [4].

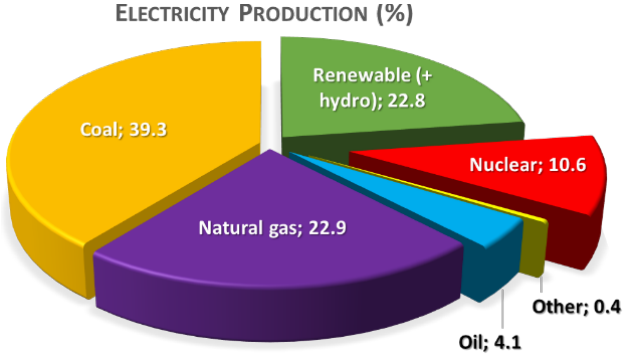

Figure 1. Worldwide electricity production (%) by fuel in 2015 [2].

One of the current challenges is to find alternative fuels to replace fossil fuels, which is the core of the perception of the hydrogen economy. Hydrogen is a promising alternative due to its high energy efficiency and lower emissions [5], [6]. There are various methods to produce hydrogen including steam reforming, gasification of fossil fuels and biomass, thermochemical water splitting using nuclear or solar energy, electrolysis using renewable energy sources, high-temperature electrolysis using nuclear energy, etc. [7]–[9]. For the realization of a hydrogen economy, nuclear power can play a crucial role by providing the electricity and/or process heat required for various water electrolysis technologies to produce clean hydrogen. The latest analysis by the Nuclear Energy Agency (NEA) shows that as a low-carbon source, nuclear energy has the potential to produce clean hydrogen on a large scale and at low costs [10].

II. NUCLEAR ENERGY – EMPOWERING HYDROGEN PRODUCTION

Nuclear power has the potential to play a significant role in empowering hydrogen production via water electrolysis and thermochemical cycling. By providing a reliable and sustainable source of electricity or heat, nuclear energy can help produce low-carbon hydrogen at a lower cost, which is essential for achieving a carbon-free future.

Water electrolysis is a process that uses electricity to split water molecules into hydrogen and oxygen. The source of electricity needed for this process includes renewable sources like solar, wind, and traditional sources like natural gas or coal. Nuclear power offers several advantages over the abovementioned sources. Nuclear power has a better chance to provide a consistent and reliable source of electricity for continuous hydrogen production, unlike intermittent renewable sources, additionally, it is almost carbon-free and the overall cost is low. In combination with water electrolysis for H production, it would produce hydrogen which is more economically viable and environmentally friendly.

Other hydrogen production technologies, such as direct thermochemical cycles, require only process heat, or hybrid

technologies such as high-temperature steam electrolysis and hybrid thermochemical cycles, require both heat and electricity [11]. Nuclear power can be used to co-produce high-temperature steam, electricity, and heat at the same time for these hydrogen production technologies.

III. NUCLEAR POWER – SOURCE OF CARBON-FREE ELECTRICITY AND HEAT

Nuclear energy generated in fission or future fusion power plants offers great potential for the large-scale production of hydrogen that is virtually emission-free. Very high temperatures or high-efficiency electricity is required to drive the most promising hydrogen production processes. Advanced nuclear systems can provide the necessary high heat to enable these processes (Figure 2).

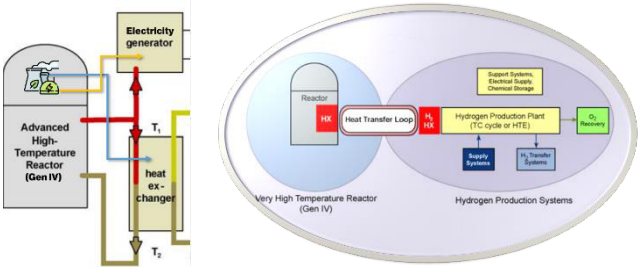

Figure 2. Schematic of the nuclear reactor as a source of emission-free electricity and heat (left). The major next-gen (IV) reactor-hydrogen interfaces and balance of plant systems (right) [12].

Generation IV Nuclear Systems can address this need, which is the next generation of innovative nuclear energy systems. Two decades ago, to gain the advantage of Generation IV Nuclear Systems for the world's future energy needs, an international collaboration led to the establishment of the Generation IV International Forum (GIF), Currently, the GIF consists of fourteen countries, namely, Argentina, Australia, Brazil, Canada, China, Euratom, France, Japan, Russia, South Africa, South Korea, Switzerland, the United Kingdom, and the United States. The GIF defines and keeps updating the goals, concepts, and R&D needs for the six most promising designs, which feature increased safety, improved economics, new products, reduced waste, and increased proliferation resistance.

Generation IV reactor's major goals are [13]:

- Sustainability: Sustainable energy generation that meets clean air objectives and promotes long-term availability of systems and effective fuel utilization for worldwide energy production.
- Economics: Clear life-cycle cost advantage over other energy sources with a level of financial risk compared to other energy projects.
- Safety and reliability: Operations excel in safety and reliability with a very low likelihood of reactor core damage and elimination of the need for offsite emergency response.
- Proliferation resistance and physical protection: Increased assurance against diversion or theft of weapons-usable materials and increased physical protection against acts of terrorism.

From the point of view of energy production the Very High-Temperature Reactor (VHTR) type of GEN IV reactor concept (one of 6 currently considered) looks most promising.

IV. NUCLEAR ENERGY FOR ADVANCED HYDROGEN PRODUCTION TECHNIQUES

Hydrogen production technologies can be classified broadly into conventional and advanced hydrogen production technologies. Conventional hydrogen production methods primarily rely on fossil fuels. For example, steam methane reforming (SMR), etc. Advanced hydrogen production technologies use alternative energy sources/processes. For example, water electrolysis, thermochemical cycles, photoelectrochemical water splitting, biomass gasification, etc. Among these water electrolysis and thermochemical cycles are well-suited for integration with nuclear energy because they can efficiently utilize the high-temperature heat generated by reactors for hydrogen production. This synergy enables continuous, large-scale, and low-emission hydrogen generation, enhancing the overall efficiency and diversification of the energy system.

A. Water electrolysis technologies:

The fundamental principle of electrolysis is to use electricity to split water into its constituent elements: oxygen and hydrogen. This process occurs through two separate reactions that take place at the two electrodes in an electrolysis cell: the cathode (-) and the anode (+). In practice, electrolyzers are made up of several interconnected electrolysis cells, also known as stacks. When voltage is applied to the cell, hydrogen is produced at the cathode and oxygen at the anode. To balance the charges between the two reactions, ion conduction occurs via an electrolyte. Additionally, a membrane is required to prevent the product gases from mixing. The type of electrolyte and ion charge varies among different electrolysis technologies. Currently, there are three main types of electrolysis (Figure 3): alkaline electrolysis (AE), proton exchange membrane electrolysis (PEME), and solid oxide electrolysis (SOE). AE and PEME operate at low temperatures, while SOE operates at high temperatures.

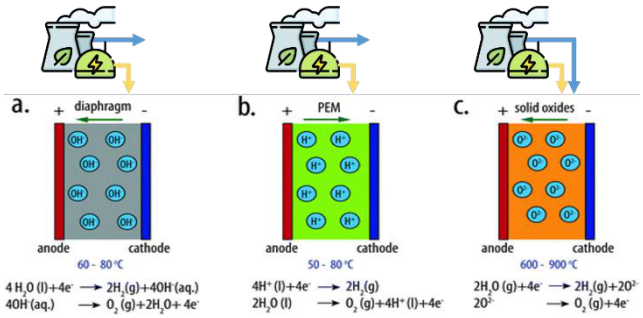

Figure 3. Schematic illustrations of (a) an alkaline electrolyzer (AE), (b) a polymer-electrolyte-membrane electrolyzer (PEME), and (c) a high-temperature solid-oxide electrolyzer (SOE) [14].

Alkaline electrolysis (AE) uses a liquid electrolyte in the form of potassium hydroxide. The electrodes in an AE system are made of metal and are separated by a diaphragm that prevents hydrogen and oxygen from mixing. AE is a well-established and efficient process, with current

efficiencies of about 70% and long-term performance expectations of about 80%. It has advantages that include lower investment costs, a longer lifetime, and the ability to achieve high nominal outputs (>100MW) without needing critical raw materials, such as expensive precious metals as catalysts. However, they are more sensitive to impurities in the product gas because gases dissolved in the electrolyte remain in the cycle and have a long cold start time of 50 minutes. These factors limit the advantages of AE compared to PEME and SOE.

The alkaline water electrolyzer typically operates at ~60–80 °C with a corresponding thermodynamic voltage for water splitting of 1.20–1.18 V. The terminal cell voltage of an alkaline water electrolyzer is 1.8–2.4 V at the typical operating current density of 0.2 to 0.4 A/cm^2 [15], [16].

Proton exchange membrane electrolysis (PEME) is a relatively new technology compared to AE. It is available on an industrial scale and can achieve nominal outputs of over 10MW. PEM electrolysis operates in an acidic environment and uses precious metals such as iridium or platinum to protect the electrodes from corrosion. A gas-proof, proton-conducting polymer membrane is used to achieve higher purity than other technologies. PEM electrolysis has good dynamic properties and is well-suited for operation with fluctuating electricity from renewable sources. It has a high load gradient, meaning it can quickly increase or decrease load absorption. Additionally, the cold start time for PEM electrolysis is only about 15 minutes.

PEM electrolyzers operate within the same temperature range (50–80 °C) as AE. The terminal cell voltage of PEM electrolyzers ranges between 1.8 V to 2.2 V under the typical operating current density of 0.6 to 2 A/cm^2 [17]. A state-of-the-art PEM electrolyzer exhibits a terminal cell voltage of ~1.70 V at an operational current density of 1.0 A/cm^2 at 80 °C [17], [18].

Solid oxide electrolysis (SOE) is currently still in the development stage. Therefore, it involves the highest capital expenditure and the smallest nominal output (150 kW) in comparison to AE and PEME. SOE technologies have been driven by the possibility to operate at high current densities (e.g., 3.6 A/cm^2 at 1.48 V and 950 °C) and efficiencies. With an external heat source, such as industrial or nuclear waste heat, SOE can achieve high-efficiency levels of approximately 80%. SOE is also suitable for co-electrolysis, which can produce synthesis gas directly for further processing for appropriate industries. SOE uses a solid oxide to separate the two electrodes and conducts oxygen ions. The oxide ions are transported from the cathode to the anode across the solid oxide electrolyte by an ionic diffusion process. It also has very long cold start times of several hours.

It operates at high temperatures of up to 1000°C and uses superheated water vapor. The thermodynamically required potential for water splitting using SOE is thus significantly lower (<1.0 V) than for other water-splitting systems.

B. Thermochemical cycles

Thermochemical cycles combine heat sources with chemical reactions to split water into its components. The term “cycle” is used because aside from water, hydrogen, and oxygen, the chemical compounds used in these processes are continuously recycled. Thermochemical cycles use a series of chemical reactions to split water at lower temperatures than can be achieved with heat alone. There are two types of thermochemical cycles, which are either direct or hybrid thermochemical cycles and Figure 4 illustrate examples of each. Direct thermochemical cycles rely solely on thermal energy to drive the reactions, with all process chemicals being fully recycled. Hybrid thermochemical cycles, on the other hand, involve both chemical reactions and an electrolysis step that produces hydrogen from a chemical compound other than water. These cycles require both thermal and electrical energy, but the energy requirements for the electrolysis step are much lower than for water electrolysis. The temperatures required for most thermochemical cycles are quite high, typically ranging from 750 to 1000°C or higher.

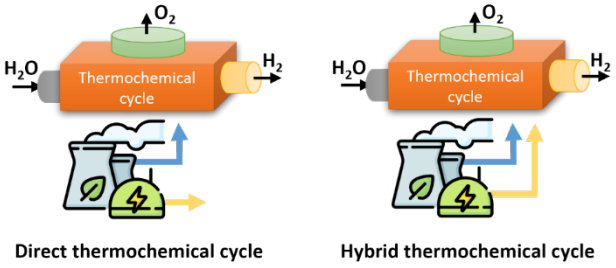

Figure 4. Schematics for direct thermochemical cycles (left) and hybrid thermochemical cycles (right).

Thermochemical cycles are seen as a promising option for hydrogen production due to their potential for high efficiency and scalability. They may also have lower costs than conventional water electrolysis because they produce hydrogen directly from thermal energy, whereas electrolysis requires the conversion of heat to electricity first. Additionally, the economics of scale for chemical plants, such as those used in thermochemical processes, have historically been beneficial compared to more modular electrolysis processes. These cycles can be driven by high-temperature heat sources such as heat from nuclear power reactions.

While thermochemical cycle technology is still relatively immature, there is significant potential for improvement. High temperature or steam electrolysis is a variation of conventional electrolysis that also has the potential for increased efficiency.

V. NUCLEAR POWER FOR ENERGY TRANSITION TO A H_2 ECONOMY

The transition to a low-carbon economy is critical for the move towards a hydrogen economy, where hydrogen replaces traditional fossil fuels as a source of energy. Simultaneous generation of electricity, heat, and high-temperature steam via nuclear energy opens the opportunity to use in hydrogen production via water electrolysis and thermochemical cycles. Low-temperature electrolysis is more suitable for compact hydrogen production at a remote location using the available local renewable resources. Therefore, low-temperature electrolysis options may not be

suitable to couple with nuclear reactors. On the other hand, the high-temperature electrolysis (SOE) or thermochemical cycling for hydrogen can take the most advantage of emission-free heat and efficient electricity produced by nuclear power plants.

Both the high-temperature electrolysis and thermochemical systems must be co-located with the nuclear heat source for such an interface. Therefore, it is essential to consider the type of nuclear power reactor technology when designing a nuclear-hydrogen plant. It is crucial to take into account the specific characteristics of the chosen nuclear power reactor technology. Each reactor technology has its unique features that can influence the efficiency and feasibility of the hydrogen production process. For example, gas-cooled reactors (GCR) tend to operate at higher temperatures, making them suitable for high-temperature electrolysis (HTE) and thermochemical hydrogen production processes. On the other hand, boiling water reactors (BWR) operate at lower temperatures, making them more appropriate for low-temperature electrolysis processes. Fast breeder reactors (FBR) can produce more fuel than they consume, making them highly efficient. Meanwhile, heavy-water reactors (HWR) use deuterium oxide (heavy water) as a moderator and coolant, which can impact the hydrogen production process.

Pressurized water reactors (PWR) are currently the most popular reactor technology in use due to their safety and operational features, making them ideal for nuclear-hydrogen plants. Currently, ca. 2/3 of reactors are in operation, and almost all reactors under construction are of PWR type. However, despite their popularity, they provide lower live-steam parameters than GCR and FBR reactors, which may limit their suitability for certain types of hydrogen production processes [19].

A. High-temperature electrolysis

High-temperature electrolysis (HTE), or steam electrolysis, has the potential for higher overall efficiency. Thermal energy is used to produce high temperature steam, which results in a reduction of the electrical energy required for electrolysis and, therefore, a reduction in the total energy required for hydrogen generation. A schematic diagram of a nuclear hydrogen plant using HTE is shown in Figure 5. The reactor (in this case HTGR) supplies both electricity and steam to the electrolytic cell. The steam generator supplies superheated steam to the cells at a temperature of 750 to 950°C.

Recently, Milewski et al. [19] carried out a theoretical analysis of the coupling of SOE and PWR-based nuclear power plants. The direct utilization of steam fed to the cathodic compartments of SOE is observed in terms of the energy consumption of hydrogen generation. The advantages to applying high-temperature electrolysis coupled with nuclear reactors: (i) there is almost no modification of the nuclear steam turbine cycle, (ii) the flexibility of the nuclear power plant rises by 20% with an almost constant thermal load of the nuclear reactor, and (iii) high-pressure hydrogen is obtained for commercial purposes.

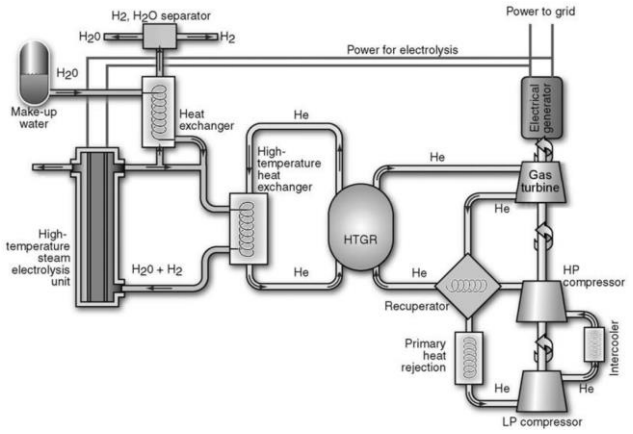

Figure 5. High-temperature electrolysis using gas-cooled reactor [20].

HTE is relatively cheaper than thermochemical cycles as it does not require large reactors or controlled cyclic processes. The highest cost contributor for the HTE cycle is the fuel cost (i.e., cost of electric power) even though the electricity consumption is over 20% less than that of low-temperature electrolysis.

B. Direct and hybrid thermochemical cycling

The main motivation behind the development of thermochemical cycles is to reduce the high cost associated with the direct electrolysis of water which is an electric-energy-intensive process. Pure thermochemical cycles require heat input at high temperatures for the water-splitting process.

The thermal decomposition of water into hydrogen and oxygen occurs at temperatures higher than 2000 °C, although the utilization of redox materials to create the reduction and oxidation cycles can effectively lower the temperature requirements down to 1000 °C [21]. Redox-material-based thermochemical water-splitting reaction cycles can be carried out within a temperature range of 900–1500 °C. These cycles involve two reactions: the first is the thermal reduction of the redox material at a temperature typically higher than the oxidation reaction to generate oxygen and oxygen vacancies within the redox material. The second reaction is the oxidation of the reduced redox material with water to regenerate the redox material and generate hydrogen. Since oxygen and hydrogen are produced in two different reactions, separation of both gases is not required, and the hydrogen produced can be directly utilized as a fuel. The reduction reaction is endothermic and favored at elevated temperatures while the oxidation reaction is exothermic and preferably operated at a lower temperature than the reduction reaction to increase the hydrogen yield.

The direct and hybrid types of thermochemical water-splitting cycles are illustrated in Figure 6. Typically, direct cycles are less complex with fewer steps, but they require higher operating temperatures compared with the more complicated hybrid cycles.

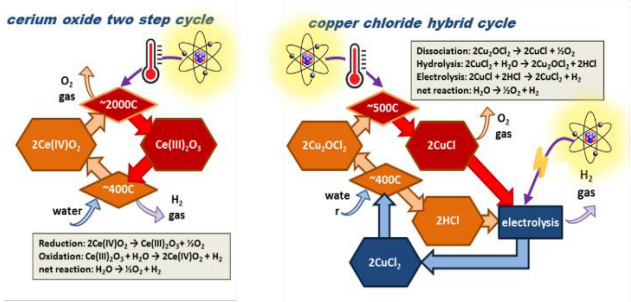

Figure 6. Two examples of thermochemical water-splitting cycles are illustrated. The "direct" two-step cerium oxide thermal cycle (left) and the "hybrid" copper chloride cycle (right) [22].

Several thermochemical cycles have been investigated for hydrogen production, including the Sulfur-Iodine (S-I) cycle, Hybrid Sulfur (HyS) cycle, Copper-Chlorine (Cu-Cl) cycle, and Magnesium-Chlorine (Mg-Cl) cycle. The hybrid Cu-Cl cycle offers great potential in terms of integration with nuclear heat or industrial process heat or renewable or waste heat [23].

The availability of a low-carbon cost-effective heat source at the necessary quality (i.e., temperature) required for the corresponding hydrogen thermochemical cycle is possible considering the advanced nuclear reactor designs. However, it's important to note that despite the potential advantages of nuclear power in hydrogen production, the current generation of nuclear power plants, as well as those under construction, are not yet equipped to support the integration of medium/high-temperature thermochemical systems. The consideration of heat-quality upgrades may facilitate such integration [24]. Research is being conducted to develop advanced nuclear reactors that can produce higher-temperature heat suitable for coupling with these hydrogen production systems. These advanced reactors include small modular reactors (SMRs), high-temperature gas-cooled reactors (HTGRs), and sodium-cooled fast reactors (SFRs). These reactors have the potential to generate heat at temperatures high enough to enable efficient hydrogen production via thermochemical and high-temperature electrolysis routes. With the development of such advanced reactors, nuclear-hydrogen plants could become a feasible option for large-scale hydrogen production in the future.

VI. CONCLUSIONS

The generation of electricity, heat, and high-temperature steam through nuclear energy provides an opportunity to produce hydrogen through high-temperature electrolysis and thermochemical cycles. High-temperature electrolysis is a relatively low-cost option compared to thermochemical cycles as it does not require large reactors or controlled cyclic processes. On the other hand, thermochemical cycles can effectively lower the temperature requirements for the water-splitting process using redox materials. The hybrid Cu-Cl cycle offers great potential for integration with nuclear heat. However, the current fleet of nuclear power plants as well as those under construction may not meet the requirements for coupling with medium/high-temperature thermochemical cycles of H_2 production.

Nevertheless, considering the advanced nuclear reactor designs, the availability of a low-carbon cost-effective heat source at the necessary temperature required for the corresponding hydrogen thermochemical cycle is possible. Thus, the combination of nuclear power with hydrogen production technologies can contribute to an H_2 economy. The goal to combine nuclear and electrochemical areas to achieve eco-friendly, cheap, and safe energy is a very promising direction, but also very challenging in the knowledge transfer aspect. In the author's perspective, it is crucial to foster dialogue between scientists and engineers from seemingly disparate research fields, such as the nuclear industry and electrochemistry/catalysis, to enhance collaboration and innovation. Thus, reaching beyond the traditional solution and offering breakthrough innovations require a constant interdisciplinary dialog among the scientific community and industry partners.

VII. ACKNOWLEDGMENTS

This research was funded by the European Union Horizon 2020 research and innovation program under Grant Agreement No. 857470 and from the European Regional Development Fund via Foundation for Polish Science International Research Agenda PLUS Program Grant No. MAB PLUS/2018/8.

VIII. REFERENCES

[1] "Global climate objectives fall short without nuclear power in the mix: UNECE | UN News." https://news.un.org/en/story/2021/08/1097572 (accessed Apr. 07, 2023).

[2] F. Sorgulu and I. Dincer, "Cost evaluation of two potential nuclear power plants for hydrogen production," *Int J Hydrogen Energy*, vol. 43, no. 23, pp. 10522–10529, Jun. 2018, doi: 10.1016/J.IJHYDENE.2017.10.165.

[3] "Nuclear power and climate change | IAEA." https://www.iaea.org/topics/nuclear-power-and-climate-change (accessed Apr. 07, 2023).

[4] "Climate Change and Nuclear Power 2022 | IAEA." https://www.iaea.org/topics/nuclear-power-and-climate-change/climate-change-and-nuclear-power-2022 (accessed Apr. 07, 2023).

[5] A. Midilli and I. Dincer, "Key strategies of hydrogen energy systems for sustainability," *Int J Hydrogen Energy*, vol. 32, no. 5, pp. 511–524, Apr. 2007, doi: 10.1016/J.IJHYDENE.2006.06.050.

[6] A. Midilli and I. Dincer, "Hydrogen as a renewable and sustainable solution in reducing global fossil fuel consumption," *Int J Hydrogen Energy*, vol. 33, no. 16, pp. 4209–4222, Aug. 2008, doi: 10.1016/J.IJHYDENE.2008.05.024.

[7] R. S. El-Emam, H. Ozcan, and I. Dincer, "Comparative cost evaluation of nuclear hydrogen production methods with the Hydrogen Economy Evaluation Program (HEEP)," *Int J Hydrogen Energy*, vol. 40, no. 34, pp. 11168–11177, Sep. 2015, doi: 10.1016/J.IJHYDENE.2014.12.098.

[8] M. F. Orhan, I. Dincer, and G. F. Naterer, "Cost analysis of a thermochemical Cu–Cl pilot plant for nuclear-based hydrogen production," *Int J Hydrogen Energy*, vol. 33, no. 21, pp. 6006–6020, Nov. 2008, doi: 10.1016/J.IJHYDENE.2008.05.038.

[9] C. Acar and I. Dincer, "Comparative assessment of hydrogen production methods from renewable and non-renewable sources," *Int J Hydrogen Energy*, vol. 39, no. 1, pp. 1–12, Jan. 2014, doi: 10.1016/J.IJHYDENE.2013.10.060.

[10] "Nuclear Energy Agency (NEA) - Nuclear energy in the hydrogen economy." https://www.oecd-nea.org/jcms/pl_20492/nuclear-energy-in-the-hydrogen-economy (accessed Apr. 07, 2023).

[11] "Nuclear hydrogen production | IAEA." https://www.iaea.org/topics/non-electric-applications/nuclear-hydrogen-production (accessed Apr. 07, 2023).

[12] C. Forsberg, "Nuclear Hydrogen R&D Plan," 2002.

[13] A. Poullikkas, "INTERNATIONAL JOURNAL OF ENERGY AND ENVIRONMENT An overview of future sustainable nuclear power reactors," Online, 2013. [Online]. Available: www.IJEE.IEEFoundation.org

[14] C. Xiang, K. M. Papadantonakis, and N. S. Lewis, "Principles and implementations of electrolysis systems for water splitting," *Mater Horiz*, vol. 3, no. 3, pp. 169–173, May 2016, doi: 10.1039/C6MH00016A.

[15] X. Li, F. C. Walsh, and D. Pletcher, "Nickel based electrocatalysts for oxygen evolution in high current density, alkaline water electrolysers," *Physical Chemistry Chemical Physics*, vol. 13, no. 3, pp. 1162–1167, Dec. 2010, doi: 10.1039/C0CP00993H.

[16] K. Zeng and D. Zhang, "Corrigendum to 'Recent progress in alkaline water electrolysis for hydrogen production and applications' [Progr Energ Combust Sci 36 (3) (2010) 307–326]," *Prog Energy Combust Sci*, vol. 37, no. 5, p. 631, Sep. 2011, doi: 10.1016/J.PECS.2011.02.002.

[17] M. Carmo, D. L. Fritz, J. Mergel, and D. Stolten, "A comprehensive review on PEM water electrolysis," *Int J Hydrogen Energy*, vol. 38, no. 12, pp. 4901–4934, Apr. 2013, doi: 10.1016/J.IJHYDENE.2013.01.151.

[18] A. Ursúa, L. M. Gandía, and P. Sanchis, "Hydrogen production from water electrolysis: Current status and future trends," *Proceedings of the IEEE*, vol. 100, no. 2, pp. 410–426, 2012, doi: 10.1109/JPROC.2011.2156750.

[19] J. Milewski, J. Kupecki, A. Szczęśniak, and N. Uzunow, "Hydrogen production in solid oxide electrolyzers coupled with nuclear reactors," *Int J Hydrogen Energy*, vol. 46, no. 72, pp. 35765–35776, Oct. 2021, doi: 10.1016/J.IJHYDENE.2020.11.217.

[20] S. Elangovan, J. Hartvigsen, J. S. Herring, P. Lessing, J. E. O'Brien, and C. Stoots, "Hydrogen Production through High-temperature Electrolysis in a Solid Oxide Cell," pp. 183–200, Apr. 2004, doi: 10.1787/9789264107717-15-EN.

[21] D. Oudejans, M. Offidani, A. Constantinou, S. Albonetti, N. Dimitratos, and A. Bansode, "A Comprehensive Review on Two-Step Thermochemical Water Splitting for Hydrogen Production in a Redox Cycle," *Energies 2022, Vol. 15, Page 3044*, vol. 15, no. 9, p. 3044, Apr. 2022, doi: 10.3390/EN15093044.

[22] "Hydrogen Production: Thermochemical Water Splitting | Department of Energy." https://www.energy.gov/eere/fuelcells/hydrogen-production-thermochemical-water-splitting (accessed Apr. 08, 2023).

[23] F. Safari and I. Dincer, "A review and comparative evaluation of thermochemical water splitting cycles for hydrogen production," *Energy Convers Manag*, vol. 205, p. 112182, Feb. 2020, doi: 10.1016/J.ENCONMAN.2019.112182.

[24] R. S. El-Emam, H. Ozcan, and C. Zamfirescu, "Updates on promising thermochemical cycles for clean hydrogen production using nuclear energy," *J Clean Prod*, vol. 262, p. 121424, Jul. 2020, doi: 10.1016/J.JCLEPRO.2020.121424.

Proceedings of the European Nuclear Young Generation Forum
ENYGF'23
May 8-12, 2023, Kraków, Poland

Design and Fabrication of a Temperature-Controlled Fueled Molten Salt Capsule Irradiation Experiment

Gregory Core*[1], Calvin Downey[1], Morgan Kroop[1], Stephen Warmann[1], Abdalla Abou-Jaoude[1], William Phillips[1], and Chuting Tan[1]

[1] Idaho National Laboratory (INL), United States

*Corresponding author: gregory.core@inl.gov

I. INTRODUCTION

Although its commercial application may be a decade or more away, liquid-fueled Molten Salt Reactor (MSR) technology has recently attracted increased attention through several demonstration efforts underway in the U.S. and abroad. While most concepts build on the legacy of the Molten Salt Reactor Experiment (MRSE) [1], several new concepts under development propose salt compounds that have never been previously tested. While several efforts are underway across the world to develop irradiation testing capabilities for molten salts [2][3][4], none has demonstrated the ability to test enriched fuel bearing salt.

Idaho National Laboratory (INL) is developing a Molten salt Research Temperature-controlled Irradiation (MRTI) experimental capsule for the Neutron Radiography (NRAD) reactor. The experiment is envisaged to be versatile and able to host a variety of salt-wall material combinations. The first test is designed to contain actinide-bearing chloride salt, which previously has not been subjected to a neutron field. The main objectives of the experiment are to produce irradiated salt samples for Post Irradiation Examination (PIE), to evaluate salt behaviour under irradiation, and to test in-situ sensors and instrumentation.

The final design for the experiment was completed in 2022, and fabrication of the experiment is underway, with a prototype completed in February 2023. The salt is double encapsulated providing insulation and redundancy in the case of leakage. A gas-gap between the inner capsule and the outer container enables tuning of thermal conduction to the NRAD coolant by altering its thickness and its gas-mixture. An inert gas mixture ratio in the gas-gap ensures the configurations reached a targeted average salt temperature of 600°C, while avoiding salt freezing or exceeding material limits. A resistive heater placed within a thermowell controls the temperature of the experiment (both when the reactor is on or off). The selected configurations can contain over 10 cm^3 of fuel-bearing chloride salt, which is sufficient for the purposes of the post-irradiation examination (PIE) and provides sufficient volume for two submerged thermocouple probes to monitor salt temperature. The capsule wall material is Inconel 625 (IN625), and weld qualifications for the assembly have been developed. A glove-box laser weld technique was refined as part of this process to ensure a leak-tight assembly for the salt-bearing assembly and reduce the risks of impurities permeating into the salt.

This paper will provide an overview of the completed final design of the experiment, including schematics of Computer Aided Designed (CAD) model. It will then discuss the recent efforts to fabricate a prototype assembly to demonstrate the manufacturing process and conduct out-of-pile testing. This prototype was loaded with non-fuel bearing salt for simplicity. The next step towards irradiation of the fuel-bearing salt experiment will be highlighted as well.

II. EXPERIMENT OVERVIEW

The irradiation experiment is planned for the Neutron Radiography (NRAD) reactor at INL [5]. The reactor is 'TRIGA-type' reactor with UZrH fuel assemblies organized in a square lattice arrangement and surrounded by graphite blocks. An illustration of the reactor is shown in Figure 1. The MRTI experiment is currently planned for the F-1 position of the NRAD core.

While the irradiation test vehicle is expected to be flexible with the ability to irradiate a variety of salt samples, the current iteration described here has been fine-tuned in order to host an enriched uranium bearing chloride salt sample. The primary goal of the experiment is to provide irradiated salt samples that can be used to study the following during Post Irradiation Examination (PIE):

1. Understand and characterize the radiological source term mechanics of salts (i.e., transport of radionuclide to the plenum vs. precipitation/wall plating vs. remaining in solution).
2. Study the evolution of thermophysical properties with burnup as fission and activation products accumulate in solution in addition to gas bubbles and suspended nanoparticles.

3. Evaluate the impact of irradiation-induced (both from neutron damage and fission product generation). corrosion on materials interfacing with the salt.

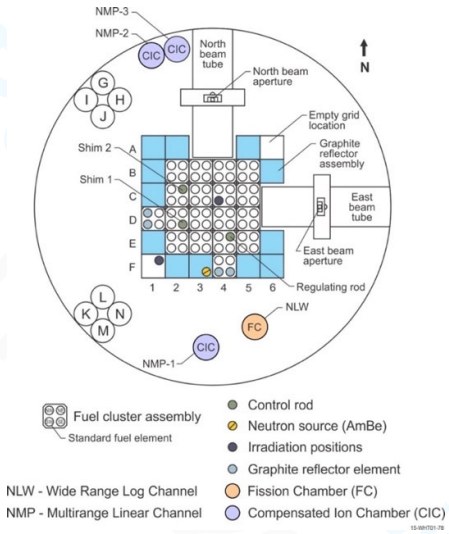

Figure 1. Overview of the NRAD Reactor core layout showing the various positions. Taken from [5].

Previous publications described parametric studies related to the experiment [6], followed by the description of the preliminary design [7]. This work will outline the final design specifications for the experiment along with the fabrication of a prototype assembly (with non-fuel salt). Detailed neutron transport and computation fluid dynamics simulations were conducted to simulate the performance of the experiment under irradiation. These analyses showed that the experiment was shown to be able to reach a targeted fission power density of above 20 W/cm^3, while staying within thermal limits (limiting salt freezing and maximum heater temperature).

III. EXPERIMENT VEHICLE DESIGN

A. Salt-Bearing Capsule Design

The MRTI capsule design features a thin-walled IN625 tube design with a substantial plenum to account for both initial powder salt packing factor (~60%) and for the accumulation of fission gas and chloride gas during irradiation. The wall thickness is designed to allow for laser-based penetration and gas retrieval of the capsule plenum in PIE. IN625 was chosen as the capsule material for its strength at high temperature, and neutronics benefits over similar alloy Inconel 617. To isolate corrosion effects on IN625 alloy, the capsule is designed such that only IN625 is in contact with the molten salt during irradiation (no dissimilar metals and potential galvanic corrosion effects). Active instrumentation is used to record in-situ temperature in the molten salt and plenum region during irradiation. Type N thermocouples with IN625 sheaths were utilized for this design for high temperature operational range and superior irradiation resistance in comparison to Type K. Additionally an optical fiber pressure sensor is utilized to measure changes in plenum pressure during irradiation. Due to size constraints regarding the optical fiber sensor, it is connected into the capsule plenum via a stainless-steel pressure extension tube.

Furnace-style heater designs were considered for initial heating of the fuel salt prior to irradiation. It was important during experimentation to maintain the fuel salt in the molten phase in order to avoid effects from salt radiolysis. For depleted uranium or low enriched uranium experiments furnace heaters are a reliable heating method. However, for higher enrichments involved in this experiment the fission heating of the molten salt would be too well insulated from the NRAD coolant water and would result in extreme temperature outside of the desired operational range of the experiment. Therefore a center cartridge heater is utilized in the MRTI capsule design in order to optimize heat transfer out of the capsule once the salt is self-heating. A high temperature Incoloy-800 sheathed 800 W heater is used as the specified heating element in the MRTI capsule. Due to the large plenum volume in the capsule only the bottom section is in contact with the salt and designed to be heated (bottom 7.6 cm). Input wattage in this heated region must be sufficient to fully melt the fuel salt and but only provide small amounts of supplemental power during irradiation. Because the heater sheath is not IN625, it is assembled into an IN625 thermowell in the axial center of the capsule.

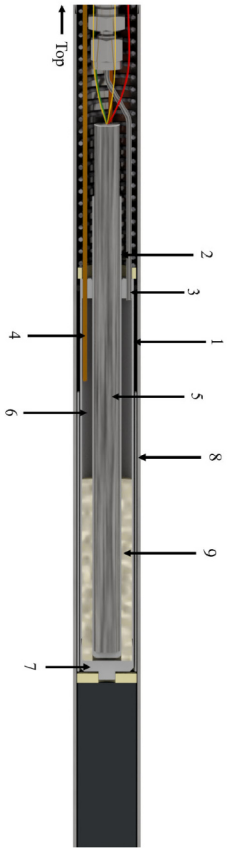

Figure 2. Half section view of MRTI capsule design. 1.) Capsule, 2.) Capsule heater thermowell, 3.) Pressure tube extension, 4.) Type-N thermocouple, 5.) Immersion heater, 6.) Plenum, argon gas, 7.) Capsule plug, 8.) Radiative Heat Shield, 9.) Molten salt volume

Heat transfer out of the capsule is controlled via an inert gas gap which is held via standoff geometries machined on the outer diameter of the capsule. Based on initial thermal hydraulic results this gas gap was designed as a 85% argon, 15% helium mixture in a total radial thickness of 0.76 mm. Further analysis utilizing STAR CMM+ revealed that at high temperatures – in the range of 1000°C – radiative heat transfer from the wall of the capsule becomes a driving mechanism of heat loss. Therefore, a radiative heat shield fabricated from 316 stainless steel (SS316) acts as an intermediate boundary between the capsule wall and the capsule containment, splitting the gas gap into two separate radial sections, and reducing radiative heat transfer.

Fuel salt with an argon atmosphere is sealed in the capsule by a combination of laser welding and induction braze procedures on the top of the capsule bulkhead and the bottom end cap.

B. Outer Can Design

The MRTI inner capsule is assembled in an outer can containment which ultimately seals the experiment from the NRAD coolant water and maintains the gas gap composition of the experiment. Outer can containment geometry is designed to resemble typical NRAD fuel pin geometries as to maintain prototypical cooling conditions on the outer diameter of the experiment. Similar to the NRAD fuel pins, the outer can containment and all welded fittings are machined from SS316L. The inner diameter of outer can containment is defined by the gas gap and capsule geometries. A top fitting on the outer can containment is welded to the outer can containment tube to interface with existing NRAD cluster assemblies shown in Section III,C.

To maximize heat generation rates of the fuel salt the midplane of the salt is aligned axially with fuel midplane of the NRAD reactor. A graphite spacer is designed with the correct height for the capsule placement at the desired axial position. Graphite was the chosen as the spacer material in order to maintain as much moderating material as possible when displacing water with the MRTI assembly. Because graphite is relatively thermally conductive a bisque-alumina is utilized as an insulative spacer between the capsule and graphite spacer. This bottom insulative spacer is designed with machined axially standoffs to create a gas gap between the capsule and most of the bisque-alumina material.

Above the capsule a SS302 compression spring holds the capsule and internals axially static during handling and irradiation, and accounts for any axial thermal expansion. To reduce potential loss of elasticity in the spring and additional axial heat loss in the in capsule a top insulative annular spacer is used between the spring and capsule. In this region above the capsule and within the inner diameter of the spring the pressure extension tube from the capsule is assembled onto the optical fiber pressure sensor via a compression swage fitting. Instrumentation and heating cabling is routed around the swage fitting and fed through a compression gland seal fitting at the top of the outer can containment assembly. Soft cabling from the heater is potted via hermetic sealing compound at the compression gland fitting. Instrumentation and extension cabling is collected and reaches approximately 3 m to the top of the NRAD coolant pool.

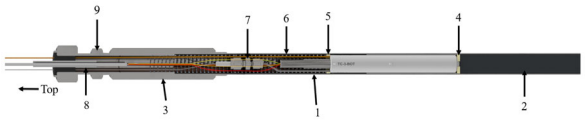

Figure 3. Cross-section view of the MRTI outer can containment design. 1.) Outer can geometry, 2.) graphite spacer, 3.) Outer can top fitting, 4.) Bottom insulation spacer, 5.) Top insulation spacer, 6.) compression springs, 7.) Swagelok fitting, 8.) Leadout potting cup, and 9.) Top compression seal fitting.

C. Experiment Assembly

The outer can containment MRTI experiment vehicle is designed to interface with typical NRAD cluster assembly hardware which interfaces with the NRAD core. To interface with the NRAD bottom cluster end fitting a male threaded bottom fitting is welded to the bottom of the outer can containment tube. Because the cluster assembly comprises four fuel pins, three other pins are required for the design. While graphite-filled or NRAD fuel pins have been considered for these cluster positions, ultimately aluminium 6061 mock pins were fabricated for the cluster assembly. In future experiments, these pins offer the opportunity for multiple MRTI experiment positions within a single cluster design. The cluster is held at the top by a lock-plate and bail assembly.

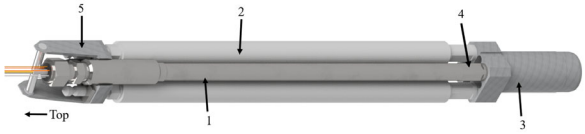

Figure 4. Isometric view of the MRTI cluster design. 1.) MRTI experiment vehicle, 2.) Aluminum pins, 3.) Bottom cluster end fitting, 4.) MRTI bottom fitting, 5.) Top cluster bail.

IV. PROTOTYPE FABRICATION

Experiment prototyping activities were conducted to improve assembly techniques and ultimately fabricate a scale surrogate-salt containing mock-up of the MRTI assembly. This assembly will then be leveraged for system commissioning testing of the MRTI heater temperature controller and expected outer can containment wall temperatures based on thermal hydraulic modelling.

A. Capsule Machining and Assembly

Capsule geometries were machined from IN625 bar for the inner capsule top and the capsule end cap. Bulkhead penetrations are drilled in the top of the inner capsule for braze assembly activities. High temperature nickel braze BNi-5 was identified as the material for the MRTI capsule with an operational temperature above 1000°C, and this material requires hole clearance of under 0.025 mm with the instrumentation and thermowell outer diameter. Induction brazing techniques were developed in accordance with American Society of Mechanical Engineers (ASME) Section IX qualification procedures for brazing IN625 sheath into IN625 bulkhead, as well as the

SS316 pressure extension tube into the bulkhead. This process was executed in one induction braze process using the high temperature BNi-5 braze. This braze is performed under purged flowing helium atmosphere at controlled pressure in order to reduce potential oxidation at the braze joint. Iterative parameter development and sample analysis was required to qualify the braze procedure for use in the experiment assembly.

Figure 5. Induction braze of an IN625 sheath instruments and thermowell in a IN625 bulkhead with prototypical thickness to MRTI capsule.

The capsule end cap is designed to be laser welded onto the capsule top. Laser welding is desirable for this application due to the thin wall of the capsule and the need to avoid potential salt melting during the welding process (laser welding provides control over local energy input in comparison to traditional hand welding techniques). An integral backer geometry with an internal interference fit is designed into the capsule wall to provide additional thermal protection of the salt during the welding process to avoid this unintended melting. This weld is performed under argon atmosphere and ultimately seals the argon plenum atmosphere in the capsule. This weld was also developed and qualified to ASME Section IX standards and testing.

Instrumentation, pressure tube extension, and the heater thermowell are induction brazed to the capsule top using the developed procedure. The compression swage fitting is installed on pressure extension tube and the fitting is capped with a union fitting or the pressure sensor is installed onto the fitting (pressure sensor is not required for surrogate salt commissioning test). From this assembly stage the capsule is filled with the surrogate LiCl-KCl salt powder using the same glovebox procedures which would be used for the fuel salt material to mock-up the assembly process. Because of leadout instrumentation a custom clamping assembly was designed to hold the capsule off the glovebox floor for salt loading. A custom metallic funnel is used to ensure catchment of salt in the capsule during loading. Once loaded, the clamp assembly also is designed to press the capsule end cap onto the capsule interference fit. Once the capsule is pressed it is ported into a laser welding glovebox and a weld is performed to seal the end cap to the capsule.

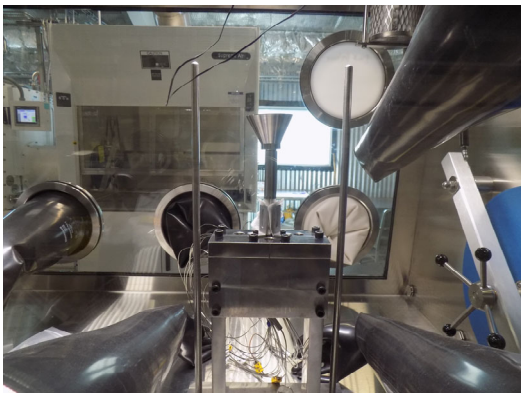

Figure 6. In-process capsule mounting, funnel and salt loading, and rails used for capsule end cap pressing.

B. Experiment Vehicle Assembly

With the completed assembly of the capsule the outer can containment assembly can be assembled. The outer can bottom fitting is pressed onto the outer can tube interference fit and welded onto the outer can tube with similar laser welding techniques for SS316L. The graphite spacer is first loaded into the outer can, followed by a pre-assembled combination of the capsule, radiative heat shield, and bottom and top insulative spacers.

Above the capsule and top insulative spacer the compression springs are slid over all instrumentation and leadouts. The outer can top fitting is then installed over the springs and pressed onto the interference fit on the outer can tube. This top fitting is then laser welded to the outer can tube. The compression seal gland fitting is then assembled over the instrumentation and onto the top can fitting. Gland internals of grafoil are carefully installed over all instrumentation and the heater cabling potting cup. The unsealed assembly is backfilled in a glovebox with the desired gas mixture. The final seal of the assembly occurs via installing the compression fitting manufacturer's instructions. After instrumentation and cabling connector installation is completed the MRTI outer can experiment vehicle is finished and inspected.

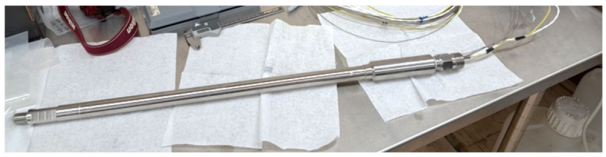

Figure 7. Completed MRTI surrogate salt experiment vehicle.

V. FUTURE WORK

Work is already underway to synthesize enriched UCl_3 to load in the final experiment assembly. Once this is completed, the fabrication process will be repeated in a controlled environment (due to the sensitive material) and loaded with enriched fuel bearing salt.

All the required documentation has also been submitted as part of the 'Experiment Safety Analysis' (ESA), and is currently under review. Once this is approved and the experiment is fully fabricated, the team can proceed to

installing the experiment within NRAD. Mimicking the layout of a TRIGA fuel cluster is expected to streamline this step. Initial zero-power testing in the reactor will then be conducted to check that the heater and all other systems (namely the controller and sensors) are operating as expected. After clearing these tests, the NRAD reactor power will be slowly ramped up and the irradiation can begin. The current plan is to commence irradiation around summer of 2023 timeframe. Around 30-days of irradiation (non-continuous) are planned. At the end of this, PIE activities can commence with the assembly transported to an INL hot cell where it will be disassembled. The initial plan is to conduct neutron radiography, gamma scan, and gas analysis. Future PIE could also include measurement of the irradiated salt properties and evaluating corrosion of salt-facing wall material.

VI. SUMMARY

The MRTI experiment design has been completed with the fabrication process demonstrated on a prototype assembly. The experiment is able to host salt samples around 10 cm^3 of salt that will be kept at temperature using an immersion heater. Salt temperature will be monitored by submerged thermocouple sensors. The salt-bearing capsule is composed of IN625 alloy and is double encapsulated for defence in-depth. The second can is made of SS316. A gas-gap separating both contains a mixture of He-Ar gas that can be fine-tuned to control the experiment temperature.

A prototype assembly was fabricated and assembled to test the manufacturing process of the experiment. It was loaded with non-fuel bearing salt for this initial phase. Welding and brazing procedures for IN625 had to be established. The final experiment assembly was conducted in an inert environment with the recommended gas mix. The next step is to repeat this process with fuel-bearing salt that will then be loaded to the NRAD reactor for irradiation.

VII. ACKNOWLEDGEMENTS

This paper was authored by Battelle Energy Alliance LLC at Idaho National Laboratory under contract no. DE-AC07-05ID14517 with the Department of Energy. This research work was funded through the INL Laboratory Directed Research and Development (LDRD) program, grant number 21A1050-016FP, under the DOE Idaho Operations Office.

The authors gratefully acknowledge the contribution of the various other colleagues as part of the design effort, namely James Chandler, Matilda Lindell, Sujong Yoon, Stacey Wilson, and Kim Davies.

VIII. REFERENCES

[1] R. E. Thoma, "Chemical Aspects of MSRE Operations," Oak Ridge National Laboratory, ORNL-4658, 1971.

[2] N. D. Ezell, J. McDuffee, K. Smith and S. Raiman, "Initial Irradiation Testing of Chloride Salts for Molten Salt Reactors," in ANS Winter Meeting, Orlando, 2018.

[3] P. R. Hania, "MSR Irradiation Program at NRG Petten," in MSR Workshop 2018, Oak Ridge, 2018.

[4] C. W. Forsberg, P. F. Peterson, K. Sridharan, L. Hu, M. Fratoni and A. Kant-Prinja, "Integrated FHR Technology Development: Trititum Management, Materials Testing, Salt Chemistry Control, Thermal Hydraulics and Neutronics, Associated Benchmarking and Commercial Basis," NEUP Report, MIT-ANP-TR-180, 2018.

[5] Bess, J. D. and Higgs, J. B. and Lell, R. M., “Neutron Radiography (NRAD) Reactor 64-Element Core Upgrade”, Idaho National Laboratory, INL/EXT-13-29628, 2014.

[6] A. Abou-Jaoude, J. Chandler, G. Core, K. Davies, C. Downey, W. Phillips, C. Tan and S. Wilson, “Conceptual Design of Temperature-Controlled Fuelled-Salt Irradiation Experiment to Support Demonstration of Advanced Nuclear Reactors”. In Proc. International Mechanical Engineering Congress and Exposition, Virtual, 2021.

[7] A. Abou-Jaoude, C. Downey, G. Core, K. Davies, W. Phillips, C. Tan, S. Yoon, and S. Wilson, “Deign and Prototyping of a Fissile-Bearing Chloride Salt Irradiation Experiment”, in *Transactions of the American Nuclear Society*, Virtual, Nov. 2021.

Proceedings of the European Nuclear Young Generation Forum
ENYGF'23
May 8-12, 2023, Kraków, Poland

Superconductivity for Nuclear Fusion

Haack, Julia[1*]

[1] UN-NYG, Vienna, Austria

*Corresponding author: *juliahaack1@gmail.com*

I. INTRODUCTION

Although mistakenly considered a technology of the distant future, fusion devices have been researched, designed, and constructed for decades, with fusion power plants anticipated as early as the 2030s. Typically, when considering fusion devices, most people with basic knowledge of the concept picture a large tokamak using magnetic fields to confine a D-T plasma within a vacuum vessel. However, fusion research encompasses many different combinations of fuel, confinement technology, and concepts. There are three main types of confinement concepts today: Magnetic Confinement Fusion (MCF), Magneto-Inertial Fusion (MIF), and Inertial Confinement Fusion (ICF). Despite the development of these alternative concepts, magnetic confinement fusion remains the most popular choice for eventual power production. However, steady power production with MCF can only be achieved using powerful superconducting magnets.

Superconductivity refers to the property of some materials to conduct electricity without resistance, typically at very low temperatures nearing 0 K. Ordinary conductors display a gradual decrease of resistance as their temperature decreases, while superconductors have a characteristic critical temperature, below which the resistance drops abruptly to zero [1]. Considering the magnetic field is proportional to the electrical current carried by the electromagnet, superconducting magnets can fulfil the extreme field requirements for confining the plasma in a MCF device, like tokamaks, stellarators, or spheromaks. Despite their great potential in nuclear fusion, superconducting magnets still present challenges that must be addressed before their widespread usage. Some of the obstacles throughout history and being researched today are manufacturing difficulties, irradiation damage, reliability with long-term use, and cost. Future applied superconductivity research aims to address these challenges, paving the way for fusion power plants. This paper reviews the historical context of superconductivity within the scope of fusion research, addresses the status of worldwide fusion projects using superconductors, and finally, identifies areas of ongoing and future research addressing these challenges.

II. HISTORY OF FUSION AND SUPERCONDUCTING MAGNETS

In the 1950s, the claims presented by German scientist Ronald Richter in his Huemel project catalysed early fusion research [2]. Despite failing to achieve nuclear fusion, it prompted the US, UK, and USSR to begin their own endeavours into fusion energy production. In the US, scientist Lyman Spitzer began research on his stellarator concept, while USSR counterparts Andrei Sakharov and Igor Tamm built their linear pinch fusion machine. By 1955, the USSR had built the first toroidal fusion device.

Simultaneously, research into superconducting materials began to gain traction. In 1954, Nb_3Sn was discovered as a superconductor and the following year, US scientist George Yntema coiled the first magnet with superconducting Nb wire, producing a field of 0.7 Tesla [3].

In 1958, the USSR began operation of the first tokamak, T-1, while Spitzer's stellarator model became the focal point of the Atoms for Peace convention in Geneva [4]. Despite growing interest in both tokamaks and stellarators, around this time all fusion devices showed high rates of plasma leakage. US physicist David Bohm had theorized that plasma diffused along lines of force at a rate inversely proportional to the magnetic field, whereas classical diffusion stated that plasma diffusion was inversely proportional to the square of the magnetic field [5].

$$D_{Bohm} = \frac{1}{16}\frac{k_B T}{eB} \quad (1)$$

where k_B is the Boltzmann constant, T is the electron gas temperature, and B is the magnetic flux density.

Bohm's diffusion rate was much higher than classical diffusion and meant that magnetic confinement fusion would not be practical. Although his theory was later replaced by neoclassical diffusion, Bohm Diffusion plunged fusion research into a period of stagnation, believing that, among other obstacles, the current magnets available could never supply the fields required for confinement.

Contrasting the pessimism surrounding fusion, superconductor research rapidly progressed with niobium-tin sustaining superconductivity at large currents and strong magnetic fields (nearly 9 T) in 1961, bridging the gap between the high magnetic field required and current materials available for MCF [3]. The following year, comparatively less brittle NbTi alloys produced fields up to 10 T, prompting commercial production of NbTi superconducting wire at Westinghouse.

After physicists in the USSR began reporting impressive 1000 eV electron temperatures in their T-3 tokamak, the tokamak spiked in popularity with a flood of new proposals in 1969 [6]. Although Spitzer's stellarator concept was originally popular in the US, MIT's Alcator, General Atomics' Doublet, UT-Austin's Texas Turbulent Tokamak, and PPPL's Symmetric Tokamak were all designed in the two years following T-3's results.

In 1978, superconductivity and fusion research finally merged with the USSR's T-7 tokamak, which used superconducting NbTi toroidal field (TF) coils [4]. Figure 1 below shows the NbTi wires placed between the grooves of the nine copper cooling channels in the T-7 tokamak. Of the two available superconducting wires at the time, NbTi offered higher ductility, hence increased manufacturability and affordability, whereas NbSn provided a stronger magnetic field at a maximum of 30 T (compared to NbTi B_{max} = 15 T) and slightly higher critical temperature of 18.3 K (NbTi T_c = 10 K).

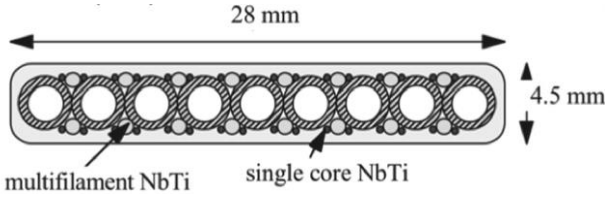

Figure 1. Cross section diagram of T-7 NbTi wire [7]

In the 1970s, Europe, Japan, and the US began designing large-scale tokamak experiments TFTR, JET, and JT-60, which each began operation in 1982, 1983, and 1985, respectively. Throughout the 1980s, the plasma operations of these large experiments revealed new plasma instability issues, requiring higher triple products than each machine was able to produce.

There had been some discussion between the USSR and US about an International Tokamak Reactor (dubbed INTOR), which was only revived during the Geneva Summit of 1985 where Reagan and Gorbachev proposed the new ITER project. In 1986, fusion research was consolidated under one multinational, massive tokamak project [8].

The next few years also brought three major discoveries in superconductivity [3]:

- 1986: Bednorz and Müller at IBM Zurich discover first high temperature superconductor (HTS) LBCO at T_c = 35 K
- 1987: University of Houston and University of Alabama discover YBCO at T_c = 93 K
- 1988: BSCCO discovered at T_c = 96 K in Japan

Finally, in 1988, design work on ITER began. Generally, ITER has three main magnet systems in their design: toroidal field (TF) coils, poloidal field (PF) coils, and the central solenoid (CS). Figure 2 shows the general design and location of each type of coil in ITER's magnet system.

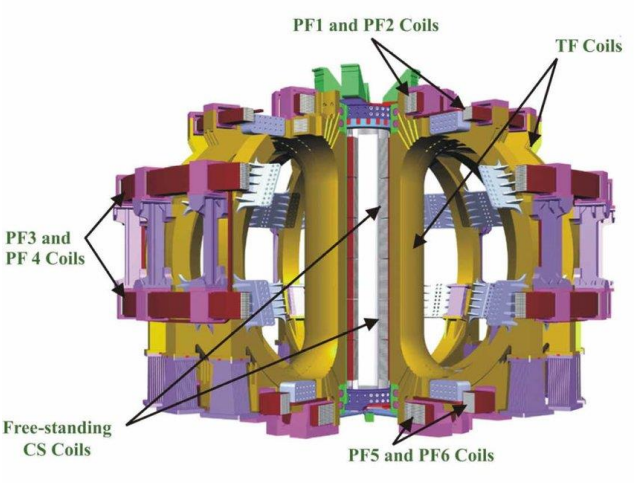

Figure 2. ITER's magnet system [9]

Reported in the 2002 design, the 18 TF coils are Nb_3Sn cables inside a stainless-steel jacket (shown in Figure 3) and held in place by grooved steel plates. To form one large TF magnet, the cables are pancake-wound in a welded SS case, treated with wind-and-react technique.

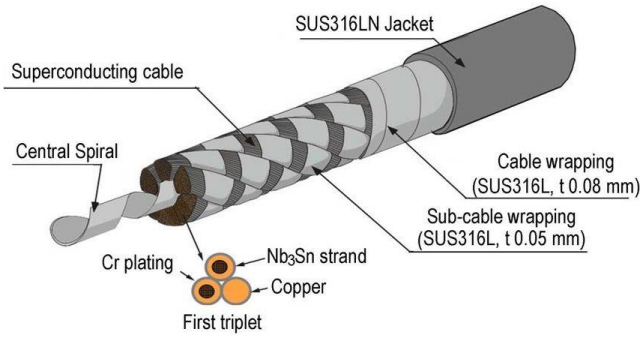

Figure 3. Schematic of ITER's TF Nb_3Sn cable-in-conduit conductor (CICC) wire [10]

The central solenoid is made of Nb_3Sn in a jacket, and split into six individual modules, built from multiple pancake layers, treated with the wind-and-react technique. Finally, the poloidal field coils are made of NbTi in a square SS conduit, constructed into double pancakes [11].

III. PRESENT STATUS

In 2022, ITER's magnet systems had the same basic materials and structure, mainly due to the limitations of ITER's design phase schedule. Despite research advances in HTS materials, low temperature superconductors (LTS), like Nb_3Sn and NbTi, are still common choices for tokamaks due to their lower cost and availability, which can also be partially attributed to the market demand created by ITER. One major change to ITER's magnet design is the replacement of conventional Cu leads for HTS current leads. Despite most suppliers switching from Generation 1 HTS materials (e.g., BSCCO) to G2 HTS materials based on rare-earth barium copper oxides (REBCO), ITER made a final design choice in 2006 to use

Bi2223 current leads, minimizing risk by avoiding the newer G2 HTS materials [12].

Currently, public tokamak research projects like ITER, EAST in China, and KSTAR in Korea still utilize LTS, however, several private and public projects have begun designing tokamaks with HTS. Today, HTS are generally defined as materials that achieve superconductivity above 77 K, with the ability to be cooled with liquid nitrogen rather than the more expensive, difficult-to-handle liquid helium. By increasing the magnetic field, MCF devices with HTS can be significantly smaller than low-field, large tokamaks like ITER. In recent years, REBCO HTS wires have become commercially available, supplied by companies like Bruker, AMSC, Fujikura, SuperOx, SuperPower, and Theva, among others. YBCO has become particularly popular for fusion applications due to the lower neutron cross section of Y (1.28 b) compared to other rare earth elements.

Commonwealth Fusion Systems (CFS), formed in the US in 2018, has begun construction on their SPARC project, a compact tokamak utilizing the high field generated from YBCO HTS magnets. For their proposed next stage fusion power plant, ARC, the major radius will be 3.3m, almost half the size of ITER's R = 6.2m. CFS's HTS magnets were made possible thanks to breakthroughs in production of $YBa_2Cu_3O_7$ with uniformly distributed Y_2O_3 nanoparticles, creating a simpler, reproducible microstructure. In 2021, SuperOx manufactured 300 km of 4mm wide YBCO tape in 9 months, making history as the largest completed order of 2G HTS tape [13].

In the UK, the private company Tokamak Energy is constructing their Demo4 magnet system, comprising of 14 TF and 2 PF coils with REBCO HTS at 20 K and expected to reach a field over 18 T. The system will demonstrate the interaction of the magnetic coils and test control and protection systems of the coils in a simple tokamak configuration, informing the design of their ST80-HTS spherical tokamak. At the UKAEA, the Spherical Tokamak for Energy Production (STEP) project is in its conceptual design phase, predicted to also utilize REBCO HTS to achieve the high field requirements.

One interesting alternative to using either HTS or LTS is the proposal of hybrid HTS-LTS magnets for EU-DEMO and the China Fusion Engineering Test Reactor (CFETR). Using hybrid magnets maintains the high-field advantage of HTS while balancing their high cost with the comparatively cheaper LTS materials. For CFETR, Nb_3Sn and NbTi strands are combined with Bi2212 and REBCO, with their placement dependant on which areas need a higher, more reliable magnetic field [14].

Renaissance Fusion, a private company based in France, has proposed direct deposition and patterning of HTS onto large cylinders to form the magnets needed for their stellarator. Multiple layers of HTS are deposited onto the cylinder to imitate multiple windings of coils. A laser then ablates the layers, forming grooves on the surface of the cylinder that act as boundaries for the current to follow. The complicated patterns will allow the HTS covering the cylinder surfaces to produce the unusual magnetic fields required for stellarators [15]. However, due to the currently pending patents, there is little public information on this process.

Although scientific breakeven (greater energy produced than required) was achieved by the National Ignition Facility in California in December 2022, breakeven with MCF has not yet been accomplished. Currently, there are MCF devices under construction which theoretically will produce Q > 1, but greater materials R&D, with emphasis on superconductivity, is required for deployment of fusion power plants.

IV. AREAS OF FUTURE RESEARCH

Fortunately, the high-field requirements for MCF have bolstered research into superconducting magnets, with a large focus on commercialization of HTS tape. However, there are still obstacles to applied superconductivity for fusion. Ongoing research on superconducting magnets for fusion aims to address these main challenges:

- Manufacturing difficulties and mechanical strength
- Irradiation and long-term availability
- Quench protection issues
- Cost of superconductors and cryogenic cooling

One of the main obstacles to mass-producing superconducting magnets is its characteristic brittleness, a property unideal for forming flexible wires and tapes in lengths of kilometres required for fusion. The majority of high temperature superconductors are also ceramics, compared to the metallic low temperature superconductors. To combat this, HTS tapes are manufactured on a metallic substrate and stacked between layers, leading to better mechanical properties (see Figure 4).

Figure 4. General stacking structure of YBCO HTS tape [16]

Since heat treatment is required for Nb and Sn to react and form Nb_3Sn, there is ongoing research on whether to wind the cable in a steel conduit first and then perform heat treatment (wind-and-react, WR) or to perform heat treatment prior to winding (react-and-wind, RW). ITER currently uses WR technique, aiming to reduce the close strain monitoring of the brittle tape as it is wound and handled. However, for EU-DEMO, the Swiss Plasma Center has proposed revisiting RW technique, indicating that the critical current of the superconductor is 30% higher than when treated with WR [17]. Since the wire jacket and welds are not exposed to heat treatment with RW method, there is also greater freedom in the jacket thickness and shape [14]. After performing a comparison, however, the Korean Institute for Fusion Energy argued that there are not clear advantages to RW technique [18], indicating there is further room for research in this topic.

Superconducting magnets are also subject to internal loads from the current and magnetic field during tokamak

operation, causing local bending of strands and eventual filament breakage. The performance degradation of the superconducting tapes will require maintenance and replacement of components that already contribute significantly to the overall cost of the tokamak. Another important factor contributing to material degradation is the irradiation of superconducting components. One of the products of the D-T fusion reaction is 14.1 MeV fast neutrons which can escape the vacuum vessel and interact with surrounding materials, especially in compact tokamak systems. The neutron radiation can affect the superconductor by creating defects in the lattice, consequently lowering the critical temperature and inducing changes in the critical current density. Annealing processes may recover the critical temperature and current in the superconductor after irradiation and future research is dedicated to finding magnet treatment methods which ensure long-term availability [14]. Additionally, continuous research into irradiation-resistant materials and magnet designs is needed to prevent degradation and costly maintenance.

Quench is the sudden loss of the superconducting state, propagating heat throughout the magnet and bringing it to a normal, discharged state. If either the field or the rate of change of the field is too large within the magnet, quenches can occur, endangering the entire magnet system. The design of quench protection systems includes two goals: to rapidly detect the quench and to immediately discharge the energy in the magnets. ITER currently tackles this by monitoring the resistive voltage of the coils, sending a signal if it begins to rise, and opening switches connecting the coil to large resistors, discharging the whole system in roughly 1.5 minutes. However, quench in HTS magnets is not as understood as LTS, prompting further research into quench protection systems for compact tokamaks.

Currently, the superconducting magnet systems make up 30% of ITER's overall cost [14]. Eventually, with demonstration power plants creating greater market demand for superconductors and increasing competition among superconductor suppliers, this cost will decrease. However, at this point, the industry is still lacking in readily available, cost-effective superconducting tape options. Further research into mass-manufacturing methods and novel superconducting materials would address this glaring obstacle to economically feasible fusion power plants.

V. CONCLUSIONS

Historically, breakthroughs in superconductivity have aided and spurred fusion research, cementing superconductors as an enabling technology for magnetic confinement fusion power plants. Today, applied superconductivity research is even more critical. By addressing current obstacles like manufacturing challenges, long-term availability, quench issues, and high cost, superconductivity research will play an important role in the realization and deployment of fusion electricity production. Multiple solutions to existing issues for fusion magnets have been proposed, but greater effort in international coordination between researchers will allow for more efficient and focused development.

VI. References

[1] M. Cyrot and D. Pavuna, *Introduction to superconductivity and high-Tc materials*. World Scientific Publishing Company, 1992.

[2] R. Arnoux, "'Proyecto Huemul:' the prank that started it all," *ITER*, Oct. 2011. [Online]. Available: https://www.iter.org/newsline/196/930.

[3] K. H. Bennemann and J. B. Ketterson, 'History of Superconductivity: Conventional, High-Transition Temperature and Novel Superconductors', in *Superconductivity: Conventional and Unconventional Superconductors*, K. H. Bennemann and J. B. Ketterson, Eds. Berlin, Heidelberg: Springer Berlin Heidelberg, 2008, pp. 3–26.

[4] V. P. Smirnov, "Tokamak Foundation in USSR/Russia 1950–1990," *Nuclear Fusion*, vol. 50, no. 1, p. 014003, 2009.

[5] D. Bohm, *The characteristics of electrical discharges in Magnetic Fields*. New York: McGraw-Hill, 1949.

[6] M. Kenwood, "Fusion Research – The Temperature Rises", *New Scientist*, vol. 82, no. 1156, p. 626, May 1979.

[7] D.P. Ivanov, *et al*., "Test results of 'Tokamak-7' superconducting magnet system (SMS) sections", *IEEE Transactions on Magnetics*, vol. 13, no. 1, pp. 694-695, Jan. 1977

[8] M. Claessens, in *ITER: The giant fusion reactor: Bringing a sun to Earth*, Cham: Springer, 2020.

[9] V. L. Tanna, 'Design and analysis of the superconducting current feeder system for the International Thermonuclear Experimental Reactor (ITER)', Oct. 2006.

[10] Y. Takahashi *et al.*, 'Technology Development for the Manufacture of Nb_3Sn Conductors for ITER Toroidal Field Coils', presented at the 23rd IAEA Fusion Energy Conf. (FEC 2010), Daejeon, Republic of Korea, Oct. 2010, pp. 558.

[11] R. Aymar, P. Barabaschi, and Y. Shimomura, "The ITER design," *Plasma Physics and Controlled Fusion*, vol. 44, no. 5, pp. 519–565, Apr. 2002.

[12] P. Bauer, *et al.,* "Development of HTS current leads for the ITER project," *IOP Conference Series: Materials Science and Engineering*, vol. 756, no. 1, p. 012032, Mar. 2020.

[13] A. Molodyk, *et al*., "Development and large volume production of extremely high current density YBa2Cu3O7 superconducting wires for fusion," *Scientific Reports*, vol. 11, no. 1, Jan. 2021.

[14] N. Mitchell, *et al*., "Superconductors for fusion: A roadmap," *Superconductor Science and Technology*, vol. 34, no. 10, p. 103001, Sep. 2021.

[15] F. Volpe, 'ICTP STI Colloquium: High-field stellarators with liquid metal walls', International Centre for Theoretical Physics, Jul. 2022.

[16] D. Yu, *et al.*, "Experimental Analysis of Critical Current and Alternating Current Losses of High-Temperature Superconductor Tape with Resin and Gallium-Indium-Tin," *Materials*, vol. 11, no. 4, p. 573, Apr. 2018.

[17] P. Bruzzone, *et al.,* 'A Prototype Conductor by React&Wind Method for the EUROfusion DEMO TF Coils', presented at the 25th International Conference on Magnet Technology (MT25), Amsterdam, Netherlands, Aug. 2017.

[18] S. Kwon, "Comparison of EU-DEMO React&Wind Nb3Sn TF CICC Current Sharing Temperature Against Wind&React Nb3Sn CICCs", *Progress in Superconductivity and Cryogenics*, vol. 24, no. 2, pp. 7-18, Jun. 2022.

Proceedings of the European Nuclear Young Generation Forum
ENYGF'23
May 8-12, 2023, Kraków, Poland

A Look Back at the Portable Nuclear Reactor that Sat on Top of the World

Hylko, James M.
Hylko Nuclear, LLC
*Corresponding author: *JHylko1@msn.com*

I. INTRODUCTION

Small Modular Reactors (SMRs) – a term used to differentiate them from larger nuclear reactors – are a newer generation understood to be smaller than 300 MW(e) per reactor in output. The SMR design concepts can be deployed in multiple module configurations within a single power plant providing flexible power generation for a wider range of users and applications, such as remote areas, district heating, desalination systems and even conventional electrolysis to support hydrogen gas production. Furthermore, these concepts provide an alternative to importing fossil fuels [1].

These ideas antedate to the 1940s, when the U.S. Air Force, Army, and Navy each initiated small-reactor research and development projects. Today's modular field concepts are most comparable to the U.S. Army Nuclear Power Program (ANPP). Its mission was to develop small, pressurized water reactors (PWRs) and boiling water reactors (BWRs) to generate electrical and space heating energy at remote, relatively inaccessible sites.

For example, electrical and heat analyses, and fuel requirements at remote installations, such as the Greenland Ice Cap, indicted nuclear power could overcome supply and transportation issues providing an overall savings compared to using conventional fuels. A conventional diesel engine plant supplying electrical energy for a remote site would require ~8,500 barrels of diesel fuel, costing ~1,510,000 zł (32,5000 €) and weighing ~1,700 metric tonnes. Transportation and deliveries would require 15 451-km round trips across the Ice Cap by six D9-type tractors having 1.4-metre tracks giving them low ground pressure over the soft snow, each pulling two tankers. The tractors delivering this fuel would consume ~852,00 litres of fuel, while a single aircraft could transport and deliver a nuclear power plant with enough fuel to operate for one to two years [2].

Of the 6 PWRs and one BWR developed and operated by the ANPP, this paper reviews the Portable Medium Power Plant (PM-2A) as part of the extensive history of portable nuclear reactors, equivalent to today's small modular reactors. The PM-2A was the first field reactor to demonstrate the feasibility to assemble and then disassemble a prefabricated nuclear plant in ice tunnels at Camp Century - referred to as the "Arctic City Under the Ice" - located 222 km inland from Thule Air Force Base on the Greenland Ice Cap, and less than 1,450 km from the North Pole [3], [4], [5].

II. CONSTRUCTING CAMP CENTURY

Camp Century was built by the U.S. Army Polar Research and Development Center (PRDC) in 1960 to learn how to construct military facilities on the Greenland Ice Cap using snow as a construction material, including prefabricated Arctic housing; power sources; steam to melt sub-surface snow as a water supply; and waste disposal, while providing a year-round habitable Arctic laboratory. The PRDC was headquartered at Camp Tuto ("Thule Take-Off") located at the foot of the Greenland Ice Cap, 29 km East of Thule Air Base, and one of the best locations to access the ice cap, and jumping off point for Camp Century.

At the time, Greenland, Northern Canada, and Alaska had become strategic military locations having the shortest air routes between the major land masses of the Northern Hemisphere. The scientific developments at Camp Century were for a defense-related operation, codenamed Project Iceworm, seeking to deploy ballistic missiles under the Greenland ice sheet. Since the ice sheet was too unstable, Project Iceworm was officially canceled in 1963 and remained a closely guarded secret until 1997 [6].

Camp Century construction materials consisted of 363 metric tonnes of pipes, machinery, and components in 27 packages, and was assembled in a series of subsurface, cut-and-cover tunnels to provide protection against the severe polar climate, since severe storms, drifting snow, and extremely low temperatures were serious disadvantages to above-surface facilities. For example, the winter season lasted from October to February, and surface temperatures were reported to reach -57 °C and wind velocities $\geq$200 km per hour. Each tunnel was constructed by cutting deep trenches with a rotary snow plow. The tunnels ranged from 46 to 335 metres long, 5.5 to 8 metres wide, and 6 to 12 metres deep. The reactor trench measured 54 metres long, 9 metres wide and 18 metres deep. The trench walls were cut to maximize tunnel floor width, and to accommodate semicircular corrugated steel roof arches. The reactor tunnel arches were 12 metres in diameter (Figure 1).

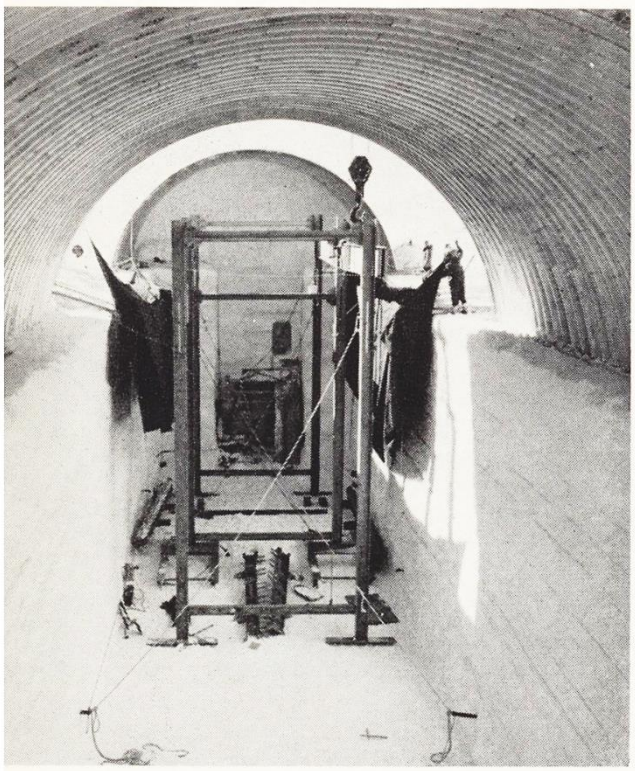

Figure 1. Reactor Cut-and-Cover Tunnel Bridged by Metallic Arches [7]

Light, insulated buildings were constructed inside tunnels housing the PM-2A nuclear reactor and all camp facilities. Annual snow tunnel temperatures were expected to stay between -32 °C and -7 °C even with building interiors maintaining temperatures between 16 °C and 21 °C. The tunnel ventilation system prevented heat losses keeping tunnel temperatures below -7 °C upholding snow wall and roofing structural integrities (Figure 2).

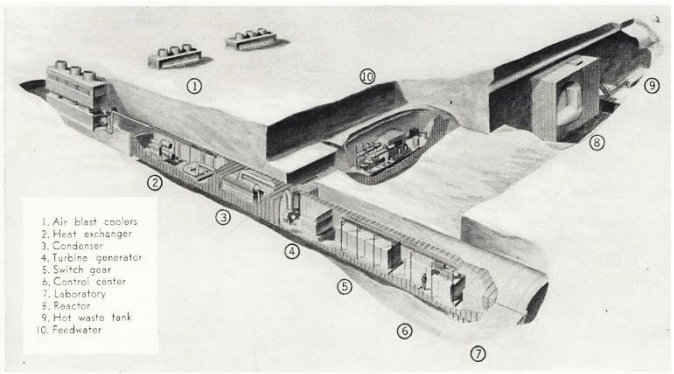

Figure 2. Sketch of PM-2A Nuclear Power Plant Installation at Camp Century [8]

Snow was then blown over the arches using the snow plow, where it would harden, permitting light traffic to cross the tunnels safely. “Timber” roadways prevented tunnel floor damage from vehicles. This enabled 105 civilian scientists and military personnel to work and live comfortably in one of the earth's most forbidding climates [2], [5], [7], [8], [9].

III. PM-2A - THE FIRST FIELD REACTOR (1960 - 1963)

A. Design, Environmental and Shipping Specifications

The PM-2A design contract was awarded January 23, 1959 to the American Locomotive Company to demonstrate the ability to assemble a nuclear power plant from prefabricated components in a remote, Arctic location. Another design feature is that the plant may be disassembled and relocated to another station extending its useful life.

The PM-2A equipment was mounted on ten skids to meet air transport weight and size restrictions. The package size limit was 2.7 metres wide, 2.7 metres high, and 9 metres long, and weight limit of ~13,600 kg. All system piping and wiring was terminated at the skid boundaries in flanged and bolted pipe connections and pin-type electrical connections. Interconnecting piping between skids were prefabricated in 9.1-metre lengths having flanged and bolted connections at each end. Interconnecting wire was contained in multiconductor cables terminating at each end in quick connectors mating with the terminals on the skids. Piping, wiring, pipe supports, cable trays, and maintenance equipment were packaged for shipment in eighteen additional crates of varying sizes below the maximum weight limits. Transporting equipment and supplies were accomplished by the D8 / D9 tractors, each pulling six or seven sleds carrying 9 and 18 metric tonnes of supplies.

B. The PM-2A Nuclear Reactor

The PM-2A nuclear reactor was a prefabricated, pressurized light-water-cooled and moderated assembly containing 32 fixed fuel elements and 5 control elements each measuring ~6.4 cm by 6.4 cm by 69 cm, and sealed inside a bolted vessel-head cover (Figure 3).

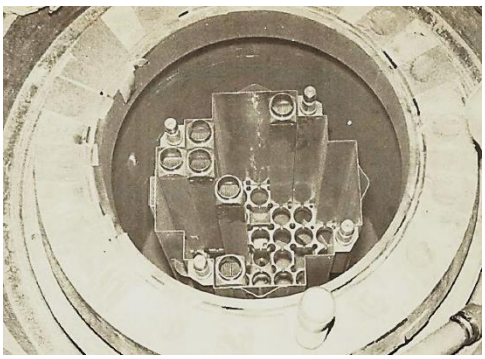

Figure 3. Six training fuel elements loaded into PM-2A reactor during testing at Dunkirk, May 1960 [10]

The fuel elements consisted of uranium dioxide (UO_2) plate assemblies at 93% uranium-235 enrichment in a stainless-steel matrix clad with low-cobalt stainless steel. Europium oxide was the absorber material used in the control rod elements. The design life of the core was 9.2 megawatt-years at an operating power level of 10 thermal megawatts. The primary loop was pressurized to 12,000 kilopascals and the coolant temperature leaving the reactor was 270 °C.

A horizontal, kettle-type heat exchanger (i.e., a horizontal U-tube or floating head bundle placed in an oversized shell; the large empty space above the tube bundle acts as a vapor disengaging space [volume] for the vapor separation of

liquid droplets), generated steam in the secondary loop at 3,450 kPa. A 7-stage steam turbine, with two extraction points, drove an AC generator producing 1,980 kw at the generator terminals. Plant auxiliaries required 420 kW, providing a net output of 1,560 kW available to the camp. In addition to the electrical output, a small heat exchanger generated 1,000,000 BTUs/hour of ~1,000 kPa steam for distribution to the camp water supply system where the steam was jetted deep into the snow to melt a subsurface pond and draw water as required. Condenser waste heat was removed using a water and ethylene glycol solution to three air blast coolers ultimately discharging this heat to the atmosphere through ducts penetrating the tunnel roof. Plant instrumentation and controls used only solid- state devices instead of electron tubes to decrease maintenance and improve resistance to damage during shipment.

C. Powered by Nuclear Power

Nineteen plant operators participated in plant assembly and testing at the factory, field installation, and assumed all power plant operational duties, and were specialists in one of four areas: mechanical, electrical, instrumentation, and process control. The training consisted of a one-year program comprised of academic and operational phases gaining hands-on experience with operating the plant's reactor and power generation equipment.

The installation of the plant equipment, buildings, utilities, and preliminary testing to permit limited operation were completed in ten weeks, and at 6:52 a.m. on October 2, 1960, the reactor achieved initial criticality for the first time. At 5:30 a.m. on November 12, 1960 - about 22 months following contract award - the plant began to generate electrical power. A short time later, it was discovered that additional shielding would be required, and a layer of two-inch-thick lead bricks was added to the primary shield tank. Total project cost for fabrication, transportation and installation of the PM-2A power plant was ~24.9 M zł (5.3 M €) [2], [5] through Fiscal Year (FY) 1961, and almost 10 times higher in FY 2022. Upon completion of the acceptance tests, which included a 400-hour run, the plant became Camp Century's primary power source. A standby diesel power plant equivalent to the PM-2A would require >1.5 million litres of fuel annually.

D. Schedule Change

In 1962, it was decided that Camp Century would operate only during the summer Arctic season. The reactor was shut down on July 9, 1963 after thirty-three months of operation for planned maintenance, and later announced the PM-2A would not resume operation. By that time, the reactor core had produced 11,232,400 kilowatt-hours of electricity for Camp Century. This included a record period of more than 2,500 consecutive hours of uninterrupted power production from October 1962 through February 1963. Factors such as: a) only needing 300-500 kW of expected energy needs compared to the original 1,560 kW design; b) prolonged shutdowns resulting from conventional turbine-generator repairs; and c) the standby diesel power plant supplying enough seasonal power, no longer made the PM-2A economically viable to operate [11]. An additional factor in shutting down the reactor was recurring damage to the tunnel support structures due to compacting snow [2].

E. Decommissioning and Relocation

Closing the Camp in the winter of 1963-1964 was contingent upon the successful removal of the nuclear reactor core by the summer of 1964. Removal of the reactor core was necessary to allow the PM-2A to be left unheated and unattended over the winter, and was also a first step in relocating the plant. An 80-day cooling period was required before the PM-2A fuel elements could be transferred to shipping casks. The morning of September 27, 1963 was the earliest date which the core unloading operation could begin. Following fuel removal, all plant systems were shut down, drained, and winterized [11]. Water from the spent fuel tank, primary system, and all shield tanks was circulated through the demineralizer and filters to reduce radioactivity to acceptable levels before being discharged into the hot waste well [3].

F. Fuel Element and Shipping Cask Removal

The process of removing the fuel began with installing a Bailey bridge, with a triple-story center section, across the reactor trench. The hoist, mounted on an overhead crane, was on running rails. The reactor's bolted, vessel-head cover was removed for unloading the fuel elements, allowing direct access with long-handled remote-actuated tools from an upper working platform. The water in the shield tank above the reactor and in the spent fuel tank shielded radioactive plant components and reduced radiation exposure of personnel on the platform. The fuel elements were moved individually from the reactor to a spent fuel tank where they were loaded into a lead-lined shipping cask. The sealed cask was raised to an upper reactor room. Hold-down bolts for the cover were replaced and the cask was washed down with detergent to remove residual radioactive contamination from the spent fuel tank water. Simultaneously, pneumatic pressure was applied to the cask interior through fittings, purging water from the cavity by siphon drain. After the water was removed from the cask, plugs were placed in the drain holes and the cask was hoisted to the snow surface.

Radiation levels and airborne radioactivity were monitored using hand survey instruments and installed instrumentation, respectively. Radiation surveys were also taken over the cask surfaces prior to release. Dose rates at the duct openings were reported as high as 3.5 Roentgens per hour, but were small in area and could be avoided. It was mentioned that all personnel working around the casks were aware of these radiation fields [11]. Thermocouple devices were installed on the casks to monitor interior temperatures after loading. Readings taken every two hours verified the absence of excessive temperature rises.

Seven casks were required to ship one entire core. The total core weight was ~340 kg, and each shipping cask weighed slightly less than 9.1 metric tonnes. The last cask was secured to its trailer by mid-afternoon, September 28, 1963. Winds up to 15 meters/second and temperatures down to -29 °C were experienced during this time [11]. The loaded casks were picked up by a crawler-crane and placed on a trailer. Figure 4 shows the PM-2A core unloading process.

small nuclear plants to provide electric power and heat in remote areas showed a vision for a technology that did not yet exist, thus providing a valuable historical perspective to the modern, land-based small modular reactor concepts.

V. REFERENCES

[1] International Atomic Energy Agency (IAEA), Technology Roadmap for Small Modular Reactor Deployment, IAEA Nuclear Energy Series No. NR-T-1.18, Vienna, Austria, August 2021.

[2] C.D. Harmon. Military Nuclear Power Plants 1958-1978, *IEEE Nuclear Power Engineering Committee*, DOI: 10.13140/RG.2.2.20664.70407, Charlotte, North Carolina, January 30, 2019.

[3] L.H. Suid, The Army's Nuclear Power Program: The Evolution of a Support Agency, New York: Greenwood Press, 1990.

[4] M.V. Ramana, The Forgotten History of Small Nuclear Reactors, *IEEE Spectrum*, 44-48, 57-58, 2015.

[5] E.F. Clark, Camp Century – Evolution of Concept and History of Design Construction and Performance, Technical Report 174, U.S. Army Material Command Cold Regions Research & Engineering Laboratory, Hanover, New Hampshire, October 1965.

[6] Camp Century, Atomic Heritage Foundation, July 19, 2018, https://ahf.nuclearmuseum.org/ahf/history/camp-century/, (accessed December 23, 2022).

[7] J. H. Kerkering, Polar Research and Development, *The Military Engineer*, Vol. 52, No. 350, 452-455, November-December 1960.

[8] J.W. Barnett, Nuclear Power Plant for Camp Century, *The Military Engineer*, Vol. 53, No. 355, 363-364, September-October 1961.

[9] National Defense Industrial Association, Atomic Energy, *Ordnance*, Vol. 45, No. 244, 472-473, 475, January-February 1961.

[10] Department of the Army, Office of the Chief of Engineers, Nuclear Power Division, Construction of the Army Nuclear Power Plant PM-2A at Camp Century, Greenland, Final Report, U. S. Army Cold Region Research and Engineering Laboratory, Hanover, New Hampshire, August 1, 1961.

[11] J.P. Franklin and W.T. Stockhausen, Removal of Nuclear Reactor Core-Camp Century, *The Military Engineer*, Vol. 56, No. 373, 328-330, September-October 1964.

[12] L.E. McKinney, Logistics of PM-2A Removal, *The Military Engineer*, Vol. 57, No. 380, 420-421, November-December 1965.

[13] T. J. Walker, PM-2A Reactor Vessel Test: Analysis of Failure Conditions, *Nucl. Eng. Des.*, Vol, 8, 71-82, 1968.

Technical Track 1
Reactor physics, Thermal hydraulics, and Simulation

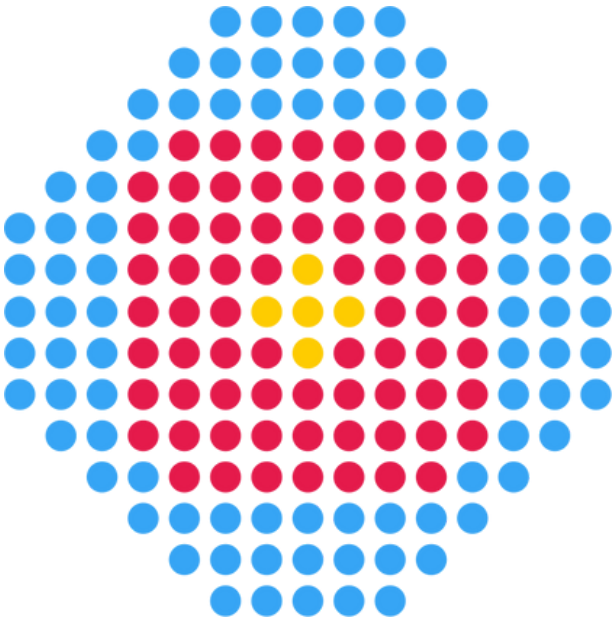

Proceedingsof the European Nuclear Young Generation Forum
ENYGF'23
May 8-12, 2023,Kraków, Poland

Large Eddy Simulation of a Simplified PressurizedThermal ShockScenario

Algazlan, Osamah[1]*, Alruwaished, Abdulaziz[1], Alsafi, Osama[1], Aljohani, Mohammed[1], Aldoughan, Abdulrahman[1], Almalki, Abdullah[1] Shams, Afaque[1,2], Kwiatkowski, Tomasz[3]

[1]King Fahad University of Petroleum & Minerals (KFUPM), Saudi Arabia

[2]Interdisciplinary ResearchCenter for RenewableEnergy and Power Systems(IRC-REPS), KFUPM, Saudi Arabia

[3]National Centre for Nuclear Research(NCBJ), Poland

*Corresponding author: s201815300@kfupm.edu.sa(O. Algazlan).

I. INTRODUCTION

There are several mechanisms that can reduce the life expectancy of a Nuclear Power Plant (NPP) components, and ultimately reduce the NPP lifetime and pose safety risks. The Reactor Pressure Vessel (RPV) is a crucial component in nuclear systems; hence it undergoes periodical analysis during its lifetime to check its integrity [1]. One of the mechanismsthat can jeopardize the integrity of RPV is a transient condition called Pressurized Thermal Shock (PTS). During accidents such as Loss of Coolant Accidents (LOCA), emergency systems are initiated to mitigate the accident. The cold water injected by the Emergency Core Cooling System (ECCS) causes a quick cooling of the downcomer and internal surface of the RPV. As a result of this rapid cooling, large temperaturegradients and thermal stresses occur, which represents the PTS phenomenon.Consequently, defects in the embrittled RPV, which can exist due to neutron irradiation, can propagate within the vessel walls. In the meantime, the pressure is either maintained or increased a little bit. These issues can be predicted through the proper use of numerical methods to simulate the thermal hydraulics of the Reactor Coolant System (RCS).

In nuclear thermal hydraulics, two categoriesof simulations can be specified, system codes and three-dimensional numerical simulations. System codes are based on one-dimensional equations that simplify flow analysis, where complex three-dimensional flows cannot be studied. On the other hand, advanced numerical simulations can represent three-dimensional complex flows, which are encountered during PTS. Direct numerical simulation (DNS) is ideal as it provides the most accurate numerical results; however, it requires very large computational resources,which makesit less practical for most of the industrial applications. On the contrary, Reynolds-Averaged Navier-Stokes (RANS) turbulence modelling approach requires less computational resources. Therefore, making it a widely used industrial tool. Nevertheless, the application of RANS methodology for any industrial scenario, such as the PTS case,requires a proper validation. In between, DNS and RANS, there exist an approach called the Large Eddy Simulation (LES) which proves to be the most suitable modelling approach for studying the PTS scenario; it is less expensive than DNS and yet it provides accurate results. Previous work has been done to simulate PTS utilizing the LES turbulence model as found in [2], where a transient single-phase TOPFLOW test case was used to validate the simulation. Following this work, Shams et al. [3] designed a simplified PTS configuration with the useof DNS. The effect of crossflow velocity on flow and heat transfer characteristics of the impinging jet was considered in [4], where Re=13400 was used. In [5], the LES of an impinging jet was performed in a heated, crossflow wall-mounted cube and a Re=5341 was used.

In 2018, a Quasi-DNS (q-DNS) numerical simulation was conducted by Shams & Komen [6] for a simplified single-phaseflow PTS case(for more details, seesection 2). This q-DNS was later used, by Shams et al. [3], as initial conditions to perform a high-quality reference DNS study. This paper adopts the exact simplified PTS casestudied by Shamset al [7], in which the cold leg is considered as square rather than a round pipe. Thus, injects a squarejet with the Re=5400, and the distance to the core barrel is 0.4865 times the jet width. Furthermore, constant fluid properties are considered. Accordingly, to mimic the buoyance effects (similar to thereal-life scenario)asthecold jet interacts with the hot core barrel, transverse-flow from the top is utilized to force the jet to flow downward, with a velocity ratio of 10. Since the jet has a square profile, the flow fields at the downcomer are non-homogeneous, which resembles a more realistic flow behaviour compared to round jets, at the expense of higher computational cost. Additionally, two boundary conditions (isothermal and adiabatic) are imposed at the downcomer walls to study the heat transfer phenomenon.The isothermal boundary condition represents the initial stage, where the temperature gradients near the wall are developing to reach high values. In contrast, the

adiabatic boundary condition resembles the steady-state behaviour of the phenomenon, where negligible temperature gradients exist near the walls. However, although DNS studies are accurate, the inherent high computational cost associated with such studies renders it unfeasible for most industrial applications. Therefore, the present paper attempts to investigate the flow fields and thermal behaviour for the aforementioned PTS case utilizing LES turbulence model. In this context, the DNS results will be used for benchmarking to assess the prediction capabilities of the obtained LES results. Accordingly, this LES method can be used to perform the PTS study at the higher Reynolds number. This will help is generating more reference numerical data, which eventually will help in validating RANS-based modelling approaches.

The rest of the article is organized as follows: In section II, the adopted numerical methodology including flow parameters, boundary conditions, meshing and turbulence modelling is given; section III discusses the obtained results, and accordingly they are summarized in section IV.

II. NUMERICAL METHODOLOGY

A. Flow Configuration

The PTS configuration used in this paper is similar to the one used by Shams et al. [3] and it is depicted in Figure 1. In this geometric configuration, a square cold leg intersects a planar downcomer of the RPV perpendicularly. For the cold leg, a square configuration is used with D_c = 0.15 m and length L = 10.15D_c. Taking the origin to be at the centre of the interface between the cold leg and the downcomer, the dimensions of the downcomer are as follow: the upper height H_1 = 10D_c, the lower height H_2 = 23.3D_c, the thickness of the downcomer D_d = 0.4865D_c, and the half width W = 10D_c. There are two inlets, inlet 1 and inlet 2. Inlet 1 is in the duct perpendicular to the downcomer, whereas the Inlet 2 is from the top of the downcomer.

B. Flow Parameters and Boundary Conditions

Reynolds number in the bulk of the fluid is chosen to be □□= $\frac{□_□□_□}{□^{□}}$ = 5400, where v is the constant fluid kinematic viscosity. It corresponds to an average friction Reynolds number □□$_{□}$= 180 in the cold leg, with □□$_{□}$= □$_{□}$ℎ$_{□}$/□, where □$_{□}$= $\sqrt{□_{□}/□}$ is the friction velocity, with τ_w the temporal and spatial averaged wall shear stress computed in the duct, and ρ is the constant fluid density. Finally, the Prandtl number is set as □□= □□= 1, where α is the constant thermal diffusivity of the fluid.

The bulk velocity U_c = 0.36 and fluid temperature T_c = 293 K are imposed in the cold leg. Recycling the velocity field in the first half of the duct with a length of 6.6D_c forces a fully developed turbulent velocity profile in the cold leg. On the secondary inlet at the top of the downcomer, a constant velocity U_2 = 0.1U_c and a constant hot fluid temperature T_h = 353 K are imposed on the surface with uniform profiles. The downcomer's vessel and barrel walls are either adiabatic or isothermal and are no-slip walls. The two side walls that encompass the downcomer in the horizontal direction are adiabatic no-slip walls. Finally, it is assumed that the downcomer's bottom surface acts as an outlet boundary.

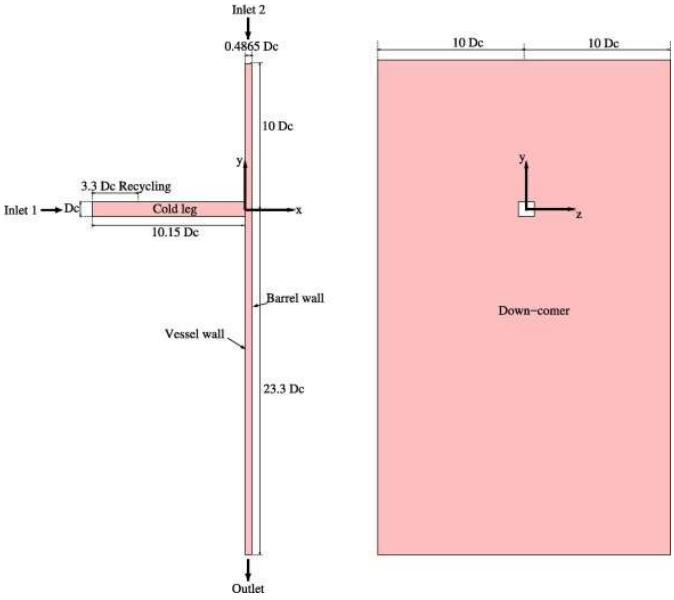

Figure 1. Sketch of the PTS geometry to be used (adopted from Shams et al. [3]).

C. Meshing Strategy

Structured hexahedral mesh was generated for the computational domain, which consists of the square duct and the downcomer. The meshing capabilities of the commercial software STAR-CCM+ version 2210 were utilized, which provides a wide range of features that facilitated the meshing process. The domain was subdivided into two regions, namely the square-duct and the downcomer. This permit manipulating the mesh easily to account for the flow physics in different regions, as shown in Figure 2.

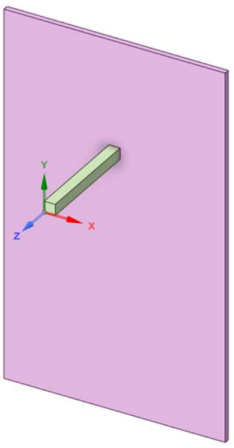

Figure2. Trimetric view of the subdivided computational domain.

Additionally, special care was devoted to the near-wall cells in each region, as to capture the large flow gradients. Following the q-DNS study of Shams et al. [6] the LES

meshing is performed, and the final meshing parameters are: the first cell $y^+ = 0.5$; ($\Delta y^+ = \Delta z^+$) < 10, $\Delta x^+ < 15$. Here, the non-dimensionalized cell size, such as y^+ is computed by using:

$$\square^{+} = \frac{\square_{\tau}\square}{\square}$$

By taking in account these meshing parameters, the overall mesh for this PTS geometry consists of ~ 20 million grid points, making it a very fine mesh to perform the LES study. Figure 3 shows a representative cross-sectional view of the square-duct mesh. The cell skewness was controlled by imposing limits on the boundary layer non-dimensional quantities:

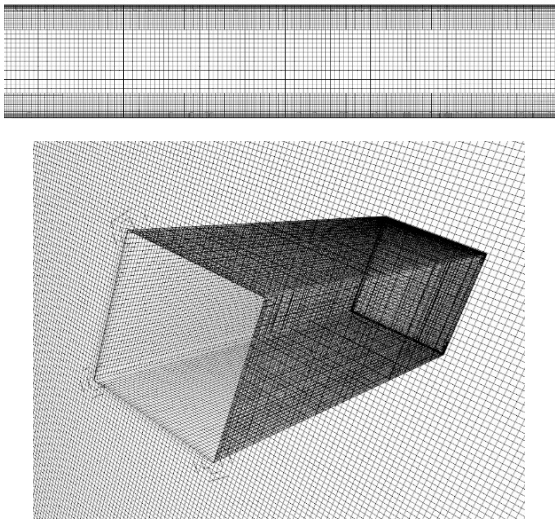

Figure 3. Representative view of the mesh in square duct.

III. NUMERICAL SCHEMES

The current simulation is run using the commercially available finite volume code STAR-CCM+ (STAR-CCM+, 2022). For this flow configuration, it was found that applying a purely central scheme causes numerical instabilities, therefore, for spatial discretization, a second order central scheme with 5% boundedness (of a second order upwind scheme) has been used. This is also consistent with the pioneering work of Shamset al. [8]. Additionally, the temporal discretization is done using a second order implicit scheme. The pressure-velocity coupling of the Rhie-and-Chow type is used in combination with a SIMPLE-type algorithm to perform the current discretization. The details of the scheme are available in the code manual (STAR-CCM+, 2022).

IV. TURBULENCE MODELING

In this study, an LES has been performed to investigate the flow in the aforementioned domain. What separates LES from the other turbulence models is the ability to solve the Navier-Stokes equations for the larger eddies and model the smaller eddies mathematically. The large eddies refer to those larger than the grid size, which depend on how fine the mesh is. On the other hand, the smaller eddies are the sub-grid scale eddies (SGS), which are assumed isotropic to simplify the modelling approach. To solve the Navier-Stokes equations, a filter is used to obtain the SGS stresses, which are represented by the turbulent stress tensor (τ_{ij}) as:

$$\square_{\square\square} - \frac{1}{3}\square_{\square\square}\square_{\square\square} = -2\square_{\text{ક}}\bar{\square}_{\square\square}$$

Here, μ_t is the SGS turbulent viscosity and S_{ij} is the strain rate tensor. To model the SGS viscosity, a Wall Adapting Local-Eddy viscosity (WALE) model is utilized, which was proposed by Nicoud and Ducros [9]. It is constructed to correct the behaviour of the SGS viscosity as it approaches the wall. This correction is done through squaring the velocity gradient tensor which accounts for both the strain and rotation rates to obtain the local-eddy viscosity. No matter if the mesh is structured or not, this model works well with both, since no dynamic procedure or explicit filtering is used. Other modelling approaches were considered such as the Lily-Smagorinsky or the Van Driest damping, yet these do not produce favourable results for wall bounded flows. Additionally, WALE produces fewer grid induced problems, and shows a y^3 behaviour of the SGS viscosity as the flow approaches the wall. Finally, since it relies on both the strain and rotation rates, it can perform exceptionally well for this study. The parameters to model the eddy viscosity using WALE are:

$$\square_{\text{ક}} = \square\square^{2}\frac{\left(\text{ઊ}_{\square\square}\text{ઊ}_{\square\square}\right)^{3}}{\left(\text{ઊ}_{\square\square}\text{ઊ}_{\square\square}\right)^{\frac{5}{2}} + \left(\text{ઊ}_{\square\square}\text{ઊ}_{\square\square}\right)^{\frac{5}{4}}}$$

$$\square_{\square\square} = \frac{1}{2}\left(\text{ઊ}_{\square\square} - \text{ઊ}_{\square\square}\right) - \frac{1}{2}\square_{\square\square}\text{ઊ}_{\square\square}$$

$$\bar{\square}_{\square\square} = \frac{\square\square_{\square}}{\square\square_{\square}}$$

$$\square_{0} = \square_{\text{ક}}\square \quad \text{where, } \square_{\text{ક}} = 0.544$$

$$\square_{\square\square}\square_{\square\square} = \frac{1}{6}\left(\square^{2}\square^{2} + \square^{2}\square^{2}\right) + \frac{2}{3}\square^{2}\square^{2} + 2\square\square_{\text{ો}\text{ા}\text{ઙ}}$$

V. RESULTS AND DISCUSSION

It is worth mentioning that the main purpose of the current LES computation is to assess its capability in reproducing the complex three-dimensional PTS scenario. In this regard, the available DNS [3] is considered as a reference. For simplicity, the obtained results are compared in two parts, i.e. (A) The square duct, and (B) the downcomer.

A. The Square Duct

Flow in a square duct exhibits non-linear behavior and is much more complex than a simple (circular) pipe flow. In Figure 4, the velocity contours at the mid cross-section of the duct are shown for LES and the reference DNS case. It can be seen that the flow is highly turbulent and fully developed. It exhibits more complex three-dimensional flow regime with systematic recirculation regions covering the whole duct. The interaction of these recirculation regions gives rise to secondary recirculation regions at each

corner of the duct. As a consequence, the flow regime is highly non-linear; hence, making it more challenging for low-order turbulence modelling approaches to predict it correctly. Furthermore, this obtained velocity field has been compared with the reference DNS and is shown as a plot in Figure 5 where the profile is taken from the wall to the center of the duct. It is worth noticing that the LES results are in very good agreement with the reference DNS data.

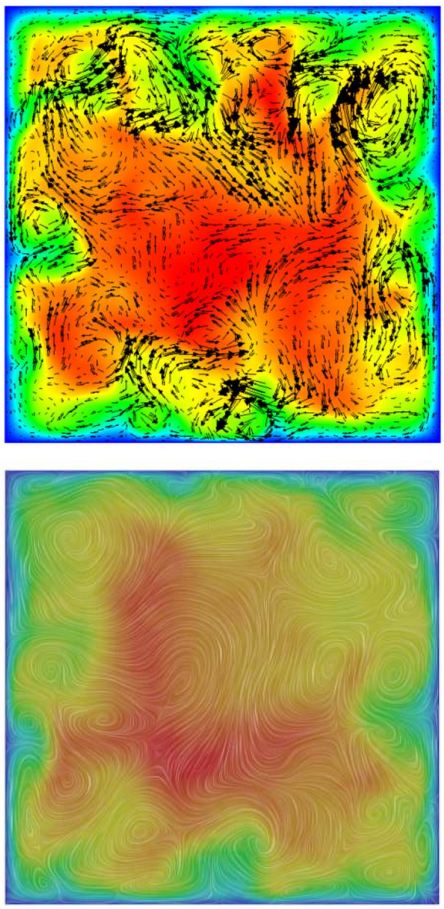

Figure 4. Iso-contours of velocity at the mid cross-section of the duct field (Top) DNS (Bottom) LES

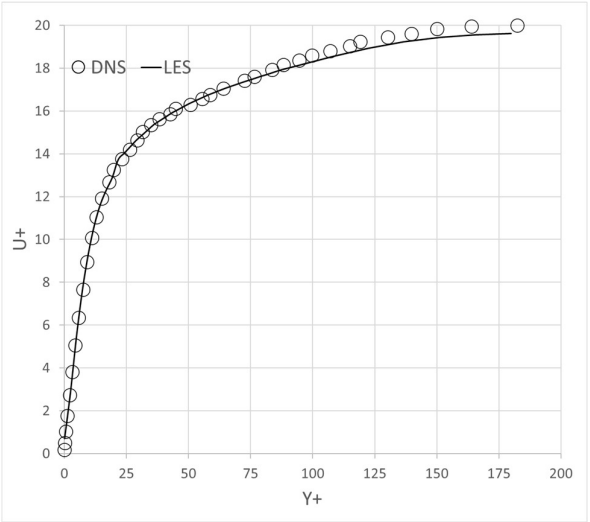

Figure 5. Comparison of velocity profile in the duct from the wall to the middle

B. The Downcomer

The fully developed turbulent flow from the duct hits the barrel wall. Accordingly, the flow field has a stagnation region and it evolves into a more complex flow and temperature fields, as depicted in Figure 6. Following the impingement region, the turbulent duct flow breaks into small turbulent scales as highlighted by the iso-surfaces of Q-criterion in Figure 7.

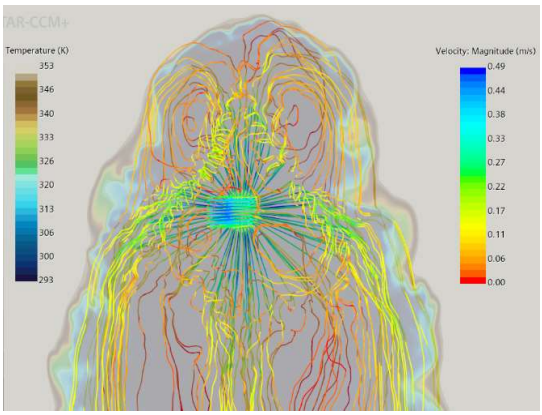

Figure6. Evolution of streamlines from duct, at the impinging region, and in the downcomer.

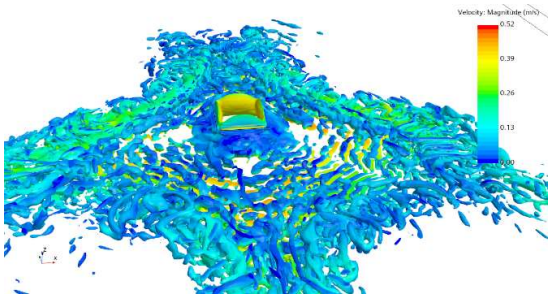

Figure7 Iso-surfaces of Q-criterion colored with velocity field.

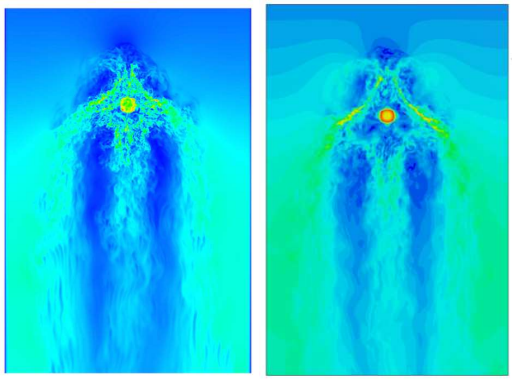

Figure 8. Iso-contours of instantaneous velocity field at the mid cross-section of the downcomer (Left) DNS (Right) LES.

These small structures undergo large shear stresses in the flow and eventually leads to the overall mixing in the downcomer. These results are consistent with the reference DNS data (for more details readers are referred to [3]). Figures 8 and 9 illustrate the instantaneous velocity and thermal fields (obtained from the adiabatic boundary condition) at the mid cross-section of the downcommer. For better understanding, these results are compared with the DNS computations. Looking at Figure 8, it is clearly noticeable that the overall turbulence flow behaviour is nicely captured by the current LES study. This highlights the supremacy of the LES method over the low-order turbulence modelling approaches to correctly predict the complex flow regimes.

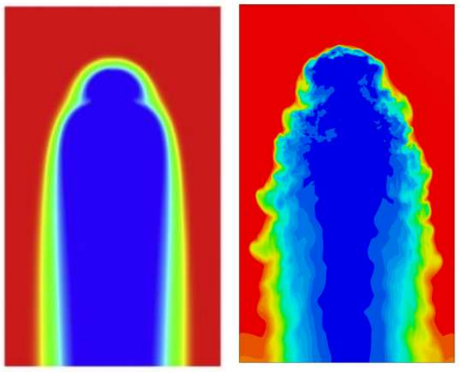

Figure 9 Iso-contour of temperature field (representing the adiabatic boundary condition) (Left) DNS (Right) LES.

In Figure 9, a qualitative comparison of the temperature field is given. Since the current LES has yet to reach statistical convergence, the instantaneous temperature field has been compared with the mean temperature field of the reference DNS. Once again, it is clear that the overall thermal field has been nicely predicted by the LES. This also validates the fact that once the LES provides a better agreement in comparison with the DNS, it has the potential to serve as a reference database if properly performed at a higher Reynold number for such complex flow regime. It is worth mentioning that the current LES simulation is still in progress and will soon yield statistical convergence of flow and thermal fields. Accordingly, they will be presented at the conference.

VI. CONCLUSION

In this paper, a simplified pressurized thermal shock scenario of flow impinging the reactor pressure vessel was numerically simulated using the LES turbulence model. This simplified configuration is based on the reference DNS work performed by Shams et al [3]. The flow configuration consists of a cold coolant flowing through a square duct and impinging towards the core barrel wall. Constant fluid properties were considered such that the Prandtl number is a unity, and the Reynold number based on the bulk velocity in the duct is Re=5400. STAR CCM+ code was used to generate a hexahedral mesh of the computational domain and has been used to run the simulation. A second order central spatial discretization scheme with 5% boundedness was considered, and a second order implicit scheme was used for the temporal discretization.

Preliminary results show similar behaviour to that found in the reference DNS in both the duct and the core barrel. The iso-contours of the velocity fields in the duct show a systematic recirculation region in the whole duct, with special consideration in the corners, indicating a complex nonlinear flow. The velocity field in the duct is in very good agreement to that of the DNS. A qualitative comparison of the obtained LES results is also done with the reference DNS data in the downcomer. In particular, the iso-contours of velocity and temperature fields are compared and has shown good agreement. This also highlights the fact that, if performed properly, LES can also serve as reference to validate low-order turbulence modelling approaches.

REFERENCES

[1] IAEA. (2019, February 28). Pressurized thermal shock in nuclear power plants: Good practices for assessment. IAEA. Retrieved November 20, 2022, from https://www.iaea.org/publications/8237/pressurized-thermal-shock-in-nuclear-power-plants-good-practices-for-assessment

[2] Bieder, U., & Rodio, M. G. (2019). Large eddy simulation of the injection of cold ECC water into the cold leg of a pressurized water reactor. Nuclear Engineering and Design, 341, 186–197. https://doi.org/10.1016/j.nucengdes.2018.10.026

[3] A. Shams, D. De Santis, D. Rosa, T. Kwiatkowski, E.J.M. Komen, Direct numerical simulation of flow and heat transfer in a simplified pressurized thermal shock scenario, Int. J. Heat Mass Transf. 135 (2019) 517–540. https://doi.org/10.1016/j.ijheatmasstransfer.2019.01.144.

[4] Wae-hayee, M., Tekasakul, P., Eiamsa-ard, S., & Nuntadusit, C. (2014). Effect of cross-flow velocity on flow and heat transfer characteristics of impinging jet with low jet-to-plate distance. Journal of Mechanical Science and Technology, 28(7), 2909–2917. https://doi.org/10.1007/s12206-014-0534-3

[5] Rundström, D., & Moshfegh, B. (2009). Large-eddy simulation of an impinging jet in a cross-flow on a heated wall-mounted cube. International Journal of Heat and Mass Transfer, 52(3-4), 921–931. https://doi.org/10.1016/j.ijheatmasstransfer.2008.03.035

[6] A. Shams, E.M. Komen, Towards a direct numerical simulation of a simplified pressurized thermal shock, Flow, Turbul. Combust. 101 (2018) 627 – 651.

[7] A. Shams, G. Damiani, D. Rosa, E.M.J. Komen, Design of a single-phase PTS numerical experiment for a reference Direct Numerical Simulation, Nucl. Eng. Des. 300 (2016) 282–296. https://doi.org/10.1016/j.nucengdes.2016.01.038

[8] Shams, A., Roelofs, F., Komen, E. M. J., & Baglietto, E. (2013). Large eddy simulation of a nuclear pebble bed configuration. Nuclear Engineering and Design, 261, 10–19. https://doi.org/10.1016/j.nucengdes.2013.03.040

[9] F. Nicoud and F. Ducros, "Subgrid-Scale Stress Modelling Based on the Square of the Velocity Gradient Tensor," Flow, Turbulence and Combustion, vol. 62, no. 3, pp. 183–200, 1999, doi: https://doi.org/10.1023/a:1009995426001.

Proceedings of the European Nuclear Young Generation Forum
ENYGF'23
May 8-12, 2023, Kraków, Poland

Three-Dimensional Numerical Simulation of a Bare Rod Bundles Fuel Assembly Configuration

Alhamdi, Abdulwahab[1*], Alotaibi, Mishari[1], Alqhtani, Saad[1], Meri, Yazan[1], Shams, Afaque[1,2] and Kwiatkowski, Tomasz[3]

[1] King Fahd University of Petroleum & Minerals (KFUPM), Saudi Arabia

[2] Interdisciplinary Research Center for Renewable Energy and Power Systems (IRC-REPS), KFUPM, Saudi Arabia

[3] National Centre for Nuclear Research (NCBJ), Poland

*Corresponding Author: s201815820@kfupm.edu.sa

I. INTRODUCTION

Flow inside nuclear reactor cores require special attention to enhance the reactor's efficiency and assure its safety. The core of nuclear reactors is a crucial location to be studied where the nuclear fuel dissipates heat to the cooling fluid. Most fuel element layouts used in nuclear reactors started with rod bundles as their basic configuration. These rod bundles are primarily distinguished by their geometric configurations; for instance, they may have square or triangular distribution. One of the primary design elements of the fuel rod assemblies is rod spacing. The pitch to rod diameter ratio (P/D) primarily serves to specify the distance between the rods, which has a significant effect on the flow.

The coolant flowing through the fuel assembly channels dissipates the heat generated by nuclear fission. Under typical operating conditions of a nuclear reactor, the temperature distribution through the fuel assemblies should, ideally, stay uniform. However, in practice, this does not occur as a result of inter-subchannel mixing. To analyze the situation and predict the lifetime of the fuel rod in terms of structural integrity and mechanical behaviour, a solid comprehension of the pulsation-induced vibrations is required. Moreover, localized flow effects like hot spots, thermo-mechanical loads, partial blockage effects, and structure deformation are frequently connected to the flow of the coolant fluid within these sub-channels. The design of reliable nuclear system operations has always depended on the understanding of flow and temperature distribution.

The bare rod bundle configuration's unstable axial flow pulsations and structures have been studied both experimentally and numerically over the past 50 years and are still a subject of research today. Hooper discovered that the P/D ratio has a significant impact on the turbulent flow structure [1]. Hooper and Rehme demonstrated that for a turbulent flow through parallel rod bundles, the azimuthal and axial turbulence intensities in the rod gap region are strongly increased with the rod spacing decreasing [2]. Additionally, they discovered that the mean secondary flow has little effect on the flow parameter.

A. The Hooper Case

The case in consideration is called the Hooper case. It refers to the specifications of the flow arrangement and Hooper's (1984, 1980) selected hydraulic experiment setup [1]-[3]. The followed experiment was performed in [3], where the setup of the rod bundle in consideration consists of a squared tight lattice configuration that contains a unit of six rods. The pitch (P) amid each rod is taken as a value of 15.5 cm and the radius of each rod (R) is taken as 7 cm. These configurations make a close-spaced rod bundle since the (P/D) ratio is equal to 1.107 (see Figure 1). The length of the unit being assessed is taken to be 9.14 m which corresponds to a factor of 128 hydraulic diameters.

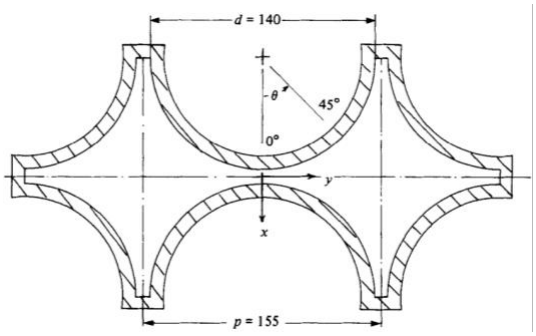

Figure 1. The geometry of a tight lattice rod bundle used in Hooper's hydraulic experiment [2].

B. Computational Fluid Dynamics (CFD)

CFD is a methodology to analyze fluid dynamics using numerical solution methods. Fluid dynamics is concerned with the physical principles of flows in the form of partial differential equations. CFD solvers convert these principles into algebraic equations and effectively solve these equations numerically. CFD's studies develop fluid-related design processes, making them less expensive and faster than conventional testing. Furthermore, in real-life tests, only a limited number of values are assessed at a time, but in a CFD study, all necessary quantities are measured at once and with excellent time and spatial resolution. Because CFD analyses approximate a real physical solution, it is crucial to emphasize that these CFD analyses cannot entirely exclude physical testing procedures. Experiments should still be undertaken for verification purposes.

The CFD methodology used in the present study is called hybrid LES-RANS. The hybrid LES-RANS method is an approach to solve fluid dynamics problems with increased

accuracy and reduced cost. It combines Large Eddy Simulation (LES) and Reynolds-Averaged Navier-Stokes (RANS) methods at regions where they best behave. The hybrid method had been initiated to solve several flow types that appear in the same region. To best understand this methodology, a comprehension of the principles, abilities and limitations of the LES and RANS methods should be developed.

LES is a simulation approach that solves large-scale eddies and models small ones. It shows a high accuracy compared to RANS and an incomparably lower computational cost to the Direct Numerical Simulations (DNS) in separated flows. However, it has a limitation in near-wall boundary regions where the eddies scale becomes smaller. It is a computational limitation as small eddies require finer meshing, which requires massive computational resources. Alternatively, RANS is constructed based on solving the Reynolds decomposition, which decomposes the flow variable into mean and fluctuating quantities. The term Reynolds Stress Tensor arises upon the application of the decomposition on the Navier-Stokes equation. The number of equations never suffice to solve as more unknown terms arise. This issue is known as the closure problem, and it is solved (closed) by a modelling methodology. The level of this modelling is classified based on the number of differential equations included. The 2-equation model has proven its efficiency in solving near-wall attached flows.

So, the hybrid method uses RANS to solve the boundary region and LES to solve the separated flow region. In between these regions, a region called the grey area exists [4]. The grey area poses a challenge to continually solve the flow. It is either solved or reduced by the different hybrid methods which are classified into zonal and non-zonal approaches. In zonal methods, flow is solved in separated regions, however, the non-zonal method solutions assure gradual transfer between RANS and LES.

C. Case description

There is plenty of research that has been done on the Hooper case such as [5]–[8]. However, this research seeks to provide a simulation for the flow between rods in nuclear reactors utilizing the advantages of an accurate and affordable method. The hybrid (LES/RANS) turbulence modelling approach has been adopted to study flow behaviour in a square lattice bare rod bundle configuration. By minimizing the overall computational cost, the best aspects of LES and RANS are employed. The obtained results are thoroughly compared with the available reference (DNS) database of a closely spaced bare rod bundle, which is based on the well-known Hooper experiment.

II. NUMERICAL METHODOLOGY

A. Flow Configuration

The computational domain is made up of two subchannels in the squarely packed rod bundle, as depicted in Figure 1. Table 1 shows the dimensions that are used for the geometry. This configuration makes a closely spaced rod bundle since the (P/D) ratio is equal to 1.107. The periodic length of the unit being assessed is taken to be 2.285 m as per [6], where a comprehensive study of the geometry length has been performed.

Table 1. Geometry dimensions

Symbol	Definition	Value
R	Rod radius	7 cm
P	Rod pitch	15.5 cm
D_h	Hydraulic diameter	0.0712 cm

B. Boundary Conditions

The boundary conditions are taken as the same boundary conditions for the numerical Hooper case in [7],[8]. The inlet mass flow rate imposed corresponds to Re = 22 600. Periodic boundary condition was set in the streamwise direction. Also, a constant heat flux of 0.1 W/m^2 has been imposed on rods.

C. Mesh Generation

The mesh for the given computational domain is generated using the ANSYS Meshing software [9]. Figure 2 shows a mesh cross-section demonstrating a completely hexahedral mesh throughout the flow domain, which gives excellent cell quality for the bulk solution. A mesh with stretched layer structure is employed in the near-wall region, which is critical for capturing the near-wall gradients. A two-step method is employed to generate the mesh. First, a 2D (in the x-y plane) mesh is generated for the cross-section. Second, this 2D mesh is then uniformly extruded in the streamwise direction assuring a high-quality mesh.

The overall mesh consists of 38 million computational cells with non-dimensional sizes Δy+ (wall-normal direction) = 0.0005 (near the wall), and 0.001 (in the bulk). The boundary mesh is structured of 20 layers with a stretching ratio of 1.15 in the near-wall region. The first layer cell size was computed to maintain the average y+ value below 1 (y+ denotes the normalized distance from the nearest wall in wall units). The mesh quality is checked through its orthogonality, skewness and aspect ratio.

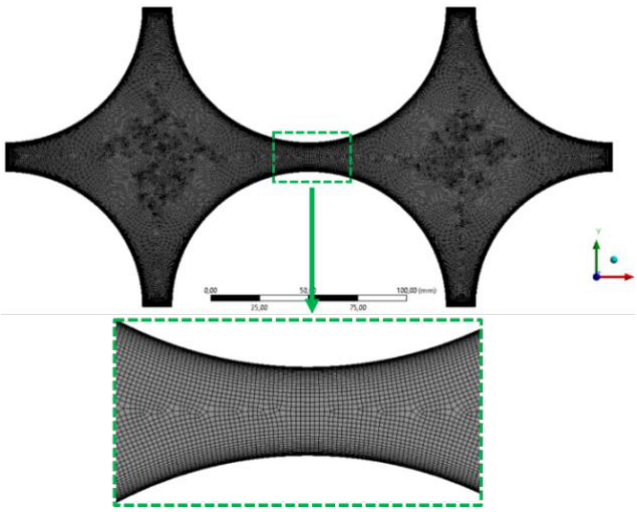

Figure 2 2D (in the x-y plane) mesh for the cross-section. The zoom mesh generated in the region between two adjected rod bundles is presented.

D. Turbulence Modelling

The commercially available Ansys Fluent Version-2022R2 [10] software was used to carry out all the numerical

simulations discussed in this paper. ANSYS Fluent is the industry-leading fluid simulation software known for its advanced physics modelling capabilities and industry-leading accuracy. It provides a cutting-edge, approachable user interface that simplifies the CFD process from pre- through post-processing inside a single window workflow.

The set turbulence modelling for this project is the hybrid approach Detached eddy simulation (DES). Unsteady RANS and LES are combined in a DES mixture in an effort to solve near-wall regions utilizing the RANS methodology and the rest of the flow with the LES. The improved version of the delayed detached eddy simulation (IDDES), which is the most recent DES formulation, is chosen for the current flow configuration.

E. Improved Delayed Detached Eddy Simulation.

The sensitivity of older DES models to Grid Induced Separation (GIS), where well-intentioned grid refining techniques may lower the quality of an LES simulation and yield findings less accurate than RANS simulations on coarser grids, was one of its weaknesses [11]. A further variation of the DES, the IDDES combines the DDES with wall modelling LES (WMLES) and blends the applied RANS and LES length scales with blending functions. A separate and essential element of IDDES is a new definition of the sub-grid length scale, which solely considers the grid spacing and explicitly accounts for wall-distance dependence [12]. Further details about the IDDES are explained in [13].

F. Flow Parameters

The rod has a 14 cm diameter (D) and a 15.5 cm pitch (P) between the two rods. As a result, the example under consideration has a pitch-to-diameter ratio (P/D) of 1.107, defining it as a close-spaced rod bundle. The test section's streamwise length is 2.285 m. The chosen configuration has a bulk Reynolds number of 22600 as done in [7].

Table 2. Summary of the simulation flow parameters

Symbol	Definition	Value
V_b	Bulk velocity	1 m/s
q	Heat flux on the rods	0.1 W/m^2
T	Temperature	100 C

III. RESULTS AND DISCUSSION

The results obtained from the simulation using the Hybrid IDDES method are presented in this section. To ensure the results are accurate, they are compared with corresponding DNS results done in [7], [8]. The validation of the results is done in two aspects: the first one is a qualitative aspect where the results are compared visually, and the second one is a quantitative aspect where the results are compared in terms of certain parameters and exact numerical results obtained from the simulation.

A. Qualitative Comparison

The data collected for the qualitative comparison includes the cross-section of the rod bundle and the axial streamwise behaviour. The presented results focus on depicting the instantaneous flow behavior to observe the qualitative prediction of the IDDES hybrid model.

B. Velocity Field Qualitative Comparison: Mean and RMS

The instantaneous velocity field is shown in Figure 3, with Figure 3a showing the cross-section flow behaviour of the domain and Figure 3b showing the axial flow behaviour. Comparing the contours of the DNS instantaneous velocity obtained by [8] in Figure 4, the turbulent eddies are well captured in the flow. The hybrid method predicts the velocity profile and captures both the turbulence and the pulsation shown in the results in Figure 4. It also produced multiscale vortexes in the flow that reached small sizes, as appeared in Figure 3a. Alongside, a sinusoidal pattern can be observed on the flow field specifically when considering the streamwise capture shown in Figure 3b. According to the findings in [14], this is an expected characteristic for bare rod bundles with a low P/D ratio. The hybrid simulation accurately represented the flow characteristics and captured fine details as compared to the DNS results in [8].

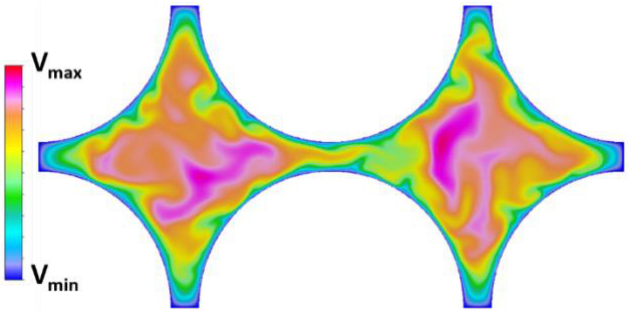

Figure 3a. XY-plane velocity field capture of hybrid IDDES simulation.

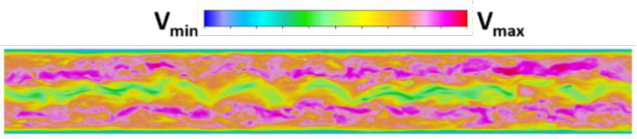

Figure 3b YZ-plane velocity field capture of hybrid IDDES simulation.

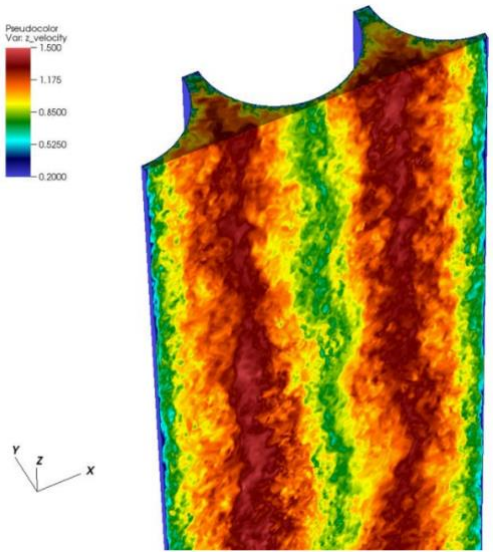

Figure 4. Instantaneous velocity field slice visualization of the DNS simulation [8].

C. Power spectral density comparison

The power spectral density (PSD) plot against the frequency of mass flow rate oscillations for the hybrid simulation is shown in Figure 5. It shows a similar behaviour compared to the PSD plot in Figure 6 done by [7]. This implies that the numerical methodology is able to predict the overall flow pulsation of the Hooper case.

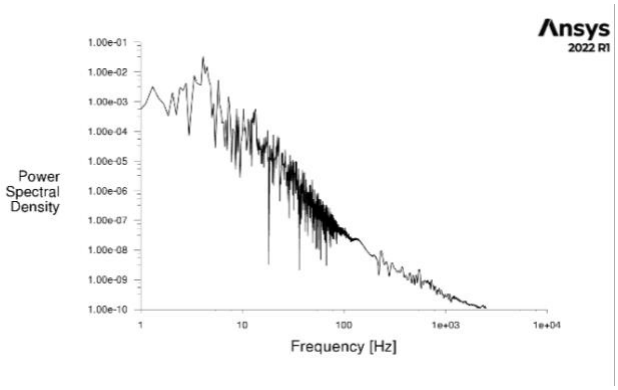

Figure 5. PSD plot for hybrid simulation.

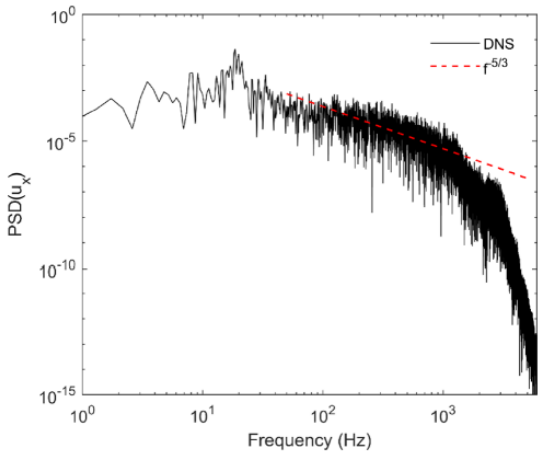

Figure 6. PSD plot for simulation done in [7]**.**

IV. CONCLUSION

Understanding the flow through the fuel assembly properly is essential considering the reliability of the nuclear reactor. So, in this study, an effort has been made to examine these aspects using CFD methods. In this context, a square lattice bare rod bundle configuration has been studied using a hybrid turbulence modelling approach. The best features of RANS and LES are used to reduce the overall computing cost. The acquired results are carefully compared with the reference DNS database that is currently available [7] and are based on the well-known Hooper experiment for a bundle of tightly packed bar rods. The chosen configuration has a (P/D) of 1.107 and a bulk (Re) of 22 600. Early simulation findings for the hybrid IDDES approach are similar to DNS results published in [7],[8]. However, to validate the hybrid IDDES method, additional simulation results must be compared to DNS results.

V. ACKNOWLEDGMENTS

This work is supported by King Fahd University of Petroleum & Minerals. All the simulations presented in this paper are performed at the National Centre for Nuclear Research.

VI. REFRENCES

[1] J. D. Hooper, “Developed single phase turbulent flow through a square-pitch rod cluster,” Nuclear Engineering and Design, vol. 60, no. 3, pp. 365–379, Oct. 1980, doi: 10.1016/0029-5493(80)90302-7.

[2] J. D. Hooper and K. Rehme, “Large-scale structural effects in developed turbulent flow through closely-spaced rod arrays,” J Fluid Mech, vol. 145, no. 1, p. 305, Aug. 1984, doi: 10.1017/S0022112084002949.

[3] J. D. Hooper and D. H. Wood, “Fully developed rod bundle flow over a large range of Reynolds number,” *Nuclear Engineering and Design*, vol. 83, no. 1, pp. 31–46, Nov. 1984, doi: 10.1016/0029-5493(84)90027-X.

[4] S. Panguluri, D. Reasor, and R. LeBeau, “Investigation of grey area construction on the performance of detached eddy simulation,” 18th AIAA Computational Fluid Dynamics Conference, 2007, doi: 10.2514/6.2007-4095.

[5] T. Kwiatkowski and A. Shams, “Towards the accurate prediction of axial flow and heat transfer in a tightly spaced bare rod bundle configuration,” Nuclear Engineering and Design, vol. 403, p. 112119, Mar. 2023, doi: 10.1016/j.nucengdes.2022.112119.

[6] A. Shams and T. Kwiatkowski, “Towards the Direct Numerical Simulation of a closely-spaced bare rod bundle,” Ann Nucl Energy, vol. 121, pp. 146–161, Nov. 2018, doi: 10.1016/j.anucene.2018.07.022.

[7] J. K. Lai, G. Busco, E. Merzari, and Y. A. Hassan, “Direct Numerical Simulation of the Flow in a Bare Rod Bundle at Different Prandtl Numbers,” J Heat Transfer, vol. 141, no. 12, Dec. 2019, doi: 10.1115/1.4044832.

[8] J. K. Lai, E. Merzari, Y. A. Hassan, and A. Obabko, “Validation and development of DNS database for low Prandtl numbers in Rod Bundle,” Volume 2: Computational Fluid Dynamics, 2019, doi: 10.1115/ajkfluids2019-5036.

[9] “Ansys meshing | mesh generation and analysis for FEA, CFD.” [Online]. Available: https://www.ansys.com/products/ [Accessed: 14-Feb-2023].

[10] “Ansys Fluent | Fluid Simulation Software.” [Online]. Available: https://www.ansys.com/products/fluids/ansys-fluent. [Accessed: 20-Nov-2022].

[11] P. R. Spalart, “Detached-Eddy Simulation,” Annu Rev Fluid Mech, vol. 41, no. 1, pp. 181–202, 2009, doi: 10.1146/annurev.fluid.010908.165130.

[12] M. L. Shur, P. R. Spalart, M. K. Strelets, and A. K. Travin, “A hybrid RANS-LES approach with delayed-DES and wall-modelled LES capabilities,” Int J Heat Fluid Flow, vol. 29, no. 6, pp. 1638–1649, Dec. 2008, doi: 10.1016/J.IJHEATFLUIDFLOW.2008.07.001.

[13] A. Shams, F. Roelofs, E. M. J. Komen, and E. Baglietto, “Numerical simulations of a pebble bed configuration using hybrid (RANS–LES) methods,” Nuclear Engineering and Design, vol. 261, pp. 201–211, Aug. 2013, doi: 10.1016/j.nucengdes.2013.04.001.

[14] S. Tavoularis, “Rod bundle vortex networks, gap vortex streets, and gap instability: A nomenclature and some comments on available methodologies,” Nuclear Engineering and Design, Oct. 2011, doi: 10.1016/j.nucengdes.2011.09.043.

Proceedings of the European Nuclear Young Generation Forum
ENYGF'23
May 8-12, 2023, Kraków, Poland

Simulating Pressurized Thermal Shock in the Reactor Pressure Vessel of Nuclear Power Plants using Hybrid (LES/URANS) Modelling

Talal, Alharbi[1], Sultan, Alshehri[1*], Mohammed, Alsultan[1], Khaled, Al-Qahtani[1], Ahmed, Al-Habib[1], Afaque, Shams[1,2], and Tomasz, Kwiatkowski[3].

[1]King Fahd University of Petroleum & Minerals (KFUPM), Saudi Arabia

[2]Interdisciplinary Research Center for Renewable Energy and Power Systems (IRC-REPS), KFUPM, Saudi Arabia

[3]National Centre for Nuclear Research (NCBJ), Otwock, Poland

*Corresponding author: *s201826100@kfupm.edu.sa*

I. INTRODUCTION

A nuclear power plant has several parts that are vulnerable to varying aging processes that might shorten its life expectancy and create safety concerns. Reactor Pressure Vessel (RPV) is one of the key components that might experience various aging processes, and the occurrence of a pressurized thermal shock (PTS) is one of these aging processes that endanger the integrity of the RPV. PTS is defined as a high-temperature gradient due to rapid cooling of RPV under high pressure. Fig. 1 shows the injected water mixed with hot fluid where the mixture flows towards the downcomer where further mixing with the ambient fluid takes place. PTS occurs during a loss of coolant accident (LOCA) when an emergency core cooling (ECC) system is activated. This accident causes interference between cold and hot water, and under a particular set of conditions, this abrupt temperature change causes thermal loads on the vessel that could cause the failure of the RPV. According to IAEA, these conditions include the occurrence of reactor transients that subject the reactor vessel to a severe thermal shock [1]. The existence of sharp flaws at the inner surface of the vessel wall, and high fast neutron fluence and concentrations of copper and nickel in the vessel wall reduce its fracture toughness. The thermal-hydraulic study of temperature distributions in the RPV, nozzles, and downcomers is one of the primary analytical types utilized to assess a PTS scenario.

For the assessment of the nuclear power plant's lifetime and the prevention of potential nuclear safety hazards, a correct understanding of the thermal loads on the RPV is crucial. The thermal-hydraulic system codes currently in use to analyse these phenomena which based on simplified one-dimensional flow representations are unable to simulate the complicated dimensional flow that takes place in a PTS scenario. In the past ten years, more complicated PTS scenarios have been simulated to predict the flow and heat fields using more complex numerical simulations based on Unsteady Reynolds Averaged Navier-Stokes (URANS) and Large Eddy Simulation (LES) techniques. The LES method is extremely costly in terms of computer resources for the domain with large dimensions or at high Reynolds numbers. On the other hand, RANS shows some weaknesses in simulating turbulent flows in which the unsteady large scales play a significant role. Hybrid RANS/LES approaches offer an alternative to RANS or LES since they attempt to combine the advantages of both RANS and LES modelling in an optimized manner that resolves both attached and separated flows effectively. The most precise method for obtaining a thorough characterization of the flow and heat fields is Direct Numerical Simulation (DNS). It can offer a reference database for thorough validation and ongoing turbulence model improvement. Even on the most advanced computational architectures currently accessible, the DNS of an actual PTS scenario remains an expensive simulation that cannot be performed. Despite this, to create accurate and thorough databases for the validation of low-order turbulence models like hybrid URANS/LES, a DNS of a simplified PTS setup is used as the reference [2]. Additionally, it will contribute to the advancement of current turbulent heat flux modelling techniques. Therefore, in this research, an effort has been put forward to study the complex phenomenon of PTS using advanced Computational Fluid Dynamics (CFD) methodology, namely, a hybrid (LES/URANS) turbulence modeling approach has been adopted.

II. Geometry

The flow complexity in geometry for pressurized thermal shock PTS requires advanced modelling of anisotropic turbulence. One of the challenging CFD simulations is PTS

due to the mixing of different phenomena such as buoyancy-driven plumes, thermally stratified flow, and turbulent thermal mixing of the T-junction type.

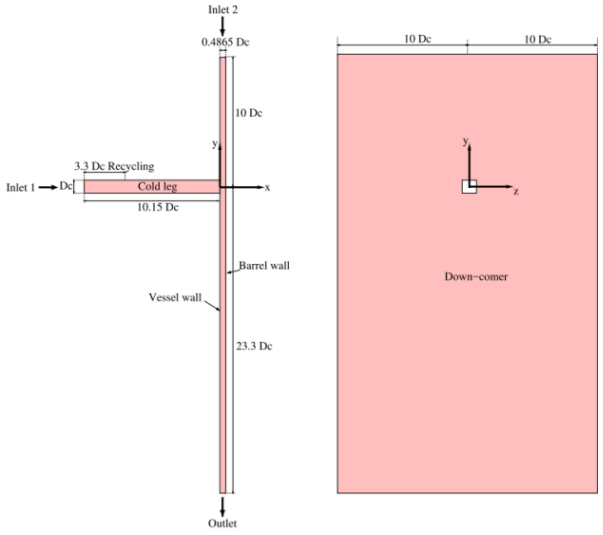

Figure 1 Geometry [2].

Therefore, choosing a geometric arrangement to mimic such a complicated flow event is a crucial initial step. To create a reduced instance that keeps the key elements of a realistic PTS scenario, the geometrical and hydrodynamic characteristics were calibrated using DNS simulations. Additionally, all the geometrical configuration and boundary conditions are adopted based on the DNS reference database. A square cold leg crosses a planar downcomer of the RPV perpendicularly in the PTS configuration will be considered. Cold water is injected into this downcomer through the cold leg. Since the current DNS utilizes constant fluid properties, another inlet above the downcomer is thought to mimic the downward flow path of cold clouds. The detailed dimensions for the geometry are shown in figure 1.

III. Flow parameters

The flow parameters which were adopted in this Hybrid simulation are based on the DNS study.Single-phase water is considered as working fluid. This produced a Prandtl number (Pr) of around 7. However, such a high number implies that Batchelor scales are far smaller than Kolmogorov scales, requiring a significantly finer mesh resolution to resolve the thermal scales. As a result, by altering the thermal characteristics of the water, the Prandtl number is reduced to one. The effects of such a modification were carefully explored, and despite minor variances, the overall topology of the thermal field was determined to be consistent. The injected cold water to the downcomer via the cold leg can be called inlet 1, while inlet 2 in the upper part of the down comer is considered to reproduce the downward flow path of the cold plume [2]. The inlet 2 velocity is chosen to be 10% of the inlet 1 bulk velocity, as detailed in [2]. Inlet 1 has a fully developed turbulent velocity profile, whereas Inlet 2 has a uniform velocity profile. The magnitude of the inlet 1 velocity is calibrated in order to set the friction Reynolds number (Re_τ) in the square duct cold leg to 180. The flow parameters of the problem are stated in table 1.

Properties	*Values*	*Units*
Density	994.58	kg/m^3
Viscosity	0.000550978	Ns/m^3
Thermal conductivity	0.65042	W/m K
Specific heat	4.1461	KJ/kg K
Outlet temperature	353	K
Inlet temperature	293	K
Reynolds number	5400	-
Friction Reynolds number	180	-

Table 1 Flow parameters

IV. CFD Code

In order to perform PTS with high accuracy, Ansys Fluent (2022R1 version) code was chosen for the analysis performed in this paper. It is considered one of the most finite element methods software used in the CFD field for modeling fluid flows, along with mass and heat transfers. It gives the user advanced physics capabilities and options to perform the desired phenomena by creating geometries and then meshing strategies. For the PTS scenarios, the hybrid turbulence model is highly recommended to use by modeling the flows near the wall by RANS and computing the large eddies by LES.

V. Mesh generation

The beginning was with the generation of the duct mesh, duct has been divided into three regions, to capture the gradient in the viscous layer. As it's known the velocity in the viscous layer is almost zero, so to capture that behavior there is a need for fine mesh near the wall. The starting point was region number 1 or close to the wall region, by calculating the first layer thickness, it was found to be less than $\Delta y^+ = 1$, then inflation was added from the first layer until the end of the second region which is the region between the first region and the central region with a stretching ratio of 1.2. And in the central region or the third region, the cell size is double the size of the last cell in the second region and all cells in the third region have the same size. The total element in the duct is 2 million – hexahedral trim mesh.

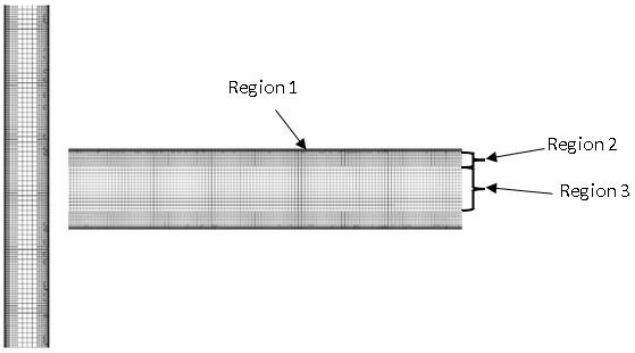

Figure 2 Side view of the mesh in the duct (right), the downcomer(left).

Let's move to the downcomer, there are two critical areas, the area where the impinging hit, and the other side of the downcomer, they are represented in the downcomer mesh by area number 1, the focus was on these two areas by having small cell size, then to have a smooth transition to the second area, inflation added starting from the first cell in the first region by a stretching ratio of 1.2. It results in downcomer a of 10 million - hexahedral trim mesh.

VI. Turbulence Modelling

The simulations of complex flow in the PTS case in this study will be conducted using a hybrid (LES/URANS) turbulence modelling approach. Mixing between unsteady (U)RANS and LES, detached eddy simulation (DES) which is one of the Hybrid modelling methods uses (U)RANS to model the flow near the wall and LES to model the bulk region of the flow. A detailed explanation was mentioned by Spalart [3], Fröhlich and von Terzi [4] about the advancement in hybrid methods. The viscosity equation of RANS eddy has a turbulence destruction term which is a function of the distance to the wall. The RANS model was modified into an LES-SGS model by substituting a length scale that depends on the grid size instead of the wall distance as mentioned in the development of the DES approach by Spalart [3]. The Figure 2 mesh of the duct length scale in this DES model alternates between wall distance (RANS) and grid size (LES). The most recent DES formulations which are delayed detached eddy simulation (DDES) and its upgraded version Improved DDES(IDDES) are chosen for the current flow configuration. k-ωSST models are taken into consideration for the IDDES formulation and are designated as IDDES-SST.

VII. Boundary conditions

According to the reference DNS case, inlet 1 uses a bulk velocity of 0.018 m/s based on the mass flow rate of one of the ROCOM test scenarios [5]. A fully formed turbulent profile is also enforced in order to maintain the turbulence level in the input pipe. The velocity at Inlet 2 is calibrated as a percentage of the velocity at Inlet 1. Inlet 1 has a relatively low temperature of T = 293K, whereas Inlet 2 has a relatively hot temperature of T = 353K. At the fluid-side walls and in the spanwise direction, standard no-slip boundary conditions are applied, however, adiabatic conditions are applied at the computational domain's outsides. It is worth noting that these boundary conditions are modified to calibrate various aspects of the specified flow arrangement.

VIII. Results and discussion

A. Analysis of the velocity field

The configuration of our geometry can be divided into two regions in terms of the flow field. The flow flowing in the square duct is the first one which then exits the square duct and hit the barrel wall. This flow is then separated in the downcomer. The flow in the downcomer is the second one which represents the area of our interest. The flow coming from the cold leg hits the barrel wall and then separated in the downcomer after making a stagnation fluid in the impingement region. These two regions can be easily seen in Figure 3. Figure 3. proves the fact that the Hybrid simulation can capture the behaviour of flow in both regions when comparing part a in the figure (results obtained by DNS) and part b (results obtained by Hybrid). Furthermore, figure 4 shows a comparison between the Hybrid simulation and the DNS reference database for the velocity profile (quantitative comparison).

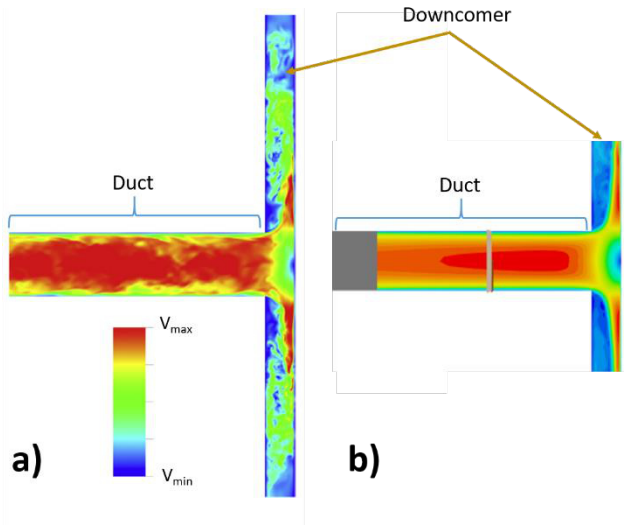

Figure 3 Velocity magnitude from a top overview of the duct and the downcomer a) DNS (left) b) Hybrid (right).

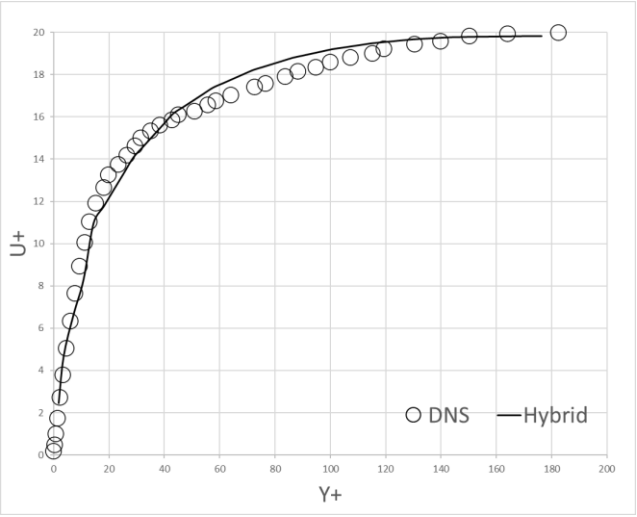

Figure 4 Comparison of the velocity profile in the duct between the Hybrid and the DNS reference.

B. The mean flow field analysis

The velocity distribution in the downcomer is more complex than in the square duct. The flow is deflected in the radial direction at the stagnation point. High velocity was observed close to the barrel wall. Figure 5 displays an overview of the velocity magnitude in the downcomer in three vertical planes at three different locations. In Figure 5 the upper

contours are for the Hybrid simulation, and the dawn ones are for the DNS simulation. An umbrella-like pattern appears in both simulations which exhibit similar trends.

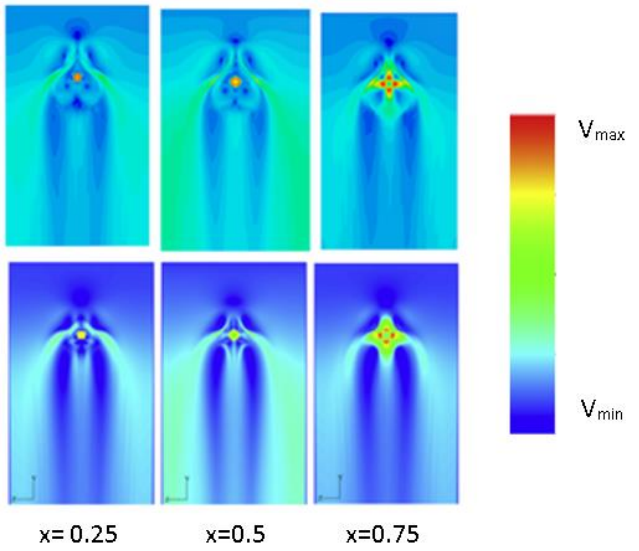

Figure 5 Contours of the mean velocity magnitude in the downcomer at different cross sections.

C. Analysis of the thermal field

Regarding the thermal field, it has a great role in PTS. The thermal field corresponding to adiabatic boundary condition is shown in figure 6. Several phenomena can be obtained from the contours of the mean temperature in the downcomer. First, the general trend of the cold fluid coming out from the duct is that it forms a radial shape on the barrel wall while interacting with the hot fluid coming from the top inside the vessel, consequently, the cold fluid is forced to flow downwards and the final mean temperature contour of the outer wall after performing the analysis is shown on figure 6.

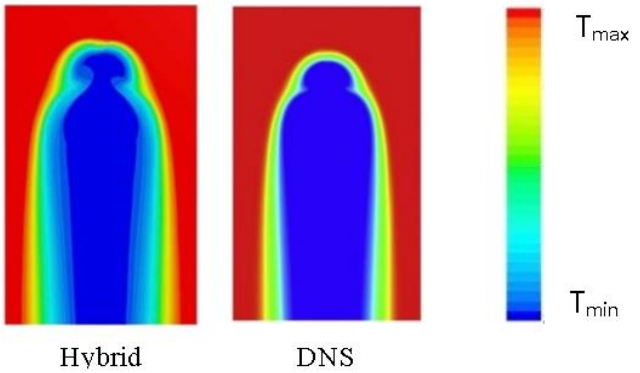

Figure 6 Contour of the outer vessel wall mean temperature in the downcomer for the case of adiabatic boundary condition.

In Figure 6, two distinct areas can be shown: the hot fluid area and the cold fluid area. Comparing the results obtained and the DNS results, the contour in figure 6 shows that the temperature is more distributed between the cold and hot fluid regions in the Hybrid simulation.

IX. Summary and conclusions

To understand the behaviour of the flow and the temperature distribution of this complex three-dimensional flow in the downcomer during ECC injection, numerical simulations using hybrid RANS-LES methods are carried out. The simulation was further validated with high-quality Direct Numerical Simulation (DNS) datasets [2]. Improved Delayed Detached Eddy Simulation (IDDES) techniques based on the k- SST model are utilized to calculate the modelling. It can be concluded that the study's findings were consistent with the references used, and the usage of hybrid (RANS/LES) models for such a complicated flow is strongly advised.

X. References

[1] A. Shams, G. Damiani, D. Rosa, and E. M. J. Komen, "Design of a single-phase PTS numerical experiment for a reference Direct Numerical Simulation," Nuclear Engineering and Design, vol. 300, pp. 282–296, Apr. 2016, doi: 10.1016/j.nucengdes.2016.01.038.

[2] A. Shams, D. De Santis, D. Rosa, T. Kwiatkowski, and E. J. M. Komen, "Direct numerical simulation of flow and heat transfer in a simplified pressurized thermal shock scenario," International Journal of Heat and Mass Transfer, vol. 135, pp. 517–540,Jun. 2019, doi: 10.1016/j.ijheatmasstransfer.2019.01.144

[3] P. R. Spalart, "Detached-Eddy Simulation," Annual Review of Fluid Mechanics, vol. 41, no. 1, pp. 181–202, Jan. 2009, doi: 10.1146/annurev.fluid.010908.165130.

[4] J. Fröhlich and D. von Terzi, "Hybrid les/Rans methods for the simulation of turbulent flows," *Progress in Aerospace Sciences*, 16-Jul-2008. [Online]. Available: https://www.sciencedirect.com/science/article/pii/S0376042108000390. [Accessed: 16-Mar-2023].

[5] "ROCOM experiments on boron mixing after restart of natural circulation - Helmholtz-Zentrum Dresden-Rossendorf, HZDR," www.hzdr.de.https://www.hzdr.de/db/Cms?pOid=24627&pNid=0&pLang=en (accessed Jan. 31, 2023).

[6] A. Shams, F. Roelofs, E. M. J. Komen, and E. Baglietto, "Numerical simulations of a pebble bed configuration using hybrid (RANS–LES) methods," Nuclear Engineering and Design, vol. 261, pp. 201–211, Aug. 2013, doi: 10.1016/j.nucengdes.2013.04.001.

[7] A. Shams, E. M. J. Komen, D. Rosa, and G. Damiani, "Design of a single-phase PTS numerical experiment for a reference Direct Numerical Simulation," ResearchGate, 2016. https://www.researchgate.net/publication/341294067_Numerical_prediction_of_a_single_phase_Pressurized_Thermal_Shock_scenario_for_crack_assessment_in_an_Reactor_Pressure_Vessel_wall (accessed Jan. 31, 2023).

[8] A. Shams and E. M. J. Komen, "Towards the Direct Numerical Simulation of a simplified Pressurized Thermal Shock," ResearchGate, 2017. https://www.researchgate.net/publication/324074143_Towards_a_Direct_Numerical_Simulation_of_a_Simplified_Pressurized_Thermal_Shock (accessed 2017).

Proceedings of the European Nuclear Young Generation Forum
ENYGF'23
May 8-12, 2023, Kraków, Poland

Numerical Simulation of Flow and Heat Transfer in A Tightly Spaced Bare Rod Bundle Configuration

Aljohani, Mohammed[1*], Alharbi, Talal[1], Shams, Afaque[1,2] and Kwiatkowski, Tomasz[3]

[1]King Fahd University of Petroleum & Minerals (KFUPM), Saudi Arabia.

[2]Interdisciplinary Research Center for Renewable Energy and Power Systems (IRC-REPS), KFUPM, Saudi Arabia

[3]National Centre for Nuclear Research (NCBJ), Otwock, Poland

*Corresponding author: *s201851520@kfupm.edu.sa*

I. INTRODUCTION

The fuel assembly's channels carry coolant, which removes the heat generated by nuclear fission. In rod bundles, the accurate prediction of flow and heat transfer is crucial for safe and reliable operation under normal and accident conditions. This prediction in tightly spaced bare rod bundles is challenging due to the complex fluid dynamics and turbulence fluctuations that occur in the small gaps between the rods.

In order to have an accurate result in a 3-dimensional geometry for mixing and heat transfer there is a need to have a step away from one-dimensional system code. This is because it will not perform well in this case, so Computational Fluid Dynamic (CFD) is considered one of the best choices to get trustful results. Also, having accurate results requires selecting an appropriate code depending on the available data and computational power.

There are various Reynolds-Averaged Navier-Stokes (RANS) turbulence models that can be used in this study however, few models have been specified and will be validated against the Direct Numerical Simulation (DNS) database. The URANS (unsteady RANS) models can predict the mixing, heat transfer, and pulsation with a reasonable percentage of error compared to DNS with less computational power and time. Numerical simulations using turbulence models have been commonly used to predict flow behaviour in these configurations. However, the accuracy and reliability of such models for simulating tightly spaced bare rod bundles are still under investigation.

Numerical investigations have shown that unsteady turbulence models capable of accounting for quasi-periodic flow pulsations are necessary for accurately predicting sub-channel mixing [1]. The URANS approach is suitable choice for this purpose. Several studies using URANS [2]-[12] have been performed to predict the appearance of flow pulsations in rod bundles, particularly in tightly-packed configurations.

In this study, the aim is to check the possibilities of the accurate prediction of turbulent flow with the use of different RANS models and compare the results with DNS reference data [13]. This will be done for simulating flow in a tightly spaced bare rod bundle configuration.

The parameters of the rod bundle configuration used in this research is based on Hooper's hydraulic experiment [14, 15] and will be further discussed in the flow configuration section.

II. NUMERICAL METHODOLOGY

A. Flow Configuration

The square packed rod bundle consists of six rods and held by spacers which create two subchannels, as shown in (Figure 1). Hooper's hydraulic experiment [14, 15] is selected as a reference case for analyzing the subchannel geometry. These details of the geometry are based on Hooper case in which six rods are spaced in a square lattice configuration with rod diameter (D) of 0.14 m and pitch to diameter ratio (P/D) of 1.107 is used. The P/D ratio of the rod bundle is considered to be close-spaced, or tightly spaced, rod bundle. The axial length (L) is 2.285m. This is to ensure that at least four wavelengths will be captured as per [16]. (Figure 1) shows the geometry of the rod and the parameters for the geometry are summarized in (Table 1).

Table 1. The parameters for the geometry

Symbol	Definition	Value	Unit
D	Rod diameter	0.14	m
P/D	Ratio of pitch to dimeter	1.107	-
L	Axial length	2.285	m

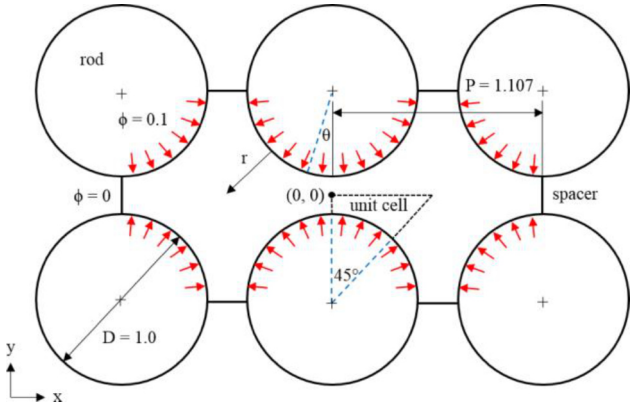

Figure 1. Flow configuration and thermal boundary condition [13]

B. Flow Parameters

For consistency, the computational domain is normalized by the rod diameter (D), bulk velocity (V_b), and Reynolds number (Re_h). Therefore, obtaining Re_h=22 600 requires V_b=1, ρ=1, D_h=0.56023, and ν=1/40341.

C. Boundary Conditions

In the streamwise direction, periodic boundary conditions (BCs) are applied such that the turbulence level is sustained. By doing so, both, the computational domain and the computational cost, will be reduced.

D. Turbulence Modelling

This study focused on the validation URANS turbulent models, which can be explained as dividing the flow parameters between Reynolds averaging equation into two terms mean and fluctuating components, then substituting these terms on Navier–Stokes equations. This study has been done using three models, and the results from each model will be validated against reference database and among each other.

a. k - ω SST

This model has been chosen in order to have an accurate prediction near the walls as well as in the bulk. This is because it composes of two models, k-ω near the walls and k-ε in the bulk. In addition, k - ω SST is a two-equation model, which will help to predict the mixing accurately.

b. RSM

The Reynolds Stress Model (RSM) is an advanced turbulence model that has been widely used in CFD simulations to predict turbulent flows. It is based on the RANS equations, which are commonly used in CFD simulations. The RSM model is more accurate than simpler turbulence models, such as the k- ε model, because it accounts for the anisotropy of turbulence by modelling the Reynolds stresses directly. This provides a more complete description of the turbulent flow field and enables more accurate predictions of complex flows.

c. GEKO

The GEKO turbulence model is a variant of the RANS equations and increasingly being commonly used in CFD simulations. It is a k- ω based model with the goal of consolidating two equation RANS models into one flexible, robust, general purpose turbulence model. Also, it has several advantages over other turbulence models. For example, it is more accurate than the standard k-epsilon model in predicting the behaviour of separated flows, and it is more robust than other models in situations where the flow is highly anisotropic.

III. Meshing Strategy

ANSYS Mesher software was used in order to create a mesh for the given computational domain. (Figure 2) is presenting generated mesh in cross-section. The mesh was generated in two subsequent steps, as mentioned below.

In step 1 a 2D mesh for the cross-section was generated. And accordingly in step 2, this 2D mesh was uniformly extruded in the streamwise direction.

The overall mesh consists of almost 6 million cells. In order to properly capture the flow gradients, the mesh contains a structured mesh boundary layer (18 grid points with a stretching ratio of 1.17) in the near wall region. The first cell was computed with the objective of maintaining the average y+ value below 1 (y+ denotes the normalized distance from the nearest wall in wall units).

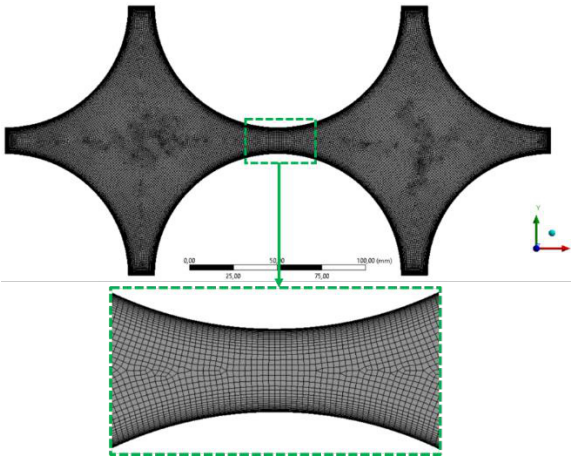

Figure 2. 2D mesh for the cross-section.

IV. RESULTS AND DISCUSSION

As a starting point, this study will focus on the analysis for a single Prandtl number, which is 0.71. This will give a basic understanding of performance of the used models, and this knowledge can be used in the investigation of the other Prandtl numbers in the future. By focusing on one Prandtl number, a more detailed analysis that can be done which will help in the future research. This study has been performed by commercial software ANSYS Fluent with the default options for all of the three previously mentioned models.

A. Velocity Field

Qualitative results for the velocity field are shown in (Figure 3). In comparison with the reference case [17], (Figure 4), all three models show pulsation, providing an indication of good momentum field prediction. Pulsations from each model have different amplitude. (Figure 3) show similar amplitudes for k-ω SST and GEKO, with RMS being noticeably thinner compared to them Low P/D rod bundles are expected to have such behaviour. These three turbulent models were included in the study done in the reference case [17] where all of them showed good prediction for the flow field.

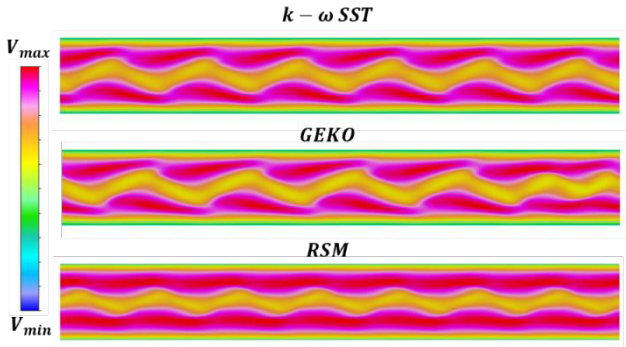

Figure 3. Contours of velocity field for different models on the streamwise plane

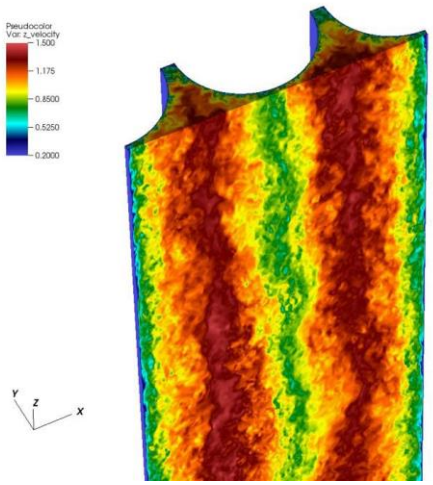

Figure 4 Contours of the velocity field on the streamwise plane captured by DNS [17]

B. Frequencies Of Momentum Field

The characteristic frequencies of momentum field for k-ω SST, GEKO, and RSM was found to be 21.3 Hz, 18.6 Hz, and 23.95 Hz, respectively, as shown in the power spectral density (PSD) (Figure 5). This difference in frequency is because different turbulence models make different assumptions and simplifications about the physics of turbulent flows. These results present a good agreement with the reference DNS data [13]. For GEKO model, several dominant peaks were obtained and the first one most dominant has the previously mentioned frequency, 18.6 Hz, which exactly match the frequency obtained from the DNS database.

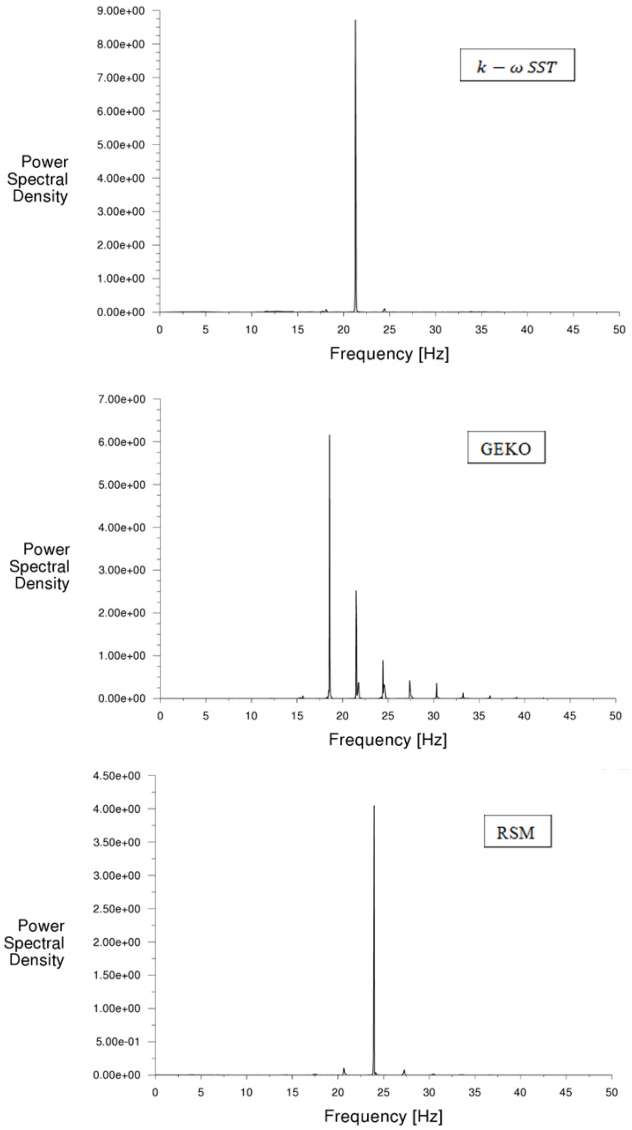

Figure 5. Characteristic frequency of momentum field for the three models

V. Conclusion

In this study, three different turbulence models, namely k-ω SST, GEKO, and RSM, were used to investigate the momentum field and its characteristic frequencies. The velocity fields of these models were compared with the reference case [17], and a high degree of similarity was observed. The results showed that all three models exhibit

pulsation, indicating a good prediction of the momentum field. The frequencies, however, varied across the models, with values of 21.3 Hz, 18.6 Hz, and 23.95 Hz, respectively. These differences in frequencies can be attributed to the underlying assumptions and simplifications made by each model in capturing turbulent flow physics. Despite this, the results showed good agreement with the reference DNS data, and the GEKO model exhibited several dominant peaks, with the most prominent frequency matching exactly with the frequency obtained from the DNS database.

VI. Acknowledgments

The authors acknowledge the support provided by Undergraduate Student Research Grant (UXplore) at King Fahd University of Petroleum and Minerals (KFUPM). All the simulations presented in this paper are performed at the National Centre for Nuclear Research, Poland.

VII. References

[1] Home, D., Arvanitis, G., Lightstone, M.F., Hamed, M.S., 2009, "Simulation of flow pulsations in a twin rectangular sub-channel geometry using unsteady Reynolds Averaged Navier – Stokes modelling," 239, 2964–2980.

[2] Baglietto, E., & Ninokata, H. (2005), "Numerical analysis of turbulent flow and heat transfer in tight-lattice rod bundles," Nuclear Engineering and Design, 235(4), 419-430.

[3] Chandra, P., Kaushik, S. C., & Saini, J. S. (2010), "Computational analysis of flow and heat transfer in square ducts with transverse ribs," Journal of Heat Transfer, 132(3), 031901.

[4] Chang, S. W., & Tavoularis, S. (2007), "Experiments on turbulent heat transfer in a square duct," Journal of Heat Transfer, 129(11), 1453-1462.

[5] Liu, W., & Ishiwatari, M. (2013), "Large eddy simulation of turbulent heat transfer in a three-dimensional wavy channel," International Journal of Heat and Mass Transfer, 57(2), 487-495.

[6] Merzari, E., & Ninokata, H. (2011), "Large eddy simulation of flow and heat transfer in a staggered tube bundle," International Journal of Heat and Fluid Flow, 32(1), 187-200.

[7] Ninokata, H., & Merzari, E. (2007), "Numerical simulation of turbulent flow and heat transfer in rod bundles," Nuclear Engineering and Design, 237(7), 755-764.

[8] Ninokata, H., Maruyama, S., & Yamamoto, T. (2009), "LES of flow and heat transfer in a 5 × 5 rod bundle," Nuclear Engineering and Design, 239(9), 1709-1720.

[9] Yan, Y. Y. (2011), "Heat transfer and pressure drop correlations for rectangular channels with pin fins," International Journal of Heat and Mass Transfer, 54(13-14), 2966-2971.

[10] Yan, Y. Y., & Gu, Y. T. (2012), "Heat transfer and flow structures in a two-pass rib-roughened channel," International Journal of Heat and Mass Transfer, 55(13-14), 3618-3631.

[11] T. Kwiatkowski and A. Shams, "Towards the accurate prediction of axial flow and heat transfer in a tightly spaced bare rod bundle configuration," Nuclear Engineering and Design, vol. 403, p. 112119, 2023.

[12] A. Shams and T. Kwiatkowski, "Towards the direct numerical simulation of a closely-spaced bare rod bundle," Annals of Nuclear Energy, vol. 121, pp. 146–161, 2018.

[13] Lai, J. K., Busco, G., Merzari, E., and Hassan, Y. A. (October 8, 2019), "Direct Numerical Simulation of the Flow in a Bare Rod Bundle at Different Prandtl Numbers," ASME. J. Heat Transfer. December 2019; 141(12): 121702.

[14] J. D. Hooper, "Developed single phase turbulent flow through a square-pitch rod cluster," Nuclear Engineering and Design, vol. 60, no. 3, pp. 365–379, 1980.

[15] J. D. Hooper and K. Rehme, "Large-scale structural effects in developed turbulent flow through closely-spaced rod arrays," Journal of Fluid Mechanics, vol. 145, pp. 305–337, 1984.

[16] E. Merzari, H. Ninokata, and E. Baglietto, "Numerical simulation of flows in tight-lattice fuel bundles Nuclear Engineering and Design," vol. 238, no. 7, pp. 1703–1719, 2008.

[17] J. K. Lai, E. Merzari, Y. A. Hassan, and A. Obabko, "Validation and development of DNS database for low Prandtl numbers in Rod Bundle," Volume 2: Computational Fluid Dynamics, 2019.

Proceedings of the European Nuclear Young Generation Forum
ENYGF'23
May 8-12, 2023, Kraków, Poland

Nuclear Safety Considerations in the Saudi Nuclear Energy Initiative Based on Historical Nuclear Reactor Events

Almalki, Abdullah[1*], Alruwaished, Abdulaziz[1], Alsubhi, Abdulaziz[1], Meri, Yazan[1], Shams, Afaque[1], Al-Athel, Khaled[1]

[1]Chemical Engineering Department, King Fahd University of Petroleum & Minerals, Saudi Arabia.

[1]Mechanical Engineering Department, King Fahd University of Petroleum & Minerals, Saudi Arabia.

** s201819080@kfupm.edu.sa*

I. INTRODUCTION

Upon the Saudi 2030 vision towards the transition of the energy sector, different clean energy sources have been considered to diversify the energy mix and reduce greenhouse gas emissions. Among these nuclear power plants was the main candidate that proves sustainability and satisfies the expected increase of energy demand in Saudi Arabia. On an international level, the nuclear energy industry is an emerging field that was first connected to the grid in 1954, making it a growing source compared to other energy production plants. Throughout the past 70 years, nuclear power plants have observed massive developments in safety, reliability, and efficiency. These development levels are a direct consequence of learning from previous historical events. Three main events have occurred in the history of nuclear energy, Three Mile Island, Chornobyl, and Fukushima. Through analyzing these events, the main causes were attributed to environmental, technical, and human factors. Proper understanding and mitigation of root causes have added to the safety and security factors of nuclear power plants and maintained their role as promising clean energy sources. It also minimizes the effects of different risks through the way they are treated. This research investigates the causes of past major events, evaluates mistakes, and provides recommendations for the Saudi Nuclear energy initiative.

II. RESEARCH METHODOLOGY

The initiation of safe nuclear power plants requires a study of possible hazards in the nuclear power plant (NPP) establishment and operation. The gathering of all possible hazards is a complicated process that greatly depends on past experiences. The area of Saudi Arabia has little experience with nuclear power plants. Many affecting factors, such as environmental factors, and their hazards vary from one area to another. Thus, the countries' experiences could not directly contribute to the methodology of reactor initiation and operation in Saudi Arabia. However, other countries' experiences can be employed to develop a local safety approach. Analyzing past major actions, the way they are treated, and how safety considerations are formed after them would add a massive experience to the local state. (Figure 1) illustrate the used methodology flowchart.

Figure 1. Research methodology flow chart.

III. BACKGROUND THROUGH THE MAJOR NUCLEAR EVENTS

A. Chernobyl

Chornobyl was a nuclear accident that caused radiological contamination in its area. It took place at reactor number 4 of the Chornobyl nuclear power plant (CNNP) in the Soviet Union (USSR) -present Ukraine- in 1986. CNNP was a type of RBMK reactor, which uses enriched uranium as its fuel and graphite as its moderator. The event happened during a safety experiment that tests the reactor safety in a loss of electricity scenario. Moments after the experiment started, a steam explosion took place. It affected the integrity of a heavy steel and concrete reactor cover and exposed the reactor core, which continued burning for more than a week [1]. The event was rated with the highest rank of a nuclear accident on the International Nuclear and Radiological Event Scale.

Going through the nuclear industry operation, nuclear-related accidents were consistently unpublished due to competitive and political reasons [2]. The lack of information transfer has created a situation for failure accumulation without monitoring. Back at the CNPP's start of the operation, the station had an unstable period of

operation that included 29 emergency shutdowns in the period 1977-1981 [3]. This shows the unsteady behavior of the station's reactors due to technical and operational causes. In performing the safety experiment, several operational human errors were noted causing the event [1]. First, experimenting was meant to be done, but it was not planned to be at run time. The experiment started at a night shift with inadequate earlier preparations [4]. This led to a reduction in operation safety and an increment in faults and accident chances. Consequently, on the day of the event, the experiment was run without its full protocol procedure and the explosion happened. In addition, there was a lack of communication and knowledge transfer between the reactor designer and operators [2]. It created a gap that caused operators to take misleading decisions. Finally, after the explosion, a lack of coordination led to delayed treatment and growth in the accident residuals.

B. Fukushima

The incident took place at Japan's Fukushima Daiichi Nuclear Power Plant. The explosion occurred on March 11, 2011, following a strong earthquake and tsunami [5]. The incident was classed as level 7 by the Fukushima Daiichi Nuclear Power Plant, which is the highest accident level characterized as a substantial discharge of radioactive material with extensive health and environmental damage. The affected reactors in Fukushima were GE Hitachi boiling water reactors (BWR-3 and -4) with Mark I and II. Fortunately, three of the six reactors, 4,5, and 6, were shut down for maintenance before the tragedy. When the earthquake was detected, the remaining three reactors were automatically shut down by the insertion of control rods. Meanwhile, the violent earthquake triggered a malfunction in the energy grid, and power to the nuclear power reactors was interrupted. Even if the reactor is shut down, reactor cooling is still required to remove residual heat. As a precaution, diesel generators began powering the water pumps. A powerful wave triggered by the earthquake swamped the plant's basement and adjacent areas in less than an hour. The flood caused a failure in the emergency cooling system.

IV. LESSONS LEARNED FROM MAJOR EVENTS AND THEIR INFLUENCE ON THE NPP OPERATION

In accident scenarios, fast handling of the situation reduces the chances of action propagation. It requires the presence of experienced operators trained to handle accident scenarios. Reviewing these scenarios, this study explores what operational behavior has changed after the Chornobyl and Fukushima incidents. It seeks emergency protocols and how the safety consideration improved after major accidents.

The major incidents had technical and environmental aspects, which may have a detrimental effect. Nevertheless, the operational and human factors would have a vital role in how the accident effect would be controlled. Examples include the technical drawback of the RBMK control rods where they have undesirable behavior at critical operational moments (start-up and shutdown). Moments before the Chornobyl core explosion, the reactor went into an irregular performance. It was not providing the amount of power it should have due to the known later situation of uranium-zirconium-silicate accumulation. If the operators were aware of the NPP situation, they would have shut down the reactor to mitigate the event. The plant had shown signs of unusual behavior, but due to the operators' low levels of transparency and bad communications, they took the incorrect decision in raising the control rods. Such a crucial decision must be taken with a full understanding of the situation with high levels of communication and transparency.

Post-Fukushima, Under the Action Plan, the International Atomic Energy Agency (IAEA) has undertaken and implemented over 1000 activities, including international expert meetings, conferences, and workshops [7]. The IAEA's safety standards have been revised to accommodate lessons gained, the IAEA's safety peer review services have been reinforced, and the number of safety peer assessments for operators and regulators in the Member States has grown. Moreover, several measurements and rules had been taken to ensure the safety of each power plant. For example, installing additional backup sources of electrical power, carrying out "stress tests" to reassess the design to simulate any possible natural hazards, and supporting the protection of plants against extreme external events. Furthermore, additional safety assessments (Stress Tests) and equipment modifications have been implemented in three phases on EDF PWRs (2012 to 2020). For example, the creation of the FARN (EDF) + FINA (AREVA). Moreover, Implementing the standard of the basic concept of safety has become more strict, redundant, diversified in integrated safety, and self-controlled in designing any new reactor. For example, in EPR (Figure 2), it is noticed that the diesel buildings are in two different places in the plant, and several implementations of safety concepts have been done.

Figure 2. EPR shows a strict application of the basic concept of safety in NPP [8].

Nuclear industry operation requires higher levels of operation and action response. It could be defined as a safety culture that includes a set of regulations and thinking processes. The safety culture may start with simple routine attitudes as stated in [6]. Developing a safety culture would take dangerous situations into safe zones rather than escalating them. Examples include having a supportive working environment. This can enhance the chances of early problem detection and having the right response for it. It develops a feedback loop from the operators to manufacturers. Moreover, developing a communication network to share the reactors' behavioral archives would create a better understanding of the reactor. It will allow

operators to have a great experience as they get exposed to more situations. In the following section, successful examples of safety attitudes are presented.

V. EXAMPLES OF SUCCESSFUL SAFETY IMPROVEMENTS EXPERIENCES

A. Nuclear power plants collaboration

Collaboration is a vital key to safe and reliable nuclear power plant operations. The international nuclear energy community observed two main forms of collaboration, national collaboration within a country and international collaboration between countries. The first collaboration was observed in the United States in 1979 when INPO (Institute of nuclear power operators) was established in response to the three-mile island accident. INPO acts as a joint for all nuclear industry utilities to promote excellence in nuclear power plant operations, by promoting information and experience exchange. Using the SEE-IN (Significant Event Evaluation and Information Network) program, INPO reviews and analyses operating and construction experiences in nuclear power plants, most significant and applicable events are communicated to other nuclear power plants in the industry [9]. As shown in (Figure 3.) the efforts of INPO have improved the net capacity factor of nuclear power plants in the United States from about 61% in 1977 to more than 91% in 2019. It is worth noting that the capacity factor has maintained a level of approximately 90% in the past 20 years, which indicates higher levels of stability through collaboration.

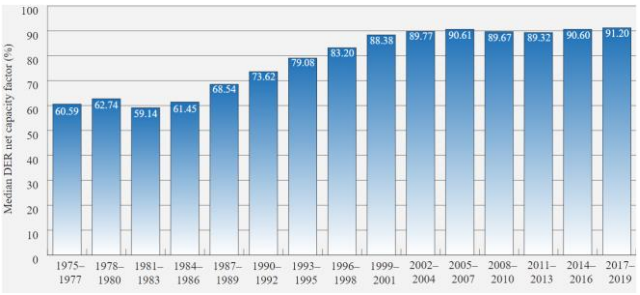

Figure 3. Median DER net capacity factor in the United States between 1975 and 2019, source ANS [10].

Based on the INPO model and as a result of the Chornobyl accident, commercial power plant operators collaborated in 1989 and established WANO (The World Association of nuclear operators). Aiming at maximizing worldwide safety and reliability of nuclear power plants, by working together to assess, benchmark, and improve the performance of nuclear power plants [11]. WANO has established many programs aimed at increasing communication and experience exchange levels between different operators internationally. WANO developed a peer review program to help members compare their operations to high excellency levels, where an independent team from outside the plant reviews the operations in the plant. The results of the review are summarized in a report indicating the main areas of improvement, this helps members learn and share operational experiences. Furthermore, a performance analysis program was created to collect and analyze data to provide members with lessons learned from events of deviation in operations.

B. FARN

French Rapid Action Force (FARN) is a safety specialized team that acts as offsite support in case of a nuclear event. FARN was created in 2011 just after the Fukushima incident to help onsite teams return electricity and water supplies within 24 hours of an event. It consists of 300 employees, formed into four nuclear power plants Bugey (Regional base), Civaux, Paluel, and Dampierre. FARN consists of experts and engineers that are professionally trained to intervene in any nuclear power plant within 12 hours to supply water, air, and electricity. Equipped with pumps, trucks, helicopters, handling machines, cranes, air compressors, electricity generators, and different probes that detect radioactivity.

FARN provides a model for maintaining and strengthening the levels of effective emergency preparedness and response capabilities in the nuclear industry. It is a one-of-a-kind entity that represents the high levels of safety and redundancy in nuclear power plant operations. Considering the approach of defense in depth (DiD) (Figure 4) found in nuclear power plants, FARN may be included in the fourth and fifth levels of DiD. The fourth DiD level aims at mitigating the severe conditions in the reactor to prevent any form of core melting. As an example, in this level, FARN has a responsibility to provide means of core cooling when the emergency core cooling system (ECCS) fails to cool the core when the core coolant is lost. The fifth level of DiD aims at limiting the consequences of radiation in the event of radioactive releases such as a case of core meltdown and containment integrity failure, in this scenario FARN is responsible for detecting the levels of radioactive releases in the environment and informing higher authorities in case of a possible evacuation plan. It can be summarized that FARN comes as a last option that would operate to protect people and the environment in the event of main and auxiliary systems failure, which is a rare event in nuclear power plants due to redundancy in their design. The presence of FARN and other similar groups makes nuclear energy the safest, cleanest, and most sustainable energy source.

Levels of defence in depth	Objective	Essential means
Level 1	Prevention of abnormal operation and failures	Conservative design and high quality in construction and operation
Level 2	Control of abnormal operation and detection of failures	Control, limiting and protection systems and other surveillance features
Level 3	Control of accidents within the design basis	Engineered safety features and accident procedures
Level 4	Control of severe plant conditions, including prevention of accident progression and mitigation of the consequences of severe accidents	Complementary measures and accident management
Level 5	Mitigation of radiological consequences of significant releases of radioactive materials	Off-site emergency response

Figure 4. Levels of Defense in Depth (DiD) [12].

VI. RECOMMENDATIONS

The importance of clear, transparent, and continuous communication is a vital aspect of the nuclear industry. Whether that communication is considered within the nuclear sector of the country, or on a wider range with nuclear sectors of neighboring countries. Sharing minuscule operating irregularities even if the issue has been resolved, can prepare other operators and prevent accidents from instigating for seemingly no reason.

Furthermore, there have been lessons for all nuclear operators from past events such as the Fukushima incident. Other than the beforementioned effective communication line, severe and rare weather conditions should be considered in the design and preparation of nuclear plants. For Saudi Arabia, the extreme weather phenomena which might not have been considered by other countries will involve extreme humidity, accompanied by extreme heat, and in even more extreme cases huge sandstorms. Thus, probabilistic safety assessment (PSA) is a tool that should be utilized greatly in estimating these unique weather conditions that might have not been considered in other climates in the design stage. On the other hand, during operation, rigorous and extensive inspections should be carried out regularly. Utilizing the country's vast knowledge and experience in the corrosion protection industry in the confines of nuclear safety culture to ensure the safe and reliable operation of their plants.

Finally, even with great preparation in the design stage and during operation, events might occur. For this, mitigation is essential. A rapid action response team, with technical knowledge of the plants, and sufficient training should be prepared before the nuclear plants are in operation. This will ensure that proper mitigation by professionals will be provided promptly in the case of accidents. This response team can even be utilized in case it is needed by neighboring countries. A choice that can strengthen relations and provide even more collaboration but most importantly, provide safety.

VII. CONCLUSION

In conclusion, the ventures of countries into the nuclear industry, as well as the shortcomings experienced in reactor operation, can all be lessons for the future of the industry. Three-mile Island, Chornobyl, and Fukushima events are incidents that have helped the nuclear industry achieve excellence and success. Through studying their major causes, a set of changes have been implemented to make sure that no such events repeat. The lessons learned from these incidents must be taken seriously, and prevention methods must be strictly adhered to. Clear communication, careful consideration in the design stage, and the readiness and preparedness to act to mitigate the harm of any possible harm in case of an accident are the most important parameters to keep and maintain within and among countries and organizations responsible for the research, design, and operation of nuclear reactors.

VIII. ACKNOWLEDGMENTS

Special thanks to Dr. Afaque Shams for his supervision and the invaluable assistance he provided. This work is supported by King Fahd University of Petroleum & Minerals.

IX. REFERENCES

[1] V. Saenko *et al.*, "The Chernobyl Accident and its Consequences," *Clin Oncol*, vol. 23, no. 4, pp. 234–243, May 2011, doi: 10.1016/j.clon.2011.01.502.

[2] S. D. Schmid, "When safe enough is not good enough: Organizing safety at Chernobyl," *Bulletin of the Atomic Scientists*, vol. 67, no. 2, pp. 19–29, Mar. 2011, doi: 10.1177/0096340211399404.

[3] D. R. Marples, "Chernobyl: A reassessment," *Eurasian Geogr Econ*, vol. 45, no. 8, pp. 588–607, 2004, doi: 10.2747/1538-7216.45.8.588.

[4] Editors of Encyclopaedia, "Chernobyl disaster," *Britannica*. Oct. 18, 2022.

[5] The Editors of Encyclopaedia, "Fukushima accident," *Britannica*. Dec. 02, 2022.

[6] N. Meshkati, "Lessons of Chernobyl and Beyond: Creation of the Safety Culture in Nuclear Power Plants."

[7] "Plant-Specific Safety Enhancements After Fukushima," *United States Nuclear Regulatory commission (U.S.NRC)*, 2021.

[8] "Introduction to EPR. Remote model," 2022.

[9] "Nuclear Regulation: NRC's Relationship with the Institute of Nuclear Power Operations," May 1991.

[10] "U.S. nuclear capacity factors: Resiliency and new realities," May 30, 2020.

[11] "World Association of Nuclear Operators (WANO) - Our Mission." https://www.wano.info/about-us/our-mission (accessed Jan. 28, 2023).

[12] "Defence in depth in nuclear safety". INSAG-10 / a report by the International Nuclear Safety Advisory group. Vienna: International Atomic Energy Agency, 1996.

Proceedings of the European Nuclear Young Generation Forum
ENYGF'23
May 8-12, 2023, Kraków, Poland

Design Investigation of NuScale Small Modular Reactor Fuel Assembly

Alsafi, Osama[1], Alqahtani, Khaled[1], Algedairi, Ahmed[1], Organji, Ramiz[1], Shams, Afaque[1,2]

[1] King Fahad University of Petroleum & Minerals (KFUPM), Saudi Arabia

[2]Interdisciplinary Research Center for Renewable Energy and Power Systems (IRC-REPS), KFUPM, Saudi Arabia

*Corresponding author: s201827080@kfupm.edu.sa *(O. Alsafi)*

I. INTRODUCTION

Small modular reactors (SMRs) are a category of nuclear reactors that are smaller and more versatile relative to large conventional nuclear reactors. They are viewed as a potential solution to many challenges facing the nuclear industry, including high capital cost and long construction times. They allow for a more efficient, safer, and cost-effective operation compared to traditional nuclear reactors, which are built on-site. Additionally, they are designed to be modular, which allows multiple SMRs to be installed at one plant and generate commercial power. This makes them an attractive option to power small and off-grid locations. However, the development of SMRs is still in the early stages. Many countries around the world are actively researching and developing various SMR concepts, yet there are still many technical and regulatory challenges to overcome before SMRs can be deployed widely. According to the IAEA [1], there are currently about 50 distinct SMR designs globally, some of which are in advanced deployable stages. Many of those designs are based on conventional Pressurized Water Reactors (PWR) that have been operated for half a century. They share common core components including fuel assemblies, control rods, core barrels, etc. Moreover, fuel assembly design is a key element to efficient and safe reactor operation. It is a grid-like structure that holds fuel rods containing nuclear fuel pellets. The fuel rods are arranged in a specific pattern to maintain and balance nuclear fission reactions, ensure efficient heat transfer, and mitigate severe dynamic responses leading to core damage.

Furthermore, a proper fuel assembly design should account for a phenomenon that commonly occurs in bounded flows known as Flow-induced Vibration (FIV). Along a fuel rod's length, the kinetic energy of the flow around it differs causing flow pulsations, especially in the region between two adjacent fuel rods. Local velocity fluctuations yield the phenomenon even more prominent, which could lead to sever rod deflection. Moreover, the pressure field of the fluid around the fuel rods is not uniform; thus, the load (pressure) exerted on the structure varies, which leads to rod vibration. The problem is amplified if the vibration frequency of the rod matches its natural frequency, the rod would then tend to resonate and possibly cause cladding permanent damage, leading to reactor shutdown. Therefore, it is crucial to study such phenomenon and develop models to counter its negative effects on reactor operation.

There have been many attempts to study FIV in the context of nuclear reactors. The dynamic response of cantilevered rods for Light Water Reactor (LWR) applications was determined by [2]. In the experimental setup, water at low velocities flows from the free end of the rods, while the other end is clamped. Utilizing an optical measurement technique to record the vibration and flow field, it was found that the rods vibrate with large amplitudes, even at low to moderate flow velocities. The data generated was particularly suited for the development of numerical models. Moreover, a thorough numerical study of FIV was conducted by [3]. The study focused on the effects of velocity pulsations on the vibration response of a bare rod, wire wrapped rod, and a rod bundle configuration. Tightly coupled finite volume and finite element solvers were used to simulate the Fluid-Structure Interaction (FSI) problem. Considering the seven-rod bundle simulation and utilizing Unsteady Reynolds Averaged Navier Stokes (URANS) turbulent model, it was found that flow caused excessive rod vibrations, resulting in rod-to-rod interactions. This article attempts to numerically study the dynamic response of a four-rod bundle in axial flow, considering NuScale's SMR fuel assembly design. The two fields (fluid and structure) are tightly coupled, following a two-way FSI approach, where the fluid and solid equations are solved simultaneously. Moreover, the vibration frequency at rated conditions is determined from the simulation results, utilizing Fast Fourier Transform (FFT) algorithms. The results found in this article can be generalized to obtain the fuel assembly performance of light water based SMRs, thus aiding the design process.

II. GEOMETRY

The fuel assembly of NuScale SMR has a 17×17 square lattice configuration of fuel rods and guide tubes. However, performing a complete FSI study on such a large domain requires high computational power and thus is not feasible. Instead, a 2×2 configuration was chosen for the study to simplify the analysis, yet still preserve the overall physics of the flow. The geometry consists of a 2×2 rod bundle, with

a rod diameter of d = 9.5 mm and a pitch of p = 12.6 mm; thus, the pitch to diameter ratio is p/d = 1.326. The outer diameter of the fluid domain is D = 50.4 mm. Figure 1 shows the geometry and the selected numerical domain for the FSI case.

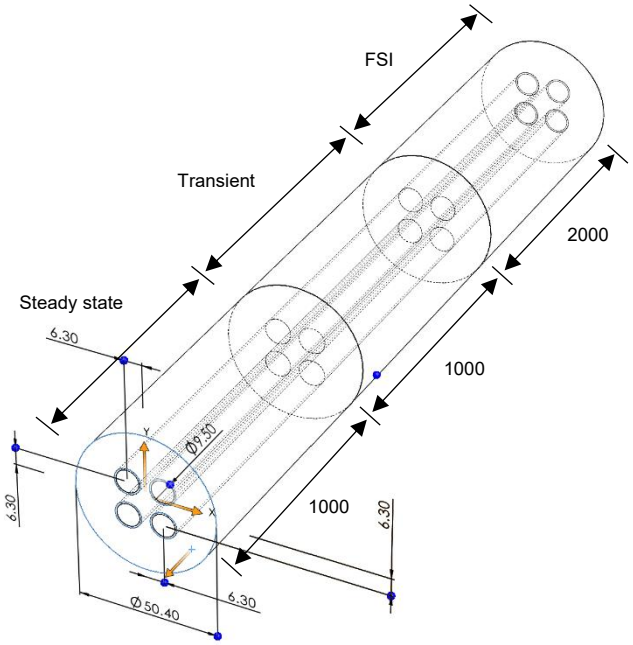

Figure 1. The computational domain used for all simulations (dimensions are in mm).

III. NUMERICAL MODLE

The numerical FSI study is performed using ANSYS Workbench 2022 R1 version, which includes several tools and solvers of which some are used. Moreover, considering the limited computational resources available, the simulations are simplified in order to save time and hold a decent accuracy. Moreover, Figure 1 illustrates the computational domain, which can be divided into three parts. It was found that performing a steady-state fluid simulation first yields a more realistic flow profile; thus, a steady-state fluid simulation with a periodic inflow outflow condition was performed, considering rigid rods. Furthermore, the obtained velocity profile was used as an inlet to the transient fluid simulation, where the rods are assumed rigid. The periodic boundary condition imposed generated well-developed velocity pulsations, which yields realistic flow physics. Finally, the velocity profile of the transient case was used as the inlet to the FSI study, where the rods are flexible.

A. Computational Grids

The fluid flow simulations were performed using the finite volume solver ANSYS Fluent version 2022 R1. The fluid domain consists of a large cylinder with four holes cut along its axis to accommodate the fuel rods. The mesh was first constructed considering a 1.5 mm length scale and hexahedral dominant mesh elements, which were judged sufficient by [4] conducting a similar kind of simulation. The 2 m long domain was divided into 220 sub-divisions in the axial direction, which yielded a mesh over 437k nodes and 417k elements. In the wall-normal direction, inflation layers were created to account for the momentum boundary layers. Moreover, the mesh statistics were compliant with the recommended values in the literature. The average element skewness was around 0.106, with an average orthogonal quality of 0.974. Furthermore, the transient structural simulation was performed utilizing ANSYS Mechanical ADPL solver version 2022 R1, which is a finite element solver type. The computational grid consists of four identical thin fuel rods spaced equally and arranged in a square lattice configuration. The mesh was generated with a total of 128k nodes and 18336 hexahedral elements, as shown in Figure 2.

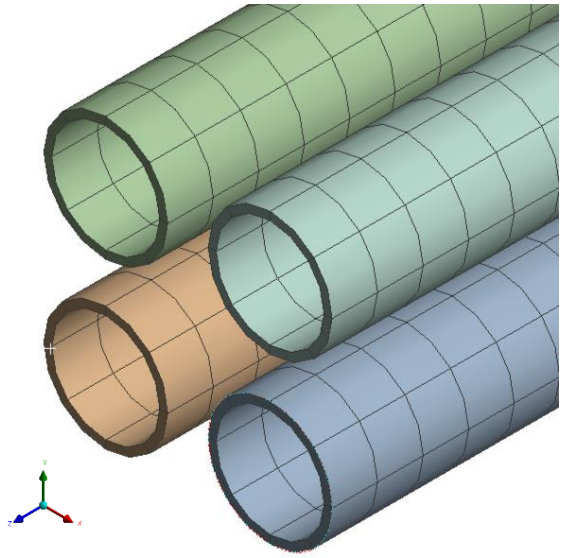

Figure 2. Computational grid for the transient structural simulation.

B. Boundary Conditions

The boundary conditions for both the fluid and the solid domains were imposed to represent the actual physical conditions in an LWR/SMR core. Moreover, since thermal analysis is not considered in this study, no thermal boundary condition is imposed. The inlet of the fluid domain has a fully developed turbulent velocity profile with a bulk velocity of u_{in}=0.823 m/s. Prior to the FSI analysis, the fluid was recirculated in two stages, each in a 1 m long channel and utilizing a periodic boundary condition. Furthermore, all walls were considered rigid non-slip walls. Additionally, an acceleration of 9.81m/s^2 opposite to the flow direction was applied to account for gravitational effects. The outflow region has a zero-gage outlet pressure boundary condition. Moreover, the external wall of the domain was considered a rigid non-slip wall, whereas the fluid-solid interfaces were deforming non-slip walls to account for rod deformation caused by the fluid flow. The properties of the fluid in use are displayed in Table 1, which were derived at the rated conditions of a particular SMR design.

Furthermore, the thin rods were considered flexible with constant mechanical properties close to the actual properties of fuel rod cladding material (M5 Zircalloy), which are listed in Table 1. The inflow and outflow sides of the rods were fixed in position; that is, deformation was judged

negligible where the rods are fixed. It should be noted that the fixed-fixed rod configuration approximately represents the actual situation of rod bundles in nuclear reactor cores, as this configuration does not allow for large movement of the rod bundles. Therefore, it provides a reasonable representation to assess the flow behavior. Moreover, the fluid-solid interface has a coupled boundary condition, which permits the transfer of loads between the two fields. Table 2 summarizes the boundary conditions for the FSI case.

Table 1. Fluid and solid properties (fluid properties at pressure and temperature of P = 12.76 MPa and T = 284 ºC, respectively).

Fluid Properties	
Density (ρ)	900Kg/m^3
Kinematic viscosity (ν)	1.248x10^{-7}m^2/s
Solid Properties	
Density	6490Kg/m^3
Elastic modulus	2x10^{11}
Poisson ratio	0.30

Table 2. Boundary conditions for the FSI domain.

Fluid Domain	
Inlet	Fully turbulent velocity profile with bulk velocity of u_{in}= 0.823m/s
Outlet	Zero-gage pressure
Outer wall	Rigid non-slip
Inner walls	Deforming non-slip
Solid Domain	
End faces	Fixed-fixed
Rod walls	System-coupling interface (allow transfer of load)

C. Numerical Schemes

The FSI simulation in this work follows the partitioned approach, where the equations of the two fields (fluid and solid) are solved simultaneously by coupling two separate solvers. Fluid flow was simulated utilizing the infamous k-ω SST (Shear Stress Transport) turbulence model, which appears capable of simulating the physics of the problem. Moreover, a pressure-based solver with a SIMPLE pressure-velocity coupling scheme were considered. The spatial discretization was set to second order, so does the transient formulation. The time scale of the simulation was an important consideration to capture the flow physics and rod deformation appropriately. However, as discussed earlier, the limited computational resources available were a major constraint; thus, the time resolution was determined as to save time and power while maintaining reasonable accuracy. Therefore, all transient simulations were performed with a constant time step of Δt = 10.0 ms, which corresponded to a maximum Courant-Friedrichs-Lewy (CFL) number of < 4.0. For the FSI case, 1124 steps were simulated, yielding a total flow time of 11.24 s.

D. Approach to Dynamics Analysis

To study the dynamic behaviour of the rod bundle, a multi-stage approach is followed. First, the frequency of the velocity pulsations (transient flow simulation) is determined by means of Fast Fourier Transform (FFT) algorithms. Second, the operating frequency is found by recording the time history of rod deformation from the FSI simulation, the applying FFT to estimate the prevailing frequency. Figure 3 shows the exact locations of all probes inserted to record time history data (for both transient flow and FSI simulations). Third, the first few natural frequencies and mode shapes of the rod bundle are determined, utilizing model analysis tools in ANSYS Workbench, and using the same mesh prescribed in section III.A. The mode at which the system is operating can be specified from the time history of rod deformations. Fourth, all the obtained frequencies are compared against each other to assess the design of the system. Finally, the global deformation behaviour of the rod bundle is analysed. It should be noted that the design assessment is based only on the dynamic response of the rod bundle at a particular coolant flow; that is, no regards are made to the heat transfer efficiency, fission rate and other factors.

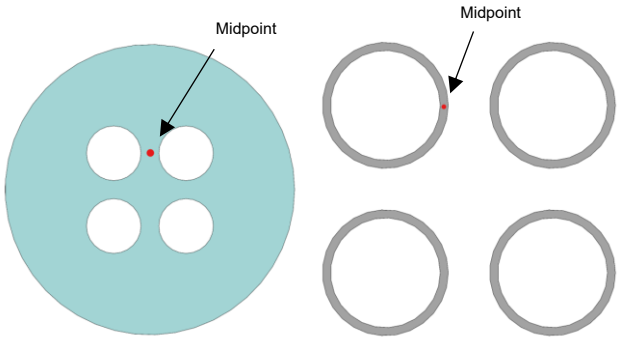

Figure 3. Probes inserted in transient flow simulation (left) and FSI simulation (right).

IV. RESULTS

The simulation results are discussed in this section, following the order stated in section III.D.

A. Flow Pulsations

Figure 4 displays the instantaneous velocity contours at two orthogonal planes, namely the YZ and ZX planes. The contours are captured at the last time step of the transient flow simulation, which corresponds to a total flow time of 20 s. The time step size appears good enough to capture the von-Kármán vortex street phenomenon, which is demonstrated by the periodic flow pulsations. Furthermore, the Reynolds number based on the hydraulic diameter (d_h = 24.65 mm) is Re = 162563, which is quite high. Consequently, the flow pulsations are continuously damped by large inertial forces and cannot sustain a uniform pattern. The time history of flow pulsation at half the domain is

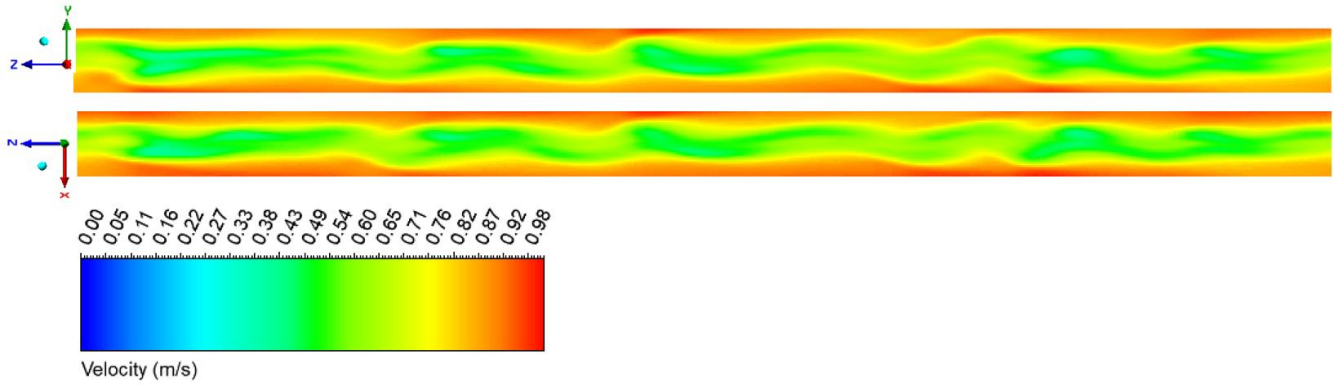

Figure 4. Instantaneous velocity contours at midplanes of the flow channel (fluid flows in the negative z-direction).

shown in Figure 5. The plot indicates the time at which the pulsations become developed. Therefore, in estimating the frequency of pulsations, the Discrete Fourier Transformation (DFT) is applied only to the time interval from 4 s to 20 s to avoid the effect of undeveloped flow. The FFT computed shows a peak corresponding to a frequency of 3.498 Hz.

B. Operating Frequency

The time history of deformation normal to the rod (in both x-direction and y-direction) is recorded. The probes used to collect the data are inserted at half the domain. It is evident from Figure 6 that considerable damping occurs. The deformation amplitude is small, and rod vibrations are negligible. Since the sinusoidal vibration behaviour exhibited by the rods is simple, the vibration frequency is determined by conventional methods (reciprocal of the oscillation period). The frequency estimated from the plots in Figure 6 is between 0.417 Hz and 0.500 Hz, which is quite small.

C. Natural Response

The natural frequency of the system is determined by acoustic modal analysis tools found in ANSYS Workbench. The natural response depends on the combined mass of the fluid and solid domains, their stiffnesses, and the boundary conditions (the type of support at the extremities of the rod bundle). The mesh used for modal analysis is similar to the one presented in section III.A, yet the element size of the fluid domain is increased to 2 mm. The first twenty vibration modes were determined from the analysis, with the natural frequency ranging from 0.4611 Hz to 2.7717 Hz. However, only the first six modes are considered since their frequencies are close to the operating frequency. Table 3 presents the first six modes of vibration, along with their frequencies.

Table 3. Natural frequencies and mode shapes of the system.

Mode	1	2	3	4	5	6
Frequency [HZ]	0.461	0.496	0.513	0.513	0.554	0.554

D. General Analysis

The mode at which the system vibrates is closely represented by the third mode, where the rods buckle towards the positive y-direction (upward), and slightly towards the negative x-direction (leftward). However, it is not the exact same mode, indicating that the actual mode of vibration is beyond the 20th mode, whose associated vibration is 2.7717 Hz. Therefore, since the operating frequency is between 0.417 Hz and 0.500 Hz, rod vibration at the rated conditions is resonance safe. Table 4 summarizes the frequencies obtained from all the simulations. Moreover, Figure 7 shows the global deformation behaviour of the rod bundles. Maximum deformation occurs withing the first few seconds, with higher deformations in the positive y-direction (upward). Nevertheless, the vibration is damped quite well, and the deformation amplitude stabilizes at low values.

Table 4. Summary of all frequencies of interest.

	Transient Fluid Flow	Operating Condition	Natural Response
Frequency [HZ]	3.498	0.417 – 0.500	0.513

V. CONCLUSION

This study was conducted to investigate the dynamic response of a particular fuel assembly design for a light water based SMR. The domain considered was a simplified four-rod bundle, preserving the exact flow physics of the original design. The results found were based on the rated conditions of operation for the targeted design. Moreover, the design analysis was made disregarding thermal conditions effects. The FSI simulation results were consistent with the modal analysis conducted afterwards. The targeted design demonstrated good dynamic behavior, having a vibration frequency well below resonance frequency. Furthermore, an experimental setup is being designed at KFUPM facilities to validate the simulation results. Additionally, to obtain a more comprehensive design assessment, parametric studies might be conducted (based on the flow velocity and p/d ratio).

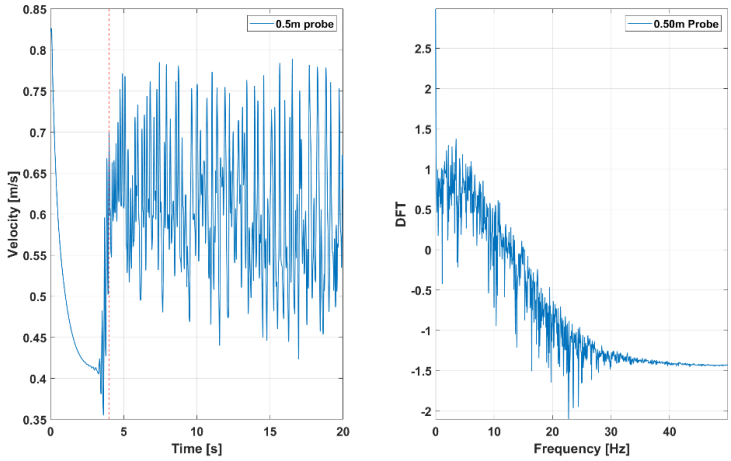

Figure 5. Time history of velocity at half the periodic domain (left), and the DFT of the signal (The DFT axis is logarithmic).

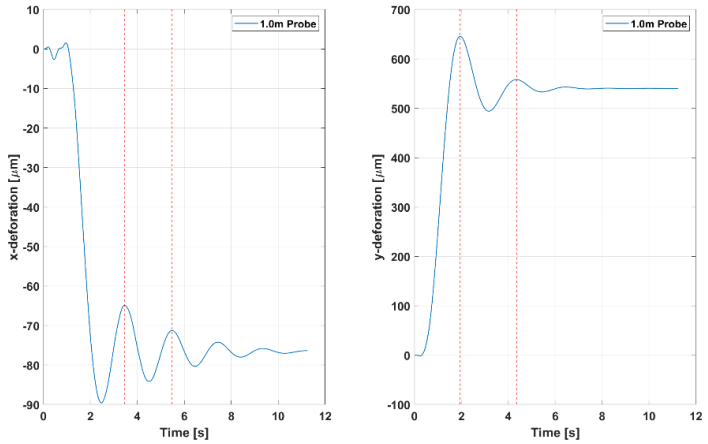

Figure 6. Time history of rod deformation in the x-direction (left) and y-direction (right).

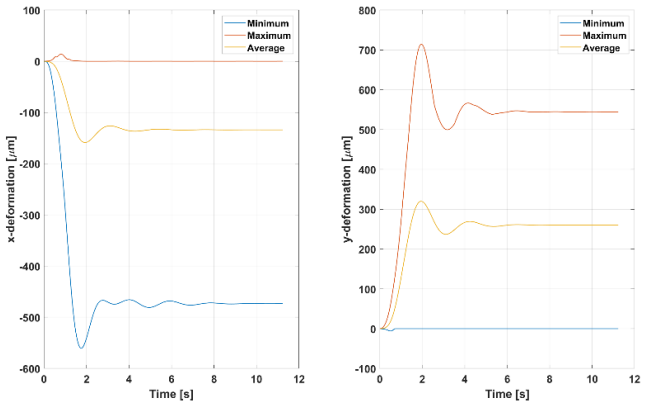

Figure 7. Deformation behavior of the rod bundles. Deformation amplitude in y-direction (right) is generally higher than in the x-direction (left).

VI. References

[1] "Small modular reactors," Apr. 13, 2016. https://www.iaea.org/topics/small-modular-reactors (accessed Mar. 16, 2023).

[2] A. Cioncolini, J. Silva-Leon, D. Cooper, M. K. Quinn, and H. Iacovides, "Axial-flow-induced vibration experiments on cantilevered rods for nuclear reactor applications," Nucl. Eng. Des., vol. 338, pp. 102–118, Nov. 2018, doi: 10.1016/j.nucengdes.2018.08.010.

[3] D. De Santis and A. Shams, "Numerical study of flow-induced vibration of fuel rods," Nucl. Eng. Des., vol. 361, p. 110547, May 2020, doi: 10.1016/j.nucengdes.2020.110547.

[4] F. Bertocchi et al., "Fluid-structure interaction of a 7-rods bundle: Benchmarking numerical simulations with experimental data," Nucl. Eng. Des., vol. 356, p. 110394, Jan. 2020, doi: 10.1016/j.nucengdes.2019.110394.

Proceedings of the European Nuclear Young Generation Forum
ENYGF'23
May 8-12, 2023, Kraków, Poland

Scoping analysis for large-scale containment experiments with GOTHIC 8.3

Arfinengo-del-Carpio, Sofía[1*], Andreani, Michele[2], Vázquez-Rodríguez, Carlos[1,3], Kapulla, Ralf[2], Paladino, Domenico[2] and Jiménez, Gonzalo[1]

[1] Universidad Politécnica de Madrid (UPM), Spain; [2] Paul Scherrer Institut (PSI), Switzerland, [3] Forschungszentrum Jülich (FZJ), Germany

*Corresponding author: *s.arfinengo@upm.es*

I. INTRODUCTION

The main function of the containment building of a nuclear power plant is to act as the last barrier to retain the radioactive materials, in case of an accident, once all the other internal protective layers have failed [1]. Some of the phenomena following a postulated severe accident may lead to hydrogen generation inside the containment building which, combined with the existing steam and air, could potentially originate flammable or explosive mixtures [2].

After the Fukushima Daiichi accident in 2011, the need to further investigate and understand hydrogen transport and mixing mechanisms within a nuclear containment building was accentuated, [3]. These studies are increasingly using three-dimensional codes, such as GOTHIC, which have been extensively validated for licensing applications. Nevertheless, their use for simulating certain complex phenomenology still requires to be addressed through detailed experiments in large scale facilities [4].

In this context, the OECD/NEA PANDA project is carried out with the main objective to continue improving the understanding of the containment phenomenology during postulated severe accidents and to extend the experimental database to phenomenology not investigated previously. It is an OECD/NEA Joint project operated by Paul Scherrer Institut (PSI), in Switzerland, with the participation of several organisations coming from different countries. This project addresses several topics, including the study of radiative heat transfer or BWR suppression pools. The series of experiments that will be specifically addressed in this paper belongs to Topic 2: "Extend the database on activation of PWR containment spray system".

The experiments that will be performed during the different phases of the project will take place in the PANDA facility, at PSI. PANDA is a large-scale, thermal-hydraulics test facility initially designed and used for investigating containment system behavior and related phenomena for different BWR designs, and for large-scale separate effect tests, but it is currently used also for experiments concerning PWR systems. PANDA is composed of six vessels - (Reactor Pressure Vessel (RPV), Gravity Driven Cooling System (GDCS), two Drywells (DW1-2) and two Wetwells (WW1-2) -, four condensers - three corresponding to the Passive Containment Cooling (PCC1-3) and the Isolation Condenser (IC) -, system lines (e.g. Main Steam Line (MSL), PCC vent lines, VB lines, etc.) and auxiliary system lines [1]. Figure 1 depicts the general configuration of the facility.

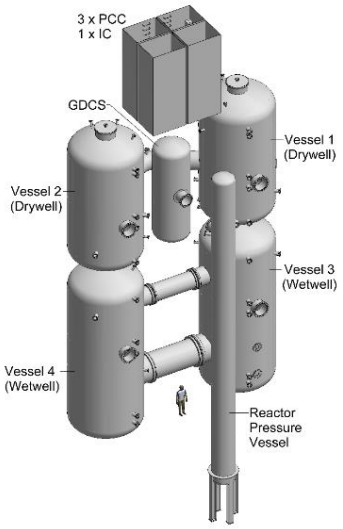

Figure 1: PANDA facility configuration.

As a precedent for the series of experiments that concerns this article (P1A3 series), P1A1 series consisted of PANDA tests addressing basic phenomena at large scale considering one steam generator compartment and a spray system, using one of the PANDA vessels (Drywell) to represent a containment building. The tests for this series were carried out at PSI in December 2022.

Following the P1A1 series, the P1A3 series is defined, with the objective of studying complex natural circulation between two compartments representing the pump/steam generator tower compartments. Figure 2 shows the configurations for both series of experiments. The compartment dimensions were geometrically scaled to be representative of a generic PWR steam generator compartment, including two openings on its upper surface, one side opening and an impingement plate that prevents the fluid to directly flow towards the upper part of the compartment. Steam and helium are injected inside the compartment to emulate the rupture of a coolant pipe.

In the case of the P1A3 series, a second compartment and a connection between both compartments are added. The size of the connection (tunnel) was calculated by defining two parameters (non-dimensional height and surface ratio), based on a generic PWR configuration. Through this method, a range for the dimensions of the tunnel was obtained.

The following sections explain how the pre-test analysis for P1A3 series was carried out by developing a 3D model of the PANDA configuration using the GOTHIC code.

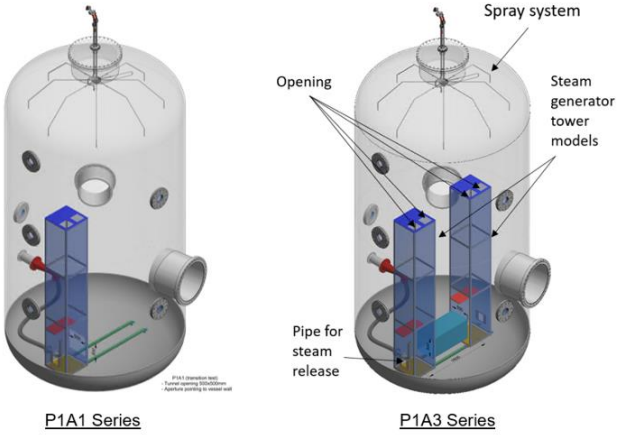

Figure 2: P1A1 and P1A3 series configurations.

II. GOTHIC MODEL

GOTHIC is a three-dimensional computational code for thermal hydraulic calculations in nuclear power plant containment buildings. Following the methodology developed by UPM ([5]), the first step towards creating the GOTHIC model was to simplify the geometry and define the working mesh in the AutoCAD environment, which are represented in Figure 3. The mesh was defined taking into account important geometrical aspects of the compartment configuration, such as the openings and the injection pipe geometry. The dimensions of the tunnel connecting both vessels that were selected for the base case were also influenced by the model geometrical aspects, using the largest transversal area that was allowed by the working mesh, and the shortest height, both laying inside the calculated ranges. The defined transversal section is 0.4 meters high and 0.267 meters wide.

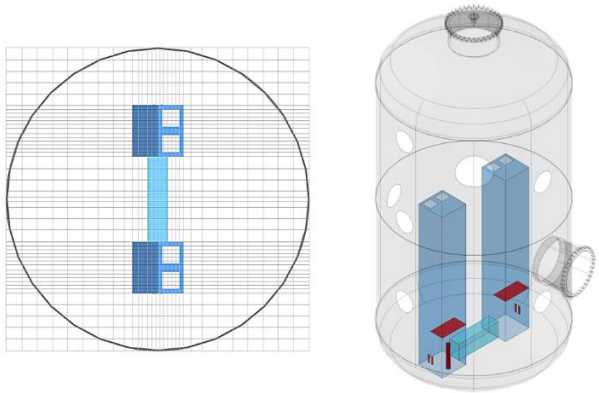

Figure 3: AutoCAD model of the simplified P1A3 series geometry.

The GOTHIC model is built using the multizone approach, where different spaces of the geometry are represented using different control volumes (CV). In total, four CVs are used – containment, two steam generator compartments and tunnel. Figure 4 shows the configuration of the model. On the left, the general CV configuration is represented, as well as the Boundary Conditions (BC), that are used to input the mass and energy release, and the Thermal Conductors (TC) that represent the heat transfer through the model structures. On the right, two views of the containment CV are represented.

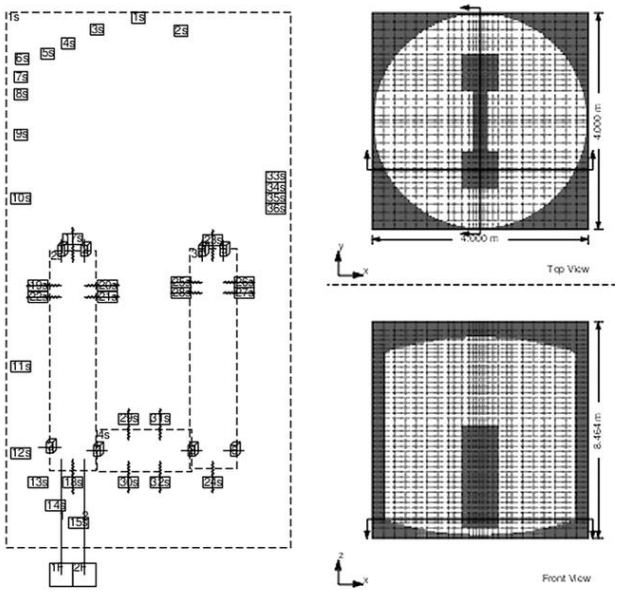

Figure 4: Configuration of the P1A3 series GOTHIC model.

The test conditions used are an initial temperature of 20 ºC, steam injection during the first 6000 seconds at 44 g/s and 150 ºC, and helium injection from 6500 to 10000 seconds at 0.54 g/s and 120 ºC. The specifications for the spray phase, which takes place from 10300 to 14000 seconds, are droplets at 40 ºC, with two possible configurations: one big nozzle with a flow rate of 0.9 kg/s or nine nozzles with a flow rate of 0.1 kg/s each. The selected configuration used as a base case for the simulations was the second one.

III. RESULTS

This section focuses on the pressure and helium stratification results that were obtained during the pre-test analysis. The pressure values provide insight on the general thermal hydraulic situation of the model, while the stratification allows to obtain local information related to fluid patterns, and it is directly tied to the study of the hydrogen risk, which is one of the main concerns of this series of experiments.

The first set of simulations that were performed was devoted to assess the effect of the addition of the second compartment and the tunnel on the model thermal-hydraulics. With this aim, the obtained results were compared with a model previously developed at PSI with the P1A1 geometry (one single compartment). Regarding the P1A3 series, three different dimensions for the tunnel were tested, all of them within the calculated range.

Figure 5 shows the pressure for the model with one compartment, corresponding to the P1A1 series (in green), and the model with the second compartment and the tunnel added, corresponding to the P1A3 series, with the three tunnel sizes variations. Even if the parameters have similar values and tendencies, during the steam and helium injection phases, as expected, pressure for the model with only one compartment grows slightly faster, reaching a higher peak value. This is caused by the inclusion of the second compartment, which added a larger amount of metallic structures, promoting the steam condensation and, therefore, softening the pressure peak. There is not an observed influence of the tunnel size in the pressure values.

Additionally, Figure 6 displays the helium distribution for the P1A1 series and the three variations of the P1A3 series. The addition of the second compartment has a slight influence on the stratification inside the vessel, being the one-compartment model the one that presents a stronger stratification. This implies that the addition of the second compartment promotes the mixing of the gases inside the vessel. On the other hand, the variation of the dimensions of the tunnel does not show a remarkable impact on the stratification.

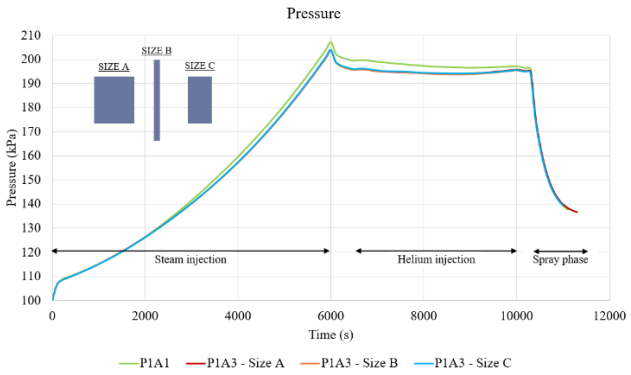

Figure 5: Comparison of the pressure for the P1A1 and the P1A3 series with three different compartment sizes.

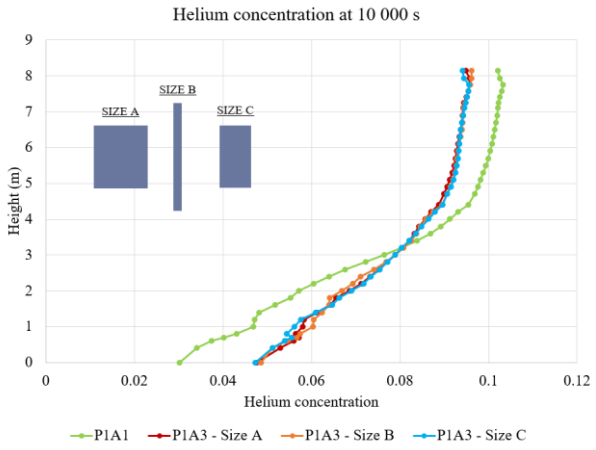

Figure 6: Comparison of the helium distribution at 10000 seconds for the P1A1 and the P1A3 series with three different compartment sizes.

After assessing the effect of the addition of the second compartment, several sensitivity analyses were performed for the P1A3 series in order to determine which parameters have a higher influence in the model phenomenology. Figure 7 and Figure 8 gather the pressure and helium concentration values inside the vessel for some of the parameter variations: a reduction of the size of the compartment side opening, removing the impingement plate and lowering its position in order to interrupt the jet earlier so more gases flow towards the second compartment.

Regarding the pressure values, all four models showed a similar behavior (Figure 7), with minimal magnitude variations. However, the effect of the mentioned modifications on the helium concentration is more remarkable (Figure 8). The scenario that presents a more homogeneous atmosphere is the base case, followed by the case with the smaller side opening. This modification results in a slightly stronger stratification, as the vapor flow rate entering the compartment through the side opening is lower and thus, promoting a weaker mixing pattern.

Additionally, the absence of the impingement plate provides a scenario comparable to the P1A1 series. Not facing an obstacle in its ascending path, the major part of the steam and helium will flow directly towards the upper part of the injection compartment, leaving the effect of the second compartment on a secondary plane. This scenario derives in a slightly more heterogeneous atmosphere inside the PANDA vessel.

However, the modification that seems to have a major effect on the model thermal hydraulic is the position of the impingement plate. If it is too close to the injection pipe, as shown with a blue line on Figure 8, the rising flow patterns are drastically interrupted, resulting in an extremely low mixing environment with a very prominent stratification. Further detailed studies will be necessary in order to determine the critical distance between injection pipe and impingement plate, where the mixing patterns stop being promoted and start being hindered.

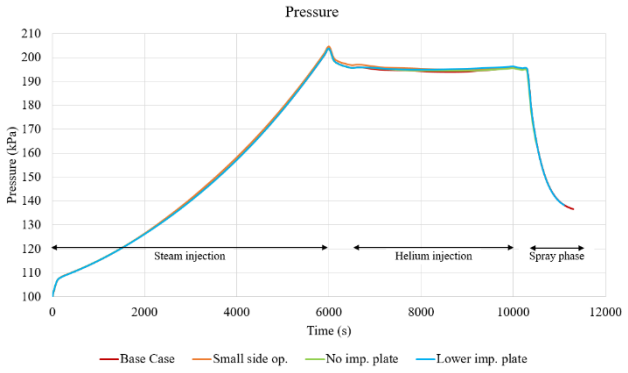

Figure 7: Comparison of the pressure for different sensitivities.

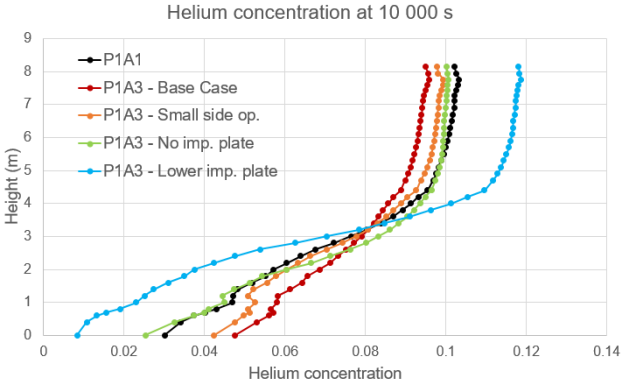

Figure 8: Comparison of the helium concentration at 10000 seconds for different sensitivities.

The last simulated sensitivity analysis was related to the temperature of the droplet phase during the spray phase of the transient. Figure 9 displays the values of the pressure for three different droplet temperatures: 20, 40 (P1A3 base case) and 60 ºC. It can be observed that as the spray temperature rises, the depressurization of the vessel occurs at a slower rate.

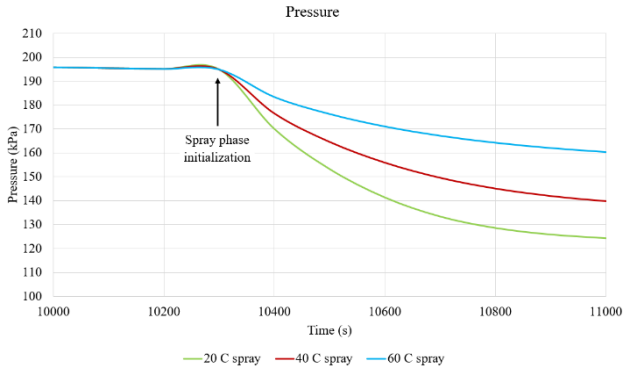

Figure 9: Comparison of the pressure during the spray phase for three different droplet temperatures.

IV. CONCLUSIONS

The objective of the P1A3 series scoping calculations is to identify how the differences in the PANDA configuration compared to the previous series (P1A1) affect the phenomenology and which parameters have a major influence on the thermal hydraulics of the system, to serve as a base for the design of the large-scale experiments. With this goal, several sensitivity analyses were performed, such as the variation of the dimensions of the tunnel between both compartments.

Regarding the pressure values, the only parameter that had a significant effect was the extra amount of metal mass that is added inside the PANDA vessel for the P1A3 series configuration, which promotes the steam condensation and, therefore, the pressure peak is lower compared to the P1A1 series.

Additionally, including the second compartment and the tunnel create a scenario where mixing patterns are enhanced, and therefore the stratification for the P1A3 series is weaker.

On the other hand, the simulations suggest that one of the most relevant parameters when it comes to physically design the experiments – the size of the tunnel – does not play an important role neither for the pressure nor the helium stratification.

In regards of the rest of the geometrical modifications, some of the parameters point out the relevance of the presence of the second compartment, especially the position of the impingement plate.

A more extensive study of the transient spray phase and the post-test analysis remain as the main future lines of this work.

V. ACKNOWLEDGEMENTS

The authors of this paper would like to acknowledge Simon Suter and Christoph Hug for carrying out the technical tasks regarding the PANDA tests and designing the images displayed on Figure 2 and Figure 3.

They also acknowledge the OECD/NEA NEST initiative for financially supporting Sofía Arfinengo's stay at the Paul Scherrer Institut, as well as the PANDA project partners, for their discussions and help designing these experiments.

VI. REFERENCES

[1] D. Paladino, R. Kapulla, S. Paranjape, S. Suter, y M. Andreani, «PANDA experiments within the OECD/NEA HYMERES-2 project on containment hydrogen distribution, thermal radiation and suppression pool phenomena», *Nucl. Eng. Des.*, vol. 392, p. 111777, jun. 2022, doi: 10.1016/j.nucengdes.2022.111777.

[2] N. Erkan, R. Kapulla, G. Mignot, R. Zboray, y D. Paladino, «Experimental investigation of spray induced gas stratification break-up and mixing in two interconnected vessels», *Nucl. Eng. Des.*, vol. 241, n.º 9, pp. 3935-3944, sep. 2011, doi: 10.1016/j.nucengdes.2011.07.025.

[3] S. Kelm, R. Kapulla, y H.-J. Allelein, «Erosion of a confined stratified layer by a vertical jet – Detailed assessment of a CFD approach against the OECD/NEA PSI benchmark», *Nucl. Eng. Des.*, vol. 312, pp. 228-238, feb. 2017, doi: 10.1016/j.nucengdes.2016.09.014.

[4] M. Andreani, D. Paladino, y D. Papini, «Multi-step planning calculations with the GOTHIC code used for the design of complex experiments in the PANDA facility», *Nucl. Eng. Des.*, vol. 339, pp. 116-125, dic. 2018, doi: 10.1016/j.nucengdes.2018.09.005.

[5] R. Bocanegra, G. Jimenez, y M. K. Fernández-Cosials, «Development of a PWR-W GOTHIC 3D model for containment accident analysis», *Ann. Nucl. Energy*, vol. 87, pp. 547-560, ene. 2016, doi: 10.1016/j.anucene.2015.10.022.

Proceedings of the European Nuclear Young Generation Forum
ENYGF'23
May 8-12, 2023, Kraków, Poland

RANS-Based CFD Modelling of Pressurized Thermal Shock in a Reactor Pressure Vessel

Alsubhi, Abdulaziz[1*], Balabaid, Abdallah[1], Almalki, Abdullah[1], Alsalhabi, Abdalaziz[1], Bahaydan, Moayad[1], Shams, Afaque[1,3] and Tomasz, Kwiatkowski[2]

[1]King Fahd University of Petroleum and Minerals (KFUPM), Saudi Arabia

[2]National Centre for Nuclear Research (NCBJ), Poland

3 Interdisciplinary Research Center for Renewable Energy and Power Systems (IRC-REPS), KFUPM, Saudi Arabia

*Corresponding author: s201761950@kfupm.edu.sa

I. INTRODUCTION

The safety of nuclear power plants is of utmost importance and requires careful consideration throughout the plant's lifetime. One key component in the reactor is the reactor pressure vessel (RPV), where fuel is located, and heat is removed. The RPV must be built to withstand temperature, pressure, and degradation caused by neutron flux. Thermal shock in the RPV, known as pressurized thermal shock, can occur during accidents such as a loss of coolant accidents (LOCA). In these cases, the Emergency Core Cooling (ECC) system is used to quickly inject cooling water into the RPV, leading to potential high stresses and temperature gradients in the walls of the RPV. In the past, simulating these events was difficult with system codes (like RELAP-5 or CATHARE), but the use of Computational Fluid Dynamics (CFD) codes has improved accuracy, though it can be costly to establish a reliable database as a reference [1]. Using three- dimensional codes for the injection of the ECC system is highly useful due to the complexity of the mixing phenomena in the downcomer [2]. Direct Numerical Simulation (DNS) modelling offers the highest level of detail in analyzing fluid flow, yet its prohibitively high computational cost makes it impractical for many applications. In contrast, CFD methods such as Large-Eddy Simulation (LES) and Hybrid offer a balance between detail and computational cost, making them useful for understanding and solving complex fluid dynamics problems. Although LES and Hybrid are less computationally expensive than DNS, they still require a significant investment of computational power and time, limiting their practicality for some industry applications.

Reynolds Averaging Navier-Stokes (RANS) models offer the most computationally efficient approach, preserving accuracy while requiring significantly less computational power and time than LES or Hybrid. RANS models are therefore useful for complementing more computationally intensive methods, providing a faster approach that can be employed in a shorter timeframe without sacrificing accuracy. The integration of RANS models with other CFD methods can lead to a more comprehensive and efficient analysis of fluid dynamics problems, allowing for a more balanced and nuanced approach to modelling fluid flow. [3]. This paper aims to validate the use of RANS in modelling the injection of the ECC system through a duct to simulate single phase Pressurized Thermal Shock (PTS) scenarios. Using the reference database compiled by [4], the results will be compared and validated.

II. NUMERICAL METHODOLOGY

A. Computational Domain

The simplified geometry for the PTS case adopted in this paper is the same configuration performed to build the DNS database by [4] and [5]. As depicted in Fig. 1, the configuration contains two main parameters intersecting normally, the square duct and the RPV's downcomer planar. The water will flow from the cold leg (inlet 1) reaching the intersection point, then impinges onto the downcomer. Also,

(inlet 2) on top of the downcomer represents gravity's effect on the flow.

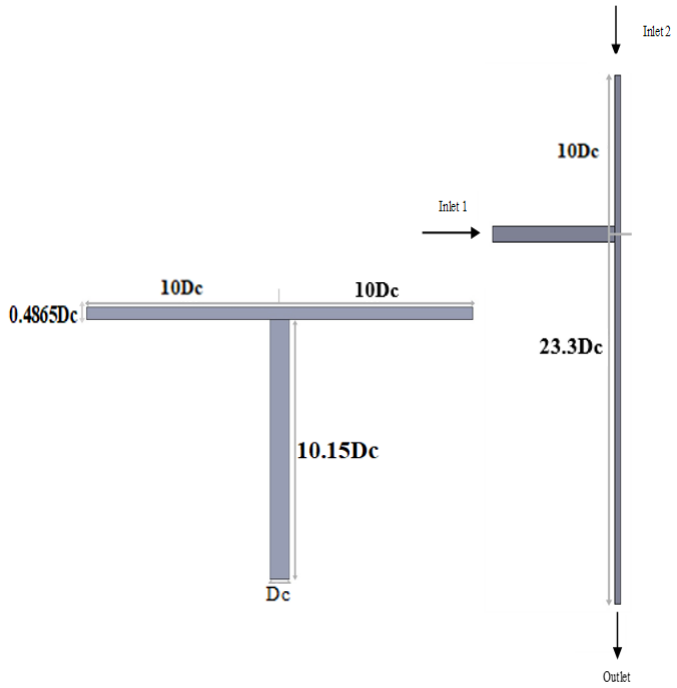

Figure 1: Geometry of the case. left (top view), right (side view).

The parameter Dc in Fig.1, is the height and width of the square duct. Furthermore, the normalised dimensions y* and z* later used in extracting data, are calculated using the Dc/2 value. It is used in the dimensions of the geometry, which are provided in table 1.

Table 1: PTS geometry dimensions with respect to Dc.

length of cold leg (L)	Width of downcomer (W)	Upper height of downcomer (H_1)	Lower height of downcomer (H_2)	Thickness of downcomer (D_d)
10.15Dc	20Dc	10Dc	23.3Dc	0.4865Dc

The simplifications employed in the configuration of the RPV was provided by [8]. Both the bulk velocity in the cold leg (U_c) and the fluid cold temperature (T_c), are imposed. While the second inlet velocity and temperature have uniform profilesthe surface and are assumed to be constant with values equal $0.1U_c$ and T_h respectively.

B. Flow Parameters and Governing Equations

The operating parameters concerning the flow are based on the following three parameters of bulk Reynolds number (Re), friction Reynolds number (Re_τ) and the Prandtl number (Pr).

$$\mathrm{Re} = \frac{\mathrm{Uc\ Dc}}{v} = 5400 \quad \textbf{(1)}$$

$$Re_\tau = \frac{u_\tau h_c}{v} = \frac{\sqrt{\frac{\overline{\tau_w}}{\rho}} h_c}{v} = 180 \quad \textbf{(2)}$$

$$Pr = \frac{v}{\alpha} = 1 \quad \textbf{(3)}$$

Where u_τ is the friction velocity, v is the kinematic viscosity, ρ is the fluid density, τ_w is the duct wall shear stress, h_c is the half height of the duct (hc = Dc 2), and α is the constant thermal diffusivity. All μ, v, ρ, and α are assumed constant. Following, these governing equations, in addition to the assumption of adiabatic boundary condition 'Q = 0', the values used for the fluid are tabulated below (table 2) [6] and [7].

Table 2: Fluid Properties.

ρ (kg/m^3)	μ (Pa·s)	v (m^2/s)	U_1 (m/s)	U_2 (m/s)	T_1 (K)	T_2 (K)	Q (W/m^2)
1000	0.01	0.00001	0.36	0.036	293	353	0

C. Boundary Conditions

The RPV wall and the Downcomer wall are adiabatic. Walls in the domain are all non-slips walls. The duct inlet has constant parameters U_1 and T_1. Along the duct, there is a parodic boundary condition, at a length of $6.6D_C$ down the duct. This allows the flow to fully develop before impinging on the Downcomer wall. The top of the domain has an inlet with constant parameters U_2 and T_2 and the bottom has a pressure-outlet boundary condition. Furthermore, the following two equations were used to obtain nondimensionalised values used in the qualitative comparison.

$$u^* = \frac{u}{U_c} \quad \textbf{(4)}$$

$$T^* = \frac{\mathrm{T} - T_c}{T_h - T_c} \quad \textbf{(5)}$$

D. CFD and Numerical Schemes

The PTS scenario is known for its complex flow, needing advanced physics modelling to be simulated accurately. The software used in this paper is Ansys Fluent [9]. This section will provide the computational setups of the simulation and the turbulence modelling methodology.

The presented paper will focus on three RANS models, namely, k-ε, k-ω SST and k-ω GEKO. These linear formulation models, give an assumption, that the Reynolds stresses and the mean flow strain has a linear constitutive relationship [10]. Default settings were used with all three models.

The standard k-ω model is based on two equations that determine the effect and properties of the turbulence flow. However, k-ω is sensitive to free stream values. Hence, more accurate results can be found performing the linear k-ω SST model [11]. The k-ω SST model is commonly used since it results in a high validation near to the wall and in the bulk flow. It can blend the two models k-ω, near to the wall, and k-ε, after the boundary layer, which enables this model to be used for both high and low Reynold numbers.

E. Meshing Strategy

The same hexahedral mesh was generated for both the duct and the downcomer. The equation used in the meshing processes shown below is to calculate y, or the distance normal to a solid boundary in a fluid flow, y_h the thickness of the first boundary layer, y_T the total height of the boundary layer, and N is the number of layers. The first cell's size has been carefully considered such that the dimensionless value of y^+, which represents the ratio of the distance from the wall to the first grid point in the fluid, to the distance from the wall where the velocity is equal to the velocity at the edge of the fluid boundary layer, is kept below 1. 45 layers with an elongation ratio of G=1.2 were used. The cross-sections of these meshes are shown in Fig. 2. From the graph we can see that the inflations on the duct and downcomer are intersecting at the corner resulting in a finer mesh at those regions. The resulting meshes are in the size of 0.0075m.

$$y^+ = \frac{y\, U_\tau}{\upsilon} \tag{6}$$

$$y_h = 2y \tag{7}$$

$$y_T = y_h \frac{1 - G^N}{1 - G} \tag{8}$$

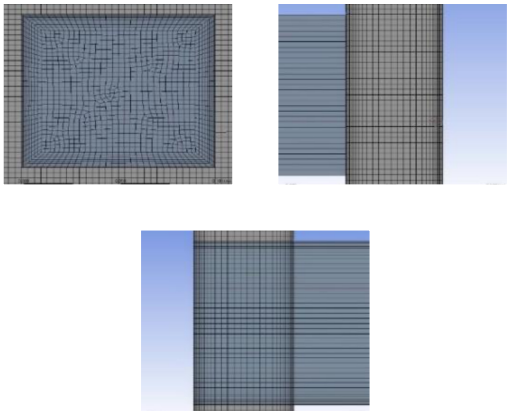

Figure 2: The meshing result a) Front view of the duct b) side view of downcomer c) cross section of the duct downcomer intersection.

III. RESULTS AND DISCUSSIONS

Based on the relevant use of the RANS models and their application, the data, obtained in this work, will be validated against the mean flow and temperature fields of the reference data [5]. As described previously in (2.A), the flow exits the duct and impinges on the downcomer wall. Therefore, those two regions will be considered mainly in the discussion.

The geometry of the duct dictates the flow to be symmetric over the x and y axis, for the sake of transparency the velocity profiles shown in Fig.3 are taken over the x-axis. Furthermore, in all graphs the following naming and colour convention will be used, reference data (Ref, Black circles), k-ω SST (SST, Orange line), k-ε (Epsilon, Grey line) and k-ω GEKO (GEKO, Blue line).

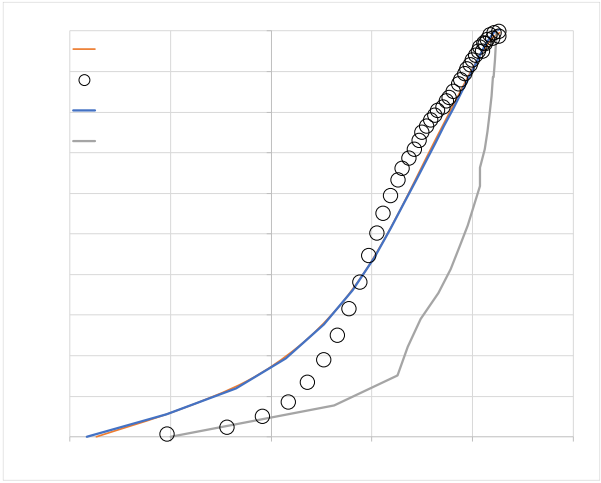

Figure 3: Velocity profiles in the duct.

All models show relative accuracy in accordance with the reference profile, except for the k- ε model. The slight error encountered is likely the effect of secondary flows in the duct. These secondary flows are induced due to the shape of the duct. All RANS models used are linear models. Thus, they are unable to capture these secondary flows in their default settings. Ansys Fluent offers options which claim to capture secondary flows, which can be investigated further in the future. For the current work, the linear models will be used with the default options. Therefore, the error encountered in the duct is logically assumed to propagate into the downcomer.

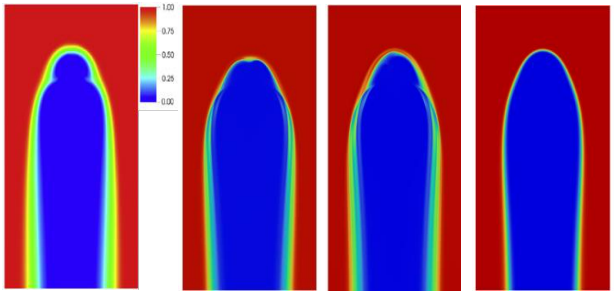

Figure 4: Iso-flux temperature contour plots at the middle of the downcomer. DNS (far-left), k-ω GEKO (middle-left)), k-ω SST (middle-right)), k-ε (far-right)

The contours of temperature shown in Fig. 4 show the same behaviour as the reference DNS. On the other hand, considering the gradient of the temperature the k-ω SST and GEKO models show a more accurate distribution of the temperature along the wall. In order to have a quantitative comparison, different lines were chosen along the Z and Y planes in accordance with the layout demonstrated in Fig.5.

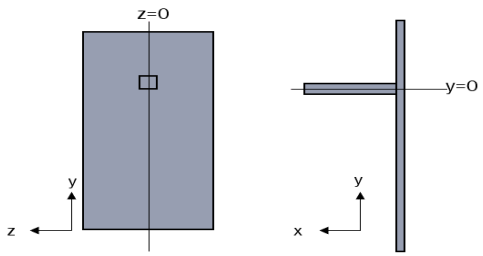

Figure 5: A sketch of the geometry showing the planes z=0 and y=0.

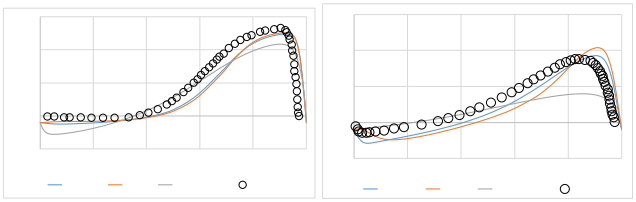

*Figure 6: Velocity profiles on the plane (y = 0) along the lines Z*2 (left), Z*4(right) .*

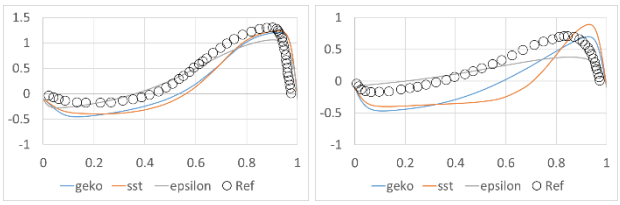

*Figure 7: Velocity profiles along the lines y*2 (right), y*4 (left).*

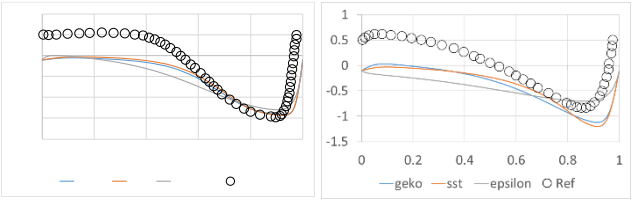

Figure 8: Velocity profiles along the lines y-2 (left), y*-4 (right).*

For profile comparison, the normalized length will be used noted by the star (*), multiplying by Dc/2 will convert these numbers back into the units used for Dc. In Fig.6, the velocity profiles along the line z*2 (i.e. z= 2 multiplied by Dc/2), generally shows very little discrepancy with the reference data, suggesting that the most significant error present is the one coming from the duct. In contrast, comparing the three models used, k- ω SST and k-ω GEKO show more accuracy than k-ε. This outcome is to be expected as the k-ε model is known to have trouble in regions with high pressure gradients, such as the ones found in the impinging region of the downcomer. Furthermore, the difference between the obtained and reference values seems to propagate in regions away from the stagnation point. Due to the beforehand mentioned, area of interest being the stagnation point. The models can be used to obtain fairly accurate results near that area, but the results get less accurate the further away you move from the area of interest.

Furthermore, with the same behaviour for the three models along y and y-, as shown in Fig. 7 and Fig. 8, the velocity profile along the lines y*2 and y*-2 in the z=0 plane provides the minimal deviation with the reference data. Where k-ω SST and k-ω GEKO show more accuracy than k-ε.

In Fig.9, the motion of fluid is identified by the instantaneous velocity contours magnitude, where (y = 0) is the horizontal plane. The result of the velocity contours in the figures show that all models follow the same behaviour as the reference DNS, where the velocity at the stagnation point is zero and increasing beside that point. Also, the contours show that the velocity in the area near the RPV wall has very low values compared to the barrel wall. To illustrate further, as the fluid exiting the duct with high speed hit the barrel wall, it will extend alongside this wall and this what make the differences in velocity between the two walls. Furthermore, the velocity gradients of k-ω GEKO and k-ω SST agree with the DNS model while the k-ε model is significantly affected due to the large, induced pressure and temperature differences in the region where the flow is impinged to the downcomer.

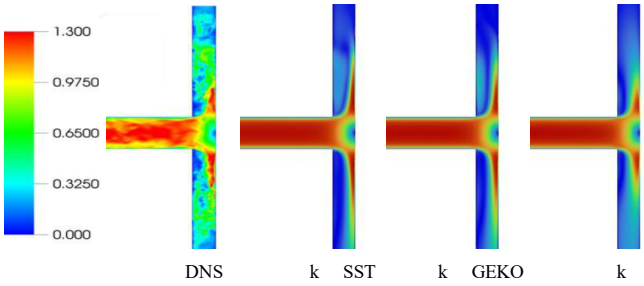

Figure 9: Instantaneous velocity magnitude contours on the horizontal (y = 0)

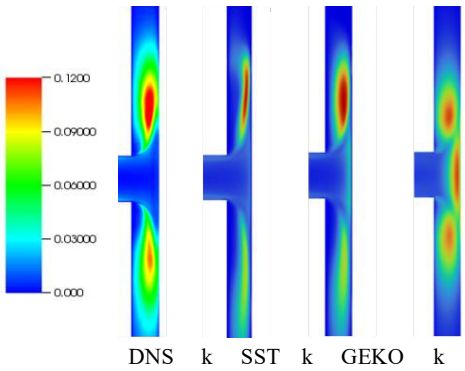

Figure 10: Turbulence kinetic energy contours on the vertical plane x=0.

The turbulence kinetic energy shows variance between the three models and the reference DNS. k-ω SST shows the most accuracy in the stagnation point. On the other hand, the k-ε shows heavy turbulence in the same area, which is not shown in the reference DNS. Away from the stagnation point, k-ε shows more accuracy than k-ω SST. The k-ω GEKO appears to show results between the two others. In the stagnation point is shows some error, while away it shows more accuracy than k-ω SST.

The contours of the mean velocity magnitude are displayed in the vertical plane between the RPV wall and the Downcomer wall in Figs. 11, give an overview of the flow field there and show the complexity of the flow. As the fluid is exiting the duct, it impinges the barrel wall and is then deflected in a radial direction. This deflected flow then interacts with the fluid that is descending from the downcomer's top, creating a complex flow pattern in the downcomer, with a shape that can be described as umbrella-like configuration. Moreover, to avoid complexity first it is easier to describe the impingement region, then the flow pattern in the other part of the downcomer can be analysed. Furthermore, near the barrel wall, there is a stagnation region where the flow is diverted from the axial to the radial direction. The jet flow leaving the cold leg is significantly diverted along the radial direction due to the close jet-to-wall distance. As a result, the flow splits off at the cold leg's borders, and a recirculation zone develops close to the vessel wall. On the other side, the fluid deflection causes a high-speed jet flow to exist close to the barrel wall. This phenomenon is a limitation for the k-ε, since it cannot deal

with complex flow with high Reynold number. Therefore, the produced configuration of the k-ε model is different from both k-ω SST and k-ω GEKO, where both k-ω SST and k-ω GEKO match the result of the DNS model.

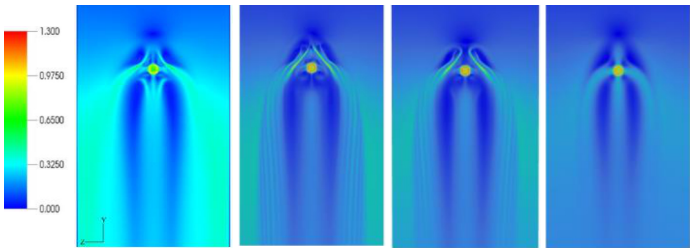

Figure 11: Contours of the mean velocity magnitude in the middle of the downcomer.

IV. CONCLUSION

In conclusion, RANS offers a valuable asset for the industry, where prompt yet well support decisions need to be made. To ensure that the use of RANS models is accurate for the case of PTS in nuclear Reactor Pressure Vessels, they need to be validated. Thus, in this work, three RANS models were validated against reference DNS data. Considering the impinging jet zone, the k-ω models were on a higher level of accuracy. But, all three models lost accuracy as the error propagated along with the flow past the past a distance of 2Dc away from the duct in both the z and y directions respectively. The k-ε model was the least accurate of the three tested here. Specifically, the k-ε turbulence model demonstrated inadequacies in accurately capturing the underlying physics of the turbulent flow, resulting in implausible predictions. This underscores the significance of diligent model selection and meticulous validation procedures, particularly when addressing intricate phenomena such as turbulence.

V. References

[1] Shams, A., Edh, N., Angele, K., Veber, P., Howard, R., Braillard, O., Chapuliot, S., Severac, E., Karabaki, E., Seichter, J., & Niceno, B. (2018, February 20). Synthesis of a CFD benchmarking exercise for a T-junction with wall. Nuclear Engineering and Design. Retrieved 2023, from https://www.sciencedirect.com/science/article/pii/S0029549318300669

[2] González-Albuixech, V. F., Qian, G., Sharabi, M., Niffenegger, M., Niceno, B., & Lafferty, N. (2015). Comparison of PTS analyses of rpvs based on 3D-CFD and RELAP5. Nuclear Engineering and Design, 291, 168–178. https://doi.org/10.1016/j.nucengdes.2015.05.025

[3] L. Wang, BB. Sundén, A. Borg, H. Abrahamsson, Heat transfer characteristics of an impinging jet in crossflow, J. Heat Transf. 133 (12) (2011) 122202. https://doi.org/10.1115/1.4004527

[4] Shams, A., De Santis, D., Rosa, D., Kwiatkowski, T., & Komen, E. J. M. (2019). Direct numerical simulation of flow and heat transfer in a simplified pressurized thermal shock scenario. International Journal of Heat and Mass Transfer, 135, 517–540. https://doi.org/10.1016/j.ijheatmasstransfer.2019.01.144

[5] Shams, A., Damiani, G., Rosa, D., & Komen, E. M. J. (2016). Design of a single-phase PTS numerical experiment for a reference direct numerical simulation. Nuclear Engineering and Design, 300, 282–296. https://doi.org/10.1016/j.nucengdes.2016.01.038

[6] Uitslag-Doolaard, H. J., Stefanini, L., Shams, A., & Blom, F. J. (2020). Numerical prediction of a single phase pressurized thermal shock scenario for crack assessment in an reactor pressure vessel wall. Annals of Nuclear Energy, 144, 107563. https://doi.org/10.1016/j.anucene.2020.107563

[7] Shams, A., & Komen, E. M. (2018). Towards a direct numerical simulation of a simplified pressurized thermal shock. Flow, Turbulence and Combustion, 101(2), 627–651. https://doi.org/10.1007/s10494-018-9902-x

[8] Kliem, S., Sühnel, T., Rohde, U., Höhne, T., Prasser, H.-M., & Weiss, F.-P. (2008). Experiments at the mixing Test Facility ROCOM for benchmarking of CFD codes. Nuclear Engineering and Design, 238(3), 566–576. https://doi.org/10.1016/j.nucengdes.2007.02.053

[9] "Ansys fluent | Fluid Simulation Software," Nov. 20, 2022.

[10] Lien, F. S. (1996). Low-Reynolds-number eddy-viscosity modelling based on non-linear stress-strain/vorticity relations. In Proc. 3rd Symp. On Engineering Turbulence Modelling and Measurements, Crete, Greece, May 27-29, 1996. https://doi.org/10.1016/B978-0-444- 82463-9.50015-0

[11] Menter, F.R., 1994. Two-equation eddy-viscosity turbulence models for engineering applications. AIAA J. 32, 1598–1605. https://doi.org/10.2514/3.12149

Proceedings of the European Nuclear Young Generation Forum
ENYGF'23
May 8-12, 2023, Kraków, Poland

Numerical Study of Natural Convection Within a molten Corium Pool for Different Turbulent Models

Balabaid, Abdallah[1], Al-Gazlan, Osamah[1], Shams, Afaque[2,3], and Siddiqui, Osman[2]

[1]Chemical Engineering Department, King Fahd University of Petroleum & Minerals (KFUPM), Dhahran 31261, Saudi Arabia
[2]Mechanical Engineering Department, KFUPM, Dhahran 31261, Saudi Arabia
[3]Interdisciplinary Research Center for Renewable Energy and Power Systems (IRC-REPS), KFUPM,Dhahran 31261, Saudi Arabia

*Corresponding author: *s201768910*@kfupm.edu.sa

I. INTRODUCTION

The safety of nuclear reactors is of the utmost importance, especially in the case of a severe accident. A severe accident condition exists when there is a loss of coolant, loss of structural integrity, and a high risk of thermal runaway with high pressure. A corium pool is formed in the case of a severe accident, where the temperature of the core rises significantly high causing the internals of the core, including the fuel, to melt and build up in the lower plenum of the reactor pressure vessel (RPV). This makes for a natural convection flow which is internally heated and characterized by an exceptionally high Rayleigh number (Ra) in the range of 10^{13}-10^{17}.

The numerical prediction of the heat transfer mechanisms for a natural convection flow in the corium pools is the focus of the current study. In 1993, the BALI-I homogeneous pool experiment [1] was conducted with the aim of creating an experimental database of the heat transfer within the corium pools.

The homogeneous pool had been designed to replicate the natural convection flow and heat transfer conditions in the corium pool at the lower head of the RPV for an internal Rayleigh number of 10^{15}-10^{16} [1]. Fig. 1 shows a slice of a typical pressurized water reactor (PWR) lower head. The slice is filled with a water-salt mixture to simulate the corium fluid. Furthermore, particle image velocimetry was used to trace the movement of the fluid, thus creating an accurate reading of the flow structure inside the slice. Fig. 2 shows the three major zones. First, a thermally stratified zone is seen in the lower part of the corium pool with low increasing velocities. While in the top of the pool, an iso-thermal and unstable region exists which is characterized by the presence of large structure eddies caused by cold plumes plunging from the cooler surface on the top. The third and final region is the flow on the cooled curved wall, where maximum velocities occur.

Various computational flow dynamics (CFD) studies were made on this topic in the past years. 2D and 3D RANS simulations using k-ε models with a low Reynolds number and a Ra of 4.9 x 10^{10} were presented by Dol and Hanjalić [2]. Additionally, Aounallah et al. [3] did a validation study on the BALI experiment using k-ω SST and k-ε with a Prandtl (Pr) number of 0.71 and Ra varying from 1.58 x 10^{9} to 10^{12}. These studies concluded that the k-ε model produced less favorable results when compared to the k-ω SST model while neither model was able to capture the flow accurately. However, studies thus far have shown that CFD models still do a much better job of predicting flow behavior than one-dimensional severe accident codes such as RELAP and ICARE.

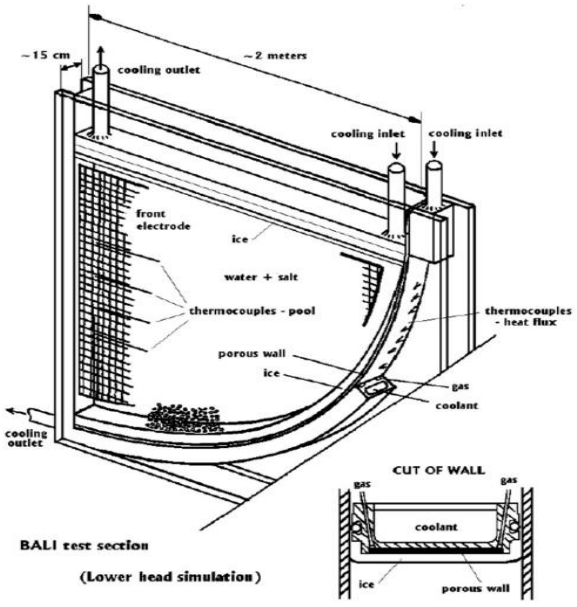

Figure 1: The BALI-I experiment test diagram, Bonnet, 1999 [1]

In this study, a CFD simulation of the flow behavior in corium pools is investigated for the BALI-I setup. Section II will discuss the numerical methodology and flow parameters. Section III will discuss the results of the study while the conclusion is presented in section IV.

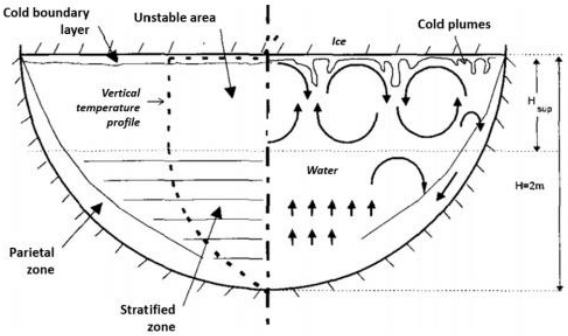

Figure 2: The three zones in the BALI-I experiment.

II. NUMERICAL METHODOLOGY

A. Computational Domain

The geometry chosen for the simulation is a 3D semi-oval with a major radius of 2 m and a minor radius of 1 m. The thickness of the slice is 0.75 m. The lower 0.1 m is truncated as it represents the ice build-up section as discussed by Shams [4]. This geometry is similar to the BALI – I experiment. The mesh was created with a boundary layer to provide sufficient resolution and capture the viscous sublayer. The y+ was kept at 0.46, this led to the first layer height of 4.87×10^{-4} m. The growth rate was set at 1.2 for 12 total layers. For the bulk volume, a triangular mesh with size 0.01 m was used.

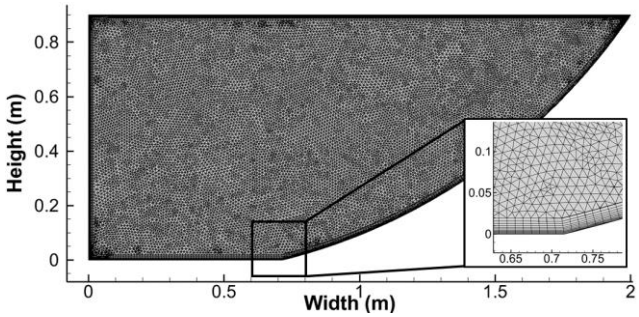

Figure 3: The 2D sectional view of the 3D mesh used.

B. Boundary Conditions

The boundary conditions used in the study are discussed in this section. First, an internal heat generation of 32,755 W/m^3 is used to simulate the heat released from the melted core and components. The thermal boundary conditions are listed in Table 1, where an isothermal temperature is imposed on the right, bottom, and top of the semi-oval structure. Additionally, an adiabatic BC is added to the front, back, and left of the semi-oval. Finally, a no-slip condition is used for the walls.

Table 1: The boundary conditions

Condition	Faces
Adiabatic (Q=0 W/m^2)	Front, Back, Left
Isothermal 273.15 (K)	Right, Bottom, Top

C. Flow Parameters

The operating parameters concerning the flow are based on the following two parameters of the Rayleigh number and the Prandtl number.

$$Ra_i = \frac{g\beta Q_v H^5}{k\nu\alpha} = 4.55 \times 10^{14} \quad \text{(Eq. 1)}$$

$$Pr = \frac{\nu}{\alpha} = 7 \quad \text{(Eq. 2)}$$

where g is the gravity constant, β is the thermal expansion coefficient, Q_v is the heat generation, H is the characteristics length, k is the thermal conductivity, ν is the kinematic viscosity, and α is the thermal diffusivity. All fluid properties are assumed constant.

Table 2: Fluid Properties.

ρ (Kg/m^3)	μ (Pa.s)	ν (m^2/s)	α (1/K)	K (W/m*K)	β (K)
998.3	0.001	1.00E-6	1.44E-7	0.6	2.07E-4

The natural convection flow is driven by the buoyancy force due to density generation and shear forces at the walls. Boussinesq approximation is used to model the density change proportional to the temperature through the thermal expansion coefficient β.

D. CFD and Numerical Schemes

The corium pool study presented in this paper was numerically modeled using the Ansys Fluent [5] software. To model the corium pool, various RANS modeling approaches were chosen to be validated. This section outlines the computational setup of the simulation and the turbulence modeling methodology.

The 4 selected models include both linear and non-linear models for a thorough study. k-ε standard, k-ω SST, GEKO, and Reynolds stress model (RSM), are the chosen models to perform this simulation. The selection of these 4models is reasoned with the following.

k-ε standard is a linear model that depends on two transport variables, namely, the turbulent kinetic energy (k) and the turbulent dissipation (ε). The model, theoretically, should perform well for wall-bounded flows. However, due to the high Rayleigh number of the flow, the model may struggle in capturing the large-scale structures developed in the corium pool.

k-ω SST is a linear model which relates the turbulent kinetic energy (k) with the specific dissipation rate (ω). This model is a combination of k-ω near the wall and k-ε in the bulk which theoretically combines the best of the two models and is expected to perform better for wall-bounded flows.

As for the k-ω GEKO model, it is a linear model but provides results similar to non-linear models. This is because it has multiple coefficients that can be tuned to the model specifications, providing the necessary customization of the model. The GEKO model customizability, especially the coefficients of mixing (CMIX) and near wall (CNW),

should in theory produce favorable results in the presence of cold plumes and flow near the wall of the lower head.

Finally, the RSM is a 7-equation model namely, the mass conservation equation, the momentum conservation equation, the turbulence kinetic energy equation, the turbulence dissipation rate equation, the Reynolds stress transport equations, the turbulence viscosity equation, and the turbulence length scale equation. RSM is a non-linear model meaning that the evolution of k and ε are dependent on the specific flow conditions. The fact that RSM is non-linear should be a great resource to face the intricate nature of a high Rayleigh number flow.

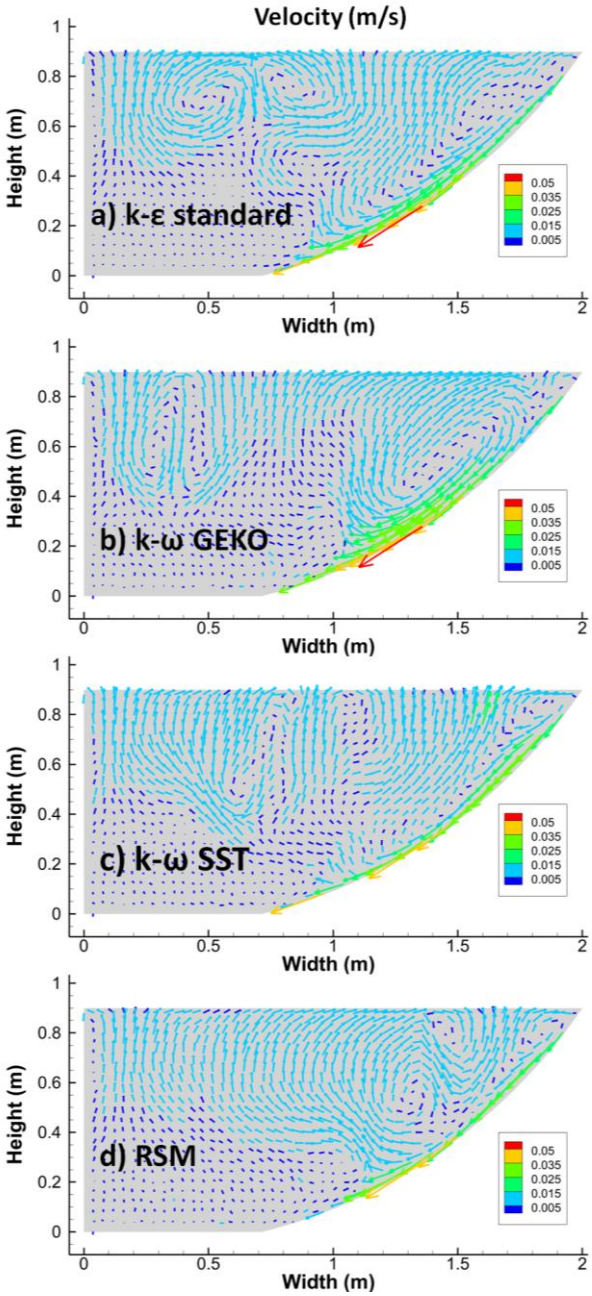

Figure 4 Velocity vectors of all models a) k-ε standard, b) k-ω GEKO, c) k-ω SST, and d) RSM)

III. RESULTS AND DISCUSSION

The velocity contours for all cases are presented in Figure4. The three regions, discussed earlier, are clearly visible for all the cases with stratified low-velocity regions at the bottom of the pool. The bulk and top of the pool show isothermal flow eddies as circulation regions. The third region is high-velocity flow along the curved surface. The k-ε standard and k-ω GEKO models show a delayed flow acceleration while the k-ω SST and RSM show earlier flow acceleration. The large circulation region is also seen to be increasing for the cases studied with RSM showing the highest amount of mixing. This high amount of mixing is due to the non-linear nature of the Reynolds stress models.

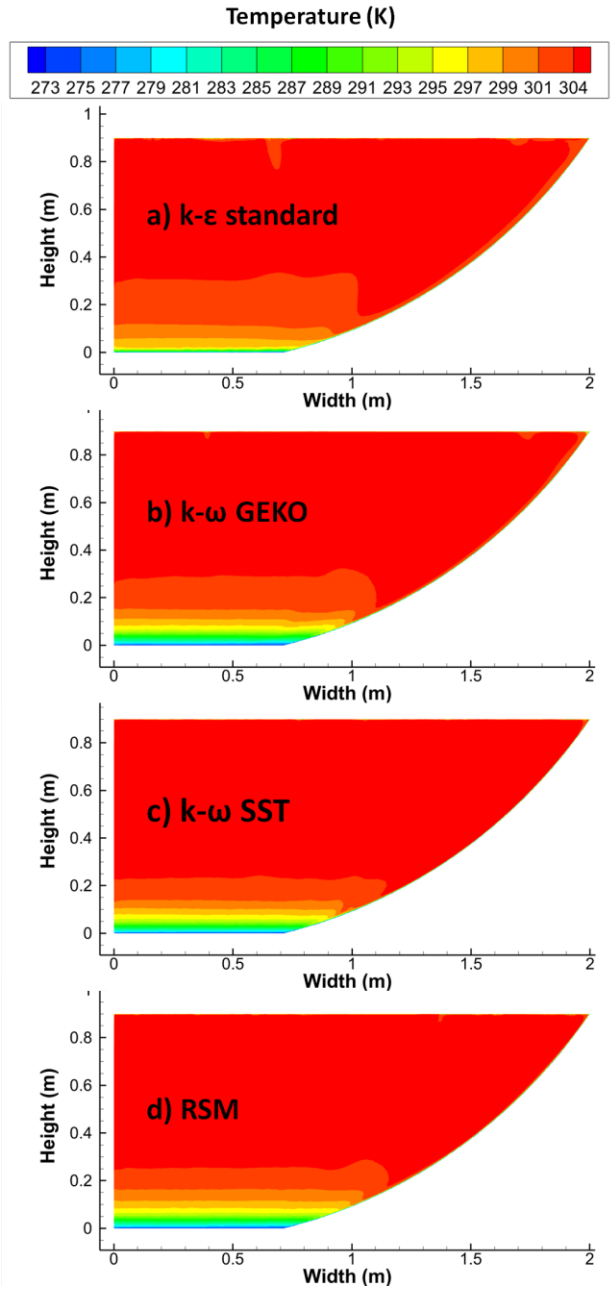

Figure 5. Temperature contours for all models a) k-ε standard, b) k-ω GEKO, c) k-ω SST, and d) RSM)

Figure 5 shows the temperature contours for all models throughout the semi-oval. Looking at the k-ε standard contour, it shows a thinner stratified region for the k-ε model while k-ω SST, GEKO, and RSM show similar thickness. These results can be further discussed with the temperature profiles presented in Fig. 6: the temperature profile is taken 0.1 m from the left and at the middle of the semi-oval

thickness. The figure shows temperature profiles for all the models, as well as AHFM-SC adopted from Shams [6], and the experimental data from BALI-I experiment. It can be seen that all models underpredict the temperature since they are based on the Reynolds analogy and their ability to include buoyancy effects is limited. As for AHFM-SC it shows a much closer agreement to the experimental data, especially in the range (0-0.6), this is due to its ability to account for buoyancy effects which are prevalent in this type of flow. In the stratified region, k-ε and AHFM-SC both predict similar temperatures as they are based on the same model, however, the latter has been calibrated to better include the buoyancy effects for high Rayleigh number flow.

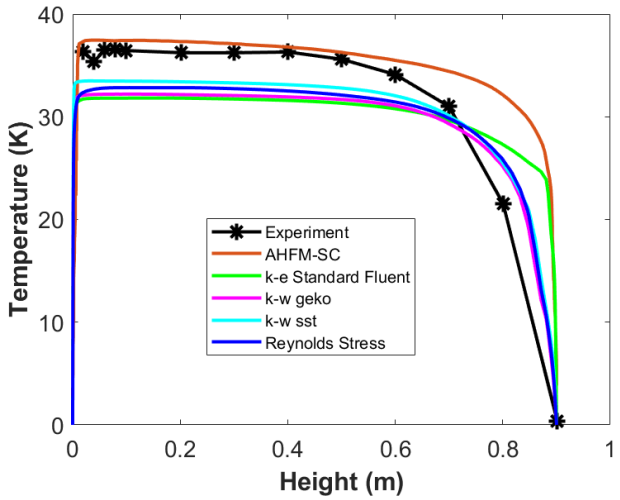

Figure 6 Quantitative comparison of temperature between all models and AHFM-SC and the experimental results.

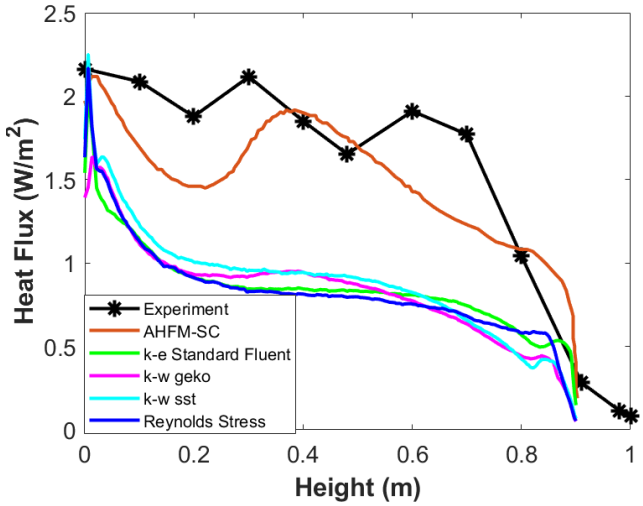

Figure 7 Quantitative comparison of heat flux between all models and AHFM-SC and the experimental results.

In figure 7, the heat flux values are plotted at the middle plane of the right curved surface. It can be seen that the AHFM-SC and experimental results match as the AHFM-SC model has been calibrated for such flows while other models tend to underpredict the heat flux which is in line with the lower temperatures as discussed in figure 6.

IV. CONCLUSIONS

In this paper, the safety aspect of a nuclear power plant in the case of a severe accident i.e. a melted core as a result of high temperatures was numerically modeled and discussed. The corium pool flow is strongly driven by buoyancy forces. This corium pool was simulated and compared to the experimental results of BALI-I and a calibrated AHFM-SC model. Four models were used, namely, k-ε standard, k-ω GEKO, k-ω SST, and RSM. All models show the low velocity, large circulation region, and high-velocity region near the curved walls. All classic models underestimated the temperature profile throughout the semi-oval while AHFM-SC was able to match the temperature of the experimental values for a significant portion of the semi-oval which is attributed to its calibration for high Rayleigh flows. The k-ε and AHFM-SC match near the bottom wall as they are both based on the same models while the k-ε shows the lowest temperature in the bulk fluid. The wall heat flux for all classical models is underpredicted while AHFM-SC follows closely to the experimental values. This shows the importance of ensuring the utility of the CFD methods by validating it with experimental results. The underprediction of temperature can be a great concern in highly critical applications like the corium pool where the safety margin is of utmost importance.

V. ACKNOWLEDGMENT

The authors acknowledge the support provided by Undergraduate Student Research Grant (UXplore) at King Fahd University of Petroleum and Minerals (KFUPM).

VI. REFERENCES

[1] J.M. Bonnet, "Thermal hydraulic phenomena in corium pools: the BALI experiment," in Proc. Workshop on Severe Accident Research (SARJ-98), Tokyo, Japan, Nov. 4–6, 1998, pp. 79–86.

[2] H. S. Dol and K. Hanjalić, "Computational study of turbulent natural convection in a side-heated near-cubic enclosure at a high Rayleigh number," International Journal of Heat and Mass Transfer, vol. 44, no. 12, pp. 2323–2344, Jun. 2001.

[3] M. Aounallah, Y. Addad, S. Benhamadouche, O. Imine, L. Adjlout, and D. Laurence, "Numerical investigation of turbulent natural convection in an inclined square cavity with a hot wavy wall," International Journal of Heat and Mass Transfer, vol. 50, no. 9–10, pp. 1683–1693, May 2007.

[4] A. Shams, "Towards the accurate numerical prediction of thermal hydraulic phenomena in corium pools," Annals of Nuclear Energy, vol. 117, pp. 234–246, Jul. 2018.

[5] "Ansys fluent | Fluid Simulation Software," Nov. 20, 2022.

[6] A. Shams, "Understanding the need for proper turbulent heat flux modelling for non-unity Prandtl number fluids" CFD4NRS Workshop, 20-23 Feb, 2023, College Station, Texas, USA.

Proceedings of the European Nuclear Young Generation Forum
ENYGF'23
May 8-12, 2023, Kraków, Poland

Convective heat transfer and critical heat flux in CO_2 at high subcritical pressures

Bronik, Jakub[1*], Theologou, Konstantinos[1] and Starflinger, Jörg[1]

[1] Institute of Nuclear Technology and Energy Systems (IKE), University of Stuttgart, Pfaffenwaldring 31, 70569, Stuttgart, Germany

*Corresponding author: *Jakub.bronik@ike.uni-stuttgart.de*

I. INTRODUCTION

Reliable models for heat transfer in both supercritical and subcritical states play an important role in safety design and safety analysis. In many transient operations of potential systems in the field of nuclear power with supercritical fluids under normal or abnormal conditions, pressure passes the critical pressure and thus leads to a transition from supercritical to subcritical states.

Figure 1 shows schematically the heat transfer in two-phase flow using the boiling curve, which represents the heat flux as a function of the superheat of the heated wall. At low heat flux, nucleate boiling takes place on the heated wall. However, if the heat flux continues to increase and reaches the critical heat flux, direct contact between the liquid and the heated wall is lost and heat transfer is significantly reduced. If the imposed heat flux remains constant, the regime changes from bubble boiling to film boiling and the wall temperature increase significantly. The point is called the boiling crisis, the corresponding heat flux is called critical heat flux (CHF), and the state after the appearance of the boiling crisis is called post-CHF.

If the heat flux is now reduced, the flow regime remains in the film boiling (post-CHF region) until the wall temperature falls below the so-called minimum film boiling temperature (Leidenfrost point). Then the wall is wetted again with liquid and a sudden drop in the wall temperature occurs. This process is called rewetting.

Heat transfer in the subcritical pressure state, including post-CHF heat transfer, has been studied very intensively in the past for the reduced pressure p_r up to $p_r = p/p_{crit} \leq 0.7$, calculated with absolute pressure p and critical pressure p_{crit}, also because of its importance in light water reactors [1]. There exists a large number of models or correlations developed for this pressure range.

However, studies of heat transfer under subcritical pressure conditions but in the high-pressure range of $0.7 < p_r < 1$ have been scarce. Analysis of the transient process in a 4-rod bundle with water cooling showed that the thermohydraulic system code ATHLET (**A**nalysis of **TH**ermal-hydraulics of **LE**aks and **T**ransients) cannot satisfactorily predict heat transfer in the high-pressure range

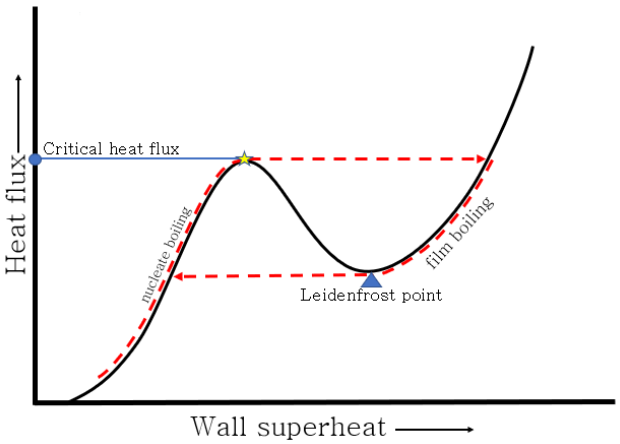

Figure 1. Boiling curve.

[2]. The experiment showed that during the transient process with decreasing pressure from 25 MPa to 17 MPa, a sharp increase in wall temperature occurs at a pressure of about 21 MPa. This corresponds to the appearance of the boiling crisis, which, however, was not predicted by ATHLET.

Within the framework of the CPC-HD project, the physical processes of heat transfer at subcritical pressures near the critical point are investigated experimentally and modelled. The main focus is on the phenomenon of boiling crisis at high steam contents (dryout) with additional investigations into the post-CHF range. For this purpose, experimental, analytical and numerical investigations are carried out. This paper concerns the experimental part of the project with CO_2 as a working fluid.

II. EXPERIMENTAL SETUP

All experiments in this publication are carried out with the SCARLETT (**S**upercritical **Car**bon dioxide **L**oop at IK**E** Stu**tt**gart) test facility at IKE. SCARLETT works as a peripheral facility used to provide CO_2 under the specified parameters: Mass flow rate, temperature and pressure near the critical point. More detailed information about SCARLETT is available in Flaig et al. [3]. For the following experiments, the facility has been modified to safely operate in subcritical pressures by the implementation of a reduction valve upstream of the test section. The simplified schematic is presented in Fig. 2.

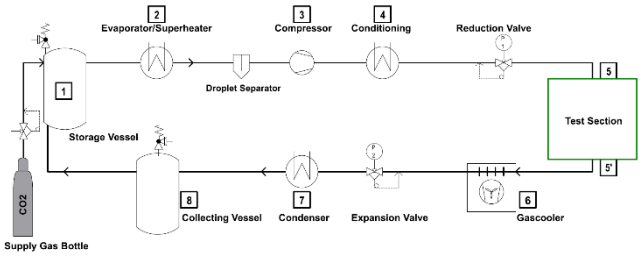

Figure 2. Simplified schematic of SCARLETT.

The test rig used for the investigations in this publication mainly consists of two test sections, which can be seen in Figure 3. The mass flow rate in each test section can be adjusted by diverting flow through the other test section. The test sections have the same structure, the only difference is the diameter of the used test tubes. The test tubes are heated up directly with a 10 kW DC power supply.

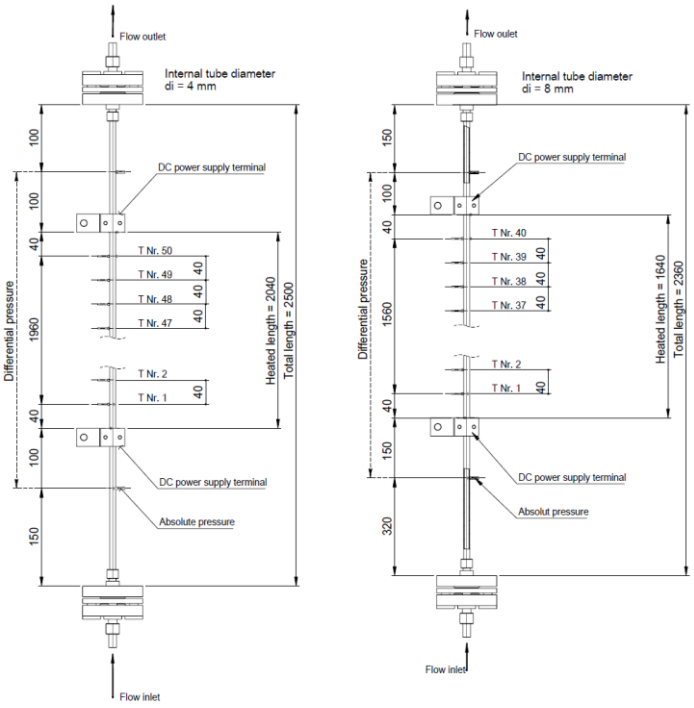

Figure 3. Dimensions of the 1st (left) and 2nd (right) test section [4].

To insulate the test rig electrically from the test tubes, special insulating flanges are used. Before the CO_2 passes the test tubes the mass flow and the bulk temperature are measured. Fig. 3 shows the dimensions of the test tubes with an inner diameter of 4 and 8 mm and an outer diameter of 6 and 10 mm. The material of the tubes is Alloy 625.

The total length of the first test tube is 2500 mm with a heated length of 2040 mm. The second test tube is 2360 mm long with a heated length of 1640 mm. 50 resistance temperature sensors are tied with a temperature-resistant yarn straight in 40 mm intervals on the outer surface of the first test tube and 40 sensors on the second test tube. The absolute pressure is measured before the heated section and the differential pressure is measured over the heated length. The pressure inside the test tube is measured through a 1 mm hole to avoid influencing the flow. More detailed information about the test rig, instrumentation and measurement accuracy is available in Theologou et al. [4].

III. EVALUATION METHODOLOGY

Table 1. gives an overview of the measured parameter ranges.

Table 1. Experimental overview

Parameter [Unit]	Value
Inner tube diameter [mm]	4, 8
Flow direction [-]	upward flow
Inlet pressure [MPa]	5.9, 6.6, 7.0, 7.3
Inlet temperature [°C]	13, 28
Mass flux [kg/m^{2}s]	750, 1250, 1300, 1650, 2000, 3600
Heat flux [kW/m^2]	25-200

In the following, a short overview of the calculations of the main variables is given. The National Institute of Science and Technology (NIST) database REFPROP provides the fluid properties [5].

$$\dot{Q}_{th} = P_{el} = U \cdot I \tag{1}$$

Heat flow rate $\dot{Q}_{th}$ gained by the fluid was calculated from the electrical power P_{el} with the voltage U and the current I.

The heat flux $\dot{q}$ is calculated with the curved surface area of the inner surface A_i of the tube and the heated length with the assumption of a uniform heat generation by direct electrical heating, the heated length L_h, and internal diameter d_i.

$$\dot{q} = \frac{\dot{Q}_{th}}{A_i} = \frac{U \cdot I}{\pi \cdot d_i \cdot L_h} \tag{2}$$

For the calculation of the bulk temperature $T_{b,y}$ across the axial position of the tube y a linear approximation of the pressure losses is assumed. Specific enthalpy at the axial position $i_{b,y}$ is calculated with enthalpy at inlet conditions $i_{b,in}$ and mass flow $\dot{m}$.

$$T_{b,y} = \mathrm{f}(i_{b,y}, p_y) \tag{3}$$

$$i_{b,y} = i_{b,in} + \left(\frac{y}{L_h}\right) \cdot \frac{\dot{Q}_{th}}{\dot{m}} \tag{4}$$

With the mathematical heat conduction model of a circular tube with uniform heat generation, an insulated outer surface and a cooled inner surface the inner wall-temperature $T_{w,i}$ can be calculated with the measured outer wall- temperature T_{625} and the volumetric heat flux $\dot{q}_v$ [6, p.152] and outer diameter d_o. The thermal conductivity λ_{625} of Alloy 625 was also approximated linearly over the temperature $\lambda_{625} = \mathrm{f}(T_{w,o})$.

$$T_{w,i} = T_{w,o} + \frac{\dot{q}_v}{4\lambda_{625}}\left[\left(\frac{d_o}{2}\right)^2 - \left(\frac{d_i}{2}\right)^2\right] - \frac{\dot{q}_v}{2\lambda_w}\left(\frac{d_o}{2}\right)^2 \cdot \ln\left(\frac{d_o}{d_i}\right) \tag{5}$$

$$\dot{q}_v = \frac{\dot{Q}_{th}}{\frac{\pi}{4}\left(d_o^{\,2} - d_i^{\,2}\right) \cdot L_h} \tag{6}$$

The inner wall temperature wall calculation has been repeated with the thermal conductivity of the tube at the mean wall temperature $\lambda_{625} = f(\bar{T}_{w,m})$, where:

$$\bar{T}_{w,m} = \frac{T_{w,i} + T_{w,o}}{2} \quad (7)$$

In the last step, the heat transfer coefficient htc can be calculated for each temperature measurement point across the axial position of the tube.

$$htc_y = \frac{\dot{q}}{T_{w,i,y} - T_{b,y}} \quad (8)$$

A. CHF experiments

The CHF experiments start with reaching steady-state conditions with certain preheating, which were assumed after pressure fluctuations less than ±0.02 MPa and inlet temperature fluctuations less than ±0.2 °C. Then the voltage imposed on the tube was raised in 0.1 V steps over two-minute intervals. CHF was assumed to occur after the first temperature rise occurred at the end of the heated length. After CHF occurred, the heat flux was further increased and the campaign continued into post-CHF experiments. Exemplary detection can be seen in Figure 7.

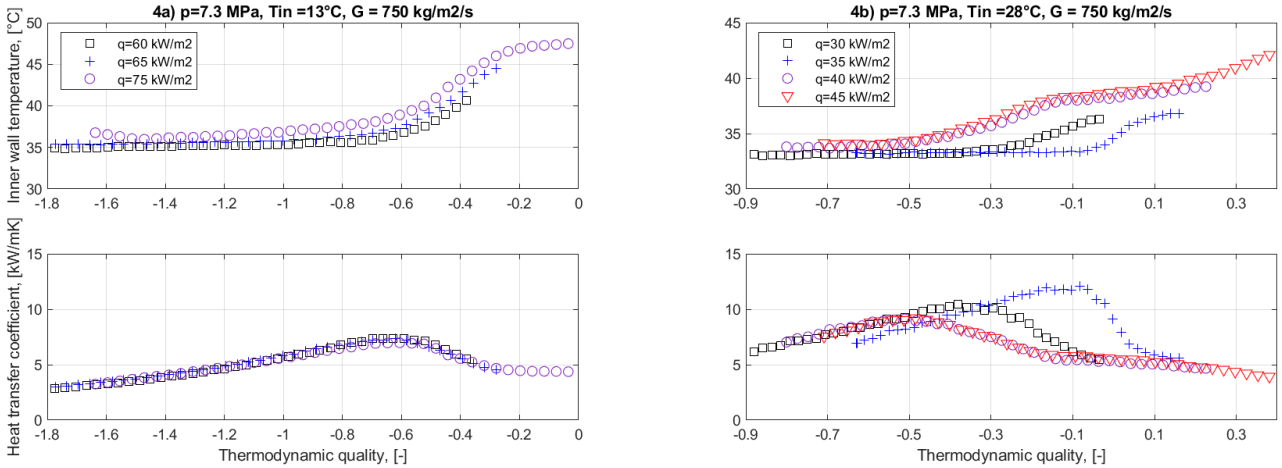

Figure 4. Heat transfer in the 8mm tube in p_r=0.99. Low subcooling in high pressures lead to fast dryout with slow decrease of htc.

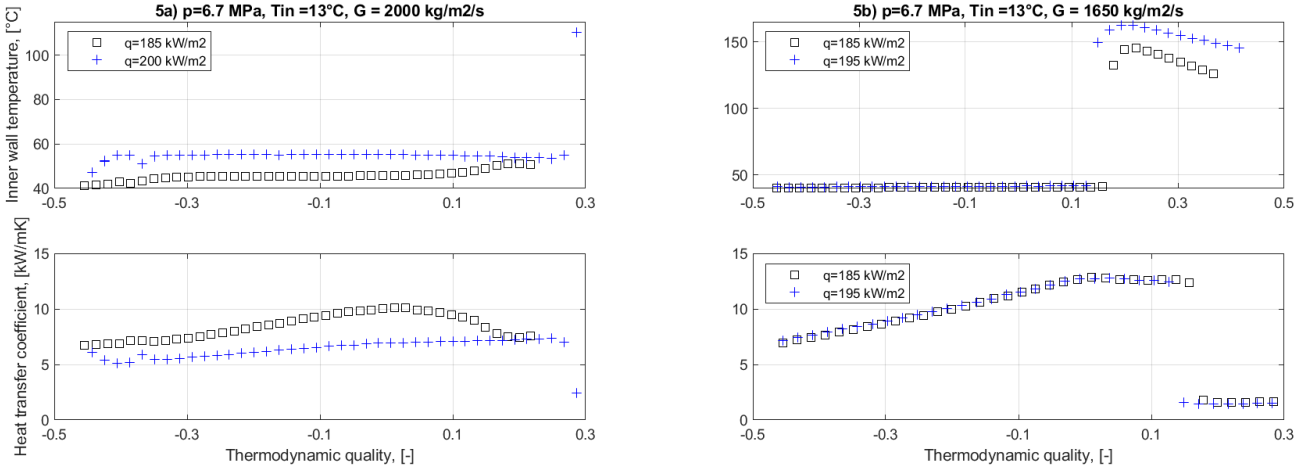

Figure 5. Heat transfer in the 8mm pipe in p_r=0.85. By high mass fluxes fast dryout occurs. It is, however, followed by more violent deterioration.

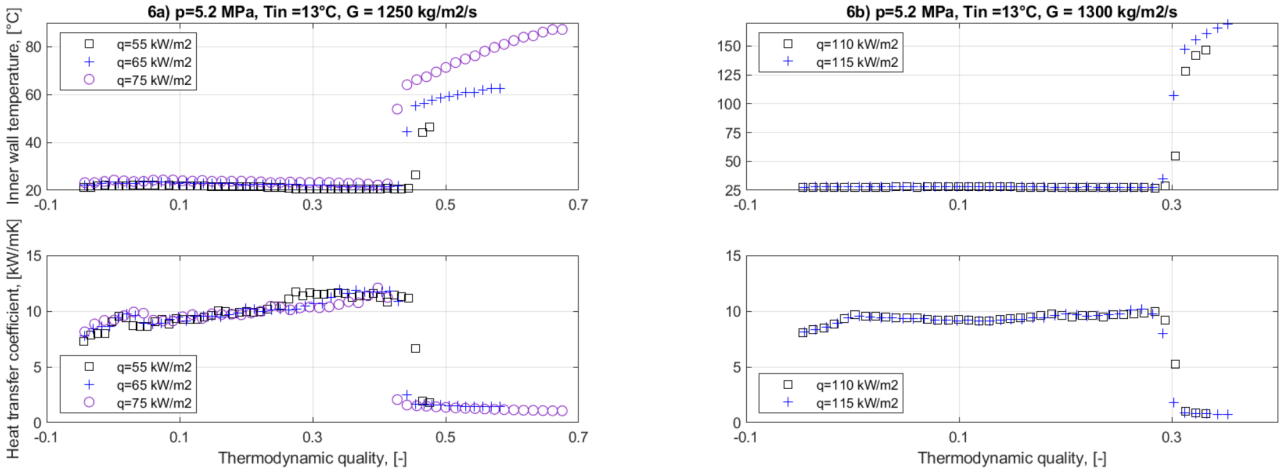

Figure 6. Heat transfer in the 8mm pipe (left) and 4mm pipe (right) in p_r=0.7.

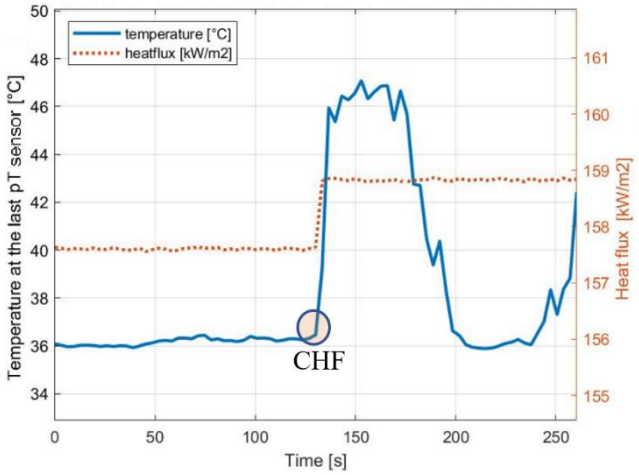

Figure 7. Exemplary detection of CHF in 4 mm pipe, 3600 kg/m²s, 7 MPa and 13 °C inlet temperature. The temperature drops due to occurence of unstable dryout.

B. Post-CHF experiments

During the experiments, the data has been collected over a 10-minute interval with a recording frequency of 0.25 to 0.5 Hz. In the next step, the arithmetic mean was calculated using measured values of each parameter. All experiments start five minutes after reaching steady-state conditions, which were assumed after pressure fluctuations less than ±0.02 MPa and inlet temperature fluctuations less than ±0.2 °C.

IV. EXPERIMENTAL RESULTS

Figures 4, 5 and 6 show the axial profiles of the wall temperature and the heat transfer coefficient for different values of heat flux, temperature, mass flux and tube diameter. The heat transfer over the thermodynamic quality is shown in an array of highly reduced pressures.

In low subcooling, the increment of wall temperature is very slow – and in the case of the highest presented heat flux in Figure 4a happened over 70% of the length (the distance between consecutive data ticks is 4 cm) of the test section which would be an indication of slow dryout [7]. The higher peak heat transfer performance $at\ p_r$=0.99 is seen in lower heat flux which is strongly visible in low subcooling. In higher subcooling the CHF happens with almost the same thermodynamic quality for different imposed heat fluxes, thus indicating a transition from entrainment controlled to deposition-controlled dryout. It is worth noting that it happens in negative thermodynamic qualities, which in this pressure might not have a strong representation in the vapor content.

For p_r=0.85 the slow dryout is not a dominant phenomenon anymore, however in Figure 5a it is still observable. With higher heat flux, however, the effect disappears. In lower mass fluxes the temperature rise in the case with the same heat flux is much higher and the slow dryout effect is not noticeable.

In p_r=0.7 slow dryout is not observed in mass fluxes <2000 kg/m²s. In the 4 mm tube, the temperature rises and the heat transfer coefficient drops much higher indicating the departure from the nucleate boiling mechanism.

V. CONCLUSION AND OUTLOOK

CHF and Post-CHF experiments have been carried out with the SCARLETT facility and a test rig with two test tubes. The results show, that while in higher pressures the CHF occurs in lower local qualities, the change of heat transfer coefficient is not as sudden and the wall temperature jumps are less pronounced than in the lower array of the investigated pressures. This is due to the heat transport properties change near the critical point, where both the thermal conductivity and the specific heat increased significantly and the mechanism of CHF being often slow dryout, which in the cases of higher reduced pressures this mechanism takes place also in mass fluxes as low as 750 kg/m²s.

In the frame of future investigations, a new test rig will be constructed to provide data for tubes with inner diameters of 6 and 10 mm – which will be instrumented with glass fibre capillaries for temperature measurement with Raman scattering technique allowing high spatial and temporal resolution for higher accuracy of CHF observation and the exact location on CHF in nonlinear heat flux distributions.

VI. ACKNOWLEDGEMENTS

The presented work was funded by the German Federal Ministry of Education and Research (BMWF. Project no. 02NUK062B) on basis of a decision by the German Bundestag.

VII. REFERENCES

[1] D. Yu, F. Feuerstein, L. Köckert, X. Cheng, "Analysis and modelling of post-dryout heat transfer in upward vertical flow" Annals of Nuclear Energy vol. 115, pp 186-194, May 2018, https://doi.org/10.1016/j.anucene.2018.01.026.

[2] M. Q. Song, X. J. Liu, X. Cheng, "Heat transfer analysis of trans-critical pressure transient" Annual Meeting of Nuclear Engineering, Berlin, Ber, Germany, May 7-8, 2019.

[3] W. Flaig, R. Mertz, J. Starflinger, "Setup of the supercritical CO2 test facility "SCARLETT" for basic experimental investigations of a compact heat exchanger for an innovative decay heat removal system", J. Nucl. Eng. Radiat. Sci., 4 (3) (2018), https://doi.org/10.1115/1.4039595.

[4] K. Theologou, R. Mertz, J. Starflinger, "Experimental investigations on heat transfer of CO2 under supercritical pressure in heated horizontal pipes", Energy vol 254, September 2022, https://doi.org/10.1016/j.energy.2022.124171.

[5] E. W. Lemmon, M. L. Huber, M. O. McLinden, REFPROP, NIST SRD 23, United States of America (2010), https://doi.org/10.18434/T4/1502528.

[6] F. P. Incropera, D. P. DeWitt; T. L. Bergman; A. S. Lavine, "Principles of heat and mass transfer", 7. ed., Wiley, Singapore (2013), ISBN: 978-1-119-38291-1.

[7] D.C. Groeneveld, "The onset of dry sheath condition – a new definition of dryout", Nuclear Engineering and Design vol. 92, p 134-140, 1985, https://doi.org/10.1016/0029-5493(86)90241-4.

Proceedings of the European Nuclear Young Generation Forum
ENYGF'23
May 8-12, 2023, Kraków, Poland

Neutronet: Loading Pattern Optimization using Machine Learning Techniques

Carrasco Sánchez, Alejandro*, Mesado Meliá, Carles and Serrano Rodríguez, José Francisco

ENUSA Industrias Avanzadas SA SME, Spain

**acas@enusa.es*

I. INTRODUCTION

For each operating cycle of a NPP the positions of fresh and burnt nuclear fuel assemblies (i.e., a Loading Pattern) must be chosen, meeting certain Nuclear Key Safety Parameters, while, at the same time, maximizing the energy delivered throughout the cycle.

The problem of Loading Pattern Optimization (LPO) has been studied for more than three decades due to its large complexity: the number of possible combinations that exist in a 3 Loop PWR plant, with quarter core symmetry and that loads 1/3 of the core with fresh fuel would be between 10^{20} and 10^{100} (one googol), as discussed in [1].

While there exist a certain number of active constraints to be considered, the fact that LPO is a discrete (integer) optimization problem (the assemblies' positions are discrete input variables of the optimization function) and the high degree of non-linearity and local phenomena affecting the core response, make it highly complex to find global minima of the optimization function. In fact, LP optimization has certain common characteristics with other classical engineering problems of exponential time solution, as described in reference [2]: it is a multimodal, non-linear, discrete optimization problem with high dimensionality and nonconvex optimization functions.

Historically, many optimization algorithms have been proposed to solve this problem, of which heuristic optimization techniques are the preferred solution. Heuristic techniques are defined by the implementation of some form of stochastic search optimization, iteratively trying to improve a candidate solution with respect to a given measure of quality and are often used when the gradient of the objective function is unknown.

Some works that have inspired the solution proposed in this paper are:

- Simulated Annealing Techniques described in [1] and [3],
- Genetic Algorithm techniques described in [4] and [5],
- Tabu Search (TS), as described in [6],
- Population Based Incremental Learning (PBIL) in [7] and [8]
- Ant Colony Optimization (ACO) in [9], and,
- Particle Swarm Optimization in [10].

Unfortunately, most solutions proposed in the research field have had only limited industrial application, where manual processes based on designer's experience still dominate. There exist several commercial products (see examples [11] and [12]), however, their use hasn't been widely adopted, due to limitations of the calculation algorithm (complex algorithms that are difficult to adapt to individual use cases), high computational costs or high calculation times.

In any case, a LPO algorithm has a large potential to result in different benefits, including:

- A significant reduction of the effort (man hours) and time (calendar days) dedicated to LP search.
- The potential for finding new, equally valid, solutions that aren't considered before because of their divergence from historic patterns.

These benefits can be of special interest in Emergency Core Redesign situations after a fuel failure (reduced time available), cycles with significant fuel changes (difficult to find LPs) and scoping Fuel Management Studies (necessity of designing multiple LPs in a short time).

A novel solution has been developed at ENUSA, based on modern Artificial Intelligence (AI) techniques and Python, that uses low computational resources and is easily adaptable to different reactor types and licenced codes, its name is Neutronet.

II. METHODS

A. Overview of Proposed Solution

The Neutronet project proposes the replacement of the licensed nodal calculation code by a neural network (NN) that will act as a surrogate model. This neural network calculates the variables that are necessary to choose a loading pattern in a fraction of the time needed by the nodal code, using negligible computational resources. The proposed neural network is described in section B.

This NN is then coupled to an optimization algorithm, described in section C, that can find one or more optimized LPs.

Finally, the licensed nodal code is executed for the proposed LP. Neutronet is therefore completely transparent for the Nuclear Authority, and there is no need to license it.

B. Surrogate Model: Created Neural Networks

A Machine Learning (ML) algorithm learns complex patterns from existing data and then uses them to make predictions on unseen data points, as defined in [13].

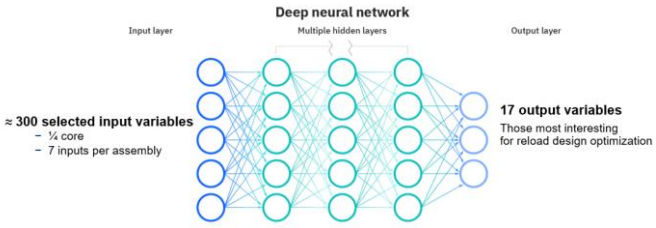

Figure 1. Proposed Deep Neural Network.

The ML algorithm proposed in this work is a type of deep neural network [14], concretely a Multi-Layer Perceptron (MLP). A simplified architecture diagram that summarises the proposed NN is shown in Figure 1.

Neural networks need a large amount of data to learn from, specifically, they must be trained with pairs of (input-output) points. In the case at hand more than 20 000 (input, output) data points were generated by randomizing the assembly positions from a set of previously evaluated loading patterns for 5 different PWR's and then each resulting LP was executed with the licensed nodal code. This resulted in more than 7 million input features and 425 000 output data labels created and saved to internal data bases. The data generation pipeline is summarised in Figure 2.

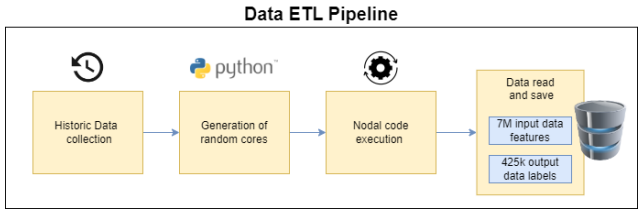

Figure 2. Data ETL (Extract, Transform and Load) pipeline for the Neutronet project.

This data was divided into train, validation and test sets and then pre-processed to ensure correct neural network training.

Table 1. Summary of Hyperparameter search

Hyperparameter	Experiments performed
NN architecture	>3000
L1, L2 and Dropout regularization	>1000
Batch size	100
Train epochs and early stopping:	100
Learning rate (LR)	50
Optimizer type	30
Activation function	30

The validation set is used in the hyperparameter tuning phase of neural network creation. Hyperparameters are defined as parameters that aren't calculated in the NN's training process, they are usually chosen manually before training (for example NN architecture, optimizer type or Learning Rate). To choose these without overfitting the available data, a separate data set is created: the validation set.

Hyperparameter tuning of the NN has included thousands of experiments, a summary is shown in Table 1. Graphic training results are shown in Figure 3 for some of the experiments performed on NN architecture.

For reference, NN training takes around 5h in an 8 core Intel Core i5 CPU processor and must be performed for each of the experiments described above. Once the neural network is trained it can produce predictions in a small fraction of time, as discussed in the results section III.A.

Hyperparameter search has been performed using both manual techniques and guided hyperparameter search algorithms. In particular, good results have been achieved with Bayesian and Grid Search Techniques with the TALOS [15] tool using in-house GPU processors.

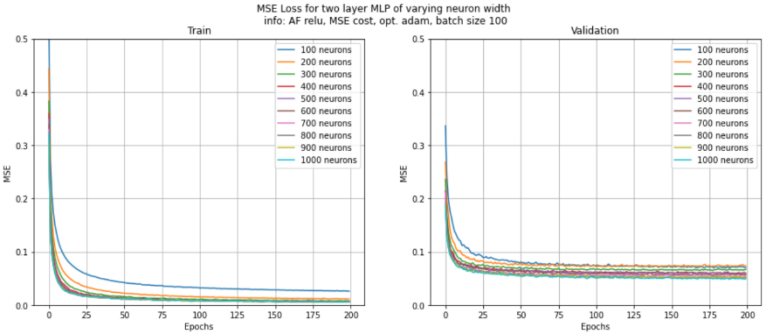

Figure 3. Example of experiments performed. The graph shows the results on the train (left) and validation set (right) of MSE (mean Square Error) reduction while training. Different lines show two-layer MLP neural networks of varying neuron width.

A library of different standardized neural networks has been created and stored for use with the Optimizer, thus, the NN that is more suited for the task at hand can be automatically accessed.

The NN results are discussed in section III.A.

C. Proposed Heuristic Optimizer Environment

As described in section I, a heuristic optimizer performs stochastic search, iteratively trying to improve (to optimize) a candidate solution regarding a given measure of quality. In Neutronet, a population of cores is proposed, and iteratively modified, executing the NN model to evaluate them at each step, resulting in a series of optimized cores. The optimization minimizes an objective function during this process, consisting mainly in reducing power peaks in the core, subject to a certain number of constraints.

To be able to perform this coupling process between the NN and the different heuristic optimizers proposed, a working environment (Figure 7) has been programmed.

The created architecture includes:

- **Input:** files that define a core model for the nodal code, and a series of parameters to perform the optimization.
- **Utilities** (represented in blue in Figure 7)**:** The inputs are loaded in an OOP (Object Oriented Programming) structure in Python, which serves as the driver for the whole program. A series of utilities (*Utils*) are used internally to execute different tasks.
- **Optimizers** (represented in grey in Figure 7)**:** a series of optimizers have been programmed from scratch, based on the optimization algorithms and bibliographical references cited in section I. These include simulated Annealing Algorithms that are currently the most common solution found in the bibliography (see section I) and novel optimization algorithms proposed by the authors, as explained below.
- **Connections** (yellow boxes in Figure 7): The program can connect both to ENUSA's internal Linux servers to execute the nodal code and to the created Neural Network Library to execute any of the saved neural networks. This enables using the ground truth execution (nodal code) to validate NN executions as well as executing hybrid optimizers that run on both engines.
- **Output:** the program outputs a series of optimized cores, which are executed with the nodal code, providing detailed execution logs and graphs for each run.

As an example, a more detailed diagram of the *Population* optimizer is shown in detail in Figure 4, this is one of the novel heuristic optimizers proposed by the authors and available in the Neutronet program.

The population optimizer is especially interesting as it is inspired by the manual process followed by the nuclear designers that work at ENUSA. The optimizer creates several random initializations and then performs a variable number of mutations, with a certain probability of performing fuel assembly swaps and rotations in different positions.

In an analogous way to the hyperparameter search described in Table 1, hundreds of experiments have been carried out to select the correct parameters and tune each of the created optimizers in this structure, some example graphs can be seen in the Optimizer results section, III.B.

III. RESULTS

A. Surrogate Model Results: Neural Networks

As discussed in section II.A, the NN is a surrogate model for the Nodal code, therefore results in this section evaluate the NN's error with respect to the Nodal code.

MSE errors are typically evaluated during the training process (Figure 3) because they are used as cost functions (error function to optimize during NN training). However, MAE (Mean Absolute Error) results are presented in this section, as this error has the same units as the calculated original variable and is a better indicator of error magnitude.

To calculate these results, the test dataset, described in Section II.B, is used. These data points are kept apart during both training and hyperparameter tunning to provide a final, independent test. MAE results represent the mean of the absolute error (*that is, value predicted by NN minus Nodal code value*) averaged over all test set data points.

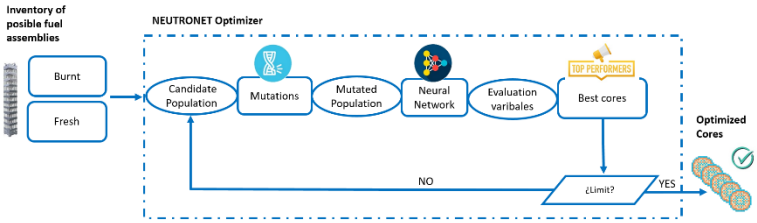

Figure 4. Detailed diagram for the *Population* optimizer.

Table 2 shows error results for the output variables of one of the created NNs, where variable names have been slightly obfuscated for confidentiality.

Table 2. Summary of NN results.

Error type	Test set results
% MAE on chemical control variable	1.4%
% MAE on energy delivered variable	0.06%
Maximum MAE of calculated FDH variables, unitless (% to limit of 1.5)	0.034 (2.3%)

FDH is defined as the enthalpy rise in the hot channel with respect to the core average, it is used as a measure of power peaks in the core and is a parameter to be optimized in the LPO process in Westinghouse NPPs. These cores must also be subject to constraints on the energy delivered and other limits set by the NPP operator and the safety authority, and therefore other output variables are also considered.

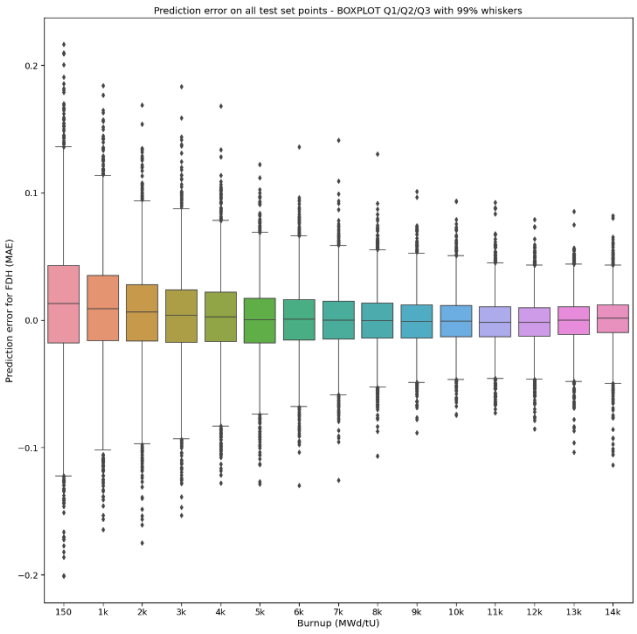

Figure 5. Boxplot of MAE error on test set data for FDH. X-axis represents cycle burnup steps, and the error is represented on the y-axis, with a Q1/Q2/Q3 boxplot and whiskers encompassing 99% of data.

A maximum MAE of 2.3% is obtained in FDH calculations. The NN error for all output variables is bounded by this 2.3% MAE value. These output variables are calculated by the NN in less than 0.1s, reducing by more than 600x the average run time of the current licensed nodal code. This is extremely interesting for their use in optimizers.

These same NN test set error results are shown in graph form in Figure 5. This boxplot represents the error distribution throughout the NPP's operation cycle (x-axis) for FDH. Larger errors are seen at the beginning of the cycle because fresh assemblies are more energetic, and therefore, more difficult to predict than depleted ones.

B. Optimizer Results

The optimization process is described in section II.C: the optimizer successively modifies cores, executing the NN seeking to minimize the objective function.

To evaluate the performance of the LPO algorithm, NN results for the optimized cores are compared against the nodal code, as these are our ground truth and are the final values that must comply with licensing limits.

The results of a single optimization run for a given cycle are shown graphically in Figure 6, comparing the best results in each generation obtained by the MLP NN (orange) to the results from the nodal code (ground truth, in blue). Successive optimizer generations are represented on the x-axis, with FDH represented on the y-axis as a measure of power peaking.

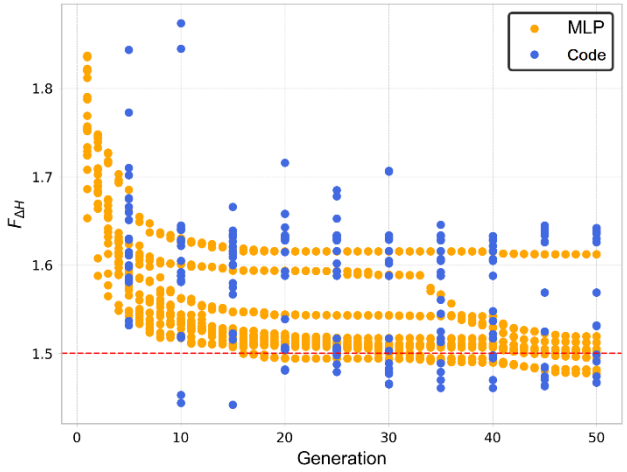

Figure 6. Graph for single optimization run.

This execution has generated more than 50k cores, running them through the optimizer, evaluating them with the NN and then checking the best candidates using the nodal code, with a total execution time of around an hour. As can be seen, the optimizer successfully reduces core power peaking during the execution, obtaining various cores with FDH values below the limit, shown in red.

Optimizer results are shown in Table 3 for 5 different real PWR NPPs. The last column in this table (bold type) shows FDH results for the best single core produced for each run, obtained with the nodal code. These results are all well below current design limits and therefore constitute successful optimizations.

Table 3. Examples of Optimizer runs for real cycles of 5 different PWR NPPs.

	FDH (neural network)		FDH (nodal code)	
	Average	**Best result**	**Average**	**Best result**
NPP1	1.5139	1.5063	1.4953	**1.4700**
NPP2	1.5376	1.5267	1.4830	**1.4590**
NPP3	1.5177	1.5069	1.4780	**1.4690**
NPP4	1.5385	1.5231	1.5093	**1.4870**
NPP5	1.4985	1.4773	1.5091	**1.4760**

IV. CONCLUSIONS

This paper proposes a novel approach to Loading Pattern Optimization using Machine Learning Techniques: Neutronet.

Several MLP neural networks have been created, for use as surrogate models, trained using augmented, randomized data from real, historic PWR LPs and saved to a Library of Neural Networks. These NNs predict the desired output variables x600 times faster than the nodal code, with an error that is small enough for optimizing.

Different heuristic optimizers have been programmed from scratch, including both classic optimizer techniques found in bibliographical references and novel optimizers proposed for the first time in this project.

A full program has been created, that, accepting cycle data as input, runs the optimizers by executing these neural networks, as well as the licensed nodal calculation code. This enables using the ground truth execution (nodal code) to validate NN runs as well as executing hybrid optimizers that run on both engines.

The results of the product created are very promising: it produces optimized cores in a fraction of the time used up in the manual process.

The main line of future work is the imposition of new constraints to the produced optimized cores, to adapt them to customer and licensing requirements.

Neutronet can reduce the effort required to obtain optimized cores, helping find new, unexplored solutions to this highly complex problem. This can be of special interest in situations of urgency or that imply a large human effort: for example, emergency redesign situations after fuel faults.

Furthermore, one of the main advantages of Neutronet is that it is highly adaptable to different licensed calculation codes and NPP types, as data can be generated for each specific case.

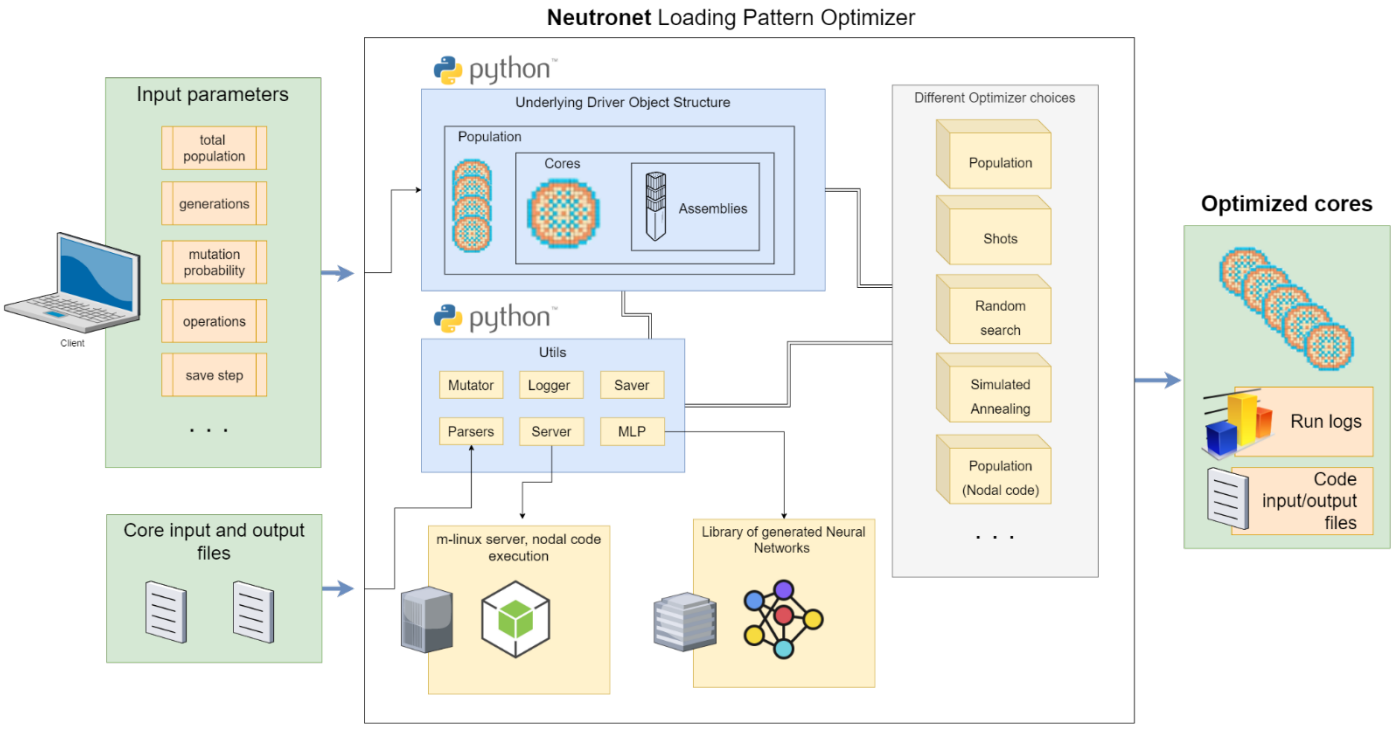

Figure 7. Created code architecture for the Neutronet Optimizer.

V. References

[1] J. G. Stevens, K. S. Smith, K. R. Rempe & T. J. Downar, «Optimization of Pressurized Water Reactor Shuffling by Simulated Annealing with Heuristics», Nuclear Science and Engineering, 121:1, 67-88, 1995, DOI: 10.13182/NSE121-67

[2] Mike Preuss, «Multimodal Optimization by Means of Evolutionary Algorithms», Springer International Publishing Switzerland 2015, ISBN 978-3-319-07406-1, https://doi.org/10.1007/978-3-319-07407-8

[3] G. T. Parks, «An Intelligent Stochastic Optimization Routine for Nuclear Fuel Cycle Design», Nuclear Technology, 89:2, 233-246, 1990, DOI: 10.13182/NT90-A34350

[4] P.W. Poon, G.T. Parks, «Application of genetic algorithms to in-core nuclear fuel management optimization » Mathematical methods and supercomputing in nuclear applications Proceedings Vol 1, (p. 878). Germany, 1993.

[5] M.D. DeChaine, M. A. Feltus, «Fuel Management Optimization Using Genetic Algorithms and Expert Knowledge», Nuclear Science and Engineering, 124:1, 188-196, 1996 DOI: 10.13182/NSE96-A24234

[6] C. Lin, J. Yang, K. Lin & Z. Wang «Pressurized Water Reactor Loading Pattern Design Using the Simple Tabu Search», Nuclear Science and Engineering, 129:1, 61-71, 1998, DOI: 10.13182/NSE98-A1963

[7] M.D. Machado, R. Dchirru, «Development of a multi-objective PBIL evolutionary algorithm applied to a nuclear reactor core reload optimization problem», Proceedings of the INAC 2005: International Nuclear Atlantic Conference.

[8] M.H da Silva, A.P Legey, A.C de A. Mol, «The evolution of PBIL algorithm when used to solve the nuclear reload optimization problem», Annals of Nuclear Energy, Volume 113, 2018, Pages 393-398, ISSN 0306-4549, https://doi.org/10.1016/j.anucene.2017.11.043.

[9] A.M de Lima, R. Schirru, «A nuclear reactor core fuel reload optimization using artificial ant colony connective networks», Annals of Nuclear Energy, Volume 35, Issue 9, 2008, Pages 1606-1612, ISSN 0306-4549, https://doi.org/10.1016/j.anucene.2008.03.002.

[10] A. A. de Moura, M. Dornellas, «Particle Swarm Optimization applied to the nuclear reload problem of a Pressurized Water Reactor», Progress in Nuclear Energy, Volume 51, Issue 2, 2009, Pages 319-326, ISSN 0149-1970, https://doi.org/10.1016/j.pnucene.2008.07.002.

[11] H.P.M. Gibcus, F.C.M. Verhagen, & P.H Wakker, «ROSA full-core and DNBR capabilities», Atw Internationale Zeitschrift fuer Kernenergie, 58(6), 353-356, 2013.

[12] H.P Vierstraete, F.C.M Verhagen, P.H. Wakker, «Loading Pattern Optimization for Standard and End-Of-Life Cycles of Ringhals PWR's with ROSA», Reunión annual de la SNE, Ávila, España, 2018.

[13] Huyen, Chip, "Designing Machine Learning Systems", O'Reilly Media, Inc., May 2022, ISBN: 9781098107963

[14] I. Goodfellow, Y. Bengio, A. Courville, «Deep Learning», Genetic Programming and Evolvable Machines 19, 305–307, 2018. https://doi.org/10.1007/s10710-017-9314-z

[15] M. Kotila, «Autonomio Talos v1.3: Hyperparameter Optimization for TensorFlow, Keras and PyTorch», open-source software package, MIT license, 2020. Available at http://github.com/autonomio/talos

Proceedings of the European Nuclear Young Generation Forum
ENYGF'23
May 8-12, 2023, Kraków, Poland

Validation of the passive autocatalytic recombiner simulation code PARUPM using experimental data from REKO-3 and THAI program tests

Domínguez-Bugarín, Araceli[1*], Reinecke, Ernst-Arndt[2], Jiménez, Miguel Ángel[3], and Jiménez, Gonzalo[1]

[1] Universidad Politécnica de Madrid (UPM), Spain; [2] Forschungszentrum Jülich GmbH (FZJ), Germany; [3]Consejo de Seguridad Nuclear (CSN), Spain

*Corresponding author: *araceli.dominguez@upm.es*

I. INTRODUCTION

Hydrogen and carbon monoxide are two combustible gases that can be generated during a severe accident (SA), posing a risk for the containment integrity in case of gas deflagration or detonation. To mitigate this risk, passive auto-catalytic recombiners (PARs) have been installed inside containment buildings of many nuclear power plants [1], [2].

These devices reduce the risk of combustion by converting these combustible gases into H_2O and CO_2, respectively. These completely passive safety devices are self-starting and contribute to the global convection and mixing of the combustible gases in the containment atmosphere. The most common PAR design consists of an array of vertical catalyst sheets located at the bottom of a rectangular housing (figure 1).

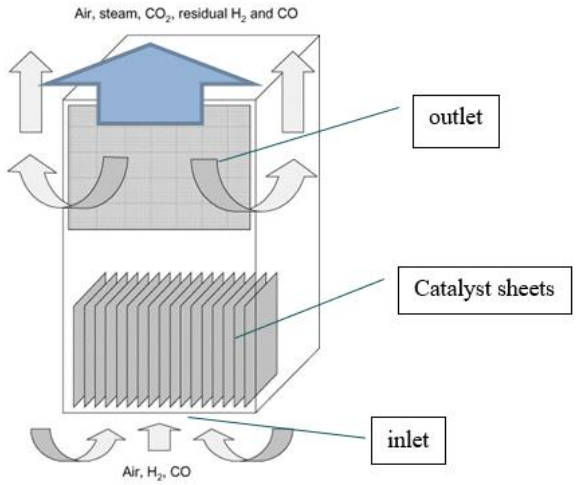

Figure 1. Scheme of a generic passive auto-catalytic recombiner (PAR)

The sheets are covered by a catalytic material (e.g., platinum or palladium) that enables the recombination reactions (1) and (2) on the surface by lowering the activation energy. Thus, reactions can occur at lower temperatures and reactant concentrations than.in the non-catalysed gaseous phase.

$$H_2 + 1/2\ O_2 \rightarrow H_2O + 242\ \text{kJ/mol} \quad (1)$$

$$CO + 1/2\ O_2 \rightarrow CO_2 + 283\ \text{kJ/mol} \quad (2)$$

To investigate the operational behaviour of PARs, a physico-chemical model of relevant processes occurring inside the housing has been developed in the context of the AMHYCO project. The model considers surface chemistry on platinum-based catalytic surfaces as well as heat and mass transfer between the catalyst and gaseous mixtures of hydrogen, carbon monoxide, air, steam, and carbon dioxide. The PARUPM code is based on this approach [3].

The European project AMHYCO (Euratom 2019-2020, GA No 945057) [4] seeks to advance the simulation capabilities to support H_2/CO combustion risk management in severe accidents based on knowledge from experimental investigations. The project's three major goals are to improve SA management, increase the predictability of numerical codes applied in explosion hazard assessment inside reactor containments, and experimentally examine SA conditions that are challenging to forecast theoretically.

II. PARUPM MODEL

Traditionally, computational models for predictive safety analysis have relied on empirical expressions that correlate the hydrogen recombination rate with fundamental environmental conditions such as temperature, pressure, and hydrogen concentration. Despite their advantages in terms of computational effort, their applicability is limited to scenarios that are within the correlation range. Thus, there is an interest in creating a mechanistic model that considers in greater detail the intricate processes that take place on the catalytic surface and that enables dealing with a variety of scenarios.

The reaction of gaseous species on the catalyst sheets produces heat that raises the catalyst sheet's temperature

(heating phase), alters the reaction rates, warms the gas mixture between the plates, and increases the flow, inducing a self-sustained natural circulation pattern. The operation of the PAR may be restricted or even prevented by the presence of poisoning species, unfavourable density gradients, and pressure losses through the device [1].

PARUPM [3] is a non-proprietary code that uses a physico-chemical model, based on surface-chemistry, to numerically simulate the behaviour of a PAR device. This model accounts for the various phenomena that take place in the recombiner, which is conceptualized as a collection of vertical flow channels separated by vertical parallel plates: the upward vertical flow driven by natural convection, which governs the transfer of heat and mass between the plates and the gas mixture, the surface processes involving adsorption and desorption of species as well as chemical reactions on the catalyst, the resulting heat release, and finally the radiative heat exchange with the surrounding space. These phenomena are closely interrelated and must be modelled accordingly. The coupling is realized using expressions for the mass and energy balance at the interface between the catalyst and the gas flow. [5].

The model is based on an adapted reaction scheme of the heterogeneous combustion of methane according to Deutschmann [6] coupled to the Elenbaas analysis [7] for the natural convection-induced heat transfer between parallel plates. In a non-dimensional set of equations, the analogy between mass and heat transfer is used to deal with the species diffusion. The proposed model is capable of simulating the heterogeneous combustion of H_2 and CO under natural convective flow conditions.

III. EXPERIMENTAL SET-UPS

A validation process of the PARUPM model was performed to study the accuracy and validity of the code. The results obtained with the physico-chemical model have been compared to experimental data obtained from both the REKO-3 facility [2] and the THAI containment [8] program tests.

A. REKO-3 installation

The experimental facility, shown in figure 2, involves a vertical flow channel equipped with 4 sheets, which are coated with a platinum-based catalyst. This setup represents a section of a PAR since commercial PARs typically contain up to 150 sheets. The primary distinction between this facility and commercial PARs is that a forced flow amongst the plates is applied. This allows to better control the flow rate of the gaseous mixture passing through the recombiner, which is very useful for validation purposes.

The purpose of the REKO-3 experiments is to study in detail relevant processes that occur in plate recombiners (conversion rates, catalyst temperatures, heat transfer, etc.) [2]. For this purpose, the natural convection effect occurring in a real PAR is removed by imposing predefined flow conditions. Thus, the experimental data obtained at this facility represent the behaviour of a recombiner under steady-state performance.

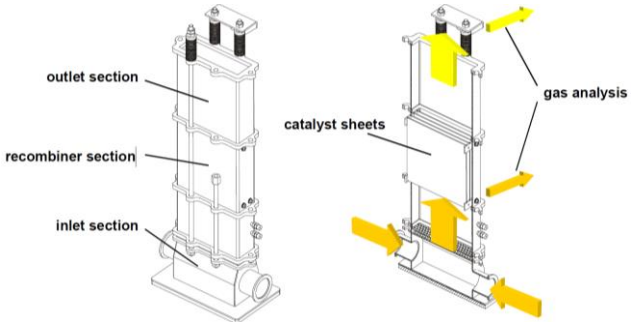

Figure 2. Scheme of the modular setup of the REKO-3 flow channel (left) and the internal flow paths (right). [2]

B. THAI containment

Several of the recombiner experiments performed by Becker Technologies in the THAI facility (figure 3) in the framework of the OECD/NEA-THAI project [8] were used for the validation exercise in this paper. The THAI containment test facility consists of a 60 m3 stainless-steel cylindrical vessel where a recombiner is located near the bottom of the structure.

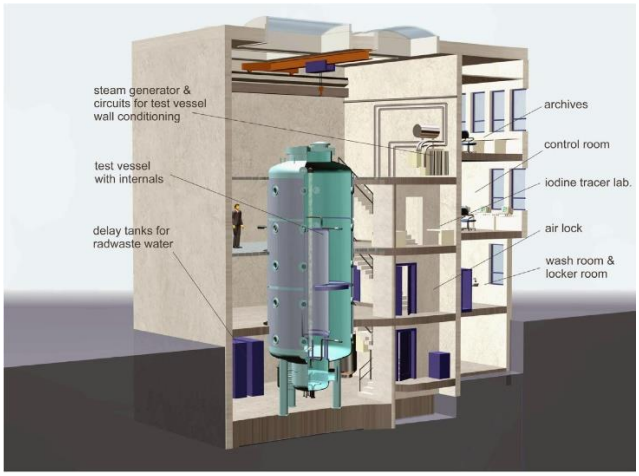

Figure 3. THAI test facility [8].

Tests considered for the validation were performed with an Areva FR90/1-380T recombiner with a 50% reduction of both the inlet cross section and the number of catalyst sheets. All tests were run with a first injection phase of hydrogen, a subsequent depletion phase, a second hydrogen injection phase, and a second and last depletion phase. The tests considered for the transient validation were the HR-1 and HR-13 from the OECD/NEA-THAI project [10]. Both tests were run at a pressure of 1 bar.

IV. CODE VALIDATION

A. O_2 starvation conditions in the REKO-3 tests

To study the effect of oxygen starvation (i.e., low oxygen/nitrogen ratio), experiments where the oxygen

molar fraction was progressively reduced were analysed. In these experiments [9], the H_2 molar fraction was kept constant at 3% while the O_2 molar fraction was gradually reduced from a 20% to a 2% of the total volumetric flow rate. The flow speed was kept constant at 1.15 m/s and the H_2 recombination rates were obtained for gas temperatures at the inlet of 20.5ºC and 80.1ºC. In table 1 the recombination rates obtained with PARUPM and from REKO-3 tests are shown.

Table 1. Recombination rates obtained with PARUPM and from REKO-3 for 5 different O_2 concentrations and 2 inlet temperatures.

X_{O2}	T(ºC)	H_{rate} PARUPM (mol/h)	H_{rate} REKO-3 (mol/h)	ΔH_{rate}
0.20	20.50	18.40	17.82	0.03
0.05	20.50	18.36	21.52	0.15
0.04	20.50	18.35	19.60	0.06
0.03	20.50	18.34	18.68	0.02
0.02	20.50	10.65	12.46	0.15
0.20	80.10	18.43	17.82	0.03
0.05	80.10	18.41	17.45	0.06
0.04	80.10	18.40	17.61	0.04
0.03	80.10	18.40	16.91	0.09
0.02	80.10	10.62	10.27	0.03

The deviations ΔH_{rate} between the recombination rates obtained with PARUPM and the experimental results show that the code is capable of accurately predict the recombiner recombination rates once the oxygen starvation stage is reached, especially for higher inlet gas temperatures.

B. CO recombination in the REKO-3 tests

To study the effect of CO on the H_2 recombination rate and the CO recombination capability of the code, several REKO-3 experiments were analysed from the series R3-A-03_CO, R3-A-04_CO, and R3-A-06_CO [10]. For 3 different H_2 concentrations, other 3 different CO concentrations where studied. The inlet flow temperature was kept at 21ºC for all the experiments and the flow velocity was 1.15 m/s for every run.

- Case 1: 2% H_2 for 0%, 0.5%, 1%, and 2% CO
- Case 2: 4% H_2 for 1%, 2%, and 4% CO
- Case 3: 5% H_2 for 1%, 2%, 3%, 3.5%, and 4% CO

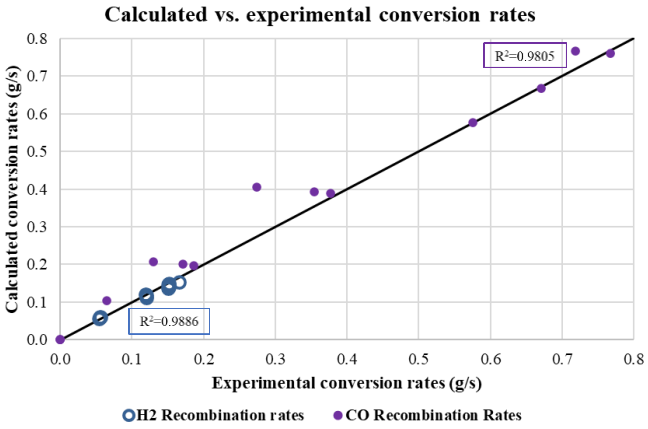

Figure 4. PARUPM H2 (blue dots) and CO (open purple dots) recombination rates against experimental recombination rates in g/s.

The average code-test deviation for the H_2 recombination rates is ~3.2% while the average deviation for the CO recombination rates is ~19.1% for case 1 although, for cases 2 and 3, the average deviation is ~5.5% and ~4.3%, respectively. Within these limits, the model is capable of calculating the recombination rates of both species in the presence of CO.

C. Transient validation. THAI tests

Test HR-1 starts with a vessel atmosphere of dry air at an ambient temperature of 25ºC. During the test first phase H_2 is injected in the vessel. After 25 minutes, the injection stops and a first depletion (recombination only) phase starts, which lasts for 60 minutes. Then, the second hydrogen injection phase takes place with a duration of 20 minutes followed by the second depletion phase which runs until the recombination stops.

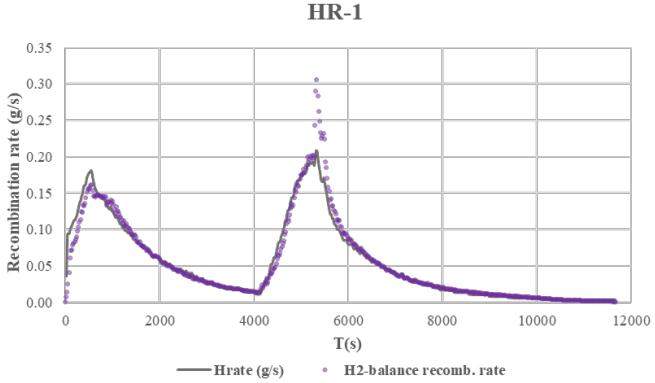

Figure 5. Recombination rate with PARUPM (grey line) and experimental recombination rates (purple dots) in g/s during the transient.

Figure 5 shows the recombination rate obtained during the experiment HR-1 as well as the recombination rates from

PARUPM using the boundary conditions from the experiment. The only significant discrepancy between the model and the experimental recombination rates occurs at the end of the second injection phase, which is due to a PAR induced ignition causing high recombination rates during the combustion process. PARUPM doesn't contain an ignition module, thus this behaviour is not analysed by the code. Overall, the comparison with experimental data confirms that the code can simulate the behaviour of a real passive autocatalytic recombiner under realistic conditions.

The initial conditions of test HR-13 include a mixture of air with 60 vol.% steam at a temperature of 86ºC. The test follows the same pattern of injection and depletion as HR-1. However, during the second injection and depletion, the recombination runs under oxygen starvation conditions.

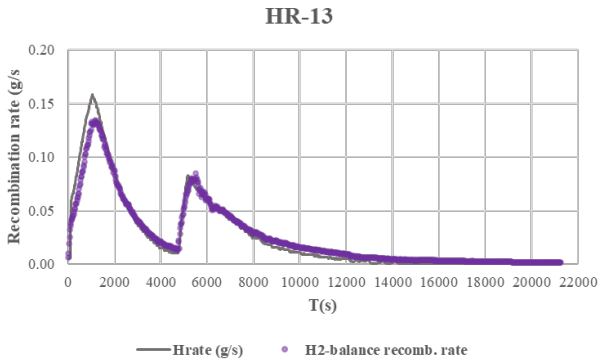

Figure 6. Recombination rate with PARUPM (grey line) and experimental recombination rates (purple dots) in g/s during the transient.

Figure 6 shows the recombination rate obtained from the experiment HR-13 as well as the recombination rates calculated with PARUPM using the boundary conditions from the experiment. The figure shows that the code reproduces well the behaviour of a real passive autocatalytic recombiner inside a containment during the second injection and depletion (as well as the rest of the transient), when the recombiner is experiencing oxygen starvation.

V. CONCLUSIONS AND FUTURE WORKS

The major goal of this work was to present the PARUPM code, along with a validation process. The results obtained and presented in this paper demonstrate that the physico-chemical strategy used in the PARUPM model can simulate the behaviour of the recombiner under a variety of conditions, from typical concentrations and settings to more extreme ones such as oxygen starvation, CO poisoning, or elevated inlet temperatures. Furthermore, the code can reproduce the behaviour of a PAR in transient conditions, where pressures, temperatures, and gas concentrations are constantly changing at the recombiner inlet.

Within the AMHYCO project, the PARUPM code has been proposed as an appropriate tool for assessing the performance of PARs in nuclear containments. The phenomenology observed in a severe accident can be examined in more detail once the PARUPM code is implemented in thermo-hydraulic analysis codes, such as GOTHIC [11], a general-purpose integrated thermo-hydraulic software package for the design, licensing, safety, and operational analysis of nuclear power plant containment and system components.

VI. ACKNOWLEDGMENTS

The authors gratefully acknowledge that the data from tests HR-1 and HR-13 (conducted in the frame of the OECD/NEA THAI project) was shared by Becker Technologies for the AMHYCO project. Furthermore, the AMHYCO project has received funding from the Euratom research and training programme 2019-2020 under Grant Agreement n°945057. The content of this paper reflects only the author's view. The European Commission is not responsible for any use that may be made of the information it contains.

VII. REFERENCES

[1] F. Arnould, "State of the Art of Passive Autocatalytic Recombiner (PARSOAR)," 2003.

[2] E.-A. Reinecke, I. M. Tragsdorf, and K. Gierling, "Studies on innovative hydrogen recombiners as safety devices in the containments of light water reactors," *Nuclear Engineering and Design*, p. 11, 2004.

[3] M. Á. Jiménez, "Recombinación del hidrógeno en dispositivos autocatalíticos pasivos y sus implicaciones en la seguridad de las centrales nucleares," 2007.

[4] G. Jiménez *et al.*, "AMHYCO project – towards advanced accident guidelines for hydrogen safety in nuclear power plants," Oct. 2020.

[5] M. A. Jiménez, J. M. Martín-Valdepeñas, F. Martín-Fuertes, and J. A. Fernández, "A detailed chemistry model for transient hydrogen and carbon monoxide catalytic recombination on parallel flat Pt surfaces implemented in an integral code," *Nuclear Engineering and Design*, vol. 237, no. 5, pp. 460–472, Mar. 2007, doi: 10.1016/j.nucengdes.2006.08.002.

[6] O. Deutschmann, F. Behrendt, and J. Warnatz, "Modelling and simulation of heterogeneous oxidation of methane on a platinum foil," *Catalysis Today*, vol. 21, no. 2, pp. 461–470, Dec. 1994, doi: 10.1016/0920-5861(94)80168-1.

[7] W. Elenbaas, "Heat dissipation of parallel plates by free convection," *Physica*, vol. 9, no. 1, pp. 1–28, Enero 1942, doi: 10.1016/S0031-8914(42)90053-3.

[8] S. Gupta, G. Poss, and M. Sonnenkalb, "OECD/NEA THAI program for containment safety research: main insights and perspectives," presented at the Eurosafe Forum 2016, Münich, Alemania, Nov. 2016.

[9] E.-A. Reinecke, S. Kelm, S. Struth, U. Schwarz, and I. M. Tragsdorf, "Performance of catalytic recombiners for hydrogen mitigation in severe accidents under oxygen depletion conditions," presented at the ICONE-15, Japan, Jul. 2007.

[10] M. Klauck, E.-A. Reinecke, S. Kelm, N. Meynet, A. Bentaïb, and H.-J. Allelein, "Passive auto-catalytic recombiners operation in the presence of hydrogen and carbon monoxide: Experimental study and model development," *Nuclear Engineering and Design*, vol. 266, pp. 137–147, Jan. 2014, doi: 10.1016/j.nucengdes.2013.10.021.

[11] EPRI, "GOTHIC 8.3 Thermal Hydraulic Analysis Package. User Manual." EPRI, Palo Alto, CA, 2018.

Proceedings of the European Nuclear Young Generation Forum
ENYGF'23
May 8-12, 2023, Kraków, Poland

Generating Latin Hypercube Sampling Design of Experiments for few-group homogenized cross-section representation with statistical learning approaches

M.-A. Dor[1*], A. Brighenti[1*], L. Graziano[1], G. Mestrot[1], W. Kubinski[1], L. Lefebvre[1], M. Segond[1] and B. Vezzoni[1]

[1] Framatome – DTIPD Codes and Methods Department, France

*Corresponding authors: marc-antoine.dor@framatome.com, alberto.brighenti@framatome.com

I. INTRODUCTION

Industrial nuclear reactor core calculations are often based on the so-called *two-level* scheme: on the first level, multiple transport calculations are performed at the assembly level in different operating conditions (e.g., fuel temperature, boron concentration, moderator density, and others) to produce multi-parameter data with homogenized microscopic cross-sections, either at the assembly, pin scale or intermediate homogenization. On the second level, the core codes interpolate the cross-sections contained in the multi-parameter data according to the operating conditions of the reactor. It turns out that for an accurate interpolation of the cross-sections in the parameter phase space, a large amount of data is needed, increasing the computational time to generate the tabulated cross-section data and to load and use them in the core code. From experience, the table loading time is a significant part of the total industrial core code computational time in the case of a standalone core flux resolution adopting the two-group diffusion approximation and coarse mesh scheme with the *two-level* scheme.

Unsurprisingly, industrial stakeholders are interested in developing fast and accurate methods to interpolate homogenized cross-sections and reduce the overall computational time and data storage of a core calculation.

The use of statistical learning models for nuclear applications started in the late 90s' [1] [2], but a growing interest in recent Machine Learning (ML) techniques appeared in the second decade of the 2000s among multiple research teams: CEA Saclay (France) has proposed an accurate multi-output ML model [3] [4], the Ulsan National Institute of Science and Technology (Korea) has proposed ML models that take in input the assembly layout to produce directly homogenized macroscopic cross-sections [5] [6] [7] [8] [9], the University of Florida (US) developed a model specifically applied to the pin-by-pin power reconstruction at the assembly scale [10] [11] and the Tsinghua University (China) developed ML models for HTGR reactor simulations [12].

This work presents the rationale and the first steps performed at Framatome (France) to develop a statistical learning method for few-group lattice homogenized cross-section representation and fast interpolation in core codes.

II. DESIGN OF EXPERIMENT

A. Methodology, tools and reference case

The first step of the proposed methodology is dedicated to modelling two-group homogenized cross-sections for all the reactions required by the core code and considering, separately, the values of the microscopic cross-sections for a specified set of isotopes and for all the other aggregated isotopes (called *residual* cross-section).

To evolve the work presented in [4] and target an industrial implementation of the present work, more realistic and challenging choices have been made, namely: using an assembly with burnable Gd pins to generate the training data, the addition of the moderator density for statistical learning models training and the modelling of equivalence parameters (nodal assembly discontinuity factors [13], *super-homogenization* equivalence factors [14]). Moreover, the current strategy is more focused on interpolation and representation performances with improved Design of computer Experiments (DoEs) random samplings to perform, in the next step of the work, a step-by-step benchmark of different ML interpolations models to validate, assess and identify the best representation strategy of few-group homogenized cross-sections. All the few-group homogenized cross-sections have been generated with the platform NEMESI [15]: a prototype of a flexible lattice calculation tool for generating multi-parameter libraries for PWR and VVER reactor assemblies based on the APOLLO3® code [16]. The gadolinium assembly considered in this exercise is publicly provided in the KAIST benchmark [17], which layout is shown in Figure 1.

The interpolation parameters of the calculation point database are the burnup (BU), the boron concentration, the moderator density, the fuel temperature and the rod configuration types.

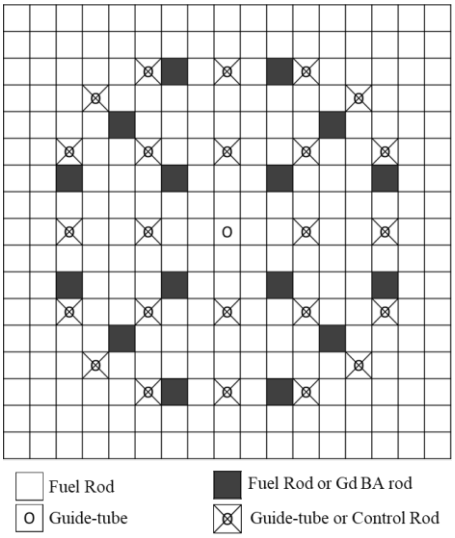

Figure 1. Sketch of the gadolinium assembly.

To compare the performances of different ML models in terms of accuracy, space occupied on disk and data loading time, two different statistical DoEs have been generated, see Table 1: the first with a cartesian grid sampling, and the second using a Latin Hypercube sampling (LHS) [18] with OpenTURNS [19] on core-state parameters, with the same number of parameters' sets as the standard sampling for each BU step. Hence, 48 LHS experiments are run: one for each BU step. The same parameters' ranges are used for LHS sampling. Each LHS experiment contains 6 (boron values) × 6 (moderator density values) × 6 (fuel temperature values) × 3 (control rod configurations) = 648 samples to ensure that there is the same number of samples for each BU step in both DoEs.

Table 1. Parameter ranges and number of calculation points for the generated DoEs.

Parameter	Range	# points Cartesian grid	# points LHS
Burnup (MWd/t)	$[0 – 20\times10^3]$	48	48
Boron concentration (ppm)	[0 – 2500]	6	648
Moderator density (g/cm^3)	[0.6 – 0.85]	6	648
Fuel temperature (C)	[250 – 1750]	6	648
Rod type[1] (no unit)	{ARO, B4C, AIC}	3	3

Hence, an LHS DoE is a clear advantage and cleanest mathematical framework besides the mainstream "cartesian-grid" sampling to build ML models: it allows for varying each parameter among more distinct values with the same number of calculation points with identical and independent distributions to sample random variables. This is the first step to deploying the statistical learning cross-section representations method. Two possible outcomes of this benchmark are listed: enhancing the interpolation accuracy with the same number of lattice calculations; or reaching the current level of accuracy with a lower number of lattice calculations, with the number of samples as a free parameter to reach the targeted accuracy level.

[1] ARO = All Rods Out; B4C = B4C control rods; AIC = Ag-In-Cd control rods.

B. Analysis

The corresponding output data is the ensemble of data required to feed a depletion calculation at a second level of the calculation scheme, i.e., the core diffusion calculation. Modelling homogenized microscopic cross-sections of major isotopes is required to ensure acceptable accuracy of the core calculation because of their contribution to defining the overall neutronic behaviour. The choice for this preliminary study considers the following significant isotopes: *U234, U235, U236, U238, Pu238, Pu239, Pu240, Pu241, Pu242, Np237, Am241, Am242, Am243, Cm242, Cm243, Cm244, Xe135, I135, Sm149, Nd148, Pm147, Pm148, Pm149, Gd152, Gd154, Gd155, Gd156, Gd157, Gd158, Gd160*. The other isotopes present in nuclear reactor cores are then grouped into three *cumulative* isotopes*: remaining fissile isotopes, remaining fission products*, and *all the remaining isotopes*.

Homogenized cross-section reactions are *ν-Fission* (for fissile isotopes), *scattering matrix*, *absorption*, and *capture*. Usually, two-group cross-sections are condensed into two energy groups: the *fast* group, from 0.625 eV to 19.64 MeV, and the *thermal* group, from 1.1×10^{-4} eV to 0.625eV. The diffusion coefficient and assembly discontinuity factors are also computed.

With some visualisation, one can note that many of the cross-sections vary smoothly in this multiparameter space, see Figure 2, while, in some cases, one can notice more significant variations, as in Figure 3, or coupled dependencies, see Figure 4.

Generally, the cross-sections behave linearly with the boron concentration, the moderator density, and the fuel temperature.

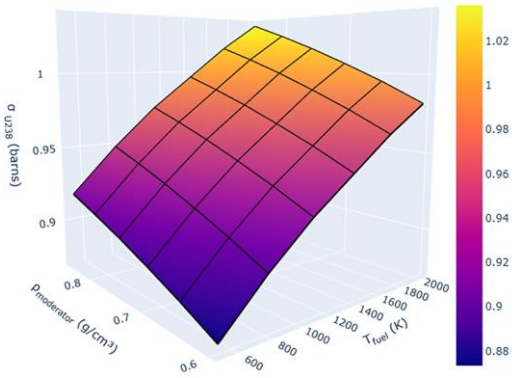

Figure 2. Fast absorption cross-section of U238 (barns) behaviour versus moderator density and fuel temperature at fixed burnup/boron concentration in an ARO configuration

On the other hand, the variations considering the burnup axis are the most erratic ones, with no linear behaviour see Figure 3; even for diffusion quantities such as the Assembly Discontinuity Factors (ADF) displayed in

Figure 4 and for the main isotopes on the Figure 5b. This is due to the assembly flux distribution and homogenization process at the assembly level. This effect is enhanced by the disappearance of absorbing gadolinium isotopes (Gd155, Gd157) when the burnup reaches about 10 GWd/t.

The statistical learning models will be tested in the next step of this work to ensure their capability of representing these different behaviours with all the state parameters for each considered cross-section: see Figure 5a and Figure 5b. Finally, some specific phenomena appear at very low burnups for some isotopes and reactions: see Figure 5b and Figure 6, where some substantial variations are noticed. This can be explained by the evolution from a non-depleted fuel (at 0 MWd/t) to a depleted fuel with equilibrium xenon (at ~150 MWd/t): this can lead to significant erratic behaviours of the homogenized cross-sections because of the samarium and xenon influence on the neutron balance.

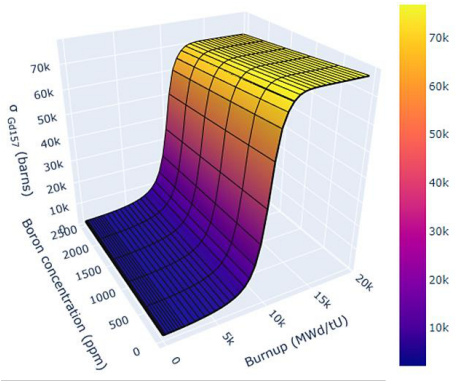

Figure 3. Thermal capture cross-section of Gd157 (barns) behaviour versus burnup and boron concentration at fixed moderator density/fuel temperature in ARO configuration.

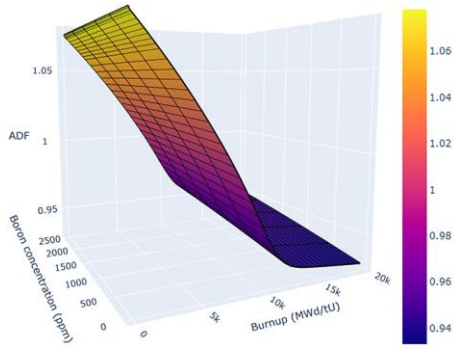

Figure 4. Thermal ADF behaviour versus burnup and boron concentration at fixed moderator density/fuel temperature in ARO configuration.

C. Perspectives

The flexibility of the tools developed so far in this work and the analysis of the results pave the way for the next steps of the methodology: it would be interesting to consider other typical variables defining the phase space, like adding parametrisations that are not currently available in our tools. Considering average xenon concentration in the assembly pins or Pu/U ratio could be added to consider the historical effects that can affect the behaviour of the assembly (see Appendix C of [3]). The ML models that will be built on the previously mentioned DoE should be tested on a dataset based on the representative distribution of core-state parameters usually required in industrial core calculations. An iterative process should be implemented, if needed, based on the accuracy obtained on this test set, that sets up an adaptive DoE sampling procedure to resolve the errors and to enhance the accuracy of the surrogate models on the corresponding regions of interest of the phase space.

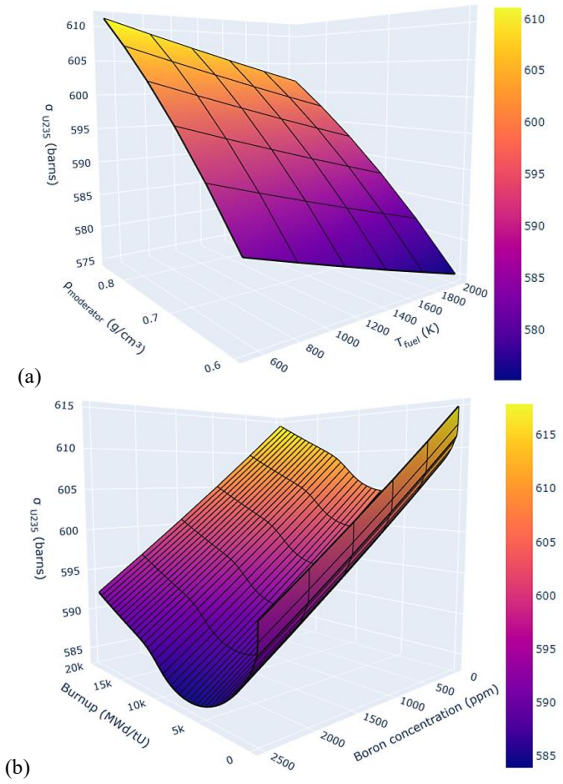

Figure 5: Thermal ν-Fission cross-section of U235 (barns) for the ARO configuration varying (a) moderator density and fuel temperature or (b) burnup and boron concentration. The parameters' vector is (2 GWd/t; 500 ppm; 0.8 g/cm^3, 1123.15 K).

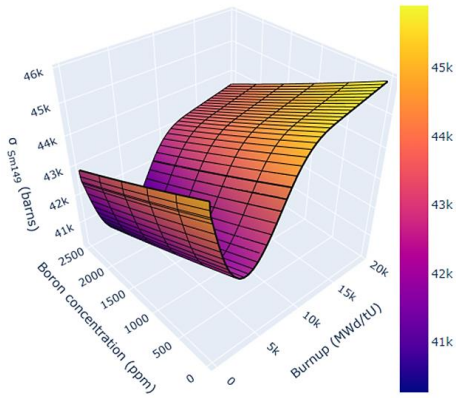

Figure 6. Thermal absorption cross-section of Sm149 versus burnup and boron concentration at fixed temperature density/fuel temperature in ARO configuration.

III. Conclusions

This paper starts by presenting the context and a bibliographic review of the use of ML techniques for nuclear applications, specifically for interpolating isotopic cross-sections. This work is the first step of the overall R&D methodology proposed by Framatome to develop cross-section data libraries representation and interpolation based on ML techniques: the use of NEMESI and APOLLO3®, wrapped with OpenTURNS is indeed proposed as a multiparameter library generator for a benchmark UGD configuration. The paper demonstrates the tool's flexibility

to cover various state parameters for cross-section calculations. Moreover, the present work shows how the cross-sections may present very different behaviours inside their phase space, e.g., smooth or with discontinuities, that can challenge the accuracy of the targeted ML models. Therefore, using the LHS for constructing the training database is advantageous given its better coverage and the statistical independence property of the parameters' phase space distributions. The paper ends by presenting this work's perspectives, namely the training and validation of the ML model and their future applications in an industrial core diffusion code at Framatome.

IV. Acknowledgments

The NEMESI prototype has been developed as part of the H2020 CAMIVVER project funded by the Euratom research and training program 2019-2020 under grant agreement No 945081. APOLLO3® is a registered trademark of the CEA developed under a long-term partnership and support of EDF and Framatome.

V. References

[1] A. Yamamoto, "Application of Neural Network for Loading Pattern Screening of In-Core Optimization," Nuclear Technology, vol. 144, no. 1, pp. 63-75, 2003.

[2] B. Leniau, B. Mouginot, N. Thiolliere, X. Doligez, A. Bidaud, F. Courtin, M. Ernoult and S. David, "A neural network approach for burn-up calculation and its application to the dynamic fuel cycle code CLASS," Annals of Nuclear Energy, vol. 81, pp. 125-133, 2015.

[3] E. Szames, Few group cross section modeling by machine learning for nuclear reactor, Université Paris-Saclay: Neural and Evolutionary Computing, 2020.

[4] E. Szames, K. Ammar, D. Tomatis and J. Martinez, "Few-group cross-sections modeling by artificial neural networks," in PHYSOR2020 – International Conference on Physics of Reactors: Transition to a Scalable Nuclear Future, 2021.

[5] S. Dzianisau, J. Choe, A. Cherezov and D. Lee, "Macroscopic Cross-Section Generation for Nodal Code RAST-K Using Artificial Neural Network," in Transactions of the Korean Nuclear Society Virtual Autumn Meeting, 2020.

[6] S. Dzianisau, K. Saeju and D. Lee, "Optimization of Training Dataset Size for Predicting Homogenized Macroscopic Cross-Sections usingDeep Neural Network," in Transactions of the Korean Nuclear Society Virtual Autumn Meeting, 2021.

[7] S. Dzianisau, F. Setiawan, K. Saeju, J. Park and D. Lee, "RAST-AI: a Standalone Nodal Diffusion/Deep Neural Network Code for Reactor Analysis and Simulation," in PHYSOR2021 - International Conference on Physics of Reactors, Pittsburgh, USA, 2022.

[8] S. Dzianisau, K. Saejua, H. Chul Leeb and D. Lee, "Development of an Artificial Neural Network Model for Generating Macroscopic Cross-Sections for Rast-Ai," Pre-print, 2022.

[9] S. Dzianisau and D. Lee, "Enhancement of RAST-AI Deep Learning Cross-Section Generation Model by Adding Gadolinia Fuel Support," in Transactions of the Korean Nuclear Society Autumn Meeting, Changwon (Korea), 2022.

[10] F. Shriver, C. Gentry and J. Watson, "Prediction of Neutronics Parameters Within a Two-Dimensional Reflective PWR Assembly Using Deep Learning," Nuclear Science and Engineering, vol. 195, no. 6, pp. 626-647, 2021.

[11] F. Shriver and J. Watson, "Scaling deep learning for whole core reactor simulation," Progress in Nuclear Energy, vol. 146, 2022.

[12] Z. Li, J. Sun, C. Wei, Z. Sui and X. Qian, "Research on the cross-section generating method in HTGR simulator based on machine learning methods," in PHYSOR2020 – International Conference on Physics of Reactors: Transition to a Scalable Nuclear Future, 2021.

[13] K. Smith, "Assembly homogenization techniques for light water reactor analysis," Progress in Nuclear Energy, vol. 17, no. 3, pp. 303-335, 1986.

[14] A. Hebert, Development of the SPH method: cell homogenization of a non-uniform lattice and reflector parameters calculation, Gif-sur-Yvette (France): CEA Centre d'Etudes Nucleaires de Saclay, 1981.

[15] A. Brighenti, A. Hebert, B. Calgaro, E.-Y. Garcia-Cervantes, G. Huccho Zavala, P. Laurent, L. Mercatali, P. Mosca, A. Previti, S. Santandrea, B. Vezzoni, J.-F. Vidal, A. Willien and I. Zmijarevic, "Development of a multi-parameter library generator prototype for VVER and PWR applications based on APOLLO3," in Submitted to The International Conference on Mathematics and Computational Methods Applied to Nuclear Science and Engineering M&C2023, Niagara Falls, Ontario, Canada, 2023.

[16] P. Mosca, L. Bourhrara, A. Calloo, A. Gammicchia, F. Goubioud, L. Lei-Mao, F. Madiot, F. Malouch, E. Masiello, F. Moreau, S. Santandrea, D. Sciannandrone, I. Zmijarevic, E. Garcias-Cervantes, G. Valocchi, J. Vidal, F. Damian, P. Laurent, A. Willien, A. Brighenti, L. Graziano and B. Vezzoni, "APOLLO3®: Overview of the new code capabilities for reactor physics analysis," in Int. Proc. M&C 2023 Conference, Niagara Falls, Ontario, Canada, August 13-17, 2023.

[17] N. Z. Cho, "Benchmark Problem 1A: MOX Fuel-Loaded Small PWR Core (MOX Fuel with Zoning)," [Online]. Available: http://nurapt.kaist.ac.kr/benchmark.

[18] R. Iman, J. Helton and J. Campbell, "An approach to sensitivity analysis of computer models, Part 1. Introduction, input variable selection and preliminary variable assessment," Journal of Quality Technology, vol. 13, no. 3, pp. 174-183, 1981.

[19] M. Baudin, A. Dutfoy, B. Ioss and A.-L. Popelin, "OpenTURNS: An Industrial Software for Uncertainty Quantification," in Handbook of Uncertainty Quantification, Ghanem, Roger; Hidgon, David; Owhadi, Houman, 2016, pp. 1-38

Proceedings of the European Nuclear Young Generation Forum
ENYGF'23
May 8-12, 2023, Kraków, Poland

Numerical validation of RANS model for low Prandtl number fluid using TALL 3D experimental data

H. Elgendy[1*]

[a] Narodowe Centrum Badań Jądrowych, NCBJ, ul. Andrzeja Sołtana 7, 05-400 Otwock, Poland

* Corresponding author: *hisham.elgendy@ncbj.gov.pl*

Keywords

k-omega model, Dual fluid reactor, mini demonstrator, Liquid lead bismuth, lead cooled reactor, Ansys fluent, thermal hydraulic analysis.

I. INTRODUCTION

As fossil fuels tend to have an end sooner or later, either due to excess consumption or the negative environmental impact, nuclear power is expected by many experts to take over this gap in the energy production sector along with other renewable energy sources [1]. A new concept of reactors namely, the Dual Fluid Reactor recently rose within the 4th generation reactors[2]. The basic feature of this type of reactor is that it uses two loops of molten materials, one fuel loop contains U-Cr, cooled by another loop of liquid lead bismuth. Significant advantages could make the DFR an excellent choice for future development and research, thus commercial production [3].

Thermal hydraulics is one of the essentials for reactor design, that's for both design and safety analysis. Several efforts have been made to find the best approach to analyze thermal hydraulics of this type of reactors. Due to the special fluids used in such type of reactors (very low Prandtl number and very high temperatures), It is important to increase our confidence towards the currently used CFD models before using any in further analysis. In this paper one of the most common turbulence models (k-omega model) is being tested and validated for the purposes mentioned above. Experimental data were used for the validation of the model. The experimental date was observed in the TALL3D facility in KTH Stockholm [4].

II. DESCRIPTION OF TEST CASE

One of few facilities in the world used to test liquid lead systems to observe the behavior of the flow in various operational conditions is the TALL-3D facility in the Royal Institute of Technology, Stockholm, Sweden. An experiment has been performed in the facility that can be used here for the purpose of validation.

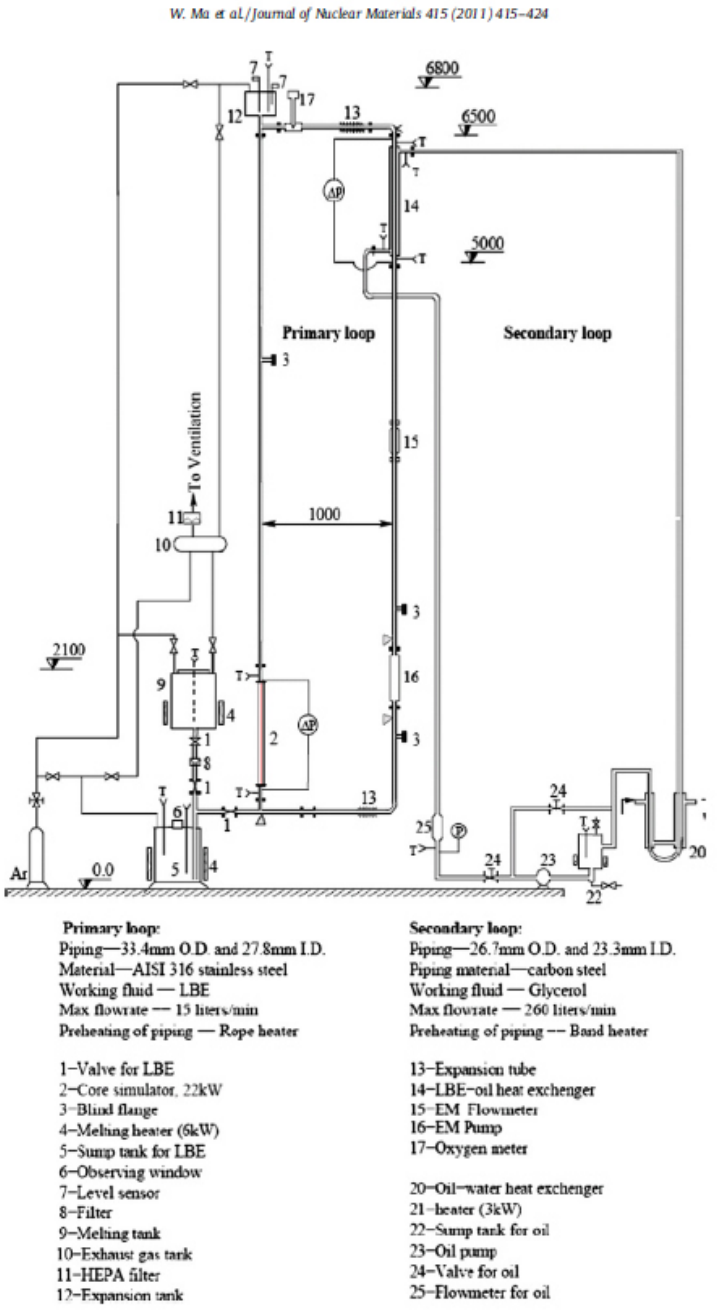

Figure 1 Schematic diagram of the TALL facility, KTH

The facility has two loops with heat exchanger between them. Liquid lead–bismuth eutectic (LBE) was used as a coolant to the primary loop while the secondary loop has glycerol oil coolant. More description can be found in [4].

The Loop has a testing section which consists of a pipe with a heater in the center along the whole testing section of 150 cm total length. The heater itself has a heating section only in 87 cm of its length located after a 60 cm length used for flow development, heater is then followed by 3 cm section as for the device constructional reasons.

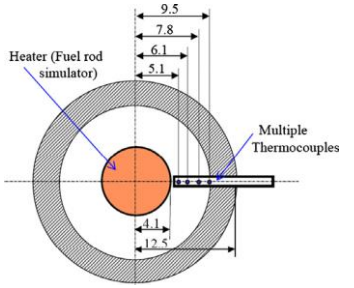

Figure 2 Positions of thermocouples in each section

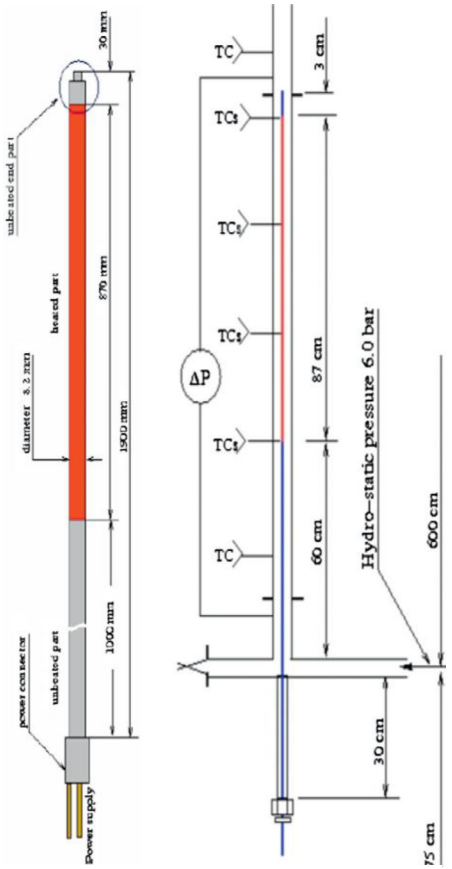

Figure 3 Testing section and thermocouple locations in the TALL facility.

The steady state experiment was set based on the nominal power of the heater, which is 21kW as a constant value, while different inlet velocities were tested (0.65, 0.93, 1.36, 1.57 and 2 m/s).

Four experimental velocities have been selected for modeling including the minimum and maximum velocities performed during the experiment corresponding to 19,000, 25,000, 45,000 and 61,000 Reynolds number respectively, have been selected for testing and Ansys fluent has been used to model the four cases using the SST k-omega model.

III. RESULTS

In the four sections temperatures were detected in four different points at different vertical plan for each section of the four sections and the average temperature was calculated for each section. The experiment was repeated for each tested velocity.

Modeling the same testing section geometry and checking the temperature in the four points in each section to follow the footsteps of the experiment for the most accurate results. See figure 2 and figure 3.

The error appeared as a difference between the SST k-omega model results and the experimental data were varying from 0% by the inlet to 3% in the second section in the tested length with highest error value corresponding to the lowest Re number. See figure 4.

Along the length of the pipe, figure 5 shows that at the highest errors were always at the beginning of the pipe, and then gradually decrease towards the exit terminal of the testing section.

One can observe that the error has the highest values in the first third of the pipe, then gradually decreasing to the end of the pipe.

The Zero error is mainly because that by the inlet of the pipe the temperature boundary condition was set to the same value in all the calculations.

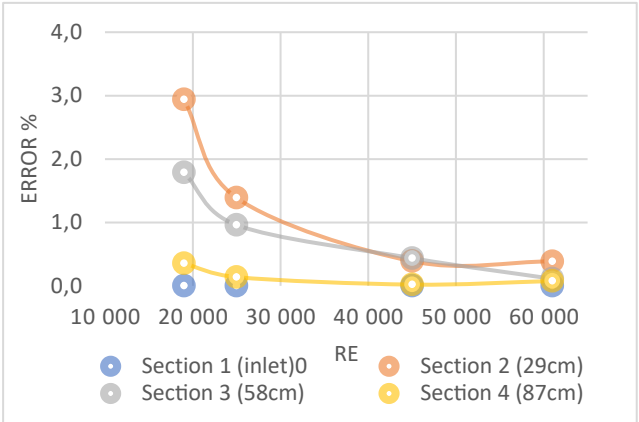

Figure 1 The change of error percentage in each section in different Re numbers

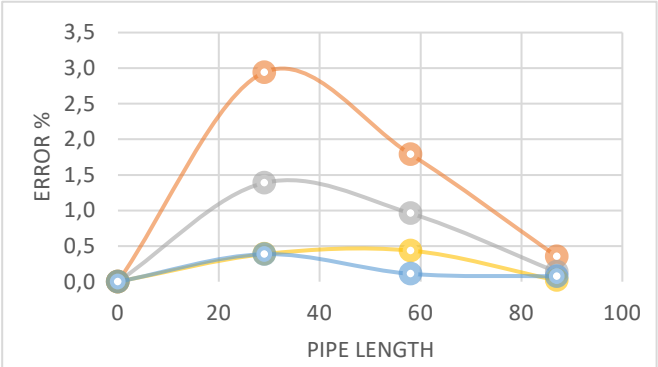

Figure 2 The change or error along the length for each tested Re number.

IV. CONCLUSIONS

The results showed that using the SST k-omega model to solve this type of flows or fluids with similar conditions can be reasonable and leads to robust results, Hence the SST k-omega model can be adopted for

further calculations for other cases having the same or similar bases.

However, the validation showed that there is a combined error clearly noticed. One part of this error is due to the developing stage of the flow. The highest error existed during the stage of flow development, however, the error decreased after that once the flow tended to be fully developed. Another part of the error is in relation to the flow velocity. The SST k-omega model showed lower error with higher Re number, on the other hand, the error tends to increase with the decrease of the Re number.

All in all, the SST k-omega model can be used in modeling the liquid metals and fluids with low Pr. But it is expected to have lower – but accepted- accuracy when it comes to low Re number flow as far as it is still considered turbulent flow.

The model needs to have further testing in more complicated geometries where the velocity of the flow changes based on the flow cross section area, for example, sudden decrease/increase in the cross-section area perpendicular to the flow direction. Another example: the changes of the flow laminas velocities due to sharp change in the flow direction which increases the sheer stress as well as the dynamic pressure irregularly within the same flow sections.

References

[1] Massachusetts Institute of Technology, *The Future of Nuclear Energy in a Carbon-Constrained World*, Revision 1. Massachusetts, 2018.

[2] "Generation IV Nuclear Reactor - an overview | ScienceDirect Topics." https://www.sciencedirect.com/topics/engineering/generation-iv-nuclear-reactor (accessed Apr. 03, 2023).

[3] A. Huke *et al.*, "Dual-fluid reactor," in *Molten Salt Reactors and Thorium Energy*, Elsevier, 2017, pp. 619–633. doi: 10.1016/B978-0-08-101126-3.00025-7.

[4] W. Ma, A. Karbojian, T. Hollands, and M. K. Koch, "Experimental and numerical study on lead-bismuth heat transfer in a fuel rod simulator," *Journal of Nuclear Materials*, vol. 415, no. 3, pp. 415–424, Aug. 2011, doi: 10.1016/j.jnucmat.2011.04.044.

Proceedings of the European Nuclear Young Generation Forum
ENYGF'23
May 8-12, 2023, Kraków, Poland

Unraveling the influence of Cr on dislocation nucleation in (011) FeNiCr alloys through nanoindentation test

Dominguez Gutierrez, F. J.[1*], Ustrzycka, A.[2], Mulewska, K[1], Xu, Q.Q.[1], Kurpaska, L[1], Papanikolaou, S[1], and Alava, M. J.[1,3]

[1]NOMATEN Centre of Excellence, National Centre for Nuclear Research, ul. A. Soltana 7, Otwock, 05-400, Poland; [2] Institute of Fundamental Technological Research, , Polish Academy of Sciences, Warsaw, Poland; [3]Department of Applied Physics, Aalto University, P.O. Box 11000, Aalto, 00076, Finland

*Corresponding author: *javier.dominguez@ncbj.gov.pl*

I. INTRODUCTION

FeNiCr alloys are typically used for their high-temperature strength and resistance to oxidation and corrosion at extreme operating conditions. They are often used in nuclear applications where harsh environments are present, such as in gas-cooled reactors or high-temperature gas-cooled reactors. These alloys have shown potential for use in extreme environments such as in new and efficient nuclear energy systems, as well as in demanding transport and construction industries [1,2]. In thermal power plants, FeNiCr alloys can be used for containers that present distortion during the process of being filled with high-level nuclear waste glass at elevated temperatures. Additionally, they can be used for manufacturing radiant tubes, thermos-wells, burners and combustion chambers, and annealing covers. Despite the high demands related to structural, mechanical and thermal properties stability at reactor environment, FeNiCr alloys are considered as an excellent candidate for applications in Generation IV - Super-Critical Water Reactors (SCWR) due to their superior corrosion resistance and high-temperature strength [3].

Nanoindentation data is commonly used to estimate plasticity properties and physical mechanisms associated with the deformation of a material and a robust computational dislocation modeling at atomistic scale is nowadays required to save financial resources for experimental trials [4-8]. Thus, large scale Molecular Dynamics (MD) simulations have proven to be a powerful tool to emulate experimental nanoindentation tests providing atomistic insights into the mechanical response of indented samples and defect mechanisms that cannot be clearly seen through Load-Displacement (L-D) curves in experiments. Furthermore, atomistic simulations can be used to study anisotropy in mechanical properties, providing a predictive tool for experiments with prohibitive technical limits and costs [7,8].

In this work, we present a combined computational and experimental study aimed at understanding the nanoscale plastic deformation mechanisms and anisotropy effects in FeNiCr alloys. We leverage electron microscopy observations of experimental indentation to develop a multiscale description, which will advance the modeling of more complex alloys.

II. COMPUTATIONAL AND EXPERIMENTAL METHODS

Atomistic computational modeling of Fe-Ni-Cr alloys is carried out based on Molecular Dynamics (MD) simulations using the Large-scale Atomic Molecular Massively Parallel Simulator (LAMMPS) [5] with interatomic potentials based on Embedded Atom Method (EAM) [6]. In this study, we generated FCC (011) Fe-Ni-Cr samples by first creating a pure FCC Fe sample with a lattice constant of 0.356 nm, followed by random substitution of Fe atoms with Ni and Cr atoms defining a numerical cell of 8 985 600 atoms with a dimension of 44.58x43.78x52.62 nm^3[7,9]. We minimized the potential energy of the structure through a series of equilibration steps to obtain a stable atomic distribution with 55% Fe, 19% Ni, and 26% Cr [9]. Next, we carried out equilibration for 100 ps with a Langevin thermostat at 300 K and a time constant of 100 fs [7-9]. This was done until the system reached a homogeneous sample temperature and pressure profile with a density of 8.0 g/cm^3[9].

To set up boundary conditions for performing nanoindentation simulations, we define three sections along the depth (*dz*): a frozen layer of atoms with a width of 0.02x*dz* for numerical stability, a thermostatic section of 0.08x*dz* to dissipate heat, and a dynamical section where the interaction of the atoms with the indenter tip modifies the surface structure. We include a 5nm vacuum region at the top of the sample as an open boundary [7-9]. The indenter tip is treated as a non-atomic repulsive imaginary rigid sphere with a force potential of $F(t) = K (r(t) - R)^2$,

where K = 236 eV/Å^3 (37.8 GPa) is the force constant, and r(t) is the position of the center of the tip as a function of time, with a radius R = 15 nm. We perform 50 simulations using the velocity Verlet algorithm with a speed of v = 20 m/s and a maximum indentation depth of 2.0nm. Each simulation is performed for 125ps with a time step of Δt = 1fs, and we randomly change the center of the indenter tip to 10 different positions for statistical significance. The x and y axes have periodic boundary conditions, while the z orientation has a fixed bottom boundary and a free top boundary in all MD simulations [7-9].

The structural analysis of the sample during nanoindentation loading was performed using the common neighbor analysis technique, which was implemented in OVITO software [?]. The analysis involved identifying the crystal structures, including FCC, BCC, HCP, and ICO, to track the stacking fault planes that formed during the test. This provided insight into the plastic deformation mechanism of the material [10].

A. Experimental nanoindentation setup

This study investigates the mechanical properties of a low carbon FeNiCr alloy known for its high-temperature corrosion resistance. Samples were polished and electro-polished to reveal grain orientation and reduce surface roughness. Nanoindentation was performed by using a NanoTest Vantage System provided by Micro Materials Ltd and utilized to measure hardness and reduced Young's modulus with different indentation loads. The Diamond Area Function (DAF) of the indenter was determined before the indentation campaign by conducting a series of indentations on a reference sample with known mechanical properties. Indentations were performed with a 20 µm distance between each indent to avoid interference of previous indents. Indentations were performed using single force mode with loads from 0.25 to 10 mN and were repeated at least 15 times at a given load. The 60 sec thermal drift measurement time at the end of each indentation cycle was recorded during the test. The methodology allowed for investigation of mechanical properties as a function of depth, taking into account the response of one grain and the cumulative effect of grains, grain boundaries, and precipitates.

III. RESULTS

The relationship between the force applied to the indenter tip and its displacement relative to the surface as it penetrates the material determines the load-displacement relationship. The load, *P*, is obtained by calculating the average of the loads obtained from different MD simulations where the indenter tip is placed at different positions on the surface. The ratio between the mean contact pressure and Young's modulus, E_Y, is shown in Fig 1 as a function of the nanoindentation strain, a/R_i, whith *a* as the contact area and Ri as the indenter tip. The ratio is calculated using a linear elastic contact mechanics formulation as [11]:

$$\frac{p}{E_Y} = \frac{2\pi}{E_Y}\left[24P\left(\frac{E_Y R}{1-\nu^2}\right)^2\right]^{1/3}$$

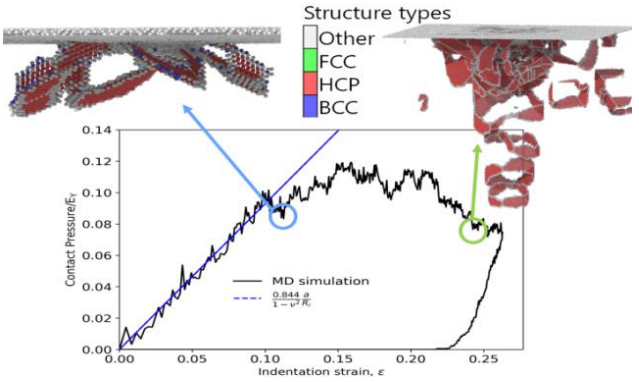

Figure 1. Average contact pressure normalized by the Young's modulus as a function of indentation strain The nucleation of material defects after the first pop-in event and the formation of prismatic dislocation loops at the maximum indentation depth are visualized and identified by different structure types.

This provides an intrinsic measure of the surface resistance to a specific defect nucleation process. The obtained results demonstrate a universal linear relationship [11]:

$$\frac{p}{E_Y} = \frac{0.844}{1-\nu^2}\frac{a}{R_i}$$

where ν is the Poisson ratio indicating that the atomic ensembles satisfy coarse-grained, linear elastic contact mechanics, and the boundary conditions do not impact the simulation dynamics. The plot also highlights the pop-in event where the contact pressure deviates from the linear geometrical fitting, triggering the first pop-in or plastic instability followed by the onset of the transitional nanoindentation regime. After the pop-in event, a pressure drop is observed, and the loading process transitions from the elastic part to the plastic deformation region.

To visualize the plastic deformation induced by nanoindentation, we examine the stacking fault nucleated at various indentation strains. Half loops oriented to the slip family planes are observed after the first pop-in event, which leads to the nucleation of prismatic dislocation loops. As the maximum indentation depth is reached, several prismatic loops are nucleated and propagate throughout the sample, characterized by stacking fault planes. The plastic region beneath the indenter tip exhibits the formation of various edge and screw dislocations, including the Shockley dislocations that are commonly found in FCC materials. To facilitate visualization, we introduce a color palette to distinguish the different types of atoms with identified structure types.

In order to validate our MD simulations, we compare to experimental observations of experimental indents obtained by scanning electron microscopy (SEM) in channeling contrast, that highlights crystal defects and orientations in a sample. It works by tilting the sample with respect to the electron beam so that the beam is aligned with specific crystallographic planes or directions. This causes the electrons to channel through the crystal in a way that is dependent on its orientation and defect structure, resulting in a contrast pattern that can be used to identify the crystal structure and defects in the sample. In Fig 2, we present results for displaced atoms at the top atomic layers of the materials at the maximum indentation depth in a)

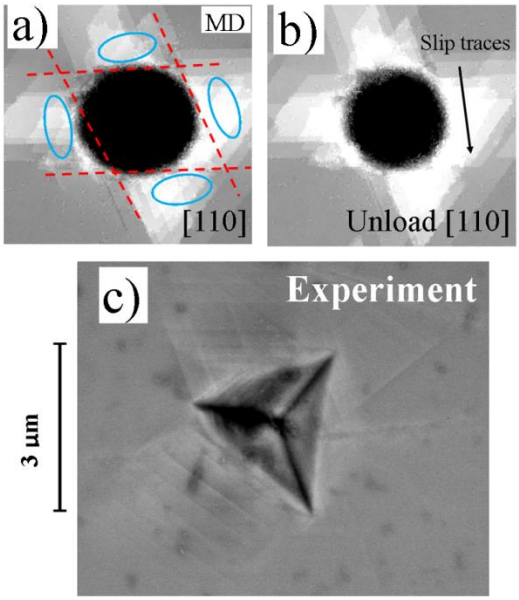

Figure 2. Displaced atoms at the top atomic layers of the material at the maximum indentation depth are shown in (a), and the same area after removing the indenter tip is shown in (b). A comparison with the SEM image is presented in (c).

and after removing the indenter tip in b), comparison to SEM image is presented in c). From our MD simulations, we can identify the typical four-folded rosette associated with the slip traces of FCC metals, as well as the identified {211} planes and symmetrical families, highlighted in Fig 2a-b) by red dashed lines. In FCC materials, {211} planes are crystallographic planes that correspond to specific directions of atomic packing, and they are commonly associated with slip planes due to their low stacking fault energy [11]. Slip on {211} planes is an important deformation mechanism in FCC materials, and it can result in dislocation slip traces that form a distinctive rosette pattern. In the SEM image, the observed slip traces are in good agreement with the numerical findings [9], confirming that the indented grain has a crystal orientation of (011) or closer to it.

IV. CONCLUDING REMARKS

In this study, we employed a combination of experimental and atomistic-based computational techniques to investigate the nanoindentation mechanisms of FeNiCr alloys. Our numerical models allowed us to simulate dislocation nucleation and dynamics at an atomistic level, resulting in excellent agreement with the trend in contact pressure and Young's modulus data obtained from experiments. We observed that the presence of Cr atoms in this type of alloy slows down the propagation of prismatic dislocation loops compared to pure Ni and FeNiCr with low concentrations of Cr [9], which we attributed to the alloy's elastic-plastic deformation transition. Our investigation revealed that the formation of dislocation loops significantly impacts the material's mechanical properties.

By characterizing the nanoindentation process and comparing our findings with experimental data, we identified prismatic dislocation loops that are mainly formed by Shockley-type dislocations and HCP structure type atoms. Our work provides insights that can inspire the design of more advanced chemically complex functional materials and contribute to a better understanding of their mechanical properties under the operating conditions of future advanced nuclear reactors.

V. Acknowledgments

We acknowledge support from the European Union Horizon 2020 research and innovation program under grant agreement no. 857470 and from the European Regional Development Fund via the Foundation for Polish Science International Research Agenda PLUS program grant No. MAB PLUS/2018/8 (L.K.,S.P., and M.A.). This work has been partially supported by the National Science Centre through the Grant No UMO-2020/38/E/ST8/00453 (F.J.D.G.,K.M., A.U.). We acknowledge the computational resources provided by the High Performance Cluster at the National Centre for Nuclear Research in Poland.

VI. References

[1] L. Malerba, “Multiscale modelling for fusion and fission materials: The M4F project,” Nucl. Materials and Energy 29, 2021, 101051.

[2] K. Lo et al., Recent developments in stainless steels, Materials Science and Engineering: R: Reports 65 (2009) 547.

[3]Oka, Yoshiaki et al., "Supercritical-pressure, Once-through Cycle Light Water Cooled Reactor Concept", Nuclear Science and Technology, 38(2001) 1081.

[4] N. Castin et al. On the equivalence of irradiation conditions on present and future facilities for fusion materials research and qualification: A computational study. J. of Nuclear Materials 562, (2022) 153589

[5] A. P. Thompson et al., Lammps - a flexible simulation tool for particle-based materials modeling at the atomic, meso, and continuum scales, Computer Physics Communications 271 (2022) 108171

[6] G. Bonny et al., Interatomic potential for studying ageing under irradiation in stainless steels: the FeNiCr model alloy, Modelling and Simulation in Materials Science and Engineering 21 (8) (2013) 085004

[7] F. Dominguez-Gutierrez et al, Nanoindentation of single crystalline Mo: Atomistic defect nucleation and thermomechanical stability, Materials Science and Engineering: A 826 (2021) 141912.

[8] L. Kurpaska et al. Effects of Fe atoms on hardening of a nickel matrix: Nanoindentation experiments and atom-scale numerical modeling, Materials & Design 217 (2022) 110639

[9] F. J. Dominguez-Gutierrez et al. Dislocation nucleation mechanisms during nanoindentation of concentrated FeNiCr alloys: unveiling the effects of Cr through molecular simulations. Modelling Simul. Mater. Sci. Eng., 30 (2022) 085010

[10] Stukowski A. Visualization and analysis of atomistic simulation data with OVITO-the Open Visualization Tool Modelling Simul. Mater. Sci. Eng., 18 (2010) 1

[11] J. Varillas et al. Unraveling deformation mechanisms around FCC and BCC nanocontacts through slip trace and pileup topography analyses Acta Mater., 125 (2017), 431

Proceedings of the European Nuclear Young Generation Forum
ENYGF'23
May 8-12, 2023, Kraków, Poland

Premixing phase in combination of melt jet breakup and premixed layer formation of melt spread

Kokalj, Janez*, Uršič, Mitja and Leskovar Matjaž

Jožef Stefan Institute (JSI), Slovenia

*Corresponding author: janez.kokalj@ijs.si

I. INTRODUCTION

During a hypothetical severe accident in a light water nuclear power plant, the molten reactor core may come in contact with the coolant water [1, 2]. The interaction between them is known as a fuel-coolant interaction (FCI). One of the consequences can be a rapid transfer of a significant part of the molten corium thermal energy to the coolant in a time scale smaller than the characteristic time of the pressure relief of the created and expanding vapour. Such a phenomenon is known as a vapour explosion [2, 3]. The process can escalate as part of the released mechanical energy enhances further fine fragmentation of the melt leading to more rapid heat transfer from the melt to the coolant. Given the possibly large amount of thermal energy, initially stored in the liquid corium melt at about 3000 K, that can potentially result in pressure peaks of the order of 100 MPa, vapour explosion can be a credible threat to the structures, systems and components inside the reactor containment [4]. It can also threaten the integrity of the reactor containment itself, which would lead to the release of radioactive material into the environment and threaten the general public safety.

The vapour explosion is commonly divided into the premixing and the explosion phase. The premixing phase covers the interaction of melt with coolant prior to vapour explosion. During this time, the continuous melt is fragmented into melt drops the size of a couple of millimetres. The melt drops and the coolant are mixed due to the density and velocity differences and also due to vapour production. If a vapour film destabilization occurs in such a system, the phenomenon is continued into a vapour explosion. The process can escalate as part of the released mechanical energy enhances further fine fragmentation of the melt leading to more rapid heat transfer from the melt to the coolant.

An important condition for the possible occurrence of strong, energetic vapour explosion and the self-sustained process of shock wave propagation is the existence of a so-called premixture of fragmented melt and coolant. In nuclear reactor safety analyses vapour explosions are primarily considered in the melt jet configuration (Figure 1) where sufficiently deep coolant pool conditions provide complete jet breakup and efficient premixture formation [5, 6]. On the other hand, stratified melt-coolant configurations, i.e. a molten corium layer below a coolant layer (Figure 2), were only recently recognized as being able to generate strong explosive interactions [7-10]. Our recent research [10] was devoted to understanding FCI in stratified configuration, especially to premixed layer formation. Namely, the previously performed experiments in the PULiMS facility (KTH, Sweden, Figure 3) with high melting temperature oxidic simulants of corium revealed that strong vapour explosions may develop spontaneously in stratified melt-coolant configuration [7, 8].

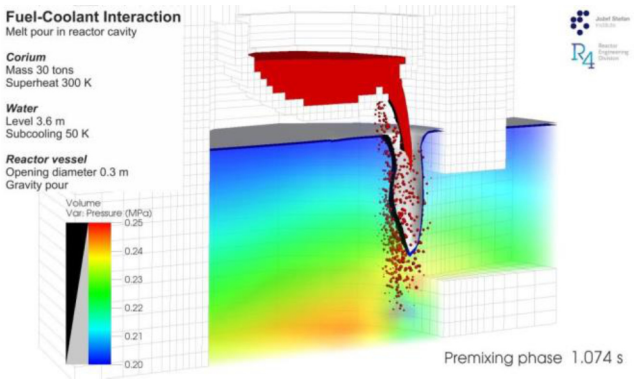

Figure 1: FCI in melt jet configuration.

Despite extensive research work, large uncertainties remain and reflect the lack of detailed understanding of the FCI processes [11]. Recently, an important safety-related uncertainty was revealed, related to the prediction of vapour explosion strength in combined stratified and melt jet configurations [10].

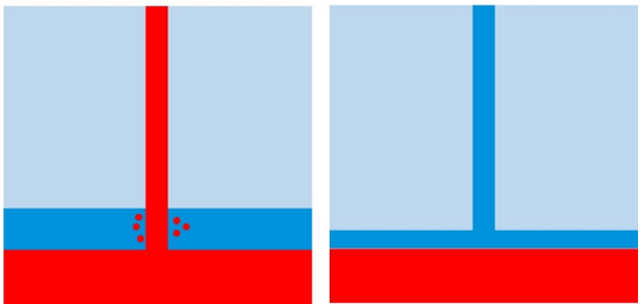

Figure 2: Possible stratified melt-coolant configuration occurrences. Red colour represents melt and darker blue water, respectively. On the left stratified geometry where poured melt jet does not break up completely in a shallow coolant pool and on the right stratified geometry where coolant is poured onto the melt.

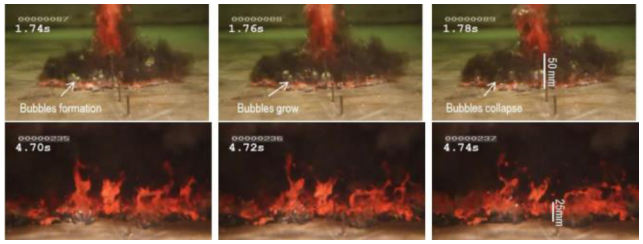

Figure 3: Melt jet and melt spreading with the formation of the premixed layer in the PULiMS-E4 experiment [8].

The observed uncertainty and lack of understanding of FCI in combined stratified and melt jet configurations have an important impact on the safety-related issue of FCI in nuclear power plants, because:

- The amount of melt in combined stratified and melt jet configurations available to participate in the explosion can be much larger than assessed before due to combined contributions of premixed layer formation in stratified melt-coolant configuration and breakup of melt jet;

- The combined stratified and melt jet configuration presents a realistic condition in e.g. nuclear power plant severe accident when the reactor cavity is only partially flooded. The possible strong vapour explosions may present an increased threat.

The objective of the paper is to analyse the possibility of modelling the melt-coolant mixing in combined stratified and melt jet configurations prior to vapour explosions, which largely defines the amount of melt, participating in the vapour explosions. Modelling, based also on the evaluation of the models for the individual phenomenon, improves the understanding of FCI.

The overview of the state-of-the-art modelling approach enables the estimation of the premixing phase in combination of melt jet breakup and premixed layer formation of melt spread, which is of high importance in nuclear safety.

II. COMBINED STRATIFIED AND MELT JET CONFIGURATION

Past research was devoted to either melt jet configuration, where the melt jet penetrates into the deep pool of coolant, or stratified configuration, where the melt is spread below the coolant. However, an intertwined configuration can be a realistic condition. If the melt is poured into the coolant pool and the coolant pool is not deep enough to provide the complete melt jet breakup, the remaining melt jet reaches the bottom and spreads. In this case, a combination of stratified and melt jet configuration can be created.

As found out, considering only the stratified configuration of spread melt under the water layer and its contribution to the mixing significantly underestimates the assessed explosion strength. In the PULiMS experiment, the melt jet, falling through the shallow, 20 cm deep pool of water created also additional mixing of melt and coolant and created a combined stratified and melt jet configuration [10].

A. Melt jet breakup

During a melt jet breakup, multiple phenomena occur simultaneously [12]. Interfacial instabilities, liquid entrainment and stripping from the interface are hydrodynamic interactions while the thermal interactions are coolant boiling and solidification of the melt surface. Jet breakup is characterized by the melt jet breakup length and melt jet breakup mode [13].

Two correlations are generally used for the melt jet breakup length. The Epstein and Fauske model (Eq. 1) [14] depends on the material properties (index j and c stand for jet and coolant, respectively) and jet diameter (D_j), with E_0 being the so-called entrainment coefficient:

$$\frac{L_{brk}}{D_j} = \frac{1}{2E_0}\sqrt{\frac{\rho_j}{\rho_c}}\,. \tag{1}$$

More widely used is the correlation by Saito (Eq. 2 and Figure 4) [15], which depends on the material properties, velocity of the melt jet (Fr is a Froude number) and its diameter:

$$\frac{L_{brk}}{D_j} = 2.1\sqrt{\frac{\rho_j}{\rho_c}}\cdot\sqrt{Fr}\,, \tag{2}$$

$$Fr = \frac{v^2}{gD_j}\,. \tag{3}$$

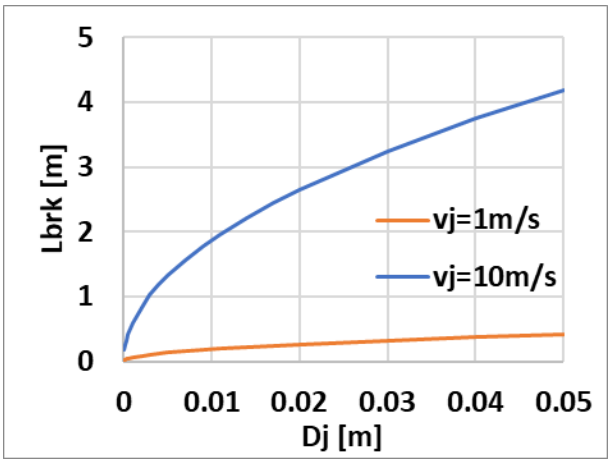

Figure 4: Illustration of the melt jet breakup length with Saito correlation for different melt jet diameters for arbitrary velocities v_j = 1 m/s and v_j = 10 m/s (with material properties ρ_j = 7800 kg/m3, ρ_c = 1000 kg/m^3,).

For the melt jet breakup mode, the initial transient of the melt jet penetration into coolant is usually related to Rayleigh-Taylor instability, while the Kelvin-Helmholtz

instability is considered for the quasi-steady regime of melt jet breakup [13]. With those models, fragmentation and melt drop size are determined according to the local conditions. Possible further breakup of the melt drops is usually modelled with consideration of the critical Weber number.

B. Melt pool fragmentation

If the melt jet breakup is not complete, the remaining melt reaches the bottom and spreads out, creating a melt pool.

The amount of melt, which does not undergo melt jet breakup can be assessed based on the breakup length, e.g. the Saito correlation, and the depth of the water pool (Figure 5).

The melt jet reaching the bottom of the test section and spreading out was clearly observed in the PULiMS experiments (Figure 3) and some other experiments [16].

The melt spreading was experimentally studied, e.g. at facilities BNL (USA), SPREAD (Japan), CORINE (France), VULCANO (France), KATS (Germany), COMAS (Germany), ISPRA (EU JRC), S3E (Sweden) [17]. Currently, from 2019 to 2024, the OECD ROSAU (Reduction Of Severe Accident Uncertainties) programme is aiming to reduce knowledge gaps and uncertainties associated with severe accident progression. Two main research areas are the spreading of melt in a cavity and in-core and the ex-core debris coolability with planned experiments at the Argonne National Laboratory (USA) with up to 300 kg of molten prototypical corium material at temperatures up to 2400 °C.

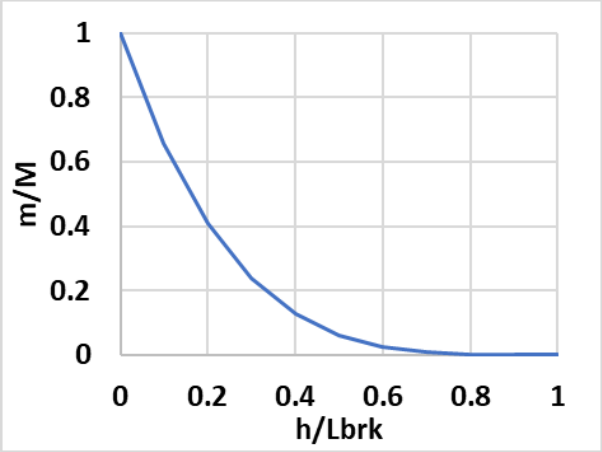

Figure 5: Amount of the initial melt jet which does not undergo breakup at a certain depth h of water compared to the melt jet breakup length L_{brk}.

As discussed by Dinh et al. [17], who were studying melt spreading at the macroscopic scale, melt spreading can be described as a hydrodynamic process. The spreading is governed by the gravitational, inertial and viscous forces. It can be divided into the gravity-viscous regime, in which viscosity plays a dominant role, while in the gravity-inertia regime, the influence of the melt viscosity may be neglected. The surface tension has an effect only for very low velocities of melt spreading. When the melt is spreading under a coolant, their interactions may influence the spreading as well [17].

The melt spreading can be terminated by melt solidification. The melt solidification during the spreading is affected by heat transfer from the melt to the structures and coolant, possible heat generation and the melt solidification behaviour [17].

The melt-coolant interaction of the melt pool under the layer of coolant is described by the model for premixed layer formation in stratified fuel-coolant configuration [10]. In geometry with a continuous layer of melt under a layer of water, called stratified configuration, the melt is usually hot enough for the coolant to vaporize. Due to the instabilities, the bubbles arise from the vapour film. In subcooled water, bubbles condense and collapse. During the asymmetric bubble collapse, water at the bubble interface accelerates towards the melt surface, creating a so-called coolant micro-jet. The pressure perturbations on the melt surface, usually due to the vaporization of the coolant micro-jets can produce the melt surface instabilities and fragmentation of the melt. This phenomenon is the so-called premixed layer formation of melt drops in the coolant layer above the melt pool. The model describes the premixed layer formation with three key characteristics, i.e. size of ejected melt drops, their initial velocity and the fragmentation rate of the continuous melt phase [8].

III. DISCUSSION AND CONCLUSIONS

Using only the model for the premixed layer formation in stratified configuration for the experiments in at least partially combined configuration of melt jet and underwater melt pool underestimates the strength of the produced vapour explosions. The possible explanation was an inadequate amount of premixing due to considering only one contribution.

This highlights the need for more complex modelling of FCI in combined configuration of melt jet and underwater melt pool. Our proposed approach is based on the modelling of the melt-coolant premixing because of the melt jet breakup and because of the premixed layer formation in stratified melt-coolant configuration.

During the melt jet breakup, multiple phenomena occur simultaneously, creating a mixture of fragmented melt jet and coolant. The melt jet breakup length indicates how much jet has been broken up at a certain coolant depth and whether there is a possibility for the combined configuration. The melt jet breakup mode describes the produced fragments.

The unfragmented melt jet reaches the bottom and spreads out. Based on the previous analysis of FCI in a stratified configuration only, a large effect on the strength of the potential vapour explosion has the surface area of the melt pool. Therefore, the accurate assessment of the spread melt is of high importance for the reliable assessment of the contribution of the premixed layer above the melt pool to the total premixing.

Only considering both the above contributions for the premixing could result in a more reliable assessment of vapour explosions in combined configuration of melt jet and underwater melt pool. However, the FCI phenomena are in general very complex. A more precise calculation of a vapour explosion, which is of high significance for nuclear safety, would be possible only by using dedicated computer codes.

IV. Acknowledgments

The authors gratefully acknowledge financial support provided by Slovenian Research Agency, grants P2-0026, Z2-4437 and L2-1828.

V. References

[1] M. L. Corradini, B. J. Kim, and M. D. Oh, "Vapor explosions in light water reactors: a review of theory and modeling," *Progress in Nuclear Energy,* vol. 22, no. 1, pp. 1-117, 1988.

[2] B. R. Seghal, B. R. Seghal, Ed. *Nuclear Safety in Light Water Reactors: Severe Accident Phenomenology*. Elsevier Inc, 2012.

[3] G. Berthoud, "Vapor explosions," *Annual Review of Fluid Mechanics,* vol. 32, no. 1, pp. 573-611, 2000.

[4] M. Leskovar and M. Uršič, "Estimation of ex-vessel steam explosion pressure loads," *Nuclear Engineering and Design,* vol. 239, no. 11, pp. 2444-2458, 2009.

[5] S.-W. Hong, P. Piluso, and M. Leskovar, "Status of the OECD-SERENA project for the resolution of ex-vessel steam explosion risks," *Journal of Energy and Power Engineering,* vol. 7, no. 3, p. 423, 2013.

[6] M. Leskovar and M. Uršič, "Analysis of PWR ex-vessel steam explosion for axial and side melt release," *Nuclear Engineering and Design,* vol. 283, pp. 40-50, 2015.

[7] P. Kudinov, D. Grishchenko, A. Konovalenko, and A. Karbojian, "Premixing and steam explosion phenomena in the tests with stratified melt-coolant configuration and binary oxidic melt simulant materials," *Nuclear Engineering and Design,* vol. 314, pp. 182-197, 4/1/ 2017.

[8] A. Konovalenko, A. Karbojian, and P. Kudinov, "Experimental results on pouring and underwater liquid melt spreading and energetic melt-coolant interaction," in *The 9th International Topical Meeting on Nuclear Thermal-Hydraulics, Operation and Safety*, Kaohsiung, Taiwan, 2012, p. 11: American Nuclear Society.

[9] M. Leskovar, V. Centrih, M. Uršič, and J. Kokalj, "Investigation of steam explosion duration in stratified configuration," *Nuclear Engineering and Design,* vol. 353, p. 110233, 2019.

[10] J. Kokalj, M. Uršič, and M. Leskovar, "Modelling of premixed layer formation in stratified fuel–coolant configuration," *Nuclear Engineering and Design,* vol. 378, pp. 111261-111277, 2021.

[11] C. Peng, "Influence of coupled factors on premixing and fragmentation of mild thermal interaction," *Annals of Nuclear Energy,* vol. 160, p. 108394, 2021/09/15/ 2021.

[12] L. Manickam, S. Bechta, and W. Ma, "On the fragmentation characteristics of melt jets quenched in water," *International Journal of Multiphase Flow,* vol. 91, pp. 262-275, 2017/05/01/ 2017.

[13] P. Kudinov and M. Davydov, "Development and validation of conservative-mechanistic and best estimate approaches to quantifying mass fractions of agglomerated debris," *Nuclear Engineering and Design,* vol. 262, pp. 452-461, 2013/09/01/ 2013.

[14] M. Epstein and H. K. Fauske, "Applications of the turbulent entrainment assumption to immiscible gas-liquid and liquid-liquid systems," *Journal of Chemical Engineering Research,* vol. 79, no. 4, pp. 453-462, 2001.

[15] M. Saito, K. Sato, and S. Imahori, "Experimental study on penetration behaviors of water jet into freon-11 and liquid nitrogen," in *ANS-Proc. 25th Natl. Heat Transfer Conf.*, 1988, pp. 173-183.

[16] D. Magallon, "Characteristics of corium debris bed generated in large-scale fuel-coolant interaction experiments," *Nuclear Engineering and Design,* vol. 236, no. 19, pp. 1998-2009, 2006/10/01/ 2006.

[17] T. N. Dinh, M. J. Konovalikhin, and B. R. Sehgal, "Core melt spreading on a reactor containment floor," *Progress in Nuclear Energy,* vol. 36, no. 4, pp. 405-468, 2000/01/01/ 2000.

Proceedings of the European Nuclear Young Generation Forum
ENYGF'23
May 8-12, 2023, Kraków, Poland

Application of the Source-Jerk Method Using a Neutron Generator at VR-1 Reactor

Mátl, Jakub[1], Rataj, Jan[1]

[1] Czech Technical University in Prague, Czech Republic

*Corresponding author: *matljaku@cvut.cz*

I. INTRODUCTION

Reactivity is one of the main operating parameters of the nuclear reactor. Therefore, it is important to continuously improve various methods of reactivity measurement and determination. The ability to obtain reactivity is essential for reactor control and maintaining a fission chain reaction.

Main experimental methods of reactivity measurement used at the VR-1 research reactor are Source-Jerk (SJ) and Rod-Drop (RD). Both methods are based on perturbation of the neutron population by dropping the control rod (RD) or sudden source removal (SJ).

The Source-Jerk method was developed in 1955 by J. O. Keppler and R. G. Givens with the following development of the Rod-Drop method. The SJ and RD methods were developed in response to the need for accurate and reliable reactivity measurement methods. Prior to these techniques, reactivity measurements were performed using manual control rods or other coarse methods. Both SJ and RD methods were later found to be highly accurate and provided a direct measurement of reactor reactivity [3].

The main theme of this work was application of the Source-Jerk method using a neutron D-D generator and its comparison with results obtained via the Source-Jerk method using a radionuclide Americium-Beryllium (AmBe) source. Unlike the first neutron source, the latter one is commonly used for SJ and RD (at VR-1 reactor).

The outcome of this study may help to optimise the reactivity measurement on the new subcritical assembly VR-2, which is currently being built.

II. SOURCE-JERK METHOD

The default assumption of the SJ method is a subcritical core driven by an external continuous neutron source. The reactor power remains constant. In time $t = 0$, the neutron source is removed, and the neutron population begins to drop. The reactivity in β_{eff} is given by Eq.*(1)*

$$\rho(\beta_{eff}) = \frac{n_0}{\int_0^\infty n(t)dt}\left[\frac{1}{\beta_{eff}}\sum_{i=1}^{8}\frac{\beta_{eff,i}}{\lambda_i} + \frac{\Lambda}{\beta_{eff}}\right], \quad (1)$$

where

- n_0 is neutron density before source removal,
- λ_i, β_{eff} and β_{eff} are kinetic parameters,
- Λ is the prompt neutron generation time.

Eight groups of delayed neutrons were considered. For experimental applications, $n(t)$ would be proportional to the detector count rate and the equation can be simplified into

$$\rho(\beta_{eff}) = \frac{n_0 - n_b}{\int_0^{300} n(t) - n_b\, dt}\left[\frac{1}{\beta_{eff}}\sum_{i=1}^{8}\frac{\beta_{eff,i}}{\lambda_i}\right], \quad (2)$$

where n_b is the background detector count rate [2]. This formula was used to measure the reactivity in this work. The kinetic parameters were determined using the Serpent2 code.

III. DESCRIPTION OF THE EXPERIMENT

The main goal of the experiment was to study the advantages and disadvantages of the D-D neutron application for the Source-Jerk method.

The whole experiment was carried out on the VR-1 reactor in shutdown mode ($\rho \approx -10\,\beta_{eff}$). Boron detectors SNM-10 and fission operational power measurement (PMV) detectors (fission chambers) were used to obtain $n(t)$. The D-D neutron generator P-385 was placed into the radial channel of the reactor and the detectors were inserted into the centre of the core at various positions (boron detectors are portable; fission chambers are in-core fixed) [1].

The application of the Source-Jerk method proceeded as follows. First, the average detection count rate before source removal n_0 was measured for 300 s. After the removal of the source, the integral $\int_0^{300} n(t)dt$ was determined using numerical integration (trapezoidal rule) and lastly, the mean value of n_B was measured (also averaged for 300 s). The same practise was used for the AmBe source. The boron detectors were set to 2 different vertical positions - to the centre of the core (position S) and to the upper edge of the core (position V) [1].

The experiment was divided into two parts.

A. Preparatory Experiment

The goal was to optimise the vertical positions of the detectors and to compare the results using both neutron sources. Since the reactor was significantly subcritical, the detector count rate in position V was low and fluctuated. This caused a high observational error of measurement and complicated the integral evaluation. Therefore, the S position was set to default. The use of neutron D-D generator caused the count rate to be roughly 2 times higher, resulting in a lower observational error. This is simply because of the generator higher emission rate. The following figures illustrate the detector count rates for different neutron sources and vertical positions [1].

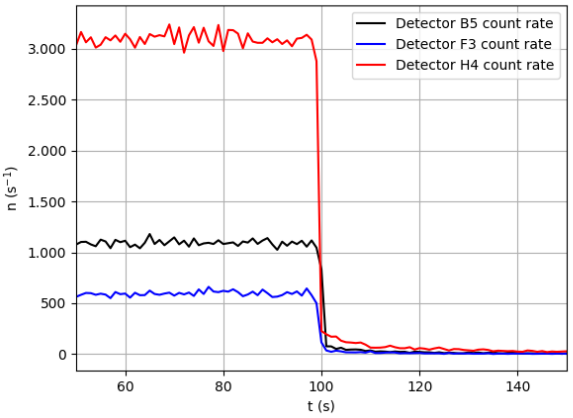

Figure 1. Boron detector count rate - D-D generator – position S.

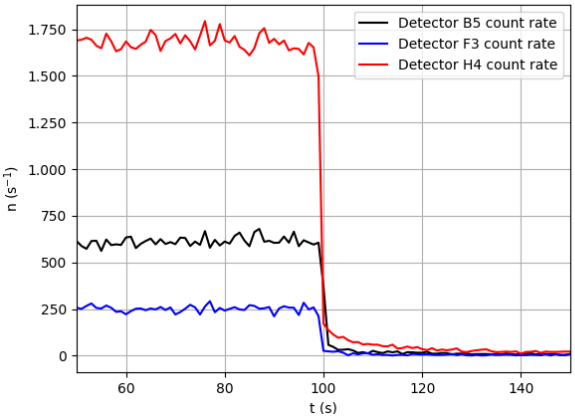

Figure 2. Boron detector count rate - AmBe source – position S.

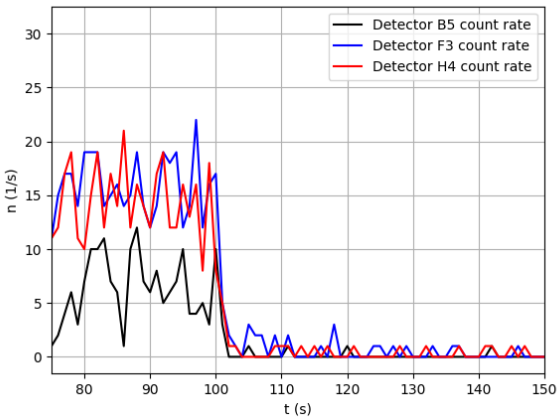

Figure 3.. Boron detector count rate - D-D generator - position V.

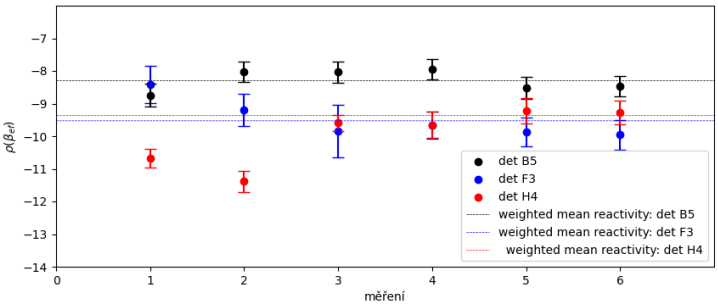

Figure 4. Reactivities obtained from boron detectors & D-D generator - time step 1 s.

B. Main Experiment

The purpose of the main experiment was to obtain enough consistent reactivity values to compare both neutron sources. The results showed that time optimisation of the neutron detection time step can lead to consistent quality results. The time step was set to 1 s and 0,1 s. Both the D-D generator and the AmBe source were used as neutron sources. The results were compared with the reactivity calculated using the Serpent2 code.

As can be seen in Fig. 4, the time step 1 s leads to random deviations in reactivity caused by insufficient determination of the neutron source removal time. Since the count rate drop in 1 s is significant, the results may differ in more than 1,5 β_{eff}. This problem was solved by reducing the time step to 0,1 s (lowest reasonable time step). Although the observational error was slightly higher, the results with the neutron generator were more consistent.

On the other hand, the error with the AmBe source was still significant. The comparison can be seen in Pic. 5 & 6, where results from one of the detectors are presented [1].

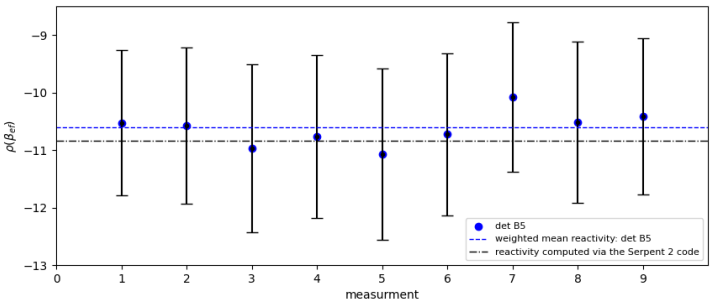

Figure 5. Reactivities obtained from boron detector B5 & D-D generator – time step 0,1 s.

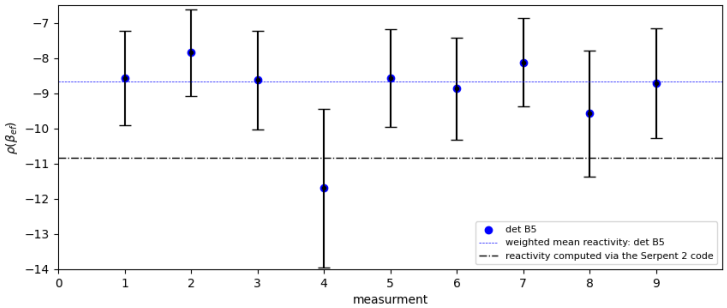

Figure 6. Reactivities obtained from boron detector B5 & AmBe source – time step 0,1 s.

IV. RESULTS

Fig. 7 & 8 illustrate the obtained reactivities from the main experiment using different neutron sources and detector positions. The thermal flux distribution through the VR-1 reactor core was obtained using the Serpent2 code. The positions of the control rods and the fuel can be easily recognised. Using this computer calculation and measurement results, it was possible to compare the spatial flux distribution and the obtained reactivities.

V. CONCLUSION

The experiment showed several interesting facts about the Source-Jerk method and its applicability using a neutron generator.

The first observation is that detector count rate with neutron D-D generator is several times higher than with the count rate with AmBe source. As was said before, this is caused by higher emission rate of the generator. This leads to lower observational error. Another observation has already been mentioned in the section before, and that is the insufficient determination of source removal time. This incapability of exact time of source removal determination is caused by long measurement time step. In the neutron generator case, the shortening of the time step led to better and more consistent results [1].

Interesting fact is the strong spatial dependence when using the generator compared to the AmBe source. Figs. 7 & 8 illustrate the spatial dependence showing the thermal

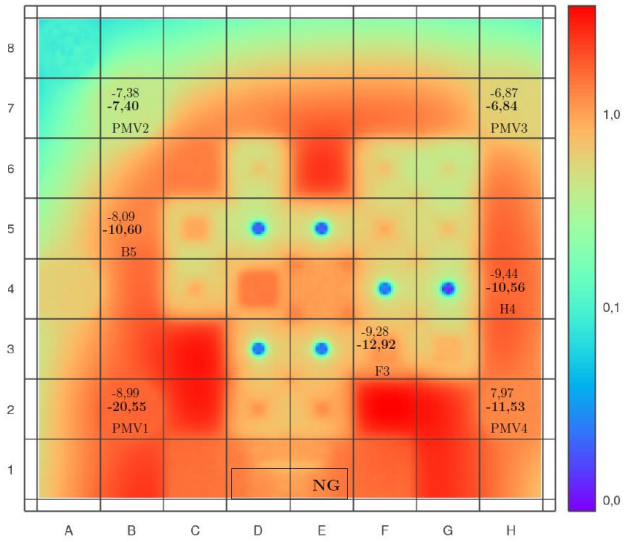

Figure 7. Neutron flux distribution & reactivities – D-D generator

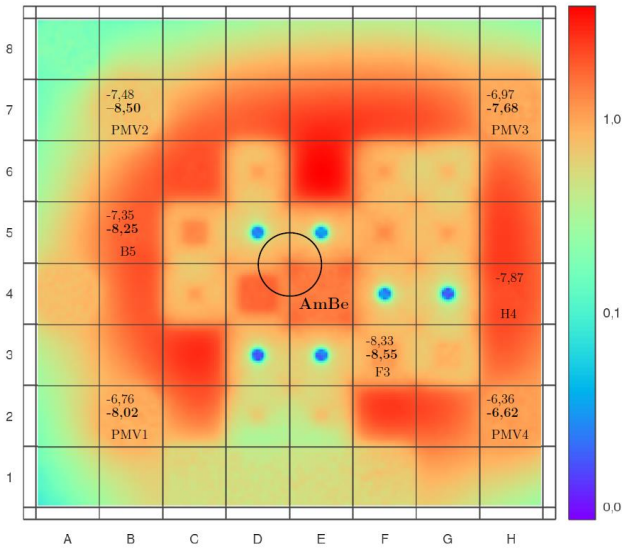

Figure 8. Neutron flux distribution & reactivities - AmBe source

neutron flux distribution in the core with measured $\rho(\beta_{eff})$ [1].

This uneven neutron flux distribution is mainly caused by the location of the source. While the AmBe neutron source is centred under the reactor vessel, the neutron generator is placed in the radial channel. This leads to an uneven neutron flux distribution, which causes different results of the Source-Jerk method depending on the position of the detector [1].

Another relevant fact is that the use of AmBe radionuclide as a neutron source caused an overestimation of the integral $\int_0^\infty n(t)dt$, which led to overestimation of reactivity. The incorrect integral evaluation was caused by the time required to remove the source. When switched on, the AmBe source is pushed through the guide tube right under the reactor core. When switched off, it takes about 0,7 s for the source to get back to the shielding box, while the radionuclide source is still emitting neutrons. This

means that the detector count after removal is overestimated. The average time for the neutron generator to turn off is in microseconds. This shows that the source removal time should be insignificant compared to measurement time step [1].

In the thesis [1], the possible usage of correction factor is discussed. This correction might help to acquire precise reactivity values with smaller spatial dependence. This correction factor would need to take into consideration the time delay of the AmBe source and should change the obtained reactivity value, so that it corresponds to reality. This correction factor would have to be estimated experimentally and might differ for each active core configuration. This might lead to even more precise and consistent reactivity measurement method. [1].

Overall, the application of the Source-Jerk method using a neutron generator with time step 100 ms has proven to be more consistent and more realistic than the usage of the AmBe source. This is mainly due to the optimisation of the time steps and the reduction of the removal time of the source. The determination of the neutron source removal time was more precise. However, spatial dependence may lead to inaccurate results. Therefore, it is more than appropriate to choose the right detector/neutron source position to get the flux distribution as uniform as possible [1].

I. References

[1] J. Mátl, "Application of the Source-Jerk Method Using a Neutron Generator at the VR-1 Reactor," DNR, FNSPE, CTU in Prague, Prague, Czech Republic, 2022.

[2] J. Rataj et al., "Experimentální neutronová a reaktorová fyzika: laboratorní cvičení," CTU in Prague, Prague, 2016, ISBN 9788001059043;8001059049.

[3] James J. Duderstadt, and Luis J. Hamilton, "Nuclear reactor análisis", Wiley, 1976.

Proceedings of the European Nuclear Young Generation Forum
ENYGF'23
May 8-12, 2023, Kraków, Poland

Amplification of HOH carrying orbital angular momentum in plasma-based amplifiers

López, Santiago[1,2*], Oliva, Eduardo[1,2], Alonso, Agustín[1,2] and De la Fuente, Elena[1,2]

[1] Universidad Politécnica de Madrid, Spain; [2] Instituto de Fusión Nuclear "Guillermo Velarde", Spain

*Corresponding author: *s.lopezg@alumnos.upm.es*

I. INTRODUCTION

Today, laser technology is as ubiquitous as the designs developed are diverse, from state-of-the-art facilities like LIGO for detecting gravitational waves to devices like the DVD. The main reason for this is the set of properties that lasers have that distinguish them from other sources of radiation. For instance, they achieve very high levels of coherence, directionality and monochromaticity. The combination of all these properties makes it possible to concentrate energy in a very short time (femtoseconds) reaching powers of up to one petawatt on very small areas (square micrometres).

Electromagnetic radiation not only carries energy, but also momentum. It can be distinguished between two contributions, linear momentum and angular momentum. Regarding angular momentum, it can again be separated into two parts: one due to polarization, known as spin angular momentum (SAM), and another that is a consequence of spatial distribution, called orbital angular momentum (OAM), a property that is as relatively novel [1] as it is clearly revolutionary. During the last 30 years, it has enabled the development of highly innovative applications, such as new coding systems [2], astrophysics techniques [3] or obtaining DNA biomolecules [4]. An example of a beam with OAM are the Laguerre-Gauss modes ($LG_{l,p}$), used in this project.

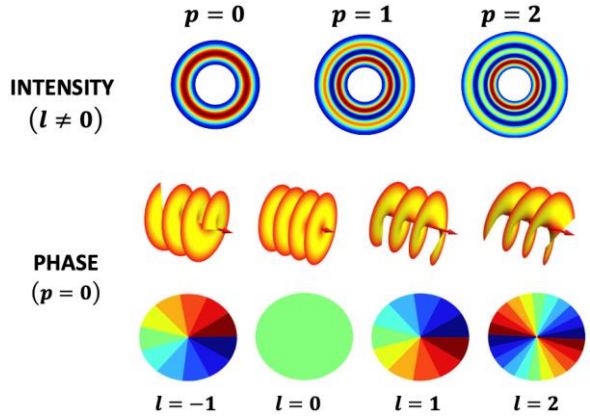

Figure 1. Intensity (up) and phase (down) Laguerre-Gauss modes [5]

On the other hand, there is currently a great interest in transposing all these properties to shorter wavelengths, such as extreme ultraviolet (XUV) or soft X-rays. Currently, free electron lasers (FEL) are the XUV sources that achieve the best performance, but their uniqueness and cost have led to the search for more compact sources. One of the most promising alternatives arises from the combination of other available sources that, by themselves, do not reach the FEL parameters. In this case, it is the injection of high order harmonics (HOH), with excellent optical properties, into krypton amplifying plasmas, capable of reaching high energies ([7], [8]).

Considering the multiple existing – and possibly future – applications related to HOHs, plasma-based X-ray lasers, and OAM itself, it is certainly attractive to combine them into a joint system. As a result, this research arises from the coupling between these concepts, whose main objective is to determine how the phenomenon of propagation and amplification in a plasma affects an OAM beam. The characterization of this property at the plasma outlet is essential for the development of possible applications, such as plasma diagnosis.

However, the scope of this work does not end here, but is more ambitious. Currently, the use of dense plasmas constitutes a strategy to increase the energy of the resulting pulses, keeping the duration below the picosecond. It is natural to consider then whether the conclusions obtained in low-density gaseous plasmas can be extrapolated to this type of systems. For this reason, the density of the plasma has been progressively increased.

II. METHODOLOGY

For this work, a methodology has been developed that, although it is true that it is based on already existing concepts, its novelty lies in how these concepts have become complementary tools to give rise to a complete, clear, and easily applicable procedure. This methodology is also unique because it allows *ab initio* simulations of the entire 4D system (spatial 3D, temporal 1D), based on the resolution of the Maxwell-Bloch equations in the Dagon code ([9], [10]). It is important to highlight here that the

studied system supposes a multiscale and multi-physics problem, and the computational structure necessary for its simulation, with the coupling of several additional codes, can be consulted in [11].

A. Maxwell-Bloch equations

The advantage provided by the Maxwell-Bloch formalism is the possibility of getting information about aspects such as the temporal dynamics of the pulse or the evolution of the OAM. It is based on the coupling of Maxwell's equations for the electromagnetic field with a quantum mechanical model (Bloch's equations) for the calculation of the elements of the density matrix of a system with two energy levels ([12], [13]). In this way, the starting point could be considered the wave equation for the electric field in a neutral plasma, within the paradigm of the paraxial approximation [14] and the slowly varying envelope [15], namely:

$$\frac{\partial E_{\pm}}{\partial t} \pm c\frac{\partial E_{\pm}}{\partial z} = i\frac{c^2}{2\omega}\nabla_{\perp}^2 E_{\pm} + \frac{i\omega}{2}\left[\mu_0 c^2 P_{\pm} - \left(\frac{\omega_{pe}}{\omega}\right)^2 E_{\pm}\right] \quad (1)$$

where $E_{\pm}$ is the electric field and $P_{\pm}$ is the polarization. This notation refers to the propagation of waves forward (positive direction) and backward (negative direction) in the direction of the z axis, respectively. For its part, ω_{pe} is the frequency of the plasma and ω that of the injected HOH; ε_0 and μ_0 are respectively the permittivity and permeability of the vacuum and $\nabla_{\perp}^2$ is the transverse Laplacian.

To calculate the polarization, a constitutive relation derived from the non-diagonal term of the density matrix can be obtained for a two-level system, such that:

$$\frac{\partial P_{\pm}}{\partial t} = \Gamma - \gamma P_{\pm} - \frac{i d_{21}^2}{\hbar} E_{\pm}(N_2 - N_1) \quad (2)$$

where γ is the rate of depolarization due to ion collisions with free electrons, providing the characteristic time of variation of the polarization; d_{21} is the corresponding non-diagonal element of the dipole matrix; $N_{1,2}$ are the populations of the levels; and Γ represents the stochastic source term associated with spontaneous emission (ASE).

Finally, the populations are calculated from standard rate equations coupled with the electric field, such that:

$$\frac{\partial N_{1,2}}{\partial t} = \sum_k C_{k_2,k_1} N_k \mp Im(E_{\pm}^* P_{\pm})\frac{1}{2\hbar} \quad (3)$$

where the coefficients C_{ij} comprise the collisional (de)excitation rates and the radiative de-excitation rates.

B. Field analysis

The resulting field has been analyzed from two points of view.

Considering potential experimental concerns, aspects such as energy or duration have been characterized, and integrated variables have been computed over the entire pulse (instead of observing specific points). Moreover, the field was propagated at a certain distance from the plasma output to simulate a laboratory detection. Finally, not only ideal, analytical seeds were used, but also experimental data were taken as input harmonics.

On the other hand, OAM was quantified using the decomposition of the output pulse into its helical components and its radial distribution, as well as its decomposition into Laguerre-Gauss modes [16]. This tool is very powerful because it allows to see which and where each mode is dominant, above the noise induced by amplification and ASE.

In addition, an innovative feature resides in how complementary simulations have been proposed to verify some of these tools or to improve the understanding of the initial results. In this way, aspects such as the electronic density profile, the energy and size of the harmonics, or the group velocity of the infrared that precedes the harmonic and generates the plasma have been modified.

Finally, to explain the obtained results, with complex intensity and phase patterns, an interference method was developed where the final field is explained as the sum of the amplified harmonic and the spontaneous emission

III. RESULTS

To assess OAM conservation, the 25th harmonic of an infrared laser – with an energy of 1 nJ and a duration of 10^{-15}s (FWHM) – has been injected into a plasma of Kr^{8+} (gas) of density $9.88 \times 10^{17}\,cm^{-3}$. This harmonic consists of a Laguerre-Gauss beam with $p = 0$ (one ring) and $l = 25$ (25 phase jumps), as shown in Figure 3 (up).

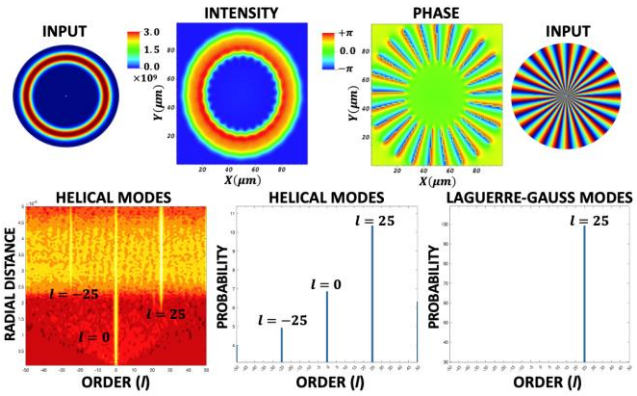

Figure 3. Left to right. Up: input intensity (Wcm-2), output intensity and phase, input phase. Down: helical mode radial distribution and decomposition, and Laguerre-Gauss mode decomposition

For the evaluation of the output pulse, parameters such as energy have been calculated, demonstrating the amplification by a factor greater than 500, or the duration, with a dilation by a factor of 20, and the characteristic oscillatory structure of the pulse has been verified, known as Rabi oscillations. They arise from the fluctuation of the population between the atomic levels involved in the laser transition of interest [17]. These features are displayed in Figure 4.

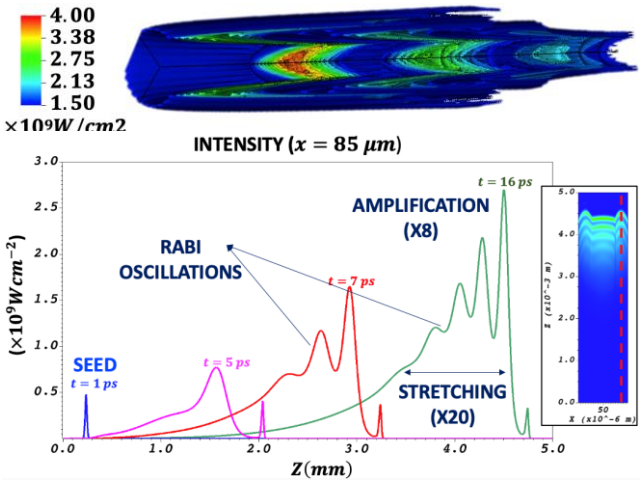

Figure 4. Up: 3D intensity structure of the seed pulse after 16 ps. Down: Evolution of the seed pulse inside a plasma amplifier.

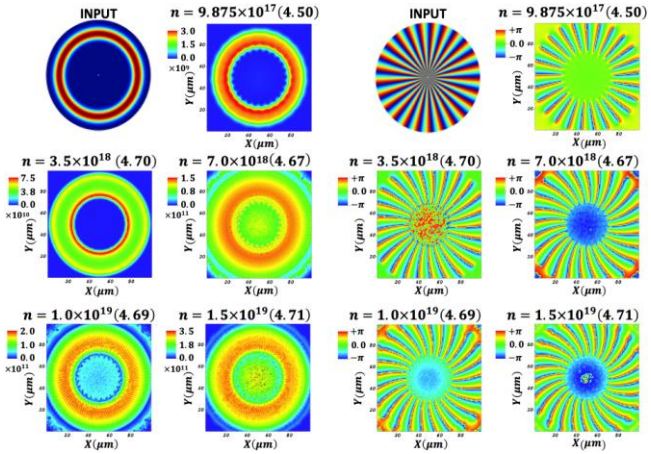

Figure 5. Intensity (left) and phase (right) at intensity maximums. Intensity is in Wcm-2, density in cm-3 and 'z' position in mm (in brackets).

On the other hand, in relation to the OAM, cross-section graphs and analysis of the output beam (Figure 3) reveal the conservation of the initial OAM, with the 25th harmonic dominance. However, this only occurs in an annulus-shaped area, because in those regions where the initial intensity of the harmonic decays notably, such as the central zone or the corners of the domain, the mode that prevails is the one corresponding to $l = 0$, associated with the ASE and not with the injected harmonic itself. This contribution could be understood as "noise" of the signal. It is precisely the contribution of this noise that causes the ripples in the inner and outer ring of the intensity, which has been verified with the interference model. In addition, both the integrated magnitudes (intensity and phase) and the propagation of the field at 1 meter, do not show notable changes in these aspects. The same can be applied to the experimental seed.

As previously mentioned, the study has been extended to higher density plasmas, up to a maximum of $1.5 \times 10^{19}\mathrm{cm}^{-3}$, due to the possibility of obtaining more energetic pulses. Thus, Figure 5 shows the changes in the intensity and phase distribution with increasing density. Regarding OAM, although the 25 phase jumps are preserved, the lines that delimit these changes begin to acquire curvature. From the interference model already mentioned, it has been verified that this phenomenon is due to the increase in the magnitude of the electron density gradients and their direction, thus inducing the refraction of the beam. For its part, in addition to increasing progressively with density, the intensity now shows a more complex pattern, which is a consequence of the greater contribution of the ASE and the different propagation speeds between the beam that heats the plasma and the harmonic beam. The first, in the infrared and therefore affected to a greater extent by the increase in density, is reached by the second, in the XUV region of the spectrum, in which the plasma slightly affects its speed.

Finally, given the interest in a scheme such as a waveguide [18], this study has been extended to plasmas with a density profile of this type (Figure 6 left), with a lower density central channel. Although again it can be affirmed the conservation of the OAM, what is interesting in this case is the clear imprint that the shape of the density profile leaves in the resulting phase (Figure 6 right). For example, changes in the direction of the gradient, such as at the edge of the channel, cause a reversal in the curvature of the phase. Although in-depth studies are required in this regard, this allows considering the use of OAM beams for applications related to the diagnosis of plasmas.

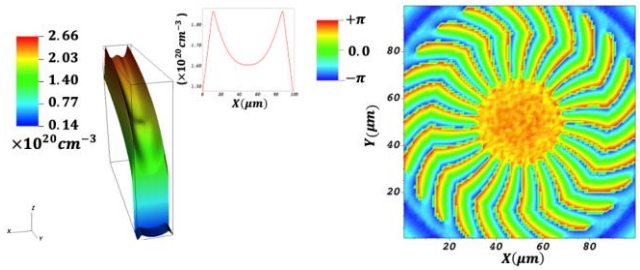

Figure 6. Waveguide electron density (left) and resulting phase footprint (right).

IV. CONCLUSIONS

First, it should be noted that this work is basic research, in which the methodology for the study of the interaction of beams with OAM in plasmas has been developed. The result is a greater understanding of the physics of laser-plasma interaction, with special emphasis on phenomena such as refraction or the interference of the HOH with the ASE.

Not only is the methodology innovative, but it has also been applied to a totally new scheme such as the amplification of HOH with OAM in plasmas. It was already known that the spin angular momentum (SAM) due to polarization was conserved under these circumstances. Thanks to this project, it is now known that OAM also does so in low-density plasmas, and it is known how changes in it induce

alterations in this property, with the impact that this can have.

In relation to the above, the approach of this project has great potential to become a highly sensitive plasma study method. The OAM constitutes an additional degree of freedom that allows characterizing the plasma density and its gradients (Figure 5 is a good example of this). This plasma diagnosis is fundamental in fields such as Nuclear Fusion by inertial confinement or laboratory astrophysics.

In addition to the above, with respect to the amplified beam as such, having coherent XUV radiation, with a known OAM, and high intensity (this would be the result of the proposed scheme), may be differential for already existing applications, or even promote new ones. In fields such as spectroscopy, endless opportunities would open, such as the optical control of Bose-Einstein condensates [19] or even nanometer-scale magnetic memory devices [20]. Other applications of interest could be in imaging techniques such as pticography, based on radiation interference patterns with the object of interest [21]. Finally, ultrashort pulses (femto or attosecond pulses) such as those that this scheme could provide, pose a new horizon in the study of ultrafast dynamics phenomena.

V. ACKNOWLEDGEMENTS

The authors thank the Community of Madrid for financial support for this work, within the *Coherent XUV and soft X-ray sources: optimization through modelling* (CROM) project. Eduardo Oliva has received support from the Ministry of Science and Innovation through a Ramón y Cajal contract RYC2018-026238-I

The authors thank the Institute of Nuclear Fusion "Guillermo Velarde" for the use of their codes and servers.

The authors thank Olivier Guilbaud and Alok Pandey, members of the Laboratoire Irène Joliot-Curie, (Paris-Saclay University, France) for their collaboration and the contribution with experimental data.

VI. REFERENCES

[1] L. Allen, M. W. Beijersbergen, R. J. C. Spreeuw, y J. P. Woerdman, «Orbital angular momentum of light and the transformation of Laguerre-Gaussian laser modes», Phys. Rev. A, vol. 45, n.o 11, pp. 8185-8189, jun. 1992, doi: 10.1103/PhysRevA.45.8185.

[2] J. Wang, «Advances in communications using optical vortices», Photonics Res., vol. 4, n.o 5, p. B14, oct. 2016, doi: 10.1364/PRJ.4.000B14.

[3] M. Harwit, «Photon Orbital Angular Momentum in Astrophysics», Astrophys. J., vol. 597, n.o 2, pp. 1266-1270, nov. 2003, doi: 10.1086/378623.

[4] X. Zhuang, «Unraveling DNA Condensation with Optical Tweezers», Science, vol. 305, n.o 5681, pp. 188-190, jul. 2004, doi: 10.1126/science.1100603.

[5] N. C. C. Gutiérrez, «Modes de Laguerre-Gauss et canalisation d'atomes froids», Université Paris-Sud, Paris, 2014.

[6] Y. Shen et al., «Optical vortices 30 years on: OAM manipulation from topological charge to multiple singularities», Light Sci. Appl., vol. 8, n.o 1, p. 90, dic. 2019, doi: 10.1038/s41377-019-0194-2.

[7] A. Depresseux et al., «Table-top femtosecond soft X-ray laser by collisional ionization gating», Nat. Photonics, vol. 9, n.o 12, pp. 817-821, dic. 2015, doi: 10.1038/nphoton.2015.225.

[8] Ph. Zeitoun et al., «A high-intensity highly coherent soft X-ray femtosecond laser seeded by a high harmonic beam», Nature, vol. 431, n.o 7007, pp. 426-429, sep. 2004, doi: 10.1038/nature02883.

[9] E. Oliva et al., «DAGON: a 3D Maxwell-Bloch code», Prague, Czech Republic, jun. 2017, p. 1024303. doi: 10.1117/12.2265044.

[10] E. Oliva, M. Cotelo, P. Martínez, J. Álvarez, y P. Velarde, «2D and 3D modelling of plasma amplifiers of UV, XUV, and soft x-rays», en X-Ray Lasers and Coherent X-Ray Sources: Development and Applications XIII, San Diego, United States, sep. 2019, p. 2. doi: 10.1117/12.2529220.

[11] E. Oliva, E. V. Fernández-Tello, M. Cotelo, P. Martínez Gil, J. A. Moreno, y P. Velarde, «3D multi-scale modelling of plasma-based seeded soft X-ray lasers», Eur. Phys. J. D, vol. 75, n.o 11, p. 290, nov. 2021, doi: 10.1140/epjd/s10053-021-00298-y.

[12] A. Sureau y P. B. Holden, «From amplification of spontaneous emission to saturation in x-ray lasers: A Maxwell-Bloch treatment», Phys. Rev. A, vol. 52, n.o 4, pp. 3110-3125, oct. 1995, doi: 10.1103/PhysRevA.52.3110.

[13] O. Larroche, D. Ros, A. Klisnick, A. Sureau, C. Möller, y H. Guennou, «Maxwell-Bloch modeling of x-ray-laser-signal buildup in single- and double-pass configurations», Phys. Rev. A, vol. 62, n.o 4, p. 043815, sep. 2000, doi: 10.1103/PhysRevA.62.043815.

[14] A. E. Siegman, Lasers, University Science Books. 1986.

[15] G. J. de Valcarcel, E. Roldan, y F. Prati, «Semiclassical theory of amplification and lasing», p. 17, 2006.

[16] A. D'Errico, R. D'Amelio, B. Piccirillo, F. Cardano, y L. Marrucci, «Measuring the complex orbital angular momentum spectrum and spatial mode decomposition of structured light beams», Optica, vol. 4, n.o 11, p. 1350, nov. 2017, doi: 10.1364/OPTICA.4.001350.

[17] C. M. Kim, K. A. Janulewicz, H. T. Kim, y J. Lee, «Amplification of a high-order harmonic pulse in an active medium of a plasma-based x-ray laser», Phys. Rev. A, vol. 80, n.o 5, p. 053811, nov. 2009, doi: 10.1103/PhysRevA.80.053811.

[18] E. Oliva et al., «Hydrodynamic evolution of plasma waveguides for soft-x-ray amplifiers», Phys. Rev. E, vol. 97, n.o 2, p. 023203, feb. 2018, doi: 10.1103/PhysRevE.97.023203.

[19] K. C. Wright, L. S. Leslie, y N. P. Bigelow, «Optical control of the internal and external angular momentum of a Bose-Einstein condensate», Phys. Rev. A, vol. 77, n.o 4, p. 041601, abr. 2008, doi: 10.1103/PhysRevA.77.041601.

[20] S. Seki, X. Z. Yu, S. Ishiwata, y Y. Tokura, «Observation of Skyrmions in a Multiferroic Material», Science, vol. 336, n.o 6078, pp. 198-201, abr. 2012, doi: 10.1126/science.1214143.

[21] K. A. Nugent, «Coherent methods in the X-ray sciences», Adv. Phys., vol. 59, n.o 1, pp. 1-99, ene. 2010, doi: 10.1080/00018730903270926

Proceedings of the European Nuclear Young Generation Forum
ENYGF'23
May 8-12, 2023, Kraków, Poland

Performance Comparison of Different Non-Condensable Gases on Pressurization Process in Gas-Steam Pressurizer

Shoghi, Abolfazl[1], Hosseini, Seyed Ali[1,2*], Shirani, Amir Saeed[1], D'Auria, Francesco[2], and Akbari, Reza[2]

[1] Shahid Beheshti University (SBU), Iran; [2] Nuclear Research Group of San Piero a Grado (GRNSPG), University of Pisa (UNIPI), Italy

*Corresponding author: *Email: ali.h.research@gmail.com, sal_hosseini@sbu.ac.ir. Tel: (+39)3463044553*

I. Brief Introduction

The Pressurizer (PRZ) plays a key role in controlling the pressure of nuclear reactors and pressurized facilities. The PRZs used in industrial processes and nuclear reactors are classified into three categories: Steam PRZ, Steam-Gas PRZ, and Gas PRZ. It is very important to quick and accurate control of pressure in the test facilities is an important feature of all PRZs. In the Gas PRZ and Gas-Steam PRZ (GS-PRZ), the pressure is normally controlled using Non-Condensable Gas (NCG). Choosing and application of NCG have important characteristics in the operation of GS-PRZ. In the primary loop of the high-pressure facilities, the pressure changes inside PRZ due to fluctuations in the mass flow rate that passes to PRZ during transients. The NCG's existence inside PRZ has a high impact on the pressurization and depressurization of PRZs. Therefore, modelling the PRZ thermal-hydraulic behaviour during transients is required with considering NCGs. PRZ dynamic model is generally nonlinear that complicates PRZ behaviour during transients. Thus, it is difficult to determine an accurate mathematical model for PRZ dynamic behaviour. This study of dynamic behaviour related to GS-PRZ is one of the most important topics in nuclear equipment design considering thermal-hydraulic aspects. Various models have been proposed for the dynamic behaviour of PRZs. In addition, many thermal-hydraulic codes are used in nuclear applications, especially in the simulation of PRZs [1-6]. Aspen HYSYS dynamic model simulates the thermal, equilibrium, and reactive behaviour of the industrial processes. The dynamic model in Aspen uses a different set of conservation equations, which account for changes occurring over time. Non-linear differential equations can be formulated to approximate the conservation principles. Therefore, numerical integration is used to determine the process behaviour at distinct time steps. Mathematical modelling is efficient for presenting the dynamic behaviour of PRZs. Comprehensive studies have been conducted in this area [7-14]. NCG has the greatest effect on the performance of the gas PRZ. These types of gases, due to their thermodynamic properties, are the main function of gas PRZ [15-16]. The GS-PRZ has been less widely researched than Steam PRZ. Therefore, the dynamic behaviour of GS-PRZ in different conditions (transient and accident conditions) is not well known. According to the developed Gas PRZ model by Shoghi et al., as the only work done in this area, this study investigated the dynamic behaviour of GS-PRZ using different NCGs [10]. This study has been evaluated for the University of Wisconsin High-Pressure Critical Heat Flux (WHPCHF) facility as the base loop. Various NCGs have been used in GS-PRZ modelling. GS-PRZ dynamic behaviour has been analysed in different transients. MATLAB is connected to Aspen HYSYS to get the simulation results. During in-surge (pressurization) and out-surge (depressurization) scenarios, the performance of different NCGs in the GS-PRZ is compared with each other.

II. Pressurizer System in Industrial Process

Steam PRZ is the most common type of PRZ in the nuclear industry. The steam PRZ operates in equilibrium with a mixture of water and steam. As shown in *Figure 1(a)*, the Steam PRZ utilizes two main strategies to control the primary loop pressure within the specified limits. The first strategy is to condense the steam through the cold-water spray to decrease the pressure, and the second strategy is to heat the water with the PRZ electrical heaters to increase the pressure. As shown in *Figure 1(b)*, the steam-gas PRZ has been composed based on the nonequilibrium two-region. The steam-gas PRZ uses a single volume consisting of two semi-independent regions, each with special thermodynamic conditions. Another presumption about steam-gas PRZ is that steam and non-condensable gas are combined in the gas region, and mass and energy are transferred between two regions at the interface area. The gas PRZ (*Figure 1(c)*) is another type of PRZ which is controlled by a non-condensable gas that does not mix with the steam.

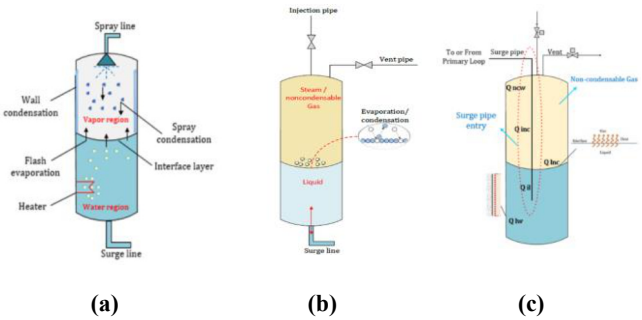

Figure 1. Different pressurizer types, (a) Steam PRZ, (b) Gas-Steam PRZ, (c) Gas PRZ.

III. Brief Description of Simulation

The Aspen HYSYS software and RELAP5 code are possible options for the thermal-hydraulic modelling of PRZ. It should be noted that the RELA5 code has imperfections in modelling the gas PRZs. In other words, the RELAP5 cannot model the pure NCG region properly. Thus, the RELAP5 just models the volume with a mixture of water/steam/NCG when the volume of NCG has a low percentage. Therefore, in this study, Aspen HYSYS software is selected to simulate gas PRZ. Aspen HYSYS is one of the unique tools for industrial processes that are used in various manufacturing processes and the dynamic behaviour of the PRZ is evaluated during the study. In this study, to evaluate different scenarios and investigate the behaviour of the PRZ, the PRZ is connected to the WHPCHF loop. It should be noted that the facility was first simulated in Steady-State and then switched to Dynamic-State to check different transitions on it. This facility is designed to operate ranges associated with low mass flux and high pressures (80-160 bar, 400-1200 kg/m^{2}s and 298-623 K). The WHPCHF components can be divided into two categories: primary and secondary Systems. A simple process flow diagram and a 3-D model of the primary system are shown in *Figure 2*. In this study, all of the components are integrated with the Aspen HYSYS. The simulated flowsheet in Aspen HYSYS software is shown in *Figure 3*.

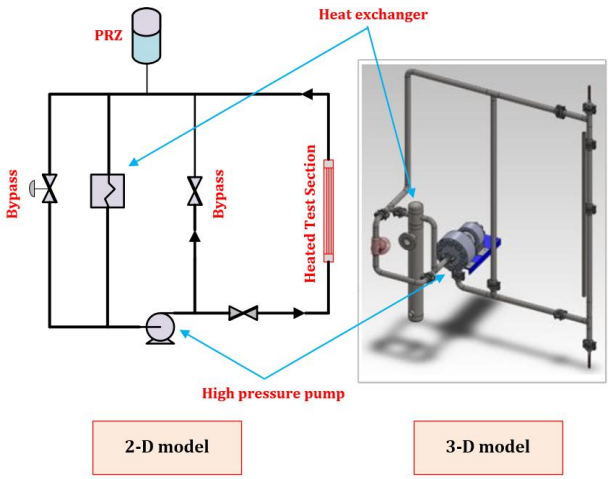

Figure 2. Process flow diagram of the primary system.

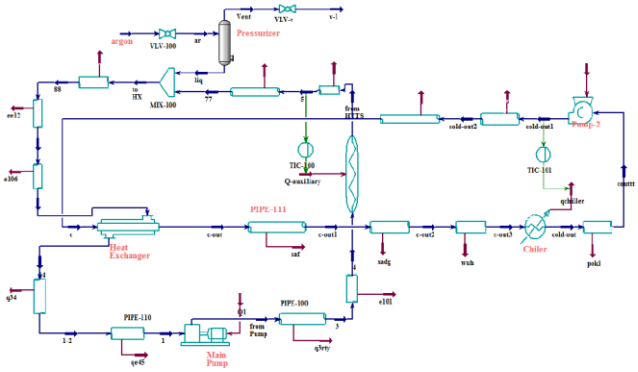

Figure 3. WHPCHF simulated flowsheet with Aspen HYSYS.

The GS-PRZ proposed for utilization in small integrated reactors has complicated thermal-hydraulic phenomena; the condensation heat transfer with NCG is an important factor in evaluating the GS-PRZ behaviour. This type of PRZ can be used in small modular reactors and high-pressure test facilities. As shown in *Figure 1(b)*, the GS-PRZ uses a single volume consisting of two semi-independent regions, each with special thermodynamic conditions. Another presumption about GS-PRZ is that NCG and steam are combined in the upper region. In this PRZ, mass and energy are transferred between two regions at the interface area. In the GS-PRZ, the NCGs are applied as controlling actuator mechanisms instead of electrical heaters and sprays (compared with steam PRZ), including the Nitrogen (N_2), Oxygen (O_2), and Argon (Ar), in the Gas-Steam mixture area.

The pressurizer is not defined in the list of Aspen HYSYS equipment. Therefore, a Separator is used to simulate the Pressurizer in the software during this work. Separator boundary conditions are selected according to GS-PRZ boundary conditions. The Separator nodalization and boundary conditions are presented in *Figure 4*. As far as quantity is concerned, only four gases are of interest for engineering applications, namely Nitrogen (N_2), Oxygen (O_2), Argon (Ar), and Carbon Dioxide (CO_2). In this study, Nitrogen, Oxygen, and Argon have been selected for use in the PRZ and have been evaluated to compare their performance. It is worth noting that different mole fractions of NCG affect the performance of the PRZ. Three different modes are considered to evaluate the PRZ performance which are given in Table 1. On each mode, three gases have been implemented and the performance of the compressor has been evaluated. Peak Pressure is one of the important parameters in PRZ performance. The presence of NCG in the mixed region has a great effect on the Peak Pressure. In this study, the Peak Pressure has been evaluated in three modes.

Table 1. Different mole fractions of NCG and Steam in GS-PRZ

Mode	NCG mole fraction	H_2O mole fraction
I	20	80
II	60	40
III	80	20

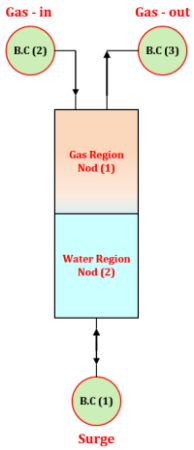

Figure 4. Separator (PRZ) nodalization and boundary conditions.

A. In-surge and out-surge scenarios for different PRZs

Two scenarios are considered to evaluate the performance of the PRZ in different conditions. The heated test section is one of the most critical components of the WHPCHF. The primary loop's temperature increases during the in-surge scenario. During this scenario, it is assumed that the thermal power given to the primary loop by the heated test section has slightly increased, then the specific volume and pressure are also increased. Therefore, some water from the primary loop enters the PRZ. Another scenario is the out-surge scenario. During this scenario, it is assumed that the thermal power given to the primary loop by the heated test section has slightly decreased. In this scenario, the specific volume and pressure are decreased and some water of PRZ enters the primary loop. During the same scenario (increasing pressure scenario), the mass input to the steam PRZ is higher than in other PRZs. The Gas PRZ also has the lowest value. In general, the pressure in the loop increases with increasing temperature. The upper region of each PRZ has a different content. The pressure changes in the gas PRZ are more than in other PRZs. This is due to the presence of NCG inside the Gas PRZ (upper region of Gas PRZ). The Gas PRZ is more sensitive to turbulence than other PRZs. After the Gas PRZ, Due to the presence of certain amounts of NCG in the mixture with steam in the upper region of PRZ, Gas-Steam PRZ is more sensitive to disturbances. NCG has the greatest effect on the performance of the PRZ. These types of gases, due to their thermodynamic properties, are the main function of PRZ. Each of the NCGs has its own thermodynamic properties and has a different performance during the PRZ operation. Choosing the type of NCG for use in systems related to pressurized water operations is very important. One of the influential parameters in this selection is the peak pressure. In similar transient conditions, the performance of various NCGs in the PRZ is evaluated.

IV. Results and Discussion

As mentioned, NCG has the greatest effect on the performance of the PRZs. The use of the NCG increases the peak pressure due to the lack of NCG condensation during transient conditions. *Figure 5* shows the simulation results with and without a NCG in the PRZ. The use of GS-PRZ makes it possible to change the pressure quickly.

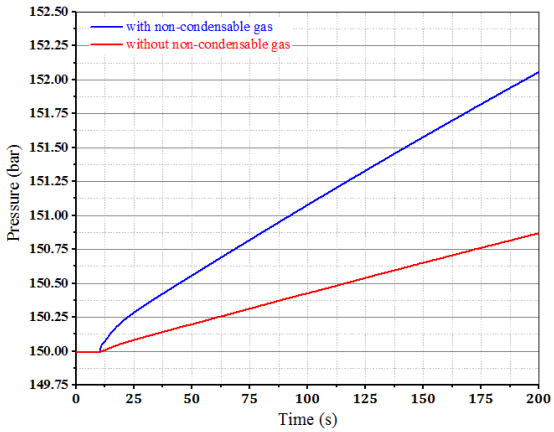

Figure 5. Pressure transient with and without NCG

The pressure change in the PRZ is apparently different when the mole fraction of Argon varies, and the peak pressure increases with the increase in Argon mole fraction (20 to 80%). This is due to the condensation heat transfer in the presence of NCG, which decreases the heat transfer coefficient with an increasing mole fraction of NCG. The pressure change ranged from 150.05 to 150.54 bar when the mole fraction of Argon is 20%. This range is 150.05 to 151.92 bar when the mole fraction of Argon is 80%. Other results are given in Table 2. The results of using N_2 and O_2 NCGs in the PRZ are also given in this table.

Table 2. Different mole fractions of NCG and Steam in GS-PRZ

NCG	NCG mole fraction (%)	Pressure change (bar)
Ar	20	0.495
	40	0.711
	60	1.268
	80	1.873
N_2	20	0.551
	40	0.982
	60	1.411
	80	1.966
O_2	20	0.248
	40	0.833
	60	1.187
	80	1.685

Choosing the type of NCG for use in systems related to pressurized water operations is very important. One of the influential parameters in this selection is the peak pressure. The peak pressure in the PRZ is very different for different types of NCG. As shown in Figure 6, there is

a difference between three NCGs (Ar, N_2, and O_2) with the same mole fraction (20%). The pressure in the presence of Nitrogen (N_2) is always larger than that in the presence of Argon (Ar) and Oxygen (O_2). This comparison has also been made for mole fractions of 60% and 80%, and the results are similar to the last scenario. The difference in peak pressure is caused by the degradation of condensation heat transfer due to the different types of NCG. It is easily seen that the pressure for N_2 will always be larger than that of Ar and O_2 at other mole fractions.

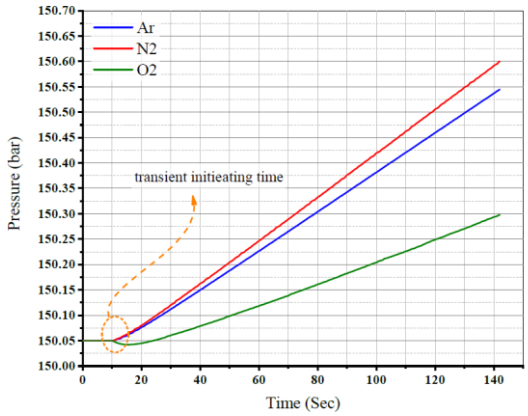

Figure 6. Comparison of pressures with different NCGs (Ar, N_2, and O_2) - mole fraction 20%.

V. Conclusion

As previously indicated, the GS-PRZ controls pressure using a mix of NCG and steam. In comparison to S-PRZ, GS-PRZ enables quicker pressure changes due to the use of NCG. The effects of various NCGs on the pressurization of the GS-PRZ are demonstrated in this research. There are numerous factors to consider while choosing the NCG type for the PRZ. The peak pressure is one of the selection's key considerations. The performance of various NCGs ((Argon, Nitrogen, and Oxygen) in the PRZ was assessed in this work under similar transient settings. Therefore, In-surge scenarios were applied to the GS-PRZ with different NCG mixing conditions. The findings demonstrated that using the NCG enhanced peak pressure due to the lack of NCG condensation during transient conditions. In the GS-PRZ, the peak pressure increased with the increase in NCG mole fraction. The peak pressure in the PRZ had different impacts on the types of NCGs. Nitrogen gas had the highest peak pressure. The difference in peak pressure is caused by the degradation of condensation heat transfer due to the different types of NCG. The proposed model can also be used to evaluate other effective parameters (solubility in water at different pressures and costs) in choosing and decision-making related to the best type of NCG for GS-PRZ. The control system design for GS-PRZ has not been discussed in this basic research study. Nonetheless, the peak pressure results using various NCGs highlight the crucial roles that NCGs will play in the development of GS-PRZs in the future.

VI. References

[1] Cheng, Y. H., Wang, J. R., Lin, H. T., & Shih, C. (2009). Benchmark calculations of pressurizer model for Maanshan nuclear power plant using TRACE code. Nuclear engineering and design, 239(11), 2343-2348.

[2] Hosseini, Seyed Ali, et al. "Design and application of supervisory control based on neural network PID controllers for pressurizer system." Progress in Nuclear Energy 130 (2020): 103570.

[3] Wu, L., Jia, H., & Liu, Y. (2013, July). Numerical Study of the Gas-Steam Transient Behavior in the Integrated Pressurizer. International Conference on Nuclear Engineering (Vol. 55799, p. V002T03A030). American Society of Mechanical Engineers..

[4] Ma, X.Z., Jia, H.J. and Liu, Y., 2017. Research on the steam–gas pressurizer model with Relap5 code. Nuclear Science and Techniques, 28(5), pp.1-8.

[5] Kim, T. W., Kim, J. W., & Park, G. C. (2006). Development of a non-equilibrium pressurizer model with non-condensable gas. Nuclear engineering and design, 236(4), 375-384.

[6] Lee, Y. G., & Park, G. C. (2013). TAPINS: a thermal-hydraulic system code for transient analysis of a fully-passive integral PWR. Nuclear Engineering and Technology, 45(4), 439-458.

[7] Moghanaki, S. K., & Rahgoshay, M. (2014). Simulation of two-region and four-region models for typical PWR pressurizer and benchmark obtained results using available results. Annals of Nuclear Energy, 63, 302-308.

[8] Zhong, X., Zhang, X., Yu, J., Saeed, M., Li, Y., Chen, Z., ... & Sun, Y. (2019). Development of an improved non-equilibrium multi-region model for pressurized water reactor pressurizer. Annals of Nuclear Energy, 126, 133-141.

[9] Kim, J. W., Lee, Y. G., & Park, G. C. (2008). Numerical Analysis on Transient of Steam-gas Pressurizer.

[10] Shoghi, A., Hosseini, S. A., Shirani, A. S., & Zangian, M. (2021). Development and verification of the mathematical modeling for the gas-pressurizer system. Annals of Nuclear Energy, 164, 108630.

[11] Shoghi, A., Hosseini, S.A., Shirani, A.S. and Zangian, M., 2022. Dynamic behavior analysis of different pressurizer types on a high-pressure test facility. Radiation Physics and Engineering.

[12] Wang, P., He, J., Wei, X., & Zhao, F. (2019). Mathematical modeling of a pressurizer in a pressurized water reactor for control design. Applied Mathematical Modelling, 65, 187-206.

[13] Lotfi, M., Menhaj, M. B., Hosseini, S. A., & Shirani, A. S. (2020). A design of switching supervisory control based on fuzzy-PID controllers for VVER-1000 pressurizer system with RELAP5 and MATLAB coupling. Annals of Nuclear Energy, 147, 107625.

[14] Pini, A., Cammi, A., Colombo, L. and Tigliole, A.B., 2018. A non-equilibrium control-oriented model for the pressurizer dynamics. Progress in Nuclear Energy, 106, pp.102-119.

[15] Ma, X.Z., Jia, H.J. and Liu, Y., 2017. Research on the steam–gas pressurizer model with Relap5 code. Nuclear Science and Techniques, 28(5), pp.1-8.

[16] Alshehri, A., Andalib, S., & Kavehpour, H. P. (2020). Numerical modeling of vapor condensation over a wide range of non-condensable gas concentrations. International Journal of Heat and Mass Transfer, 151, 119405.

Proceedings of the European Nuclear Young Generation Forum
ENYGF'23
May 8-12, 2023, Kraków, Poland

ATHLET-validation for simulating SMART's passive residual heat removal system featuring indefinite cooling via loop-thermosyphons

Rincon Soto, Nelson Felipe[1*]

[1] University of Stuttgart, Institute of Nuclear Technology and Energy Systems (IKE), Germany

*rincon@ike.uni-stuttgart.de

I. INTRODUCTION

Interest in Small Modular Reactors (SMRs) is gaining momentum, as they offer an attractive alternative for a vast range of energy markets due to their flexibility, transportability and simplified manufacturing. Inherent reactor safety in combination with passive residual heat removal systems (PRHRS) are common design features in emerging SMRs [1].

PRHRS are responsible for the removal of residual core-generated heat after plant shutdown [2]. PRHRS rely on naturally-driven forces to transfer the residual heat to an intermediate heat sink, usually a water-filled emergency cooling tank (ECT) with a limited grace period. To avoid ECT-water depletion due to evaporation, the residual heat must be transferred via an additional loop to an ultimate heat sink (UHS), such as the environment or to an air-cooling tower (ACT). Multiple process schemes and models for indefinite PRHRS-operation in SMRs considering an UHS have been extensively studied [3]. A representative example is shown in figure 1, where the core decay heat is transferred to the secondary loop producing steam, which flows upwards to the ECT via the PRHRS. Then, the surplus heat of the ECT-water is removed by the LTS system and transported to an UHS, in this case an ACT.

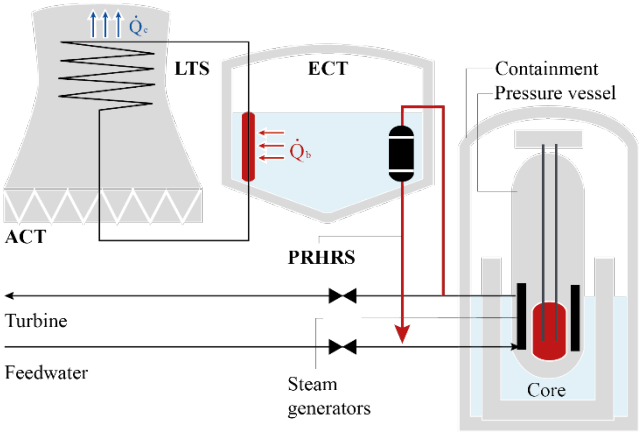

Figure 1. Indefinite cooling concept for a PRHRS

Loop thermosyphons (LTS) are considered suitable secondary loops for this heat transport purpose. LTS are a type of wickless two-phase operated heat pipes, featuring a closed-loop configuration with an evaporation and a condensation zone connected by two independent flow channels for the gas and liquid phase, respectively [4].

After incorporating additional built-in features (Such as two-phase pressure drop models and heat transfer correlations for air surroundings) in the 1D-Code ATHLET (Analysis of Thermal-hydraulics of Leaks and Transients, developed by GRS) to properly simulate the thermal-hydraulics of LTS systems, indefinite cooling concepts for SMRs are to be tested [5]. Several experimental facilities have been built to test PRHRS in emerging SMRs. For instance, the VISTA-ITL is a downscaled facility representing the PRHRS of the 330MWt advanced integral pressurized water reactor, SMART. The VISTA-ITL is able to simulate a small-break loss of coolant accident (SBLOCA), complete loss of reactor coolant system flow rate (CLOF), allowing assessment of the PRHRS-performance [6]. Existing models developed with the MARS can accurate represent the thermal-hydraulics of the VISTA-ITL facility, but do not simulate the accident scenarios featuring an indefinite cooling concept [7].

Within this research, ATHLET will be used to simulate the steady states and transients of the VISTA-ITL facility during the experimental campaigns carried out by [8]. After code-validation, several arrangements for an indefinite cooling via LTS are evaluated to ensure a long-lasting safe operation of the ECT within the PRHRS.

II. MODEL DESCRIPTION

A. Experimental campaign at the VISTA-ITL

The VISTA-ITL is a 1/2.77-height downscaled facility of SMART's PRHRS. It consists of an electrically-heated primary system (up to 818 kW), featuring a core, riser,

reactor coolant pump, and a pressurizer; a secondary system that removes the heat from the primary system through a helical steam generator (SG); and a PRHRS that transfers the residual heat to an ECT via a tube and shell heat exchanger (HX). Figure 2 shows the process flowsheet of the VISTA-ITL facility with some additional auxiliary components needed for operation. A detailed description of the facility can be found in [8].

Two stationary states from the experimental campaigns were selected for model validation: At 100% (818 kW) and 20% (165 kW) input power. After reaching the stationary states, the complete loss of coolant transient was further induced by following the experimental sequence of events: Once the primary coolant pump (RCP) coasts down, the inlet power is reduced to 5% of its initial value, and the valves to the PRHRS open to direct the secondary steam to the HX. The inlet power is then reduced to 3% and 1% after 780 s and 1400s in the transient, respectively.

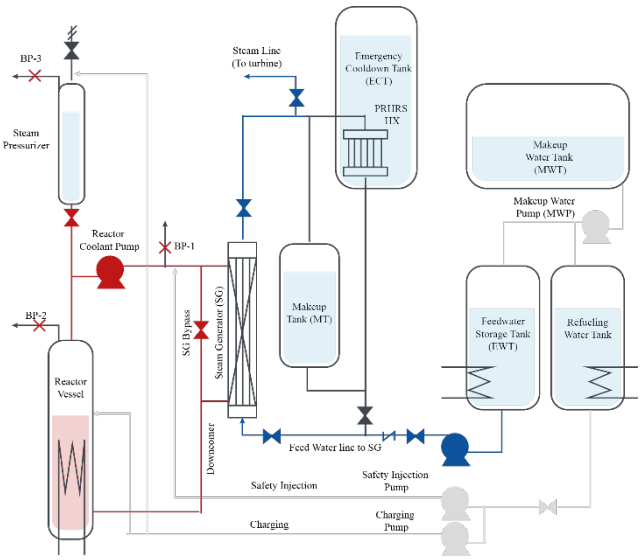

Figure 2. Process flowsheet of the VISTA-ITL facility

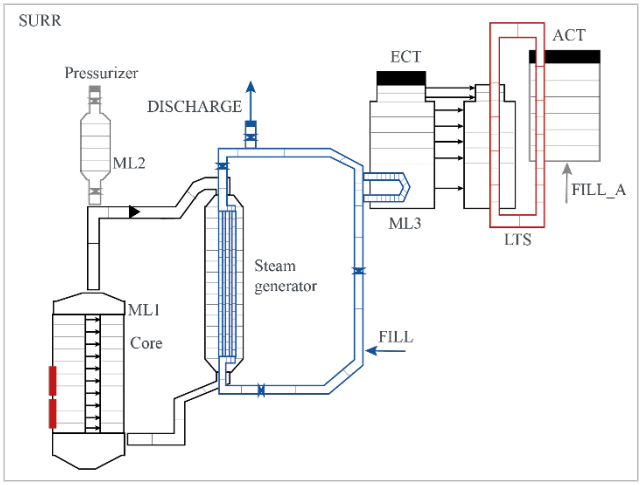

Figure 3. ATHLET-Nodalization of major plant components and LTS attached system

B. ATHLET modelling

The main heat transfer loops of the VISTA-ITL facility were modelled in ATHLET using the initial and boundary conditions specified for each operation point. The nodalization can be seen in Figure 3, where the Thermal-fluid objects (TFOs) of every priority chain (PR) of the model are depicted. The primary loop (depicted in black) consists of three PRs as follows: main and auxiliary core channels, and the connection to the pressurizer. The secondary loop (depicted in blue) consists of three priority: the main steam generator loop, which features a SG modelled via a set of parallel tubes equipped with pressure-loss coefficients for helical tubes; the connection to the discharge pipe, and the attachment of the HX. The ECT is modelled as a set of TFO bound by cross-connection objects to enable bi-directional flow, characteristic of natural circulating systems.

The LTS were not built in the experimental facility, but they will be added to the model as an attachment to the ECT. Their evaporator's side is submerged in the ECT and their condenser's side is attached to an ACT. Both, ECT and ACT are connected to time-dependant volumes as boundary conditions (surroundings). A set of 10 LTS of 12m total loop length was implemented. Model-relevant geometry parameters are summarized in Table 1.

Table 1. Geometry input deck for main model components

Parameter	Value	Parameter	Value
No. of PRHRS trains	1	ECT: ID	0.4 [m]
No. of HX tubes/train	6	PRHRS steam line: volume	0.000912 [m3]
HX: tube length (ID)	1.2 [m]	PRHRS feed water line: volume	0.000342 [m3]
HX tube outer/inner diameter (OD)/(ID)	0.018/0.013 [m]	LTS (OD/ID)	0.008/0.006 [m]
SG-PRHRS HX: height gap	3.1 [m]	LTS total loop length	12 [m]
ECT: height	3.4 [m]	N° of LTS	10

III. RESULTS AND DISCUSSIONS

The obtained simulated stationary states (sim) are compared with the experimental values (exp) and shown in Table 2. Results for 100% and 20% input power are displayed for the main parameters of the primary and secondary systems. An overall agreement with the experimental values was obtained for most parameters, including inlet/outlet temperatures, pressures and flow rates.

Table 2. Experimental and simulated stationary states of the VISTA-ITL facility

	Primary system				Secondary system			
	SG inlet T (°C)	SG outlet T (°C)	Pressure in pressurizer (MPa)	Flow rate (kg/s)	SG inlet T (°C)	SG outlet T (°C)	Flow rate (kg/s)	SG outlet P (MPa)
100% exp	324	296	14.92	2.54	50	318	0.15	5.20
100% sim	326	299	14.91	2.52	50	320	0.13	5.21
20% exp.	314	309	15.0	2.70	50	314	0.039	5.01
20% sim.	312	308	14.99	2.61	50	313.5	0.033	5.01

Once transient is induced, the dynamics of the process was further analyzed. Figure 4 illustrates the experimental and

simulated results for the PRHRS HX inlet temperature and Figure 5 the average ECT pool temperature over time. An overall agreement over time between the data sets was found for both, the PRHRS HX inlet temperature and the ECT average pool temperature. Moreover, no stationary state was reached for the pool temperature, as it continues to rise over time and may surpass the recommended operation value of 70°C after some more operation time at 1% input power.

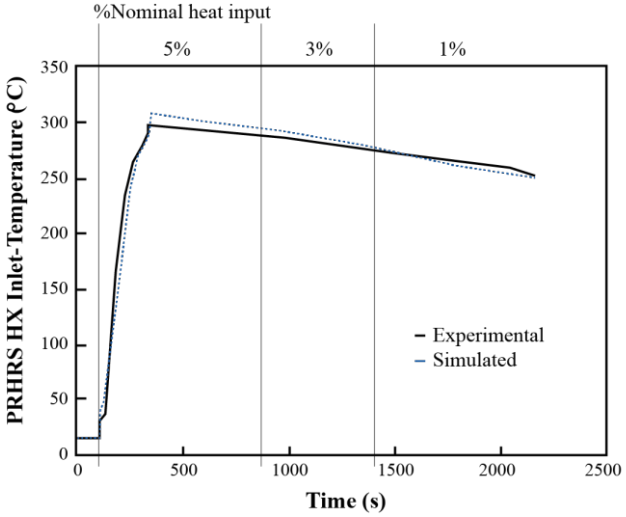

Figure 4. Complete loss of coolant: PRHRS HX inlet temperature

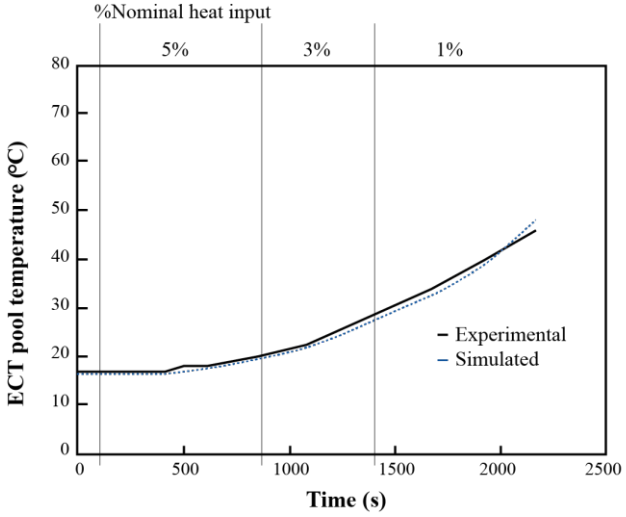

Figure 5. Complete loss of coolant: ECT average temperature

To evaluate the indefinite cooling via a bundle of LTS, the simulation time was extended up to 4500s and a set of 10 LTS was attached to the ECT and to an air-cooling tower as ultimate heat sink. Figures 6 and 7 show the results of the ECT pool average temperature for a filling ratio (FR) of 40% and 27%, respectively at 1.5 m/s air inlet velocity in the ACT. The FR is defined as the volume of working fluid over the total volume of the inner piping of each LTS. Low FRs might induce dry-out and therefore, inefficient single-phase operation of the LTS. On the other hand, larger FRs might reach a two-phase operation at higher loop pressures, where the saturation temperature of the working fluid might be too close to the ECT-average temperature, complicating heat removal. Hence, the FR is a parameter to be further tuned for every heat removal scenario.

The dotted red and blue lines in Figures 6 and 7 depict the pool temperature with and without attached LTS, respectively. The grey solid line corresponds to the working fluid (water) temperature inside of the LTS in its evaporating section. It is clear that the FR impacts the LTS-operating pressure and determines the two-phase saturation state. In the case of a 40% FR, the LTS reached an average saturation temperature of 64°C and it was able to slow-down the pool's temperature increase, but not able to maintain the pool temperature under 70°C. In contrast, a FR of 27% reached an average saturation temperature of 47°C and was able to minimize the time where the water inventory sits above 70°C

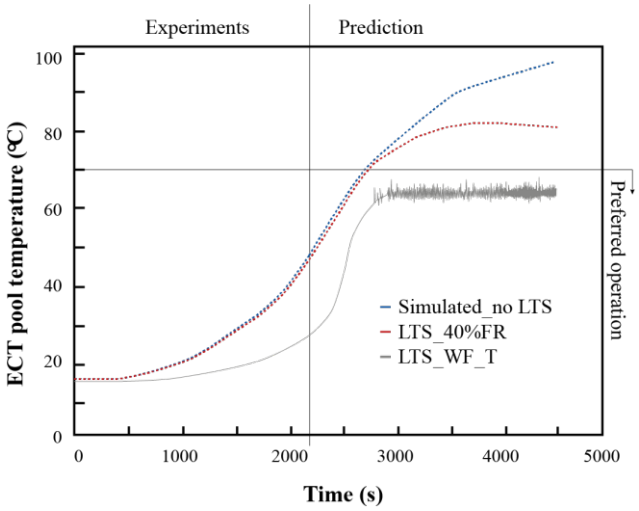

Figure 6. Complete loss of coolant transient after adding LTS at 40% filling ratio and 1.5 m/s air velocity in ACT

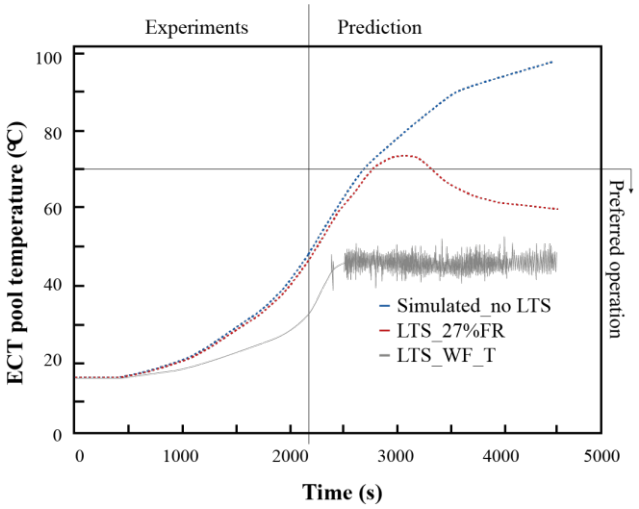

Figure 7. Complete loss of coolant transient after adding LTS at 27% filling ratio and 1.5 m/s air velocity in ACT

The effect of further LTS-related variables, such as the air velocity and temperature in the ACT was also studied. Selected results will be Figure 8 displays the transient results at FR 27% and 2.5 m/s air inlet velocity in the ACT. It is clear that relative variations in the air velocity do not impact the LTS-performance as much as variations in the FR, as the dynamic output of the models is comparable in Figures 7 and 8. Nevertheless, the peak values of the ECT average temperatures are slightly lower when higher velocities are used in the ACT. Further increases in the inlet air velocities showed no considerable influence in the model output.

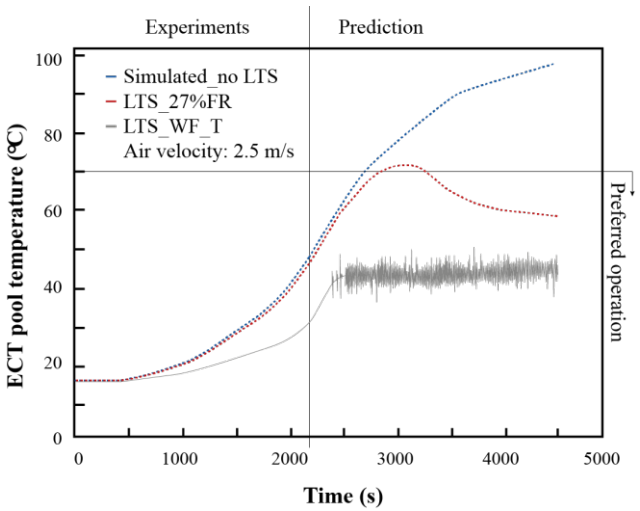

Figure 8. Complete loss of coolant transient after adding LTS at 27% filling ratio and 2.5 m/s air velocity in ACT

IV. SUMMARY AND CONCLUSIONS

A 1D-model of the VISTA-ITL facility was developed using the ATHLET code. The model was validated via stationary and transient experimental campaigns. LTS systems were attached to the model to evaluate an indefinite cooling concept for the PRHRS.

In terms of fluid temperatures, pressures and mass flows; the ATHLET-model of the VISTA-ITL facility reached the experimental stationary states values for different power inputs. Once the transient was induced (Complete loss of coolant, CLOF), the model's output yielded an accurate agreement to the experimental data over the course of the transient. Without any further heat removal loops, the model also predicts a considerable increase in the ECT-water temperature of the after 2.500 s of transient, surpassing the recommended 70°C design threshold. After assessing multiple LTS-arrangements to transfer the residual heat from the ECT to an ultimate heat sink, it was found that filling ratios (FR) between 27-35% in the LTS deliver enhanced performances for the ECT-indefinite cooling. Some other variables, such as surrounding air temperature and velocity did not impact the indefinite cooling as much as the LTS-filling ratio.

V. ACKNOWLEDGMENTS

Supported by:
Federal Ministry for Economic Affairs and Climate Action
on the basis of a decision by the German Bundestag

In this paper results of the research project VASiL were shown. It was financed by the Federal Ministry for Ecomonic Affairs and Climate Action.

VI. List of Abbreviations

Abbreviation	Meaning
ACT	Air cooling tower
CLOF	Complete loss of flow rate
ECT	Emergency cooling tank
FR	Filling ratio
HX	Heat exchanger in ECT
LTS	Loop thermosyphon
MARS	Multi-dimensional Analysis of Reactor Safet
PR	Priority chain
PRHRS	Passive residual heat removal system
RCP	Reactor coolant pump
SBLOCA	Small break loss of coolant accident
SG	Steam generator
SMRs	Small modular reactors
UHS	Ultimate heat sink

VII. References

[1] International Atomic Energy Agency – IAEA, "Advances in Small Modular Reactor Technology Developments". Austria, September 2018.

[2] K. H. Bae, H. C. Kim, M. H. Chang, S. K. Sim, "Safety evaluation of the inherent and passive safety features of the smart design". Annals of Nuclear Energy, vol. 28, no. 4, 2001, 333-349.

[3] K. H. Bae, H. C. Kim, M. H. Chang, S. K. Sim, "Indefinite sustainability of passive residual heat removal system of small modular reactor using dry air cooling tower". Nuclear Engineering and Technology, vol. 52, no. 5, 2020, 964-974.

[4] R. Swart, R.T. Dobson, "Thermal-hydraulic simulation and evaluation of a natural circulation thermosyphon loop for a reactor cavity cooling system of a high-temperature reactor". Nuclear Engineering and Technology, vol. 52, no. 2, 2020, 271-278.

[5] N. F. Rincon Soto, F. Ramirez Carrasco, "Applicability of local heat transfer correlations for residual heat removal via loop thermosyphons in Small Modular Reactors (SMRs)". Proceedings of ENYGF'21, Tarragona, Spain, September 27-30, 2021.

[6] H. S. Park, B. Y. Min, Y. C. Shin, S. J. Yi "Major results from safety-related integral effect tests with VISTA-ITL for the SMART design". Proceedings of ICAPP'12, Chicago, USA, No. 12457, June 24–28, 2012.

[7] Y.J. Chung, H. C. Kim, B. D. Chung, M. K. Chung, S. Q. Zee, "Two phase natural circulation and the heat transfer in the passive residual heat removal system of an integral type reactor". Annals of Nuclear Energy, vol. 33, 2006, 267–270.

[8] B. Y. Min, H. S. Park, Y. C. Shin, S. J. Yi, "Experimental verification on the integrity and performance of the passive residual heat removal system for a SMART design with VISTA-ITL". Annals of Nuclear Energy, vol. 71, 2014, 118-124.

Proceedings of the European Nuclear Young Generation Forum
ENYGF'23
May 8-12, 2023, Kraków, Poland

Towards a collaborative open-source platform for accident analysis with containmentFOAM and OpenModelica

Sturm, Karl J. X.[1,2*] and Kelm, Stephan[2]

[1] Department of Electrical Engineering and Information Technology, RWTH Aachen University, Germany;
[2] Institute for Energy and Climate Research (IEK-14), Forschungszentrum Jülich GmbH, Germany

*Corresponding author: *karl.sturm@rwth-aachen.de*

I. INTRODUCTION

High-resolution analysis of containment phenomena in nuclear reactor accident scenarios require customized computational fluid dynamic (CFD) codes [1]. Yet, these codes are not able to fully resolve effects from connected safety systems like the primary coolant circuit, pressure suppression pools (PSPs) or passive auto-catalytic recombiners (PARs). To tackle this multi-scale problem, the current go-to solution is a domain decomposition approach with coupling of CFD and system codes [2]. In the past, multiple efforts have been undertaken to couple various combinations of CFD codes with system code packages [3], [4]. However, none of the currently available system codes is fully openly available, either due to access restrictions or the proprietary nature of the codes [5]. Therefore, education and training of young nuclear engineers and the collaboration between researchers is hindered; modification of existing simulation tools and implementation of new ideas can be difficult [6]. To resolve this issue, this work proposes to pair two open-source packages – containmentFOAM [1] and OpenModelica [7] – to create a collaborative platform for accident analysis. containmentFoam is a custom OpenFOAM-based CFD solution for containment phenomena. OpenModelica implements the general-purpose modeling language Modelica, with an accompanying simulator, and is successfully used in reactor design research and education [5], [6], [8].

The paper is organized as follows: Section II elaborates on the vision for an open co-simulation platform, Section III shows an approach towards implementing this platform and Section IV reports on the results of this proof-of-concept implementation. Section V concludes this work and identifies points of further development.

II. PLATFORM

To bring together both the CFD and system domain, a platform concept as illustrated in Figure 1 is envisioned. Here, the three-dimensional (3D) CFD domain simulates containment atmosphere mixing (combustible gas and aerosol transport, pressurization, etc.). In the system domain, safety system models such as PARs, PSPs and venting systems are instantiated. To connect them, a plug-in infrastructure couples the two partitioned domains and enables co-simulation. Additionally, the interface for plug-ins shall be well-defined and open, such that users have full flexibility in implementing and coupling their self-created system models with the CFD simulation. Furthermore, by using a standard interface, packaging and sharing of system models is simplified, aiding in cross-institutional collaboration.

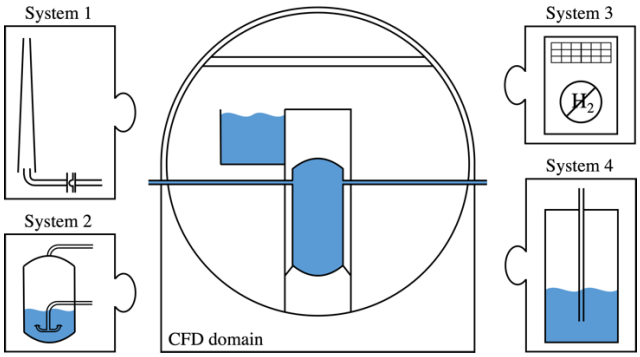

Figure 1. Accident analysis platform with plug-in infrastructure. Containment phenomena are covered by a CFD simulation (middle). Plug-in system models: (filtered) containment venting (system 1), pool scrubber (system 2), PAR (system 3) and PSP (system 4).

III. IMPLEMENTATION

To set a first step towards the above-mentioned platform, this section details our proof-of-concept implementation that covers the creation of system models, plugging them into the CFD domain, and running coupled simulations.

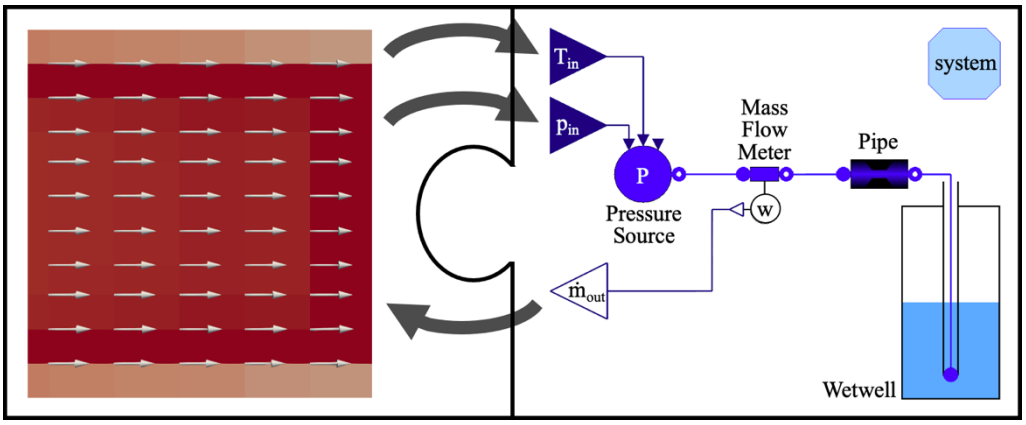

Figure 2. Test case: Flow through pipe (CFD domain, left) coupled with a wetwell system model (right). Boundary conditions are exchanged through a coupling interface (middle).

A. System Model Creation

For safety system model creation and export, OpenModelica [7] is used. The programming environment and simulator enables users to rapidly model technical systems. Model creation is achieved through either programming Modelica code (consisting of an equation-based description of a system's technical behavior), or by connecting multiple pre-existing sub-systems graphically. An example of an OpenModelica schematic is shown in Figure 2 (right). Examplary Modelica code is given in Figure 5 (left); it closely matches the formulation of an equation system (Figure 5, right). To aid rapid model development, various libraries with multiple ready-to-use components are currently available. Here, in in the given example, ThermoPower [9] is employed. It is an open-source zero-dimensional (0D) thermal hydraulics library which has previously been used in reactor analysis [5], [8].

B. Plug-in Infrastructure

With a component modeled to sufficient accuracy, OpenModelica provides the ability to package and export it as an executable simulator in accordance with the Functional Mockup Interface 2.0 (FMI2) standard [10]. The output is a so-called Functional Mockup Unit (FMU). Besides packaging for model exchange, FMI2 acts as a well-defined interface for systems co-simulation.

On the CFD side, containmentFOAM is extended with the capability to load FMUs through an OpenFOAM-native implementation in C/C++. FMU configuration and loading is orchestrated though a dictionary file. Figure 3 shows an example for a 'systemCoupling' dictionary. Here, choices are made on activation of the coupling interface, and which coupling scheme to use. Section 'FMU' declares one or more plug-in instances, and contains information on the FMU file path, data logging and initial values for FMU inputs. Afterwards, the section 'boundary' describes field values that are exchanged between the CFD domain boundaries and system models. This includes the connection between individual patches on the CFD side and input/output variables of a particular FMU instance.

This clear and open interface effectively enables a plug-in infrastructure, where not only self-created system models can be used, but also ones that are provided by collaborators and third parties.

C. Coupled Code Simulation

For the prototype implementation, containmentFOAM and a component FMU are coupled in a serial, explicit fashion as shown in Figure 4. Each the CFD simulation and the FMU take their turn in simulating a fixed time-step, one after another. Between their individual turns, the simulators exchange data that act as boundary conditions (BCs) for the opposing simulator's next time-step. The data include mass flow rate, temperature and pressure. Field quantities (T and p) are converted between 0D and 3D by mass flow rate averaging at their respective boundary area on CFD side.

```
coupling    true;
scheme      explicit; // explicit, implicit
algorithm   none;     // none, Aitken, Quasi-Newton

FMU {
    pss0 {
        name    PSS;
        path    "$FOAM_USER_LIBBIN/FMUs/
                 PressureSuppression";
        log     ( p_in T_in mdot_out );
        init {
                T_in    400;
                p_in    118500;
        }
    }
}

boundary {
    OUTLET_PATCH {
        pressure {
            direction   output;
            extVar      p_in;
            fmu         pss0;
        }
        temperature {
            direction   output;
            extVar      T_in;
            fmu         pss0;
        }
        massflow {
            direction   input;
            extVar      mdot_out;
            fmu         pss0;
        }
    }
}
```

definition of FMU

definition of interfaces CFD ⇔FMU

Figure 3. Example of 'systemCoupling' dictionary file.

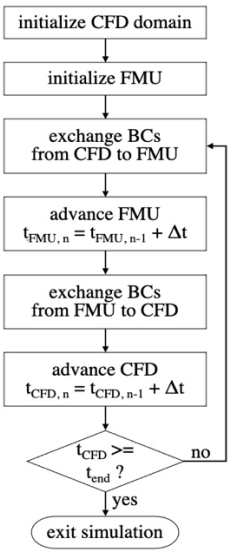

Figure 4. Serial-explicit code coupling scheme.

Table 1. PSP test case simulation parameters

CFD Parameters	
Steam mass flow inlet	$\dot{m} = 0.963$ kg/s
Steam temperature	$T_{CFD} = 400$ K
Pipe diameter	$\emptyset = 0.6$ m
System Model Parameters	
Wetwell cross-section	$A_c = 9$ m^2
Wetwell initial volume	$V_{water} = V_{gas} = 27$ m^3
Wetwell initial temperature	$T_{water} = T_{gas} = 300$ K
Water-gas interface heat transfer coeff.	$\alpha = 5$ W/(m^2·K)
Downcomer outlet above pool bottom	$l_{in} = 1$ m

IV. RESULTS

The implemented code coupling scheme is currently extensively verified and validated. However, for brevity, the focus of this paper lies on the motivation of possible application scenarios. For this reason, the prototypical implementation of a PSP is shown.

To further illustrate the previously-mentioned coupling, Figure 2 shows the implementation of a simple PSP test case. In the CFD domain, a steam flow at constant rate and temperature through a pipe is simulated. In the system model, a wetwell similar to the one described in [11] is implemented (see Figure 5), and subsequently exported as FMU. Data exchange between the two works as follows: At the pipe outlet, massflow-averaged temperature and pressure are evaluated in CFD and forwarded as boundary condition to the FMU. The FMU in turn internally applies these values to a ThermoPower "SourcePressure" component, as shown in Figure 2 (right). Thereby, a mass flow results from the pressure difference between pressure source, downcomer pipe flow resistance, and wetwell water pool pressure. By adding a mass flow meter component to the circuit, the measured value is transferred back to the CFD domain to act as pipe outlet BC.

Running the simulation with the parameters in Table 1 leads to the results as shown in Figure 6. Steam exits the CFD domain and enters the system model at a temperature of 400 K. The water volume in the wetwell then is heated by a rate of approximately 0.02 K per 1000 s. Through conductive heat transfer at the free surface between water and gas space in the wetwell, the gas space (air) temperature closely follows this trend. With the gradual increase in water mass and temperature, the pressure in the wetwell rises as well (Figure 6, bottom). The difference in pressure between pressure at the outlet in the CFD domain and the wetwell downcomer pipe outlet is due to the modeled pipe flow resistance in the system model. The wetwell heating rate is slightly higher than a first-order approximation ($\Delta Q = m \cdot c_p \cdot \Delta T$); thereby it can be concluded that the coupling is conservative and plausible.

```
// Water and air volumes
V_w = A_c*l_w;
V_g = A_c*(l_t - l_w);

// Water-Air heat transfer
Q_w_g = alpha*A_c*(Medium.temperature(waterState) - T_g);


// Water mass and energy balance
rho_w*A_c*der(l_w) = w_w_in;
rho_w*V_w*der(h_w) = w_w_in*(h_w_in + (l_i - 0.5*l_w)*g)
                     - Q_w_g;

// Water pressure of lumped volume and
// at blowdown pipe outlet
p_w = p_g + 0.5 * l_w * rho_w *g;
p_i = p_w + (0.5*l_w - l_i) * rho_w * g;


// Air mass and energy balance
m_g = V_g*rho_g;
der(m_g) = 0;
rho_g*V_g*cp_g*der(T_g) = V_g*der(p_g) + Q_w_g;
```

$$V_{water} = A_c \cdot l_{water}$$
$$V_{gas} = A_c \cdot (l_{total} - l_{water})$$

$$Q_{water \Leftrightarrow gas} = \alpha \cdot A_c \cdot (T_{water} - T_{gas})$$

$$\rho_{water} \cdot A_c \cdot \frac{\mathrm{d}l_{water}}{\mathrm{d}t} = w_{water,in}$$
$$\rho_{water} \cdot V_{water} \cdot \frac{\mathrm{d}h_{water}}{\mathrm{d}t} = w_{water,in} \cdot (h_{water,in} + (l_{in} - \frac{1}{2} l_{water}) \cdot g) - Q_{water \Leftrightarrow gas}$$

$$p_{water} = p_{gas} + \frac{1}{2} l_{water} \cdot \rho_{water} \cdot g$$
$$p_{in} = p_{water} + (\frac{1}{2} l_{water} - l_{in}) \cdot \rho_{water} \cdot g$$

$$m_{gas} = V_{gas} \cdot \rho_{gas}$$
$$\frac{\mathrm{d}m_{gas}}{\mathrm{d}t} = 0$$
$$\rho_{gas} \cdot V_{gas} \cdot c_{p,gas} \cdot \frac{\mathrm{d}T_{gas}}{\mathrm{d}t} = V_{gas} \cdot \frac{\mathrm{d}p_{gas}}{\mathrm{d}t} + Q_{water \Leftrightarrow gas}$$

Figure 5. Excerpt of simple wetwell model implementation in OpenModelica (left), and its formulation analogous to [11] (right).

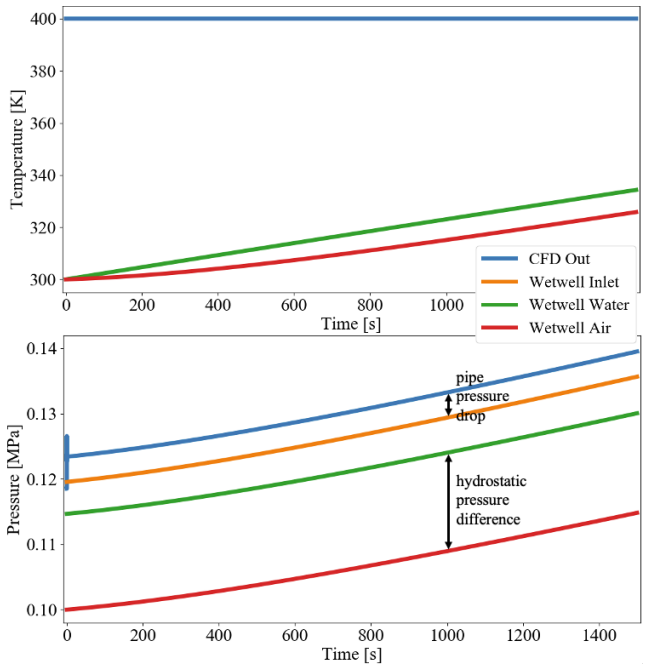

Figure 5. Simulation results: Temperature (top) and pressure (bottom).

V. CONCLUSION AND FURTHER WORK

A concept for an open accident analysis platform with a coupling between CFD and thermo-fluid dynamic system models was presented. Through standardized interfaces and code access, collaboration through model exchange is promoted. To give an application example, the prototypic simulation of a pressure suppression system is shown.

As further work to enhance the platform, stability improvements for simulation cases with large transients will be needed, as discussed by [12]. In particular, a step forwards from the serial-explicit coupling towards a stabilized semi-implicit approach.

Finally, to foster and further promote sharing and re-use of implemented system models in the community, the plug-in infrastructure can be ported to other OpenFoam-based simulators [13].

VI. Acknowlegdements

This work is complementary to and partly motivated by the IAEA Open-source Nuclear Codes for Reactor Analysis (ONCORE) initiative, a collaborative framework for the development and application of open-source multiphysics to support research, education, and training in analysis of advanced reactor designs.

The authors gratefully acknowledge professor Stefano Lorenzi for his help in getting started with Modelica.

VII. References

[1] S. Kelm et al., "The Tailored CFD Package 'containmentFOAM' for Analysis of Containment Atmosphere Mixing, H2/CO Mitigation and Aerosol Transport," Fluids, vol. 6, no. 3, 100, Mar. 2021.

[2] A. Gerschenfeld, "Introduction to Multiscale Approach," presented at the Joint ICTP-IAEA Course Theor. Found. Appl. Comput. Fluid Dyn. Nucl. Eng., Trieste, Italy, Sep. 2021.

[3] J. Long, B. Zhang, B.-W. Yang, and S. Wang, "Review of Researches on Coupled System and CFD Codes," Nucl. Eng. Techn., vol. 53, no. 9, pp. 2775–2787, Sep. 2021.

[4] K. Zhang, "The Multiscale Thermal-Hydraulic Simulation for Nuclear Reactors: A Classification of the Coupling Approaches and a Review of the Coupled Codes," Int. J. Energy Res., vol. 44, no. 5, pp. 3295–3315, Apr. 2020.

[5] S. Lorenzi and A. Cammi, "Use of Open-Source Modelica-based Li- braries as System Code for Nuclear Power Plant Simulation," presented at the IAEA Tech. Meeting Develop. Appl. Open-Source Model. Simul. Tools Nucl. React., Milano, Italy, Jun. 2022.

[6] S. Lorenzi, A. Cammi, and C. Fiorina, "Use of Open-Source Tools in Education and Training: Experience from POLIMI and EPFL," presented at the IAEA Tech. Meeting Develop. Appl. Open-Source Model. Simul. Tools Nucl. React., Milano, Italy, Jun. 2022.

[7] P. Fritzson et al., "The OpenModelica Integrated Environment for Modeling, Simulation, and Model-Based Development," Model. Identification Control: Norwegian Res. Bull., vol. 41, no. 4, pp. 241–295, 2020.

[8] A. Cammi, F. Casella, M. Ricotti, and F. Schiavo, "Object-Oriented Modeling, Simulation and Control of the IRIS Nuclear Power Plant with Modelica," presented at the 4th Int. Modelica Conf., Hamburg, Germany, Mar. 2005.

[9] F. Casella and A. Leva, "Modelica Open Library for Power Plant Simulation: Design and Experimental Validation," presented at the 3rd Int. Modelica Conf., Linköping, Nov. 2003.

[10] "Functional Mockup Interface for Model Exchange and Co-Simulation, Version 2.0.2," Modelica Association, Tech. Rep., Dec. 2020.

[11] R. A. Berry et al., "RELAP-7 Theory Manual," Idaho National Laboratory, Idaho Falls, Idaho, Tech. Rep, Feb. 2014.

[12] A. Toti, J. Vierendeels, and F. Belloni, "Improved Numerical Algorithm and Experimental Validation of a System Thermal-Hydraulic/CFD Coupling Method for Multi-Scale Transient Simulations of Pool-Type Reactors," Ann. Nucl. Energy, vol. 103, pp. 36–48, May 2017.

[13] C. Fiorina, I. Clifford, S. Kelm, and S. Lorenzi, "On the development of multi-physics tools for nuclear reactor analysis based on OpenFOAM®: state of the art, lessons learned and perspectives," Nucl. Eng. Des., vol. 387, p. 111604, Feb. 2022.

This project has received funding from the Euratom research and training programme 2014-2018 under Grant Agreement No. 847553.

+Proceedings of the European Nuclear Young Generation Forum ENYGF'23
May 8-12, 2023, Kraków, Poland

ELSMOR – towards European Licensing of Small Modular Reactors

Szogradi, Marton[1*], Buchholz, Sebastian[2], Lansou, Sylvain[3], Lombardo, Calogera[4], Ferri, Roberta[5], Reinke, Nils[2], De Angelis, Alessandro[6], Davelaar, Frans[7], Liegeard, Clément[8], Bittan, Jeremy[7], Värri, Konsta[9], Ricotti, Marco[10], Tulkki, Ville[1]

[1] VTT Technical Research Centre of Finland Ltd. (VTT), Finland, [2] Gesellschaft für Anlagen- und Reaktorsicherheit (GRS), Germany, [3] Framatome, France, [4] Agenzia Nazionale per le nuove tecnologie, l'energia e lo sviluppo economico sostenibile (ENEA), Italy, [5] SIET S.p.A., Italy, [6] University of Pisa (UNIPI), Italy, [7] Électricité de France S.A. (EDF), France, [8] Commissariat à l'Energie Atomique (CEA), France, [9] Fortum, Finland, [10] Politecnico di Milano (Polimi/CIRTEN), Italy

*Corresponding author: *marton.szogradi@vtt.fi*

I. Introduction

In recent years more and more high-level goals have been articulated on the global stage by governments, utility companies and other stakeholders, considering the decarbonization of energy production [1]. The efficacy of such developments will depend on the success of low-level projects, which aim to reform our energy systems. A practical candidate, replacing fossil fuels in these future energy mixes, is nuclear energy. Besides heavy-duty electricity production other industrial and communal needs could be served by integrating novel nuclear systems e.g. microreactors and small modular plants.

The ELSMOR (towards European Licensing of Small Modular Reactors) project addresses the latter topic as an answer to the Horizon 2020 Euratom NFRP-2018-3 call, titled "Research on the safety of Light Water Small Modular Reactors" [2]. The consortium comprises 15 partners from 8 European countries, involving research institutes, major European nuclear companies and technical support organizations. The 3.5-year project, launched in September 2019, investigates selected safety features of light-water (LW) small modular reactors (SMRs) with focus on licensing aspects. Providing a comprehensive compliance framework that regulators can adopt and operate, the licensing process of such SMRs could be streamlined and optimized enabling early deployment.

II. Project structure and progress

Activities have been thematised in 7+1 work packages (WPs), 7 targeting different topics of SMRs and their specific safety features relevant for safety analyses, plus one WP dedicated to project coordination. For demonstrative purposes, a new European SMR (E-SMR) design has been developed in WP5. This master model was shared among participants and work packages thus the activities have been revolving around the E-SMR primarily while taking into account industrial expertise e.g. with respect to multi-unit operation and transient management.

A. WP1: Identification of improved safety features of LW SMRs

Practices on light-water reactor safety assessment had been reviewed with respect to international and state-level regulations and guidelines. European Union (EU) directives establish a high-level and technology-neutral framework that can be directly applied to SMRs. The International Atomic Energy Agency (IAEA) has not published any safety guidance explicitly dedicated to SMRs, regardless, available LW pressurized water reactor (PWR) criteria and guidance should apply to SMRs, based on the same technology. The Western European Nuclear Regulators' Association (WENRA) outlines safety objectives concerning design, site, construction, commissioning and operation. These objectives call for extended safety demonstration, considering new reactors as well as the reinforcement of the Defence-in-Depth (DiD) concept. Some accident scenarios which had been considered beyond design basis accidents for existing reactors (e.g. multiple failure and core melt scenarios) are now enshrined in the design process of new plants, hence these cases are regarded as design extension conditions (DEC).

European Nuclear Safety Regulators Group (ENSREG) directives are based on and updated according to international, legally binding safety conventions and EU legislation. These directives are in line with regulatory methodologies, developed under the auspices of international bodies e.g. IAEA, Organisation for Economic Co-operation and Development Nuclear Energy Agency (OECD NEA) and WENRA. Therefore, ENSREG reiterates the previously noted remarks on SMR safety features. State-level nuclear regulations were found to be applicable to LW SMRs in general, where the review considered EU member states (France, Germany, Lithuania) and non-EU countries (Canada, UK, USA). It has to be noted that approaches

differ regarding safety philosophy, e.g. Canada and the UK adopted non-prescriptive methodologies while the US legislation is more prescriptive. This implies that design specific reviews have to be performed by a given regulatory body in a case-by-case manner, which might be highly unpractical.

A review of the most advanced LW SMR designs was carried out, focusing on for instance reactivity control, decay heat removal, containment integrity and multi-unit operation. Strong differences between SMR concepts and operating large PWRs were noted, e.g. with respect to fuel cycle management. Several new designs foresee 48- and 72-month fuel cycles, having further implications on reactivity control. In some cases the operation is planned to be boron-free in order to reduce construction costs while simplifying primary system chemistry (e.g. reduced ^{3}H-production and corrosion rates). Instead of boric acid these concepts strongly depend on burnable absorbers and control rods, such design decision raises the question, how do these fuel characteristics affect safety demonstration methods? Another important issue is the extensive use of passive safety systems for decay heat removal. These systems incorporate a large degree of uncertainty in terms of analytical capabilities and experimental know-how. Thus, validation and verification (V&V) efforts require more attention from all stakeholders of the nuclear sector.

The prescribed safety demonstration methodologies face potential challenges, depending on technology and plant-specific attributes. Some of the most prominent features were found to be multi-unit siting (using a single control room with reduced staff), high burn-up cores (aging issues), severe accident (SA) mitigation (affecting practical elimination and emergency planning zones (EPZs)) and the impact of passive safety system on reliability assessments.

B. WP2: Development of safety case methodology

Addressing the outlined licensing challenges, WP2 focused on the development of methodologies, supporting the safety demonstration with qualitative and quantitative recommendations. Regarding multi-unit siting, new initiating events should be considered which might lead to more complex accidental sequences, depending on the level of independence between the units. Since a single event could impact several units simultaneously, there could be a higher risk of potential radiological releases which would also require more stringent mitigation. The impact of one unit on the whole plant (cross-effect) should be limited, especially with respect to shared equipment. Propagation of events, especially internal hazards, from one unit to others shall be prevented. The sizing of a shared safety equipment must suffice to secure its function simultaneously on several units. Considering probabilistic safety assessment (PSA), the traditional risk matrix should be extended to incorporate multi-unit sequences. As one of the major factors in PSA, common cause failure quantification has to be revisited, taking into account the number of impacted equipment (which may be too high on a modular site to provide an accurate quantification) and their nature (whether the equipment is shared or not by several units). These profound modifications of the risk matrix would also justify the need for new numerical targets i.e. event frequency limitations.

A general ELSMOR methodology was developed to help the safety assessment of innovative light-water reactor designs. This method is accompanied by principles, appropriated from other methodologies, the complete algorithm is presented in Figure 1.

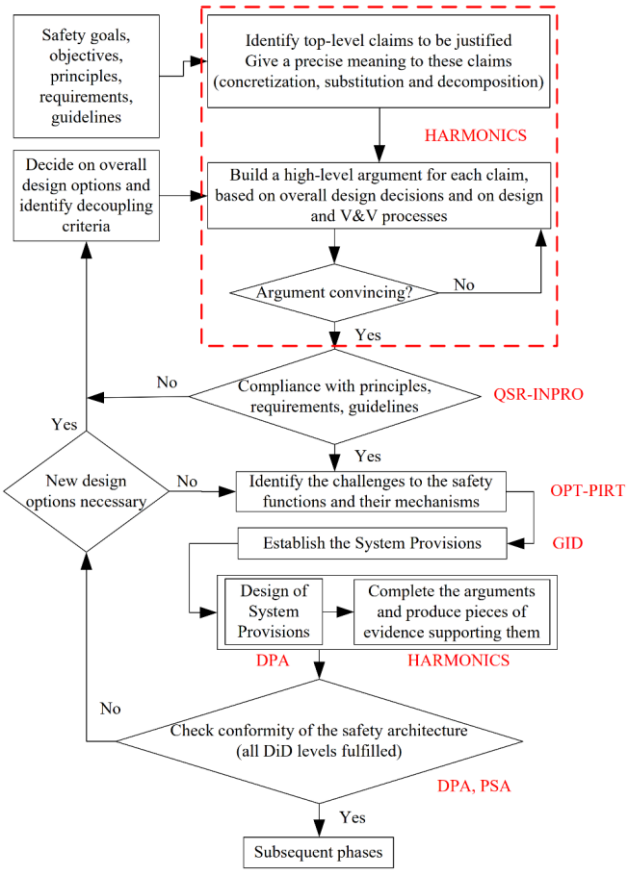

Figure 1. The proposed safety case methodology for ELSMOR (provided by Framatome)

As part of the general ELSMOR approach, a flexible, non-accident specific method, called Graphical Independence of DiD assessment (GID), has been developed by Framatome for subsequent safety demonstration. GID is applicable to pre-conceptual, conceptual and final designs. The method tests the functions (e.g. reactivity control) and sub-functions (e.g. ensuring core subcriticality, preventing uncontrolled reactivity insertion) which have to be ensured to control fundamental safety functions during accidents by assessing the degree of system independence at various DiD levels. In practice this means that the postulated initiating events are paired up graphically with provisions at each level of DiD from design basis to extension conditions in order to check the robustness of the plant. In our case, GID will be applied in WP5 to the heat removal function of the E-SMR. Referring to severe accident scenarios, an EPZ methodology was conceived to evaluate multi-unit plants. For the E-SMR, the determination of EPZ distances can be performed using the DEC analyses of WP5, if the SA data show substantial release of fission products.

C. WP3: Core cooling safety functions

The work package consists of 5 tasks which address uncertainties related to the assessment and modelling of passive safety systems. The first task was dedicated to the compilation of a phenomena identification ranking table

(PIRT) on passive safety systems of integrated pressurized-water SMRs for decay heat removal. The second task represented a literature review with the summary of SMR-relevant experiments concerning safety. The third task incorporated the design, installation and operation of a new experimental facility at SIET's facility in Piacenza, Italy. The main goal of the campaign is to provide a versatile database for subsequent validation activities with respect to plate-type heat exchangers (HXs) by perturbing various parameters e.g. flow rates, pool level, non-condensable (NC) injection, secondary side filling ratio, etc. The test facility was commissioned in Q4 2022, single- and two-phase tests are planned for Q1 2023. The test loop consists of a primary circuit, a plate-type compact steam generator (CSG), a secondary circuit and a large water pool with an in-pool safety condenser. The E-SMR design was used as reference for the scaling of the facility, nominal parameters and the schematics are depicted in Figure 2.

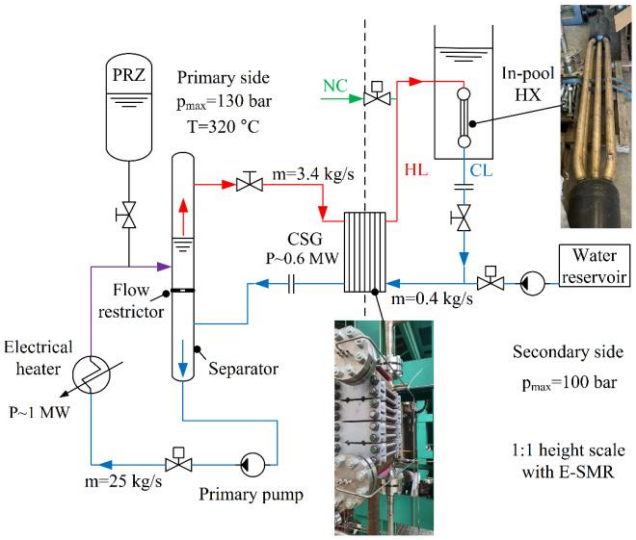

Figure 2. Layout of the ELSMOR facility (photos by SIET)

The facility operates in a natural circulation regime on the secondary side while the primary pump delivers the primary coolant to the electrical heater. Under single-phase conditions (filled separator) a flow restrictor divides the coolant flow between the CSG and the pump. Under two-phase conditions (flow restrictor removed, separator partially filled) steam can reach the CSG, the fresh condensate then returns to the separator.

The fourth task explores code capabilities and possible options for further development with extra attention to passive safety systems. The figure of merit contains lumped-parameter (LP) codes such as AC^2, Apros, CATHARE and RELAP5. As a result of benchmarking and validating with measurement data, the shortcomings of various system codes will be identified considering such plate-type heat exchanger with regards to natural circulation. In order to study the multiphase fluid dynamics of the CSG, a test loop was assembled at Polimi featuring a Chevron-type compact plate HX. Besides obtaining a versatile flow pattern map, pressure characteristics and high-speed video footage, the data also aided computational fluid dynamics (CFD) modelling activities focusing on cross-periodic flows.

D. WP4: Containment safety functions

The submerged containment concept of the E-SMR is investigated in this WP with emphasis on CFD and LP code assessment. Prior to modelling activities, a PIRT was established featuring 42 phenomena, ranked by relevance and level of expertise. The table was centered on the NUWARD™ and NuScale™ SMRs with respect to station blackout (SBO), loss-of-coolant accident (LOCA) and DECs. The major sources of uncertainty were related to the water wall, heat transfer processes in the containment and the late phase of an accident with core degradation. Establishing a robust V&V library required the survey of available experimental data. It was found that data on large water pool tests are still scarce or proprietary. Even though downscaled facilities exist, mimicking the behaviour of containments with water-wall (e.g. INKA [3], PANDA [4], PASI [5]), the suitability of the data for code validation purposes is questionable due to low Rayleigh numbers ($Ra < 10^{14}$) characterising free convection heat transfer. Nonetheless, the validity range of some valuable data might be extended to a range of Ra numbers of higher interest for ELSMOR.

Regarding code applications, a single-phase (#1) and a more ambitious, possibly two-phase flow case (#2) were defined resembling the submerged containment of the E-SMR. In both cases, the atmosphere was assumed to be the ultimate heat sink, dominating heat losses on the concrete walls of the pool. Since the evaluation of the results is ongoing, only an excerpt of preliminary results can be given hereby. Case #1 Ansys CFD results of GRS suggested that small structural components on the containment outer wall have small influence on the overall temperature and velocity fields in the water wall. The Lithuanian Energy Institute (LEI) adopted a coarser 3D Cartesian-grid for spatial discretization in ATHLET to compare the model against high-fidelity codes. Even though 3D effects were captured in the pool, due to the scale of the nodalization micro-scale phenomena e.g. boundary layer effects could not be depicted adequately. University of Pisa deployed CATHARE and STAR-CCM+ to compare 0D and 3D simulations using integral parameters. Average pool temperatures highlighted growing discrepancies between the two approaches from early on (see Figure 3).

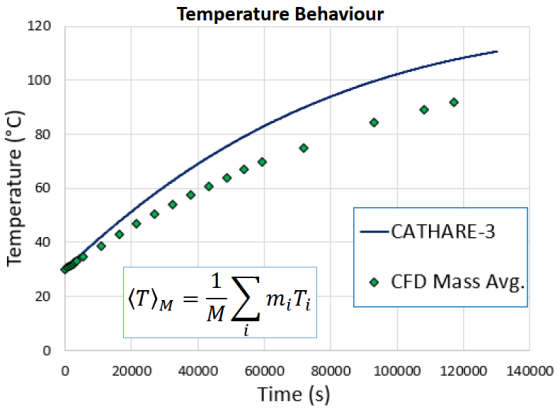

Figure 3. Bulk pool temperature trends in LP and CFD models (provided by UNIPI)

Despite profound differences in the approaches of CFD and LP models, the results showed consistency with respect to

fluid flow fields (mixing vs. stratification) and grace time until saturated conditions. 3D analyses supported simplifying assumptions, considered in 2D simulations in which an axisymmetric domain was used. Broader plant analyses require the coupling of the RPV, containment and water wall, these studies are subjects of WP5.

E. WP5: Example of application of safety case methodology

In order to demonstrate the safety assessment methodology and modelling capabilities in design basis accident (DBA) and DEC scenarios a novel reactor design was established by a core group of partners, including notably Polimi and VTT. The unit specifications heavily rely on the conceptual version of the NUWARD™ SMR [6] albeit numerous modifications were made in terms of geometry and passive safety systems for example. The reactor is an integrated pressurized-water SMR featuring plate-type compact steam generators (6xCSGs). No active safety systems have been implemented, decay heat removal is realized via the passive condenser (P-COND) and safety CSGs (2xS-CSG) while additional coolant inventory is provided by low-pressure hydroaccumulators (4xACCs). The input deck describes the containment, the water wall and rudimentary control logics, besides the RPV and its auxiliary systems. Main parameters of the plant are given in Table 1, the schematics of the unit are illustrated in Figure 4.

Table 1. Main attributes of the E-SMR (nominal conditions)

Property	Value
Core/CSG power	540/90 MWth
Primary/secondary coolant pressures	150/45 bar
Primary/secondary flow rates	3700/240 kg/s
Core inlet/outlet temperatures	300.0/324.5 °C
Containment/water wall free volumes	1732/5481 m^3
Containment/water wall coolant inventories	125/5457 t

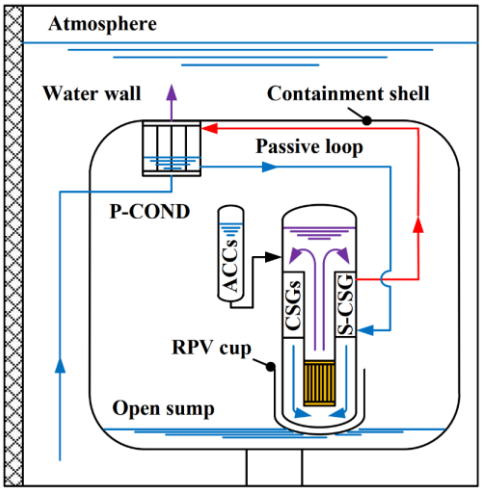

Figure 4. The onion structure of the E-SMR unit (provided by VTT)

As decay heat function, the ANS94-3a curve was chosen and extended since DBA calculations envelope 72-hr transients while DEC simulations cover a timeframe of 15 days. Regarding the core, a 76-assembly configuration was selected with AREVA-NuScale inspired fuel properties.

Ongoing DBA analyses with the Apros code at VTT have shown promising performance. During station blackout transients the passive loop activates as the S-CSG loads-up after reactor shutdown. A pilot-operated relief valve on the top of the RPV is responsible for fast-response primary depressurization, this actuation yielded a ~700 kg (1.1 %) primary inventory loss in the Apros model. Afterwards the reactor pressure gradually decreased and the RPV water level fell. At 15 bar the ACCs started to refill the RPV with room-temperature water. Such low pressure was proven sufficient considering ACC utilization while preventing rapid transients e.g. related to pressurized thermal shock. By the end of the 3-day simulation not even the upmost water wall nodes could reach saturation. Pool temperatures are depicted in Figure 5 where the maximum node temperature was 92.6 °C. The LOCA case considers a ⌀40 mm guillotine break on an ACC injection line as the most conservative location. Apart from the initiating event, the model will not be altered, the same boundary conditions will be applied as for SBO.

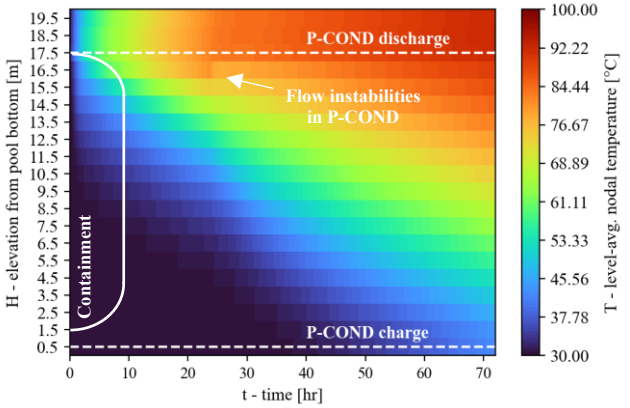

Figure 5. Temperature trends in the Apros water wall during SBO (provided by VTT)

DEC analyses reiterate the DBA scenarios without the passive condenser, allowing partners to assess core degradation with ASTEC and MAAP. The results will provide information on containment response (e.g. non-condensable gas plugging) while long-term trends will depict the behaviour of the corium. These studies are crucial in evaluating in-vessel retention strategies, H_2 combustion risks and mitigating options.

F. WP6-7: Dissemination - Education & training

The consortium is preparing a collection of articles by Summer 2023, in which 10 articles will outline the work, performed in ELSMOR. WP materials, discussed in the present paper, are continuously uploaded to the project's website [2]. In 2022, Polimi organized the "International Summer School on early-deployable SMRs" with 63 students from 24 countries. The lecture materials, prepared by international experts, will be published at [2] along with additional video materials by the end of the project.

III. Synopsis & outlook

ELSMOR tackles an array of critical aspects of light-water SMR licensing. The project establishes a thorough assessment methodology for such purposes, based on extensive experimental and analytical work. The upcoming TANDEM project [7] will utilize the E-SMR design for subsequent cogeneration plant studies, considering H_2 production, district heating and power supply for urban areas. These projects establish a platform for a more active dialogue between regulatory bodies and representatives of the nuclear industry in order to accelerate the deployment of LW SMRs. Engagement from all stakeholders will be required after these projects to utilize the results and obtained expertise.

IV. List of abbreviations

ACC – Accumulator

Apros – Advanced Process Simulation Software

ASTEC – Accident Source Term Evaluation Code

CEA – Commissariat à l'Energie Atomique

CFD – Computational Fluid Dynamics

CIRTEN – Consorzio Interuniversitario per la Ricerca TEcnologica Nucleare

CSG – Compact Steam Generator

DBA – Design Basis Accident

DEC – Design Extension Condition

DiD – Defence-in-Depth

DPA – Deterministic and Phenomenological Analyses

EDF – Électricité de France

ELSMOR – towards European Licensing of Small Modular Reactors

ENEA – Agenzia Nazionale per le nuove tecnologie, l'energia e lo sviluppo economico sostenibile

ENSREG – European Nuclear Safety Regulators Group

EPZ – Emergency Planning Zone

E-SMR – European Small Modular Reactor

EU – European Union

GID – Graphical Independence of DiD

HARMONICS – Harmonised Assessment of Reliability of MOdern Nuclear I&C Software

HX – Heat Exchanger

LEI – Lithuanian Energy Institute

LOCA – Loss-Of-Coolant Accident

LP – Lumped-Parameter

LW – Light-Water

MAAP – Modular Accident Analysis Program

NC – Non-Condensable

NEA – Nuclear Energy Agency

OECD – Organisation for Economic Co-operation and Development

OPT – Objective Provision Tree

P-COND – Passive Condenser

PIRT – Phenomena Identification Ranking Table

Polimi – Politecnico di Milano

PSA – Probabilistic Safety Assessment

PWR – Pressurized Water Reactor

QSR-INPRO – Qualitative Safety features Review - International Project on Innovative Nuclear Reactor and Fuel Cycle

RELAP – Reactor Excursion and Leak Analysis Program

RPV – Reactor Pressure Vessel

SA – Severe Accident

SMR – Small Modular Reactor

TANDEM – Small Modular ReacTor for a European sAfe aNd Decarbonised Energy Mix

UNIPI – University of Pisa

V&V – Validation & Verification

VTT – Valtion Teknillinen Tutkimuskeskus

WP – Work Package

V. References

[1] M. Paloneva, S. Takamäki, “Summary of sectoral low-carbon road maps, Finnish Government,” Ministry of Economic Affairs and Employment, February 2021.

[2] “ELSMOR official website,” 14 January 2023. [Online]. Available: http://www.elsmor.eu/about/.

[3] S. Leyer, M. Wich, “The Integral Test Facility Karlstein,” *Science and Technology of Nuclear Installations,* vol. 2012, 2011.

[4] D. Paladino, J. Dreier, “PANDA: A Multipurpose Integral Test Facility for,” *Science and Technology of Nuclear Installations,* vol. 2012, p. 239319, 2011.

[5] V. Kouhia, V. Riikonen, O.-P. Kauppinen, et al., “PASI – A test facility for research on passive heat removal,” *Nuclear Engineering and Design,* vol. 383, p. 111417, 2021.

[6] IAEA ARIS database, “Status report - NUWARD (EDF lead consortium),” [Online]. Available: https://aris.iaea.org/PDF/F-SMR_2020.pdf. [Accessed 17 01 2023].

[7] “TANDEM official website,” [Online]. Available: https://tandemproject.eu/. [Accessed 20 01 2023].

Proceedings of the European Nuclear Young Generation Forum
ENYGF'23
May 8-12, 2023, Kraków, Poland

Impact of the spray safety system on the hydrogen risk based on a GOTHIC 3D containment model

Vázquez-Rodríguez, Carlos[1,2*], Fontanet, Joan[3], Jimenez, Gonzalo[2], Herranz, Luis Enrique[3], Domínguez-Bugarín, Araceli[2], Serra, Luis[2], and Kelm, Stephan[1]

[1] Forschungszentrum Jülich GmbH, Germany; [2] Universidad Politécnica de Madrid, Spain; [3] CIEMAT, Spain

*Corresponding author: *c.vazquez-rodriguez@fz-juelich.de*

I. INTRODUCTION

During a severe accident in a nuclear power plant, combustible gases such as hydrogen (H2) and carbon monoxide (CO) can be released, leading to a potential combustion risk in the nuclear containment building. The interest in the combustion risk evaluation was revived by the explosions recorded in Unit-1, Unit-3, and Unit-4 reactor buildings of Fukushima Daichii in 2011. The AMHYCO Project (EU-funded Horizon 2020 project) aims to improve the understanding of H2/CO combustion and incorporates this knowledge into the Severe Accident Management Guidelines (SAMGs) [1]. The potential improvement for the H2/CO combustion risk evaluation must rely on the close interaction of multiple disciplines: experimental investigations of H2/CO mixtures under realistic accidental conditions, modelling of the involved phenomena using different analytical tools with a wide range of thermal-hydraulic resolution, and an in-depth review of the actions scoped at the current SAMGs [1].

Among the several needs of the project, the work presented in this article falls between two of its main tasks: (i) the identification of sequences with significant H2/CO combustion risk; and (ii) the detailed numerical analysis of these sequences with state-of-the-art computational codes of different thermal-hydraulic resolution (LP, 3D, and CFD). Specifically, this article will present the preliminary implementation of a sequence identified in task (i), a Large Break Loss of Coolant Accident (LBLOCA) calculated with MELCOR, in a 3D GOTHIC containment model of a generic PWR-W that will be used for the simulations of task (ii).

Task (i) was the main objective of the Work Package (WP) 2 of AMHYCO. The selection of Severe Accident (SA) sequences was based on a set of agreed criteria [2]: high molar fractions of combustible gases (H2 + CO) in control volumes which conditions are within flammability limits; large total mass of combustible gas within the containment; and, fast combustible gas release rates. The sequences evaluation is concluded by a qualitative assessment process.

Task (ii) was the core of WP4 of AMHYCO, whose final objective is to support the assessment, revision, or extension of existing SAMGs in WP5. The SA sequences are long transients, and the SAMGs evaluation will require to perform several sensitivities for the safety system actuations. WP4 foresees the use of full-containment 3D models to perform part of these evaluation. Therefore, the development of models with affordable computational times, which should have the ability to represent the safety systems actuation, may be one of the critical issues of the project.

The development of a 3D GOTHIC model of a PWR-W containment is covered in section II, and it relied on previous works addressing the challenges of AMHYCO WP4. For example, the methodology to handle the geometrical database for the models is described in [3]. The specific modelling guidelines to decrease the computational cost of the GOTHIC model is summarized in [4]. Finally, the validation of GOTHIC to simulate one of the principal safety system, the spray cooling system, based on PANDA experiments was published in [5], and the implementation of the system in the coarser mesh of a containment model was studied in [6].

All the points discussed above evidence that the work presented in this article is just a small piece of all the multiple fields of knowledge needed to comply with AMHYCO's objectives. The simulations presented in section III are focus on evaluating the performance of the model during the in-vessel phase in terms of computational cost. Furthermore, a preliminary evaluation of the implementation of different safety system and the impact of their actuation in the combustible gases risk are briefly discussed.

II. PWR-W GOTHIC 3D MODEL

The containment of the generic PWR-W is a steel-lined post-tensioned reinforced concrete structure, which accommodates a Westinghouse 3-loops PWR. The reinforced concrete structure consists of a vertical cylindrical wall and a semi-ellipsoidal dome. The principal characteristics of the PWR-W containment safety analysis are included in Table 1.

The PWR-W is modelled with GOTHIC8.3(QA), which is a thermal-hydraulics code based on a two-phase, multi-fluid formulation, solving separate conservation equations for mass, momentum, and energy for three fields: vapor, continuous liquid, and droplets (Euler-Euler) [7]. The 3D discretisation of the spatial domain is limited to Cartesian meshes. GOTHIC is a porous media code where the presence of the solids is represented by the inclusion of porosity factors to the cells' volume and cells' faces surface, which are included in the conservation equations. The coupling between the fluid and the solid relies on correlations for all the heat transfer modes. Using correlations and fluid bulk values, rather than attempting to model the boundary layers in detail, the code permits to combine a 3D thermal-hydraulic resolutions with relatively coarse meshes.

The basic methodology used to build the PWR-W GOTHIC model was already presented in 2016 [8]. From the available plant layouts, the model development starts from the creation of a detailed CAD model, which is later modified to a simplified CAD using the geometrical bodies compatible with GOTHIC. Though respecting its fundamentals, the modelling methodology has been progressively updated. The model used in this paper was built following the latest update, which was already presented in the previous edition of ENYGF [3], [4].

The most relevant characteristics of the latest modelling methodology are the use of homogeneous meshes and the considerable simplification of the real geometry to adapt it to the defined mesh. Both features have demonstrated their potential to considerably decrease the computational cost of the simulations while keeping the level of accuracy of the models [4]. Essentially, the presence of solids mostly occupying cells or cell faces created challenging numerical conditions slowing down the calculations [4]. Therefore, the geometry is adapted to the mesh, as shown in Figure 1, avoiding the problematic cells. The simplifications of the geometry are performed while keeping the figures relevant to the containment thermal-hydraulics (free volumes, heat transfer surfaces, size of the connection between compartments, etc.).

Table 1. PWR-W main characteristics for containment analysis

3-loops PWR-W			
Thermal Power	2 940 MW	PARs FR-1500	20
Free Volume	61 293 m^3	PARs FR-960	20
Liner Surface	7 754 m^2	Spray Nozzles	208
Concrete Surface	13 988 m^2	Spray Flow Rate	208 kg/s
Steel Surface	18 178 m^2	Drop Diameter	700 µm

The PWR-W has been discretised using a relatively coarse 1x1x1.5 m homogeneous mesh, giving 42700 active cells. GOTHIC includes a drop breakup model representing the water flashing during the reactor blowdown. The condensation in the presence of non-condensable gases uses a diffusion layer model (heat-mass transfer analogy). The turbulence is modelled using the STD k-ε model. The droplets are represented with a mono-dispersed population, using the Sauter mean diameter to characterise the mass, heat, and momentum transfer between the droplets and the vapor phase.

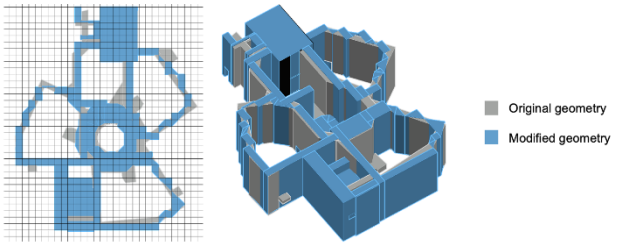

Figure 1. Geometrical modification to adapt the geometry to the Cartesian mesh

The spray system consists of three rings of nozzles located at different heights. The lower, medium, and upper rings have 104, 60, and 44 nozzles, respectively. Each nozzle injects 1 kg/s of droplets with a Sauter mean diameter of 700 µm. During the Direct Spray injection phase (DSpray) the system is fed from the Water Storage Tank (WST) at 30 ºC. When the tank is empty, the system takes water from the bottom of the containment. In this version of the model, the temperature of the water during the spray recirculation phase was defined as a boundary condition (approx. 75 ºC, an approximate value for a situation without intermediate cooling between the water source and the nozzles). The modelling of the recirculation phase was an important step of these preliminary simulations since sinking > 200 kg/s of water in a single cell (replicating the real system) hindered the stability of the solution. The numerical efficiency of the implemented solution is evaluated in section III.

Last, the model includes a total of 40 Passive Autocatalytic Recombiners (PARs) of Framatome types FR-1500 (x20) and FR-960 (x20). According to the PAR vendor [9], and for the conditions chosen to measure the nominal recombination rate, these PAR types recombine 5.36 kg/h and 1.2 kg/h of H2, respectively. This gives a total hydrogen recombination rate of 131.2 kg/s .

III. RESULTS

When the simulations included in this chapter were performed, the priority was to check the numerical stability of the model and the expected performance of the different safety systems. From the list of sequences produced during WP2, the most challenging for the model stability was the Large Break Loss Of Coolant Accident (LBLOCA) due to the high velocities and the extreme gradients associated with the blowdown phase. The mass and energy releases of the LBLOCA calculated with MELCOR [2] are introduced in the 3D PWR-W GOTHIC model as boundary conditions. First, an unmitigated transient without PARs nor sprays is simulated as a reference scenario (*wo PAR&Spray*). Next, the performance of the safety systems is evaluated with three additional cases with a single parametric change: a case activating the PARs (*wPAR*), a case with the direct injection phase of the sprays (*woPAR/wDSpray*) without the spray recirculation phase, and a case including the spray recirculation phase (*woPAR/wSprayR*).

The postulated LBLOCA was a double-ended break in the cold leg. The break was followed by a failure of all redundancies of the high- and low-pressure injections. Thus, the accumulators are the only remaining water source for cooling the reactor core. The containment pressure reached the spray activation criteria (260 kPa) within three seconds;

however, the system response took approximately 100 seconds (time needed to activate the pump and feed the system). The core uncovery started 550 seconds after the break, and considerable amounts of hydrogen reached the containment approximately at 1500 seconds. The switch to the spray recirculation phase occurred at 6670 seconds, and the simulation was stopped at 9600 seconds, just before the beginning of the molten core concrete interaction, which was out of the scope of these preliminary simulations.

As stated in chapter I, the main objective of these simulations was to check the numerical stability of the 3D model with the large flow velocities and mass and energy gradients induced by the LBLOCA. Figure 2 is used to evaluate the computational cost of the simulations providing the real time (*CPU time*) needed to simulate each second of the transient *(LBLOCA time*) by using 3 Intel i7-8700 cores (3.2 GHz) of a desktop computer. The timestep of the simulation is automatically controlled by GOTHIC according to several numerical criteria. As shown in Figure 1, the most time-consuming period of the simulation was the blowdown phase of the LBLOCA. This fact was due to the high velocities induced close to the break, which lowers the time step in GOTHIC to comply with the limitations on the Courant number. The computational cost for all the cases was driven by the high velocities near the break location during the first 200 seconds. The four cases of Figure 2 were split into two pairs of curves: the squares&diamonds with lower computational cost and the slower cases of triangle&circle. The common feature of the last two cases was the spray activation, which induced more restrictive conditions for the courant limiter from 200 seconds onwards. Indeed, the activation of the spray considerably increased the total simulation time (from 47 hours for the cases without spray to 90 and 104 hours for the cases with spray). The case including the spray recirculation phase (*wSprayR,* had the highest computational cost.

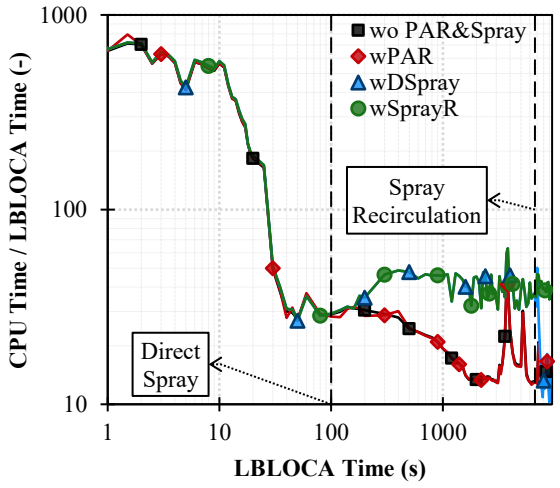

Figure 2. PWR-W LBLOCA computational cost for different safety system activation criteria (3 x Intel i7-8700 CPU @ 3.20GHz)

Figure 3 shows the pressure evolution of the four cases presented in this article. The pressure results are divided into two graphs: on the left, the x-axis represents the time after the break in logarithmic scale to enhance the visibility of the fast pressure increase related to the LBLOCA blowdown phase; on the right, the time is in linear scale also for easing the interpretations of the results. The double-ended LBLOCA induced a pressure increase from the initial 100 kPa to 380 kPa in 25 seconds, when the condensation in the cold surfaces of the containment balanced the steam injection. Later, the condensation rate was larger than the steam source rate, decreasing the pressure to 366 kPa 100 seconds after the break, when the spray system was activated in two of the four cases. The spray cooling induced two very different pressure evolutions. The pressure for the two cases without the spray was ≈ 280 kPa 3000 seconds after the break, whereas the pressure for the two cases with spray was 150 kPa.

The non-monotonic behaviour of the pressure shown in Figure 3 after 3000 seconds was related to intermittent injections of significant masses of steam from the reactor pressure vessel. In the late phase of the transient, the pressure differences between the two cases without spray were due to the heat released by the PARs recombination, which increased the average temperature of the containment. The final pressures for the cases without spray were 298 kPa and 310 kPa. For the cases using the spray, the final pressures were 185 kPa and 182 kPa. It is important to note that the case that included the spray recirculation phase injected the water at the sump temperature without intermediate cooling, and therefore its pressure evolution was similar to the case postulating the failure of the spray recirculation (*wDSpray).*

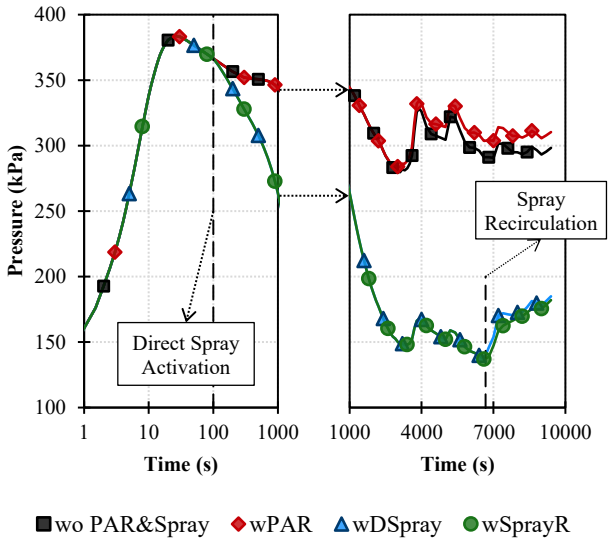

Figure 3. PWR-W LBLOCA Containment pressure with different safety system activation criteria. Log scale on the left and linear on the right.

Figure 4 shows the last result of the section, which is a volume-averaged volumetric concentration of hydrogen for the full PWR-W containment. The hydrogen concentrations shown in Figure 4 were linked to the spray and PAR operation. The lower pressures of the cases using the spray system meant lower steam concentrations and, therefore, higher values for hydrogen volume fractions. The PARs demonstrated their ability to decrease the hydrogen concentration in the late phase, ending with a hydrogen concentration below 3% - lower than the low flammability limit – versus the value close to 5% of the reference case (*wo PAR&Spray*). The case postulating the failure of the spray recirculation (usually when changing the system alignment from the WST to the containment sump) had a

final hydrogen fraction of 7.4% *(wDSpray)*, 0.6% higher than the case with spray recirculation *(wSprayR)*. Since the droplets injected during the recirculation phase were approximately at 75º C, their saturation pressure was higher than the steam partial pressure. Therefore, the droplets injected during the recirculation phase were evaporated, increasing the steam concentration, and consequently decreasing the hydrogen volume fraction.

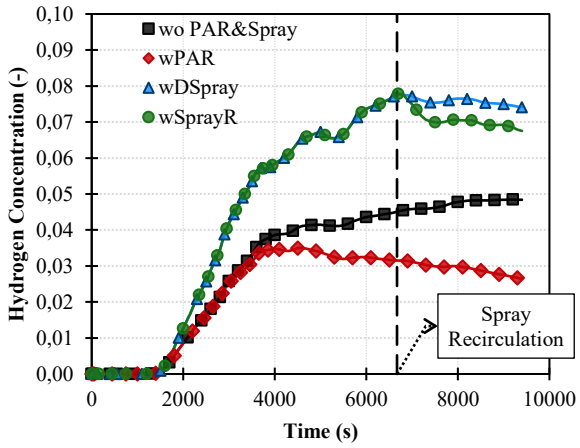

Figure 4. PWR-W LBLOCA hydrogen average fraction with different safety system activation criteria.

IV. CONCLUSIONS

In the context of the EU-funded Horizon 2020 AMHYCO project, a 3D containment model of a generic PWR-W has been developed with GOTHIC8.3(QA). The stability of the model and its optimisation in terms of computational cost have been tested with a challenging transient, an LBLOCA calculated within the framework of AMHYCO. Furthermore, most of the main systems for the containment safety analysis, such as the PARs and the spray, have been successfully implemented. Without needing a cluster (3 x i7 cores), the calculations of a ~10 000 seconds long LBLOCA took between 2 and 4.5 days, depending on the hypotheses on the safety system actuation. These are affordable computational costs for the scope of the AMHYCO project.

The evaluation of some of the main thermal-hydraulic variables of the containment, such as the pressure and the hydrogen concentration, offered the first insights into the impact of the safety systems actuation on the hydrogen risk. The PARs induced a slightly larger pressure, but this fact is less relevant than its ability to decrease the average concentration of hydrogen. The spray system condensed most of the steam released to the containment atmosphere, consequently increasing the average hydrogen concentration. Though this article only included global/averaged variables, the local information offered by the 3D discretisation will offer a more detailed quantification of the combustion risk than the traditional approaches (0D). These comprehensive analyses will be included in future dissemination of the results of AMHYCO.

Further developments of the 3D model presented in this work are currently ongoing. The filtered containment venting system, which will also be assessed within AMHYCO, is being implemented in the model. Furthermore, there is work in progress to define the optimal way to introduce the molten corium concrete interaction data, which is calculated by severe accident codes for the ex-vessel phase, as boundary conditions for the containment codes. Finally, new correlation and mechanistic physical models are being coupled with the containment models to give more representative recombination rates for the PARs in an ex-vessel atmosphere (H2, CO, CO2, and potential O2 starvation).

V. ACKNOWLEDGMENTS

The AMHYCO project has received funding from the Euratom research and training programme 2019-2020 under Grant Agreement n°945057. The content of this paper reflects only the author's view. The European Commission is not responsible for any use that may be made of the information it contains.

VI. REFERENCES

[1] G. Jiménez *et al.*, 'AMHYCO PROJECT – Towards an enhanced accident management of the H2/CO combustion risk', in *NURETH-19*, 2022.

[2] L. Herranz *et al.*, 'High Combustion Risk Sequences. Identification and Characterization', in *10th European Review Meeting on Severe Accident Research (ERMSAR2022)*, Karlsruhe, Germany, May 2022.

[3] L. Serra, A. Domínguez-Bugarín, C. Vázquez-Rodríguez, G. Jiménez, S. Kelm, and L. E. Herranz, 'Development of a detailed 3D CAD model of a generic PWR-KWU containment as a basis for a better assessment of H2/CO combustion risk', in *ENYGF21*, Tarragona, 2021.

[4] S. Arfinengo-del-Carpio, C. Vázquez-Rodríguez, and G. Jiménez, 'Preventive methodology: geometric simplifications a priori for containment models optimization with the GOTHIC code', in *ENYGF21*, 2021.

[5] C. Vázquez-Rodríguez *et al.*, 'Assessment of the depressurisation and mixing effects of two spray systems in the PANDA facility, part II – Simulations using GOTHIC8.3(QA)', *Nucl. Eng. Des.*, vol. 403, p. 112120, Mar. 2023, doi: 10.1016/j.nucengdes.2022.112120.

[6] C. Vázquez-Rodríguez, M. Andreani, J. M. Martín-Valdepeñas, and G. Jimenez, 'Implementation of the spray safety system on a 3D containment model of a generic PWR-W', in *47ª Reunión Anual de la Sociedad Nuclear Española, Cartagena, Región de Murcia*, 2022.

[7] EPRI, 'Thermal Hydraulic Analysis Package, Version 8.3(QA)', EPRI, Palo Alto, CA, 2018.

[8] R. Bocanegra, G. Jimenez, and M. K. Fernández-Cosials, 'Development of a PWR-W GOTHIC 3D model for containment accident analysis', *Ann. Nucl. Energy*, vol. 87, pp. 547–560, Jan. 2016, doi: 10.1016/j.anucene.2015.10.022.

[9] Framatome, 'Framatome Passive Autocatalytic Recombiners'. https://www.framatome.com/solutions-portfolio/docs/default-source/default-document-library/product-sheets/a0642-p-ge-g-en-201908-par.pdf?sfvrsn=748c9be2_2 (accessed Feb. 04, 2022).

Technical track 2
Nuclear Safety and Security

Proceedings of the European Nuclear Young Generation Forum
ENYGF'23
May 8-12, 2023, Kraków, Poland

Proposing a methodology for evaluating multi-unit risks of novel small modular reactors

Ibrahim A. Alrammah[1*]

[1] King Abdulaziz City for Science and Technology (KACST), Riyadh, Saudi Arabia

*Corresponding author: irammah@kacst.edu.sa

I. INTRODUCTION

Probabilistic safety assessment (PSA) provides a reliable framework for safety decision making. It allows modifications in a NPP elements and systems to be compared to a common quantitative basis of risk estimate. PSA aims to find out design weaknesses and main risk contributors the NPP, and this helps to enhance the robustness of the plant [1].

PSA has to date been effectively utilised in several fields of technology and various industries [2]. It is mainly used in nuclear activities, and aerospace and aviation industries [3]. PSA is also used for process industry, marine and civil engineering structures [4]. The first successful application of PSA in nuclear power industry is the Reactor Safety Study WASH-1400 carried out for nuclear safety. Since then, PSA has been applied for safety study of many existing NPPs, and for the design and licensing of new plants [5].

PSA has gained good experience from application to large light water reactors (LWRs). While for small modular reactors (SMRs) that grasp increasing attention nowadays, the application of PSA should be refined according to the special characteristics of such concepts. PSA presents an integrated tool of a plant safety. It is a logical and mathematical technique for estimating numerical figures that represent the safety case of an NPP and other industrial installations. The design of SMRs takes place with multiple modules that can share components and structures or not at a single site within a full plant. The consideration of multi-unit site risk including the operation of plant sites in the commercial or the regulatory authorities needs to be emphasised.

There is an increasing tendency to consider innovative SMRs planned either as single modules in distant sites or as multi-units constructed in a single site, as this option is more practical and resource efficient. Some of these projects are modular reactors with a collection of four to eight reactor modules that share some supporting and auxiliary systems and structures. Multi-unit sites include reactors with essentially separate facilities as well as several that employ highly integrated and shared support systems. Some have the capability to cross connect the emergency core cooling systems and others have shared control rooms. Though, such sites have probable risks of concurrent multiple plant hazards mainly due to external events.

The current paper aims to present considerations for a proposed approach to multi-unit PSA. It also introduces insights that considers PSA approaches in order to evaluate the hazards that could threaten a multi-unit nuclear site. The proposed framework could assist as a roadmap to support the process of using PSA in licensing evolutionary SMRs.

II. HOT TOPICS

For multi-unit sites there has been limited development in terms of evaluating and assessing the safety significance of multi-unit risks and the consequences of substitute measures such as core damage frequency (CDF) and large early frequency release (LERF) despite the acknowledgement of its importance by organisations such as the IAEA. There were several events that affected multi-unit sites. Examples include:

- The Oconee Turbine Building Flood (1976): that resulted in near miss core damage on three units.
- Le Blayais External Flood (1999): that caused degradation of safety systems at four reactor units.
- The Great Japan Earthquake and Tsunami (2011): this event resulted in: loss of offsite power; tsunami site inundation at two sites; core damage on three reactor units and major challenge to protect three units and spent fuel storage.
- Loss of offsite power events (1970-2015): in many sites worldwide and several regional events [6].

What is known publicly by Fukushima disaster has led to a plenty of studies and lessons learned. Some of these insights follow:

- Tsunami inundated the Daini and Dai-ichi sites and resulted in major damage at both sites; seismic induced loss of power at several other sites.
- Core damage at Dai-ichi Units 1, 2, 3 had core damage; containment breach; site contamination; wide radioactive material releases; shortage in accident management resources.
- Main causes of accident comprised flood damage to emergency switchgear in Units 1-4; weakness in emergency preparedness for multi-unit loss of AC and DC power; problematic containment venting procedures, disorder in the facility command and control; multi-unit interactions.
- Ad hoc and heroic operator actions instrumental in protecting cores and spent fuel in Units 4,5, and 6 and preventing releases during evacuation.
- Missed opportunities to identify and fix vulnerabilities from PSA:
  - Explicit evidence from tsunami hazard studies not considered.
  - Internal flood PSA would have identified issue with lack of flood protection inside the plant [6,7].

Simultaneous event sequences on two or more modules on a site can be the result of events such as seismic events, the event of loss of service and power offsite lost events. Using shared and dependent systems as well as CCFs in redundant systems at multi-unit sites can considerably influence the likelihood of multiple concurrent reactor accidents. At an NPP there are a number of critical inter-unit dependencies which have an impact on forming an integral risk statement. Such systems as those for service water supply and electric power. Compared with the linear combination of single reactor accidents at each unit, multi-unit accident sequences are predicted to be one of the main factors in multi-unit risk and therefore needs to be considered [8], also an exclusive event on one unit could impact other units.

In comparison with single-unit PSA studies, there is limited discussion in the available literature on the subject of multi-unit effect. The common consensus is that it is a "good practice", although it is also accepted that conducting such an assessment and interpreting the results represent significant methodological challenges [9]. Today, the multi-unit probabilistic safety assessment (MUPSA) is not explicitly considered when assessing the risks of a NPP [10].

There are recommendations as to how various different aspects of a MUPSA; yet there is still a lack of established comprehensive methods that can account for dependencies relating to multi-unit sites during the construction of a MUPSA [11].

There have been few PSA applications that investigate the potential for event sequences that may involve accidents on two or more reactors simultaneously. One example is the original Seabrook PSA [12] which included a limited examination of such sequences initiated from full power operation [13].

The first PSA results for Seabrook Station were issued in 1983 before the cancellation of Unit 2 and before the operating license for Unit 1 was issued [12]. The project specification called for a state-of-the art PSA which was ultimately utilized to handle emergency planning subjects that caused delaying the licensing of that plant. It was a PSA of accidents initiated from full power and full investigation of internal and external events like fires, floods, and seismic events. That PSA comprised quantification of the integrated risk from operation of both units.

Since the original PSA for Seabrook Station was issued there have been a number of updates for external events analysis and supporting various risk informed applications. The CDF outcomes for the more recent updates are considerably lower than those developed in the original issue to account for design changes, modelling enhancements, risk management actions and updates to include various generic and plant specific data. However, some of the insights extracted from the original PSA are still valid when reviewing the results from a relative perspective. It is to be noted that the updated PSA results did not involve the multi-unit PSA since the Unit 2 was cancelled before the updates were issued. There are various crucial inter-unit dependencies at Seabrook Station that were found to affect the development of an integrated safety assessment.

III. CONSIDERATIONS FOR THE APPROACH

A. Sources of Dependencies between Units at a Site

Since there are about 100 systems in an NPP, there are several ways in which two or more units can be linked. A review of PSA applications displayed that the explicit target of a PSA at site level was to treat the dependencies that are between the units on that site. Dependencies have been split into seven main dependence classifications for the sake of adequately considering the risks in a MUPSA, as described below:

1) Initiating Events (IEs):

Initiating events (IEs) account for single events that have the capability of affecting multiple units within an NPP site. Despite the fact that several IEs that are integrated into a usual PSA have the capability to affect in excess of one unit at a site, not all do so. The IEs can therefore be split into two subclasses; namely definite and conditional

IEs. The definite IEs are those that can, for the most cases, affect multiple units; whereas conditional IEs will impact multiple units only under specific conditions.
The events which can always affect multiple units can be listed as the following: power offsite loss and ultimate heat sink loss in addition to several external events such as fires, tsunamis, floods, hurricanes, earthquakes, very high winds and temperatures. For conditional events which are capable to impact multiple units but under certain conditions they can be events like loss of service water, internal fire and flood, turbine missiles and vacuum loss [11].

2) **Shared connections:**

Shared connections represent the links between components that connect multiple units, so the cables, power divisions, piping etc. The most commonly considered interaction between units is that results from the sharing of systems. Shared systems are potential to:

- affect the success criteria for an individual system or group of systems,
- alter the frequencies of IEs previously considered (i.e., the frequency of occurrence is impacted by multi-reactor plant operation),
- introduce IEs not previously considered (i.e., new initiator categories due to multi-reactor plant operation), or
- change dependencies or present new dependencies between systems, or otherwise impact the response of the plant to initiating events [14].

Connections can be classified into three different classes:

1. A single Structure, System & Component (SSC). It is where a single SSC is relied upon for support by multiple units. For instance, in safety injection having a common header or the same plant exhaust stack.
2. Cross-connected or time sequential sharing SSCs. This is where a single unit is fully supported by an SSC yet it cannot support multiple units simultaneously. This is seen for instance in NPPs between electrical power supplies.
3. Standby sharing where a standby is shared between multiple units or a spare SSC which can only be utilised for single unit support. Such a method is often observed within systems used for safety such as fire water systems.

3) **Identical components:**

These are the components that are for multiple units and have the same design and operating conditions. The level of similarity means that the design, installation or maintenance is similar for the components making them prone to CCFs which are taken into account for single units. It includes digital Instrumentation and Control (I&C) systems along with conventional systems.

4) **Proximity dependencies:**

They are demonstrated in various ways. Such dependencies occur when multiple units can be affected by shared environment. This common situation can be created deliberately or unintentionally. The proximity can be positions between or within systems, within a room or may happen as a result of the site layout. In addition to this, independent areas may become connected due to doors and conduits. For example, a fire could catch multiple units in the instance where the chemical and volume control system. Similarly, if two adjacent units exist and an explosion was to occur onsite, this would affect both units.

5) **Human dependencies:**

They are also demonstrated in different ways. This is where multiple units are affected by the human interaction with machines. This could refer to any personnel who have direct contact with the machines such as the operator, maintenance team, installation team etc. Human dependencies can be divided into two categories known as post and pre-event actions. Latent conditions are usually created before an event such as when the same task is carried out by the maintenance team and therefore a similar failure environment is induced on multiple units for an operating plant. After an event happens it is usually the human factors that result in immediate consequences such as in the example of the control of multiple plants at the same time by the same operator causing a difficulty in terms of controlling or even noticing a developing problem on another unit [15].

6) **Organisational dependencies:**

These have several different factors. This occurs during the connection of multiple units by an organisation in the form of programmes such as procedures for operations, surveillance and emergencies, simulators for training, reliability assurance etc., where a logic error of some sort infiltrates the organisation. It may be inferred that organisational and human related dependencies have similarities however the root cause of the failure is where the distinction lies. For organisational dependencies it is usually caused by the culture of the organisation whereas for human dependencies these are caused by the interaction between humans and machines. In the case of the organisational culture this can refer to that within the whole plant or a particular department. It can also be from a contractor which supplies systems to a plant. Such dependencies can exist due to the same culture which is common among groups and impact several units and even several sites.

7) **Independent events:**

These are events which do not result in a dependency between multiple units. They comprise events where the occurrence is only for a single unit. Such events which are not part of the mentioned classifications would go under this category with a lot of SSCs for each unit falling into

this class. An example of an independent event would be Loss Of Coolant Accidents (LOCAs) [15].

B. Assumptions and Boundaries of the MUPSA Model

1. It is possible to form multi-unit accident sequences by combining sequences from the single-unit PSA models. This premise entails that:
    i. The set of single-unit Initiating Events (IEs) and sequences is collectively exhaustive. As a consequence, supplementary IEs or more single-unit accident sequences will not be required within the MUPSA procedure.
    ii. Site configurations are formed by applying the operation configurations allocated within each single-unit PSA (SUPSA) model with any necessary adjustments in order to account for any logically impossible combinations or combinations that are prevented by technical specifications.
    iii. Site Radiological Release States (RRSs) can be determined by merging the RRSs developed within the SUPSA models with any necessary adjustments to account for differences in release timing.
2. The MUPSA procedure will focus on detecting and evaluating risk-influencer multi-unit sequences. As a consequence:
    i. The MUPSA procedure will underscore the breadth of the analysis. It will first count all possible multi-unit accident sequences and consequences and then utilise various screening and scoping techniques to ascertain and concentrate on risk-influencer multi-unit sequences.
    ii. The screening and scoping methods used to focus on risk-influencer multi-unit sequences must take both the sequence frequency and sequence consequence into consideration.
    iii. In order to determine the objectives of screening and ranking, the consequences of a multi-unit accident can be roughly calculated by summing up the consequence scenarios of each unit which makes a contribution to the multi-unit accident.
3. The MUPSA procedure is a largely iterative in nature, such that intermediate findings can be used to enhance previously completed steps. The iterative nature of the procedure is not limited to the MUPSA procedure. On the contrary it simply pertains to the fact that SUPSA has always involved some form of iteration among the various analysis subtasks. The necessity for iteration within the MUPSA procedure should be carefully carried out to ensure that the dependencies are properly taken into account in the model and that an appropriate level of detail is used to produce valuable analyses.

C. Risk Metrics

The risk assessed for the current large light water reactors (LWRs) is mostly described in terms of risk objectives such as LERF and CDF which provide a sufficient risk metric for current LWRs as they can be used a substitute metric for the safety objective. However, for new modular reactors, quantitative values of CDF and LERF are so small and may therefore be meaningless [16]. Therefore, "Site level" metrics are needed as the single reactor risk metrics are insufficient in terms of capturing integrated risks of multi-unit sites [6]. There are limitations to CDF and LERF as the following issues are not addressed:

- The probability of single reactor events increases
- New accident sequences with multiple releases
- Non-core source release

The consequences arising due to the increasing of source term from multi-unit releases are:

- Latent health effects scale with source term as a result of linear dose response models
- Complex impacts due to differences in the release timing and points
- Early health effects not to scale as a result of non-linear dose response models

So, capturing risk from multiple unit NPPs has no basic way of manipulating CDF and LERF from single-unit PSAs. As a result, it is required to define new site level risk metrics [17]. A set of "site risk metrics" were proposed. Examples include [6]:

- Multi-unit CDF (MUCDF): the frequency of core damage involving two or more reactor units simultaneously.
- Site CDF (SCDF): the frequency of core damage where one or more reactor units are involved.
- Site LERF (SLERF): the frequency of a large early release from an accident encompassing one or more reactor units on the site.
- Individual risks to people in the close proximity of the site (Quantitative Health Objectives 'QHOs') may represent the integrated risks from all the units on the site.

IV. CONCLUSION

The purpose of a MUPSA approach is to estimate the total site risk and to determine the most significant contributors to the total site risk. The expression "total site risk" denotes the risk from accidents that impact one or more of the reactor units located at a site. The first step in MUPSA is to identify the risk influencers and estimate the risk from accidents that only impact a single reactor unit (by

'SUPSA'); consequently, the MUPSA process will focus on the risks arising from accidents that impact combinations of and interactions between the on-site radiological sources. The findings of the MUPSA process are expected to afford new insights to improve regulatory decision-making.

V. References

[1] S. Kondo, Lessons learned for PSA from the SGTR incident at Mihama, unit 2, in 1991, Reliability Engineering & System Safety. 45 (1994) 57–65. https://doi.org/10.1016/0951-8320(94)90076-0.

[2] P. Kafka, Probabilistic safety assessment: quantitative process to balance design, manufacturing and operation for safety of plant structures and systems, Nuclear Engineering and Design. 165 (1996) 333–350. https://doi.org/10.1016/0029-5493(96)01207-1.

[3] M. Čepin, Advantages and difficulties with the application of methods of probabilistic safety assessment to the power systems reliability, Nuclear Engineering and Design. 246 (2012) 136–140. https://doi.org/10.1016/J.NUCENGDES.2011.08.082.

[4] P. Kafka, Important issues using PSA technology for design of new systems and plants, Reliability Engineering & System Safety. 45 (1994) 205–213. https://doi.org/10.1016/0951-8320(94)90087-6.

[5] H. Tang, Development of a PSA-based safety assessment and management framework for a nuclear-based hydrogen generation system, 2014.

[6] K. Fleming, Expanding capabilities of PSA to address multi- unit sites, in: CRA's 2015 Risk Forum: Risk Analysis in an Uncertain World, 2015.

[7] V. Hassija, C. Senthil Kumar, K. Velusamy, Probabilistic safety assessment of multi-unit nuclear power plant sites – An integrated approach, Journal of Loss Prevention in the Process Industries. 32 (2014) 52–62. https://doi.org/10.1016/J.JLP.2014.07.013.

[8] L. Burgazzi, RL. Frano, Application of risk-informed probabilistic and deterministic safety approach to estimate the risk of external events, 2015.

[9] J. Vecchiarelli, K. Dinnie, J. Luxat, Development of a whole-site PSA methodology, 2014.

[10] M. Dennis, Framework for assessing integrated nuclear power plant site risk using dynamic probabilistic safety assessment, In: Technical analysis approach plan for level 3 PRA project., 2013.

[11] S. Schroer, An event classification schema for considering site risk in a multi-unit nuclear power plant probabilistic risk assessment, 2012.

[12] P. Lowe, Seabrook station probabilistic safety assessment, 1983.

[13] K. Fleming, On the issue of integrated risk – a PRA practitioners perspective, in: The ANS International Topical Meeting on Probabilistic Safety Analysis, San Francisco, 2005.

[14] M. Muhlheim, G. Flanagan, W. Poore, Initiating Events for Multi-Reactor Plant Sites, 2014.

[15] S. Schroer, M. Modarres, Initial classification of events to consider in a multi-unit PRA, in: The 20th International Conference on Nuclear Engineering, Anaheim, California, 2012.

[16] U.S.NRC, Feasibility study for a risk-informed and performance-based regulatory structure for future plant licensing, 2007.

[17] K. Fleming, Application of probabilistic risk assessment to multi-unit

Proceedings of the European Nuclear Young Generation Forum
ENYGF'23
May 8-12, 2023, Kraków, Poland

Integration of Automated Radiation Detectors into the Physical Protection System of Nuclear and Radiological Facilities in Handling Radioactive Sources; Potential Implications to Security of Nuclear and Radioactive Materials/Sources.

Gochera, Tinashe*

[1] Office of the president of Zimbabwe, Zimbabwe

*Corresponding author: *tinashegochera5@gmail.com*

I. INTRODUCTION

Management of nuclear and radioactive material in use and storage and of associated facilities embraces the establishment and implementation of policies, plans, procedures and processes. These in turn provide personnel with the needed authority and resources to establish and maintain an effective security system.

Radiation detectors have been used for nuclear safety and security purposes for a prolonged time especially in physical protection system in cases such as intrusion detection systems and radiation environmental monitoring systems. For radiation protection purposes intrusion detection system and radiation monitoring systems are usually parallel and independent systems. The dependent component of the operator's management in the PPS is usually integrated into the overall PPS in a manner that circumvents, or at least minimizes, conflicts with other elements of security management system, such as nuclear and radiation safety. In particular, the operator always ensures that security measures and safety measures do not conflict with one another and are mutually supportive. A good PPS management has the following three main resolutions: Ensuring the effectiveness and sustainability of the security system; Ensuring that personnel, procedures and equipment function effectively as a system (integration); Promoting a robust nuclear security culture.

Therefore, the objective of this synopsis is to explore the possibility of integrating and automating radiation detectors to improve work effectiveness and efficiency capabilities of the nuclear detection system.

II. BACKGROUND

Integration of radiation detectors equipped with various algorithms is now being used in various applications across the nuclear and radiation industry. These are being installed at checkpoints, but can also be mobile systems, vehicle-mounted or the detector itself can be mounted directly on a wall or a stand. The basic components of these integrated systems are the radiation detectors, alarms, control units, network systems and display units, but the system can be customized with optional components like access and barrier control interface to prevent a contaminated vehicle or person from leaving or entering the area. The display unit of this system is often supervised by security personnel, so as to the monitor the conventional security systems. The user interface of integrated radiation detectors provides useful information about the current and historical radiological situation also, it generates automatically reports and seldom provides support decisions to make life easier for operators.

Threat due to insiders should be paid attention since they could take advantage of their access rights, complemented by their authority and knowledge, to bypass dedicated physical protection elements or other provisions, i.e. safety procedures. The PPS is usually assisted by nuclear material accountancy and control (NMAC) measures to deter and detect the protracted theft of nuclear material by an insider.

A. PHYSICAL PROTECTION SYSTEMS IN NUCLEAR FACILITIES

This is an integrated system of detection, delay and response measures, and should be effective against both unauthorized removal and sabotage. It consists of people, procedures and equipment to provide defense in depth, with a graded approach, to address the range of threats identified in the applicable threat statement and to protect against both unauthorized removal and sabotage. Guidance on threat assessment and design basis threat is provided in IAEA Nuclear Security Series No. 10-G (Rev. 1), National Nuclear Security Threat Assessment, Design Basis Threats and Representative Threat Statements.

B. Automation of Physical Protection Systems

Automation is the key factor that will be increasingly present in the factories of the future, these are characterized by a set of software and hardware components that allows computer systems, network devices or machines to function without any manual intervention. Processes are completely automatic with the help of control loops and special logic therefore; operations can be performed without a human operator physically located at the site where the system is installed. These type of systems are being used in a wide range of applications, such as control and monitoring systems, data security applications, factory automation systems, automated message response systems.

Since a PPS includes interior and exterior intrusion detection sensors, cameras for assessment, delay measures, access control devices and response measures, it can also have several automated subsystems designed to pass information and video images to a central alarm station (CAS). The integration of these components can be used by operators as a basis to respond appropriately. The PPS integrates all physical protection measures and subsystems, but subsystems may be integrated together within the PPS. Therefore, there are boundless possibilities of integrating the entire PPS so as to come up with one unit connected by a network.

C. Regulatory Considerations

The operation of PPS defines the scope of the evaluation and identifies the security requirements against which compliance is to be verified, such as regulatory requirements, license conditions and provisions of the facility security. The scope should include the security system and security management elements to be evaluated. Evaluation criteria and methods of evaluation should be agreed with the regulatory body.

The State is responsible for establishing and maintaining a legislative and regulatory framework to govern physical protection. This framework provides for the establishment of applicable physical protection requirements and include a system of evaluation and licensing or other procedures to grant authorization. This framework includes a system of inspection of nuclear facilities and transport to verify compliance with applicable requirements and conditions of the license or other authorizing document, and to establish a means to enforce applicable requirements and conditions, including effective sanctions.

D. PPS Network, Information and Computer Security

Access to sensitive information might give an advantage to adversaries wishing to carry out unauthorized removal of nuclear material or sabotage of nuclear material and nuclear facilities. Sensitive information exists in many forms, such as software (unauthorized disclosure, modification, alteration, destruction or denial of use), these in-turn could compromise physical protection. Before designing and evaluating a PPS, operators need to establish internal policies, plans and procedures for protecting the confidentiality, integrity and availability of the sensitive information they hold or handle, in compliance with national security policy and the relevant national laws and requirements on information security.

PPS network design addresses the needs for both information security and physical protection of communication lines and network nodes. The system should have means of detecting and registering both explicit and implicit failures of components (e.g. devices, algorithms, signals). Special attention should be given to the protection measures at computer security zone boundaries (i.e. firewalls, limitation of data traffic) as well as physical and administrative controls. PPS network devices are continuously exposed to operating conditions that can reduce the life of the components (e.g. weather conditions, mechanical impacts, voltage variations, radiation fields). Periodic preventive maintenance of the physical protection network will increase PPS availability and extend the operational life. PPS network maintenance and testing activities should comply with computer security requirements.

Guidance on information security in a nuclear security context, including an example classification guide to assist in identifying sensitive information, is provided in IAEA Nuclear Security Series No. 23-G, Security of Nuclear Information [19], and Refs [1, 2] provide more specific guidance on the security of sensitive information relating to physical protection.

III. IMPLEMENTATION MODEL

The process for PPS design and evaluation should be systematic and preferably should employ a systems engineering approach. Systems engineering is an approach used to design and build complex systems, and includes processes for defining requirements, designing systems and evaluating designs. An integrated management system is used by facility managers to monitor and control all activities throughout a nuclear facility, including the PPS. Operation of a PPS includes all of the activities associated with the PPS, including maintenance and testing. Application of the management system helps to ensure that the PPS continues to meet its original design specifications and is modified as needed to address changes in requirements. An integrated management system can be applied to the PPS at a nuclear facility through a series of elements: requirements management; work direction and control; resource management; and assurance activities (Figure 1).

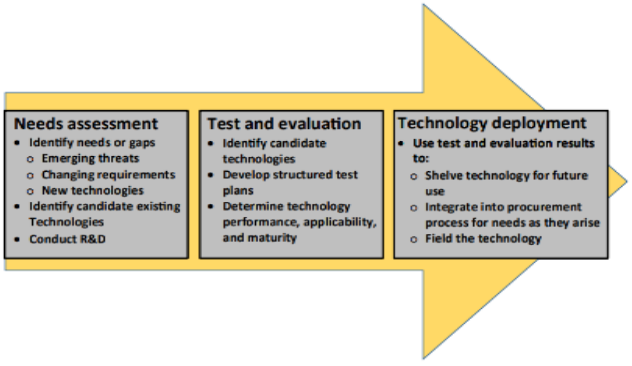

Figure 1. ***Technology development and management framework***

IV. SECURITY IMPLICATIONS AND POTENTIAL HAZARDS OF AUTOMATED DETECTION SYSTEMS,

The adoption of automation leads to significant advantages in economic and safety terms, these include the elimination of the risk of human errors, the improvement of user productivity, the development of standardized operations and a greater operations management. Automated systems must have high security standards since, if they can get exposed to spam, virus and other computer security threats, therefore they need a precise degree of protection. Regarding cyber security, threats against automation networks are haphazard, they can potentially yield destructive results. Attacks on networks include spoofing and denial of service which can cause the loss of process alarms and potential cause serious safety issues which can effect damages to the system but also to the external environment (other systems, workers).

Insiders are also a great challenge to a PPS because they have detailed information and are capable of using defeat methods not available to external adversaries.

In cases of computer network security, encryption of transmitted data might be used if physical access to PPS communications lines cannot be controlled. However, encryption can cause significant delays in communication as signals are encrypted and decrypted. The risks associated with increased communication times should be evaluated and taken into account while designing the PPS network. Use of encryption should be evaluated during the comprehensive asset inventory undertaken as the basis for a classification of computer systems according to importance.

V. CONCLUSION/ SUMMARY

The main focus of this paper was on highlighting the potential vulnerabilities and inequities that the use of Automation imposes on the dimensions of society. Automation reduces labor demand for people with the skills in question, workers reorient away from learning skills that have already been automated during their training. After this consideration there a strong need to evaluate new and emerging technologies to address technology development and new and emerging threats. This evaluation can facilitate the adoption of technologies that reduce costs, improve effectiveness, mitigate risk associated with new and emerging threats, and improve overall PPS functionality and capability.

In the event of insiders, the adoption of automated systems has proven to have an elimination effect to dependency of the human element which could take advantage of their access rights, authority and knowledge, to bypass dedicated physical protection elements.

A common weakness of integrated automated security and safety systems methods is that they all employ a reductionist approach to the identification of harm scenarios. The scenarios are predicted by examination of system's individual parts. This way, emergent hazard scenarios cannot be identified, as they emerge from a system without arising from any part of the system alone, but because of interactions between parts. They are often manifested in complex, highly coupled, systems, possibly in catastrophic ways. This, view, is a remaining challenge of a great importance that is left for future research.

VI. References

[1]. INTERNATIONAL ATOMIC ENERGY AGENCY, Nuclear Security Recommendations on Physical Protection of Nuclear Material and Nuclear Facilities (INFCIRC/225/Revision 5), IAEA Nuclear Security Series No. 13, IAEA, Vienna (2011).

[2]. INTERNATIONAL ATOMIC ENERGY AGENCY, Security of Radioactive Material in Use and Storage and of Associated Facilities, IAEA Nuclear Security Series № 11-G, IAEA, Vienna (rev.1, 2019)

[3]. NTERNATIONAL ATOMIC ENERGY AGENCY, Physical Protection of Nuclear Material and Nuclear Facilities (Implementation of INFCIRC/225/Rev.5), IAEA Nuclear Security Series No. 27-G, Vienna (2018)

[4]. INTERNATIONAL ATOMIC ENERGY AGENCY, Handbook on the Design of Physical Protection Systems for Nuclear Material and Nuclear Facilities, IAEA Nuclear Security Series No 40, Vienna (2021).

[5]. Tran-Quang, V., Dao-Viet, H. An internet of radiation sensor system (IoRSS) to detect radioactive sources out of regulatory control. *Sci Rep* 12, 7195 (2022). https://doi.org/10.1038/s41598-022-11264-y .

[6]. D. Hugon. Security of Automated systems – exploiting risk assessment as countermeasure against cyber-threats Mar 5, 2021 | Blog. https://valu3s.eu/security-of-automated-systems-exploiting-risk-assessment-as-countermeasure-against-cyber-threats/ .

Proceedings of the European Nuclear Young Generation Forum
ENYGF'23
May 8-12, 2023, Kraków, Poland

Numerical simulation of fast depressurization using a homogeneous model

GUN, Anıl Kemal[1*], GONCALVES, Eric[2] and HOARAU, Yannick [1]

[1] University of Strasbourg ICUBE laboratory, France; [2] ISAE-ENSMA Insitut Pprime, France

*Corresponding author: *anil-kemal.gun@etu.unistra.fr*

I. INTRODUCTION

Numerous industrial sectors, including the petroleum industry, turbomachinery, power generation plants, and naval engineering, can benefit from theoretical and numerical modeling of compressible two-phase fluid problems. There are various techniques for modeling two-phase flow in the literature, from one-fluid homogeneous mixture models [1] to complete models with seven equations [2].

Under normal operating conditions, the coolant in Pressurized Water Reactors (PWRs) is a liquid. However, in the event of an accident, it may change into a mixture of liquid and gas phases. Since the 1960s, a number of models for predicting two-phase flow in nuclear thermal hydraulics have been developed. However, the accuracy and complexity of these models and the numerical simulations based on them may vary due to the hyperbolic nature of the system. Many modeling efforts in nuclear thermal hydraulics have focused on predicting the behavior of PWRs during a Loss-Of-Coolant-Accident (LOCA), which is one of the most severe accident scenarios that can occur in a nuclear power plant. In these transient steam-water flows, two main physical phenomena are at play and interact with each other: the propagation of pressure waves and the transfer of mass. These phenomena are important to understand in order to accurately predict the behavior of the system. Therefore, it is expected that numerical models would deliver precise data about mechanical efforts on both nuclear fuel and other reactor components.

To obtain safety licensing for reactors, safety analyses usually concentrate on double-ended guillotine breaks at the cold leg because these types of breaks lead to the maximum flow out of the reactor coolant system. A sudden rupture of a pipe in the primary circuit leads to the rapid depressurization of the system. During the process of depressurization, the high-pressure coolant in the primary circuit comes into contact with the low-pressure atmosphere inside the containment structure. This can cause a rarefaction wave to propagate through the primary circuit and the Reactor Pressure Vessel (RPV). The depressurization wave moves in a single-phase liquid flow for the first few milliseconds of the accident and then transitions to a two-phase flow. At the beginning of a depressurization event, the coolant flow in the reactor core is reversed; however, once the break flow becomes saturated, the core flow is restored. The speed of the coolant flow is restricted by the liquid sonic velocity when it is in a subcooled state. However, when the coolant reaches a saturated state and flows through the break in two phases, the sonic velocity is significantly reduced. If the flow velocity at the break is equal to the sonic velocity, the flow is considered to be choked. During the saturated blowdown, the pressure waves become damped and the coolant exits the primary circuit in two phases at a critical flow rate [3]. When the primary system pressure falls to a specific level, the Emergency Core Cooling System (ECCS) releases a significant amount of borated coolant water to the primary system to ensure the cladding temperature remains within the allowed limits and for long-term cooling [4].

In this work, the numerical solution of the fast depressurization of water will be investigated using the reduced Kapila model [5], a four-equation model [6], which is three conservation laws for mixture quantities and void ratio for transport equation. CANON and SUPERCANON experiments [7], which could be assimilated to a two-phase tube with a mass transfer, are simulated through this model. These experiments, which were carried out in the late 1970s, were created to be a representation of LOCA in a PWR primary circuit in order to assess the depressurization of heated water.

II. GOVERNING EQUATIONS

The model consists in three conservation laws for mixture quantities and an additional equation for the void ratio. We present below the inviscid two-dimensional equations, expressed in variables $w = (\rho, \rho\vec{\vec{V}}, \rho E, \alpha)$:

$$\frac{d\rho}{dt} + div\,(\rho\vec{V}) = 0 \tag{1}$$

$$\frac{\partial(\rho\vec{V})}{\partial t} + div(\rho\vec{V} \otimes \vec{V} + PId) = 0 \tag{2}$$

$$\frac{\partial(\rho E)}{\partial t} + div\,(\rho \vec{V} H) = 0 \tag{3}$$

$$\frac{\partial \alpha}{\partial t} + \vec{V}.grad(\alpha) = K div(\vec{V}) \tag{4}$$

$$K = \frac{\rho_l c_l^2 - \rho_v c_v^2}{\frac{\rho_l c_l^2}{1-\alpha} - \frac{\rho_v c_v^2}{\alpha}} \tag{5}$$

where $\vec{V} = (u, v)$ denotes the centre of mass velocity, $E = e + V^2/2$ is the total energy of the mixture and $H = h + V^2/2$ is the entalphy of the mixture. The term K refers to the sound of the speed of pure phases and it reflects the effects of changes in the volume of each phase.

An equation of state (EOS), which connects the pressure and temperature to the internal energy and density, is required to complete the system. For this purpose, stiffened gas EOS was used:

$$P(\rho, e) = (\gamma - 1)\rho(e - q) - \gamma P_\infty \tag{6}$$

$$P(\rho, T) = \rho(\gamma - 1)C_v T - P_\infty \tag{7}$$

$$T(\rho, h) = (h - q)/C_p \tag{8}$$

$$c^2 = \gamma(P + P_\infty)/\rho = (\gamma - 1)C_p T \tag{9}$$

where $\gamma = C_p/C_v$ is the heat capacity ratio, C_p and C_v are thermal capacities, q is the energy of formation, and P_∞ is a constant reference pressure. The mass transfer term is activated when the local pressure P is smaller than the vapour pressure $P_v(T)$ which is calculated as:

$$P_v(T) = P_v(T_{ref}) + \frac{dP}{dT}(T - T_{ref}) \tag{10}$$

A thermodynamic table is used to evaluate the constant quantity dP/dT. When the mass transfer between phases takes places, the void ratio equation expression changes and becomes:

$$\frac{\partial \alpha}{\partial t} + div(\alpha \vec{V}) = (K + \alpha) div(\vec{V}) + \left(\frac{\frac{c_v^2}{\alpha} + \frac{c_l^2}{1-\alpha}}{\frac{\rho_l c_l^2}{1-\alpha} + \frac{\rho_v c_v^2}{\alpha}}\right) \dot{m} \tag{11}$$

Assuming that the mass transfer is proportional to the divergence of the velocity:

$$\dot{m} = \frac{\rho_l \rho_v}{\rho_l - \rho_v} + \left(1 - \frac{c^2}{c_{wallis}^2}\right) div(\vec{V}) \tag{12}$$

$$\frac{1}{\rho c_{wallis}^2} = \frac{\alpha}{\rho_v c_v^2} + \frac{1-\alpha}{\rho_l c_l^2} \tag{13}$$

The entalphy of each phase can be used to describe the speed of sound in the mixture:

$$\rho c^2 = (\gamma(\alpha) - 1)\left[\frac{\rho_v \rho_l}{(\rho_l - \rho_v)}(h_v - h_l)\right] \tag{14}$$

III. NUMERICAL METHOD

The four-equation model can be written in one-dimensional space as:

$$\frac{\partial U}{\partial t} + \frac{\partial G(U)}{\partial x} + B(U)\frac{\partial u}{\partial x} = 0$$
$$U = \begin{pmatrix} w \\ \alpha \end{pmatrix}, G(U) = \begin{pmatrix} F(w) \\ \alpha u \end{pmatrix}, B(U) = \begin{pmatrix} 0 \\ -K - \alpha \end{pmatrix} \tag{15}$$

Using finite-volume method, spatial and temporal domains are divided into regular meshes of the uniform length Δx and uniform intervals Δt, respectively;

$$\frac{U_i^{n+1} - U_i^n}{\Delta t \backslash \Delta x} + G_{i+\frac{1}{2}}^n - G_{i-\frac{1}{2}}^n + \int_{x_{i-\frac{1}{2}}}^{x_{i+\frac{1}{2}}} B(U)\frac{\partial u}{\partial x} = 0 \tag{16}$$

where i and n stand for discretization in space and time. The Riemann problem solution or any other numerical approach can be used to calculate numerical flux $G_{i+1/2}^n$. In this study, explicit time integration is used to perform numerical simulations, and Harten-Lax-van Leer Contact approximate Riemann solver (HLLC) is used to compute the convective flux through the cell interface [8]:

$$F_{i+\frac{1}{2}} = \begin{cases} F(w_L) & \text{if } S_L > 0 \\ F(w_L^*) & \text{if } S_L \le 0 < S_M \\ F(w_R^*) & \text{if } S_M \le 0 \le S_R \\ F(w_R) & \text{if } S_R < 0 \end{cases} \tag{17}$$

where S_L and S_R are the smallest and largest speed waves at the cell interface, respectively. The left *(K=L)* and right *(K=R)* states of corresponding fluxes (w_K^*) :

$$F(w_K^*) = \begin{pmatrix} \rho_k^* S_M \\ (\rho u)_K^* S_M + P^* \\ (\rho E)_K^* S_M + P^* S_M \\ \alpha_K^* S_M \end{pmatrix} \tag{18}$$

where the pressure P^* and the contact-wave speed S_M are given by:

$$P^* = P_L + \rho_L(u_L - S_L)(u_L - S_M) \tag{19}$$

$$S_M = \frac{P_R - P_L + \rho_L u_L(S_L - u_L) - \rho_R u_R(S_R - u_R)}{\rho_L(S_L - u_L) - \rho_R(S_R - u_R)} \tag{20}$$

Although there are different approaches related to determination of wave speed S_L and S_R in literature, simple wave speed estimation is used due to its computational efficiency and ease of implementation:

$$S_L = \min(u_L - c_L, u_R - c_R)$$
$$S_R = \max(u_L + c_L, u_R + c_R) \tag{21}$$

On the other hand, the discretization of the non-conservative section is based on the strategy suggested in [9]. The *B(U)* term is formulated as :

$$\int_{x_{i-1/2}}^{x_{i+1/2}} B(U)\frac{\partial u}{\partial x} \cong B(U_i)(u_{i+1/2} - u_{i-1/2}) \tag{22}$$

The interface cell value is then derived;

$$u_{i+1/2} = \begin{cases} u_L & \text{if } S_L > 0 \\ \dfrac{S_L - u_L}{S_L - S_M} S_M & \text{if } S_L \leq 0 < S_M \\ \dfrac{S_R - u_R}{S_R - S_M} S_M & \text{if } S_M \leq 0 \leq S_R \\ u_R & \text{if } S_R < 0 \end{cases} \quad (23)$$

IV. TEST CASES

To simulate a complete break LOCA of a PWR primary circuit, the Canon and Super-Canon experiments were set up. It entails opening a 100% break to rapidly depressurize a horizontal pipe. As can be seen Fig.1 the pipe is 4.389 m long with an internal diameter of 102.3 mm. The pipe has a membrane on one side and a closed end on the other. These studies of the LOCA are typical test cases for nuclear safety codes. At time zero, the tube is filled with under-saturated water, after the membrane is ruptured a rarefaction wave begins to travel up the pipe. In the experiments, whilst the void fraction is only measured at one location, the pressure is monitored along the pipe at many points.

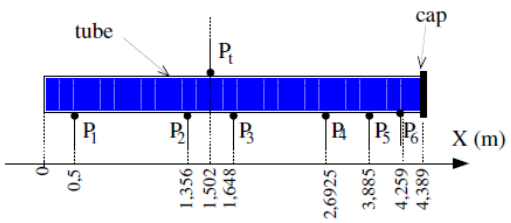

Figure 1. Schematic of experiment facility [10].

For the Canon test case $(p_0, T_0) = (32\ \text{bar}, 220℃)$, the stiffened gas EOS paramaters are given in Table 1. The computational domain is 10 m and on the right is a tank at atmospheric pressure. Initial conditions are given in Table 2.

Table 1. EOS paramaters for liquid and vapour for the Canon experiment

	Liquid	Vapour
γ	1.66	1.34
P_∞ (Pa)	769317123.86	0.00
q (kJ.kg^{-1})	-1359.57	2032.35
C_v (kJ.kg^{-1}.K^{-1})	2.80	1.16
q' (kJ.kg^{-1}.K^{-1})	11.67	2.35

In the second test case, Super-Canon, the pressure and temperature values were chosen to represent the PWR's primary loop exactly, and these values are 150 bar and 300 ℃. Stiffened gas EOS parameters are shared in Table 3, while initial conditions are given in Table 4.

Table 2. Initial conditions for the Canon experiment

		Pipe	Tank
α	liquid	.1-10^{-3}	10^{-3}
	vapour	10^{-3}	1-10^{-3}
ρ (kg.m^{-3})	liquid	841.12	837.74
	vapour	16.72	0.52
P (bar)	liquid	32	1
	vapour	32	1

Table 3. EOS paramaters for liquid and vapour for the Super-Canon experiment

	Liquid	Vapour
γ	.1.38	1.49
P_∞ (Pa)	570798395.20	0.00
q (kJ.kg^{-1})	-1530.70	2288.30
C_v (kJ.kg^{-1}.K^{-1})	3.61	0.60
q' (kJ.kg^{-1}.K^{-1})	-0.51	4.82

Table 4. Initial conditions for the Super-Canon experiment

		Pipe	Tank
α	liquid	.1-10^{-3}	10^{-3}
	vapour	10^{-3}	1-10^{-3}
ρ (kg.m^{-3})	liquid	736.45	717.72
	vapour	88.23	0.59
P (bar)	liquid	150	1
	vapour	150	1

As can be seen in the figures below, although the results obtained from the 4-equation model (shown as 4 Eq.) correctly predicted the pressure drop in the first few milliseconds for the Canon test case, they gave quite different results compared to the experimental results (shown as Exp.) in the following process. The main reason for this is based on the assumption of thermal and mechanical equilibrium in the 4-equation model, while thermal and chemical non equilibrium should be taken into account in fast depressurization systems. These test cases involve fluid conditions that are rapidly changing. Metastable conditions result from a delay in vaporization when a fluid enters the two-phase domain. Thus, in order to obtain the experimental data from the model, the metastable states of water must be considered. The Navier-Stokes Multi-blocks (NSMB) was used as a numerical solver. The NSMB solver is a program that uses the finite volume method to solve the compressible or incompressible Navier-Stokes equations on multi-block

structured grids. For more information about the solver, one can consult the NSMB Handbook [11].

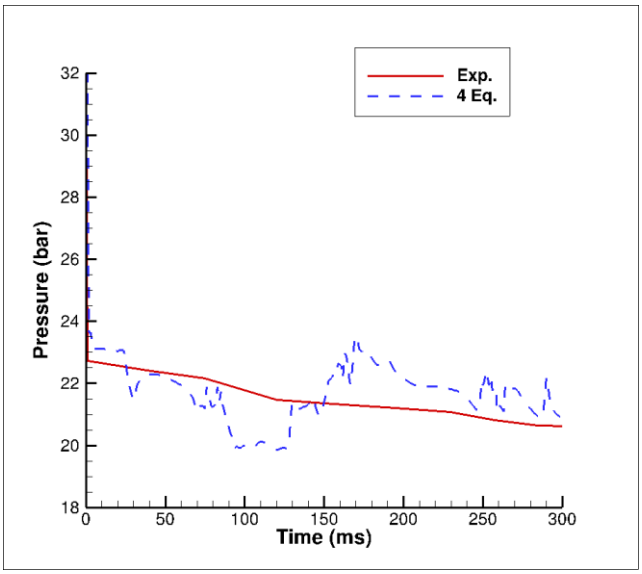

Figure 2. Pressure vs time at P1 location in Canon experiment.

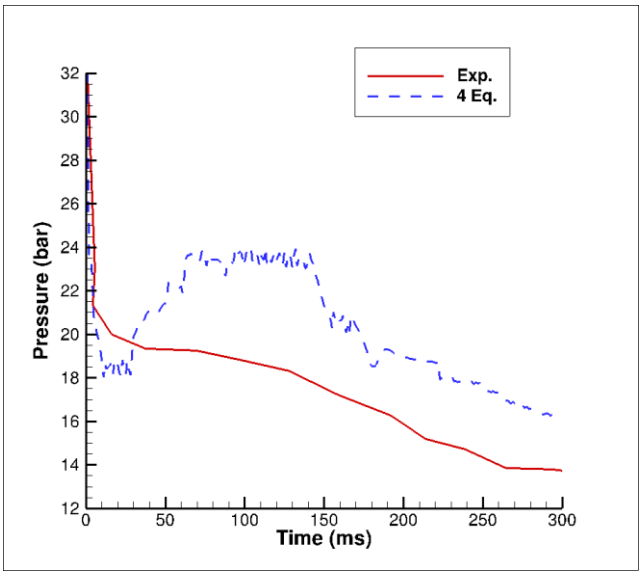

Figure 3. Pressure vs time at P5 location in Canon experiment.

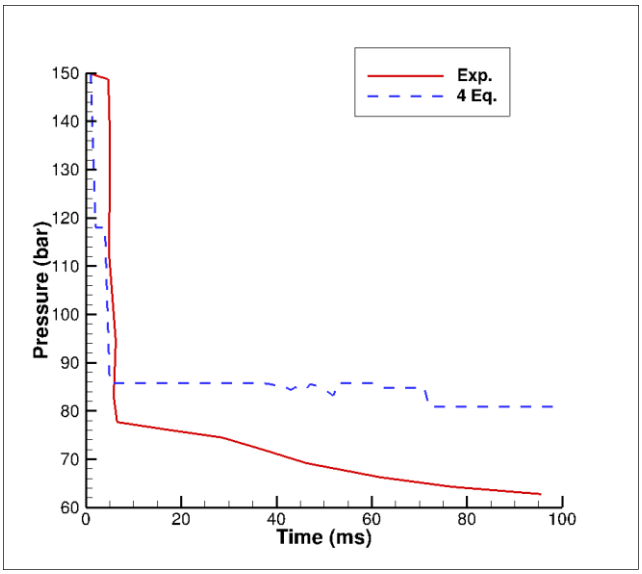

Figure 4. Pressure vs time at P1 location in Super-Canon experiment.

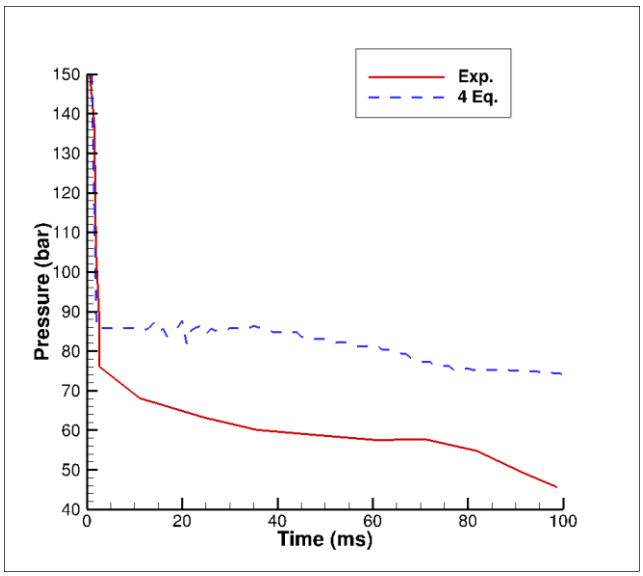

Figure 5. Pressure vs time at P5 location in Super-Canon experiment.

V. CONCLUSION

This work is preliminary work for simulating fast depressurization in PWRs. Using the four-equation model, the numerical solution of two-phase problems is examined. This model was evaluated on test cases using the HLLC numerical scheme. Although the model correctly predicted the pressure drop in the first moments, different results were obtained compared to the reference results in the following. A more complete methodology is desired to increase the accuracy of numerical simulations of nuclear safety accidents, and for this, it is crucial to take into account thermal and chemical non-equilibrium. For this purpose, two new models are planned to be added to the solver, the homogeneous relaxation model, and the single velocity six-equation model. These models have been shown to provide accurate predictions of the behavior of two-phase flow systems during LOCA events and are used in a variety of applications, including the design and optimization of safety systems for nuclear power plants.

VI. References

[1] H. Bruce Stewart and B. Wendroff, “Two-phase flow: Models and methods,” Journal of Computational Physics, vol. 56, no. 3, Dec. 1984, pp. 363–409.

[2] M. R. Baer and J. W. Nunziato, “A two-phase mixture theory for the deflagration-to-detonation transition (ddt) in reactive granular materials,” International Journal of Multiphase Flow, vol. 12, no. 6, Nov. 1986, pp. 861–889.

[3] F. Huang, M. Takahashi, and L. Guo, “Pressure wave propagation in air-water bubbly and slug flow,” Progress in Nuclear Energy, vol. 47, no. 1–4, Jan. 2005, pp. 648–655.

[4] L. S. Tong and J. Weisman, “Thermal analysis of pressurized water reactors,” www.osti.gov, Jan. 1979.

[5] A. K. Kapila, R. Menikoff, J. B. Bdzil, S. F. Son, and D. S. Stewart, “Two-phase modeling of deflagration-to-detonation transition in granular materials: Reduced equations,” Physics of Fluids, vol. 13, no. 10, Oct. 2001, pp. 3002–3024.

[6] E. Goncalves and D. Zeidan, “Simulation of Compressible Two-Phase Flows Using a Void Ratio Transport Equation,” Communications in Computational Physics, vol. 24, no. 1, 2018.

[7] B. Riegel. “Contribution à l’étude de la décompression d’une capacité en régime diphasique.” PhD thesis, L’Université Scientifique et Médicale et l’Institut National Polytechnique de Grenoble,1978.
[8] E. F. Toro, “The equations of fluid dynamics. In Riemann Solvers and Numerical Methods for Fluid Dynamics,” Springer, 1999, pages 1–40.

[9] F. Daude, P. Galon, Z. Gao, and E. Blaud, “Numerical experiments using a HLLC-type scheme with ALE formulation for compressible two-phase flows five-equation models with phase transition,” Computers & Fluids, vol. 94, May 2014, pp. 112–138.

[10] O. Hurisse and L. Quibel, “Simulations of water-vapor two-phase flows with non-condensable gas using a Noble-Able-Chemkin stiffened gas equation of state,” Computers & Fluids, vol. 239, May 2022.

[11] JB Vos et al. “NSMB Handbook 6.07”. In: Lausanne: EPFL, March (2014), pp. 601–97

Proceedings of the European Nuclear Young Generation Forum
ENYGF'23
May 8-12, 2023, Kraków, Poland

Is there a future for online HAZOP beyond the COVID-19 pandemic? A qualitative analysis of online HAZOP participant experience.

Hill, Jenny

[1] Abbott Risk Consulting (ARC), United Kingdom

I. INTRODUCTION

Successful risk management in the high hazard industries is dependent on rigorous and systematic hazard identification [1]. There are a number of established methods for hazard identification, which are selected and applied based on the requirements and phase of the project or operation for which the study is carried out [2]. Hazard and Operability (HAZOP) studies are an example of a hazard identification method.

HAZOP studies are a collaborative, multidisciplinary activity [3], conducted by a team of participants with diverse experience and knowledge of the process studied, as well as an independent leader, referred to as a 'Facilitator' throughout this study and a secretary or 'Scribe' [4]. Team members include representatives of operations and maintenance personnel, designers, relevant engineering disciplines and those with specialist knowledge in safety or particular aspects of the equipment or operations to be studied [1]. Crawley and Tyler [5] write that the validity of the analysis drawn from a HAZOP study depends on having the right people in the team, a view shared by Mokhtarname et al. [3], as the findings of HAZOP studies are relatively subjective, based on the judgement and experience of the team members.

Stamatis [6] describes the importance of the setting of the HAZOP study, including a spacious and well ventilated location with equipment including wall projection and flip charts, indicating that the assumption is that the studies should be carried out in person. This is supported by other literature on the application of the method such as that from the IEC [7] and Crawley and Tyler [5] which contain no reference to performing studies in an online setting.

The COVID-19 pandemic was announced as a "Public Health Emergency of International Concern" by the World Health Organisation (WHO) in January 2020 [8]. The impact of the pandemic was on a global scale with strict policies introduced to manage the spread of the virus [9]. A dramatic and large-scale shift to working from home took place due to workplace and travel restrictions, as described by George et al. [10]. Although there is existing knowledge on the concept of remote working, Wang et al. [11] highlighted that the extraordinary context of the pandemic would put that knowledge into question.

In addition to the requirement for workers to carry out their individual roles online, there has been a rapid shift to virtual collaboration, where workers have been forced to use technology in new ways to communicate with their peers [12] within virtual teams; an approach that has been used to continue to carry out HAZOP studies in the context of the COVID-19 pandemic. Virtual teams are defined by Garro-Abarca et al. [13, p. 2] as "a group of people or stakeholders working together from different locations and possibly different time zones, who are collaborating on a common project and use information and communication technologies intensively to co-create". Research into virtual or online team work in a range of contexts identifies a number of themes that influence outcomes of virtual team exercises. Much of the literature, however, focusses on virtual team working amongst university students, for example studies by Ku et al. [14] and Rauer et al. [15]. The participants of these studies are likely to be "digital natives", defined by Garro-Abarca et al. (2021) [13, p. 2] as those born after 1990 with "…the naturalness to the adaptation to the use of ICTs", meaning that fewer studies have looked at participants who are "digital migrants" (born before 1990), a term which could represent the experienced collaborators within a HAZOP study team. The research also focussed on teams that collaborate regularly, rather than those who gather for one-off or discontinuous activities such as HAZOP studies. The existing research on virtual collaboration cannot, therefore, be directly applied or used to inform the process of online HAZOP.

While some guidance exists for carrying out HAZOP studies online, most is based on the anecdotal experience of the Facilitator adapting the traditional face-to-face methods to an online setting. Examples include Younes [16] and Burwood [17]. In 2021, the IChemE Safety Centre (ISC) [18] published guidance on good practice in online HAZOP based on survey data, although the validity of the data is not clear.

Views presented in the literature on the efficacy of online HAZOP and it's future application differ. The ISC guidance [18] suggests that online HAZOP should not reduce the need for face-to-face meetings in the future, whereas some anecdotal evidence such as that from Younes [16] suggests that virtual HAZOPs can prove useful and could be considered as an alternative to face-to-face studies in the future.

In light of the gaps identified in the existing literature on virtual team work and online HAZOP studies, the purpose of this study was to determine if online HAZOP is a suitable process to be continued beyond the context of the COVID-19 pandemic. The aims of the study were as follows:

Aim 1: to understand participant experience of online HAZOP studies.

Aim 2: to identify positive and negative themes relating to individual experience with the process.

Aim 3: to identify the key factors that make the process suitable for online application.

II. METHODOLOGY

The study was qualitative and phenomenological in nature, seeking to understand the online HAZOP process from the point of view of those who experience it.

Data was collected from 14 particpants who had taken part in HAZOPs as Facilitators, Scribes and wider team members to gain a more comprehensive understanding of how online HAZOPs have been carried out.

Semi-structured interviews were conducted in which open questions were used as prompts to encourage the participants to talk about their experiences surrounding the research question. Participants were asked: *"Please can you describe the method used when you took part in an online HAZOP study?", "What, if any, are your perceived benefits of carrying out the HAZOP study online?", "What, if any, are your perceived drawbacks of carrying out the HAZOP study online?",* and *"Do you think that HAZOP studies should continue to take place online in the future?".*

The data collected was transcribed and the research technique of thematic analysis was conducted following the process outlined by Braun & Clarke [19]. The data was reviewed to firstly identify key words to produce a list of initial codes. The initial codes were further refined considering their corresponding extracts in the data set and frequency of occurrence, and collated into key themes and sub-themes. This was an iterative process as the data was reviewed and the key codes and themes were continuously refined as the data was analysed.

III. ANALYSIS

Analysis of the data identified five key themes that represent the key factors associated with participant experience in online HAZOP studies. The factors impacted on both the participants' perception of online HAZOP studies, and how the studies themselves were carried out in an online setting.

Theme 1: Attitudes to Online HAZOP

The data indicated that, overall, participation in online HAZOP studies was a positive experience, and that the perception of online HAZOP had changed from a negative one to a positive one during the course of the COVID-19 pandemic. The shift to a more positive perception was linked to a number of factors at different scales. At an organisational level, companies became more supportive of online HAZOP due to monetary savings linked to a reduction in travel, and were encouraged by the overall quality of the online studies, which was reported to be consistent with the quality of studies carried out in-person. On an individual level, the positive perception was linked to the personal values of the participants, including the reduction of carbon footprint and improvement to work-life balance, both of which are facilitated by a reduction in travel.

As a result of the large majority of responses being positive, the overall feeling from participants was that there is a strong future for HAZOPs to be carried out online, and many participants highlighted that the HAZOP methodology was easily adapted to an online setting. However it was noted that there would be some circumstances where an in-person HAZOP study could be the preferred option in the absence of any COVID-19 related restrictions. These include where information security requirements would limit online participation, as well as the study length and the complexity of the subject matter, as discussed under Theme 2 below.

Theme 2: Scheduling and Session Structure

Many participants reported that the duration of online HAZOP studies, and how they were scheduled and structured, had a significant impact on their experience of the process.

Participants agreed that HAZOPs carried out online generally took longer to complete than those carried out in-person, as conversation is more carefully facilitated and managed in order for individuals to speak in turn.

It was observed by several participants that there was a preference from organisations and team members for longer HAZOP studies to be divided into a number of shorter online sessions that are carried out over time, rather than requiring team members to spend consecutive full days in attendance. This is because scheduling in this manner was more likely to secure the attendance of team members, and that shorter sessions were perceived to be more beneficial in terms of maintaining focus on the subject matter; participants reported feeling more "fresh" and "invigorated" in shorter sessions. It is however noted that some participants felt that this approach is more suitable for shorter studies on more simple processes and that longer duration HAZOPs for complex processes may still be better carried out in-person over consecutive days in the absence of COVID-19 restrictions.

Theme 3: Preparation

Many of the study participants emphasised the importance of the tasks involved in preparing for online HAZOPs. This was particularly in relation to the preparation and distribution of supporting information, including large drawings and plant layouts, that would previously have been given to team members in hardcopy at the beginning of an in-person HAZOP. It was highlighted by a number of participants that it was more important to distribute the information to individuals at an earlier stage when the HAZOP was to be conducted online compared to if it was conducted in-person, in order for the team members to familiarise themselves with the contents. Participants found this beneficial to the online HAZOP for efficiency, as it allowed team members to navigate the information more effectively during the session and it was also perceived as beneficial for engagement.

Theme 4: Use of IT

Videoconferencing software was discussed by all participants, indicating that software has a significant influence on online HAZOP studies. Several videoconferencing platforms were reported to be used, and were selected depending on factors such as accessibility, functionality and the requirements of the client or organisation.

Software functions that were reported by participants as being particularly useful for online HAZOP studies included those that enabled the Facilitator to manage discussions and prevent over-talking, which would result in inefficiencies in the process. For example the "raise your hand" reaction was commonly used to indicate when a participant wished to speak. The ability to mute microphones was also reported to be useful in preventing over-talking and excessive background noise, however this was acknowledged by some participants to have the potential to limit engagement.

Most participants discussed the importance of the IT hardware set up of the HAZOP team members as being important to their HAZOP experience. Home IT set ups were reported to have improved vastly as the COVID-19 pandemic continued, evolving from the use of a single laptop to a set up more comparable to an office setting, including multiple display screens. The use of multiple display screens was highlighted by many of the study participants as particularly useful for online HAZOP sessions, because team members were able to quickly and easily navigate between different sources of information, such as the HAZOP record sheet and supporting references. In particular, the participants that had experienced online HAZOPs as a Scribe reported that the use of multiple display screens allowed them to perform their role much more efficiently, as they had quick access to reference materials including equipment identifiers. The ability to share and change between different information sources was cited as a particular benefit of carrying out HAZOP studies online compared to in-person.

The use of cameras by HAZOP study team members was mentioned by most participants. Those who had experienced online HAZOP studies as Facilitators reported that it was beneficial for team members to have their cameras turned on during the sessions. This allowed Facilitators to pick up on non-verbal cues that can indicate how team members are feeling, and when they want to make a contribution. The preference for having cameras turned on was not shared by all participants, however, as it was reported that the use of cameras can contribute to a feeling of intensity and fatigue. The preference for camera use may therefore vary depending on personal preference and role within the HAZOP study team.

Theme 5: Participant Engagement

Most of the study participants commented on the level of engagement of team members when discussing their experiences in online HAZOP studies.

In general, it was noted that individuals were more focused on the subject of the HAZOP and conversations were less likely to digress into other topics when carrying out the study online. Furthermore, as team members were in a remote location, it was observed by several participants that there were fewer occurrences of individuals being called away from the session to deal with issues in the workplace in comparison to when studies are carried out in-person and onsite. Conducting HAZOPs online therefore improved attendance, presence and engagement. It was however highlighted by some participants that it was easier to carry out other desk-based work such as checking emails while attending a HAZOP session online, which impacted on how engaged individuals were with the session, and potentially resulting in them failing to provide important information.

Those who reported on engagement agreed that it was important for Facilitators to ask questions and check in with each team member in turn to focus their attention and facilitate conversation.

IV. DISCUSSION

Interviews with 14 participants provided an understanding of how the HAZOP methodology has been applied in an online setting throughout the COVID-19 pandemic. Despite a lack of previous research into virtual collaboration in the context of hazard identification, and limited guidance on online HAZOP application, participants demonstrated that, in general, online HAZOP studies have proven to be positive experiences.

Particularly positive aspects of online HAZOP application involved a reduction in necessary travel, improved participant attendance and engagement and the ability to share and navigate information.

Negative aspects of online HAZOP application largely related to individual behaviours such as over-talking and dividing attention between the study and other desk based tasks, however these were reported to be effectively managed by Facilitator involvement.

The findings of the research indicate that the prescribed HAZOP method is easily adapted to an online setting, provided that adequate time is provided to facilitate conversation, that supporting information is shared in advance of the study and that team members have adequate provisions for IT including multiple display screens. This suggests that there is a strong future for online HAZOP, with

the majority of participants agreeing that this is the case. In the absence of COVID-19 related restrictions, however, factors such as study length, site or process complexity and security requirements may influence the decision to carry out some HAZOPs in-person.

V. References

[1] F. Crawley, *A Guide to Hazard Identification Methods,* 2nd ed. Elsevier, 2020.

[2] S. Mannan, *Lee's Process Safety Essentials: Hazard Identification, Assessment and Control.* Elsevier, 2014.

[3] R. Mokhtarname, A. A. Safavi, L. Urbas, F. Salimi, M. M Zerafat, N. Harasi, N. (2020). "Toward HAZOP 4.0 approach for managing the complexities of the hazard and operability of an industrial polymerization reactor". *IFAC-PapersOnLine* [Online]. vol. 53, issue 2. Available: https://doi.org/10.1016/j.ifacol.2020.12.852

[4] J. Ahn, D. Chang, „Fuzzy-based HAZOP study for process industry", *Journal of Hazardous Materials,* vol. 317*,* pp. 303-311, 2016.

[5] F. Crawley, and B .Tyler, *HAZOP: Guide to Best Practice,* 3rd ed. Elsevier, 2015.

[6] D. H. Stamatis, *Introduction to Risk and Failures.* Taylor & Francis Group, 2014.

[7] *Hazard and operability studies (HAZOP studies) – Application guide,* IEC Standard 61882, 2016.

[8] World Health Organisation. (2020, January 30). *Statement on the second meeting of the International Health Regulations (2005) Emergency Committee regarding the outbreak of novel coronavirus (2019-nCoV)* [Online]. Available : https://www.who.int/news/item/30-01-2020-statement-on-the-second-meeting-of-the-international-health-regulations-(2005)-emergency-committee-regarding-the-outbreak-of-novel-coronavirus-(2019-ncov)

[9] H. Sun, H. Wang, M. Yang, G. Reniers, "On the application of the window of opportunity and complex network to risk analysis of process plants operations during a pandemic," *Journal of Loss Prevention in the Process Industries,* vol. 68, article 104322, 2022.

[10] T. J. George, L. E. Atwater, D. Maneethai, J. M. Madera, "Supporting the productivity and wellbeing of remote workers: Lessons from COVID-19," *Organizational Dynamics,* vol. 51, pp. 1-9, 2022.

[11] B. Wang, Y. Liu, J. Qian, S. K. Parker, "Achieving effective remote working during the COVID-19 pandemic: a work design perspective," *Applied Psychology: An International Review,* vol. 70, issue 1, pp. 16-59, 2021.

[12] L. Waizenegger, B. McKenna, W. Cai, T. Bendz, "An affordance perspective of team collaboration and enforced working from home during COVID-19," *European Journal of Information Systems,* vol. 29, issue 4, pp. 429-442, 2020.

[13] V. Garro-Abarca, P. Palos-Sanchez, M. Aguayo-Camacho, "Virtual Teams in Times of Pandemic: Factors That Influence Performance," *Frontiers in Psychology,* vol. 12, 2021.

[14] H. Ku, H. W. Tseng, C. Akarasriworn, "Collaboration factors, teamwork satisfaction, and student attitudes toward online collaborative learning," *Computers in Human Behaviour,* vol. 29, pp. 922-929, 2013.

[15] J. N. Rauer, M. Kroiss, N. Kryvinska, C. Engelhardt-Nowitzki, M. Aburaia, "Cross-university virtual teamwork as a means of internationalization at home," *The International Journal of Management Education,* vol. 19, article 100512, 2021.

[16] A. Younes, "Lessons Learned and the Pros and Cons of Virtual HAZOP" in *IChemE Hazards31 Conference*, Online, 2021.

[17] S. Burwood. (2020, May. 1). *Remote HAZOP Workshops: Top tips* [Online]. Available: https://esc.uk.net/remote-hazop-workshops-top-tips/

[18] *Good practice in virtual HAZOP,* IChemE Safety Centre, 2021.

[19] V. Braun, V. Clarke, "Using thematic analysis in psychology," *Qualitative Research in Psychology,* vol. 3, issue 2, pp. 77-101, 2006.

Proceedings of the European Nuclear Young Generation Forum
ENYGF'23
May 8-12, 2023, Kraków, Poland

Safety in the Nuclear and Aeronautic Sectors: A Comparison for possible Future Insights

Suárez Ortiz, Francisco[1*]

[1] Tecnatom S.A., Spain.

*Corresponding author: *fsuarez@tecnatom.es*

I. INTRODUCTION – Level 1 (Times

Nuclear safety standards and practices are integrated in the foundations of any activity within the nuclear sector. Safety is also of capital importance in other sectors, such as the aeronautic industry. This paper presents some of the similar safety-related aspects between both sectors and reviews some of the differences in the licensing approaches. The comparison is focused on possible insights for the deployment of advanced nuclear reactors, particularly considering Small Modular Reactors (SMRs).

The main technological advances for the development and deployment of both civil sectors took place less than a century ago. Not forgetting about previous valuable research efforts, without which the later development would have been difficult to conceive or achieve, two important milestones can be highlighted in each sector as the respective kick-offs: 1903 Flyer-1 (Wright Brothers first sustained flight by tripulated heavier-than-air powered and controlled aircraft) and 1942 Chicago Pile-1 (Fermi's first human-made controlled self-sustaining nuclear chain reaction). In a matter of decades since their respective "proof of concept", and leaving the role of military motivations out of the scope of this review, substantial technological development took place to internationally deploy the civil benefits that both air transportation and nuclear electricity generation bring to Society.

Within this development, the role of safety also became prominent leading first to the foundation of the International Civil Aviation Organization (ICAO), as a result of the Chicago Convention in 1944 and the International Atomic Energy Agency (IAEA) in 1957, as a result of Eisenhower's earlier "Atoms for Peace" address to the United Nations (UN). Conceivably by the nature of the Agency's objective and original motivation, it has a greater level of authority in the establishment and administration of safeguards (although the establishment of standards of safety is also within its original functions, per its Statute). Both institutions are somewhat sister organizations within the UN umbrella.

Moving on from their historical parallelisms, the following sections identify further common ground regarding safety and consider some differences between both sectors.

II. COMMON GROUND BETWEEN NUCLEAR AND AVIATION

Safety provisions aim to reduce the risk of accidents to very low levels, ultimately a low enough or acceptable level as perceived by Society for the normal development of the activity. Regarding risk mitigation, although both sectors deal with prominent consequences when considering possible accidents, safety measures reduce the probability factor in such a degree that position them within the safest options for electricity generation and transportation respectively.

Close similarities between how safety is factored into analogous areas in nuclear and aviation can be observed by considering general phases in the lifecycle of a nuclear power plant (NPP) and an aircraft. The following analysis is not meant to be exhaustive, but rather aims to identify and present some examples of common approaches.

A. Design

The design of structures, systems and components include safety margins, understood as an extra capacity they must have to assure their integrity and operability beyond the expected conditions they will have to function in. In essence, the design could cope with more demanding conditions than the ones they will be expected to deal with.

Particularly when regarding the systems design philosophy, two common attributes arise in nuclear and aviation (commercial jet airliners are considered as reference): redundancy and independency. Safety-related systems of NPPs consider redundancy to fulfil a safety function by providing different ways to assure the given function and also consider independency such that a particular system (or train within a system) can act independently of another one (eliminating common cause failure). This can be found in current operating NPPs in

systems, such as the emergency core cooling systems (ECCS) and other safety systems, where the different systems consider several redundant and independent features to assure the control of reactivity, core cooling and containment. This same approach can be found in passenger airliner aircraft, where for example in the Airbus A320, three different and fully independent hydraulic systems are considered to provide the necessary hydraulic pressure to operate main components. Consumer loads are shared with a degree of overlap between the three hydraulic systems (referred to as: Green, Yellow and Blue –the Boeing analogous hydraulic systems are named: A, B and Standby–) such that control of the aircraft is ensured even when one system is inoperative [1]. The following table and figure describe the main components of these hydraulic systems.

Table 1. Fundamental characteristics of the three independent hydraulic systems of the A320. Information from [1].

Hydraulic System	Main Characteristics
Green	▪ Powered by: Engine#1 driven pump, Power Transfer Unit (PTU) from Yellow. ▪ Services: flight controls, landing gear, brakes, nose wheel steering, reverser Eng#1.
Yellow	▪ Powered by: Engine#2 driven pump, Yellow electrical pump, PTU from Green. ▪ Services: flight controls, brakes, parking brake, reverser Eng#2
Blue	▪ Powered by: Blue electrical pump, RAM Air Turbine. ▪ Services: flight controls, emergency electrical generator.

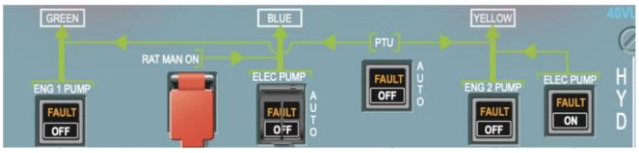

Figure 1. Schematic of the A320 Hydraulic overhead panel [2].

As can be depicted above, an essential system for the safe operation of the aircraft is based on redundancy and independency, like the safety-related systems of NPPs. An additional interesting feature of the A320 hydraulic system is the powering of the blue system under emergency conditions. In the unlikely case of dual engine failure (meaning that both engine driven pumps become inoperative) and electrical failure (which would zero the buses from which both yellow and blue electrical pumps hang, considering also the failure of the Auxiliary Power Unit), the RAM Air Turbine (RAT) can be deployed. The RAT consists of a propeller type turbine, see Figure 2, that is lowered in emergency conditions and is powered by the stream of air flowing around the aircraft in flight. The RAT is coupled to a hydraulic pump that thereby powers the blue hydraulic system which in turn, as can be seen from Table 1, would power the emergency electrical generator restoring electrical power to essential buses. This emergency arrangement during flight, that makes use of available airstream energy to re-establish essential power, is very similar to turbine driven pumps of ECCS [direct in BWRs and via Steam Generators in PWRs], where available steam is used to drive pumps that maintain core cooling. In addition, the Auxiliary Power Units of airliners could be seen in a way as the emergency diesel generators of NPPs. In this regard, the electrical system architecture for NPPs and airliner aircraft (involving both AC and DC buses, emergency buses, etc.) also show several parallelisms in design.

Figure 2. RAT deployed in a grounded aircraft [3].

Finally, another area that can be noteworthy to highlight is the consideration of human factors in designing control rooms and cockpits. Adequate human-machine interface designs support the enhancement of safety by systematically supporting the operators/pilots tasks as they interact with the corresponding displays and controls by considering task attributes such as the importance and frequency of operations. Such designs factor in both the human factor and operational considerations [4], thereby minimizing potential error.

B. Operation

Considering the operation of NPPs and aircraft, several areas of common ground can be identified:

- Procedures: Both sectors rely heavily on procedures to operate. No room is left for improvisation. NPP operators adhere to procedures that cover all operational circumstances (normal, abnormal and emergency) much alike pilots who must also follow operational procedures and checklists every day, regardless of their degree of experience.
- Team operation: At least two persons will be always working together in control room (reactor operator, turbine operator, shift supervisor, etc.) and in the cockpit (captain, first officer, sometimes a second officer, etc.), who in turn also interact with other teams.
- Communications: Operators and pilots must communicate with other persons to operate (e.g.: NPP field technicians or Air Traffic Control, among others) where it is essential that information is communicated effectively. Both sectors apply 3-way communications and the phonetic alphabet (taken originally from aviation, as initial radio transmission quality required clarity and a common international

understanding), to reduce the chances of misinterpretation and error.

- Training: The training processes for operators and pilots share a common structure. Both lay their foundations with generic fundamentals (physics, basic components, reactor theory, flight theory, meteorology, etc.), followed by specific systems training which are then trained together with procedures and technical specifications or limitations in full-scope real-time simulators, where normal, abnormal and emergency scenarios are practiced. This process, featuring also additional topics, takes several years. Once they gain their initial license / certificate, continuous training is extended throughout their entire career. Both NPP operators and airliner pilots continue to re-train on simulators at least yearly.

Finally, a case study that presents certain operational analogy is presented, which is related to guaranteeing the capability of "stopping". A technical specification requirement in NPPs is to always ensure the availability of sufficient shutdown margin to assure that a safe subcritical condition can be reached (have control rod worth for insertion of sufficient negative reactivity). Conversely, aircraft must ensure sufficient landing distance margin [5] to bring the airplane to a stop within the runway (evaluated considering aspects such as weight on landing, runway length and conditions, wind, elevation, etc.).

C. Maintenance

Both NPPs and commercial airliners operate practically continuously and have design lifetimes of several decades. Maintenance therefore becomes an important aspect in both sectors to ensure all components keep functioning over time as expected. Ageing monitoring, replacements, design modifications, etc. are subject to high levels of control as they are closely related to ensuring safety standards. In this regard, another close parallelism can be seen in the area of inspection. Both sectors rely heavily on non-destructive inspections conducted periodically.

As an example, Tecnatom (Spanish nuclear engineering firm mainly dedicated to inspection, training and operational support services) created a division for aeronautical components inspection based on such parallelisms, where the developed experience with ultra-sound inspection processes for reactor pressure vessels could be applied to carbon-fibre components of aircraft.

D. Operating Experience

Sharing of international Operating Experience (OE) is a common practice in both nuclear and aviation. Cumulative experience on the operation of similar technologies (within nuclear and aviation respectively) can be enhanced by making lessons learned available to all relevant involved stakeholders, to implement them across the sector thus together further mitigating identified risks. As pointed out in [6], this OE sharing was implemented first in the aviation sector, but with the creation of the Institute for Nuclear Power Operations (INPO) in1979 and furthermore in 1989 that of the World Association of Nuclear Operators (WANO), international nuclear OE distribution was systematically implemented too.

In both sectors, accidents and incidents are analysed in detail to extract all lessons learned that can lead to measures of avoiding future occurrences such that they can be implemented where applicable. There are even cases that are studied between these sectors (e.g.: Los Rodeos airport accident of 1977 is also studied as a nuclear safety training). Tackling the unknown-unknowns presents its challenges, however the transverse knowledge and application of OE reinforces safety in both sectors.

E. Security

When it comes to security, both the aviation and the nuclear sectors are usually considered as national critical infrastructures which face equivalent types of threats (both consider physical security, cybersecurity and insiders), as pointed out in a recent review by the World Institute for Nuclear Security (WINS) benchmarking security for both sectors [7].

F. Regulations

Nuclear and aviation are highly regulated industries. Regulations apply for all the previously presented areas and more, which are watched over by competent national regulators. Although many parallelisms apply between regulations in each sector (licenses/certificates must be issued by regulators for designs to be able operate, including licenses for personnel, etc.) some differences exist as will be summarized next.

III. LICENSING FUNDAMENTALS IN THE AVIATION AND NUCLEAR SECTORS

A licensing and lifetime management comparison between both sectors was conducted by the World Nuclear Association (WNA) in report [8]. The following summary is mainly derived from their analysis:

Licensing of aircraft designs is based on binding international minimum standards defined in Annex 8 of ICAO's Chicago Convention (whose first edition was adopted in 1949 [9]), supplemented by national airworthiness regulations. Although ICAO does not replace national regulations nor reduce national regulator's sovereignty, it is empowered to adopt and amend safety standards, and these are binding on Member States. This international regulatory architecture is not analogous in nuclear as depicted in Figure 3.

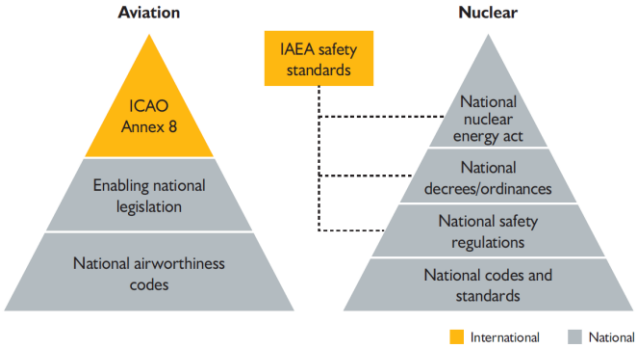

Figure 3. Safety regulation hierarchy in aviation and nuclear [8].

In a nutshell, for a given type of aircraft design to be certified as fit to fly, the designer must firstly obtain a

"Type Certificate" which is issued by the authority of the State of design (country in which the designer is established). This would generally require subsequent applications to States of registry for the issuing of analogous certificates in other countries. Secondly, each aircraft manufactured according to the approved type certificate design will have to obtain an "Airworthiness Certificate" issued to the aircraft owner, thereby granting it is compliant with the approved design and ready for safe operation. The international nature is present in the aviation industry (planes will often operate across a range of different countries) and regulations count on international harmonization allowing commercial aircraft designers to apply for type certificates in several countries simultaneously.

For NPPs, the definition of licenses is not so consistent internationally. Each country is free to define the scope of their licenses, leading to a variety of licensing formats across countries (e.g.: a given country can integrate into one license several stages of the NPP lifecycle whilst another has a different multi-step licensing process. In addition, as depicted in [10], pre-licensing processes also vary greatly between countries and have different design maturity expectations). Those that have more generic design approval procedures could be compared to the type certificate of aviation.

The following bullets summarize some additional points treated further in [8]:

- IAEA safety standards are not binding on Member States.
- National aviation regulators, although part of an international framework for aviation regulation, have the same degree of authority and responsibility as their counterparts in nuclear.
- In aviation the instrument of bilateral airworthiness agreements between countries establish that national regulators accept design review work done by the regulator of the state of design. Although nuclear regulators from different countries do cooperate (e.g.: WENRA) voluntarily, there is no counterpart to bilateral airworthiness agreements.
- The European Aviation Safety Agency (EASA), grouping national regulators, signed in 1990 the Cyprus Arrangements where they agreed, among other points, on joint certification of products designed in their countries or imported from others, which for designers would mean that in practice the evaluation process would happen once with its corresponding technical findings, although each regulator would issue its own license.

WNA points out that the Cyprus Arrangements could serve as inspiration for analogous joint licensing procedures in nuclear. In addition, considering regulatory expectations for SMRs [10], it identifies as a good practice/ recommendation the engagement with international bodies thereby improving harmonization in safety standards and licensing approaches.

IV. DISCUSSION AND CONCLUSIONS

The successful deployment of future SMRs will necessarily require production of many factory-built modules to make the business case and enhance their economic competitiveness. Like aircraft, the design development process will require initial investments which once finished and certified would be recovered by producing and selling many units of that specific design to a range of customers. For that, access to the international market (several countries with potential candidate sites) by SMR designs would foster their deployment and competition. Considering that several SMR designs are being considered for development which can serve (very low carbon) energy needs around the world, harmonized and joint licensing processes, similar to those in aviation, could reasonably be expected to ease and enhance their deployment.

From the side of overseeing safety throughout the lifecycle of SMRs, an aspect of interest when considering joint licensing can be the analogous provisions for continuing airworthiness of aircraft [9], where flow of information found necessary for continued safe operation between State of Design and State of Registry is established, jointly accumulating oversight experience over the same type design (modular philosophy) across different countries.

The present general overview has considered only certain factors of parallelism in safety between both sectors, and for example has not considered possible technical or legal barriers to adapting the aviation certification structure into the nuclear domain, should they exist.

Finally, given the high degree of correspondence between how safety is factored into analogous areas of both sectors, it can be reasonable to consider that inter-sector collaborations, furthering transfer of experiences, could be mutually beneficial. For example, within the training domain, potential for combined safety related practical exercises combining operators and pilots, and how they could reciprocally strengthen their practices can be explored. A possibility could be a "simulators-exchange" experience, that would consist in the mutual demonstration of analogous scenarios in an NPP and an aircraft, enhancing experience exchange and reinforcement in the operational safety domain.

V. ACKNOWLEDGMENTS

I express my gratitude to Mr. Raul Herranz, for sharing his valuable experience in both the nuclear and aeronautic sectors in discussions with me. I also thank the designers and developers of the MS Flight Simulator series for integrating the engaging learning by exploring philosophy.

DISCLAIMER

Any views reflected in this article are of the author alone and should not be interpreted as necessarily representing those of Tecnatom S. A.

VI. References

[1] M. Palomeque, “A320 – Dual Hydraulic Loss”, Safety First (Airbus Magazine), vol. 4, June 2017.

[2] 320 Pilots Website, https://320pilots.com/hydraulic-system/, consulted March 2023.

[3] Aviation Matters Website, https://www.aviationmatters.co/airbus-a320-ram-air-turbine-rat-a-pilots-guide/, consulted March 2023.

[4] Airbus, “The Airbus Cockpit Philosophy”, Flight Operations Safety Awareness Seminar (FOSAS), September 2017. Taken from ICAO Website consulted March 2023.

[5] US Federal Aviation Administration, “Mitigating the Risks of a Runway Overrun Upon Landing”, Advisory Circular 91-79A, September 2014.

[6] L.F. Franzen, E. Iansity, “The Safety Activities of the ICAO and the IAEA”, IAEA Bulletin, Vol. 25, No.4, December 1983. (Note: this article was written pre-Chernobyl).

[7] R. Howsley, R. Delgado, “Security in the Civil Nuclear and Aviation Sectors: Identifying Transferrable Best Practices”, IAEA International Conference on Nuclear Security (ICONS), February 2020.

[8] World Nuclear Association, “Aviation Licensing and Lifetime Management – What can Nuclear Learn?”, CORDEL Group, Report No.2013/001, January 2013.

[9] ICAO, “The Convention on International Civil Aviation. Annexes 1 to 18”, October 2012. Taken from ICAO Website consulted March 2023.

[10] World Nuclear Association, “Design Maturity and Regulatory Expectations for Small Modular Reactors” CORDEL Group, Report No. 2021/001, June 2021.

Proceedings of the European Nuclear Young Generation Forum
ENYGF'23
May 8-12, 2023, Kraków, Poland

Numerical Modeling of Mixed Convection Flow Regime in Low-Prandtl Number Fluids

Alsubhi, Abdulaziz[1*], Meri, Yazan[1], Al-Athel, Khaled[1,2], Shams, Afaque[1,3] and Siddiqui, Osman[1]

[1] Mechanical Engineering Department, King Fahd University of Petroleum & Minerals (KFUPM), Saudi Arabia.

[2]Interdisciplinary Research Center for Advanced Materials (IRC-AM), KFUPM, Saudi Arabia

[3]Interdisciplinary Research Center for Renewable Energy and Power Systems (IRC-REPS), KFUPM, Saudi Arabia

*Corresponding author: s201761950@kfupm.edu.sa

I. INTRODUCTION

In most thermofluidic applications, mixed convection exists which is constituted of forced and natural convection components. The forced component of the mixed convection appears due to external sources such as pressure and frictional effects. Natural convection is driven by an internal property of fluids which is density variance as a function of temperature. Mixed convection is present in several applications where pressure and temperature difference exist such as power generation, electronics cooling, and product manufacturing. The study of the behavior would contribute to the modeling of scientific, industrial, and technological applications. An area of interest in studying mixed convection is its behavior as a function of changes in thermofluidic properties. The understanding of fluid behavior is enhanced by studying the momentum and heat transfer of flowing fluids. The fluid momentum transfer investigates the fluid particles' motion and the forces they pose and are exposed to. However, heat transfer studies the ability of these particles to transmit thermal energy.

A. Mixed convection case development

The pressure-driven turbulent flow in a planar channel (also known as the Poiseuille flow) is a standard configuration concerning the forced convection regime. On the other hand, the widely regarded phenomena of the natural convection regime is the Rayleigh-Bénard convection (RBC). Since Poiseuille-Rayleigh-Bénard (PRB) flow (Figure 1) combines the key characteristics of the paradigmatic situations of forced and natural convection, it is the suitable option for mixed convection studies. The PRB is indeed a pressure-driven Poiseuille flow in which buoyancy effects are created by a temperature difference between the top and bottom walls of the channel [1].

B. Numerical Modeling and Analysis Methodology

The approaches to study flow and heat transfer are experimental, numerical, and computational methods. Experimental methods have stayed the essence of thermofluidic science throughout history as they are the reliable research methodology and many current theories have been constructed on an experimental basis. However, they have limitations in explaining several scientific advances. The limitations could be constituted in measurement ability, measurement resolution, experiment construction and replicability, practicability, and accuracy. Analytical solutions are possible with several simplifications and assumptions to result in simple fundamental studies, however, as the research statements advanced with higher complexities, the application of the Analytical methods became restricted. This brought focus to the computational tools that aim to solve numerical models for complex domains. Computational fluid dynamics (CFD) is a model approach that solves complex problems based on the fundamental numerical models implemented on smaller elements of the domain. Turbulent fluid flow models are mathematical models to simulate and predict the disturbance effects for real-life flows with practical results. One of the CFD approaches is Direct Numerical Simulation (DNS), which solves the actual Navier–Stokes equations even for turbulent flows without requiring a turbulence model. Thus, having DNS as a reference allows the numerical comparison of various turbulence models.

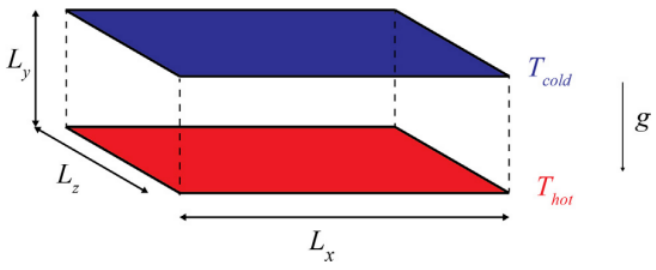

Figure 1. An illustration of the Poiseuille-Rayleigh-Bénard mixed convection computational domain [2].

Analysis of the fundamental governing equations gave rise to non-dimensional numbers that combine various

thermofluidic conditions and properties. They express the physical behavior of fluids with the ability to generalize the analysis. The study analyzes the impact of varying the Prandtl number (Pr) for a constant Reynolds number (Re) and Richardson number (Ri).

C. Prandtl Number Effect

The Prandtl number defines the ratio of momentum diffusivity to thermal diffusivity. It infers the thickness and development of thermal and momentum boundary layers. As a fluid's Prandtl number deviates from unity, the difference in boundary layer thickness gets expanded resulting in one boundary layer being small when compared to the other as illustrated in Figure 2. Examples of low Prandtl numbers include liquid metal flows (i.e. small momentum boundary layer). Capturing the boundary layer is one requirement to be addressed in computational modeling. This process is highly dependent on discretization elements' size as smaller elements can model more accurate flow features [3]. The dimensionless wall distance y^+ is used to denote the wall regions namely: the viscous sublayer ($y^+ < 5$), the buffer layer ($5 < y^+ < 30$), and the logarithmic layer ($y^+ > 30$). The y^+ for this flow is kept below 0.5 to capture the flow within the viscous sublayer near the wall and is calculated as:

$$y^+ = \frac{\rho y u_\tau}{\mu} \quad (1)$$

where ρ is density, μ is dynamic viscosity, y is wall distance and u_τ is the friction velocity.

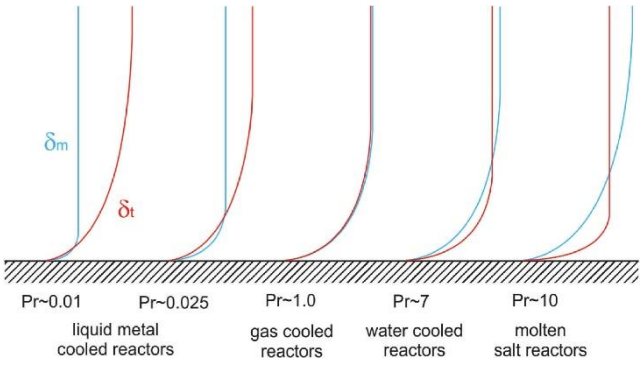

Figure 2. Momentum and thermal boundary layer development for multiple Prandtl numbers [4].

D. Recent Studies

The solution of turbulent mixed convection is a challenging numerical case that is highly dependent on the turbulence model used. To establish a reference case, De Santis et al. [2] presented DNS solutions that do not require a turbulent model. The turbulence level was reported to be increasing near the wall due to the buoyancy effect which resulted in large gradients near the wall and remaining nearly constant in the bulk fluid region. In addition, the DNS results showed that as the Prandtl number is reduced the temperature gradient extends further within the bulk fluid. Guo et al. [5] similarly reported the reduction in thermal boundary layer thickness with buoyancy effects for mixed convection study using DNS. The reduced thickness resulted in high thermal gradients near the wall.

Pucciarelli et al. [6] studied the mixed convection in a vertical channel. Upon comparison with DNS, the AHFM-SC (Algebraic Heat Flux Model based on Shams Correlation) model gave the closest temperature field in comparison to the other RANS (Reynolds-Averaged Navier-Stokes) models. It was concluded that the simple gradient heat flux models have limitations when modeling buoyancy forces while advanced models like AHFM-SC have shown their ability to match the DNS results.

II. CASE DESCRIPTION

The analyzed domain consists of a 2D rectangular planner channel as illustrated in Figure 1. The geometry is specified with the wall-normal dimension ($L_Y = 2\delta$) and streamwise dimension ($L_X = 4\pi\delta$) with δ representing the boundary layer thickness. A constant wall temperature boundary condition is applied at the top wall (T_C) and the bottom wall (T_H). The difference in temperatures ($\Delta T = T_C - T_H$) induces a buoyancy effect along the y-axis direction due to density variation. The buoyancy flow is constant due to the fixed temperature difference ($\Delta T = 2.6$ K). A forced flow is introduced in the x-axis direction with a constant flow rate maintaining $Re_b = 5{,}639$, $Re_\tau = 180$, and $Ri = 0.5$. This resulted in flow with the bulk velocity of $U_b = 0.1128$ m/s. The periodic boundary condition is applied to ensure a fully developed flow with the no-slip condition at the walls. In addition, the low Prandtl flow behavior is studied with Prandtl number values of 1, 0.1, and 0.01. In doing so, the various turbulent models' capabilities to attain accurate results are examined. All flow parameters are presented in Table 1.

Table 1. Summary of the simulation fluid parameters

Symbol	Definition	Value
Re_b	Bulk Reynolds number	5639
Re_τ	Friction Reynolds number	180
Pr	Prandtl Number	1, 0.1, 0.01
Ri	Richardson Number	0.5
U_b	Bulk velocity	0.1128 m/s
μ	Dynamic viscosity	1e-6 Pa·s
K	Thermal conductivity	1e-3 W/m·K
ρ	Density	1 kg/m^3
β	Thermal expansion coefficient	1e-3 K^{-1}

A. Numerical Solution

All numerical simulations have been conducted utilizing the commercially available software Ansys Fluent 2022 [7]. Ansys Fluent is a CFD software that is known for its

advanced physics modeling capabilities and accuracy. The selected turbulent flow models were based on the Reynolds analogy, which relates heat transfer to turbulent momentum. The particular turbulent models studied are:

- k-ε
- k-ω SST (Shear Stress Transport)
- Reynolds Stress Models (RSM)

k-ε is among the most common model that uses two additional transport equations for turbulent kinetic energy and turbulent dissipation. The k-ω SST is a two equations model that combines the best of k-ω and k-ε formulations. It uses the k-ω formulation close to the wall (low Reynolds within the viscous sublayer) while using the k-ε formulation away from the wall in the free stream where k-ω has a high sensitivity to the turbulence properties. The RSM is a second-order closure model, and its formulation follows the precise Reynolds stress transfer equation.

B. Mesh Generation

The mesh has been produced for the computational domain utilizing the meshing software provided by ANSYS, Inc. As demonstrated in Figure 3, the mesh is constructed with inflation layers near the walls in the wall-normal direction. The main purpose of inflation is to capture momentum and thermal boundary layers across the top and bottom walls. The first layer size is set to have a thickness of 0.006 m considering y^+ less than 0.5. The inflation between layers extended with a stretching ratio of 1.2. Along flow direction, the mesh is of 0.01 m element size resulting in total elements of 22,600.

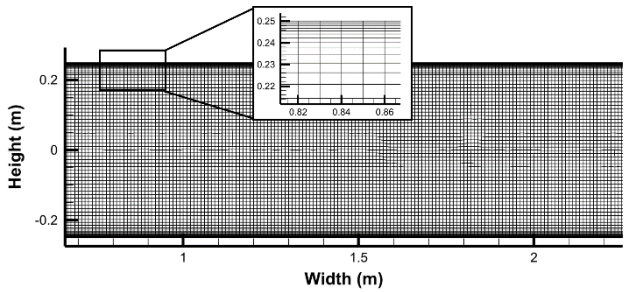

Figure 3. A cross-sectional capture of the case upper half mesh.

III. RESULTS AND DISCUSSION

In this section, the results obtained with the use of k-ε, RANS k-ω SST, and RSM turbulent models will be presented with a thorough assessment of the simulation results for the mixed convection case. The case will be evaluated through a qualitative review and a quantitative data validation with the DNS and AFHM-SC taken as reference data [2]. The AFHM-SC is the most advanced and up-to-date model available in the nuclear industry and is able to predict the mixed convection behavior better than the other RANS-based models. The evaluation will consider both Turbulent Momentum Flux (TMF) and Turbulent Heat Flux (THF).

A. Qualitative Results Assessment

The obtained qualitative results for both TMF represented in the velocity distribution and THF represented in the temperature distribution are shown in (Figure 4). The RANS model k-ω SST was able to predict the average behavior of the flow. A typical turbulent flow where the bulk flow has maximum speed is shown with the no-slip condition effect in the near-wall region. Because of the limitations of the RANS models, they cannot capture turbulent eddies. This is due to the averaged effect of RANS. In a similar manner, the heat diffused from the top and bottom walls can be visualized in Figure 4 (b). The temperature shows a similar effect to the velocity gradient. This effect is mainly due to the shortcoming of the Reynolds analogy where the heat transfer is related to the momentum flux.

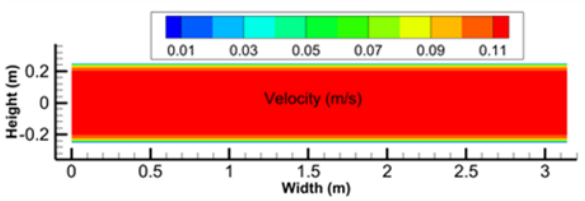

Figure 4 (a). Velocity field capture of RANS simulation.

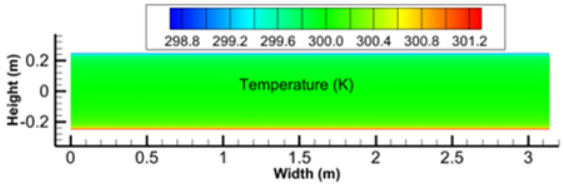

Figure 4 (b). Temperature field capture of RANS simulation.

B. Quantitative Results Assessment

Quantitative comparisons are performed to the temperature fields at variable Prandtl numbers. The temperature field is analyzed to examine the mixed convection effects in the channel. Results are compared with the reference DNS database [2] as shown in Figure 5. The selected parameter for comparison is the vertical normalized temperature profile calculated as follows:

$$T^* = \frac{(T - T_{cold})}{T_{hot} - T_{cold}} \quad (2)$$

Results are extracted at the mid-vertical cross-section of the flow domain. The normalization is done for both temperature and vertical height.

Figure 5 (a) shows the temperature profile along the vertical flow axis for different models. As the DNS model solves the full Navier–Stokes equation without using any turbulence model, it is taken as the reference to compare other models. The AHFM-SC model has been calibrated for a wide range of test cases, as highlighted in Shams [8]. It is also evident from Figure 5 that this model is able to predict the temperature within the thermal boundary layer as well as the bulk of the fluid. In comparison, the k-ε model based on the Reynolds analogy shows the most deviant temperature

profile. The model is overestimating the thermal boundary layer and is unable to predict the sudden temperature changes near the walls. It should be further noted that for the turbulent flow, the temperature and velocity profiles remain relatively flat in the middle of the channel due to the inherent turbulent flow as opposed to the laminar flow that has parabolic profiles. The k-ε model lacks the ability to predict this linear profile in the middle section but rather shows a non-zero slope. The k-ω SST model performance is in between the other two models and shows the results relatively closer to the reference. Similar patterns are evident for the Pr = 0.1 case shown in Figure 5 (b) and Pr= 0.01 shown in Figure 5 (c). At lower Prandtl numbers, the thermal boundary layer is larger in comparison to the momentum boundary layer. This is visible as the constant linear middle section reduces as the Prandtl number increases. For the lowest Prandtl number, the k-ε model almost predicts a linear temperature variation while the DNS and AHFM-SC show constant temperature for the middle section. Whereas, the RSM and k-ω SST models show results similar to each other.

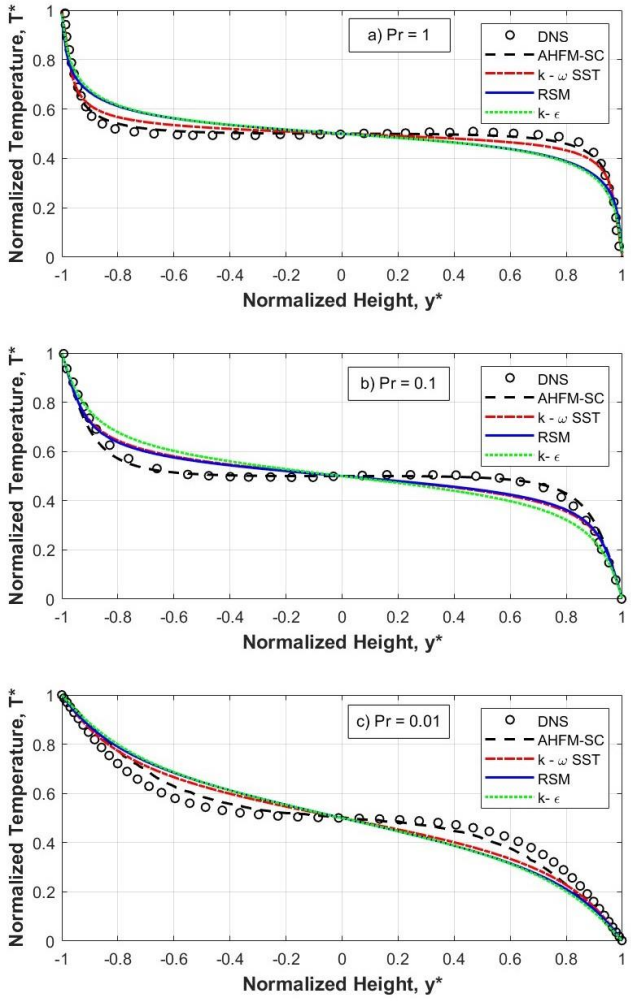

Figure 5. The normalized temperature variation along the vertical cross-section for a) Pr = 1, b) Pr = 0.1, and c) Pr = 0.01.

IV. CONCLUSIONS

This work focuses on the mixed convection flow regime that exists in almost all real-world applications and the buoyancy-driven, i.e. natural and mixed convection, elements make it challenging especially for turbulent flows. CFD simulations have been performed to address the ability of RANS-based turbulence models to predict the mixed convection regime at non-unity Prandtl numbers. A 2D forced flow was modeled between differentially heated walls inducing the buoyancy effect. The mixed convection was studied at multiple Prandtl numbers and validated against the reference DNS databse. The results obtained from three different turbulence models are also compared with an advanced turbulent heat flux model, called AHFM-SC, to assess different turbulence models and their respective limitations. It has been found that the AHFM-SC shows superior results compare to the other RANS models (k-ε, k-ω SST and RSM). This is mainly because the AHFM-SC takes into account the explicit modeling of turbulent heat flux and is well-calibrated for low-Prandtl number fluids. Whereas, the other considered models model the THF based on the simplest assumption of Reynolds analogy.

V. ACKNOWLEDGMENT

The authors acknowledge the support provided by Undergraduate Student Research Grant (UXplore) at King Fahd University of Petroleum and Minerals (KFUPM).

VI. REFERENCES

[1] R. Taher, M. M. Ahmed, Z. Haddad, and C. Abid, "Poiseuille-Rayleigh-Bénard mixed convection flow in a channel: Heat transfer and fluid flow patterns," International Journal of Heat and Mass Transfer, vol. 180, p. 121745, 2021.

[2] D. De Santis, A. De Santis, A. Shams, and T. Kwiatkowski, "The influence of low prandtl numbers on the turbulent mixed convection in an horizontal channel flow: DNS and assessment of Rans Turbulence models," International Journal of Heat and Mass Transfer, vol. 127, pp. 345–358, 2018.

[3] K. Hanjalić, "One-Point Closure Models for Buoyancy-Driven Turbulent Flows," Annual Review of Fluid Mechanics, vol. 34, no. 1, pp. 321–347, 2002.

[4] A. Shams, F. Roelofs, I. Tiselj, J. Oder, Y. Bartosiewicz, M. Duponcheel, B. Niceno, W. Guo, E. Stalio, D. Angeli, A. Fregni, S. Buckingham, L. K. Koloszar, A. Villa Ortiz, P. Planquart, C. Narayanan, D. Lakehal, K. van Tichelen, W. Jäger, and T. Schaub, "A collaborative effort towards the accurate prediction of turbulent flow and heat transfer in low-prandtl number fluids," Nuclear Engineering and Design, vol. 366, p. 110750, 2020.

[5] W. Guo, A. Shams, Y. Sato, and B. Niceno, "Influence of buoyancy in a mixed convection liquid metal flow for a horizontal channel configuration," Int. J. Heat Fluid Flow, vol. 85, no. June, p.108630, 2020, DOI:10.1016/j.ijheatfluidflow.2020.108630.

[6] A. Pucciarelli, A. Shams, and N. Forgione, "Numerical prediction of turbulent flow and heat transfer in buoyancy-affected liquid metal flows," Ann. Nucl. Energy, vol. 186, no. November 2022, p. 109773, 2023, DOI:10.1016/j.anucene.2023.109773.

[7] "Ansys Fluent | Fluid Simulation Software." [Online]. Available: https://www.ansys.com/products/fluids/ansys-fluent. [Accessed: 20-Nov-2022].

[8] A. Shams, "Understanding the need for proper turbulent heat flux modelling for non-unity Prandtl number fluids" CFD4NRS-9, 20-23 February, 2023, College Station, Texas, USA.

Proceedings of the European Nuclear Young Generation Forum
ENYGF'23
May 8-12, 2023, Kraków, Poland

Collaboration – the key to streamlining nuclear regulation

Tanguy, Ronan[1*]

[1] World Nuclear Association, United Kingdom;

*Corresponding author: *ronan.tanguy@world-nuclear.org*

I. INTRODUCTION

A climate emergency has been declared by multiple countries and jurisdictions around the world, indicating the need for rapid and immediate action if we are to mitigate against the worst effects of climate change. The 2015 Paris Agreement's temperature goal is to keep the rise in mean global temperature to well below 2°C above pre-industrial levels, and preferably limit the increase to 1.5°C. To do so emissions should be reduced as soon as possible and reach net-zero by the middle of the 21st century [1]. To stay below 1.5°C of global warming, emissions need to be cut by roughly 50% by 2030.

Recent International Energy Agency (IEA) roadmap to Net Zero by 2050 [2] and Intergovernmental Panel on Climate Change (IPCC) reports [3] calls for increases in nuclear power generation alongside other low carbon sources of energy such as wind, solar and hydro.

Nuclear energy is currently the second largest source of low-carbon electricity generation in the world and largest among OECD countries [4]. Nuclear energy can help in achieving these targets by maintaining existing assets and seeking to safely extend their current operating lives. Maintaining existing plants will simply not be enough however and therefore there is a need to build significantly more nuclear capacity, and do so at a much faster rate than current efforts.

In September 2022, the IAEA updated its nuclear power requirement estimates [5] identifying that the contribution of nuclear to the world electricity market could more than double to about 873 GW(e) by 2050. The World Nuclear Association Harmony programme [6] and the median IPCC scenario [7] both indicate that nuclear capacity needs to rise to approximately 1250GW by 2050 to support a realistic transition to Net Zero electrical production (note these estimates do not account for use of nuclear energy in heat and steam for non-electrical applications).

Notably, the need for energy security has also increased in urgency recently, as energy prices are dramatically impacted in many parts of the world. Nuclear power, by providing a distinct low-carbon energy form, can greatly benefit the energy security of many nations and therefore this driver has increased in strength of late.

There are currently over 100 new reactor units planned across the world and a further 325 units proposed by governments. To meet the goal of a total of 1250GWe of nuclear generation by 2050, an additional 1000GWe of nuclear to be installed. If half of that were to come from Small Modular Reactors (SMRs) and the other half from traditional large scale reactors a total of 2250 new reactor would need to be connected to the grid. This would be mean around 85 new reactors, each year, every year until 2050. Over the past decade, the world has averaged just 10 new connections a year [8]. There is therefore a significant need to scale up and speed up deployments.

II. REGULATORY CHALLENGES

In order to achieve these ambitious targets on time, there are significant challenges to overcome, notably those involving regulatory approval, or licensing.

A. Different Interpretations and Application

Current emerging reactor design business models are based on n^{th}-of-kind deployment costs that are based on standardised modules being deployed at every site around the world. However, given current national regulatory practises, it is unlikely that every module designed for a new plant in one country will be identical in every other country.

As outlined in the World Nuclear Association report *Different Interpretations of Regulatory Requirements* [9], nuclear safety fundamental objectives have been well harmonised between countries and national regulators through cooperation at an international level and the creation of standards such as the International Atomic Energy Agency (IAEA) Safety Standards series, and the Western European Nuclear Regulators Association (WENRA) safety reference levels for existing reactors or safety objectives for new power reactors.

These standards have been developed by consensus between nuclear regulators using historical national standards, however those standards were developed without much if any consideration for the global nuclear industry that currently exists. These standards are often referred to as a baseline and although IAEA member states claim that their regulatory frameworks conform with fundamental safety

standards, differences in how the IAEA standards are interpreted and applied nationally in relation to nuclear power plant design continue to persist.

The different ways in which the IAEA standards are interpreted and applied often lead to design changes from one country to another. These differences are often a result of the acceptance criteria used by different regulators, which can be difficult to discern as they are not always part of the written requirements but may result from the deliberation of a group of individuals or be strongly influenced by the interpretations of specific inspectors/assessors.

In addition to the differences in acceptance criteria, the method of demonstrating a safety case can vary widely among national regulators (e.g. prescriptive versus non-prescriptive regulatory approaches). When a reactor vendor seeks to license its design in a country with a different regulatory framework, the form of the regulations and guidance can lead to a complete reframing of the original safety case and ultimately a significant amount of effort from the reactor vendor to produce new documentation that was not required by other national regulators.

Ultimately these changes can turn what should be an n^{th}-of-a-kind (NOAK) project into another first-of-a-kind (FOAK), incurring the risks and costs associated with new projects.

B. Financial Implications

Obtaining a design certification or licence from a nuclear regulator is an expensive venture for reactor designers. While the regulatory processes, fee structures and licensing durations vary between countries, the overall cost to the reactor vendor has two components.

The first of these are the fees paid to the regulator for their review work, which based upon multiple reactor vendor estimates and regulatory reports from the USA and UK, World Nuclear Association has calculated to be around 60 million USD. The second component is the cost of the work undertaken or contracted by the reactor vendor to support licensing. This cost is estimated at between 180 to 240 million USD, based upon a 1:3 or 1:4 ratio of regulatory fees to support internal costs.

It can easily be seen that licensing a reactor across multiple countries can quickly become very expensive, potentially reaching a billion USD when a vendor aims to enter four markets. It should also be noted that this work not does achieve a construction and/or operating licence and that other costs such as technology development costs and license application fees are not included.

C. Regulatory Readiness

Differences in regulatory requirements and financial implications are not the only barriers to scaling up and speeding up new nuclear deployment however. As outlined in World Nuclear Association report *Design Maturity and Regulatory Expectations for Small Modular Reactors* [10], there is limited regulatory experience with a lot of new, innovative designs.

A majority of regulatory frameworks are currently based around large-scale water-cooled reactors, which may not be suitable for emerging reactor designs. Regulators are adapting their frameworks to increase flexibility, which also brings FOAK challenges as the first designs try to navigate these new frameworks.

There is also a regulatory resource challenge to the extent that whether the number of reviews that can be undertaken concurrently by current regulatory staffing levels, would be sufficient to meet the deployment demand required to achieve net zero targets. The most recent IAEA Advanced Reactors Information System (ARIS) Advances in Small Modular Reactor Technology Developments booklet [11] lists over 80 different reactor designs under development. While it is unrealistic to expect all these designs to reach the market and apply for regulatory review it provides a clear indication of the scale of the challenge to be faced by regulators. There are currently 14 reactor designs at various stages of review with the US Nuclear Regulatory Commission (NRC) and 6 designs have been submitted in the UK to enter the Office for Nuclear Regulation's (ONR) generic design assessment process. It is not unfeasible to expect further submissions to regulators over the coming years.

Unless regulators can find a way to overcome this capacity challenge, the people and environment that they importantly protect against radiation and nuclear related risks could face the consequences of risks that emerge from insufficient reduction in carbon emissions.

III. Regulatory Harmonisation

World Nuclear Association's Cooperation in Reactor Design Evaluation and Licensing (CORDEL) Working Group has long argued the benefits of harmonising design criteria and aligning regulatory requirements [12]. Successful examples of international harmonisation of nuclear regulation also exist, such as nuclear transportation [13], and should look to be built upon.

The main objective for this harmonisation should be to reduce the size of the obstacles presented in Section II, which can be achieved by facilitating the ability of a regulator to assess and accept all, or part, of the outcomes from reviews undertaken by other regulators to support their own regulatory process. This would not remove any sovereignty from national regulators but it would provide an opportunity to considerably reduce the work to be undertaken by both regulators and reactor vendors during licensing.

A. Harmonisation proposal

CORDEL proposes that regulatory harmonisation could happen in a phased process that would work towards demonstrating equivalence between the outputs from different regulatory reviews. The ultimate goal being that regulators could pool resources to review different parts of reactor designs and accept the elements of review from other regulators.

In this three phased approach, the focus would initially be on aligning existing harmonisation activities, developing joint understanding of regulatory working practices, sharing information and agreeing common terms. This would then evolve into a second phase in which greater emphasis would be placed on key areas of focus to drive harmonisation, greater collaboration between regulatory bodies to define

the areas that can be easily accepted from one to another and developing approaches to mitigate gaps in the other areas.

The final, third aspirational phase would focus on the alignment of requirements, mechanisms for validation and acceptance of other regulatory review outputs and how these would be incorporated into the national regulatory frameworks.

To support this proposal, CORDEL has undertaken a review of US and UK regulatory requirements, benchmarking them against IAEA safety requirements in SSR-2/1 [14]. This review identified ten influential areas in which alignment between regulators would have the most beneficial impact.

These areas are: general licensing, defence-in-depth, postulated initiating events (including DBA & DEC), internal & external hazards, common cause failure, design limits, engineering design rules, safety classification, control systems, and protection systems.

B. Harmonisation Initiatives

2022 marked a renewed appetite for harmonisation initiatives not seen since the start of the multi-national design evaluation programme (MDEP). The IAEA launched its Nuclear Harmonization and Standardization Initiative (NHSI), aiming to bring together industry and regulators across seven topics (three for regulatory approaches and four for industrial approaches). CORDEL is leading the industry track on codes and standards alongside the IAEA and is actively contributing to all but one of the seven topics. Publications from NHSI are scheduled for the end of 2024.

Alongside large international initiatives, small groups of national regulators have initiated joint review efforts on SMR designs. The US NRC and the Canadian Nuclear Safety Commission (CNSC) signed a memorandum of cooperation (MoC) [15] to enhance their cooperative work by working on regulatory and safety issues in the licensing review of the GE-Hitachi BWRX-300 SMR design. Three initial topics have been chosen for review, reactor fuel verification and validation, safety strategy, and advanced construction techniques. The first two topics are familiar to one of the regulators but not the other and the third topic is unfamiliar to both. This choice of topics will allow the US NRC and CNSC to evaluate how they can work together using complementary knowledge and how they can jointly approach a new challenge. On the other side of the Atlantic, the Czech, Finnish and French nuclear regulators have agreed to jointly review the EDF NUWARD SMR design across six topics; safety objectives and study rules, list of design basis conditions (DBC), use of passive cooling systems in the DBC/ design extension conditions (DEC), development plan for scientific calculation tools (Computer Codes), incorporation of two reactors into one NUWARD installation, and probabilistic safety assessment (PSA).

CORDEL is aiming to gather lessons learnt from these initiatives along with feedback from other international collaborative efforts such as the success of the UAE's Korean designed Barakah plant and Russian export programmes in Turkey and Egypt to help assist the efficient growth of international regulatory collaboration.

IV. Conclusion

Net-zero and emissions goals will require a significant and rapid increase in nuclear power deployment not only for electricity production but also the decarbonisation of industry. Harmonising regulatory requirements is critical to enabling this growth.

While there is a level of cooperation between the organisations undertaking harmonisation initiatives, the activities are not coordinated at a higher, nor do they share a clear common goal.

There is an urgent need for a paradigm shift towards greater harmonisation of approaches to licensing and that will require all stakeholders to move forward together. The nuclear industry, nuclear regulators and nuclear organisations cannot respond to his alone however. Government leadership is essential for leadership for the development of suitable legal frameworks, polices and capabilities that enable the shift. Mechanisms to use lessons learnt in previous and existing harmonisation activities need to be established. Initiatives to support existing and newcomer countries to optimize their approach to regulation are equally a must.

These can only be achieved through effective collaboration between governments, international organisations, regulators, and industry, all working together with the shared objective of streamlining international licensing and regulatory approaches.

V. References

[1] UNFCCC, "The Paris Agreement," United Nations, 2015.

[2] IEA, "Net Zero by 20250," 2021.

[3] IPCC, "Special Report on the impacts of global warming of 1.5°C above pre industrial levels and related global greenhouse gas emission pathways, in the context of strengthening the global response to the threat of climate change," 2018.

[4] IEA, "Nuclear Power in a Clean Energy System," 2019.

[5] IAEA, "Energy, Electricity and Nuclear Power Estimates for the Period up to 2050," 2022.

[6] World Nuclear Association, "https://world-nuclear.org/our-association/what-we-do/the-harmony-programme.aspx," [Online].

[7] IPCC, "Emissions Scenarios," 2018.

[8] IAEA, "Power Reactor Information System," [Online]. Available: https://pris.iaea.org/pris/home.aspx.

[9] World Nuclear Association, "Different Interpretations of Regulatory Requirements," 2021.

[10] World Nuclear Association, "SMR Design Maturity and Licensing Expectations," World Nuclear Association, London, 2021.

[11] IAEA, "Advances in Small Modular Reactor Technology Developments," 2022.

[12] World Nuclear Association, "International Standardization of Nuclear Reactor Designs," 2010.

[13] World Nuclear Association, "Harmonization of Reactor Design Evaluation and Licensing: Lessons Learned from Transport," World Nuclear Association, London, 2020.

Technical Track 3
Operation and Maintenance

Proceedings of the European Nuclear Young Generation Forum
ENYGF'23
May 8-12, 2023, Kraków, Poland

Risk Exposure for the Proposed Bataan Nuclear Power Plant Rehabilitation

Aliperio, Mark Gino[1*]

[1] Department of Science and Technology – Philippine Nuclear Research Institute, Commonwealth Avenue, Quezon City, Philippines

*Corresponding author: *mgealiperio@pnri.dost.gov.ph*

I. INTRODUCTION

Developing countries like the Philippines experience increasing energy demands to support economic growth, and with the worldwide calls for reducing greenhouse gas emissions, alternative sources like nuclear are explored and harnessed to replace fossil fuels for baseload generation. The signing of Executive Order No. 164 [1] aims to include nuclear in the country's energy mix by pursuing nuclear power installations. One option to achieve this is to rehabilitate the mothballed Bataan Nuclear Power Plant (BNPP) in the province of Bataan. BNPP is the first nuclear plant in the Southeast Asian region and is a 621 MWe pressurized water reactor built by Westinghouse. The construction was completed in 1984 but the plant was never operated due to political reasons. It is currently under a preservation mode maintained by the National Power Corporation. There have been attempts by the government to commission and operate the plant but to no avail due to some uncertainties, questions to the safety of operation, and strong opposition from various sectors of the society. Recently, South Korean government-owned companies, Korea Electric Power Corporation (KEPCO) and Korea Hydro & Nuclear Power Co. (KHNP) offered to rehabilitate BNPP at a cost of one billion US dollars with an estimated timeline of 4 to 5 years [2].

By nature, any project can be filled with uncertainties that can significantly impact its objectives, which is why Project Planning is needed for a successful project delivery. Some unplanned events are usually associated with the project delivery and are characterized by their effects either positively or negatively. Risk items are described by its state of being vulnerable or exposed. Risk Exposure is defined as risk probability multiplied to its corresponding impact [3]. It is a means of comparing risks to determine which have the greatest threat or opportunity to the project, and which risks should receive the most management. To achieve success in a project, best practices such as Project Risk Management must be adopted as it is the only way to remain safe from adverse effects of project risks and to deliver sustainable benefits.

In this paper, risks from different categories are identified and evaluated to determine the risk exposures in the case of the Bataan Nuclear Power Plant (BNPP) $1B rehabilitation project as proposed by KEPCO and KHNP.

II. METHODOLOGY

The mechanism employed in this paper is based on the risk process as defined in the Project Management Institutes' (PMI) Project Management Body of Knowledge (PMBOK) [4], which describes a series of steps that are cyclic and continuously applied at each stage in the Project Life Cycle. The six-step process are defined as (1) Risk Management Planning; (2) Risk Identification; (3) Qualitative Risk Analysis; (4) Quantitative Risk Analysis; (5) Risk Response Planning; and (6) Risk Monitoring and Control.

Each of the six (6) steps is completed in each phase of the project and each step has a defined process and a defined outcome. As the scope of this project, steps one (1) to four (4) are employed to identify the risk exposure of BNPP rehabilitation project. The results of this four-step process will then be used as baseline for the remaining steps which are Risk Response Planning and Risk Monitoring and Control.

A. Risk Identification

Risks are captured in this step which is most effective when done in the early stage of the project because the cost of managing the risk is lower as there are more possible ways to address the risk. The Risk Breakdown Structure and Risk Register present 65 risk items under 10 categories (Financial; Technical and Engineering; Project Delivery; Operational; People; Strategic; Legal; Markets/External; Political/Policy; Region/Environment) for evaluation that are based from International Project Risk Assessment [3].

Table 1. Risk Register of the 65 risk items under 10 categories

ID	Risk Item	Category
1	Cost/Benefit Estimation Accuracy	Financial
2	Business Case Analysis	Financial
3	Change in Engineering Design	Technical and Engineering
4	Constructability	Technical and Engineering

5	Information & Documentation	Technical and Engineering
6	Technology & R&D	Technical and Engineering
7	Operability	Technical and Engineering
8	Reliability	Technical and Engineering
9	Conformance to Standard	Technical and Engineering
10	Technical Support	Technical and Engineering
11	Complexity of Design	Technical and Engineering
12	Unclear Specifications	Technical and Engineering
13	Design Criteria and Standard	Technical and Engineering
14	EPC Capability	Project Delivery
15	Project Scope	Project Delivery
16	Resource Availability	Project Delivery
17	Communications & Reporting	Project Delivery
18	Design and Construction Planning	Project Delivery
19	Availability of Utility Services	Project Delivery
20	Quality	Project Delivery
21	Operations Acceptance	Operational
22	Interruption/disruption	Operational
23	Commissioning Knowledge Transfer	Operational
24	IT Management	Operational
25	Data Security	Operational
26	Project Portfolio Interdependence & Coordination	People
27	Stakeholder Management	People
28	Health & Safety	People
29	Localizing operational workforce	People
30	Workforce availability and skill	People
31	Workforce logistics and support	People
32	Planning & Resource Management	Strategic
33	Project Governance	Strategic
34	Social Responsibility (Public Opinion)	Strategic
35	Organizational Structure	Strategic
36	Relationship with owner	Strategic
37	Regulatory environment	Legal
38	Contract Management	Legal
39	Visa Requirements	Legal
40	Government Participation	Legal
41	Permitting	Legal
42	Immigration Control	Legal
43	Regulate import and export	Legal
44	Tax/Customs	Legal
45	Supply Chain Dynamics	Markets/External
46	Contractor Viability	Markets/External
47	Local Community	Markets/External
48	Infrastructure support	Markets/External
49	Environment - Religion	Markets/External
50	Environment - Climate	Markets/External
51	Language	Markets/External
52	Unstable government	Political/Policy
53	Political stability	Political/Policy
54	Nationalism	Political/Policy
55	Consistency of Policy	Political/Policy
56	Intervene and control of government	Political/Policy
57	Geographical distance	Region/Environment
58	International relations with host country	Region/Environment
59	Environmental requirements	Region/Environment
60	Project Viability and Selection Criteria	Financial
61	Interface to Existing Equipment	Project Delivery
62	Project Manager Resource Pool	People
63	Risk Management appetite	Strategic
64	Financial/Capital Market dynamics	Markets/External
65	Supply/Production Market dynamics	Markets/External

B. Qualitative Risk Analysis

Qualitative Risk Analysis is the step whereby each risk is analyzed based on the probability of its occurrence and its potential impact on the project. Impact is assessed in many areas such as schedule, cost, safety, and quality but in this paper, impact on cost is only considered. Both Impact and Probability are assessed on a five (5) level scale from very low to very high as presented in Tables 2 and 3. This process normalizes risks between different areas so they can be further analyzed side-by-side.

Table 2. Division for Likelihood of Occurrence

Occurrence	Probability
NA – Not applicable to this project	Zero
1 – Very low chance of occurrence, rare and occurs only in exceptional circumstances.	(<5% chance)
2 – Low chance and unlikely to occur in most circumstances.	(5% chance of occurrence < 10%)
3 – Medium chance and possible to occur in most circumstances.	(10% chance of occurrence < 30%)
4 – High chance of happening and will probably occur in more circumstances.	(30% chance of occurrence < 40%)
5 – Very high chance of occurrence and almost certain and expected in most circumstances.	(40% or greater chance of occurrence)

Table 2 shows a suggested probability division for the Likelihood of Occurrence. Elements that have a Very High, High, or Medium level probability of occurrence generally require the project team's attention when the Relative Impacts are Low or greater.

Table 3. Relative Impact Definition

A	Negligible consequence that routine procedure would be sufficient to deal with the consequences.
B	Low consequence that would threaten an element of the project. Normal control and monitoring measures are sufficient
C	Moderate consequence would necessitate significant adjustment to the project. Requires identification and control of all contributing factors by monitoring conditions and reassessment at project milestone
D	Significant consequence that would threaten goals and objectives; requires close management. Could substantially delay the project schedule or significantly affect technical performance of costs, and requires a plan to handle
E	Extreme consequence would stop achievement of project or organizational goals and objectives. Most likely to occur and prevent achievement of objectives, causing unacceptable cost overruns, schedule slippage, or project failure

Table 4. Impact Matrix

Rank	Cost
Very High	US $22.23M – $25.35M
High	US $19.10M – $22.23M
Moderate	US $15.97M – $19.10M
Low	US $14.76M – $15.97M
Very Low	US $14.17M – $14.76M

Table 4 presents the impact matric where values are based from the proposed US $1 billion rehabilitation cost of BNPP and from a correspondence report summarizing construction overrun data for 175 nuclear power projects [5]. The values for the "Moderate" ranking is reflected from the mode of the statistical data, whereas for "Very High" and "Very Low" are based on the maximum and minimum data entries respectively. Having assessed each risk for the probability of its occurrence and impact on project objectives, each risk is then plotted on a risk matrix or a heat map. The risks that fall in the red areas are considered 'hot' or critical risks and these become the highest priority for risk management.

Probability and Impact values are allocated based on comprehensive literature review and KEPCO's NPP experience in UAE, KHNP's operational experience of Kori-2 NPP which has the same design as BNPP. After designating the probability and impact scales of the 65 risk items, a Risk Register is then developed that contains information related to the risks. This includes risk coordinate on the risk matrix, its baseline category, associated ranking, and cause. This Risk Register will then be utilized as the basis for managing risk and responding to them.

C. Quantitative Risk Analysis

Having collected detailed risk information from the previous steps, Quantitative Analysis then proceeds. Project Risk Management software – @RISK by Palisade [6] specifically, is used to accomplish this step. Techniques include Sensitivity Analysis, Simulation and Decision Trees. The analysis provides information such as degree of confidence, milestones sensitivity, and main risk drivers to name a few. This process allowed the project to understand the degree of impact from a particular risk, and to determine which risks drive the project. Risk Exposure of each of the 65 risk items are calculated by multiplying the probability distribution with its corresponding impact distribution. Then the sum of these risk exposures is used to determine probability and sensitivity analyses through @RISK software. Simulations are set with 50,000 iterations for improved accuracy. The resulting graphs will be used as baseline for risk mitigation planning and decision making.

III. Results and Discussion

NPP Project Risk Management provide the Risk Breakdown Structure (RBS). The Risk Registers refers to International Project Risk Assessment (IPRA) for baseline, while the probability & impact matrix for likelihood of occurrence and relative impact are based on Section II.B. Table 4 presents the Risk Register of the 65 risk items for the BNPP rehabilitation project.

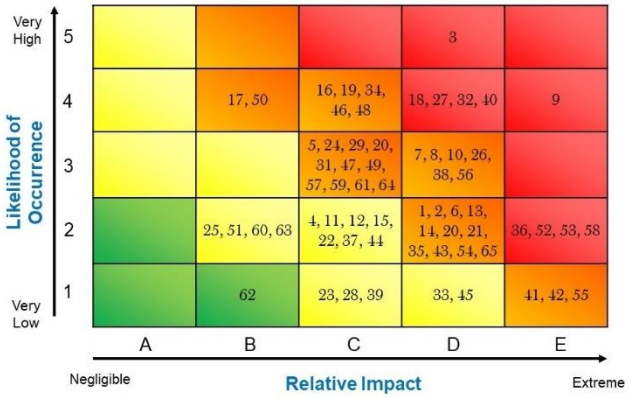

Figure 1. Risk Matrix or Heat Map of the 65 risk items

Figure 1 presents the Risk Matrix or Heat Map of the 65 risk items in the BNPP rehabilitation project, where 10 risk items are classified as Critical Risks; 38 as Major Risks; 16 as Moderate Risks; and one Minor Risk. The purpose of this project is to provide early insights for decision making

whether the proposed BNPP rehabilitation is to be pursued. Monte Carlo simulation was executed to determine cost overrun and terms of percentage to reduce the impact of risk events. Based on 50,000 iterations, Figure 2 shows the simulation results of probability distribution graph for the 65 risk items. The simulation using @RISK software set at 90% confidence level shows that the Mean Cost Overrun for the BNPP rehabilitation is approximately US $199.1

$224.8 M while the Minimum Cost Overrun is US $172.3 M.

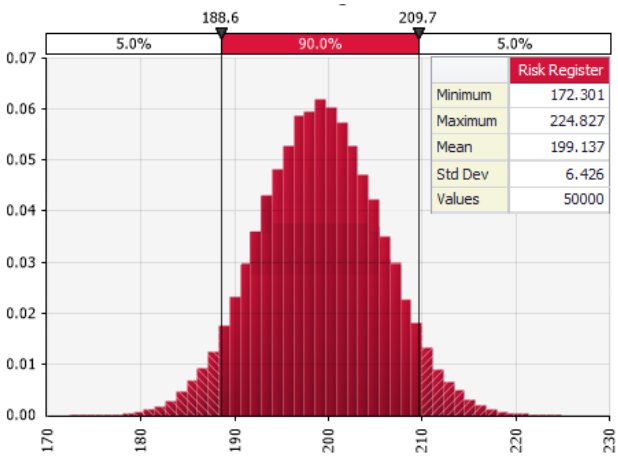

Figure 2. Probability Distribution Graph for 65 Risk Items

In order to reduce the impact of risks, a sensitivity analysis is conducted to detect the most key cost overrun elements affecting the BNPP rehabilitation to aid the mitigation approach. The bars in Figure 3 show the risk which contribute the most overrun on the project. As shown below, Change in Engineering Design is the most contributing factor to the project cost overrun. However, there are a number of different response types that can be taken for the risk items particularly the key risk items. For example, Change in Engineering Design risk can be mitigated by reducing the probability of its occurrence by re-evaluating the plant design of the decades-old BNPP and ensuring it conforms to current standards and regulations. Moreover, risk items in general can be transferred by shifting some or all of the impact, along with ownership and management, to a third party that has a higher expertise in the risk area. Also, risks can be accepted though it would need to have some contingency reserves.

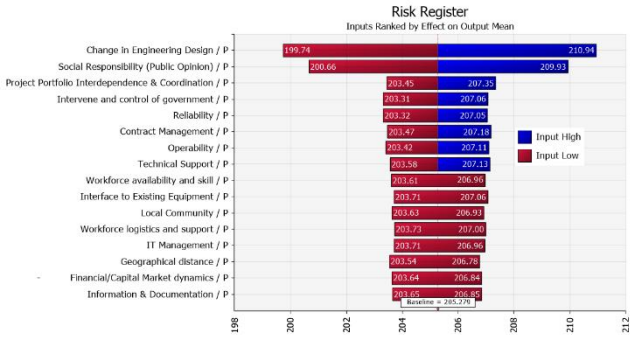

Figure 3. Tornado Graph for Overrun Cost Analysis

IV. Conclusion

In general, the results of this study show the sources of risk from different factors and show the visibility of risks through risk exposures calculation. Furthermore, this provides early insights for risk mitigation plan and/or decision making whether the BNPP rehabilitation project to be pursued is viable or not, thus saving significant effort and resources. After all, effective and efficient Risk Management increases the chances of project success up to a great extent.

V. References

[1] Official Gazette, “Executive Order No. 164 s. 2022”, Manila, Philippines, 2022

[2] C. Luci-Atienza, "South Korea’s offer to rehabilitate Bataan Nuclear Power Plant still stands, says PNRI exec" Manila Bulletin (2021)

[3] Construction Industry Institute, International Project Risk Assessment, Implementation Resource 181–2 (2003).

[4] Project Management Institute (PMI), “A Guide to the Project Management Body of Knowledge (PMBOK® Guide)”, 6th ed. 2016 Implementation Resource 181 – 2 (2003), USA

[5] A. Gilbert, BK Sovacool, P. Johnstone, A. Stirling, “Cost overruns and financial risk in the construction of nuclear power reactors: A critical appraisal”, Energy Policy 102 (2017) 644–64

[6] Palisade, “@RISK: Probabilistic Risk Analysis in Excel” https://www.palisade.com/risk/ (accessed: 2022)

Proceedings of the European Nuclear Young Generation Forum
ENYGF'23
May 8-12, 2023, Kraków, Poland

Combined Simulations to Plan Liquid Waste Remediation at the Savannah River Site

Bas, Jeremy[1*], Woodward, Simon[1], Georgiou, Andreas[1], Jung, Andrew[2] and Williamson-Owens, Scott[1]

[1] DBD Limited, United Kingdom; [2] Savannah River Mission Completion (SRMC), United States of America

*Corresponding author: jbas@dbdinternational.com

I. INTRODUCTION

The Savannah River Site (SRS) in South Carolina houses various forms of nuclear waste, by-products from nuclear materials processing for the United States' national defence, research, medical programmes, and outer space missions. The group of companies comprising Savannah River Mission Completion (SRMC) have been designated to manage the remediation the liquid waste stored in multiple tanks at the site. This includes 'sludge', an insoluble mixture of uranium fission products, and 'salt cake', a soluble mixture resulting from the neutralisation of nitric acid solutions, also contaminated with fission products.

To retrieve waste from a tank, SRMC will extract its contents and stabilise the sludge through vitrification. The process also dissolves the salt cake in water before separating out most of its radionuclides, which are vitrified along with the sludge. This leaves behind a decontaminated salt solution (DSS), which is converted to grout and stored permanently on site. Once a tank is empty, it can be filled with grout and closed [1].

The tanks are located at various areas of SRS, and at different heights above and below ground level. Radionuclide concentrations vary widely between tanks. The diversity of circumstances makes choosing which tanks to empty first a challenge. The impacts of any decision could allow risks in underserved areas to become realised, or increase the duration of the overall programme, generating cost overruns [2].

For many years, engineers at SRS have used computational methods to predict the impact of decisions on the liquid waste remediation programme. In 2022, SRMC requested for DBD Limited (DBD) to produce an updated version of this modelling capability, that this paper will describe [3].

II. MODELS DESCRIPTION

DBD chose to use two separate technologies to simulate the operations covered by SRMC. In one instance, DBD built an operational research (OR) model to represent the logistics of moving large volumes of liquid between tanks and the resources needed to run the operation: the Programme Optimisation Model. This uses the Discrete Event Simulation (DES) engine Anylogic. In the other, DBD built a process chemical model (PC) to study material, energetic and chemical balances occurring in individual unit operations: the Technical Optimisation Model. This uses the differential equation-based process modelling engine gPROMS.

A. Programme Optimisation Model (POM)

The POM covers the entire SRMC project. This can be divided into four large areas.

The Tank Farm is the storage location for the waste. In the POM, each tank is represented as an individual instance of a Tank object built identically to all others. This allows a tank to fulfil multiple roles throughout its lifetime: dissolving the salt it contains, holding salt solution generated in other tanks, or feeding the processing plants. Tanks can also fulfil different roles in successive iterations of the model with little development work. The Tank Farm also includes diversion boxes that connect tanks and control flows between them, and evaporators to concentrate solutions and reduce occupied volume [2].

The Salt Waste Processing Facility (SWPF) separates radionuclides from salt solutions using several operations: adsorption onto Mono-Sodium Titanate (MST) and filtration, and liquid-liquid solvent extraction. Its products are a DSS largely depleted of radioactive contaminants, and radionuclide streams transferred to the Defense Waste Processing Facility (DWPF).

The DWPF vitrifies the most active wastes: sludge from the tank farm and radionuclides extracted at the SWPF. The process includes multiple evaporation steps, addition of borosilicate material, melting and pouring into steel canisters. The canisters are also welded shut and temporarily stored on site.

The DSS from the SWPF is pumped to the Saltstone Production facility, where slag and fly ash are combined with DSS to form grout. The grout is poured into large

Saltstone Disposal Units (SDUs) at SRS, where it is permanently stored.

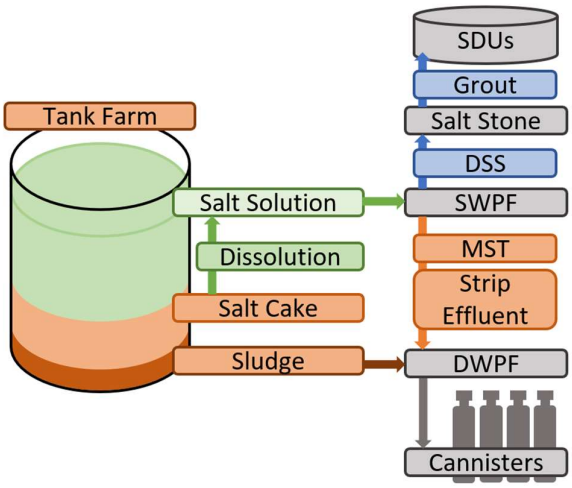

Figure 1. Block Diagram for the tank remediation process

Each of the four areas have their own processing rate and can be affected by a range of outages and upgrades throughout the project. The POM allows SRMC to predict where the bottlenecks in its process will appear, and which modifications are effective in clearing them. SRMC can also study the order of tank waste retrieval in the tank farm, and its impact on the overall project [1].

B. Technical Optimisation Model (TOM)

Whereas the most complex areas of the POM are linked to the tank farm and movements of waste between tanks, the TOM shines when it comes to the intricacies taking place in the SWPF and the DWPF.

In the SWPF, salt solution is mixed with MST, which adsorbs radionuclides such as Strontium-90 and Plutonium isotopes and is separated from the solution via filtration. The TOM can calculate decontamination factors for various initial concentrations resulting from mixing salt from multiple tanks, as well as single MST strike and multiple strike operating modes.

The SWPF also operates a Caustic-side Solvent Extraction (CSSX) process to strip radioactive Caesium and other isotopes from the salt solution. The TOM can calculate radionuclide concentrations in the resulting strip effluent, as well as volumes generated depending on the type of solvent used.

In the DWPF, sludge from the tank farm is combined with radionuclide-loaded MST and strip effluent from the SWPF, as well as borosilicate glass frit. The mixture is heated to form a homogenous melt, which is poured into steel canisters. The concentrations calculated in the SWPF and tank sludge data are combined by the TOM to forecast the amount of heat generated by each canister, depending on the origin of its contents. The TOM can also examine the condensate generated from the DWPF off gasses and predict contaminants present in this stream before it is returned to the tank farm.

C. Benefits of Combining Modelling Approaches

DES modelling excels at representing processes with many discontinuities, such as the many relatively small transfers occurring between tanks in the POM. On the other hand, Process Modelling struggles with discontinuities which force it to restart its solvers from a new set of initial conditions. Therefore, DBD applied this simulation method to focus on continuous processes, such as the gradual loading of radionuclides onto MST with time, which is best described with differential equations. The POM and the TOM complement each other to give a more complete picture of the SRS remediation process.

III. MODEL APPLICATIONS

SRMC and DBD intend to use results of the models to improve their understanding of as many areas as possible. In many cases, interactions between the POM and the TOM can increase the detail and value of information extracted. Three examples are described in summary in the following section.

A. Tank Transfers

One key feature of the POM's tank farm is to follow a user-defined strategy rather than individual instructions. For example, the user will request for specific types of tanks to be emptied first (notably with higher environmental risk). The user does not specify where the contents of the emptied tanks should go next. The POM will autonomously choose which interim tanks should receive the contents of the emptied ones. The POM bases its choices on factors such as how often a transfer route is used, or how complex it is to operate. If the most ideal destination tank is unavailable, it can find the next best one at that moment.

This feature is intended to imitate the real-life decisions that SRMC operations and planning teams will make in the future when the contents of the tanks will differ significantly from their current status. In later iterations of the POM, this should also help in quantifying the effect of unexpected events, such as equipment failures that make certain tanks temporarily unavailable.

DBD can examine all of the transfers made over a simulated lifetime of the remediation programme to extract information useful to operate and maintain the facilities. For example, the instantaneous rate at which salt cake can be dissolved is known to SRMC. However, to accurately forecast the operational dissolution rate, the POM also considers the amount of tank space available at any given time to store the produced salt solution. In the results, the accounting of tank transfers made by the POM shows that SRMC can produce salt solution faster than it can decontaminate it in the SWPF. It also shows how quickly the interim storage capacity of the tank farm will be filled up with salt solution. With current assumptions, results show that improving the throughput rate of solution in SWPF will provide a greater benefit than further improving salt cake dissolution rates.

The list of transfers generated by the POM also predicts how often specific assets that help move liquid between tanks will be used. When frequently used assets undergo maintenance and repairs, their downtime has a greater detrimental effect on the overall programme end date.

Therefore, results from the POM have encouraged SRMC to invest in improving the reliability and maintainability of plant that is expected to see higher utilisation than average. Figure 2 illustrates the difference in the utilisation rate of tanks for transfers (represented by the size of the arc) The chords between arcs of the circle represent the volume transferred from the starting tank to another. The volume received by a tank is not represented on the figure.

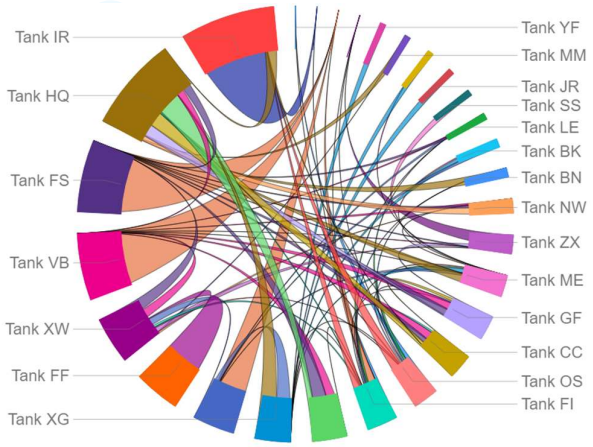

Figure 2. Chord chart aggregating transfer volumes between tanks

B. Salt Solution Batching

The salt solution sent to the SWPF must meet specific chemical concentration limits. There are some tanks that do not meet these limits without intervention. Therefore, solution from several tanks is mixed together to obtain an acceptable blend before sending it for treatment. It is difficult to predict contents of the tanks more than a few years in the future, and hence just as with transfers, the POM must be capable of choosing which tanks to blend autonomously.

The POM assumes that no reactions occur when a blend is mixed and that the key variables are the volumes to extract from each original tank, and the concentrations of four key chemicals within them. In effect, this can be summarised to a linear programme which the POM solves and optimises for a user defined objective. The user can choose whether to optimise for batches with the most radionuclides, or that require the least caustic addition for pH correction. The POM runs this optimisation on all mechanically feasible batches and can chooses the best available one.

The results of batching years in the future by the POM can be used as input to the TOM to compute the expected composition of the materials eventually sent for vitrification in the DWPF. The TOM can then calculate the effect of different salt solution blends on the heat expected to be produced by the glass canisters filled in the DWPF. This information helps establish the impact of activities in the tank farm on the wider programme.

With the results of simulation, SRMC will have a better idea what to expect depending on which strategies it chooses to adopt. The models offer a preview on what operational circumstances may occur, and operators can prepare responses well in advance in order to address them.

C. SWPF Throughput

The SWPF uses consecutive adsorption, filtration and solvent extraction steps to remove active contaminants from the salt solution. The first two steps are operated batch-wise whereas the final extraction step is a continuous process. In ideal conditions, average throughput rates through the two sections should be roughly identical; otherwise, a slowdown in the batch-wise process can be exacerbated if the continuous process must be shut down and then restarted.

This pattern of slower adsorption and filtration has become realised in recent activities, and therefore simulations have focussed on how changes to this process could improve the overall throughput of the SWPF. Specifically, the TOM can test different versions of the adsorption step, where radionuclides bind to MST. The user can choose whether MST should be added a second time after filtration in a pattern named 'double strike'. The benefit here is that fresh MST will adsorb radionuclides faster, resulting in a greater decontamination factor of the salt solution, a reduction in the overall amount of adsorption time, or both. Additionally, observing the adsorption curve can help adjust the amount and time of the MST strike used in the facility.

Once the user is satisfied with a particular operating method, the TOM can produce parameters that serve as inputs for the POM. This alternate simulation engine can test the impact of the efficiencies found over the long term, and how they interact with the continuous section of the SWPF. The operators can use the simulation tools to determine which upgrades being considered are most likely to bring the greatest benefit over the lifetime of the project.

IV. FURTHER DEVELOPMENT

In many areas, SRMC's processes are much more complex than currently described in the POM are TOM. The modelling capability will continue to develop further detail where required, to investigate proposed improvements and troubleshoot individual areas. This type of work is beyond the scope of this paper.

Therefore, this section will focus on more holistic changes foreseen for the capability, specifically by harnessing the flexibility and repeatability of the simulations developed so far.

A. Stochastic Modelling

In its current form, the POM is used exclusively as a deterministic simulation. Its objectives are to help forecast operational timelines required to meet SRMC's objectives and support the development of a System Plan. A clear improvement to the POM would be to insert uncertainties where they can be quantified, such as maintenance events and dates of plant upgrades. This feature would allow the POM to express operational timelines at varying levels of probability. A sooner completion date could be suggested at a 50% certainty level, and a more conservative estimate at 70% probability.

One obstacle to overcome is the availability of data to enable stochastic modelling, and efforts are underway to begin collecting the required inputs. Another obstacle is the technology currently in use to run the POM. Although a

single model iteration is relatively fast, effective stochastic modelling requires many more iterations, adding up to a large amount of time if operated on the same machines. This and other benefits described below is why DBD sees virtualisation as one of the key next steps in the development of SRMC's modelling capability.

B. Virtualisation

In future versions, the simulations described previously will be installed on shared virtual hardware controlled remotely by the team's developers and analysts. This approach provides many benefits that are described below.

The first gain relates to the increased centralisation inherent to virtualisation. The system can keep track of all runs ordered by users and store them in a common database, containing not only the results of runs, but also inputs essential to understanding outcomes. Advanced visualisation tools can also be shared to a wider group. This helps organise the work completed by the development team and will later facilitate presenting results to stakeholders in a consistent manner.

Another benefit is that the team can share advanced hardware and execute many runs without compromising the availability of their own workstations. They can order large stochastic runs to take place with minimal monitoring requirements, that can still produce results relatively quickly.

Beyond stochastic runs, virtualised simulations could more easily be connected with a range of optimisation engines. Classic non-linear programming could be used, or even machine learning algorithms if deemed appropriate and worthwhile.

Finally, as mentioned as part of the Modelling Applications, there are a few situations where outputs from one of the two simulation engines can be used as inputs for the other. With virtualisation, this opportunity can be seized in an automated way, without relying on users manually transcribing data between the POM and the TOM. Other than decreasing the chance of errors, it opens the possibility for combined runs with feedback loops between the models.

V. CONCLUSION

The POM and TOM have provided SRMC with a sandbox to test its approach to remediating the SRS tank farm and the liquid waste within it. The toolset is being used to forecast an operational timeline that meets SRMC's and its stakeholders' needs and objectives. The simulations will be continually updated as information becomes available and will keep informing plans in the years to come.

VI. REFERENCES

[1] SavannahRiver Site, "Facts from the SavannahRiver Site: Liquid Waste Facilities," SavannahRiver Mission Completion, May 2022. https://www.savannahrivermissioncompletion.com/_files/ugd/b25c55_25c6d25558584e4cbc9b1259273b16a4.pdf

[2] SavannahRiver Site, "Facts from the SavannahRiver Site: Liquid Waste Tank Farms," SavannahRiver Mission Completion, May 2022. https://www.savannahrivermissioncompletion.com/_files/ugd/b25c55_7750be8d40dd49c093558c2a2ad929be.pdf

[3] D. P. Chew, B. A. Hamm, and M. N. Wells, "Liquid Waste System Plan Revision 21," US Department of Energy, Jan. 31, 2019. https://www.energy.gov/sites/default/files/2019/05/f62/SRS-Liquid-Waste-System-Plan-January-2019-0.pdf

OPTIMOV®: from project to successfully fully implemented in-service test program

Bernat, Hugo[1*], Van Nuffel, Diederik[2] and Vanderstappen , Geoffrey[3]

[1] Tractebel, ENIGE group, Belgium

*Corresponding author: *hugo.bernat@tractebel.engie.com*

I. TRACTEBEL

TRACTEBEL, a subsidiary of ENGIE (formerly GDF SUEZ), is a global engineering consultancy active in the fields of electricity production, transmission and distribution, energy efficiency and civil infrastructure. Its areas of expertise cover nuclear and thermal power generation, renewable energies, transport of electricity and gas, hydropower and energy market transition. TRACTEBEL employs +5,000 staff and is active in over 70 countries.

TRACTEBEL has been providing a full scope engineering support to the seven nuclear reactor units in Belgium ever since their conception in the early 1970s. This long-term partnership with Nuclear Power Plant operator Electrabel has placed TRACTEBEL at the forefront of the development of technical solutions for nuclear infrastructure, effectively addressing operational issues and minimizing plant downtime.

II. WHAT IS OPTIMOV?

OPTIMOV® stands for Optimization Program for Testing without Intrusion Motor Operated Valve. It complies with GL 96-05 using electrical power measurements.

A. Origins

The Long-Term Operation program for Belgium's fleet of nuclear power plants required, among others, compliance with US NRC GL 96-05 generic letter on the justification of the operability of safety-critical valves.

Justifying the operability of safety-critical valves is a difficult and time-consuming process. The strain gauges traditionally used must be installed onto the valves by experienced staff and then again removed after the test sequence. The environment in which this is done requires the procedure to be foreseen during a planned shut-down of the reactor, while the test results may lead to unforeseen interventions affecting the total duration of downtime.

TRACTEBEL has developed a method to justify the operability of Motor Operated Valves (MOVs) that is compliant with US NRC GL 96-05, is safe in its use, and greatly speeds up the testing sequence. It allows a close and detailed monitoring of all types of MOVs as a system and of its individual parts.

This greatly enhances the visibility needed to evaluate the amount of work required for upcoming maintenance interventions, improving planning, optimizing operational expenditures over time and providing an overall safer operation, as well as minimizing plant downtime.

An additional feature of OPTIMOV®'s model is its recognized capability to extrapolate measurements to Design Basis Conditions, justifying operability even in accident conditions.

B. Calculation

OPTIMOV®'s calculation method is used to determine the forces occurring inside the MOV during actuation. A precise and complete data gathering must be previously conducted on all the MOVs (actuator, gearbox, valve, efficiency, …). The results of this analysis allows to determine the minimum required torque to operate the valve, and the maximum allowable torque (actuator limitation or valve's structural integrity). Knowing the boundaries of the equipment, engineers can advise a setting torque.

The comparison between the minimum required torque and the advised setting torque gives the theoretical margin. This overview of all the MOV's state enables the NPPs licensees to focus their testing campaigns on critical equipment and ensure efficiency without compromising safety.

C. Measurements

The OPTIMOV® methodology is based on the remote measurement of active power-to-torque of a MOV, which is fed to a purpose-built model. It ties in to the plant's existing I&C system and the MOV's Active Power Measurement (APM) unit. If not readily present, such an APM can easily be back-fitted at a fraction of the time and cost of a single strain gauge measurement.

Calibration of the actuator of the valve is prerequired to monitor the torque as a function of the electrical power (see Figure 1). To do so, it must be placed on a test bench (note: disassembly of the actuator occurs during normal plant operations to change the torque switch settings).

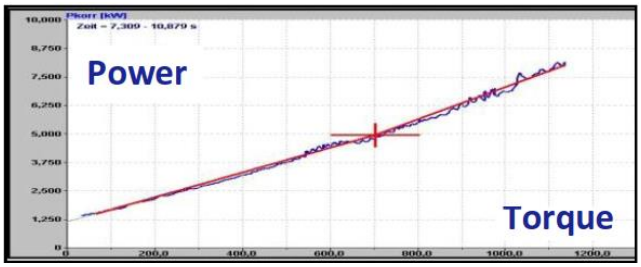

Figure 1. Reference power-to-torque measurement

The testing model itself has been developed by TRACTEBEL using 280 different parameters of some 1300 MOVs to date. The MOV's APM records the power-to-torque trace during each stroke, and a one stroke test sequence is fed into the model's algorithm that compares this trace to the reference measurement taken on the actuator in its initial state. The model then calculates the MOV's actual operational margin.

Discrepancies between the two traces provide an immediate insight into the MOV's ageing and wear, identifying eventual problems as well as their source. The OPTIMOV system is often precise enough to pin-point which individual component of the MOV is at fault, including the actuator or the gearbox.

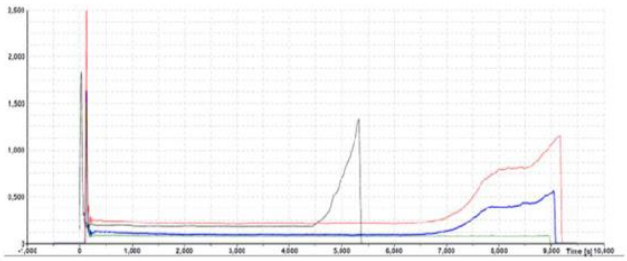

Figure 2. Active Power Measurement trace

The different testing campaign add up throughout the years and feed the model's algorithm. Recent test traces also display the results of previous testing campaign (see Figure 2). Ageing and wear at a glance!

D. Justification of MOV operability at operating and design conditions

The OPTIMOV® methodology has been approved by the Belgian Federal Authority for Nuclear Control to demonstrate operability of MOVs, or justify alternative interventions such as closer monitoring, during plant operation.

Furthermore, the methodology's model allows extrapolating from test conditions to accident conditions, which provides justification of operability in Design Basis Conditions.

E. Optimization of the plant maintenance plan

With such quantitative and qualitative data on the condition of the each of the plant's MOV, the operator can then anticipate either of the following options:

- Continue operating the MOV as is, with the model providing justification of its operability,
- Continue operating the MOV, with regular monitoring at set intervals to provide an advance notice of any further degradation,
- Replace individual parts of the MOV (actuator, packings, bearings, gears, etc.),
- Replace the entire unit.

This presents the major advantage that the maintenance strategy can be developed prior to any intervention on the MOVs, with minimal risk of diagnostic error.

A broad view on the condition of the plant's fleet of MOVs also allows an improved spare parts inventory management, and overall reduced plant maintenance downtime.

III. REAL LIFE APPLICATION

The OPTIMOV® program has been live for several years now and permitted to test hundreds of MOVs in nuclear power plants. It allowed to detect a number of valves with insufficient operability margin.

In the first phase of the implementation of this program, operability calculations were performed and validated by static and dynamic testing on a various number of valves. Nowadays, as the methodology and the corresponding calculations are completely up to date, the OPTIMOV® project has been converted to a fully implemented in-service test program for all the Belgian units.

OPTIMOV® made it possible to qualitatively assess the condition of each MOV resulting in a differentiated maintenance strategy, considering replacement of MOV, replacement of actuator, repair of components, or close monitoring. By using this program, the operator has been able to avoid replacing over half of MOVs with insufficient margin.

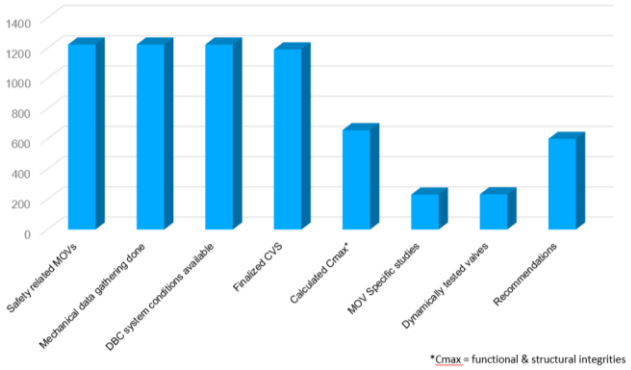

Figure 3. Achievements (in number of valves per action)

For more than 1300 safety related MOV's analysed, only 200 were tested dynamically (see Figure 3), drastically reducing maintenance cost.

III. CONCLUSION

Since the beginning of the project in 2010, to its implementation in Doel and Tihange NPP's in 2016, OPTIMOV® is now a fully operating program ensuring the operability of Motor Operated Valves of any type (gate,

wedge, globe, butterfly, plug, 3-way, …) and reducing maintenance cost. With a complete methodology and the return on experience of Tractebel's engineers, it would only take 3 years to transpose the program on a new NPP with around 300 MOV's.

IV. REFERENCES

[1] U.S. NRC, "PERIODIC VERIFICATION OF DESIGN-BASIS CAPABILITY OF SAFETY-RELATED MOTOR-OPERATED VALVES" Generic Letter 96-05, USA, September 18, 1996.

Proceedings of the European Nuclear Young Generation Forum
ENYGF'23
May 8-12, 2023, Kraków, Poland

Experimental techniques for the destruction of oxalic acid after use as a decontaminant to clean out reprocessing plants

Hopkin, Jessica[1*]; Carey, Thomas[1]; Dunnett, Barbara[1] and Street, Jonathan[2]

[1] National Nuclear Laboratory (NNL), United Kingdom; [2] Sellafield Ltd, United Kingdom

*Corresponding author: *Jessica.Hopkin@uknnl.com*

I. INTRODUCTION

Sellafield, previously one of the largest reprocessing sites in the world, has ceased reprocessing operations. As a result, the Magnox and Thermal Oxide Reprocessing Plants (THORP) are now in a state of Post Operational Clean Out (POCO) prior to decommissioning. The implementation of non-native reagents (i.e. those not previously utilised on-plant) may be required for POCO of the contaminated reprocessing plants on the Sellafield site. Oxalic acid has been identified as a possible option due to its known ability to solubilise remnant contaminants [1], [2], as well as its potential to aid in the removal of solids, such as molybdates. A range of decontamination options exist, e.g., chemical gels [3] and laser ablation [4], however the relative ease of deployment of strong complexing reagents via existing access routes make them desirable [2]. However, oxalic acid is potentially incompatible with the downstream effluent waste plants; therefore, it is necessary to understand how it could be destroyed after use in the reprocessing plant. This knowledge is required for the safety and efficiency of downstream operations.

Laboratory scale experiments for the destruction of oxalic acid were performed via the following methods: thermal destruction in nitric acid, photocatalysis, and ozonation [5]–[7]. The results from these experiments are presented here.

II. METHODS AND MATERIALS

In order to first identify methods which may be appropriate for the destruction of oxalic acid as a secondary wasteform, a comprehensive literature review was first carried out. This was used to identify destruction methods used for oxalic acid, or other simple carboxylic acids such as formic acid or citric acid, across multiple industries. The methods from this literature search which were appropriate for consideration were a) heating with nitric acid (HNO_3), b) photocatalysis, c) purging with ozone gas, d) catalytic wet air oxidation, e) electrolysis and f) ultrasonic degradation. Deliberation over which of these identified destruction techniques may be most suitable for existing plant infrastructure at the Sellafield site resulted in small scale, non-active laboratory experiments being carried out on methods a, b and c. For these experiments, a starting concentration of 0.52 M oxalic acid dihydrate was used to allow for comparison between the destruction methods; this was found to be the approximate solubility limit of oxalic acid in 8 M HNO_3. All chemicals and reagents were sourced from Fisher Scientific UK.

a. Heating with nitric acid

A temperature of either 50°C, 75°C or 100°C was used for these experiments as they were representative of available evaporator systems across the Sellafield site, in which oxalic acid may destroyed. The 250 ml oxalic acid (0.52 M) and nitric acid (8 M) solution was heated to the desired temperature in a glass round bottom flask placed within a thermostatically controlled isomantle system, accurate to ±3°C. This was regularly checked by the operator by viewing the thermostat display, and manually by inserting a glass thermometer into the solution. A condenser system was applied to the vessel to ensure that the liquor did not evaporate, which would impact the concentration of oxalic acid observed in the solution.

For some experiments, manganese nitrate ($Mn(NO_3)_2$) was added to catalyse the destruction of oxalic acid. This was added at a concentration ranging from 0.00025 M to 0.05 M. Such low concentrations were used to ascertain the minimum concentration which could be used to achieve destruction of 0.52 M oxalic acid within a 14 day period (representative of evaporator residence time) whilst generating the minimum amount of Mn-containing waste which would require storage and, eventually, disposal.

These experiments continued until all of the oxalic acid was destroyed, a run time of up to 2 weeks. Throughout the experiments, samples of 1 ml were taken from the round bottom flask to analyse the oxalic acid concentration.

b. Photocatalysis

Photocatalysis experiments were carried out with the objective of generating a photo-Fenton reaction. A 250 ml solution containing 0.52 M oxalic acid and 0.0052 M ammonium iron (II) sulfate (Mohr salt) were placed into a clear glass vessel. At ambient temperature, the solution was then exposed to either 1 or 2 UVP UVGL-58 handheld UV lamps at a wavelength of 365 nm; using either 1 or 2 lamps allowed for the control of the amount of UV the experiment was exposed to. The solutions were then periodically dosed with either 23 mmoles or 12 mmoles of 30 %w/v hydrogen peroxide (H_2O_2) to allow for the photo-Fenton mechanism to develop. In addition to these experiments exposed to UV light, control experiments were also carried out. These controls (referred to as 'dark' in the results) were covered with aluminium foil to prevent any exposure of the solution to environmental light. Control experiments also followed the same H_2O_2 dosing pattern as the experiments exposed to UV light.

The same method of tracking the oxalic acid destruction as stated in the previous section was applied.

c. Purging with ozone gas

Ozonation (purging with ozone gas) was performed at ambient temperature using a Triogen® LAB2B ozone generator and compressed air. The generated ozone was then bubbled into a 250 ml 0.52 M oxalic acid solution via glass frit bubblers. Ozone was produced at either 2 g/hr (low) or 4 g/hr (high) from the generator for these experiments.

Due to the evaporation of the experimental liquor caused by the bubbling of ozone, it was necessary to frequently add 18 MΩ deionised water to maintain a constant volume and obtain representative results from analysis.

d. Analysis of samples

All samples taken during the experiments were subject to analysis of their oxalic acid concentration by two techniques. UV-vis spectrophotometry using 0.1 M potassium permanganate, 3 M nitric acid and 0.03 M sulfamic acid was carried out at 526 nm on a Thermo Scientific™ GENESYS™ 40 UV-Vis spectrophotometer. The absorbance reading from the spectrophotometer was used to calculate the oxalic acid concentration using a calibration of known concentrations. A titration using 0.005 M potassium permanganate was also used as an analytical method. The volume of potassium permanganate required to titrate the oxalic acid while a colour change from colourless to pale pink was observed was used to calculate the oxalic acid concentration of the sample. This was done based on the molar ratio of oxalic acid and potassium permanganate in the titration reaction. For both of these analysis techniques, the limit of detection was found to be 0.003 M of oxalic acid.

For experiments where H_2O_2 was used, an additional titration was also necessary due to the reaction of H_2O_2 with potassium permanganate, thereby affecting the oxalic acid analysis. Oxalic acid samples containing H_2O_2 were added to 18 MΩ deionised water, 3.5 M sulfuric acid, 0.09 M potassium iodide and ammonium molybdate; this mixture was then titrated from colourless to pale yellow using 0.001 M sodium thiosulfate. At this point, starch solution was added which turned the mixture black, and then sodium thiosulfate was continuously added until a further colour-change back to colourless was observed. The H_2O_2 concentration was then calculated from this titration and was subtracted from the oxalic acid concentration determined by the other analysis method. This subtraction allowed for an accurate value for oxalic acid concentration.

III. RESULTS AND DISCUSSION

The results for the destruction of oxalic acid by heating with nitric acid along with $Mn(NO_3)_2$ are presented in Figure 1 (50 °C), Figure 2 (75 °C) and Figure 3 (100 °C).

Data presented in these figures clearly show that as the temperature of the nitric acid heating system was increased, the time taken to destroy the oxalic acid also decreased. This is consistent with similar work carried out, where it was also determined that this destruction follows first-order kinetics [5]. At 50°C without the presence of $Mn(NO_3)_2$ (Figure 1), no significant oxalic degradation was observed. However, at all other temperatures and $Mn(NO_3)_2$ concentrations, the oxalic acid was destroyed.

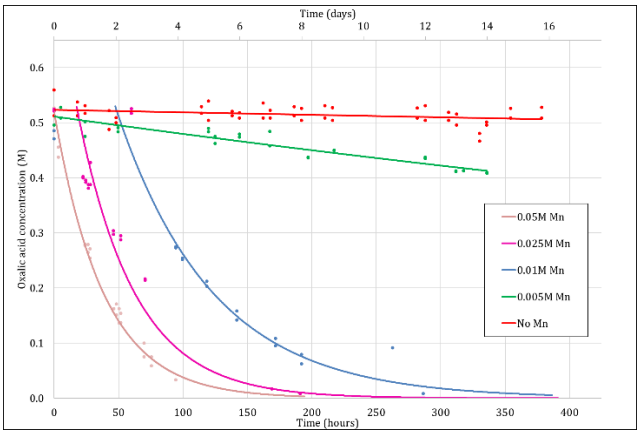

Figure 1. Destruction of oxalic acid by heating with nitric acid and $Mn(NO_3)_2$ at 50°C.

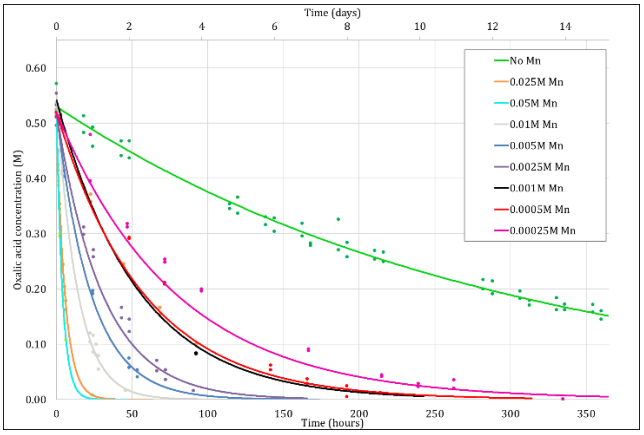

Figure 2. Destruction of oxalic acid by heating with nitric acid and $Mn(NO_3)_2$ at 75°C.

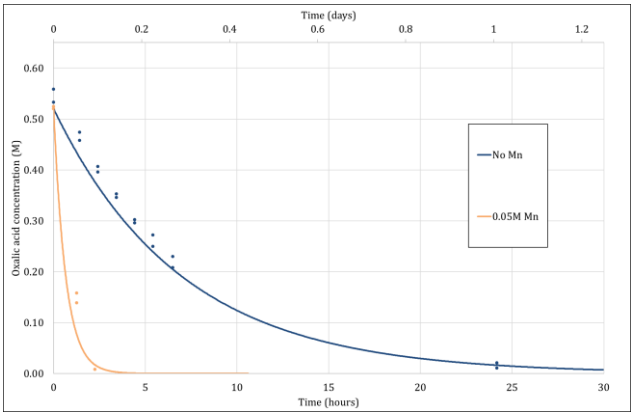

Figure 3. Destruction of oxalic acid by heating with nitric acid and $Mn(NO_3)_2$ at 100°C.

The use manganese in the form of $Mn(NO_3)_2$ was found to be an effective catalyst for these reactions. The time taken for decomposition of the oxalic acid decreased as the concentration of the $Mn(NO_3)_2$ increased. Employment of the $Mn(NO_3)_2$ catalyst at 0.05 M lowered the activation energy for the destruction reaction from 154 kJ mol^{-1} to 81 kJ mol^{-1}, as calculated by the Arrhenius equation [8]. Throughout this destruction process, production of NOx gas was observed. Therefore, implementation of this technique on a reprocessing plant would require sufficient off-gas treatment to be in place.

While the experiments were carried out at the selected temperatures due to their representativeness of evaporators present on the Sellafield site, most experiments were carried out at 75°C (Figure 2) due to particular interest in the Medium Active evaporators, which operate at approximately this temperature. The residence time of the oxalic acid liquor within this evaporator would be 14 days, therefore the oxalic acid would need to be destroyed within this time before the liquor is moved downstream. A $Mn(NO_3)_2$ concentration of 0.0005 M was found to be the minimum catalyst concentration capable of destroying the oxalic acid down to the limit of detection. Following the oxalic acid destruction, the Mn containing waste would then likely be stored in bulk storage vessels before vitrification. High concentrations of Mn compounds is known to have a negative impact on the performance of glass melters used for vitrification [9]. Therefore, it would be beneficial to this process to use the lowest possible concentration of Mn upstream. Use of 0.0005 M Mn is understood to have an insignificant impact on the downstream operation of reprocessing plants.

While the thermal destruction method was determined to be successful for destruction of oxalic acid, this methodology may involve routing of the oxalate containing liquor through reprocessing plants to a location where this destruction method could be carried out. Therefore, destruction via a photo-Fenton reaction or ozonation has the potential advantage of in-situ/local implementation. Data from the photo-Fenton experiments are shown in Figure 4.

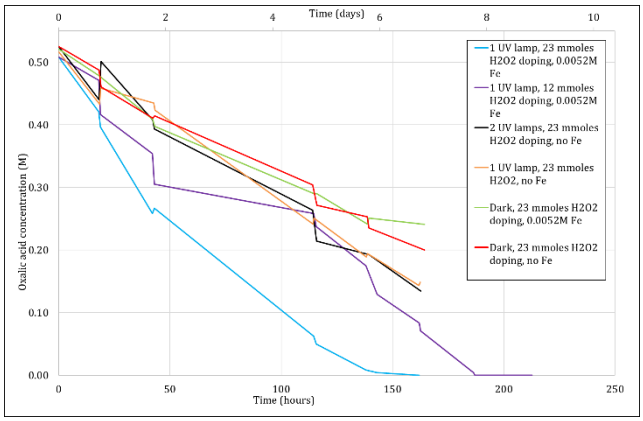

Figure 4. Destruction of oxalic acid for a photo-Fenton mechanism.

Figure 5 shows that while the destruction of oxalic acid was accelerated by the presence of UV light and Fe (Mohr salt), it was also possible without these catalysts via the addition of hydrogen peroxide (red line in Figure 4), as has been previously reported in literature for aqueous solutions [10] and nitric acid based solutions [11]. The presence of Fe and UV light act as catalysts for the photo-Fenton process. The Fe^{2+} is oxidised to Fe^{3+} by the H_2O_2 under UV conditions and initiates the production of radical species, which in turn lead to the oxidation and destruction of oxalic acid. Figure 4 shows that a higher concentration of H_2O_2 achieves destruction quicker, however the intensity of the UV light (use of 1 or 2 lamps) appeared to have no significant effect.

Repeated dosing of the experiments with H_2O_2 was found to be necessary for maintaining oxalic acid destruction, as it was used up during the oxidation process. Therefore, were this technique to be used for in-situ oxalic acid destruction on a reprocessing site, the location would need to permit frequent access for dosing. In literature, other catalysts such as titanium dioxide (TiO_2) have been looked at for the photocatalytic destruction of oxalic acid [12]–[14]. However, as this catalyst would be added as a solid, this may pose operational difficulties downstream. Therefore, an aqueous mechanism, as described in this work, was identified ideal for reprocessing plants, such as Sellafield.

Destruction via ozonation was an attractive technique, due to its perceived simplicity from the addition of a singular gaseous component. Data from ozonation experiments, where ozone was produced at 2 g/hr or 4 g/hr, are shown in Figure 5.

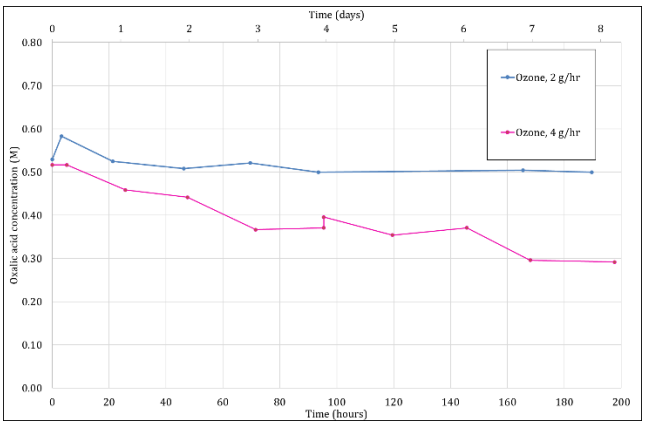

Figure 5. Destruction of oxalic acid by generated ozone gas.

Unfortunately, the ozonation experiments were unable to be optimised to the extent of the other destruction techniques examined during this work. However, this data was useful for some initial scoping regarding this technique. Figure 5 shows that at the higher ozone production rate (4 g/hr), oxalic acid was consistently destroyed. Whereas at a lower generation rate of 2 g/hr, no change in the oxalic acid concentration was observed. These results suggested that increasing the ozone production beyond what has been used in these experiments could yield more rapid oxalic acid destruction.

Implementation of ozone as used in this work would be relatively simple on a reprocessing plant, as this could be carried out at ambient temperatures in suitable vessels with a permitting gas route. However, increased efficiency of this method has been shown through pairing with catalysts such as UV and H_2O_2 [7], [15] and TiO_2 [16]. If efficiency and destruction rate are desired over simplicity of implementation, pairing ozonation with catalytic systems would likely be required.

Due to the limitations of existing plant infrastructure (i.e. evaporators) on the Sellafield site and the destruction seen in these experiments, the destruction of oxalic acid via heating with nitric acid with a Mn catalyst was deemed the most desirable option. A negligible concentration of 0.0005 M Mn in evaporator-representative conditions (75°C) was deemed the best option and poses minimal risk to downstream waste treatment. The other destruction methods assessed in this work may prove to be useful options for future decommissioning operations at the Sellafield site.

IV. CONCLUSIONS

Destruction of oxalic acid, used as a decontaminant during the decontamination and decommissioning of Sellafield's reprocessing plants, was found to be possible via heating with nitric acid and photocatalysis. The efficiency of the destruction using these techniques can be improved by using catalysts – $Mn(NO_3)_2$ for heating with nitric acid, and Fe/H_2O_2 for photocatalysis. The limited experiments performed for ozonation as a destruction method were not optimised in order to reasonably assess the effectiveness of this method.

V. References

[1] R. M. Orr, H. E. Sims, and R. J. Taylor, "A review of plutonium oxalate decomposition reactions and effects of decomposition temperature on the surface area of the plutonium dioxide product," *J. Nucl. Mater.*, no. 465, 2015.

[2] L. Zhong, J. Lei, J. Deng, Z. Lei, L. Lei, and X. Xu, "Existing and potential decontamination methods for radioactively contaminated metals - A Review," *Prog. Nucl. Energy*, no. 139, 2021.

[3] A. Gossard, A. Lilin, and S. Faure, "Gels, coatings and foams for radioactive surface decontamination: State of the art and challenges for the nuclear industry," *Prog. Nucl. Energy*, no. 149, 2022.

[4] Q. Wang *et al.*, "Laser decontamination for radioactive contaminated metal surface: A review," *Nucl. Eng. Technol.*, no. 55, 2023.

[5] C. Mason, T. L. Brown, D. Buchanan, C. J. Maher, D. Morris, and R. J. Taylor, "The Decomposition of Oxalic Acid in Nitric Acid," *J. Solut. Chem.*, no. 45, pp. 325–333, 2016, doi: 10.1007/s10953-016-0437-2.

[6] N. Quici, M. E. Morgada, G. Piperata, P. Babay, R. T. Gettar, and M. I. Litter, "Oxalic acid destruction at high concentrations by combined heterogeneous photocatalysis and photo-Fenton processes," *Catal. Today*, vol. 101, pp. 253–260, Apr. 2005, doi: 10.1016/j.cattod.2005.03.002.

[7] E. Ketusky and K. Subramanian, "Advanced Oxidation Oxalate Decomposition Testing with Ozone," Waste Management Conference, Phoenix, Arizona, USA, Paper 12534, 2012.

[8] A. Youssef, A. Salas, N. Al-Harbi, N. Basfer, and D. Nassr, "Determination of chemical kinetic parameters in Arrhenqius equation of constant heating rate: Theoretical method," *Alex. Eng. J.*, no. 67, pp. 461–472, 2023.

[9] A. Goel, J. S. McCloy, R. Pokorny, and A. A. Kruger, "Challenges with vitrification of Hanford High-Level Waste (HLW) to borosilicate glass - An overview," *J. Non-Cryst. Solids X*, vol. 4, no. 4, 2019.

[10] D. Y. Chung, E. H. Kim, Y. J. Shin, J. H. Yoo, C. S. Choi, and J. D. Kim, "Decomposition of Oxalate by Hydrogen Peroxide in Aqueous Solution," *J. Radioanal. Nucl. Chem.*, vol. 201, pp. 495–507, 1995.

[11] E. H. Kim, D. Y. Chung, J. H. Park, and J. H. Yoo, "Dissolution of Oxalate Precipitate and Destruction of Oxalate Ion by Hydrogen Peroxide in Nitric Acid Solution," *J. Nucl. Sci. Technol.*, vol. 37, pp. 601–607, 2000, doi: 10.1080/18811248.2000.9714936.

[12] T. A. McMurray, J. A. Byrne, P. S. M. Dunlop, J. G. M. Winkelman, B. R. Eggins, and E. T. McAdams, "Intrinsic kinetics of photocatalytic oxidation of formic and oxalic acid on immobilised TiO2 films," *Appl. Catal. Gen.*, vol. 262, pp. 105–110, 2004.

[13] D. Tomova, V. Illiev, A. Eliyas, and S. Rakovsky, "Promoting the oxidative removal rate of oxalic acid on gold-doped CeO2/TiO2 photocatalysts under UV and visible light irradiation," *Sep. Purif. Technol.*, vol. 156, pp. 715–723, 2015, doi: http://dx.doi.org/10.1016/j.seppur.2015.10.070.

[14] C. B. Mendive, D. W. Bahnemann, and M. A. Blesa, “Microscopic characterization of the photocatalytic oxidation of oxalic acid adsorbed onto TiO2 by FTIR-ATR,” *Catal. Today*, vol. 101, no. 3–4, pp. 237–244, Apr. 2005, doi: 10.1016/j.cattod.2005.03.016.

[15] C. Martino, W. King, and E. Ketusky, “Actual-Waste Tests of Enhanced Chemical Cleaning for Retrieval of SRS HLW Sludge Tank Heels and Decomposition of Oxalic Acid,” Waste Management Conference, Phoenix, Arizona, USA, Paper 12256, 2012.

[16] F. J. Beltrán, F. J. Rivas, and R. Montero-de-Espinosa, “Catalytic ozonation of oxalic acid in an aqueous TiO2 slurry reactor,” *Appl. Catal. B Environ.*, vol. 39, pp. 221–231, 2002, doi: 10.1016/S0926-3373(02)00102-9.

Proceedings of the European Nuclear Young Generation Forum
ENYGF'23
May 8-12, 2023, Kraków, Poland

DigiDECOM- Innovative training on decommissioning solutions in nuclear as well as other industries.

Rajkumari, Archita[1*], Szőke, István [1], Szőke, Réka [1] and Porsmyr, Jan Otto[1]

[1] Institute for Energy Technology, Os Alle 5, NO-1777 Halden, Norway

*Corresponding author: *Archita.Rajkumari@ife.no*

I. INTRODUCTION

The nuclear industry is facing a critical challenge regarding the decommissioning and waste management of nuclear sites. Unlike some other industries, decommissioning in the nuclear sector is still in its infancy, with a lack of standardization and reuse. Additionally, the industry needs to maintain and develop relevant skills and competencies for the many years that a plant operates, as well as create and maintain new specific skills required for decommissioning and waste management. The specialized knowledge and experience required for these tasks, along with the ability to effectively address obstacles and issues, cannot be met without a greater number of young academics and professionals.

The nuclear industry is facing two significant issues: 1) how to maintain relevant skills and competences for the 50+ years that a plant is operating when no new builds are planned in the country; and 2) how to create and maintain new specific skills required for decommissioning and waste management. However, the current training programs on practical nuclear applications, decommissioning, and waste management have been phased out during the last decade in many countries. [2]

To address these challenges, an innovative and holistic training solution called the DigiDECOM Training program is proposed. This program aims to provide young academics and workers with the necessary theoretical knowledge and practical experience to enable them to continue their professional development independently, learn from seasoned professionals, and develop critical thinking skills. In addition to teaching technical skills, this program emphasizes a Human Technology Organization (HTO) aspect for approaching decommissioning and waste management, including understanding the human component, coping with leading teams and personnel, successful methods of leading interdisciplinary staff, as well as intersystem thinking. The use of Artificial Intelligence (AI), data, and robotics-based innovation is also emphasized as applicable across many industries. The Institute for Energy Technology (IFE) in Norway is leading the way in competence building for nuclear decommissioning and has established the HADRON laboratory for cross-sectional research and development. The DECOM Cluster for Decommissioning and Repurposing is also established to connect innovations for decommissioning and reuse from IFE and other partners with the industry for higher safety, efficiency, and sustainability. The paper aims to promote the need for the DigiDECOM Training program and highlight the importance of creating and maintaining specialized competence trainings for vocational subjects in the nuclear industry and other industries that require work in potentially hazardous environments.

The nuclear sector has some of the strictest requirements for risk management and security. The standards, services, and products that are developed within nuclear decommissioning and waste management will be applicable in many other industries where removal and recovery of buildings or facilities is required. We believe that the foundations for IFE taking a key international role in competence building for nuclear decommissioning are already in place, IFE being the first organization designated by the International Atomic Energy Agency (IAEA) as an International Collaborating Centre in the field of digitalization for nuclear decommissioning.

IFE having led the longest international undertaking related to nuclear safety, the Halden Reactor Project (HRP), and leading the Halden HTO project born from the HRP, has an exceptionally good basis for supporting nuclear safety on an international level. There is also a considerable potential for collaborating with other industries where safety critical processes and work in potentially hazardous environments are involved.

Norway has decided to close and decommission the nuclear research reactors at Kjeller and in Halden, with an estimated cost of NOK 25 billion. Furthermore, several other businesses and facilities will be decommissioned (oil and gas platforms, ships, ports, etc.). Decommissioning is a new industry in Norway that can contribute to creating many new jobs and opportunities.

II. Vision behind DigiDECOM

Halden (hosting the HRP and HTO projects, an IAEA designated centre, DigiDECOM workshops, and the

DECOM Cluster), is an important competence centre to meet the challenges related to decommissioning of nuclear installation as well as supporting current and future nuclear energy solutions.

IFE has 60+ years of experience in supporting the safe operation of nuclear facilities along with specific expertise and fully developed technology components. The DECOM cluster has been established to ensure a Private Public Partnership (PPP) approach to the application of innovative technology, with a focus on improving safety, efficiency, and sustainability in decommissioning. The aim of the cluster is also to apply knowledge across industries, pilot innovative technology, create sustainable business development, offer competence development, facilitate collaboration, and joint projects. The international network of the Cluster will provide increased learning, innovation, and technology development along the entire value chain.

III. Methodology

An increasing number of national and international experts and practitioners have been actively supporting the DigiDECOM workshops and trainings since 2017. The systemic approach of DigiDECOM includes technical, as well as human and organizational considerations for Nuclear Decommissioning and Waste Management. A very special emphasis is placed on the active involvement of the young generation and professionals, who can later influence the ongoing research activities. Due to previous studies highlighting the power of digital learning, DigiDECOM training takes full advantage of XR (eXtended Reality) experiences for exchanging knowledge and providing a learn by doing approach. However, traditional classroom learning approaches are also applied.

This training is designed as a modular, coherent, and commonly qualified training program in nuclear decommissioning with the fundamentals of radiation protection and nuclear physics and working in hazardous environments to the usage of Artificial Intelligence (AI), data and robotics in the nuclear back end. DigiDECOM Training also aims to raise the interest of students and professionals to stimulate careers in this important and emerging field, by offering attractive theoretical and practical learning opportunities applicable across industries.

The use of Virtual Reality (VR) and XR opens tremendous new possibilities in training and education, especially teaching complex or specialized tasks where traditional approaches are complex, time-consuming, and expensive. We take advantage of advanced technologies like XR, AI, Digital Twins, robotics, etc for better, more efficient, safe, and sustainable disposal solutions in the future. DigiDECOM focuses on integration of AI, data, and robotics technologies with nuclear/radiological and other physics models.

The main mandate of DigiDECOM is to improve the processes related to decommissioning in nuclear and other industries using digitalization and robotics. DigiDECOM has been supporting various EURATOM projects (e.g., on SHARE, PLEIADES, PREDIS and HARPERS) focusing on addressing digital transformation, robotics, and other possible trends in nuclear decommissioning and waste management. DigiDECOM 2021 and 2022 had a very fruitful exchange with NEA's EGRRS (Expert Group on the application of Robotics and Remote-Systems in the nuclear back end).

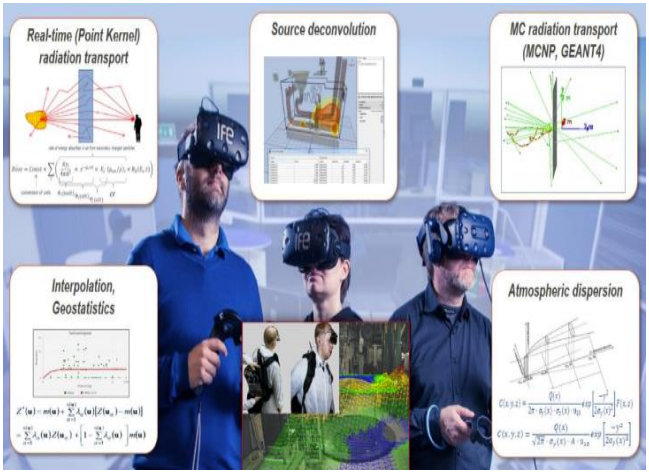

Figure 1. Radiological hazard modelling including XR. [3]

Figure 1 explains the physics behind the resource tool IFE has developed for radiological modelling including XR.

A. Importance and challenges of competence building

The current landscape of nuclear competence varies greatly between nations. While certain competencies and talents may be in danger in one nation, they may be far more secure in another. Experts who previously worked in the nuclear industry have moved to other industries in countries where nuclear has been declining. Hence, international cooperation will be needed more than ever before to ensure all the nuclear expertise and capabilities that the industry needs on an international level. Since the number of workers needed in the nuclear sector only make up a small portion of all graduates, replenishing the pool of nuclear professionals shouldn't be an issue. However, it is getting increasingly difficult to attract highly qualified technical graduates in the face of competition from other, seemingly more alluring industries.

IFE in Norway has been one of the very few international beacons for the development and early real-life application of advanced support systems powered by a combination of 3D modelling/simulation and 3D real-time radiation physics modelling and visualization (advanced Digital Twins) for nuclear maintenance and decommissioning. Nuclear physics aided XR based training has proven to be a superior training method for nuclear competence building due to providing an improved engagement, understanding, learning retention rate, and attraction of the young generation. IFE is building up a library of digital learning modules that can be delivered anywhere and can be

integrated into training programs for various audiences, learning objectives, and certifications.

Hence, DigiDECOM Training offers both the opportunity to learn taking advantage of advanced AI, data, and robotics technologies, as well as an engaging learning experience using XR training technologies. Due to this innovative approach, DigiDECOM Training is very appealing for the young generation looking for engaging courses and long-term career opportunities. The 3D radiological modelling assisted XR learning technology offered by DigiDECOM with digital models and data, capabilities for developing and delivering digital training content, as well as lessons learned from previous activities in the nuclear sector in other countries is attracting an increasing number of young professionals to the nuclear field. As indicated before, skills offered by DigiDECOM training are also applicable in several non-nuclear application areas. The library of training modules is being extended with modules specifically designed for non-nuclear industries, like decommissioning in the oil & gas sector and other hazardous environments where people or expensive equipment (e.g., robots) can be impacted negatively. Some examples are shown below in figure 2 from the application of VRdose used for training purposes in Ukraine and Russia.

Figure 2. Examples of 3D simulation-based evaluation for designs and procedures in nuclear environments.

B. Resource: IFE VRdose™

HVRC VRdose is a real-time software tool for modelling and characterising various nuclear environments, planning a sequence of activities in creating task plan reports with dosage estimates, optimizing radiation, and modelling the environment. It provides the option to customize the offered dosimetry output and adjust the radiological model to increase the accuracy of estimates. The program can also be used to help create post-work review reports that incorporate actual measurements. Additionally, the platform supports information presentation to various user types for briefing and decision-making, facilitating communication across intervention stakeholders.

The VRdose Planner offers charts, graphs, and 3D radiation visualisation to assist the user in understanding the results of calculations. These are updated instantly to reflect any changes to the modelled radiological state, such as changing shielding materials and human activities over time. The VRdose Briefer is a dedicated presentation tool for communicating scenarios prepared using the Planner as shown in figure 3.[3]

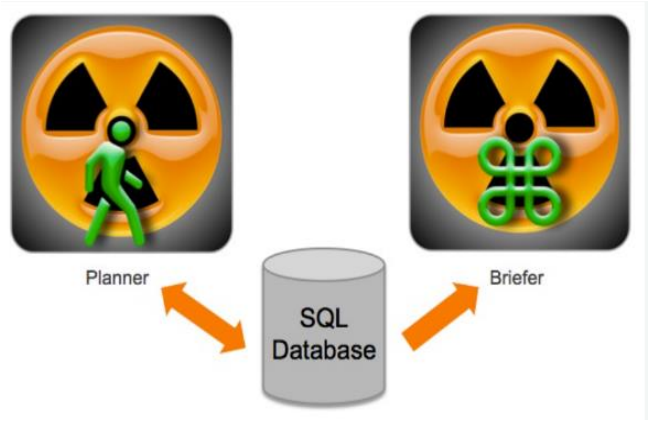

Figure 3. The VRdose Briefer and Planner tool [3]

The VRdose system is a sophisticated piece of desktop 3D simulation software, suitable for planning and training for work involving possible exposure of humans to ionizing radiation and other hazards. The technologies applied are powerful tools for the support of work involving radiation risks, as they enable many possibilities, including the following:

- invisible radiation can be visualized in a virtual (or augmented reality) environment in real time.
- work scenarios can be taught and practiced cost-effectively in a safe but realistic environment.
- communication between workers, regulators and other remote participants can be greatly enhanced.

To create a radiological environment in software simulations, specific requirements must be met by tools such as the Halden Planner and VRdose system. The first requirement is input data, which describes the environment to be modeled, including radiation sources, barriers that affect radiation transport, instruments for measuring the radiation field, worker movement, etc. The algorithms use these data to evaluate radiation risks, which is known as the 'dosimetric approach.' In the next step, the dosimetric approach results are presented in a user-friendly, sophisticated manner. The purpose of these codes is to assist experts in making informed decisions, minimize human exposure to radiation, and support the ALARA dose planning principle. The VRdose is part of a VR tool ecosystem offering an integrated approach to decommissioning and waste management through supporting facility information management, risk management, ALARA based work planning, safety demonstration, training, documentation, and other tasks. This integrated approach allows for the training to be part of an integrated digital capability supporting the entire project. In this approach, digital content is prepared not only for training, but for supporting safety planning, regulatory communication, internal communications, and other tasks.

IFE assisted the operator improving safety in operation through better training in Leningrad, Kola, and Rivine Nuclear Power Plants. In the UD projects, better planning the use of personnel working in radioactive environments in cooperation with Radiation Safety Department and Decommissioning Department were done. A better safety strategy was designed through higher quality of work due to easier and more exact planning of dose. The **LNPP (Leningrad Nuclear power Plant) Planner** for work planning including radiation visualisation and dose calculation (dosimetry) was developed with VRdose.

IV. Conclusion

In conclusion, the preservation of nuclear knowledge held by senior experts and the capacity of universities to teach nuclear subjects to young professionals is crucial to ensuring the continued research and development of this important field. The decrease in public support for nuclear research and development has created a need for industry and government support to guarantee the availability of professionals and resources in research institutes and universities. With the nuclear industry responsible for supporting R&D, it is urgent to gather competencies and knowledge from experts and provide them to the next generation of professionals and students. The DigiDECOM Workshops and Trainings aim to address this need by reinstating interest in careers in the nuclear field and building new competencies with a specific focus on the application of AI, data, and robotics in decommissioning and waste management in the nuclear and other industries.

V. References

[1] NEA (2004), Nuclear Competence Building, OECD Publishing, Paris

[2] Rajkumari Archita, Ziemons Karl, Paulßen Elisabeth, Langer Christoph, & Steinmetz Hans-Jürgen (2021). The International Master Program on Nuclear Applications at FH Aachen- Nuclear Waste Management as a Part of Holistic Education A Student Contribution to the IAEA International Conference on Radioactive Waste Management (IAEA-CN--294). International Atomic Energy Agency (IAEA)

[3] I Szőke and M N Louka and T R Bryntesen and J Bratteli and S T Edvardsen and K K RøEitrheim and K Bodor, “Real-time 3D radiation risk assessment supporting simulation of work in nuclear environments,” Journal of Radiological Protection, vol. 34, no. 2, April 2014, 10.1088/0952-4746/34/2/389.

Proceedings of the European Nuclear Young Generation Forum
ENYGF'23
May 8-12, 2023, Kraków, Poland

Development of the Material Testing Program Within the DELISA-LTO Project

Rusnakova Katerina[1*], Smola Vojtech[1], Kozakova Veronika[1], Kopriva Radim[1], Adamech Marek[2], Petzova Jana[2], Slnek David[2,3], Ildiko Szenthe[4,] Maksym Zarazovskii[5]

[1]UJV Rez, a. s., Hlavni 130, Rez, 250 68 Husinec, Czech Republic; [2]VUJE, a. s., Okruzna 5, 918 64 Trnava, Slovakia; [3]STU, MTF, Jana Bottu 2781/25, 917 24, Trnava, Slovakia; [4]EK-CER, Konkoly Thege Miklos UT 29-33, Budapest 1121, Hungary; [5]IPP Centre, Bolsunovska Street 8, Kyiv 01014, Ukraine

**katerina.rusnakova@ujv.cz*

I. INTRODUCTION

DELISA-LTO (DEscription of the extended LIfetime and its influence on the SAfety operation and construction materials performance - Long Term Operation with no compromises in the safety) is an international project with the four years duration under the HORIZON-EURATOM-NRT-01 call (2022-2026). The main aim is to obtain important information about material degradation of structural materials harvested from selected decommissioned WWER type Nuclear Power Plants (NPP).

Combination of the simulation tools and experimental techniques – e. g., mechanical testing and NDT inspection methods will help to understand materials degradation phenomena like thermal ageing and swelling which are significant materials degradation processes of the NPPs components. Testing of the harvested material subjected to real operating conditions is a promising opportunity to acquire new information about material degradation in real operated NPPs. Obtained information will be important to assure Long Term Operation (LTO) in case of lifetime extension of currently operated NPP.

II. MATERIAL TESTING PROGRAM WITHIN DELISA-LTO PROJECT

There are 7 Work Packages (WPs) in the DELISA-LTO Project. This paper is primarily focused on material testing program within DELISA-LTO Project.

Methodology and assessment are included into the WP2 and Experimental validation and tests into the WP4. Both WPs are connected and based on permanent connection.

The goal of WP2 is to define experimental testing methodology. WP2 is responsible for selected structural components materials. Tasks included in the WP2 are in the Table 1. The leader of WP2 is VUJE (Slovakia).

Table 1. Tasks included in the WP2

Task	Title
Task 2.1	Critical analysis of the primary circuit components important to LTO safe operation of NPP WWER 440 and WWER 1000
Task 2.2	Methodology for the NDT
Task 2.3	Methodology for the evaluation of structural and substructural changes
Task 2.4	Methodology for the mechanical testing

The goal of WP4 is to establish experimental works based on obtained information from participating laboratories and development of the Experimental Matrix. Tasks included in the WP4 are in the Table 2. The leader of WP4 is UJV Rez, a. s. (Czech Republic).

Table 2. Tasks included in the WP4

Task	Title
Task 4.1	Characterization of the relevant specimens and methods
Task 4.2	Thermal Ageing
Task 4.3	NDT methods – industrial implementation
Task 4.4	Screening of the results and data from the past/ongoing projects

A. Selected structural components and materials

Original purpose of the DELISA-LTO Project was to use only harvested materials from decommissioned Jaslovske Bohunice NPP in Slovakia (Figure 1) - Unit 1 and Unit 2, that were operating for 28 years (WWER 440 V230 type). Materials included in the experimental program are in the Table 3 (extended by material in initial state - Pressurizer surge line from Unit 3 Jaslovske Bohunice NPP).

Table 3. Materials included in the Experimental Matrix in DELISA-LTO Project

Component	Material and state
Main circulation piping	08Ch18N12T - NPP EBO V1 – initial state; BM
Main circulation piping	08Ch18N12T+WM - NPP EBO V1 – after 28 years in operation; BM, WM, HAZ
Main circulation piping – triple T-junction	08Ch18N12T+WM – NPP EBO V1 – after 28 years in operation; BM, WM, HAZ
Pressurizer surge line	08Ch18N10T - NPP EBO V1 – after 28 years in operation; BM
Pressurizer surge line	08Ch18N10T - NPP EBO3 – initial state; BM

Collaborating partners in WP2 and WP4 - IPP Centre (Ukraine) and EK-CER (Hungary) extended the volume of other available materials usable for material testing thereafter. These supplemented materials are included in the Table 4.

Table 4. Supplemented materials in the Experimental Matrix in DELISA-LTO Project

Component	Material and state
WWER-1000 - Reactor flange fastening parts	after 30 years in operation (IPP-C)
WWER-1000 - Steam generator collector with HE tubes	08Ch18N10T - operated (IPP-C)
WWER-1000 - Main circulation piping	10GN2MFA+SS cladding - NPP V1 – initial state (IPP-C)
WWER-440 - Capsules of the thermal specimens	Paks NPP (2 pcs), 08Ch18N10T - 24 years in operation (EK-CER)
WWER-440 - Capsules of the thermal specimens	Paks NPP (2 pcs), 08Ch18N10T - 32 years in operation (EK-CER)
WWER-440 - Main circulation pump - Guide wheel	10H18N9TL - 27 years in operation (EK-CER)

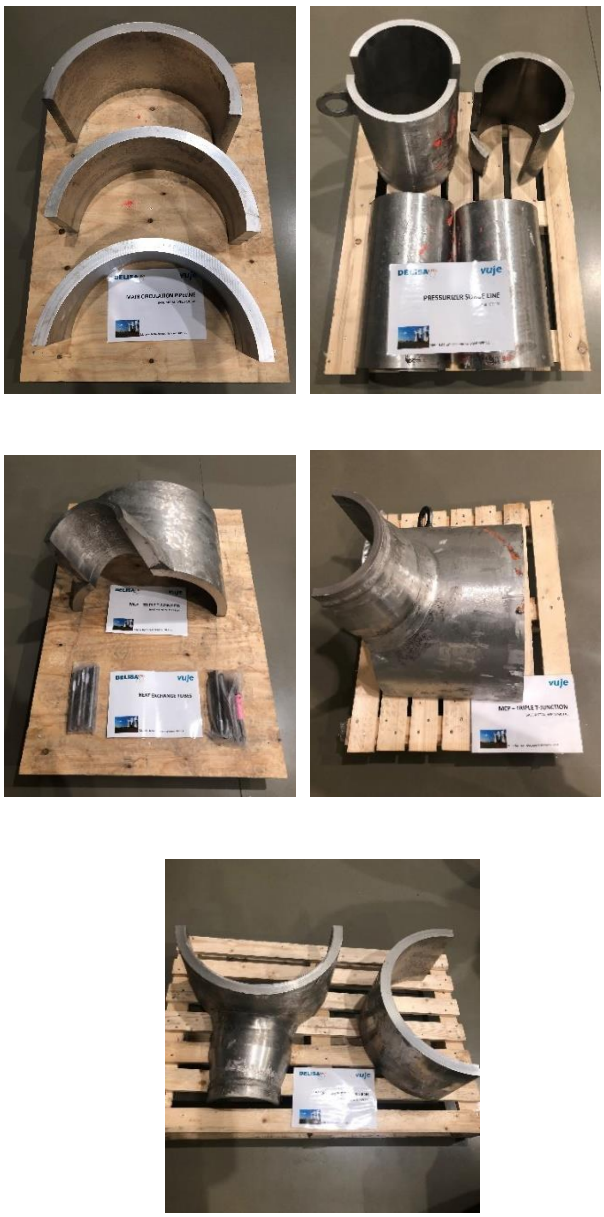

Figure 1. Material from V1 Jaslovske Bohunice NPP stored in VUJE (Slovakia)

B. Laboratory equipment, testing procedures and quality assurance system Questionnaires

The first step to define experimental works was to obtain necessary information from participating laboratories. All participating laboratories were asked about their laboratory equipment, testing procedures and quality assurance system though the questionnaire. First evaluated data provided basis for the next round of questionnaires. Second round was more detailed and was based on information from the first round of the survey.

For every experimental testing method additional more detailed questionnaire was created. These more comprehensive questionnaires were sent to contributing partners in WP4 - VUJE (Slovakia), STUBA (Slovakia), CVR (Czech Republic), IPP (Ukraine), BZN (Hungary), EK-CER (Hungary), VTT (Finland). Completed questionnaires were subsequently evaluated and were summarized in the prepared Experimental matrix frame.

The first part of the two round questionnaire was divided into two parts - “Experimental testing” and “Non-destructive testing”. The sub-part one includes information about experimental testing accreditation or non-destructive testing certification and site qualification. The subpart two includes experimental testing methods or non-destructive testing methods.

The second part of the survey – more detailed questionnaires were sent to contributing partners based on data from the first questionnaires. Each laboratory obtained detailed questionnaires for every experimental method (mechanical testing / NDT / Microscopy) which were indicated in the first round.

Detailed questionnaires were used for the frame of experimental testing matrix preparation. Within European research projects the precise preparation of the experimental interlaboratory studies using surveys and questionnaires has not been used in such extent before.

C. Experimental Matrix

The Experimental matrix is a table where collaborating laboratories, materials and their states, testing methods, specimen types and geometry are included. It is a suitable tool for finding common cross-cutting areas for interlaboratory comparisons too.

In general, the experimental matrix frame combines experimental testing and analytical techniques, participating laboratories, experimental archive material and preferred specimen type of each contributing partner and testing methodology. Specimen types are divided into standard and miniaturized testing sample types for the planned comparison of conventional methods with perspective approaches using sub-sized specimens. Selected experimental and analytical methods will be connected with the available archive material inventory to create the detailed system of experimental interlaboratory studies. Included experimental techniques are

- Impact testing,
- Tensile testing,
- Static Fracture testing,
- Hardness,
- Small Punch Test (SPT),
- Scanning Electron Microscope (SEM),
- Optical Microscopy,
- Transmission Electron Microscopy (TEM),
- Non-destructive Testing (NDT),
- Other methods (e. g. Positron annihilation spectroscopy, Mössbauer spectroscopy, Replicas).

Materials were selected within the WP2 from different primary circuit components of the NPP Jaslovske Bohunice (EBO) (Units 1 and 2) with respect to the structural material state (initial state / number of years in operation) and material type – base metal (BM), weld metal (WM) and heat affective zone (HAZ). Experimental matrix will also serve as a basis for the thermal ageing phenomenon evaluation, thus accelerated thermal ageing in laboratory conditions is also planned within the WP4.

III. PREPARATION FOR EXPERIMENTAL TESTING

Experimental testing preparation is in progress. Next steps will be activities like cutting plans creation, samples drawings, unification of mechanical testing conditions and preparation of interlaboratory comparison etc.

Presentation about this topic Development of the Material Testing Program Within the DELISA-LTO Project will give more information about next steps in WP2 and WP4.

IV. CONCLUSION

Testing of the harvested material subjected to real operating conditions is important to assure Long Term Operation (LTO) in case of lifetime extension of currently operated NPPs. Obtained data will help to understand material degradation phenomena like thermal ageing in the primary circuit components.

V. ACKNOWLEDGEMENT

This paper was supported by the DELISA-LTO project n°101061201 funded by the European Union.

Funded by the European Union

VI. REFERENCES

[1] GRANT AGREEMENT: Project 101061201 — DELISA-LTO. In: EUROPEAN COMMISSION: Directorate-General for Research and Innovation, 2022, 23/5/2022

Technical Track 4
Fuel Cycle and Radiation Protection

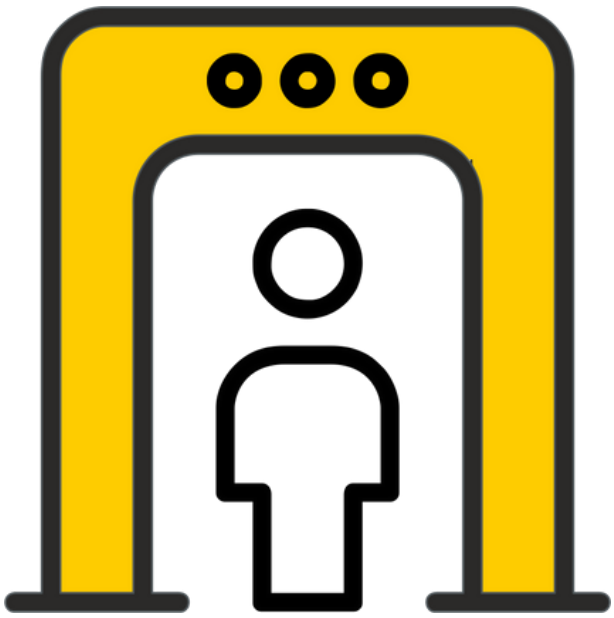

Proceedings of the European Nuclear Young Generation Forum
ENYGF'23
May 8-12, 2023, Kraków, Poland

An application of graphene oxide in spent nuclear fuel interim storage

Aragón, Pau[1], Milena-Pérez, Abel[1] and Sánchez-García, Iván[1*]

[1] Centro de Investigaciones Energéticas Medioambientales y Tecnológicas (CIEMAT), Spain

*Corresponding author: *ivan.sanchez@ciemat.es*

I. INTRODUCTION

The nuclear fuel employed in most reactors currently in operation consists of cylindrical ceramic pellets made of uranium oxide (UO_2) enriched with less than 5% of ^{235}U. These pellets are then arranged in tubes composed of a Zr alloy (Zircaloy) that are approximately 4 meters in length. While within the reactor, the fuel undergoes high-energy neutron irradiation, which induces substantial alterations in its composition and thermo-mechanical properties.

The fuel pellets contain fission products (FP), which are nuclides produced during the fission of heavy elements or the radioactive decay of others, also created during the fission reaction in the reactor. Generally, FP are beta and gamma emitters, and their concentration in the fuel post-irradiation is around 5-6%, including volatile components (I, Br, Cs, Ru, noble gases), metallic aggregates (Mo, Tc, Cd, In), oxide precipitates (Rb, Ba, Zr), and rare earth elements that are dissolved in the UO_2 matrix (La, Ce, Nd). Conversely, due to neutron capture reactions, some of the ^{235}U transforms into ^{236}U, while part of the ^{238}U is converted into heavy elements known as transuranic elements (TRU), such as Pu, Np, Am, and Cm. The last three are considered the minor actinides (MA). TRU are alpha emitters, and most of them can replace uranium atoms in the UO_2 matrix since they are completely miscible in the structure. Following irradiation, their concentration in the fuel varies between 1-2%. The generated plutonium, mainly ^{239}Pu, undergoes fission reactions, contributing to energy generation and the radiotoxic inventory. Moreover, some elements present in the structural materials, which make up the fuel elements, undergo neutron capture reactions, generating activation products. The most representative are ^{60}Co, ^{63}Ni, ^{93}Zr, and ^{94}Nb.

As irradiation cycles progress, the concentration of neutron poisons such as ^{236}U, FP, and TRU may inhibit the fission chain reaction, thereby limiting the degree of burnup. For this reason, a reload must be performed, typically every 12, 18, or 24 months, depending on the fuel type and reactor technology. During the reload, approximately one-third of the total number of fuel elements are renewed. The discharged material is referred to as spent nuclear fuel (SNF), which includes both the irradiated pellets and cladding.

After a wet storage period in the cooling pools of a nuclear power plant, SNF is transferred to dry storage containers for final management, such as the ENUN 32P design shown in Figure 1. These containers are required to comply with safety functions established by Nuclear Regulatory Authorities, which include subcriticality control, confinement of radioactive material, radiation shielding, residual heat evacuation, and fuel recovery capacity. Typically, a rack inside the container holds fuel assemblies in a vertical position within a cylindrical stainless-steel vessel surrounded by a neutron-absorbing shield. This structure is then placed inside a concrete module to provide additional radiation protection. To prevent a chemical reaction that could lead to corrosion or degradation of the fuel cladding, the interior atmosphere in contact with the SNF is filled with inert helium gas.

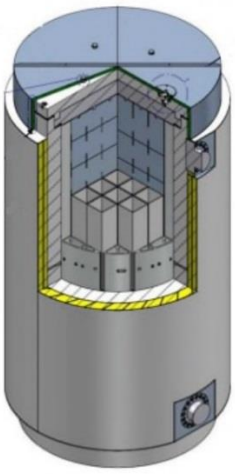

Figure 1. Schematic design of an ENUN 32P container [1].

II. STORAGE AND DISPOSAL OF HIGH-LEVEL WASTE

Nuclear fission reactors generate high-level waste (HLW) primarily composed of SNF, which poses significant radiological risks due to the presence of FP and TRU. The

heat generated by their radioactive decay impacts all stages of HLW management. FP primarily contributes to the radiotoxicity of HLW during the first few hundred years after irradiation, while TRU become responsible for the total activity due to their long half-life periods. Therefore, responsible and safe management of SNF is crucial to avoid imposing undue burdens on future generations and protect the public and environment from ionizing radiation hazards.

Selecting an appropriate strategy for managing HLW is highly complex and involves considering several factors such as political context, economic feasibility, natural resource conservation, environmental protection, and public opinion. This complexity arises primarily due to the long-term implications associated with the proliferation risk and the presence of fissionable materials like U and Pu in SNF. In addition to that, the activity and concentration of the aforementioned radionuclides in SNF are also key factors in the design of the HLW management programs as they determine the storage methods and warehouse design [2].

Currently, a technically valid long-term management option for SNF is confining it in metal containers; of the same type that the one shown in Figure 1. These containers are temporarily stored in a centralized or decentralized interim storage facility for cooling and radioactive decay before being permanently disposed in a deep geological repository (DGR). In those storage scenarios, and in the case of container or cladding failure during the early stages of disposal, a release of HLW can be produced resulting in a radiation hazard for the public and environment. In such a case, volatile FPs, such as I, Br, Cs, and Ru, are the most important from a safety perspective as they will be the first to be released in the mentioned event. In order to ensure the safe management of the HLW, it is crucial to have an additional barrier capable of retaining these elements and even more important, to indicate if a leak is occurring in spent fuel management.

III. GRAPHENE OXIDE: A NEW BARRIER

In 1986, the term "graphene" was proposed to describe each layer of graphite [3, 4]. Prior to its discovery in 2004, it was believed that graphene only existed as a constituent of other graphite materials due to the incorrect hypothesis that two-dimensional crystals would be thermodynamically unstable [5]. Graphene is a two-dimensional material where each carbon atom is covalently bonded to three other carbon atoms, forming a flat sheet with a hexagonal structure similar to a honeycomb. It is considered the basic unit of different carbon structures (Figure 2) as it can be rolled up to form carbon nanotubes (2D) or stacked to form graphite (3D).

Graphene oxide (GO) is a compound derived from graphene that consists of a graphene sheet with various oxygen groups on the basal planes and edges. GO is obtained through an oxidation process of graphite with chemical agents in an acidic medium, resulting in graphite oxide. This oxide then undergoes an exfoliation process to produce GO, which is a highly hydrophilic, hygroscopic material with a high oxygen content and a high specific surface area [6]. Like graphene, GO is a two-dimensional material that can be used in various applications.

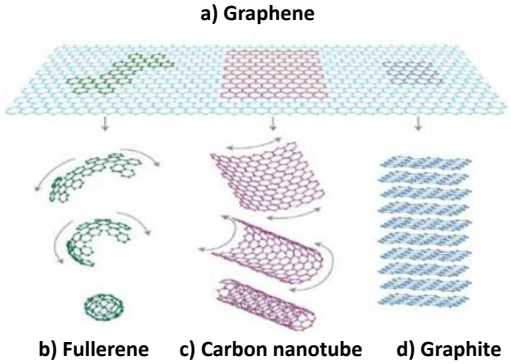

Figure 2. Formation of carbon structures from graphene [5].

Due to its high specific surface area and oxygen group presence, GO is an attractive adsorbent for the nuclear field where it can be used to adsorb radionuclides. This material has excellent adsorption capacity for various radionuclides in liquid media such as ^{233}U, TRU (^{239}Pu, ^{241}Am, ^{237}Np), and relevant FP (^{90}Sr, ^{137}Cs, ^{95m}Tc, ^{152}Eu) achieving higher retention yields than conventional materials like bentonite and activated carbon [7-9]. GO's adsorption capacity makes it suitable for use in radioactive water treatment during dismantling operations or accidents such as the Fukushima accident.

In addition to liquid media, GO can also adsorb gases such as CO_2, NH_3, and NO_2, among others. Although GO is an insulating material, it can be transformed into a conductive material through a reduction technique that involves removing some oxygen functional groups via chemical or physical methods. The resulting material, reduced graphene oxide (rGO), has lower electrical properties than pristine graphene but is still conductive enough to be used in electronic devices. rGO also maintains comparable adsorption properties to GO, making it a suitable adsorbent.

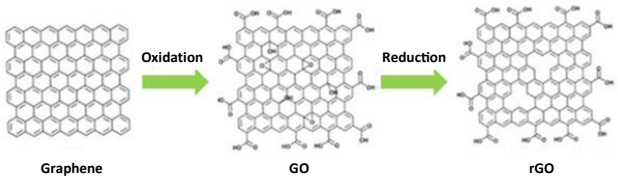

Figure 3. Structural model of graphene, GO, and rGO.

rGO's application as a gas sensor has generated a lot of interest due to its gas adsorption properties. Gas sensors produce electrical signals that indicate the presence of a gas and are widely used in fields like environmental monitoring. Studies have shown that rGO's conductivity changes appreciably when exposed to different gases and undergoes adsorption, making it a suitable gas sensor.

In the application of radioactive waste adsorbent, rGO must have high resistance to radiation emitted by radionuclides present in radioactive waste to perform its function satisfactorily. HLW consists of radionuclides that emit alpha, beta, and gamma radiation, so this material must have good radiation resistance. Studies have investigated rGO's

radiation resistance and adsorption capacity for certain radionuclides, concluding that it has good radiation resistance (up to an absorbed dose of 600 kGy of gamma radiation) while maintaining an acceptable adsorption capacity [10]. Additionally, there is significant interest in using radiation as a method to reduce GO to rGO, potentially making it even better as a sensor.

IV. APPLICABILITY

Given the composition of the radioactive waste to be stored in containers and the excellent properties of graphene oxide, our work explores two novel applications of this material in the field of radioactive waste storage. The first application involves using rGO as an additional barrier to retain radionuclides in the event of a container breach, minimizing potential environmental emissions. The second application involves using rGO as a sensor to detect container leaks and take appropriate measures, considering the associated risks. These applications are crucial in the management of radioactive waste and highlight rGO's significance in this field.

A. Applicability as a barrier

To utilize rGO as a barrier, GO could be acquired as a suspension in water and subjected to thermal treatment in a high-pressure oven at 200 °C and 20 atm for an hour, yielding rGO. As the temperature may be reached without water evaporation, the resulting rGO would be in suspension and ready to be used as a spray. The objective is to apply rGO as an external coating for containers during manufacturing, acting as the final physical barrier in the container (Figure 4). The sprayed layer would be 150 µm thick, typical for sprayed paints. In the event of a container breach, volatile fission products (I, Br, Cs, Ru,) would interact with the oxygenated groups of rGO, resulting in their retention.

B. Applicability as a sensor

Regarding the sensor application, a circuit that monitors changes in resistivity will be required, where the sensor functions as a variable resistance over time, connected by two terminals to the circuit. These terminals will be situated in different parts of the container to continuously measure its electrical resistivity (Figure 4), and the value will be monitored through equipment located in the control room. It is important to note that this material can adsorb water from the air, resulting in a conductivity signal, necessitating a control point to serve as a reference. This will detect changes in resistivity caused by adsorption resulting from container leaks.

Furthermore, the gas sensor inside the container can be designed for online signal transmission without cables, such as through Wi-Fi connection, to optimize communication and minimize contact with the containers. Each container will have a circuit that measures changes in resistivity, transmitting that data to a receiver in the control room for processing. This enables online quality control and monitoring of container conditions, improving the safety of the interim storage facility.

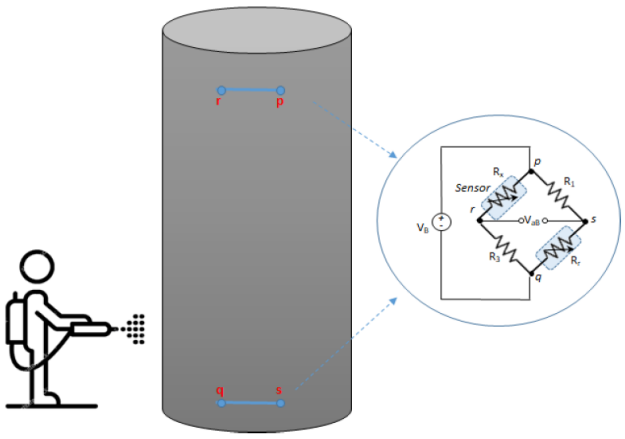

Figure 4. Application of reduced graphene oxide as paint and as a sensor in the spent fuel storage container.

V. CONCLUSIONS

This paper proposes using reduced graphene oxide (rGO) as a new containment barrier in case of a potential incident during the interim storage of spent nuclear fuel. The use of rGO serves a dual purpose. Firstly, its excellent adsorption properties are utilized to trap potential gaseous fission products that could be released into the environment following a container rupture, as they are the first to be released due to their volatility. Secondly, the structural changes that occur in rGO when adsorption occurs are utilized as a gas sensor. When wirelessly connected to a receiver, the containers' integrity can be monitored, and a signal is produced when an unexpected event occurs. The technical feasibility of this project is supported by the previous use of this material in adsorbing radionuclides. Finally, the project would have broad social acceptance, as it establishes an additional barrier to existing ones, reinforcing the safety of these types of facilities, which is a primary concern of nuclear power opponents.

VI. References

[1] CSN, "Propuesta de dictamen técnico sobre la solicitud de ENSA de modificacion de la aprobacion del diseño del contenedor ENUN 32p para almacenamiento de combustible gastado en base a la revision 4 del estudio de seguridad y la revision 9 del plan de calidad," Consejo de Seguridad Nuclear2018.

[2] NEA, *National Inventories and Management Strategies for Spent Nuclear Fuel and Radioactive Waste*, 2016.

[3] J. Jegoudez, C. Mazieres, and R. Setton, "A study of some alkali metal-furangraphite compounds and of their charge transfer characteristics," *Carbon,* vol. 24, pp. 747-756, 1986.

[4] V. Singh, D. Joung, L. Zhai, S. Das, S. I. Khondaker, and S. Seal, "Graphene based

materials: past, present and future," *Progress in Materials Science,* vol. 56, pp. 1178-1271, 2011.

[5] A. K. Geim and K. S. Novoselov, "The rise of graphene," *Nature Materials,* vol. 6, pp. 183-191, 2007.

[6] D. Chen, H. Feng, and J. Li, "Graphene oxide: preparation, functionalization, and electrochemical applications," *Chemical Reviews,* vol. 112, pp. 6027-6053, 2012.

[7] A. Y. Romanchuk, A. S. Slesarev, S. N. Kalmykov, D. V. Kosynkin, and J. M. Tour, "Graphene oxide for effective radionuclide removal," *Physical Chemistry Chemical Physics,* vol. 15, pp. 2321-2327, 2013.

[8] Z. Li, F. Chen, L. Yuan, Y. Liu, Y. Zhao, Z. Chai, *et al.*, "Uranium (VI) adsorption on graphene oxide nanosheets from aqueous solutions," *Chemical Engineering Journal,* vol. 210, pp. 539-546, 2012.

[9] S. Yu, X. Wang, X. Tan, and X. Wang, "Sorption of radionuclides from aqueous systems onto graphene oxide-based materials: a review," *Inorganic Chemistry Frontiers,* vol. 2, pp. 593-612, 2015.

[10] I. Sánchez-García, A. Nunez, L. J. Bonales, J. M. Perlado, and J. Cobos, "Study of the adsorption capacity of graphene oxide under gamma radiation in different media," *Radiation Physics and Chemistry,* vol. 165, p. 108395, 2019.

Proceedings of the European Nuclear Young Generation Forum
ENYGF'23
May 8-12, 2023, Kraków, Poland

New Focus for New Fuel: How nuclear transport approaches may need to adapt to support the deployment of advanced nuclear fuels

Burnett, George[1*]

[1] Nuclear Transport Solutions (NTS), United Kingdom;

*George Burnett: *george.burnett@ntsglobal.uk*

I. BACKGROUND

The global nuclear industry is poised to contribute to efforts to mitigate climate change and address energy security concerns. Reactor technology has seen significant innovation to adopt modular manufacturing and installation principles for Generation III+ and IV reactor systems, which are currently seeing extensive investment to make them available for demonstration or wide scale deployment. Many developing reactor systems are also looking to adopt new fuel types to capitalise on a myriad of potential benefits. These new fuel types include:

- High Assay Low Enriched Uranium (HALEU)
- Tri-Structural Isotropic (TRISO) / Coated Particle Fuel (CPF)
- Molten Salt

Each novel fuel type brings about its own nuances in practice, and this remains the case for nuclear transport operations. Nuclear transport forms a fundamental enabling element of the nuclear industry, connecting nuclear facilities across the entire fuel cycle. Naturally, the challenges faced by safety and security during transport are distinct to those face by a licensed nuclear site. Moving nuclear material within the public domain requires a bespoke approach to ensure safe and secure operations involving nuclear materials. Developing the appropriate nuclear transport safety and security arrangements begins with one fundamental question '*What is being transported?*'. Therefore, the advancements being seen within the fuel cycle will bear significant influence on the approaches required for transport.

II. NUCLEAR TRANSPORT SAFETY & SECURITY

A. Nuclear Safety in Transport

The principal regulations for radioactive transport are the IAEA Regulations for the Safe Transport of Radioactive Material (SSR-6) [1]. These regulations are aimed at ensuring safety primarily through the capability of the transport package, irrespective of the mode of transport. Transport packages are diligently designed and licensed against these regulations, subsequently encompassing the majority of radioactive safety credit that can be taken for the entire transport. Safety claims of the package require significant substantiation to be justified for licensing, through modelling and real-world testing against:

- Routine Conditions of Transport
- Normal Conditions of Transport (NCT)
- Accident Conditions of Transport (ACT)

The series of transport conditions see transport package designs tested against parameters deemed credible under each title. Accident conditions of transport see the packages undergo the most stringent testing that is considered equivalent to a severe and credible transport accident. These include a fully engulfing fire up to 800 ºC, 9 metre drop onto an unyielding target, 1 metre drop onto a punch bar and immersion in water.

Figure 1. M4/12 Transport package, used to transport Mixed Oxide (MOX) fuels

B. Nuclear Security in Transport

The Convention on the Physical Protection of Nuclear Material (CPPNM) [2] and its Amendment [3] are the only legally binding international instruments in the area of physical protection of nuclear material. The original convention concerns international transport, while the recent amendment extends its application to domestic use, storage, and transport. The convention places several legal obligations on states who are party to the convention, to protect nuclear material in transport.

Annex I of the CPPNM and its Amendment detail the level of protection that must be afforded to nuclear material based on what is known as the material "Category". Annex II provides a tabulated categorisation method for nuclear material based upon the type, form, and quantity of material in transport. Category I material is afforded the highest levels of physical protection.

Theft and sabotage are the 2 key considerations for nuclear security. Theft being a 2-stage process in which physical protection systems are overcome and control of the material is lost, and adversaries escape with the material. Sabotage is considered a 1 stage event, in which Unacceptable Radiological Consequences (URCs) occur. The material type, form, and quantity in transport have a substantial influence on the arrangements that could be in place for how attract the material is for theft, and how vulnerable the material is to sabotage.

C. Safety and Security Interface

Common goals are shared by safety and security, in that both are looking to protect the public, the environment and property (safety concerning accidents and security via protection from malicious acts). Therefore, an important interface exists that must be considered in practice, one that is cognisant of the influence each area bears on the other.

III. AN INSIGHT FROM FUEL

Although not yet commercially available, numerous reactor vendors have developed designs incorporating HALEU fuel types. Utilising HALEU is allowing reactors to capitalise on longer operating cycles, achieve smaller designs and increased efficiencies. In the United States (US) alone, Idaho National Laboratory produced a paper estimating HALEU requirements at a cumulative total of 5,350 Metric Tonnes (MT) for a net-zero economy by 2050 [4]. Similarly, the Nuclear Energy Institute (NEI) issued an open letter the (then) Secretary of Energy estimating a total cumulative requirement of 1972.6 MT to support US nuclear energy requirements up to 2035 [5]. To that end, the US has launched the HALEU availability programme, tasked with securing a supply of HALEU for the US and declaring investment of $2.5 billion in funding for 2 demonstration projects [6]. These sources demonstrate that one of the key nuclear powers in the world is committed to adopting and utilising HALEU as a future fuel source. HALEU may be fabricated into conventional UO2 forms, TRISO / CPF or incorporated into molten salts, and data from SMR development suggests this is the case.

In the coming years SMRs are expected to make a significant contribution to the nuclear capacity installed globally. The International Atomic Energy Agency's (IAEA) 2022 publication, The Advances in Small Modular Reactor Technology Developments [7] is supplementary to the IAEA's Advanced Reactor Information System (ARIS), and details fact sheets for the known SMR designs under development. Analysis of the listed fuel types within this publication demonstrates the uptake in novel fuel types within the SMR space.

Table 1. Number of SMRs listing the use of novel fuel types [7]

	Number of Listings
Total SMRs	83
HALEU	46
TRISO / CPF	25
Molten Salt	10

The data in Table 1 represents SMRs alone, however does give insight into the momentum that has gathered behind using novel fuel types at a larger scale. Further, the large investment in HALEU production for current nuclear states is a telling sign of the direction of the industry.

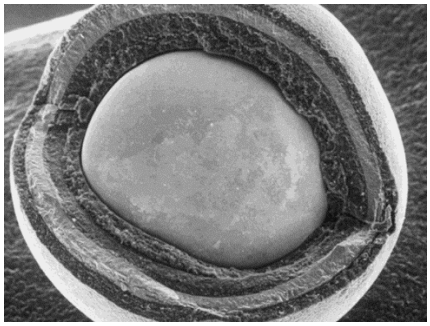

Figure 2. Microscope image of TRISO fuel particle

IV. TRANSPORT GAPS

Assessment of the material in transport forms the first step in determining: safety requirements of the transport package and security requirements of the associated physical protection system (PPS). The variety of fuel options proposed for next generation reactor systems brings with it complexity in planning for nuclear transport operators and developing the assets required. When considering UO2 fuels, operational experience of moving LEU at $\leq$5% is vast given the use in the majority of commercial power reactors, while experience with HEU at $\leq$ 90% for military and research reactor purposes is also well established. Therefore, a substantial gap in experimental data and operational experience exists, due to a historical lack of need for such data. However, as we are approaching the adoption of HALEU fuels at scale, the nuclear industry is working to address this information gap, to bring the theoretical into the physical and substantiate designs and claims.

The most prominent barrier to transporting advanced nuclear fuel types at scale is the licensing process. Current regulations are still geared towards conventional reactor types with clear definitions of the material and packages being transported. As we near deployment dates, the ability to conduct more specific analysis on the fuel types to determine capability and asset requirements is needed. However, until these fuels are more widely available this is difficult to achieve. This puts the onus on national laboratory facilities or state funded research programmes to begin producing this data.

Undertaking transport criticality and shielding assessments requires a large amount of data to be collated to enable the production of suitable models, such as:

- Design drawings
- Fissile material contents
- Fuel details
- NCT and ACT damage conditions
- Stress conditions
- Temperature profiles
- Fuel break up
- Fissile release

For NCT and ACT modelling, shielding and criticality assessments utilise this data to investigate the characteristics of the fuel material in these scenarios to demonstrate that the transport package achieves the required safety performance. In lieu of this specific data being available, any efforts to produce or identify credible transport packages are too speculative to be considered viable.

The availability of packages capable of moving novel material in significant quantities is considered low, with none currently capable of moving this material in significant quantities, as the need for these packages has only developed in recent years. Without real world data underpinning the modelling software, any simulations, and subsequent claims, again, cannot be substantiated.

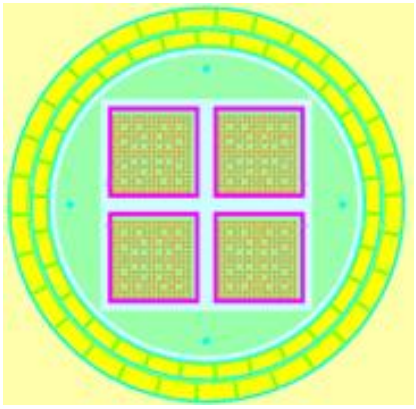

Figure 2. An example of a criticality modelling M4/12 flask containing 4x fuel assemblies

The data gap does not only impact arrangements for package substantiation in transport safety, but also those of transport security requirements. Moving from "conventional" being consider below 5% enrichment to being considered up to 20% enrichment, increases the security category from category III to category II, thus requiring more stringent security arrangements. 55% of the SMR designs listed within [7] have HALEU listed as a fuel, demonstrating that a significant number of SMRs under development are going to have at least some of the associated fuel cycle attracting a higher level of security and in turn, cost increases. Although the application of Category II security requirements is not a novel task in itself, the amount of these transport taking place looks set to increase massively. There is also great potential for these transports to be taking place in states with limited experience above conducting Category III (less onerous security) operations.

Given that HALEU covers a broad range of fuel types, the material may also be further fabricated into TRIOS / CPF or molten salt types. While similar issues arise for these fuel types within the context of transport safety (i.e. data gaps), unique considerations come to light when considering the ideas of theft and sabotage.

When nuclear security practitioners consider theft, the known threat is considered, often represented as a Design Basis Threat (DBT), a threat statement or informed through specific threat intelligence. This enables an appropriate and proportionate PPS to be developed against a specified capability, and it is understanding this capability that is paramount to designing transport PPS' for advanced nuclear fuel.

Molten salt fuel has fissile material contained within a fluoride or chloride salt medium. In designing a PPS to protect molten salt proportionately, the malicious actor's capability to separate the fissile material from the salt medium must be identified. If it is determined impossible to separate for any malicious actor or facility other than a state sponsored laboratory, the fuel could be considered inherently secure (subject to a state's assessment of the threat). This type of assumption requires significant experimentation to make such a claim. This consideration is also true for TRISO / CPF, a fuel designed with inherent safety features and accident tolerance, that may likely serve a security benefit when measured against the threat. To determine the attractiveness of these materials to theft, we must understand how obtainable the fissile material contained within the TRISO / CPF particle is.

Now if we consider a scenario in which separating the fissile material from the medium (be it a ceramic coating or a salt) is not taking place, acts of sabotage bring about additional considerations. Dispersibility (or release fraction) is a key factor in the determination of URCs and the extent of these consequences. Due to its design, TRISO / CPF fuel is considered less dispersible and considered too large and dense to travel in the atmosphere except in extreme weather conditions [8], which is particularly favourable when compared to any powdered materials. Beyond this, TRISO / CPF particles are designed to contain fission products within them, an element of the safety feature and robustness that also serves a security purpose. Fission products are the biggest contributors to what could create URCs, as such spent fuel and waste materials are considered higher sabotage risks than unirradiated fuel. A particle that contains fission products within it is inherently sabotage resistant to the extent that this boundary of containment can remain intact. Molten salt fuels share this benefit of containing fission products within them also, again further demonstrating a potential sabotage resistance by design. However, these claims are still to be substantiated and measured against what could be credible threat scenarios. Security regulators require well evidenced claims, therefore until such data is available, no viable credit can be taken for what could be described as inherent fuel security.

V. TRANSPORT ADAPTATIONS

The approaches to modelling for transport conditions of a package are expected to see significant evolutions. Conventional fuel types such as UO2 enriched to the levels considered HALEU will have an impact on the payload achievable in any package that currently exists. The higher levels of enrichment, broadly, adversely impact the

payload mass due to shielding and criticality requirements, although these relationships are not linear and subject to many influencing factors. This means licensing a package to move significant quantities of HALEU material may require a variety of new package designs. Transport packages in circulation today will likely need investment to be altered, or redesigning, to be able to move fuel quantities associated with an operating reactor. It is more likely that transport operators will (and are) investing in developing new transport packages that may be versatile to transport a range of novel fuel types, or purpose built to transport a singular element of the advanced fuel cycle. However, to sufficiently design such a package, substantiation of the safety claims is paramount. This can only be achieved with the appropriate modelling, underpinned by experimental data. To date this is not widely available, however work in the industry globally is underway to address this, as experimental data on these fuels will serve the entire fuel cycle and not just transport requirements.

The security process of categorisation is currently based on fissile contents, with additional arrangements being determined subsequently. Transport security professionals are soon going to be required to design a PPS that accounts for any inherent security benefit that could be provided by the specific fuel type. Before this can happen though, specific security experimentation must take place against credible threats, to determine the security credibility of the fuel types.

Across both safety and security, the issue is a requirement of specific data. Given the expedited deployment timescales, many states are engaged in specific testing of fuel types they expect to deploy. However, an opportunity for industry collaboration would see an efficient response to this issue. The sharing of experimental data across borders will serve to further substantiate safety and security claims, while giving industry the ability to develop and evolve at a pace that meets the demand for new nuclear.

VI. SUMMARY

While adjustments must be made and there is much work to be done to fully capitalise on the potential of new nuclear fuels, the drivers for success far surpass any anticipated barriers. Energy security is fundamental for any state to develop and mitigating climate change needs a reliable low carbon source of energy. Therefore, the importance of the role of new nuclear technologies coming to the forefront and delivering cannot be understated. The future is indeed bright, with much more of it powered by fission.

A. References

[1] IAEA. (2018). Regulations for the Safe Transport of Radioactive Material. Available: 17-45271_PUB1798_body.indb (iaea.org)

[2] IAEA. (1980, May). Convention on the Physical Protection of Nuclear Material, INFCIRC/274/Rev.1/Mod.1. Available: INFCIRC/274/Rev.1 - The Convention on the Physical Protection of Nuclear Material (iaea.org)

[3] IAEA. (2021, October 18th) Amendment to the Convention on the Physical Protection of Nuclear Material, INFCIRC/274/Rev.1/Mod. Available: INFCIRC/274/Rev.1/Mod. 1 (Corrected) - Amendment to the Convention on the Physical Protection of Nuclear Material (iaea.org)

[4] Idaho National Laboratory (2021, December), Estimated Requirements for Advanced Reactors to Support a Net-Zero Emissions Economy by 2050. Available: DOE/ID-Number (inl.gov)

[5] M. Korsnick, Nuclear Energy Institute (2020, July 23rd), Updated Need for High-Assay Low Enriched Uranium. Available: Updated Need for HALEU (nei.org)

[6] Office of Nuclear Energy. (2021, December 14th). *U.S Department of Energy Seeks Input on Creation of HALEU Availability Program* [Online]. Available: U.S. Department of Energy Seeks Input on Creation of HALEU Availability Program | Department of Energy

[7] IAEA. (2022) Advances in Small Modular Reactor Technology Developments. Available: https://aris.iaea.org/Publications/SMR_booklet_2022.pdf

[8] C.A. Condon *et* al., "Fate and transport of unruptured tri-structural isotropic (TRISO) fuel particles in the event of environmental release for advanced and microreactor applications" *Journal of Environmental Radioactivity,* vol. 234, p. 106630, 2021.

Proceedings of the European Nuclear Young Generation Forum
ENYGF'23
May 8-12, 2023, Kraków, Poland

Decay Heat Estimation And Comparison With Experimental Data

Herrera, Enrique A.[1,2*]; Fiorito, Luca[1]; Romojaro, Pablo[1] and Garcia, Nuria[2]

[1]SCK-CEN, Belgium; [2]Universidad Politécnica de Madrid (UPM), Spain

*Corresponding author: *enhergom@gmail.com*

I. INTRODUCTION

The Decay Heat (DH) generated by Spent Nuclear Fuel (SNF) is a critical parameter in the safe and efficient operation of nuclear reactors. An accurate prediction of its evolution over time is essential for the management of spent fuel, including its cooling, storage and disposal. In recent years, Monte Carlo (MC) codes have been widely used to simulate the DH of spent fuel, providing valuable insights into its behaviour. In this study, we compare the DH obtained from experimental data against the obtained through MC simulations using the Serpent code. Our goal is to assess the accuracy and reliability of stochastic MC methods in predicting the DH of SNF, and to identify potential sources of error and uncertainty in the simulations. Additionally, many other institutions will repeat such calculations with different MC codes, so that a benchmark of several codes can be made and their speed and accuracy compared against each other.

To carry out this study, several UO_2 fuelled reactor assemblies coming from second generation Swedish Nuclear Power Plants will be used for both experimental and modelling purposes. We will consider the loading, discharging, and cooling time data before performing DH measurements, as well as their nominal power throughout their life cycles. DH measurements are performed at the Swedish Nuclear Fuel and Waste Management Company's (SKB) CLAB facility inside a calorimeter, which will host the measured assembly inside while being submerged in water. The calorimeter will measure the water temperature increase due to the radioactive decay of the assembly's fuel and components, as well as the gamma radiation being emitted from the assembly and that will eventually end up transforming into heat. Simulations are performed at the SCK-CEN with the use of Newton, their supercomputer.

II. DECAY HEAT ESTIMATION

Decay Heat occurs when the radioactive isotopes inside the assembly decay in search of stability, releasing energy in the process [1]. Some of this energy is released as heat, and can be characterized by using the following equation:

$$DH = \sum_i E_{ri}\lambda_i n_i \qquad (1)$$

Where E_{ri} represents the energy emitted by decay, λ_i the decay constant and n_i the isotopic density of the given isotope. It becomes clear then that to correctly model DH we must have a good understanding of the isotopic concentration of each nuclide residing on the given assemblies at the end of their life cycle.

To calculate the isotopic concentration at any given point in time all decay chains must be considered for every individual isotope, as well as the activity of every nuclide decaying into the wanted isotope, and the decay of the isotope itself, resulting into a balance equation known as Bateman's Equation written below.

$$\frac{dN_i(t)}{dt} = -\lambda_i N_i(t) + \lambda_{i-1} N_{i-1}(t) \qquad (2)$$

This equation remains true for any given isotope while the reactor is offline (i.e. there is no neutronic flux present). However, many reactions take place inside the reactor due to the movement of neutrons, this fact forces us to take the neutron flux, as well as all the existing cross sections into account, modifying Bateman's equation to do so in the following way:

$$\frac{d}{dt}N_i(t) = (\lambda_{j\to i} + \sigma_{j\to i}\psi)N_j(t) - (\lambda_i + \sigma_i\psi)N_i(t) \qquad (3)$$

We can then achieve a comprehensive estimation of all isotopic densities if the neutron flux is correctly calculated. To estimate the flux we make use of Boltzman's Transport Eq. (4). This equation strives to obtain the balance between the neutron sources at any given point of the reactor, such as fission reactions, in-scattering neutrons coming from different regions and other external sources; and the neutron losses occurring because of reactions such as absorptions and out-scattering.

$$\frac{DN_i(\vec{r},\vec{v},t)}{Dt} = \frac{1}{v}\frac{d\psi}{dt} + \vec{\Omega}\nabla\cdot\psi$$
$$= \frac{\chi_{fiss}(E)}{4\pi}\iint_{E\ \vec{\Omega}} \sigma_{fiss}(E')N_i(\vec{r})\psi(\vec{r},E,\vec{\Omega},t)dE'd\vec{\Omega}'$$
$$+ S(\vec{r},E) + \qquad (4)$$
$$\iint_{E\ \vec{\Omega}} \sigma_S(E')N_i(\vec{r})(\bar{r},E'\to E,\Omega' \to \Omega,t)\psi(\vec{r},E,\vec{\Omega},t)\,dE'd\vec{\Omega}'$$
$$- \sigma_{S,i}(E')N_i(\vec{r})\psi(\vec{r},E,\vec{\Omega},t)$$
$$- \sigma_{T,i}(E')N_i(\vec{r})\psi(\vec{r},E,\vec{\Omega},t)$$

As it can be seen in Eq. (4), isotopic concentration (N_i) is also needed to determine the flux, thus an iterative process between Transport and Depletion equations will be needed. We can use the initial fuel composition as a first step towards determining the flux, recalculate the isotopic concentration with the obtained flux, and so on, continuing this process throughout the assembly's life.

It should also be noted that fission products continue to decay while the reactor remains in operation, which will inevitably affect the neutron flux and introduce an additional error in our calculations if not properly accounted for. Also, the evolution of the isotopic composition on the reactor's materials affect the transmutation cross sections, which ends up affecting the depletion rate. To address this issue, MC codes make use of a Predictor Corrector [2], this tool allows MC codes to account for the variation in isotopic concentration (and thus neutron flux) in each step. In our chosen code, Serpent, this process can be done in a certain number of ways:

- Constant Extrapolation (CE): Simplest burn-up algorithm, assumes steady flux and cross sections on each interval.
- Constant Extrapolation with Linear Interpolation (CE/LI): Consists on a Predictor calculation, where the flux and cross sections are obtained at the beginning of the step, and a Corrector calculation, where the material is depleted during the step's interval and its flux and cross sections obtained at the end of the step. Values from the Predictor and Corrector calculations are averaged and used as the total value throughout the step.
- Linear Extrapolation (LE): rather than performing 2 calculations as the CE/CI method does, this method uses the calculation at the next step as the Corrector calculation for the step before, predicting the first step with CE.
- Linear Extrapolation with Linear Interpolation (LE/LI): the method chosen for our given set of simulations. Much like CE/LI, this method works in the same way, only that it will be using LE to obtain the flux and cross sections at the beginning of the step.
- Linear Extrapolation with Quadratic Interpolation (LE/QI): Very similar to LE/LI, only that this time it will also be using the previous-step (PS) interpolation value, using a second-order polynomia.

III. ASSEMBLY MODELING

As the experiment organizers, information on all 50 Swedish assemblies coming from Ringhals, Barsebäck and Forksmark Nuclear Power Plant (NPP) emplacements was provided for us to model. Half of the assemblies are used on PWR's, and the other half on BWR's. There are 6 different types of assemblies:

ASSEMBLY	REACTOR	N
15x15	PWR	5
17x17	PWR	20
SVEA-96	BWR	9
SVEA-100	BWR	4
Atrium 10B	BWR	1
AA 8x8-1	BWR	11

Table 1: Types of modeled assemblies.

A. Information provided

In order to perform accurate burnup calculations, the SKB provided us with nominal power and days in operation per cycle values for each assembly. However, we do not have access to the axial power distribution, so we will be performing a two-dimensional simulation using all nominal values. We will then upscale the results, such as DH, by multiplying them by the active height of the reactor. The downtime days in-between reactor cycles, as well as the cooling time before DH measurement at the CLAB facility is also listed individually per assembly.

Other important aspects of each assembly included in the data provided are [3]:

- U-235 concentration.
- Fuel pin layout and geometry.
- Fuel temperature and density.
- Assembly walls and cladding geometry.
- Cladding material and density.
- Boron concentration per cycle.
- Reactor's pressure and temperature.

B. Model Assumptions

However, the information given to us does not always prove enough for us to adequately model an assembly, we must then make assumptions based on our reactor's design and operation knowledge, which are critical for the correct characterization of DH. There will be general assumptions, taken for all modelled assemblies, and individual assumptions taken separately for each assembly type.

It is a known fact that all models must use enriched UO_2 as fuel, but for our simulations we will also assume that all enriched uranium comes from non-reprocessed sources, i.e. the fuel is fresh and does not contain any trace of U-236, which cannot be found in nature. U-234 weight percentage concentration also had to be estimated by using Eq. (5) shown below.

$$U_{234}\ (wt.\%) = \frac{(\ 1.036\ x\ U_{235}(wt.\%) - 0.449\ )}{100\ (wt.\%)} \qquad (5)$$

Information regarding pin by pin enrichment percentages was also missing, it was decided to use a single type of pin, with average fuel enrichment levels for all fuel assembly rods. The pins where burnt homogeneously throughout the assembly so that simulations were simpler and faster to perform by the supercomputer. Additionally, each pin was burnt as a whole, rather than being subdivided into crown like segments to take into account the difference in neutron moderation on each region. This was done like so to help the supercomputer deal with any possible memory storage issues.

Cladding material also had some information missing concerning important factors such as alloy temperature and composition. The temperature was estimated by using a simple linear interpolation between the moderator and fuel temperatures, while the used materials were found in relevant data that can be seen in reference [4].

It should also be noted that all the given dimensions were measured with the assemblies outside the reactor's core, which means that the thermal expansion of the materials due to the operating temperature of the reactor was not taken into consideration when modeling the assemblies.

For BWR's, another critical unknown factor is the Void Fraction (α), this factor determines the flow composition in a two-phase mixture. In a fluid such as water, a high α number indicates a larger steam or "void" presence in the mixture. The Cross Sectional Void fraction can be estimated using the equation below, where A_g refers to the cross sectional area being occupied by the gaseous phase, and A_l the area occupied by the liquid phase.

$$\alpha = \frac{A_g}{A_l + A_g} \qquad (6)$$

Since our simulations are made in two dimensions, we must use the correct void fraction to estimate the average power of the reactor. As shown in Fig. 1, α varies depending on the altitude we are at, it would not be wise to take the α found at the middle of the reactor, since a lower α means higher coolant density, indicating a much stronger moderation towards the bottom of the reactor, which results in a higher power output [5].

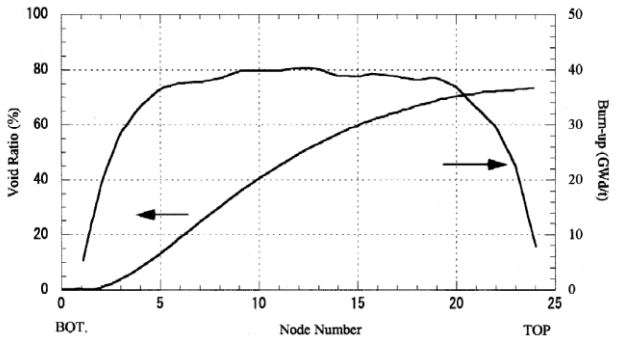

Figure 1: Variation in Void Fraction and Burn-up.

It was decided to use a void fraction of 40% for our assemblies to estimate the total coolant density.

Lastly, assembly AA8x8-1 also lacked some information. Although it was said that the material used as support for the control rods was made out of stainless steel, the specific type was never specified. To model our assemblies we used SS 304L, since is one of the most common types used on similar second generation reactors.

C. Results

Although information and results obtained in the studied assemblies is confidential and cannot be disclosed, there is, however, information about the CLAB set of experiments published in 2010 [6] performed to solve the same kind of questions.

On these set of experiments, up to 198 assemblies were measured on the Swedish CLAB, GE-Morris and HEDL facilities. Their predicted decay heat was estimated using ORIGEN-S code, using cross section libraries generated with the 2-D TRITON depletion sequence.

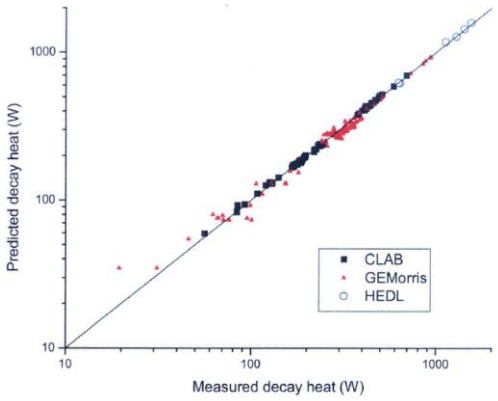

Figure 2: Measured vs predicted decay heat for all assemblies.

The graph shown in Fig. 2 shows how the Measured DH compares against the Predicted DH, with the diagonal representing the perfect match between the two sets of data. It is clear that the results are fairly accurate for most cases, with the relative error being as low as ~0.10% on some cases. There are, nevertheless, some outliers coming from GE-Morris measurements, like the one coming from assembly MT228, with its relative error going as high as 27.38%.

IV. CONCLUSIONS

Results in DH are for the most part satisfactory, and show a good understanding of DH from burnup simulation codes. Nevertheless, some results do not match the measured data, because there is also some error involved in the measurements, it is hard to know if the miss prediction in DH occurs because of the Burn-up code or because the measurement themselves, it is because of this fact that more experiments such as these are needed to ensure the accuracy of our simulations so SNF can be properly managed without the need of expensive and time consuming measurements.

V. REFERENCES

[1] G. Žerovnik et al., Observables of interest for the characterisation of Spent Nuclear Fuel. European Commission, 2018.

[2] J. Leppänen and A. Isotalo, 'Burnup calculation methodology in the Serpent 2 Monte Carlo code', American Nuclear Society, Inc., 555 N. Kensington Avenue, La Grange Park …, 2012.

[3] G. Ilas and H. Liljenfeldt, 'Decay heat uncertainty for BWR used fuel due to modeling and nuclear data uncertainties', Nuclear Engineering and Design, vol. 319, pp. 176–184, 2017.

[4] McConn, Ronald J., et al. Compendium of material composition data for radiation transport modeling. No. PNNL-15870 Rev. 1. Pacific Northwest National Lab.(PNNL), Richland, WA (United States), 2011.

[5] Y. Nakahara et al., 'Nuclide composition benchmark data set for verifying burnup codes on spent light water reactor fuels', Nuclear Technology, vol. 137, no. 2, pp. 111–126, 2002.

[6] I. C. Gauld, G. Ilas, B. D. Murphy, and C. F. Weber, 'Validation of SCALE 5 decay heat predictions for LWR spent nuclear fuel', Nuclear Regulatory Commission report (ORNL/TM-2006/13), in preparation, 2010.

Proceedings of the European Nuclear Young Generation Forum
ENYGF'23
May 8-12, 2023, Kraków, Poland

Preliminary studies on a method of uranium extraction from dusty fractions of fly ash for the fabrication of nuclear fuel

Jędrzejek Filip*, Szarłowicz Katarzyna, Stobiński Marcin and Mendera Weronika

[1] AGH University of Science and Technology, Faculty of Energy and Fuels, Kraków, Poland

*Corresponding author: *jedrzejek@agh.edu.pl*

I. INTRODUCTION

Hard coal and lignite are the main sources of electricity in Poland. At the same time, coal-fired power plants are among the largest producers of carbon dioxide and ash. Every year, Polish power plants produce approximately 4 million tons of fly ash and only 9% is used [1]. Coal combustion residues contain trace concentrations of naturally occurring radioactive materials, including thorium, uranium, and their radioactive decay products. Mobile fractions of radioactive elements, or their condensates, tend to be retained in fine-grained ash particles. In addition, equivalent amounts of uranium and its progeny remain directly associated with bottom ashes. There is also a concentration of uranium isotopes as a result of mass loss, associated with the loss of combustion products during the industrial process. The concentration of these isotopes will occur at higher levels in the waste than in the raw materials being burnt. Therefore, wastes from coal-fired power plants is termed Technologically Enhanced Naturally Occurring Radioactive Materials (TENORM). An increased concentration of radionuclides, including uranium in the waste material, may create the possibility of using the ashes to extract uranium as a valuable energy resource.

The average amounts of uranium in the ashes are not at high levels, but based on the scale of this industry, these materials could be a viable alternative source of nuclear fuel. In addition, considering that waste with similar physical and chemical characteristics is also produced in other industries, there is a high potential for uranium production from waste materials of this type.

One of the problems associated with the leaching of uranium from dusty waste materials, such as coal combustion ash, is its amorphous nature. The ashes in the acid solutions form suspensions. In order to make separation less challenging, this work proposes a new method using a semipermeable membrane. It is important to emphasise that the study is only an initial step in the introduction of a new method and was verified only on a small laboratory scale. However, the results may show the potential of the proposed solution.

II. URANIUM IN COAL AND ASHES

Uranium is mainly found in the mineral fraction of coal and can also be found in the organic part, low-grade coals. Increased uranium mineralisation in coal deposits occurs mainly in edge zones, in spaces where sedimentary disturbances have occurred, or in areas of tectonic intrusion, as well as in zones of contact between coal and sandstone beds [2]. The coal was mineralized by infiltration of leached uranium from feldspar-enriched sandstone complexes. Increased uranium concentrations occur in more oxidized components of the organic matter. On the other hand, the maximum uranium content is noticeable in fractions with densities ranging from 1.7 to 2 $g \cdot cm^{-3}$ [2]. Experimental results have shown that uranium is found mainly in the glassy phase of carbons, more precisely it is embedded in aluminosilicates and ferric oxides [3].

Table 1 shows examples of uranium concentrations in coal used in coal-fired power plants. The values are not large, but it should be noted that the concentration of uranium in fly ash can be between 5 and 10 times higher, as a result of the concentration in the combustion process [4].

Table 1. Uranium concentrations in different coals [5-10].

Origin	Uranium
Brazil	80 $mg \cdot kg^{-1}$
Turkey	11-20 $mg \cdot kg^{-1}$
China	39-376 $mg \cdot kg^{-1}$
Greece	4-20 $mg \cdot kg^{-1}$
India	1-6 $mg \cdot kg^{-1}$
Poland (Lower and Upper Silesia)	2-9 $mg \cdot kg^{-1}$

III. URANIUM EXTRACTION FROM FLY ASHES

Most research on uranium extraction processes has focused on bottom ashes, which are less challenging than fly ashes.

The mean particle size of fly ash is about 5µm, an order of magnitude smaller than that of the bottom ash [11]. Therefore, the separation of the final product requires an additional process related to agglomeration and synthesis of aerogels [12]. Generally, in the literature, the use of sulfuric or nitric acid is recommended for uranium extraction. An additional problem in this area is the optimal performance for particles with a grain size distribution in the 48-75µm range, which corresponds to the conditions of bottom ash [13]. Consequently, for bottom ash, the recovery of uranium is in the range of 60-90%, when for fly ash it is 20-50%, depending on the conditions and type of raw material [13-15].

IV. MATERIAL AND METHODS

This paper describes an attempt to separate uranium from fly ash, based on the study of an exemplary fly ash sample. The material was obtained from one of the Polish thermal power plants. The first stage of the research was to analyse the composition and radioactivity of the initial ash sample.

A gamma-ray spectrometer with an HPGe semiconductor detector (Canberra BE3830) was used for the analysis. The detector was efficiency calibrated with reference materials: IAEA447, IAEA RG-U, IAEA RG-Th. The measurement time lasted at least 3 days.

Individual samples, separated from the raw material, were leached with 5M nitric acid to separate the uranium fraction. Uranium oxides were deposited on a column of selective sorbent.

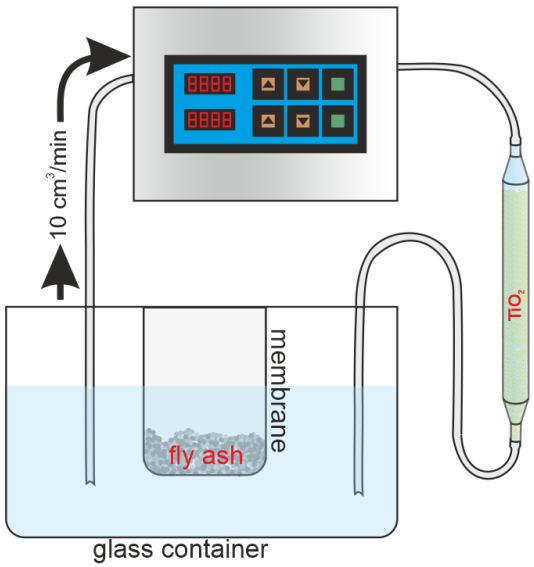

Figure 1. Diagram of the experimental setup

The experimental system was developed on a membrane of regenerated cellulose, which was placed in a chemical reactor. The membrane separates the leaching solution from the ash suspension, preventing mixing. Only oxidized metal ions are allowed to move outside the membrane by diffusion forces. The experiment was carried out in a closed circuit, where the solvent solution was also circulated through a column with an ion exchange resin (titanium oxide TiO_2) selective to uranium ions. Selective uranium sorption on a column, increased concentration gradient, and diffusion forces. The diagram of the experimental system is presented in Figure 1. The experiment was carried out under the following parameters:

- 10 $cm^3 \cdot min^{-1}$ Flow rate
- 20 g of fly ashe single probe
- 5g of TiO_2 ion exchenge resin and 2g for ex. 6

The experiment was carried out in two time regimes, 5 and 8 days. Some of the samples were also calcined with calcium chloride, at 900 Celsius degrees. As inferred from the literature, calcination affects the availability of uranium ions for the leaching process, breaking some chemical structures in the ash [14]. The experimental parameters used for each sample are listed in Table 2.

Table 2. List of prepared samples and experimental conditions

ID	Operating time	Chemical preparation and other operations
1	5 days	-
2	8 days	-
3	5 days	900°C calcination
4	8 days	900°C calcination
5	8 days	-
6	5 days	continuous mixing on a magnetic stirrer

The total uranium content, obtained by leaching of the ash, was determined from the concentration of the ^{235}U isotope in the sorbent bed and its abundance. The radioactivity concentration of the uranium isotope was determined from the 186 keV line by gamma spectrometry, on the same spectrometric track as the initial sample. This allowed measurements of the direct activity of uranium isotope, regardless of the radioactive equilibrium that must be established for determination of ^{238}U isotope. The abundance of ^{235}U isotope is low (about 0.7%), and the analyte line is affected by interference from a ^{226}Ra isotope. However, statistically correct results were obtained and the time-consuming step of waiting for equilibrium in uranium-radium series was avoided. The interference problem was solved using a method available in the literature [16].

V. RESULTS AND DISCUSSION

Figure 2 shows the characteristics of the initial sample, including selected gamma isotopes. The examined ash was characterized by a significant radioactivity of the ^{40}K isotope, while the other isotopes from uranium and thorium series remained at similar and about four times lower levels.

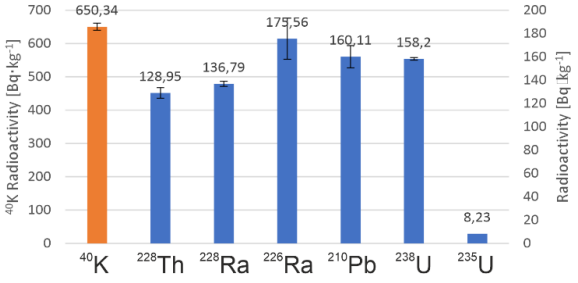

Figure 2. Radioactivity of selected isotopes in the initial sample

The calculation results of the total uranium content are presented in Figure 3. The average concentration of total uranium in the initial ash sample was 13,6 ±1,1 mg·kg^{-1}. The enrichment in ash, relative to coal, increases by 5 to 10 times [4]. When comparing the result with the data in the literature (Table 1), it could be predicted that the coal combusted in the power plant was characterized by contents at the lower limit for Polish origin. In general, a relatively low uranium content should be assumed in the ash sample.

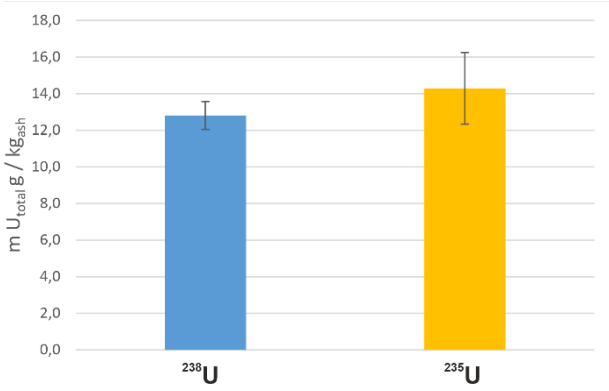

Figure 3. Total concentration of uranium

Figure 3 also presents the differences in the calculated total uranium concentration, using isotope radioactivity of ^{238}U and ^{235}U for calculations. The differences between both cases were within the uncertainties. The purpose of this exercise was to validate the assumptions of the adopted analytical method. By referring to the constant contributions of isotope, the correctness of gamma spectrometric determination was confirmed. Therefore, it was statistically correct to base the calculation on the radioactivity of ^{235}U only. In the case of measurements based on ^{238}U, equilibrium would be required to establish itself in the series, which would require a delay of about 6 months.

Figure 4 shows the total uranium content in the ashes and sorbents, after the leaching process, for each experiment.

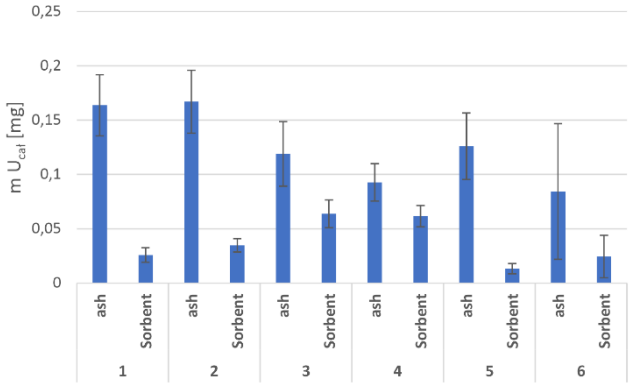

Figure 4. Total concentration of uranium in ash and sorbent, after the leaching process.

A noticeably higher loss was observed for calcined ash samples (Ex. 3 and 4). The mean values were 0.11 mg U$_{total}$ and 0.15 mg U$_{total}$ respectively for calcined and uncalcined ash samples. For the uranium content of the sorbent, a similar relation was observed for experiments 3 and 4 (calcination), the retained mass of total uranium was higher. The differences in content for these sorbent samples were significantly different from those of the others. The positive effect of calcination was evident. Samples from experiment No. 6 were additionally stirred, and this did not significantly affect the result of the experiment. The diffusion forces provide sufficient movement of ions in solution; therefore, the additional energy expense for stirring the reactor volume seems unnecessary.

Figure 5 presents the recovery of total uranium relative to the initial ash sample. The value was calculated as the ratio of total uranium in the sorbent sample to total mass in raw ash.

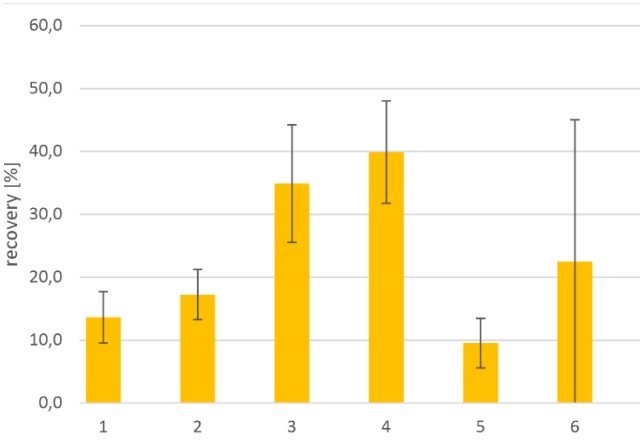

Figure 5. Uranium Recovery Factor

The highest recovery was seen for Experiments 3 and 4, 34.9% and 39.9%, respectively. These were samples treated with earlier calcination. It can be concluded that earlier chemical activation leads to a noticeable increase in process efficiency. For the remaining samples, without calcination, the average recovery was 15.7%.

For experiment 6, conducted without calcination, the recovery factor was above average. However, the result revealed significant uncertainty, due to the small mass of TiO_2 used in the experiment. The goal was to verify the economically optimal conditions. However, reducing the mass of the sorbent significantly increased the uncertainty of the measurement, which is mainly due to the specifics of the measurement. Therefore, no conclusions can be reached in that field.

A minimal increase in radioactivity can be seen, with the process extended by 3 days, the recovery value increased by an average of 4 percentage points. However, measurement uncertainties exceeded change, so the results do not allow clear conclusions to be drawn.

To examine the dynamics of the process, it would be necessary to carry out tests in a different time regime, using a different analytical method. Most likely, the liquid scintillation counting technique. It would possible to measure the concentration increase, directly in the leached acid solution. This technique has a higher sensitivity and the possibility of a direct measurement of the ^{238}U isotope.

VI. CONCLUSION

A successful experiment has been conducted. The method still needs to be optimized, but this research has recognized its potential. However, these were only preliminary studies and lack of correct statistics in the data is visible.

The preliminary uranium yield of 40% seems satisfactory, which is in agreement with the previously presented literature data (20 – 50% for fly ash). It can certainly be improved e.g. sulfuric acid extraction.

Assuming the given yield level, it is possible to calculate which range of uranium content in coal is the threshold value. From an industrial point of view, conventional sources are classified as those with a concentration of more than 400 ppm uranium [17]. Based on this value, the percentage recovery yield and the typical enrichments of ash, the optimum uranium concentration in the coal is in range of 100 – 200 $mg \cdot kg^{-1}$. It is an unfavourable range compared to reported in a polish coals, but in worldwide perspective quite common. Additionally, there are other sources, e.g. copper mining dump waste, which can also be suitable for the proposed method.

One important disadvantage is associated with calcination, which is a very energy-consuming process. It drastically reduces the potential of the method. This should be an area of necessary improvement to obtain an economically competitive uranium source.

The work did not fully answer the possibility of providing a competitive source of uranium for nuclear fuel production. However, the proposed method using semi-permeable membranes provides an effective solution. It also provided critical issues to be resolved in future studies, e.g. chemical activation (calcination) and minimal concentration in source material.

VII. REFERENCES

[1] Stoch A., “Fly Ash From Coal Combustion Characterization.”, Instituto Superior Técnico, 2015

[2] Olkuski T., Stala-Szlugaj K., “Występowanie pierwiastków promieniotwórczych w węglach, kamiennych pochodzących z GZW, w skałach przywęglowych, w wodach kopalnianych oraz w odpadach.,” Gospodarka surowcami mineralnymi, 2009, in polish

[3] Z. R. a. B. J. R., „Radionuclides in fly ash and bottom ash: improved characterization based on radiography and low energy gamma-ray spectrometry.,” 1997.

[4] Monnet A., Percebois J., Gabriel S., “Assessing the potential production of uranium from coal-ash milling in the long term”, Resources Policy, Volume 45, 2015

[5] Flues, M., et. All, “Evaluation of radionuclides concentration in Brazilian coals.” Fuel 86, 807, 2007

[6] Turhan, Ş., et. All. “Radiometric measurement of lignite coal and its by-products and assessment of the usability of fly ash as raw materials in Turkey. Radiochimica Acta, 106(7), 611–621, 2018

[7] Chen, J., et all. “Abundance, Distribution, and Modes of Occurrence of Uranium in Chinese Coals.” Minerals 7, 239, 2017

[8] Papastefanou, C. “Escaping radioactivity from coal-fired power plants (CPPs) due to coal burning and the associated hazards: a review.” J. Environ. Radioact. 101(3), 191, 2009

[9] Mahur, A. et. All. “Estimation of radon exhalation rate, natural radioactivity and radiation doses in fly ash samples from Durgapur thermal power plant, West Bengal, India.” J. Environ. Radiact. 99, 128, 2008

[10] Bojakowska I., Lech D., Wołkowicz S., „Uran i tor w węgla ch kamiennych i brunatnych ze złóż polskich”, Gospodarka Suro wcami Mineralnymi t. 24, 2008

[11] F.J., C.M., F., R.C., V.G. “Natural radioactive elements and heavy metals in coal, fly ash and bottom ash from a thermal power plant” Journal of Environmental Science and Health, 1993

[12] Q.Li., T.Xi., J.L., Y.Z.,"Explorations on efficient extraction of uranium with porous coal fly ash aerogels", Science of The Total Environment, V 839, 2022

[13] Y.Z., L.Y., N.Y. et al. “Effects of oxidant and particle size on uranium leaching from coal ash”, J Radioanal Nucl Chem 317, 801–810, 2018

[14] Q. G. L. X. X. H. W. Y. Sun Y., „Extraction of uranium in bottom ash derived from high-germanium coals,” Procedia environmental sciences, 2016.

[15] M. S., M.P., "Acid leaching of coal and coal-ashes", Fuel,82:1721-1734,14,2003

[16] M. Z. Magdalena Długosz-Lisiecka, „Direct determination of radionuclides in building materials with self-absorption corection for thw 63 and 186 keV gamma energy lines,” Journal of Environmental Radioactivity, pp. 44-48, 2015.

[17] NEA (2018), Uranium 2018: Resources, Production and Demand, OECD Publishing, Paris

VIII. Acknowledgment

This work was partially supported by research subvention supported by the Polish Ministry of Education and Science grant number 16.16.210.476.

Proceedings of the European Nuclear Young Generation Forum
ENYGF'23
May 8-12, 2023, Kraków, Poland

Modelling and experimental determination of surface and volume activity in different geometry metallic waste samples

Lagzdina, Elena[1*], Plukienė, Rita[1], Germanas, Darius[1], Mikalauskienė, Kristina[1], Konstantinova, Marina[1], Plukis, Artūras[1] and Remeikis, Vidmantas[1]

[1]Center for Physical Sciences and Technology (CPST), Lithuania

*Corresponding author: *elena.lagzdina@ftmc.lt*

I. INTRODUCTION

The decommissioning process of RBMK-1500 reactors operated in Ignalina Nuclear Power Plant (NPP) started in 2004 when the first unit was shut down, while the second one was shut down in 2009. Like in other nuclear reactors, the RBMK-1500 reactor core is the main source of radionuclides generated in the NPP [1]. The RBMK-1500 reactor shield and support plates are made of constructional quality grade 20 carbon-steel. There are about 504.1 t of this steel in one RBMK-1500 type reactor. These plates are located close to the reactor active core (graphite stack) and become radioactive due to relatively intensive neutron activation and can be contaminated too.

The main radionuclides associated with the activation of metal structures of a reactor facility are ^{55}Fe and ^{60}Co isotopes. These radionuclides have the highest activity levels in the cooling period of about 30 years and in the cooling period of 30 to 150 years practically all activity is caused by ^{63}Ni [2], which is beta emitter. The list of radionuclides related to surface contamination contains isotopes of Cs, Eu, actinides and others.

One of important tasks for smooth and successful decommissioning process of NPP is optimization of metal radioactive waste (MRW) management by applying grouping and separation of MRW. For this purpose different approaches may be used which meet requirements of lowcosts for purchase and maintenance for the use in gamma-ray analysis.

Gamma-ray spectrometry dealing with low and very low-level gamma-ray activities of different samples is a fundamental part of radiological environmental monitoring programmes. For efficient characterization of very low-level metallic waste the determination of surface contamination part is needed by application of simple and non destructive γ-spectrometry measurements.

In recent years there has been a growing interest in the development of new scintillator materials, like bromide scintillators. $CeBr_3$ can be particularly attractive for medium to high energy resolution gamma-ray spectrometry at room temperature as it's resolution is better than that of a typical NaI(Tl) detector, but worse than a HPGe detector. The medium resolution of $CeBr_3$ detectors could be sufficient to satisfy the quality requirements (uncertainties and detection limits) concerning the determination of the main radionuclides, like a quantitative activity concentration measurement of ^{137}Cs by gamma-ray spectrometry [3].

The aim of this work is to investigate the γ-spectra of ^{60}Co (activation) and ^{137}Cs (surface contamination) model sources in different shielding geometries.

The preliminary analysis using MCNP6 modelling and experimental analysis by using both HPGe and $CeBr_3$ detectors measurements of home-made different geometry metallic waste samples with ^{60}Co and ^{137}Cs sources have been performed. Modelling, inter-comparison of experimental γ-spectra and analysis of the nuclides peaks and Compton scattering edges for samples with sources of ^{60}Co and ^{137}Cs in different iron shielding conditions is presented below.

II. MATERIALS AND METHODS

Usually both computer modelling and spectrometric measurement methods are used for assessing the activity of reactor activated structures. Modelling tools (MCNP6, SCALE6.2) are used for obtaining activation of materials in the reactor core for characterization and separation of waste streams of highly activated zones, zone of intermediate and low activation metal waste and also non-activated materials for which only surface contamination is relevant [4]. Control of ^{137}Cs isotope activity in radioactive waste is important due to high mobility of ^{137}Cs which appears due to damage of cladding of fuel elements in the core. γ-spectrometry is very important for characterization and monitoring of different activity level radioactive waste. For many radionuclides, γ-spectrometry is a precise and often the only possible method of measurement.

A. γ-spectrometry

Interacting with matter gamma rays can collide with an electron and bounce off it (Compton scatter) or it can push an electron to a higher energy level (photoelectric ejection). Also, part of this energy can be transformed into matter directly by creating an electron and a positron (pair production). These interactions create an electric current in the detector, which are amplified and measured to estimate the energy and direction of the original γ-ray.

Gamma-ray spectrometric measurements of the known-home-made different geometry metallic waste samples were carried out using both HPGe detector coupled to the MCA Canberra DSA1000 with Genie-2000 gamma ray spectroscopy analysis software (Canberra Industries, USA) and a standard high resolution $CeBr_3$ scintillation detector 51B51/2M-CEBR-X (Scionix, Netherlands). Detectors have been efficiency-calibrated for the standard geometry of the measurement. For the efficiency calibration the reference standards with ^{137}Cs, ^{60}Co and ^{152}Eu were used.

^{137}Cs and ^{60}Co point sources were measured, which were placed on several steel plates of 50x71x10 mm between the detector and source (Figure 1b). When the source was between the plates, it was placed inside an Al disk with an inner diameter of 26 mm, an outer diameter of 75 mm, and a thickness of 3 mm.

B. MCNP modelling

In order to understand the gamma detector response in the different contamination - radioactive source - geometry and background conditions MCNP6 code and ENDF-VII cross-section libraries were used [5], [6]. Monte Carlo particle transport is based on the explicit tracking of particles. Probability distributions are randomly sampled using transport data. In calculations these distributions are used to determine the type of interaction, energy of particles if it scatters and leakage. In our case MCNP6 has been used for gamma rays interaction calculation with radioactive source shielding materials, detectors materials and Fe-Pb protective shields of the detector (see Figure 1a) in different source cases: point source, volume source and planar source. This was accomplished by using the F8 tally (pulse height distribution in cell) from MCNP6. The modelling of efficiency calibration of particular HPGe detector using Monte Carlo simulations including coincidence-summing corrections for two peaks was done in [7]. The similar procedure was performed also with $CeBr_3$ detector (Figure 1b).

I. RESULTS AND DISCUSSION

Analysis of experimental measurement and modelling of the different geometry metallic waste samples was performed for ^{60}Co and ^{137}Cs point sources shielded by different thickness of iron plates (Table 1). The sensitivity and gamma peak resolution is ~10 times better for HPGe detector, thus the peak/Compton ratio also is better expressed for HPGe detector, but $CeBr_3$ could be also used for surface/volume activity determination but with less accuracy.

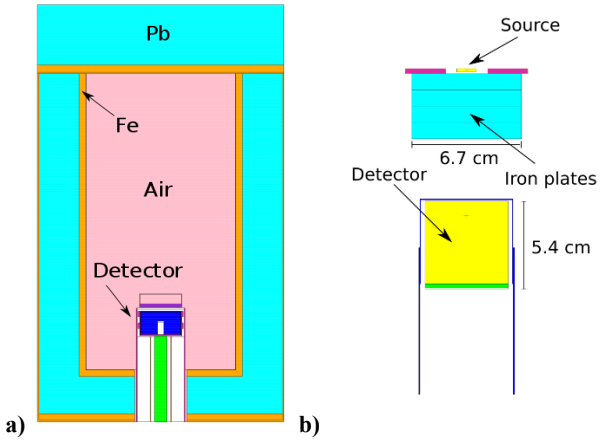

Figure 1. Scheme of the simulated a) HPGe detector with iron-lead shield and b) $CeBr_3$ detector with shielded point source.

Table 1. Compton/peak ratio values using various thickness of metal plates placed between the source and the detector (h, cm) depending on the energy and the detector type (measured)

h, cm	HPGe detector		$CeBr_3$ detector	
	661.6 keV	1173.2 keV	661.6 keV	1173.2 keV
0	0.023±0.002	0.024±0.007	0.16±0.02	0.21±0.05
1	0.026±0.004	0.035±0.008	0.25±0.02	0.26±0.05
2	0.029±0.004	0.039±0.006	0.35±0.04	0.29±0.06
3	0.034±0.006	0.045±0.007	0.46±0.05	0.3±0.1
4	0.040±0.007	0.05±0.01	0.6±0.1	0.4±0.2

The comparison of measured with HPGe detector and modelled γ-spectra of point sources shielded by 1cm thickness iron shields is presented in Figure 2. One can notice, what a good consistency of experimental and modelled results have been obtained and this allows investigating of γ-spectra of surface contaminated, and volume activated metallic waste samples of various shapes.

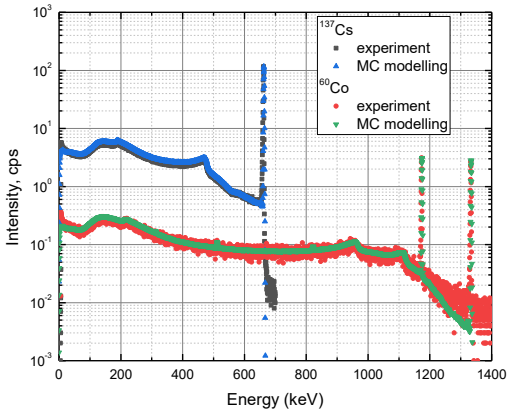

Figure 2. Inter-comparison of measured with HPGe detector and modelled γ-spectra of ^{60}Co and ^{137}Cs point sources shielded by 1cm thickness iron shields.

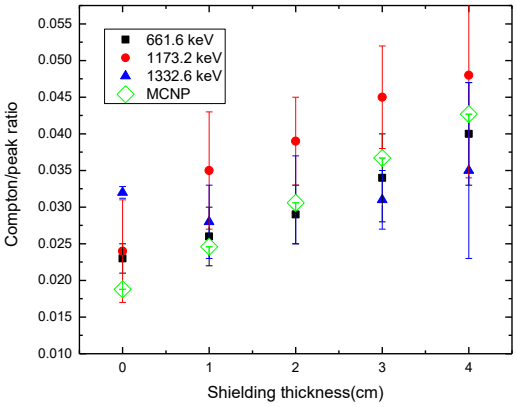

Figure 3. Experimental Compton/peak ratio for different ^{60}Co and ^{137}Cs point sources shielding geometries measured by HPGe detector and compared to MCNP modelling results.

The dependence of Compton/peak ratio values for different thickness of shielding metal plates (at bottom and on top) of the ^{60}Co and ^{137}Cs point sources is presented in Figure 3. The analysis shows that one can clearly distinguish between non shielded source and source shielded with different thickness of iron. The strongest dependence has been obtained for bottom shielding case (this would represent the inner surface of half cut pipe in the reality) – comparing with surface source: 0.023±0.002 unshielded case with 0.04±0.007 for 4 cm shielding case for ^{137}Cs. The similar result was obtained also in case of ^{60}Co source 0.024±0.001 comparing with 0.048±0.014 for 4 cm shielding case. The good agreement (up to 8%) have been obtained between ^{137}Cs modelling and experimental cases with shielding, the higher discrepancies (about 23%) occurred in non-shielded case due to point source activity and measurement dead time.

Figure 4 shows the comparison of γ-spectra of ^{137}Cs source in non-shielded geometry obtained by using both $CeBr_3$ scintillation detector and MCNP modelling. A good consistency of experimental and modelled results have been obtained and this shows that $CeBr_3$ scintillation detector is suitable for investigation of MRW samples.

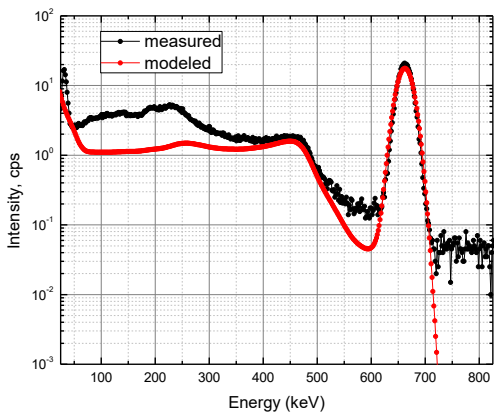

Figure 4. Inter-comparison of γ-spectra of ^{137}Cs measured with $CeBr_3$ detector and modelled in case of non-shielded source.

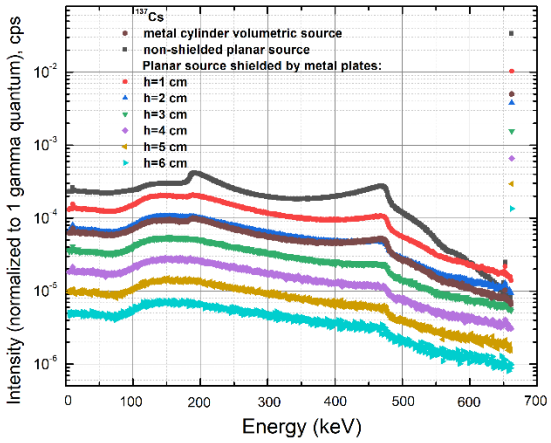

Figure 5. Comparison of modelled ^{137}Cs γ-spectra in HPGe for different source cases: volumetric source (homogeneously distributed in the h=6cm r=3.36cm metal cylinder) and planar source shielded with metal plates of different thickness.

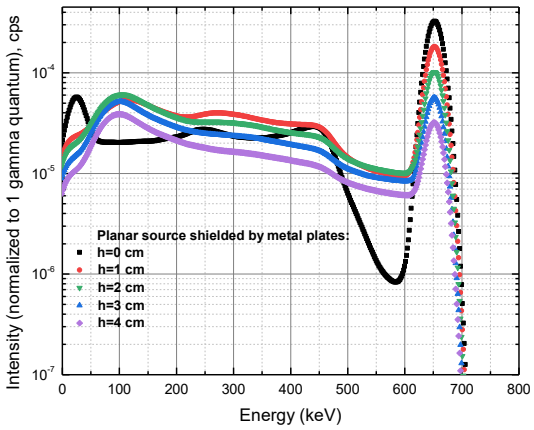

Figure 6. Comparison of modelled ^{60}Co γ-spectra in $CeBr_3$ detector for point source shielded with metal plates of different thickness.

The modelling shows that planar surface contaminated ^{137}Cs source could be distinguished from shielded or volumetric source by the shape/intensity of photo peak and Compton/peak ratio of γ-spectra as it is presented in Figure 5. The intensity of photo peak decreases with shielding material thickness from 3 to 250 times comparing 1 cm – to 6 cm shielding plates, the Compton/peak ratio changes from 0.021±0.0001 and 0.06±0.009 for non-shielded source and shielded by 6 cm metal plate source respectively. We should note that h=6 cm metal cylinder ^{137}Cs volumetric source γ-spectrum looks quite similar with planar source shielded by 2 cm metal plate: the photo peak intensity ratio is 0.8, but Compton/peak ratio stands out better 0.033±0.0002 and 0.027±0.001 for 2 cm shielded planar source and volumetric source respectively. Figure 6 shows the comparison of modelled ^{60}Co γ-spectra in $CeBr_3$ detector for point source shielded with metal plates of different thickness.

II. CONCLUSIONS

The identification and analysis of surface and volume activity by using both HPGe and $CeBr_3$ detectors is

performed. A good consistency of experimental and modelled results is obtained during comparison of measured and modelled γ-spectra of ^{60}Co and ^{137}Cs point sources shielded by different thickness of iron for both analysed detectors, but in $CeBr_3$ case 10 times lower sensitivity was obtained. $CeBr_3$ is more suitable for in-situ measurements and could be used for investigating of γ-spectra of surface contaminated and volume activated different geometry metallic surfaces at the place.

Analysis of HPGe experimental measurement and modelling of the ^{60}Co and ^{137}Cs point source samples have shown, that there is peak/Compton ratio dependence for different thickness iron shield environment of ^{60}Co and ^{137}Cs point sources. The possibility to use this type of analysis could be useful for detail radioactive metallic waste samples surface activation identification (both on the surface and on the inner surface of the tube) after sample collection.

MCNP modelling of different source cases: planar source shielded with different metal plates and volume source have revealed, that surface contamination ^{137}Cs source can be distinguished if compared with reference source case by using modelling and measurement techniques from the shape/intensity and peak/Compton ratio of γ-spectra analysis for both HPGe and $CeBr_3$ detectors.

Acknowledgements

This research is part of a project that has received funding from the EU HORIZON 2020 Euratom research and training programme PREDIS under grant agreement No. 945098.

III. References

[1] R. Plukienė, A. Plukis, A. Puzas, V. Remeikis, G. Duškesas, and D. Germanas, "Modelling of Impurity Activation in the RBMK Reactor Graphite Using MCNPX," *Prog. Nucl. Sci. Technol.*, vol. 2, no. 0, pp. 421–426, 2011.

[2] E. Narkūnas*et al.*, "Neutron Activation in the Metal Structures of anRBMK-1500 Reactor" *Nucl. Technol.*, vol. 168, no. 2, pp. 533-536, 2017, DOI: 10.13182/NT09-A9239.

[3] R. Idoeta*et al.*, "Possibilities of the use of $CeBr_3$ scintillation detectors for the measurementof the contentof radionuclides in samples for environmental monitoring",*Appl. Rad. and Isotopes*,vol. 176,109881, 2021, DOI:10.1016/j.apradiso.2021.109881.

[4] V. Remeikis *et al.*, "Characterisation of RBMK-1500 graphite: A method to identify the neutron activation and surface contamination terms," *Nucl. Eng. Des.*, vol. 361, 2020.

[5] M. B. Chadwick *et al.*, "ENDF/B-VII.0 : Next Generation Evaluated Nuclear Data Library for Nuclear Science and Technology," vol. 107, pp. 2931–3060, 2006.

[6] B. Colling, I. Kodeli, S. Lilley, and L. W. Packer, "Benchmarking comparison and validation of MCNP photon," vol. 06024, 2017.

[7] M. Konstantinova, D. Germanas, A. Gudelis, and A. Plukis, "Efficiency Calibration of High-Purity Germanium Detector Using Monte Carlo Simulations Including Coincidence-Summing Corrections : Volume Source Case," vol. 61, no. 1, pp. 66–73, 2021.

Proceedings of the European Nuclear Young Generation Forum
ENYGF'23
May 8-12, 2023, Kraków, Poland

In-situ monitoring by Raman spectroscopy of spent nuclear fuel oxidation under dry storage conditions

Milena-Pérez, Abel[1*], J. Bonales, Laura[1], Rodríguez-Villagra, Nieves[1] and Galán, Hitos[1]

[1] Centro de Investigaciones Energética, Medioambientales y Tecnológicas (CIEMAT), Spain

*Corresponding author: *abel.milena@ciemat.es*

I. INTRODUCTION

There is an international and increased concern on the Spent Nuclear Fuel (SNF) integrity during its management for pre-disposal activities, being the interim dry storage the intermediate step before the final disposal. Dry storage of fuel constitutes a well-proved stage in which security is demonstrated. Nevertheless, fundamental research can lead to vary certain design options that could improve some aspects of the fuel management, and thus they must be considered. In dry storage conditions, the safety of the fuel must be ensured mainly in front of oxidation, which can occur at high-enough temperature in presence of oxygen, and may possibly lead to a potential degradation mechanism affecting the clad integrity driven by the formation of U_3O_8. Therefore, the formation of U_3O_8 and other intermediate oxides from the oxidation of UO_2, the main constituent of current nuclear fuels (and thus called SNF matrix), has received considerable attention [1-3]. The reason is that U_3O_8 entails an increase in volume around 36% with respect to UO_2, and comes along with spallation and pulverization of the initial UO_2 sample [1]. Therefore, the formation of U_3O_8 could lead, depending on the condition of a pre-existent failure in the clad, to failure propagation, splitting the clad and even allowing certain release of radioactive material [4].

Due to its practical importance from the nuclear safety point of view, the boundary conditions in current nuclear storage facilities at which U_3O_8 does not form are widely studied (*i.e.* low temperature and lack of oxygen). Other conditions impacting on the formation of U_3O_8 have been studied under the circumstances expected during dry storage of the fuel. In this regard, the upper limit temperature allowed for LWR fuel stored in dry conditions is 400ºC [4], in order to protect the fuel cladding [5]. This is the reason why most of the studies regarding the oxidation of SNF have been conducted at this temperature or below [6, 7]. Most of these works have been carried out by using thermogravimetric analysis and flowing air as the oxidant phase.

In fact, regarding the atmosphere, the fuel has been mainly studied after being exposed to air. Investigating the potential oxidation of the fuel matrix at lower oxygen partial pressures, *i.e.*, with specific loading cells being partially inert, might bring to other alternatives to air that might delay or even prevent this oxidation. However, the literature regarding the effect of lower oxygen partial pressures than air on UO_2 oxidation is scarce [8-10]. In addition, traditional techniques such as thermogravimetry have been mostly used in those studies published up to date. This method gives the "bulk" oxidation of the sample, providing an average O/M value reached by UO_2 after the experiment. Taking into account the possible security controls at storage facilities, it could be interesting to detect the potential early apparition of U_3O_8 and follow the progress of the reaction even if the entire sample is not yet oxidized. In this regard, Raman spectroscopy is presented as a non-destructive technique able to measure the oxidation progress from really short times (2 minutes), to provide a fingerprint to distinguish between similar uranium oxides, and to perform *in-situ* measurements, allowing studying the materials in real conditions. The methodology developed here can also be applied in the analysis of SNF for example in hot cells, as some Raman instruments have already being used in those conditions.

Thus, in this work we use Raman spectroscopy to study the effect of three temperatures of interest (200, 300 and 400ºC), each one at four different atmospheres (0.1, 1, 10, and 21% O_2) on the formation of U_3O_8 from a fresh UO_2 surrogate. The measurement protocols developed here to carry out the reaction *in-situ* can be directly applied in the study of irradiated fuel.

II. EXPERIMENTAL SETUP

The fuel analogues studied consisted of powdered UO_2 samples coming from monoliths of unirradiated sintered UO_2 pellets that were crushed into powder in a Mixer Mill MM 400 (Retsch). This material has been characterized in detail in our laboratory, and we have been able to prove that it is a UO_2 surrogate whose representativeness is given

in terms of its conservatism in relation to actual SNF. The material is labelled as P3 in [11].

Raman spectra were acquired by means of a Horiba LabRam HR Evolution spectrometer (Jobin Yvon Technology). A red He-Ne laser beam (λ=632.8 nm) with 50 mW of nominal power was used, focused on to the sample by an Olympus BX41 microscope (50x objective). For the *in-situ* measurements, the sample was placed inside a Linkam THMS600 temperature-controlled pressure stage. A frontal view of this stage is shown in Figure 1. This chamber allows maintaining the sample in a closed environment and focusing the incident radiation through a central overture in order to acquire the spectra (central part in Figure 1). The connections correspond to the inlet/outlet gas quick-fits, as well as inlet/outlet water circuit for refrigerating the stage. The sample temperature is controlled by using a T95 Linkpad temperature controller, which provides temperature stability better than 0.2ºC.

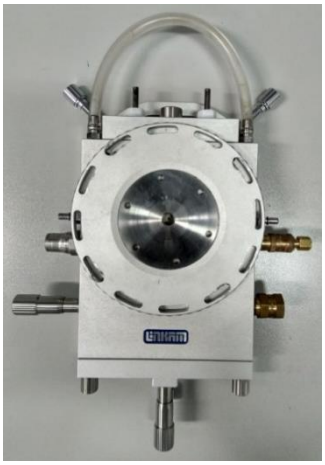

Figure 1. Frontal view of the Linkam stage.

The optimized protocol for ensuring a correct measurement during the experiments has involved a number of steps. They are summarized in Table 1.

Table 1. Optimized measurement protocol for carrying out oxidation experiments with the Linkam stage.

Step	Description
Initial	Place the sample and close the lid assembly. Determine the measurement conditions (acquisition time and accumulations)
Inertization	Overnight low flow of Ar gas in order to remove oxygen
Heating	10ºC·min^{-1} up to the experimental temperature still with the Ar atmosphere (to prevent early oxidation)
Stabilization	10 minutes of isothermal at the experiment temperature with Ar
Gas change	Ar is replaced by the desired atmosphere (0.1-21%O_2), the reaction begins
Oxidation	Spectra acquisition during the isothermal reaction
Gas change	When the oxidation is finished, Ar is set again to prevent further changes
Cooling	Oxidized sample is cooled to room temperature to store it

III. MONITORING OF THE SNF OXIDATION

This stage has involved two main steps: identification of the Raman spectra of the uranium oxides of interest and application of the optimized protocols described.

A. Raman signature of the uranium compounds

Prior to the *in-situ* reaction, we first establish the criteria to identify the different uranium phases involved in the oxidation from UO_2 to U_3O_8. Figure 2 shows these spectra:

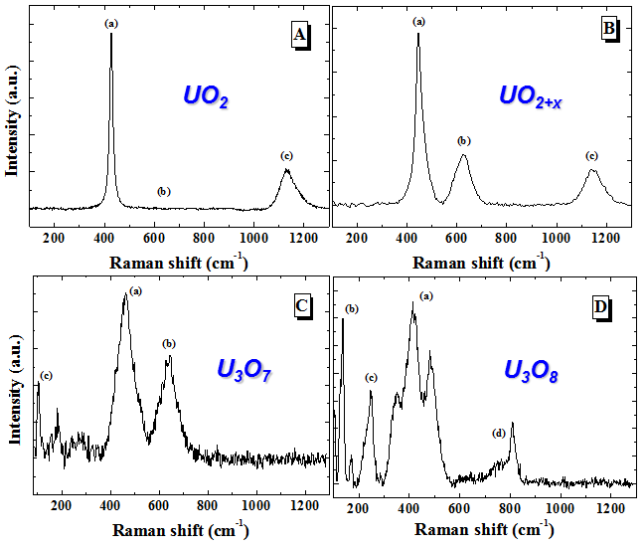

Figure 2. Raman reference spectrum for A) UO_2 B) UO_{2+x} C), U_3O_7 and D) U_3O_8.

In Figure 2, the letters between parentheses represent the main Raman bands of each phase. They have been assigned by other authors through the decades, giving as a result a solid knowledge about the transformation among phases and the associated changes in the spectrum [12-15].

From Figure 2, the evolution of the Raman spectra with the oxidation can be described as follows: the initial UO_2 spectrum varies by increasing the intensity of the band located above 600 cm^{-1} and decreasing the intensity of the band at 1140 cm^{-1} (2LO band) when oxidized to UO_{2+x}. Thereafter, when U_3O_7 is formed, the 2LO band disappears and therefore the spectrum has two intense features at 445 cm^{-1} and above 600 cm^{-1}. The change that occurs when the oxidation proceeds up to U_3O_8 is evidenced by the triplet of bands in the 300-500 cm^{-1} region. These transitions have been used as a fast, visual indicator of a change in the reaction, and therefore they are studied as a function of time in the oxidation experiments.

B. *In-situ* Raman acquisition and spectral analysis

The optimized protocol described above has been systematically applied to the UO_2 selected substrate at the testing conditions (0.1, 1, 10 and 21% O_2 and temperatures of 200, 300 and 400ºC). With this procedure, we have been

able to follow the reaction since the very beginning (2 minutes) up to a temporal range of several days. Each spectrum was measured during 50 seconds of acquisition time and using 3 accumulations. In order not to damage the sample, the laser power was reduced to a 5% of the nominal power [13]. Here we show some representative results selected at some of the conditions.

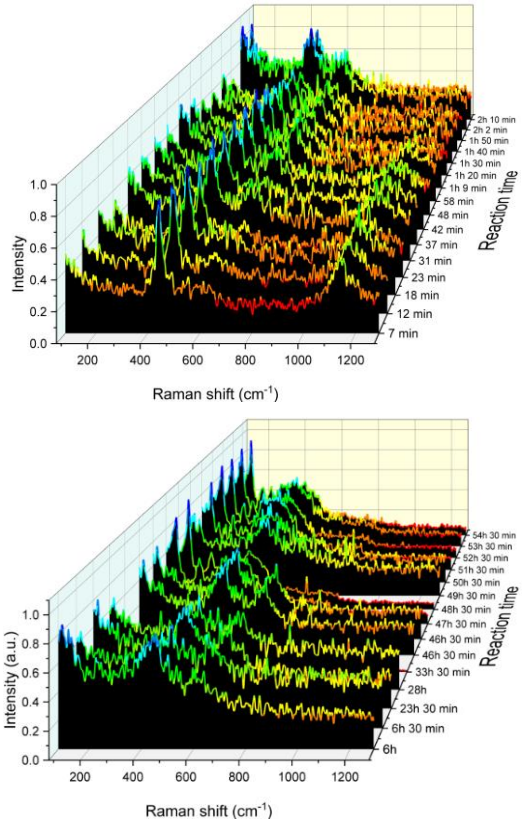

Figure 3. Raman spectra acquired during the experiment at 300ºC and 1%O_2 from 0 min to 2h (top), and from 6 to 54h (bottom).

The uranium phases described before are clearly visible in Figure 3. In the figure, the transformation from the initial UO_2 proceeds through the UO_{2+x} phase, which is reflected in the spectra by a continuous increase in the band at around 600 cm^{-1}, related to defects in the cubic lattice of UO_2 [16]. The opposite trend is found for the 2LO band at 1150 cm^{-1}, decreasing its intensity with time. The disappearance of this feature has been associated to the formation of U_3O_7. From 6 hours on, Figure 3 at the bottom, the spectrum of U_3O_8 (with the Raman bands described in Figure 2D) is obtained until the end of the experiment, confirming that the reaction has finished at these conditions.

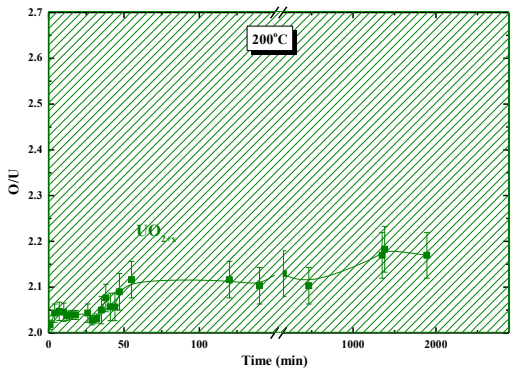

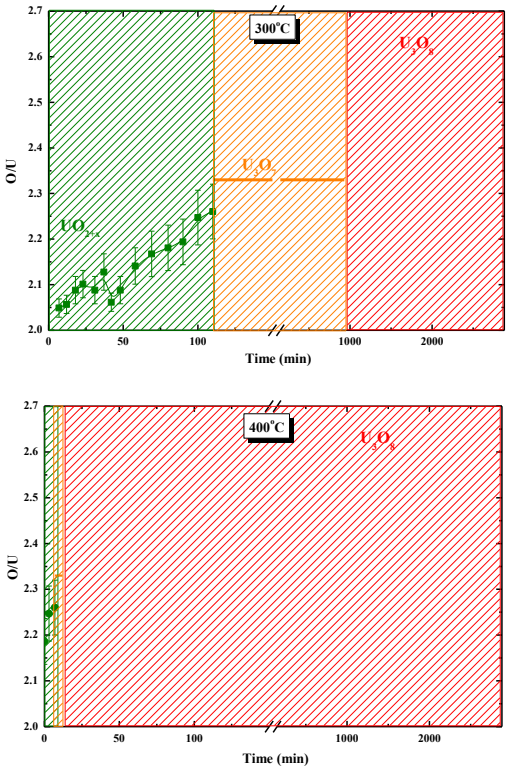

Figure 4. O/U ratio vs reaction time at 1%O_2 in the three temperatures of interest.

The spectra acquired at the different experimental conditions, and previously presented, have been analyzed in terms of the oxidation degree of UO_2. In this regard, the O/U ratio has been estimated according to the evolution of the Raman spectra with time. This assessment has allowed us characterizing the overall reaction and to divide it into three different phases: UO_{2+x}, U_3O_7 and U_3O_8. First of all, the initial step of the reaction has been evaluated by determination of "*x*" in the structure UO_{2+x}. With this purpose, we have used a previous analysis of the Raman spectra as a function of *x* [13], taking also into account the temperature correction factor [17]. In the second step of the reaction, the intermediate U_3O_7 phase is mainly obtained and interpreted as a stabilization phase of the reaction before reaching the final oxidation product. This phase has been associated with an O/U between 2.25 and 2.40, according to different values reported in literature [12, 18]. Finally, a third step in the reaction is defined by the presence of acquired spectra corresponding to the U_3O_8 phase, which is associated with the final of the oxidation process (O/U=2.67). This analysis has allowed us plotting the evolution of O/U with time, as in the form shown in Figure 4. From the figure, it is seen that, at 200ºC, the UO_{2+x} phase is obtained throughout the duration of the entire experiment, with an O/U ratio stabilized around 2.2. On the other hand, at 400ºC U_3O_8 is prevalent, in spite of carrying out the reaction in at atmosphere with only 1% O_2 present. This result is obtained for the rest of oxygen concentrations. At 300ºC, the different phases are discernible, following the known oxidation of UO_2. This major temperature effect has been also observed in other studies using traditional methods, such as TGA [6, 7], and the kinetics obtained for the UO_2 oxidation resembles the curves plotted here for the O/U evolution (Figure 4). This

fact reinforces the validity of this method for studying this reaction.

IV. CONCLUSIONS

In this work, we have developed a procedure that allows *in-situ* detecting the different uranium phases involved in the oxidation of UO_2, unlike other traditional techniques, such as TGA. This method is based on the use of the Linkam stage, coupled to the Raman spectrometer, which allows controlling the experimental conditions, not only in terms of temperature but also the different gaseous atmospheres. In the case of the UO_2 oxidation, this control is of particular importance in new designs for dry storage facilities of spent nuclear fuel, including an operational lifespan of the existing facilities.

In fact, the detailed analysis of the spectra obtained at the different conditions has allowed us following the reaction progress in an easy way, and thus determine the time at which U_3O_8 appears. Another conclusion of this analysis is that temperature (up to 400ºC) is a much-more affecting factor to the fuel oxidation, rather than the studied oxygen concentrations. All in all, this measurement protocol that ensures a reliable monitoring of the reaction has been optimized, being directly applicable to irradiated fuel.

V. ACKNOWLEDGEMENTS

The work presented here has been funded by ENRESA in the project: Nº 079-CO-IA-2018-0007 “Unirradiated UO_2 Oxidation Tests and associated analyses”.

VI. REFERENCES

[1] R. J. McEachern and P. Taylor, "A review of the oxidation of uranium dioxide at temperatures below 400°C," *Journal of Nuclear Materials,* vol. 254, pp. 87-121, 1998.

[2] S. Aronson, R. Roof, and J. Belle, "Kinetic Study of the Oxidation of Uranium Dioxide," *The Journal of Chemical Physics,* vol. 27, pp. 137-144, 1957.

[3] L. Quémard, L. Desgranges, V. Bouineau, M. Pijolat, G. Baldinozzi, N. Millot*, et al.*, "On the origin of the sigmoid shape in the UO2 oxidation weight gain curves," *Journal of the European Ceramic Society,* vol. 29, 2009.

[4] U.S.NRC, *Spent Fuel Project Interim Staff Guidance - 11: Cladding Considerations for the Transportation and Storage of Spent Fuel*: Nuclear Regulatory Commission, 2003.

[5] D. J. Richmond and K. J. Geelhood, "FRAPCON analysis of cladding performance during dry storage operations," *Nuclear Engineering and Technology,* vol. 50, pp. 306-312, 2018.

[6] R. E. Einziger and J. A. Cook, "LWR Spent Fuel Dry Storage Behavior at 229ºC," 1984.

[7] I. J. Hastings, D. McCracken, J. Novak, and K. Nash, "Behaviour in air at 175-400 degrees C of irradiated UO2 fuel," Canada1984.

[8] J. Nakamura, T. Otomo, T. Kikuchi, and S. Kawasaki, "Oxidation of Fuel Rod under Dry Storage Condition," *Journal of Nuclear Science and Technology,* vol. 32, pp. 321-332, 04/01 1995.

[9] A. B. Kolyadin, V. Y. Mishin, K. Y. Mishin, A. S. Aloy, and T. I. Koltsova, "Behavior of UO2 in the RBMK-1000 Spent Fuel under Oxidizing Conditions," *MRS Proceedings,* vol. 824, p. CC8.51, 2011.

[10] P. Tucker, "The effect of oxygen partial pressure on the kinetics of unirradiated UO2 oxidation," in *Proceedings of a workshop held at Berkeley Nuclear Laboratories*, 1987, pp. 7-9.

[11] A. Milena-Pérez, N. Rodríguez-Villagra, S. Fernández-Carretero, and A. Núñez, "Thermal air oxidation of UO2: Joint effect of precursor's nature and particle size distribution," *Progress in Nuclear Energy,* vol. 159, p. 104629, 2023.

[12] H. He and D. Shoesmith, "Raman Spectroscopic Studies of Defect Structures and Phase Transition in Hyper-Stoichiometric UO2+x," *Physical chemistry chemical physics : PCCP,* vol. 12, pp. 8108-17, 07/28 2010.

[13] J. M. Elorrieta, L. J. Bonales, N. Rodríguez-Villagra, V. G. Baonza, and J. Cobos, "A detailed Raman and X-ray study of UO2+x oxides and related structure transitions," *Physical Chemistry Chemical Physics,* vol. 18, pp. 28209-28216, 2016.

[14] T. Livneh, "Resonant Raman scattering in UO_2 revisited," *Physical Review B,* vol. 105, p. 045115, 01/11/ 2022.

[15] G. C. Allen, I. S. Butler, and T. Nguyen Anh, "Characterisation of uranium oxides by micro-Raman spectroscopy," *Journal of Nuclear Materials,* vol. 144, pp. 17-19, 1987/01/01/ 1987.

[16] J. M. Elorrieta, A. Milena-Pérez, J.-F. Vigier, L. J. Bonales, and N. Rodríguez-Villagra, "New insights into the structural transition from UO2+x to U3O7 by quantitative Raman spectroscopy," *Physical Chemistry Chemical Physics,* vol. 24, pp. 28394-28402, 2022.

[17] J. M. Elorrieta, L. J. Bonales, N. Rodríguez-Villagra, V. G. Baonza, and J. Cobos, "Spent fuel matrix oxidation studies under dry storage conditions," *MRS Advances,* vol. 2, pp. 675-680, 2017.

[18] G. Leinders, R. Bes, K. O. Kvashnina, and M. Verwerft, "Local Structure in U(IV) and U(V) Environments: The Case of U3O7," *Inorganic Chemistry,* 2020.

Proceedings of the European Nuclear Young Generation Forum
ENYGF'23
May 8-12, 2023, Kraków, Poland

Evaluation of the radiolytic effects affecting nuclear fuel reprocessing performance

Sánchez-García, Iván[1*], Núñez, Ana[1], Vacas-Arquero, Pablo[1], Serrano, Lorena[1] and Galán, Hitos[1]

[1] Centro de Investigaciones Energéticas, Medioambientales y Tecnológicas (CIEMAT), Avda. Complutense 40, 28040, Madrid (Spain).

*Corresponding author: *Ivan.sanchez@ciemat.es*

I. INTRODUCTION

One of the main issues nowadays towards the future of nuclear power is the proper and efficient management of nuclear waste. As one of the most sustainable solutions, the scientific community is working on advanced nuclear fuel cycles and particularly on the demonstration of closed fuel cycles, where the recovery of valuable fissile and fertile materials are not the only main goals, but also the reduction of the volume and radiotoxicity of the waste to be emplaced in the geological disposal facility. This strategy implies the reprocessing of the spent nuclear fuel in order to recycle the minor actinides (MAs: Am, Cm, Np) (which are together with the Pu, the main contributors of the long-term radiotoxicity) with the aim to produce fuels or transmutation blankets for advanced reactors [1, 2].

Currently, the aqueous processes (hydrometallurgical processes) are the most mature technology able to address actinides recycling. However, its development implies some important challenges like dealing with the degradation and regeneration of the extraction systems due to the effect of the highly radioactive field and nitric acid concentration where spent nuclear fuel must be dissolved. In fact, one limiting point for the hydrometallurgical strategy is that the organic extractants typically used for the selective separation are susceptible to radiolysis-induced breakdown, increasing both the cost and the amount of secondary wastes produced. Radiolytic and hydrolytic degradation during the extraction procedure give place the formation of degradation compounds, which can modify the extraction performance of the system by extracting undesirable elements, and/or the formation of insolubilities that produce the formation of third phases, which is considered as one of the main causes for criticality accidents during the handling of radioactive fuel solutions [3]. For that reason, the resistance of solvents must be carefully studied and optimized.

Among the organic extractants proposed for MAs partitioning applications, diglycolamides (DGAs) are known to be highly selective ligands for trivalent actinides (An(III)) and lanthanides (Ln(III)), reason why several compounds of this family of ligands have been studied over the last decades [4]. Particularly TODGA (*N,N,N',N'*-tetraoctyldiglycolamide, which structure is shown in Figure 1), [5, 6] is a well-known efficient co-extractant of An(III) and Ln(III) and consequently, several solvent extraction processes are currently under development based on the use of TODGA for MAs separations such as the European *i*-SANEX [7], the EURO-EXAM [8] and the EURO-GANEX [9] processes.

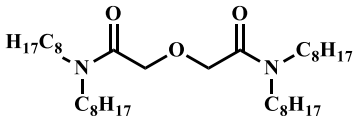

Figure 1. Structure of *N,N,N',N'*-tetraoctyldiglycolamide (TODGA).

It is desirable that organic phases be recycled as much as possible. In that sense, TODGA-based solvents have been the focus of many stability in the last years, concluding that TODGA solvents show, in general, a resistance enough to the harsh operational conditions expected [10-13]. However, the formation of degradation compounds (DCs) and their effects must be assessed in depth for each process, since the experimental conditions can modify the proportion and accumulation of these by-products.

The current trend is going towards more realistic studies, taking into account relevant process conditions. In that sense, the effects of metal complexation is one of the aspects to be considered since it is one of the major responsible of ligand environment. Up to now, from all studies abou TODGA degradation, only in a recent study performed by Kimberlin et al. [13], the radiolytic stability of TODGA-M complexes (neodymium and americium) has been reported. From this study, it can be concluded a higher resistance of the ligand when the complex between ligand and metal is formed, nevertheless, there is no information about the quantification of the degradation compounds.

The study of the DCs is relevant form the poinf of view of the extraction process because as DCs are formed due to TODGA degradation, the physico-chemical properties of the solvent may be modified as consequence of the individual properties of these compounds being able to

produce 3rd phase formation or solubility problems. In addition, some DCs could have different extraction properties than the initial ligand, resulting in an efficiency loss of the process. Therefore, the DCs study is the vital importance for the long-term operation of the extraction process.

In this work, the evaluation of the gamma radiolytic resistance of the TODGA ligand was studied taking into account the complexation with the Eu metal, varying the ratio of the ligand:metal with the aim to study after irradiation the degradation of TODGA as well as identifying and quantifying its degradation compounds by the HPLC-MS technique.

II. EXPERIMENTAL

A. Materials

The extractant used in the organic phase was TODGA, (purchased in Technocomm Ltd) diluted in odourless kerosene (OK), which was supplied from Alfa Aesar (Germany). $Eu(NO_3)_3 \cdot 6H_2O$ with a purity of 99.9 % was purchased from Aldrich (Germany). Nitric acid used as the aqueous diluent was obtained from VWR Chemical as nitric acid (HNO_3) 65% with the grade AnalaR NORMAPUR for analysis. The reagents were used without further purification except for HNO_3, which was additionally purified twice by a Quartz subboiling distillation system (MLS-Milestone) and used within a short period of time. The TODGA degradation compounds I-VIII were prepared according to the procedure described in previous works [16].

B. Irradiation procedure

Irradiation experiments were performed at the Náyade irradiation facility (CIEMAT). This facility consists of a pool of a 1.2 m^2 by 4.5 m deep that uses water as biological shield. At the bottom of the pool, 60 sources of ^{60}Co (15 mm diam. x 135 mm long each) can be distributed in six lots and using a cylindrical irradiation container provides a homogeneous irradiation flux.

Different samples of TODGA (0.1 mol/L in OK) pre-equilibrated with 3 mol/L HNO_3 were irradiated in steps of 50 kGy up to 500 kGy at dose rate of 9.23 kGy/h, as determined by Fricke dosimetry. In order to assess the effect of a metal in the degradation of this compound, samples of TODGA were submitted to gamma radiation at the same absorbed doses using an identical dose rate after a extraction with two different concentration of europium (17 mmol/L and 33 mmol/L $Eu(NO_3)_3 \cdot 6H_2O$ in 3 mol/L HNO_3, respectively). The pre-equilibration and the extraction experiments were performed by mixing both phases, aqueous and organic, for 30 min at room temperature (22 ± 2 ºC). Then, the phases were separated by centrifugation (5 min at 5000 rpm) and aliquots of only organic phase were taken for the irradiation experiment.

C. HPLC-MS analysis

The chemical composition of the irradiated organic samples was characterised by HPLC-MS. These measurements were performed by using an HPLC-MS Bruker EVOQTM (Triple Quadrupole detector) with an ACE 3 C18-PFP column (50 mm × 2.1 mm) at 40 °C, using a gradient of mobile phase [(A: 0.1% HCOOH in H_2O), (B: 0.1% HCOOH in CH_3CN)]. $APCI^+$ ionization mode was used for the quantification of TODGA and ESI^+ ionization mode for its DCs. Samples for HPLC-MS studies were analysed without preevaporation and diluted 1:30,000 in HPLC grade MeOH. Calibration curves were performed for TODGA and each TODGA DCs, from 10 to 1000 ppb, and the correlation coefficients in all cases were in the range of 0.992-0.999. All measurements were performed in duplicate to have an uncertainty analysis where results show a maximum error of ±4%.

III. RESULTS AND DISCUSSION

In the present study, the gamma irradiation was performed up to 500 kGy of 0.1 mol/L TODGA in OK in three different conditions: pre-equilibrated with 3 mol/L HNO_3, and after the extraction with 17 mmol/L and 33 mmol/L $Eu(NO_3)_3 \cdot 6H_2O$ in 3 mol/L HNO_3. The pre-equilibration was carried out with the aim to saturate with HNO_3 the organic phase in order to compare with the conditions where the metal is included. During the irradiation process, a small colour change from slightly yellow to dark yellow was found in all samples, but no third phase formation, precipitate, or other physical changes were observed.

After irradiation, all samples were characterized by HPLC-MS in order to assess the TODGA stability. First, the qualitative HPLC-MS analysis of the reference and the most irradiated (500 kGy) samples of TODGA in the three studied conditions were examined. In the non-irradiated samples, only the signal corresponding to TODGA was observed. As expected, when samples are irradiated, results show an intensity decrease of the TODGA signal as a consequence of degradation and the presence of several DCs (DC I-IX), which all of them are in agreement with the literature [10-13]. The structure of these DCs is shown in Figure 2. All irradiated samples analysed show practically the same chromatogram profile, but it is important to highlight that the relative intensities of DCs and TODGA changes as a function of the Eu concentration present in the irradiated samples. These observations seem to indicate a lower degradation of TODGA when the metal Eu is forming the complex with TODGA during the irradiation.

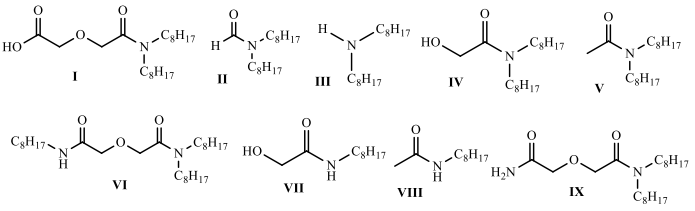

Figure 2 TODGA degradation compounds (DCs) identified in the qualitative analysis by HPLC-MS.

In order to clarify this hypothesis, quantitative HPLC-MS measurements not only for TODGA but also its DCs were carried out for all irradiated samples. Figure 3 shows the concentrations of TODGA as a function of the absorbed

dose for the three experimental conditions used: TODGA pre-equilibrated with 3 mol/L HNO_3 (called a) *TODGA w/o Eu*), TODGA after extraction with 17 mmol/L and with 33 mmol/L $Eu(NO_3)_3 \cdot 6H_2O$ in 3 mol/L HNO_3 (named b) *TODGA + 17 mmol/L Eu and c) TODGA + 33 mmol/L Eu*, respectively). Quantitative results confirm a decrease of TODGA concentration as a function of the absorbed dose, but also a lower degradation as Eu concentration increases.

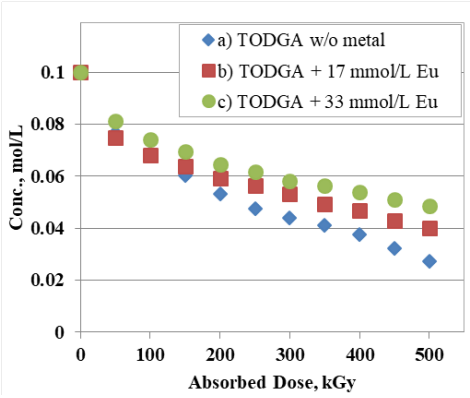

Figure 3. Concentration of TODGA as function of the dose for 0.1 mol/L TODGA irradiated in different conditions.

Taking into account the consideration of an exponential decrease of TODGA concentration as a function of absorbed dose suggesting a pseudo-first order kinetic, the dose constant was calculated following the next equation: $C = C_0 e^{-k'dos}$, where C_0 and C are the initial and final concentration of TODGA in mol/L, k' is the dose constant and *dos* is the absorbed dose by solvent in kGy. The results are given in Table 1. The *k'* value obtained for TODGA without metal is in agreement with the obtained for TODGA degradation in literature when it is irradiated pre-equilibrated with HNO_3 [11, 14]. Regarding the samples with metal, the trend is similar than the obtained by Kimberlin *et al.* [13] using Nd and the values are higher in that work probably because of they used a lower concentration of nitric acid (2.5 mol/L). The presence of a high Eu concentration (33 mmol/L) in the organic phase seems to have a higher protective effect than a low metal concentration (17 mmol/L). It can be found in literature a stoichiometry of 1:3 for Eu:TODGA complexes, which show a high constant association [15-17]. Therefore, when Eu concentration is about 30 mmol/L in the organic phase, every TODGA molecule should be involved in the Eu complex. However, for a half Eu concentration it still exits a high proportion of free TODGA in the media. These results can conclude that when TODGA is involved in a complex is less affected by gamma radiation. This behaviour could be explained by a steric protective effect of the weakest point of the molecule because of the complexation phenomena.

In addition to TODGA quantification, the TODGA DCs were also quantified at the same conditions. From nine DCs observed in the qualitative chromatograms, the quantification from DC I to DC VIII as a function of absorbed dose was represented in Figure 4 for all studied samples. DC IX quantification was not carried out due to the unavailability of the isolated product for the corresponding calibration curves. From Figure 4, as a consequence of TODGA degradation, an increase of all DCs concentrations as a function of the absorbed dose can be observed.

From all previous studies, it can be said that DCs formed are mainly IV and III, V and VI, due to the radiation effect over the weakest bonds of TODGA (C-O_{ether} and N-C) [10, 11]. As DCs are formed, they are also susceptible to radiolysis producing more DCs, reaching an equilibrium between its formation/degradation. This phenomenon can be observed in the figure with variations of concentrations of all DCs as a function of absorbed dose. First, a sharp increase of their concentration (until 250-300 kGy) and after that, the concentration slightly decreases and continues to growth indicating an equilibrium between their formation and own degradation. Moreover, it can be seen that as the concentration of europium increases during the irradiation (and therefore the formation of the TODGA-Eu complex), the concentration obtained for all DCs is lower, corroborating again the higher stability of TODGA when Eu is present, and always the more abundant DCs are mainly IV and III, V and VI. Therefore, it can be concluded from these results that there is no change in the degradation pathway of TODGA although there is europium in the medium and the complex is formed.

Table 1. Dose constants for TODGA degradation in different conditions.

Sample type	k' (kGy^{-1})
a) TODGA w/o Eu	0.00232
b) TODGA + 17 mmol/L Eu	0.00156
c) TODGA + 33 mmol/L Eu	0.00126

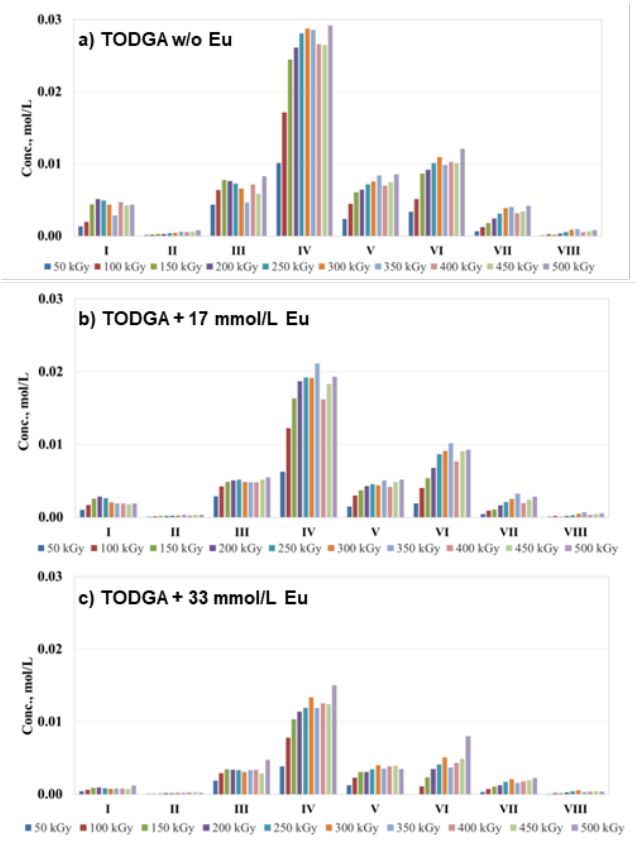

Figure 4. HPLC-MS quantitative studies of different TODGA degradation compounds at different experimental conditions.

IV. CONCLUSIONS

TODGA is a relevant molecule employed in several partitioning processes focused in the actinides recovery, included in the advanced fuel cycle strategy. The radiolytic resistance of these extractants is a limiting factor in the development of the processes, with special attention to its DCs. In this work, the radiolytic stability of TODGA in odourless kerosene was analysed taking into account the effect of the metal complexation during the irradiation process evaluating its degradation and the formation of its DCs. From the results obtained in this study, it can be concluded that metal complexation protects TODGA molecules from degradation, being particularly more stable when all TODGA molecules are involved in the Eu-complex formation.

As a consequence of TODGA degradation, the TODGA degradation compounds are also analysed and quantified, concluding that the most abundant are DCs IV, V and VI, which are products of the breakdown of the weakest bonds of TODGA, in agreement with the literature. Furthermore, this behaviour is always observed, regardless of whether there is Europium in the organic phase or not, so it can be concluded that there is no change in the degradation pathway because of metal complexation. As future work, deepest studies should be addressed in order to clarify what is the effect responsible for this protection observed.

V. References

[1] *Spent Fuel Reprocessing Options*. Vienna: INTERNATIONAL ATOMIC ENERGY AGENCY, 2009.

[2] E. Collins, G. DelCul, B. Spencer, R. Jubin, C. Maher, I.-T. Kim*, et al.*, "State-of-the-Art Report on the Progress of Nuclear Fuel Cycle Chemistry," Organisation for Economic Co-Operation and Development2018.

[3] B. J. Mincher, "Radiation chemistry in the reprocessing and recycling of spent nuclear fuels," in *Reprocessing and recycling of spent nuclear fuel*, ed: Elsevier, 2015, pp. 191-211.

[4] S. A. Ansari, P. Pathak, P. K. Mohapatra, and V. K. Manchanda, "Chemistry of diglycolamides: promising extractants for actinide partitioning," *Chemical reviews,* vol. 112, pp. 1751-1772, 2012.

[5] S. Ansari, P. Pathak, V. Manchanda, M. Husain, A. Prasad, and V. Parmar, "N, N, N′, N′-Tetraoctyl diglycolamide (TODGA): a promising extractant for actinide-partitioning from high-level waste (HLW)," *Solvent extraction and ion exchange,* vol. 23, pp. 463-479, 2005.

[6] D. Whittaker, A. Geist, G. Modolo, R. Taylor, M. Sarsfield, and A. Wilden, "Applications of diglycolamide based solvent extraction processes in spent nuclear fuel reprocessing, part 1: TODGA," *Solvent Extraction and Ion Exchange,* vol. 36, pp. 223-256, 2018.

[7] G. Modolo, A. Wilden, P. Kaufholz, and D. Bosbach, "Development and demonstration of innovative partitioning processes (i-SANEX and 1-cycle SANEX) for actinide partitioning. vol. 72," *Prog Nucl Energy,* pp. 107-114, 2014.

[8] C. Marie, P. Kaufholz, V. Vanel, M.-T. Duchesne, E. Russello, F. Faroldi*, et al.*, "Development of a selective americium separation process using H4TPAEN as water-soluble stripping agent," *Solvent extraction and ion exchange,* vol. 37, pp. 313-327, 2019.

[9] K. Bell, C. Carpentier, M. Carrott, A. Geist, C. Gregson, X. Hérès*, et al.*, "Progress towards the development of a new GANEX process," *Procedia Chemistry,* vol. 7, pp. 392-397, 2012.

[10] H. Galán, A. Núñez, A. G. Espartero, R. Sedano, A. Durana, and J. de Mendoza, "Radiolytic stability of TODGA: characterization of degraded samples under different experimental conditions," *Procedia Chemistry,* vol. 7, pp. 195-201, 2012.

[11] I. Sánchez-García, H. Galán, J. M. Perlado, and J. Cobos, "Stability studies of GANEX system under different irradiation conditions," *EPJ Nuclear Sciences & Technologies,* vol. 5, p. 19, 2019.

[12] A. Kimberlin, D. Guillaumont, S. Arpigny, B. Camès, P. Guilbaud, G. Saint-Louis*, et al.*, "An experimental and computational look at the radiolytic degradation of TODGA and the effect on metal complexation," *New Journal of Chemistry,* vol. 45, pp. 12479-12493, 2021.

[13] A. Kimberlin, G. Saint-Louis, D. Guillaumont, B. Camès, P. Guilbaud, and L. Berthon, "Effect of metal complexation on diglycolamide radiolysis: a comparison between ex situ gamma and in situ alpha irradiation," *Physical Chemistry Chemical Physics,* vol. 24, pp. 9213-9228, 2022.

[14] H. Galán, C. A. Zarzana, A. Wilden, A. Núñez, H. Schmidt, R. J. Egberink*, et al.*, "Gamma-radiolytic stability of new methylated TODGA derivatives for minor actinide recycling," *Dalton transactions,* vol. 44, pp. 18049-18056, 2015.

[15] M. R. Antonio, D. R. McAlister, and E. P. Horwitz, "An europium (III) diglycolamide complex: insights into the coordination chemistry of lanthanides in solvent extraction," *Dalton Transactions,* vol. 44, pp. 515-521, 2015.

[16] Y. Sasaki, P. Rapold, M. Arisaka, M. Hirata, T. Kimura, C. Hill*, et al.*, "An additional insight into the correlation between the distribution ratios and the aqueous acidity of the TODGA system," *Solvent Extraction and Ion Exchange,* vol. 25, pp. 187-204, 2007.

[17] A. Sengupta, S. M. Ali, and K. Shenoy, "Understanding the complexation of the Eu3+ ion with TODGA, CMPO, TOPO and DMDBTDMA: Extraction, luminescence and theoretical investigation," *Polyhedron,* vol. 117, pp. 612-622, 2016.

Proceedingsof the European Nuclear Young Generation Forum
ENYGF'23
May 8-12, 2023, Kraków, Poland

Progress on the adaptation and validation of the Incremental Centre Hole Drilling (ICHD) method for useon spentAGR fuel cladding

van Heule, Xavier[1*], Truman, Christopher[1], Coules, Harry[1] and Clark, Ronald[2]

[1] University of Bristol, United Kingdo; [2] National Nuclear Laboratory (NNL), United Kingdom

*Corresponding author: xavier.vanheule@bristol.ac.uk

I. INTRODUCTION

Since the strategic decision of the UK's Nuclear Decommissioning Authority (NDA), to cease the reprocessing of spent Advanced Gas-cooled Reactor fuel [1], any remaining spent fuel pins, as well as future ones to come out of the piles are to be kept in interim storage until a geological disposal facility becomesoperational.

The fuel pools of the former reprocessing facility THORP at Sellafield are being used for this interim storage. However, under these aqueous conditions, stress corrosion cracking (SCC) has been observed on some of the pins [2]. The driving force behind this SCC is thought to be the residual stress state in the fuel cladding. However, in order to make an optimal decision concerning prevention or mitigation, data about the affected fraction of the inventory is required.

Unfortunately, there is currently no readily available method for measuring residual stresses on the highly radioactive spent fuel pins. Therefore, research to adapt the Incremental Centre Hole Drilling (ICHD) method for application on spentAGR fuel pins is carried out.

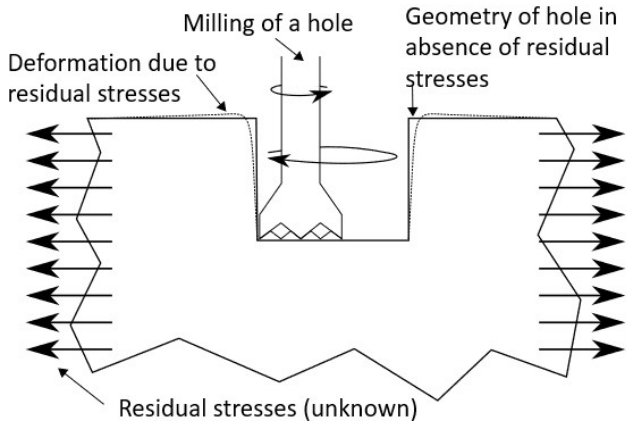

Figure 1. Schematic representation of Incremental Centre Hole Drilling (ICHD)

ICHD is a well-known [3-5] and standardized [6] technique. It is a semi-destructive relaxation method illustrated by figure 1. Stressesat the walls of the hole are relaxed, resulting in deformation at the surface around the hole. By measuring these deformations, the relaxed stresses can be determined. The thickness of the cladding (0.38 mm) and pitch of the ribs (2.77 mm) would allow up to seven 50 µm increments of a 1 mm diameter hole.

However, the ICHD technique, as prescribed by the standard, is not directly applicable to AGR fuel cladding. Frist off, the deformations are to be measured using three strain gauges, laid out in a rosette pattern. Unfortunately, the geometry of AGR fuel cladding (shown in figure 2) renders it impossible to accommodate such a strain gauge rosette. Furthermore, the calibration data used to calculate the stress profile from these strains, is also not applicable due to the curvature and presence of helicoidal ribs. In addition to this, the high radioactivity of spent fuel complicates matters even more in that all operations must be executed remotely, shielded from the radiation.

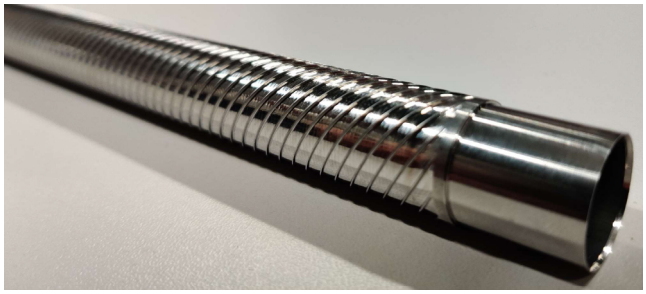

Figure 2. AGR Fuel cladding tube

To circumvent these issues, the use of Digital Image Correlation (DIC) instead of strain gauges is proposed. DIC correlates different photographs of a random pattern applied to the sample to determine displacement fields between these images. Although literature has already proven the successful combination of DIC and ICHD before [7], it is far from trivial to simply substitute strain gaugesfor DIC.

First off, new calibration has been generated and has been presented in [8]. Then, to combine DIC and ICHD, a specific stagewill be required [9]. This measurementstage will needto be remotely operableand fully resilient to high radiation doses. Finally, in irradiated fuel pins, the cladding interacts with the fuel, influencing and potentially skewing the results of an ICHD measurement.

Rather than providing an in-depth discussion for all these topics, this paper aims to give a brief summary of the research progress for each of these aspects.

II. LAB-BASEDVALIDATION

The first validation step consists of lab-based experiments performed on unirradiated pieces of cladding to demonstrate the feasibility of the method of measuring stresses in AGR fuel cladding. As the method combines ICHD and DIC, the sample must be reoriented between the drill and the camera system between each increment high repeatability, for which a specific experimental stage was developed. The successful use of this stage shall demonstrate the feasibility of the ICHD-DIC method.

The experiments are performed on short, 20 mm long sections of empty fuel cladding tube. To ensure stresses are present inside these samples they are mounted on a radial expander. This radial expander is designed to apply a uniform radial load on the inner surface of the tube.

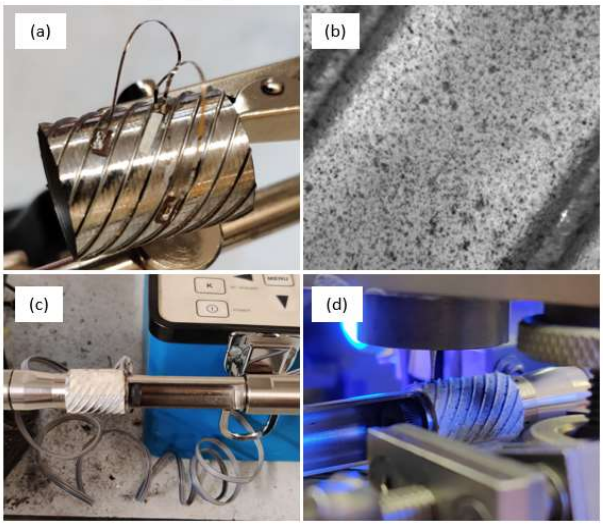

Figure 3. (a) application of a strain gauge between two ribs, (b) application of speckle pattern, (c) mounting and loading on radial expander, (d) hole drilling procedure.

Before the experiment, as shown in figure 3, a small strain gauge is attached to the cladding between two ribs as an independent measurement for the level of stress in the sample. Then, before mounting the sample on the radial expander, a speckle pattern is applied for the DIC, and finally, the ICHD experiment is executed.

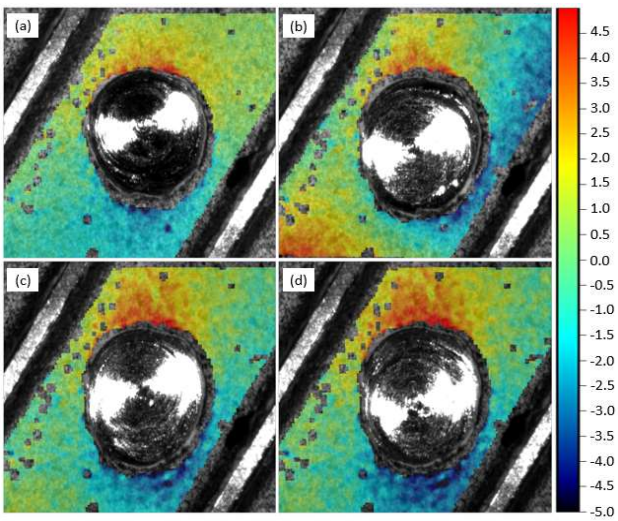

Figure 4. Hoop displacement fields [µm] for four depth increments

Typically, the radial expander results in a hoop stress of 400 - 450 MPa, and displacement fields such as the ones in figure 4 are obtained. After calculation of the hoop stress with the calibration data, the stress is overestimated by 2 orders of magnitude. Upon comparison of the measured displacement fields with the calibration data for 100 MPa (shown in figure 5), the origin of the discrepancy becomes clear.

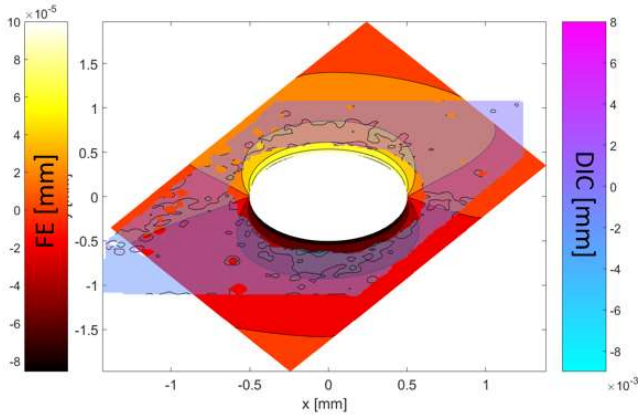

Figure 5. Comparison of the hoop displacement fields (in mm) for the calibration data at 100 MPa at the first increment with the measured DIC displacement field. A difference of two orders of magnitude is observed.

These seemingly unrealistic deformations are thought to be the cause of plastic deformation. Although the stress in the cladding (~450 MPa) is well below the yield strength (600-700 MPa), the presence of the hole causes a stress concentration of up to 3x the original stress [10], bringing the material well into the plastic domain.

In case of plasticity, the inverse calculation of the stresses with the calibration data becomes impossible. However, a potential solution has been identified under the form of the Neuber plastic strain correction [11]. This approach proposes a method to calculate estimates of the real stress and strain from an infinitely linear elastic material. The underlying assumption is that the energy required to deform both materials should be equal.

This, however, requires the tensile properties and plastic behaviour of the material to be well characterized, which is currently not the case. Future work will therefore aim to properly characterize the material and investigate the accuracy of the Neuber correction.

III. IN-SITUVALIDATION

Ultimately, these measurements are to be performed on active fuel pins, whose high activity introduces further difficulties. Any work on highly active material is remotely performed in shielded cells also known as 'hot cells' or 'caves', using tele-manipulators.

As a result, the feasibility of the method in hot cell environment is to be demonstrated as well. For this purpose, a new prototype for remotely applying ICHD with DIC on AGR fuel pins is designed. Besides being resilient with regards to high radiation doses, this prototype should be able to:

- retain a fuel pin immobile during drilling;

- Reorient the pin between the drill and the camera.
- Position the drill relative to the pin to drill in the desired location.
- Aim and focus the camera system at the drilling site.
- Drill the 50 µm increments with high precision.

The initial design of the prototype is shown in Figure 6. Two clamps, suspended on bearings, are used to grip the sample. Due to the bearings, the grips rotate freely, and two cams at either side limit their rotation to 90°. This fixes the rotation to two discrete positions: the drill and camera system. Since AGR fuel pins can be bent under irradiation, the drill needs 3 axes of movement: two horizontals (X3 and Z3) to align with the camera and drilling site, and one vertical (Y3) to perform the increments. The camera has two axes of movement: one vertical to align with the fuel pin, and one horizontal to focus the image. All actuation is done manually to avoid electronics as these are prone to failure under irradiation.

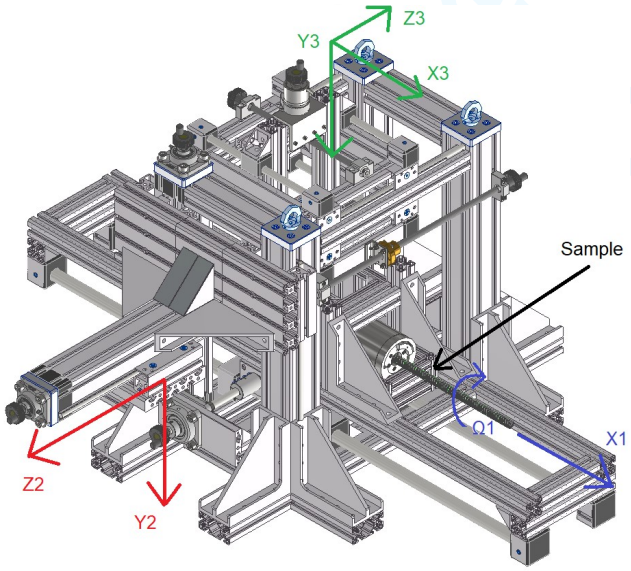

Figure 6. Initial design of the in-cave ICHD-DIC prototype. Red arrows indicate degrees of freedom for the camera, green for the drill, and blue for the sample.

Before bringing new rigs or inside a hot cell, these are first tested in a mock-up cell, free from radiation. Inside these mock-up cells, the rigs are tested extensively to identify any potential issues and demonstrate the reliability of the machine. This is to ensure interventions inside the cell will not be required.

Therefore, the in-cave ICHD-DIC prototype was sent to NNL facilities in Workington where such a mock-up hot cell is set up. Inside this mock-up cell, the prototype is subjected to a series of tests. These tests consist of verifying the operability of all controls, as well as performing a hole drilling procedure. Figure 7 displays some pictures of these tests.

The trials identified a series of issues with the operability of the rig. In the meantime, these have been resolved and the modified prototype is awaiting availability of the MSM test station for a second round of trials.

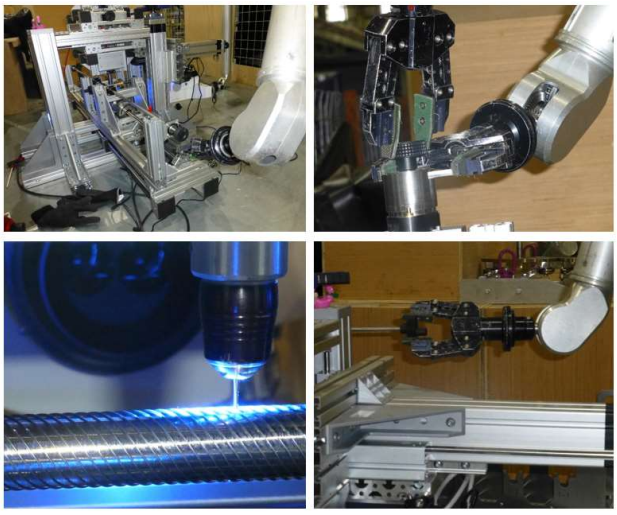

Figure 7. Testing of the CIHD-DIC prototype in a mock-up hot cell at NNL in Workington

IV. INFLUENCE OF THE FUEL

Finally, the presence of fuel pellets inside the fuel cladding tube is suspected to have a significant influence on the deformations at the surface of the material, and as such, must be subjected to further investigation.

For this purpose, pieces of cladding with simulant fuel pellets shrink fitted inside are brought to a synchrotron beamline facility (ESRF in Grenoble) for X-ray diffraction measurements. With X-ray diffraction, distances between crystal lattice planes are measured which are then converted to strain using the strain-free lattice parameter.

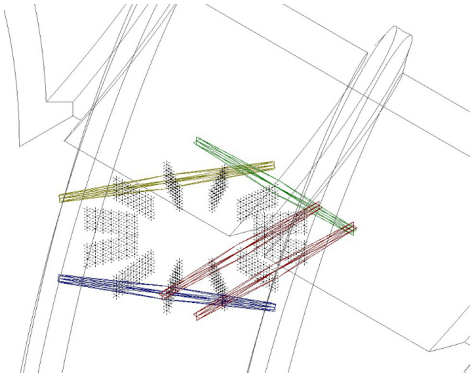

Figure 8. Rosette pattern for X-ray diffraction measurements, the position of the hole is at the center of the rosette, and the highlighted volumes illustrate some gauge volumes.

At the beamline, the strains are measured in the rosette pattern shown in figure 8, first before drilling the hole, and then after. It should be noted that the strains are measured in the direction radially outwards from the hole.

The resulting measurement data is shown in figure 9. Near the surface a strain relaxation is observed in the hoop direction, which is expected as the tensile hoop stress resulting from the shrink fit relaxes when the hole is drilled. What is less expected is that deeper inside the cladding, this relaxation decreases and becomes even positive (increase in strain). While it is remarkable that the strain would increase after drilling a hole, there is a plausible explanation for it.

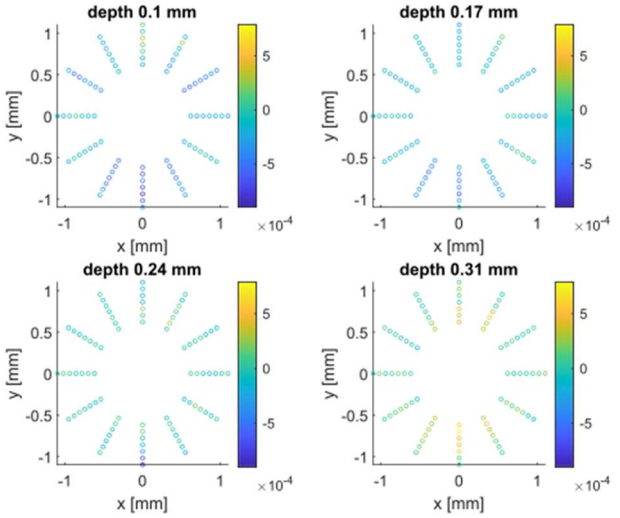

Figure 9. Rosettes of strain relaxation (μstrain) at different depths. Points on the x-axis show strain in the axial direction, points on the y-axis in the hoop direction. Points in between are measured in a direction in between hoop and axial, corresponding to their polar angle.

The pellet shrink fitted inside the cladding is pushing radially outward on the cladding, which is equilibrated by a tensile hoop stress inside the cladding. This radially outwards force is still present after the hole is drilled and must still be equilibrated, however with less material present near the hole. Therefore, the hole acts as a stress concentrator, explaining the increase in hoop strain underneath it.

The next steps consist of replicating the stress state prior to drilling in FE and investigating the strain relaxation with the hole as a function of the boundary conditions at the fuel-cladding interface such that the FE model behaves as closely as possible to the measured data.

V. CONCLUSIONS

The ICHD method for measuring residual stresses is being adapted for application on spent AGR fuel pins. For this purpose, DIC has been identified as a potential alternative to strain gauge rosettes for measuring surface deformation.

Firstly, lab-based validation experiments have been performed, demonstrating the feasibility of applying combined ICHD and DIC on AGR fuel cladding, successfully resolving the deformation fields using DIC.

However, these experiments have identified plasticity as a potential issue, and a solution based on the Neuber plastic strain correction is being investigated.

Next, to also demonstrate the feasibility of the method in a relevant environment, an in-cave prototype was designed and tested. The trials identified several operability issues, for which solutions have been worked out and implemented. The adapted prototype is currently awaiting its second round of tests to verify that the identified issues have indeed been solved.

Finally, it has been established that the presence of fuel inside the cladding has a significant influence on the measurement results. To quantify this influence, X-ray diffraction measurements with surrogate fuel pellets have been performed. The resulting data will be used to correct the FE calibration model, resulting in validated calibration data for cladding with fuel.

VI. ACKNOWLEDGEMENT

The authors would like to express their gratitude to NDA for providing funding for this project, and to NNL for industrial supervision. We would also like to thank EPSRC for providing the funds to develop the in-cave prototype, and NNL for providing access to their facilities and expertise.

Further thanks to ESRF in Grenoble for granting the beamtime, as well as the beamline scientists for their time and assistance.

VII. REFERENCES

[1] Nuclear Decommissioning Authority, "Oxide fuels: Preferred option," Tech. Rep. SMS/TS/C2-OF/001/Preferred Option, 2012.

[2] National Nuclear Laboratory, "Summary of AGR wet storage," Tech. Rep. NNL IP200709-6-10-01, 2009.

[3] G. S. Schajer, "Advances in hole-drilling residual stress measurements," Experimental Mechanics, vol. 50, no. 2, pp. 159–168, 2010. DOI: 10.1007/s11340-009-9228-7.

[4] M. B. Prime and M. R. Hill, "Uncertainty, model error, and order selection for series-expanded, residual-stress inverse solutions," Journal of Engineering Materials and Technology, vol. 128, no. 2, pp. 175–185, 2006. DOI: 10.1115/1.2172278.

[5] M. Steinzig, D. Upshaw, and J. Rasty, "Influence of drilling parameters on the accuracy of hole-drilling residual stress measurements," Journal of Engineering Materials and Technology, vol. 54, no. 9,pp. 1537–1543, 2014. DOI: 10.1007/s11340-014-9923-x.

[6] "Standard Test Method for Determining Residual Stresses by the Hole-Drilling Strain-Gage Method," American Society for Testing and Materials, Pennsylvania, USA, Standard ASTM E837-13a, 2013.

[7] M. J. McGinnis, S. Pessiki, and H. Turker, "Application of three-dimensional digital image correlation to the core-drilling method," Experimental Mechanics, vol. 45, no. 4, pp. 359–367, 2005. DOI: 10.1177/0014485105055435.

[8] X. van Heule, C. Truman, H. Coules, and R. Clark, "Measurement of residual stress in spent AGR fuel cladding using Incremental Centre Hole Drilling", Proceedings of the European Nuclear Young Generation Forum, 2021, pp. 138-143, ISBN-13: 978-84-09-24743-1.

[9] M. Pastor, M. Hagara, I. Virgala, A. Kalavsky, A. Sapietova, and L. Hagarova, "Design of a unique device for residual stresses quantification by the drilling method combining the photostress and digital image correlation," Materials, vol. 14, no. 2, pp. 1–27, 2021. DOI: 10.3390/ma14020314.

[10] G. Kirsch, "Die Theorie der Elastizitat und die Bedurfnisse der Festigkeitslehre," Zantralblatt Verlin Deutscher Ingenieure, Vol. 42, pp. 797-807, 1898.

[11] H. Neuber, "Theory of stress concentration for shear-strained prismatical bodies with arbitrary nonlinear stress-strain law," Journal of Applied Mechanics, vol. 28, pp. 544-550, 1961. DOI: 10.1115/1.3641780

List of Articles

Hot Topic 1 – Energy Transition: The Role of Nuclear

Hot Topic 2 – Neutrons for Progress

Hot Topic 3 – Communication, Policy, and Education

Hot Topic 4 – Future Nuclear

Technical Track 1 – Reactor physics, Thermal hydraulics, and Simulations

Technical Track 2 – Nuclear Safety and Security

Technical Track 4 – Fuel Cycle and Radiation Protection

ENYGF
KRAKÓW 2023

This book of proceedings compiles the articles of the European Nuclear Young Generation Forum 2023. The conference organizers did not ask for any intellectual property or exclusive use of the articles include herein. The materials in the articles have been used under the responsibility of the authors.

Graphic design, layout, compilation and editing:
Maciej Lipka
Front cover design:
Anna Talarowska

ISBN 978-83-66559-08-0

Instytut Zrównoważonej Energetyki and nuclear.pl

Kraków–Warszawa 2023

www.instytutze.org
www.nuclear.pl

ENYCF

KRAKÓW 2023

9 788366 559080

EUROPEAN NUCLEAR SOCIETY